

Friction Characteristic Prediction within a Carbon-Carbon Race Clutch

Gemma Lawrence (2008)

<https://radar.brookes.ac.uk/radar/items/4cb87f3e-58d7-4744-b67c-cd696f5e5c7d/1/>

Note if anything has been removed from thesis: pages XXXIX-LII

Copyright © and Moral Rights for this thesis are retained by the author and/or other copyright owners. A copy can be downloaded for personal non-commercial research or study, without prior permission or charge. This thesis cannot be reproduced or quoted extensively from without first obtaining permission in writing from the copyright holder(s). The content must not be changed in any way or sold commercially in any format or medium without the formal permission of the copyright holders.

When referring to this work, the full bibliographic details must be given as follows:

Lawrence, G (2008)

*Friction Characteristic Prediction within a Carbon-Carbon Race Clutch*, PhD, Oxford Brookes University

# **Friction Characteristic Prediction within a Carbon – Carbon Race Clutch**

by

Gemma Lawrence

A thesis submitted in partial fulfilment for the requirements of the degree of Doctor of Philosophy. Awarded by Oxford Brookes University in collaboration with AP Racing, Coventry and Honda Racing F1, Brackley

February 2008



## Abstract

Clutches are devices for disengaging the connection between the driveshafts and power units, and hence transferring rotational energy. Two inertias travelling with different angular velocities are brought to the same speed by engaging the clutch. The dissipation of energy during the operation results in a rise in temperature. When considering the parameters which contribute to the effectiveness of clutches, the properties of carbon fibre reinforced carbon (known as carbon-carbon) composites are considered to be superior to any other candidate materials available. The cost of devices made from such materials has precluded their use in “everyday” applications and limited them to “high end” motor sport use such as Formula 1.

This work considers the frictional properties of carbon-carbon composites in race clutch applications when combined with launch control systems, and how by improving the modelling of the co-efficient of friction of the material would lead to improved race starts. The work investigates the causes of frictional instability and how to promote more consistent coefficient of friction values through both bedding analysis and mathematical modelling.

Physical testing was undertaken using a clutch dynamometer to explore the effects of temperature, input speed and clamp loads upon the friction coefficient. Using infra-red sensors, a novel method was developed for the direct measurement of surface temperature of the plates. Banding of the clutches was also investigated. Materials testing was undertaken on the carbon-carbon clutch material to characterise its properties for thermal expansion, emissivity, specific heat and thermal conduction and this was novel in its contribution to the access of this data to the wider research community. The influence of carbon structure, physical, thermal, mechanical and chemical properties, as well as friction films, on the performance of carbon-carbon friction materials were modelled using MATLAB®. This was novel in the incorporation of surface behaviours into the full model. This model was then used to replicate clutch dynamometer data and predict coefficient of friction values. Results gave good predictions, with small errors in comparison with experimental data.

## Acknowledgements

I would like to thank AP Racing and The Engineering and Physical Sciences Research Council (EPSRC) for their funding of this project and Honda Racing F1 for the use of their test facilities.

I would like to acknowledge and thank my University supervisors, Prof. Denise Morrey and Prof. Geoff Goddard for their help, patience and knowledge. The encouragement and belief that they displayed throughout each stage kept project momentum going, and their understanding of all things engineering kept a broad vision of the subject matter. Thank you!

To Craig Dawson; my fellow research student, office cohabiter and best friend. Thank you for pulling me through the early stages; for the laughter and inspiration, the wise head and the broad shoulders. You are remembered every day.

Finally; a very special thankyou is reserved for my Grandad, for teaching me that its fine to pull everything apart in search of the answers to the question: "Why?"

# Table of Contents

Abstract	I
Acknowledgements	II
Table of Contents	III
List of Figures	IX
List of Tables	XVII
List of Abbreviations	XVIII
Nomenclature	XIX

## **Chapter 1: Introduction**

1.1	General Background	2
1.2	Aims and Objectives	3
1.3	Original Contributions as Outcomes from the Project	4

## **Chapter 2: Clutches and Control Systems; History, Development and Design**

2.1	What is a Clutch?	6
2.2	History of Development of Race Clutches	9
2.3	Clutch Design Process	13
2.4	Control Systems	16

## **Chapter 3: Literature Review**

3.1	Clutch Design and Carbon-Carbon Manufacture	21
3.2	Microstructures of Carbon	32
3.3	Material Properties and Behaviour	35
3.4	Factors Affecting Carbon – Carbon Material Behaviour	39
3.5	Surface Properties of Carbon-Carbon	42
3.6	Friction Film and Wear Mechanisms	57

3.7	Surface Tribological Behaviour and Oxidation	62
3.8	Surface and Heat Treatments	68
3.9	Heat Measurement Sensors	71
3.10	Experimental Testing	76
3.11	Mathematical Modelling and Prediction	78
3.12	Control System Development	86
3.13	Motorsport Applications	87
3.14	Summary	87
3.15	Gaps Identified in Previous Research	88

## **Chapter 4: Race Start Analysis**

4.1	Background	90
4.1.1	Qualifying Position	93
4.1.2	Grid Position (R/D)	93
4.1.3	0 – 100kph Time	94
4.1.4	Position Change	94
4.1.5	Time on Grid	94
4.1.6	Race Start (RS) Fuel	94
4.1.7	Tyre Temperatures: Initial & Race Start	95
4.1.8	Clutch Mode: Formation Start and Race Start	95
4.1.9	Clutch Friction: Formation Start, Race Start and Delta	96
4.1.10	Energy; Formation Start, Formation Lap and Race Start	96
4.1.11	Number of Clutch Events for Stack	96
4.1.12	Number of Race Starts	96
4.1.13	Weather	97
4.1.14	Air Temperature	97
4.1.15	Track Temperature	97
4.1.16	Friction Co-efficient of the Grid	97
4.2	Race Start Data	98
4.2.1	Melbourne	99
4.2.2	Barcelona	100
4.2.3	Budapest	101
4.3	Analysis of Starts	102

4.4	Results Analysis	105
4.4.1	Race Start 0-100kph	107
4.4.2	Number of Clutch Events Performed during Formation Lap	109
4.4.3	Race Start Energy	111
4.4.4	Race Start Coefficient of Friction	113
4.5	Conclusions from the Race Start Analysis	115

## **Chapter 5 : Bedding**

5.1	What is Bedding?	116
5.1.1	Friction Mechanisms During Bedding	117
5.1.2	Problems Created by Little or No Bedding In	118
5.1.3	Effect of Bedding Process on Actual Clutch Behaviour	
5.2	How are Clutches Bedded?	121
5.2.1	Variation of Kinetic Energy Through the Bedding Process	124
5.2.1	Variation of Bedding across Different Clutch Packs	125
5.2.3	Clutch Bedding and Bite Point Learns at the Track	126

## **Chapter 6 : Design of Experiments and Instrumentation**

6.1	Overview of Clutch Dynamometer and Current Testing Procedures	129
6.1.1	Temperature Measurement of the Clutch on the Dynamometer	130
6.2	IR Vs. Fibre Optics for The Application	132
6.3	Determination of the Emissivity of the Carbon Material	137
6.3.1	Emissivity Materials Testing	137
6.3.2	Results from Emissivity Materials Testing	142
6.4	Dynamometer Adaption for Accomodation of the Infrared Sensor	143
6.5	Dynamometer Rig Modifications	140
6.6	Structural FEA modelling of the adapted dynamometer test rig	148
6.7	Clutch Adaption	149
6.8	Experimental Validation of the Initial Setup	151
6.8.1	Analysis of Validation Test Data	151
6.9	Test Plan	154
6.10	Results	155

6.10.1	Temperature Analysis	156
6.10.2	Torque Analysis	159
6.10.3	Torque Vs. Temperature Analysis	160
6.10.4	Infrared Sensor Alignment	163
6.11	Conclusions and Recommendations for the Further Experimental Work	164

## **Chapter 7: Experimental Testing**

7.1	Adaptions from the Initial Testing	166
7.1.1	Experimental Investigation into the Effects of Banding	166
7.2	Test Plan	169
7.3	Initial Result Observations	173
7.3.1	Results for Enforced Banding Plate A	176
7.3.2	Results for Enforced Banding Plate B	177
7.3.3	Results for Enforced Banding Plate C	178
7.3.4	Results for Enforced Banding Plate D	179
7.3.5	Results for Enforced Banding Plate E	180
7.3.6	Results for Enforced Banding Plate F	181
7.3.7	Results for Enforced Banding Plate G	182
7.3.8	Results for Standard Plate with no Enforced Banding	183

## **Chapter 8: Experimental Results Analysis**

8.1	Constraints of the Experimental Programme	184
8.2	Estimation of Experimental Error	185
8.2.1	Sensor Errors	185
8.2.2	Apparatus Errors	188
8.2.3	Post Processing Errors	188
8.3	Processing of Raw Experimental Data	190
8.4	Experimental Data Results	190
8.4.1	Experimental results for the Effects of Initial Heat Soak	190
8.4.2	Experimental results for the Effects of Clamp Load	194
8.3.3	Experimental results for the Effects of Initial Speed	198
8.5	Discussion of Results Obtained from Experimental Testing	201



8.5.1	The Use of Scanning Electron Microscopy to Determine Oxidisation	204
8.6	Processing of 'Banding' Raw Data	207
8.7	'Banding' Data Results	210
8.8	Conclusions from Experimental Testing	220

## **Chapter 9: Input Modelling**

9.1	Rig Model Overview	222
9.2	Clutch Dynamometers: Overview	223
9.3	Schematic of the Clutch Dynamometer	224
9.4	Clutch Dynamometer Modelling	227
9.5	Model Code Validation	229

## **Chapter 10: Thermal Modelling**

10.1	Thermal Modelling Background	231
10.2	Materials Characterisation	232
10.2.1	Specific Heat	233
10.2.2	Thermal Diffisivity / Conductivity	234
10.3	Thermal Model Code Generation and Structure	238
10.4	Validation of the Thermal Model	240

## **Chapter 11: Surface Modelling**

11.1	Surface Characteristics	243
11.2	Materials Characterisation	245
11.3	Modelling of the Surface	247
11.4	Surface State Look Up Table Generation	249
11.5	Surface Model Code Generation	254
11.6	Model Validation	257

## **Chapter 12: Final Model**

12.1	Final Model Overview	258
12.2	Final Model Code for Thermal Characteristic Generation	259

## **Chapter 13: Model Results and Discussion**

13.1	Input Model Results	263
13.1.1	Input Model Results Discussion	264
13.2	Final Model Results and Assessment	266
13.3	Discussion, Discrepancies and Errors	268

## **Chapter 14: Further Work**

14.1	Follow-On Work as a Result of the Literature Review	270
14.2	Reccomendations for Further Experimental Work	271
14.2.1	Plate Profile	271
14.2.2	Saturation and Oxidation Temperature Investigation	271
14.3	Reccomendations for Further Modelling Work	272
14.3.1	Improvements the coule be made to the Existing Model	272
14.3.2	Further Investigation of Surface Behaviour	275

## **Chapter 15: Conclusions**

15.1	Conclusions	276
------	-------------	-----

<b>References</b>	XXII
-------------------	------

## **Copies of Published Materials**

Paper A	LAWRENCE, G; MACE, G; BOWLER, N; GODDARD, G; MORREY, D: (2006). <i>Measurement of the Interfacial Plate Temperatures within a Carbon Clutch, and Determination of Effects upon its Friction Characteristics.</i> (2006-01-3634) Warrendale, PA: Society of Automotive Engineers.	XXXVIII
---------	--	---------

## Appendices

Appendix A	2006 Race Starts Data Plots	LI
Appendix B	Race Start Analysis MATLAB Code	LXIX
Appendix C	Rig Part Drawings.	XC
Appendix D	140mm Clutch Technical Information	XCIX
Appendix E	Initial Testing Graphs.	CIV
Appendix F	Final Testing Banded Plate Graphs	CVIII
Appendix G	MATLAB® Code for Data Extraction	CXVI
Appendix H	Temperature Effects of Initial Temperature	CXXIX
Appendix I	Friction Effects of Initial Temperature	CXXXVIII
Appendix J	Temperature Effects of Clamp Load	CXLVI
Appendix K	Friction Effects of Clamp Load	CLV
Appendix L	Temperature Effects of Input Speed	CLXIII
Appendix M	Friction Effects of Input Speed	CLXXII
Appendix N	Friction vs. Temperature Plots for sub 400°C	CLXXX
Appendix O	MATLAB® Code for Results Analysis Model	CLXXXVIII
Appendix P	Results Analysis Model Initial Plots	CXCVIII
Appendix Q	Results Analysis Model Evaluated Plots	CCV
Appendix R	Technical Drawings of a Clutch Dynamometer	CCVIII
Appendix S	Rig Modelling MATLAB® Code	CCXII
Appendix T	Specific Heat and Thermal Diffisivity and Conductivity Test Results	CCXV
Appendix U	Thermal Modelling MATLAB® Code	CCXVII
Appendix V	Thermal Decomposition Test Results	CCXXI
Appendix W	Surface Modelling MATLAB® Code	CCXXIV
Appendix X	Final MATLAB® Model Code	CCXLIII

## List of Figures

Figure 1.1a	A Multi-plate Clutch Arrangement – as used in F1 applications	2
Figure 2.1a	Drivetrain Schematic – with the engine, transmission and exhaust systems	7
Figure 2.1b	A typical torque (red) / power (blue) curve	7
Figure 2.1c	Zeroshift System	8
Figure 2.3a	AP Racing’s first 140mm and most recent 97mm carbon-carbon clutches	11
Figure 2.4b	A typical SimuLink model for F1 clutch Mu calculation	16
Figure 2.4c	Mu calculation control conditions.	17
Figure 3.1a	The PAN Precursor Fibre Process [19]	24
Figure 3.1b	Basic Elements Required to Produce Carbon Fibres from Rayon [19]	24
Figure 3.1c	The Processing Sequence for PAN and Mesophase Pitch-based Precursor Carbon Fibres [19]	25
Figure 3.1d	The balance of diffusion and surface kinetics [19]: idealized depictions: (a) surface reaction rate is greater than diffusion rate; (b) diffusion rate is greater than the reaction rate.	26
Figure 3.1e	The Carbon – Carbon Manufacturing Process [22]	29
Figure 3.2a	Eight allotropes of Carbon [19]	32
Figure 3.5a	Diagrammatic representation of graphine layers [19]	44
Figure 3.5d	Schematic diagram of changes in the lamellar structure of a graphitizing carbon with increasing HTT [19]	54
Figure 3.5f	XRD spectra of CVI-densified carbon-carbon composite before and after HTT (intensity on log scale) [59]	55
Figure 3.6a	The SEM cross-sectional profile of carbon-carbon material [64]	60
Figure 4.2a	A Typical F1 Steering Wheel.	85
Figure 4.2b	Typical Race Start Graph with Plot Explanations	98
Figure 4.2.1a	Race Start, Car One, Melbourne Circuit	99
Figure 4.2.1b	Race Start, Car Two, Melbourne Circuit	99

Figure 4.2.2a	Race Start, Car One, Barcelona Circuit	100
Figure 4.2.2b	Race Start, Car Two, Barcelona Circuit	100
Figure 4.2.3a	Race Start, Car One, Budapest Circuit	101
Figure 4.2.3bi	Race Start, Car Two, Budapest Circuit	101
Figure 4.3b	Anscombes Quartet	104
Figure 4.4.1a	Mu calculation control conditions - Race Start 0 – 100kph	107
Figure 4.4.2a	Mu calculation control conditions – Number of Events	109
Figure 4.4.3a	Mu calculation control conditions - Race Start Energy.	111
Figure 4.4.4a	Mu calculation control conditions - Race Start Friction.	113
Figure 5.1.3a	Peak coefficient of friction values for a typical new F1 clutch at the start and end of clutch engagement [164].	119
Figure 5.1.3b	Peak coefficient of friction values at the start and end of a clamping event after approximately 20 bedding cycles [164]	120
Figure 5.1.3c	Peak coefficient of friction values at the start and end of a clamping event after approximately 70 bedding cycles[164].	120
Figure 5.2a	Bedding cycle for Sachs 3209 clutch: Friction Co-Efficient [164]	122
Figure 5.2b	Calculation of Peak Friction Values [164]	122
Figure 5.2.1a	Bedding cycle for Sachs 3207 clutch – Initial Kinetic Energy [164]	125
Figure 5.2.2a	Measured mu for selected clutch packs [164]	125
Figure 5.2.3a	Pi Toolbox screen grab of single event from Sachs 3556 [164]	127
Figure 6.1a	Representation of the Clutch Dynamometer at AP Racing	130
Figure 6.1b	The Clutch Dynamometer at AP Racing, Coventry	130
Figure 6.1.1a	Thermocouple Mountings on the clutch in the dynamometer	131
Figure 6.1.1b	Heat Dissipated by a Clutch Whilst Slipping (taken during initial clutch testing)	132
Figure 6.2a	Possible Fibre Optic Signal Converter Mounting Point.	133
Figure 6.2b	Proposed Sensor Exit Location	134
Figure 6.2c	The infrared sensor, as used in the dynamometer testing	136
Figure 6.2d	The mirrored head, used in the infrared sensor	136
Figure 6.2e	The Infrared sensor dimensions, as supplied by Radir	136
Figure 6.3.1a	Emissivity Test Apparatus at the National Physical Laboratory Teddington UK	138

Figure 6.3.1b	Close up of the Graphite Block Used to Hold the Sample (taken at the National Physical Laboratory – Teddington)	138
Figure 6.3.1c	The Emissivity Vacuum Chamber and Window (taken at the National Physical Laboratory – Teddington)	139
Figure 6.3.1d	The Emissivity Spectrometer / Detector (taken at the National Physical Laboratory – Teddington)	140
Figure 6.5a	Infrared sensor configuration on the adaptor plate for the clutch on the dynamometer (taken during initial testing)	145
Figure 6.5b	a. Drive torque motor, b. Body of infrared sensor, with right angled mirror attached, c. Clutch assembly, d. Actuator (taken during initial testing).	146
Figure 6.5c	Spring Cushioning between Actuator Plate and Actuator	147
Figure 6.5d	Overview of Spring Cushioning between Actuator Plate and Actuator	147
Figure 6.7a	A typical AP Racing multi plate clutch arrangement (Solidworks screen grab)	149
Figure 6.7b	The Old Clutch Configuration prior to modification (parts with a red dot rotate)	150
Figure 6.7c	The New Clutch Configuration after modification (parts with a red dot rotate)	151
Figure 6.8.1a	Drive Torque Vs. Output Torque.	152
Figure 6.8.1b	Drive Torque Vs. Output Torque During Clamping	153
Figure 6.9b	Thermocouple Radial Depth Locations	155
Figure 6.10.1a	Thermocouple Profile	156
Figure 6.10.1b	Infrared vs. Thermocouples at initial temperature of 100°C	157
Figure 6.10.1c	Infrared vs. Thermocouples at initial temperature of 200°C	157
Figure 6.10.1d	Brake Banding Taken on the brakes dynamometer. (Courtesy of AP Racing)	159
Figure 6.10.2a	Torque analysis at initial temperature of 100°C	159
Figure 6.10.3a	Torque vs. temperature analysis from initial temperature of 100°C	161
Figure 6.10.3b	Torque vs. temperature analysis during the ‘cool down’ phase from a 7000rpm, 3500N slip with initial soak of 100°C	162

Figure 7.1.1b	SolidWorks Model of a Typical Banded Plate	167
Figure 7.1.1c	A Typical Plate with enforced banding as used in testing	168
Figure 7.1.1d	Damage Caused by the Cutting out of the Material by the Enforced Banding Plate	169
Figure 7.2c	The Configuration of enforced banding plate D	172
Figure 7.2d	Thermocouple Arrangements on Driving Plate	173
Figure 7.3a	Plate A at 3000rpm, 1500N Clamp Load at 100°C (red), 200°C (green) and 300°C (blue) soak temperatures	174
Figure 7.3b	Plate A at 5000rpm, 3500N Clamp Load at 100°C (red), 200°C (green) and 300°C (blue) soak temperatures	175
Figure 7.3.1a	Graph of drive speed in rpm and input torque x 10 Nm on y1 and temperature °C and mu x 1000 on y2 against log number (100 = 1 second) for Plate A at an input speed of 5000rpm, clamp load of 2500N and an initial soak temperature of 200°C	176
Figure 7.3.2a	Graph of drive speed in rpm and input torque x 10 Nm on y1 and temperature °C and mu x 1000 on y2 against log number (100 = 1 second) for Plate B at an input speed of 5000rpm, clamp load of 2500N and an initial soak temperature of 200°C	177
Figure 7.3.3a	Graph of drive speed in rpm and input torque x 10 Nm on y1 and temperature °C and mu x 1000 on y2 against log number (100 = 1 second) for Plate C at an input speed of 5000rpm, clamp load of 2500N and an initial soak temperature of 200°C	178
Figure 7.3.4a	Graph of drive speed in rpm and input torque x 10 Nm on y1 and temperature °C and mu x 1000 on y2 against log number (100 = 1 second) for Plate D at an input speed of 5000rpm, clamp load of 2500N and an initial soak temperature of 200°C	179
Figure 7.3.5a	Graph of drive speed in rpm and input torque x 10 Nm on y1 and temperature °C and mu x 1000 on y2 against log number (100 = 1 second) for Plate E at an input speed of 5000rpm, clamp load of 2500N and an initial soak temperature of	180

	200°C	
Figure 7.3.6a	Graph of drive speed in rpm and input torque x 10 Nm on y1 and temperature °C and mu x 1000 on y2 against log number (100 = 1 second) for Plate F at an input speed of 5000rpm, clamp load of 2500N and an initial soak temperature of 200°C	181
Figure 7.3.7a	Graph of drive speed in rpm and input torque x 10 Nm on y1 and temperature °C and mu x 1000 on y2 against log number (100 = 1 second) for Plate G at an input speed of 5000rpm, clamp load of 2500N and an initial soak temperature of 200°C	182
Figure 7.3.8a	Graph of drive speed in rpm and input torque x 10 Nm on y1 and temperature °C and mu x 1000 on y2 against log number (100 = 1 second) for the Standard Plate at an input speed of 5000rpm, clamp load of 2500N and an initial soak temperature of 200°C	183
Figure 8.2.1a	Torque Sensor (Courtesy of Variohm Sensors – Daventry UK)	186
Figure 8.2.3a	Temperatures due to Emissivity Uncertainty	189
Figure 8.2.3b	IR Transmission Spectra of Polyethylene	189
Figure 8.4.1b	Example of plots created for different initial soak temperatures with respect to time versus temperature on a scale of initial speed versus clamp load for enforced banding Plate A	192
Figure 8.4.1c	Graph of Initial Soak Temperature against Time to reach 800°C for the Standard Plate, Plate B, Plate D and Plate F	191
Figure 8.4.1d	Example of plots created for different initial soak temperatures with respect to coefficient of friction versus temperature on a scale of initial speed versus clamp load for forced banding Plate A	192
Figure 8.4.2b	Example of plots created for different clamp loads with respect to temperature versus time on a scale of initial speed versus initial soak temperature for forced banding Plate A	196
Figure 8.4.2c	Graph of Clamp Load against Time to reach 800°C for the	197



	Standard Plate, Plate B, Plate D and Plate F.	
Figure 8.4.2d	Example of plots created for clamp load with respect to coefficient of friction versus temperature on a scale of initial speed versus initial soak temperature for forced banding Plate A	197
Figure 8.4.3b	Example of plots created for different initial input speeds with respect to temperature versus time on a scale of initial clamp load versus soak temperature for forced banding Plate A	200
Figure 8.4.3c	Graph of Input Speed against Time to reach 800°C for the Standard Plate, Plate B, Plate D and Plate F	200
Figure 8.4.3d	Example of plots created for initial input speeds with respect to coefficient of friction versus temperature on a scale of clamp load versus initial soak temperature for forced banding Plate A	201
Figure 8.5a	Graph of Clamp Load vs. Log Number (time) for Plate B at 5000rpm, 2500N and 200°C	202
Figure 8.5b	Graph of Friction vs. Temperature up to 400°C for Plate A at 5000rpm and 3500N Clamp Load	203
Figure 8.5c	Graph of Friction vs. Temperature up to 1500°C for Plate A at 5000rpm and 3500N Clamp Load	203
Figure 8.5.1a	SEM Photo Showing a Dull Banded, Oxidised Area, Moving Into an Un-oxidised Area of a Carbon-Carbon Clutch Disc (taken using the SEM at Honda Racing F1)	205
Figure 8.5.1b	SEM Photo of an Oxidised Area of a Carbon-Carbon Clutch Disc (taken using the SEM at Honda Racing F1)	206
Figure 8.5.1c	SEM Photo of an Un-oxidised Area of a Carbon-Carbon Clutch Disc (taken using the SEM at Honda Racing F1)	206
Figure 8.5.1d	SEM Photo of a Pore in an Oxidised Area of a Carbon-Carbon Clutch Disc (taken using the SEM at Honda Racing F1)	206
Figure 8.7c	Bar Chart Illustrating the Correlation Coefficients of Banded Plates	215
Figure 8.7f	Bar Chart illustrating the two Highest Correlation Coefficients of Standard Plate Compared to the Banded	218

	Plates	
Figure 8.7g	Bar Chart Illustrating the Highest Correlation Coefficients of Standard Plate Compared to the Banded Plates	219
Figure 9a	Initial Schematic of the Mathematical Model.	221
Figure 9b	Free body diagram of the system to be mathematically modelled	222
Figure 9.2a	The model schematic and where the rig model fits into it.	222
Figure 9.2a	Diagrammatic Representation of the Clutch Dynamometer at AP Racing	223
Figure 9.2b	The Clutch Dynamometer at HGT (Japan) [164])	224
Figure 9.3a	Schematic diagram of the HGT Clutch Dynamometer [164]	225
Figure 9.3b	Block Diagram of the Clutch Dynamometer at HGT	225
Figure 9.3c	Block diagram of the clutch dynamometer at HGT in inertial absorption configuration	226
Figure 9.3d	Block diagram of the clutch dynamometer at HGT in constant slip configuration	226
Figure 9.5a	Dynamometer data versus. Modelled data for clutch speed difference for different values of clutch actuation pressure	230
Figure 10a	The model schematic and where the thermal model fits into it.	231
Figure 10.2.2b	Thermal Diffusivity Test Signal	235
Figure 10.2.2c	Thermal Diffusivity Sample Holder	236
Figure 10.2.2d	Thermal Diffusivity Test Apparatus	236
Figure 10.2.2e	Thermal Diffusivity of a Carbon Clutch Plate Material	237
Figure 10.2.2f	Thermal Conductivity of a Carbon Clutch Plate Material	237
Figure11a	The model schematic and where the surface model fits into it	242
Figure 11.1a	SEM highlighting the surface morphology of as-polished disc (Type I) [50]	243
Figure 11.1b	SEM highlighting the surface morphology of bedded material (Type II/Type III transition) [51]	244
Figure 11.1c	SEM highlighting Type III surface morphology (lubricating friction film) [50]	244
Figure 11.2a	Sample Decomposition Summary	247

Figure 11.4b	Generation of 3D lookup table with defined points highlighted (known = red, generated = green)	252
Figure 11.4c	Example of a poorly generated lookup table	252
Figure 11.4d	Change in Surface State Coefficient Due to Normalised Power and Normalised Temperature	253
Figure 12a	The overall model schematic	258
Figure 13.1a	Actual and Simulation Clutch Speed Difference for Bedding Pressures	264
Figure 13.1.1a	Simulated Rig Speed / Torque Profile	265
Figure 13.1.1b	Actual Rig Speed / Clamp Load Profile	265
Figure 13.2a	Actual and Simulation Clutch Speed Differences during a clamping event from 8000rpm at varying clamp loads.	266
Figure 13.2b	Error in Mu Ave (s1), Start Mu (s2) and End Mu (s3) for a Single Event Using 44,000 different look up tables.	267
Figure 13.2c	A Simulation Result for Clutch Friction from the full model	267
Figure 13.2d	Rig Data for Clutch Friction	268
Figure 14.3.1b	DMA Sample and Sample Holder	273
Figure 14.3.1c	Perkin Elmer DMA Machine	274
Figure 14.3.1d	Perkin Elmer DMA Test Program	274
Figure 14.3.1e	Thermal Expansion Graph	275

## List of Tables

Table 3.5b	Descriptions of the surface morphology classifications as suggested by Ju et al. [51]	46
Table 3.5c	XRD analysis of wear debris by Hutton et al. [57]	50
Table 3.5e	XRD analysis of HTT specimens by Luo et al. [58]	54
Table 3.5g	Experimental data from testing of HTT specimens by Luo et al. [59]	55
Table 6.3.2a	Normal Spectral Emissivity Results Obtained from Emissivity Testing at NPL, Teddington UK	142
Table 6.3g	Emissivity Measurement Uncertainty (Percent)	143
Table 6.9a.	Test Plan for varying initial temperatures, clamp loads and input speeds	154
Table 6.10.3c.	Percentage heat reduction and its effects on the reduction in torque from initial testing.	162
Table 7.1.1a	Radial locations of the enforced bands	167
Table 7.2a.	Variables Showing the Clamp Load, Input Speed and Initial Soak Temperature for all tests	170
Table 7.3c.	Thermocouple Legend for use in Graphs in Section 7.3	175
Table 8.4.1a	Clamp Load Duration for all Variable Plates at Temperatures of 100°C, 200°C and 300°C, Grouped by Input Speed and Clamp Load	191
Table 8.4.2a	Clamp Load Time for all Variable Plates for Clamp Loads of 1500N, 2500N and 3500N, Grouped by Input Speed and Temperature	195
Table 8.4.3a	Clamp Load Time for all Variable Plates for Speeds of 3000rpm, 5000rpm and 7000rpm, Grouped by Temperature and Clamp Load	199
Table 8.6b	Table illustrating the correlation coefficients required for each set of test parameters and each banded test plate	208
Table 8.6c	Banded Plates and Their Corresponding Thermocouples	209
Table 8.7a	Correlation Coefficients of the Banded Plates Compared to the Standard Flat Plate	210
Table 8.7b.	Slip ID Numbers, as used by the MATLAB® Model.	213

Table 8.7d	Correlation Coefficients of the Banded Plates Compared to the Standard Flat Plate	216
Table 8.7e	Maximum and Minimum Correlation Coefficients of the Banded Plates Compared to the Standard Plate	217
Table 9.2c	Motor specifications for the clutch dynamometer at HGT (Japan) [164]	224

## List of Abbreviations

AP	Automotive Products Limited
ATLAS	Advanced Telemetry and Logging Acquisition System
bhp	Brake horse power
C-C	Carbon-carbon material
CVD	Chemical Vapour Deposition
DPC	Direct Push Clutch
EPSRC	Engineering and Physical Sciences Research Council
F1	Formula One
fos	Factor of safety
HIP	Hot Isostatic Pressing
LM	Low Modulus
MESL	McLaren Electronic Systems Limited
MMC	Metal Matrix Composite
NPL	National Physical Laboratory
PAN	Polyacrylonitrile
rpm	Revolutions per minute
RS	Race start
SEM	Scanning Electron Microscope
TGA	Thermo-gravimetric Analysis

## Nomenclature

$\alpha$	Thermal expansion
$C_p$	Specific heat
$\delta L$	Change in length
$\delta T$	Change in temperature
$D_e$	Outer diameter of diaphragm spring
$D_i$	Inner diameter of diaphragm spring
$E$	Modulus of elasticity
$\epsilon(\lambda)$	Emissivity (at wavelength)
$F$	Clamp load
$h$	Thickness of diaphragm spring
$h_d$	Thermal diffusivity
$h_o$	Free height of diaphragm spring
$ID$	Inner diameter of the friction surface
$I_s$	Infrared Specimen signal
$I_B$	Infrared Blackbody signal
$I_0$	Infrared Signal at $T_0$
$K$	Thermal conductivity
$K_1$	Constant dependant upon the ratio of $D_e / D_i$
$kg$	Kilogram
$L$	Initial length
$n$	Number of friction surfaces
$N_{rpm}$	Rpm of engine
$OD$	Outer diameter of the friction surface
$\mu$	Coefficient of friction
$\pi$	3.14159
$\rho$	Density
$R_g$	Radius of gyration
$r$	Radius
$s$	Deflection of diaphragm spring
$t_{slip}$	Slip time
$t$	Thickness of diaphragm spring
$T_c$	Clutch torque capacity (normally $T_e \times$ factor of safety)

$T_e$	Maximum engine torque
$T_0$	Known temperature
$W_{\text{engine}}$	Energy of engine
$W_{\text{lost}}$	Energy lost during start up
$W_t$	Energy transmitted
$V_i$	Initial angular velocity



# Chapter 1

## Introduction

The success of a F1 launch is determined by many factors like driver response time, the grip of the tyres (and in turn, wheel spin), the torque of the engine and how that torque is transmitted through the drive train onto the track. Part of that drive train is the clutch, which is used to transmit the torque from the engine to the gearbox. The clutch is made up of a series of carbon-carbon plates; 4 driven plates and 3 drive plates, that when clamped together, transmit the torque from the engine to the gearbox. Due to the nature of its mechanism, the friction characteristics of the clutch plates play a large part in the overall efficiency of the clutch, and in turn, the race start. However, the friction co-efficient of the carbon-carbon material not only changes with the material temperature, but is also found to be inconsistent from launch to launch.

The thesis describes why carbon-carbon (C-C) composites are used as friction materials. It discusses the frictional properties of C-C composites as related to their use in race clutch applications when combined with launch control systems, and how improving the calculation of the friction co-efficient of the material would lead to improved race launches. This work investigates the causes of the frictional ( $\mu$ ) instability, differences in the friction coefficient caused by different bedding procedures and how to enable the clutch material to be subject to more consistent coefficient of friction values through both bedding analysis and mathematical modelling. Physical testing is undertaken to explore a range of variables whilst the friction and wear mechanisms of carbon and the influence of carbon structure, physical, thermal, mechanical and chemical properties, as well as friction films, on the performance of C-C friction materials are described and modelled and then compared to real car data to assess the suitability of the model for the calculation of friction co-efficient in a launch control program.

## 1.1 General Background

The Oxford English Dictionary defines a clutch as: 'A mechanism for connecting and disconnecting the engine and the transmission system in a vehicle.' [1]

A race car clutch is generally made up of two sets of plates, a driving plate set; which is connected to the engine, and a driven plate set; which is connected to the gearbox. At most times the two sets of clutch plates are held in contact with each other by a spring. A clutch is needed because the engine spins all of the time, but the wheels don't. The clutch allows the spinning engine and the stationary wheels to engage smoothly by controlling the slippage between them during a gear change or when the car 'pulls away'.

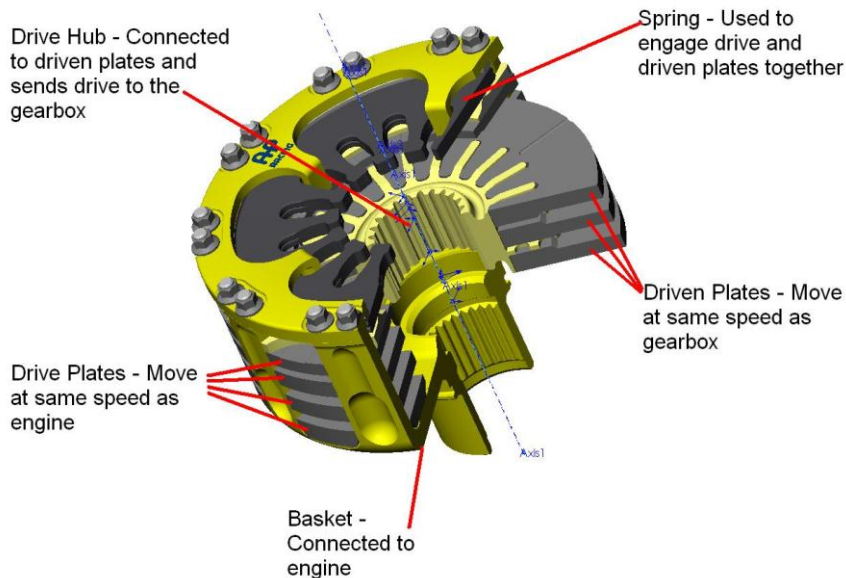


Figure 1.1a – A Multi-plate Clutch Arrangement, as used in F1 Applications

Race clutches are much smaller than normal road use clutches. In motorsport, everything is kept to a minimum due to the weight and performance restrictions placed upon the designs meaning that a typical Formula One clutch assembly will be in the region of 97mm diameter and 1.5kg and be capable of transferring up to 1000bhp, whilst its road car counterpart will be approximately 250mm in diameter and weigh 4kg, whilst only transmitting a fraction of the horse power [2]. These extreme conditions mean that race clutches are changed often, so where a clutch on a road car may have a serviceable life of up to 100,000 miles in

its lifetime, a race clutch will have a maximum of 1500 miles life. The space restrictions placed upon a race clutch mean that multi plate clutches have been developed to allow for a smaller diameter to be used whilst maintaining the same friction area. The smaller diameter is also a key design factor in aiding the inertia as the larger the diameter, the larger the turning moment acting upon the clutch, and therefore, the larger amount of energy is required to change its angular velocity.

In race clutch applications carbon-carbon composites fulfil three functions including:

- a) Heat sink - The C-C composite friction material acts as the heat sink to convert the kinetic energy of the slipping plates into heat. Carbon is an attractive material because the heat capacity of carbon is 2.5 times greater than that of steel.
- b) Friction - Sufficient friction must also be generated by the friction plate material to transmit the torque in a smooth, controlled manner under different kinetic energy conditions (launches and gear changes).
- c) Structural member - High mechanical strength is also required at elevated temperatures since the friction material also acts as the structural member and transfers the frictional torque to the gearbox during normal driving. The strength of carbon at normal atmospheric temperatures is comparable to that of steel, while at high temperatures, carbon is nearly twice as strong.

Overall, carbon race clutches are highly tuned components, which are specified and manufactured for use with one specific set of parameters. An F1 clutch is very different to that of a production sports car, which is turn, is different to that of a Formula 3. However, one thing remains; that the increased predictability of the carbon-carbon friction characteristic means that the clutch can be further optimised for more efficient race starts and launches.

## **1.2 Aims and Objectives**

The overall aim of the project was to produce and validate, a working clutch model which accounts for surface characteristics and frictional, thermal and wear affects. This was achieved through a series of objectives:

- Analysing a series of race starts and observing the accuracy of the current methods of carbon-carbon clutch friction prediction
- Investigating into current methods of friction stabilisation
- Research into the Tribological behaviours of the carbon-carbon materials
- Undertaking physical testing of the clutch on a dynamometer to directly measure the inter plate temperatures over a range of conditions
- Conducting materials testing to understand thermal effects
- Developing a mathematical model of the clutch; separating it into two separate models for bulk and surface
- Correlating the mathematical model to results obtained through experimental testing
- Drawing conclusions and making recommendations based on the outcomes of the work

### **1.3 Original Contributions as Outcomes from the Project**

Three main original contributions have been established as a result of this work, the first being an addition to the general understanding of carbon-carbon materials within the scientific and engineering community. A suite of materials testing was undertaken and has experimentally determined values for a variety of thermal properties of carbon-carbon clutch material. The work has also investigated and proposed theories regarding the destruction and formation of transfer films that act between the two mating carbon-carbon clutch faces, as well as investigating and experimentally determining and mathematically modelling the effects of thermal decomposition within the clutch.

The second original contribution of this project is the development of a proven novel method of direct clutch plate surface temperature measurements using infra-red sensors. This could be further adapted for installation on a race car for testing purposes and more accurate temperature readings, enabling more accurate friction calculations and better race starts. Presently, there is no other method of clutch plate surface temperature measurement that has the capability to be utilised in this way.

In conjunction to with the two main original contributions, the Formula One industry has also benefitted from the work undertaken as part of this project by significantly aiding the prediction of the coefficient of the clutch before a race start. Moving on from this work, procedures have been able to be developed and used to condition the clutch during the formation sequence to an optimal state for a race launch, resulting in faster acceleration from the line and improved race starts.

## **Chapter 2**

# **Clutches and Control Systems; History, Development and Design**

This chapter looks into clutches; how they work, their development and design.

### **2.1 What is a Clutch?**

A clutch is a mechanism which is used for 'holding apart' two components which are rotating at different speeds, and then bringing them together to rotate at the same speed.

The main focus of this work is upon clutches for automotive, and more specifically, motorsport use. Within a motor vehicle motion of the wheels from the power source is delivered via the drive train. The drivetrain (sometimes known as the powertrain) consists of the engine, flywheel, clutch, gearbox, output shaft, differential, drive shafts, hubs and finally the wheels. This configuration can change depending on whether the vehicle is front wheel drive, rear wheel drive or four wheel drive, but the principle remains the same: to transfer the power from the engine, to the wheels. This can be observed in figure 2.1a [3]. The clutch is a very important part of this system, as it is the only part that can be used to disconnect the drive train at the demand of the driver (or electronics system). The ability to disconnect the drive train is a crucial one, as the engine is spinning all the time and producing an output movement. It is necessary to connect a stationary object to the spinning engine to allow the drive train to become complete and for the vehicle to move.

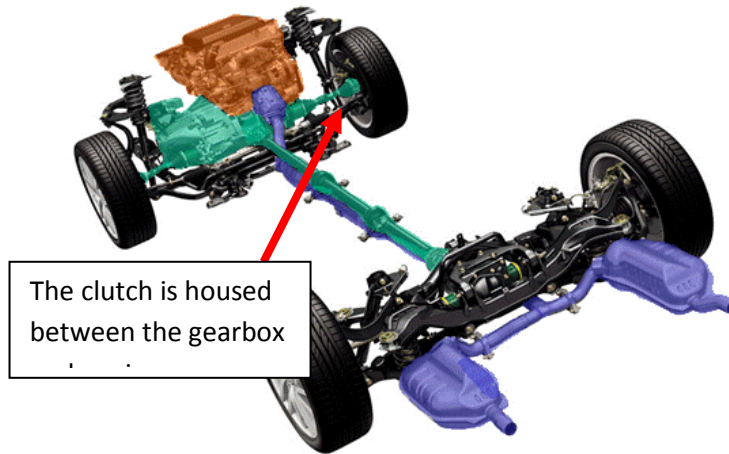


Figure 2.1a – Drivetrain Schematic – with the engine (orange), transmission (green) and exhaust systems (blue)

A typical race car engine will turn at speeds of up to 20,000 rpm (revolutions per minute) and its peak power will generally fall at about 18,500 rpm. At this peak power, the torque is around 285Nm. Torque is produced by the pressure from the crankshaft on the pistons and tends to be low at idle speeds, but as the engine speed increases so does the torque (as shown in figure 2.1b) until it reaches a peak and then decreases as the engine speed continues to increase. Because of this gears are used, so that regardless of wheel speed the engine is always kept within the optimum revs range.

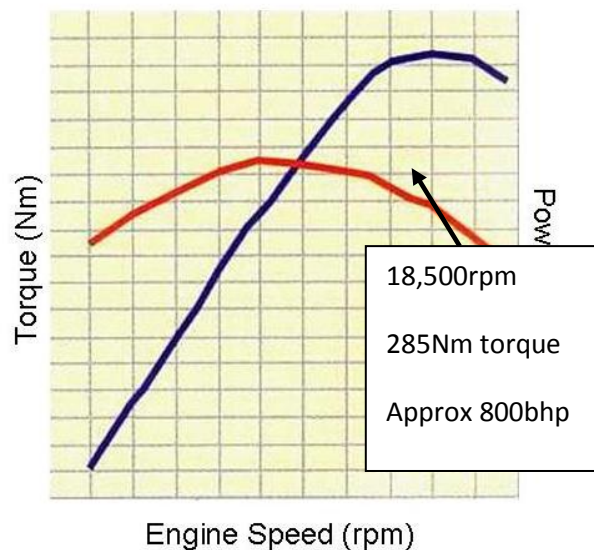


Figure 2.1b – A typical torque (red) / power (blue) curve

This is done in order to utilise the optimum torque band (that is, where the engine speeds are such that peak torque is produced) to its full extent and to prevent damage the engine. When the engine is revving at a high speed and the gear needs to be changed the clutch is first disengaged, separating the engine from the gearbox. This allows the engine to continue moving and the car to 'free wheel' with drive no longer being transmitted from the engine to the gearbox and wheels. When the clutch is re-engaged, the gearbox and the engine will now be rotating at different speeds, so the two friction plates within the clutch (one is connected to the flywheel, and the other connected to the gearbox) will slip over each other and the friction between them creates heat. This friction allows the engine to lose some of its speed through heat dissipation, and it also allows the other friction plate to begin moving.

A development within F1 in the past 10 years is the introduction of 'Zeroshift' systems – which is almost identical to the standard shift system described as above, except that the system uses a series of bullets to essentially hold the car in two gears at once, and is seen in figure 2.1c below courtesy of Zeroshift Systems [4].

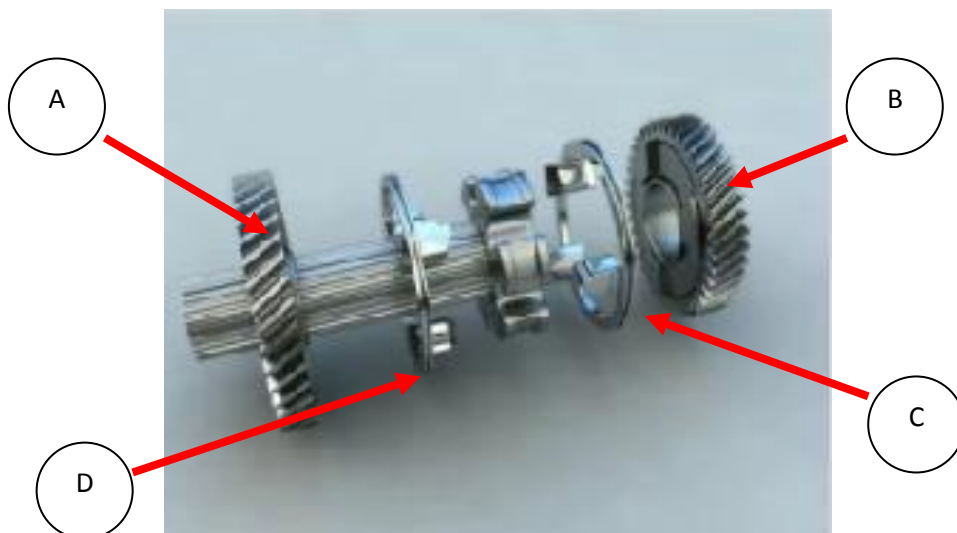


Figure 2.1c – Zeroshift System

Both gears float on the output shaft shown and are driven via mating gears connected to the input shaft with 1st gear on the left (a) and 2nd gear on the right (b). Drive is taken up when the drive ring on the right (c) moves left and connects with 1st gear. Overrun backlash is taken up when the drive ring on the left (d) moves left and connects with 1st gear. To change into gear, the unloaded drive



ring on the left is shifted through into 2nd gear, while still driving in 1st. As 2nd gear is rotating faster, drive is only handed over when the drive faces connect. At this instant, drive is relieved from 1st gear and to complete the shift, the now unloaded drive ring on the right is shifted through to take up overrun backlash in 2nd gear.

When two shafts are rotating at different speeds, and need to move to a speed differential ( $\Delta v$ ) of zero either one of two methods can be used. Either the slower of the two shafts needs to speed up or the faster of the two shafts needs to lose speed. Making the slower shaft speed up would require extra energy to be introduced into the system, which is not practical in a vehicle, as it is usually the gearbox shaft that is the slower shaft of the two and has no means of being powered. The other option of slowing down the faster of the shafts is far more practical and energy is lost by the formation of heat, generated by slippage due to the friction of the clutch, which is converted into heat.

## **2.2 History of Development of Race Clutches**

For racing applications, direct push clutches are the actuation method of choice. Direct push clutches (DPC's) allow for more controlled operation. The direct push mechanism makes it easier to map and program the exact position of the clutch engagement, which is of particular importance under launch conditions.

During the early 1980's carbon-carbon clutches for F1 applications were first investigated but this material had already been in use for more than thirty years. Carbon composites were used as the fins of Second World War German rockets in the form of polygranular synthetic graphite [10], for the materials superior retention of mechanical properties at high temperatures. However, fibres were not introduced to the material until the late 1950's when fibre technology had advanced to a stage where their potential for addition to structural components was fully understood.

Carbon-carbon had begun to emerge as a major new genre of materials by the late 1960's and by the 1970's, was being developed on both sides of the Atlantic,

primarily for military use. Mainly used in rocket nozzles and re-entry parts, early carbon-carbon was produced using low modulus rayon fibre weaves in a pyrolysed (decomposed by heat) resin, such as phenolic.

Carbon-Carbon brakes inspired by those used in aircraft, were introduced into [Formula One](#) by the Brabham team in conjunction with Dunlop in 1976. Carbon-Carbon braking is now used in most top-level motorsport worldwide, reducing unsprung weight and giving better frictional performance compared to cast iron.

In 1982, AP Racing first began to look at carbon-carbon clutches as a potential option by substituting the conventional sintered material with carbon plates. These investigations were halted due to the discovery of the very low co-efficient of friction at cold temperatures. After further investigations by Tilton race engineering [5] in 1984, a modified drive hub was used to distribute the 800bhp engine power into the clutch.

By the mid 80's high boost, high torque 1.5 litre engines took over from their 3.0 litre atmospheric counterparts. Pressure plates thickened up to cope with the increased torque input, double bolt fixings (12 from the usual 6) were introduced and weight increased from 4.15 kg to 4.45 kg. However, the addition of a cross drilled intermediate plate and an aluminium end cover subsequently reduced the weight to 3.85kg.

In 1986, AP Racing was nearing the completion of the development of their 140mm race clutch, which was lug drive, rather than gear drive. Outer plates were driven by the lugs that were protruding from the end cover, whilst the integral cover and lug assembly was machined from a solid billet of aluminium, with a bolt passed through each of the lugs to attach the assembly to the flywheel.

1987 was the year that Honda began using a quadruple plate version of the 140mm AP clutch with its turbocharged F1 engine. By using the smaller diameter plate, the weight of the clutch was concentrated towards the centre, significantly reducing the inertia. This permitted the use of a lighter crankshaft, allowing for a quicker uptake of the engine and quicker gearshifts. In the same year, AP started

using carbon-carbon clutch plates with the 140mm clutch which again reduced the weight and inertia. The carbon-carbon material didn't warp, offering cleaner engagement than its sintered counterpart, and the friction ( $\mu$ ) value of the plates increased with temperature (0.15 cold to 0.55 hot), allowing for a better withstanding of the extreme heat increases seen at a standing start. By 1988, this clutch configuration was standard equipment in AP's range. In 1989, Tilton [5] patented the first carbon racing clutch, which was the first carbon clutch to be used [6], and the first to win in F1, soon after this virtually all F1 teams began using carbon-carbon clutches.

In 1991 a gear drive for the 140mm clutch was introduced, after discovering that the lug drive type, was producing an area of high stress where the lug joined the end cover. The gear drive teeth were machined into the carbon plate, and meshed with the teeth machined onto the aluminium adaptor ring. By switching the drive type, the clutch weight was dramatically reduced, as was the overall diameter, which went from 165mm (known as the 140mm clutch due to its effective radius) to 159.5mm in 1994.

In 1996 AP reverted to running a lug drive type clutch, when the diameter was reduced further to 115mm. Metal matrix composite (MMC) was used as the materials cover, but this offered too much thermal resistance, so in 1997 the switch to a machined billet of titanium was made.

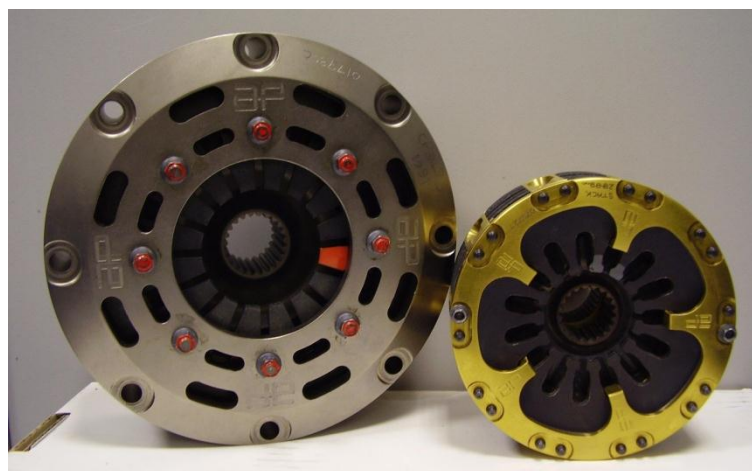


Figure 2.3a – AP Racing's first 140mm and most recent 97mm carbon-carbon clutches

The most important factors in the carbon-carbon clutch materials are the stability of  $\mu$  (friction co-efficient) with the rising temperature, the wear rate and the tensile strength. The 2D material which AP racing had been using up until 1999 was merely a material based on structural fibres of carbon embedded in a carbon matrix. This material was simply laminated in sheets to the required thickness. The construction of the material meant that under extreme temperature loading situations, the clutch face material could become saturated. The introduction of 3D weave carbon-carbon, developed by McLaren Racing and Allied Signal, meant that the heat could be conducted away from the face of the material and into its core.

In 2000, the 97.5mm triple plate clutch was introduced, of which, only 13.5mm wasn't friction surface diameter. By 2003, the diameter had shrunk even further to 87mm (3.43 inch), of which only 12mm was non friction diameter. This tiny clutch was a 4 plate configuration, so whilst it was a smaller diameter, it was actually longer. As a consequence of their reduced diameter a multi-plate clutch is much harder to control, as described by Race Car Engineering's 'Insight' article [7]. Despite weighing the same as its 97.5mm counterpart, the 87mm clutch offered lower inertia, due to its decreased diameter.

However, *"With each decrease in clutch diameter, comes an increase in the difficulty of controlling it"* – Jon Grant, Head of Clutch Design, AP Racing.

## 2.3 Clutch Design Process

Initially clutch size is determined by its required torque carrying ability. The remaining system parameters are optimised with regards to functional requirements, such as pedal effort and gear shifts.

When starting to develop a clutch for a new application, an essential place to start is by estimating the largest clutch size possible by considering the flywheel bolt circle diameter and the attaching bolt size. This information can then be used as a reference point in estimating the clutch diameter.

The next step is to establish the specific heat stress, which is defined as '*the ratio of friction work lost due to launching the car, to the friction material area*', Shaver [8] pp 65. There are no industry standards regarding heat stress limits, but it can be calculated using equations (2.3a) and (2.3b);

$$\text{Heat Stress} = \frac{W_{\text{lost}}}{n \times (\pi/4) (OD^2 - ID^2)} \quad \text{Equation(2.3a)}$$

Where;

$$W_{\text{lost}} = W_t = \frac{W_{\text{engine}}}{2} = \frac{(\pi) T_e N_{\text{rpm}} t_{\text{slip}}}{60} \quad \text{Equation (2.4b)}$$

Where:

$W_{\text{lost}}$	Energy lost during start up
$W_t$	Energy Transmitted
$n$	Number of friction surfaces
$OD$	Outer diameter of the friction surface
$ID$	Inner diameter of the friction surface
$W_{\text{engine}}$	Energy of engine
$T_e$	Maximum engine torque
$N_{\text{rpm}}$	Rpm of engine
$t_{\text{slip}}$	Slip time

Assuming that;

- The engine speed is constant under launch
- The torque transmitted during launch is constant and causes constant acceleration
- Resistance torque is a constant
- Start up occurs from  $V_i$  (initial angular velocity) = 0
- Elasticity of the drivetrain is disregarded
- Thermal influences are disregarded
- Energy absorbed by the clutch system is assumed to be half of the expected energy during start up

These equations may be used to determine the amount of heat energy dissipated through the clutch during a launch, which is dependant upon the rolling resistance, engine torque and rpm, elasticity of the drivetrain, clutch housing temperature, thermal transfer, vehicle mass, gearbox ratios and drivetrain losses, but many of these elements are factored out using the assumptions above, to allow for consistency in the calculations.

Once the outside diameter of the clutch has been established, and the inside diameter determined by the specific heat stress, it is possible to calculate the clamp load using equation (2.3c):

$$F = \frac{T_c}{n \times R_g \times \mu} \quad \text{Equation (2.3c)}$$

Where;

$$R_g = \frac{\int_{r_i}^{r_o} \int_0^{2\pi} r \, dA \, dr}{3 (OD^2 - ID^2)} = \frac{(OD^3 - ID^3) \times 1000}{3 (OD^2 - ID^2)} \quad \text{Equation (2.3d)}$$

Where;

- $T_c$  Clutch Torque Capacity (Nm)
- $n$  Number of friction surfaces
- $R_g$  Radius of Gyration
- $\mu$  Co-efficient of Friction

Once the clamp load is determined, the diaphragm spring needs to be specified. This utilises the clamp load, along with the bearing travel to specify the basic dimensions for the spring. By using a diaphragm spring high clamp loads can be achieved with relatively little deflection. The spring is simply a stamped steel ring, with multiple fingers, or levers, which is heat treated to achieve the required stiffness. The spring features can be determined using equation (2.3e).

$$F = \left( \frac{4E}{1 - \mu^2} \right) \left( \frac{s t^3}{K_1 D_e^2} \right) \left[ \frac{(h_o - s)}{h} - \frac{(h_o - 0.5s)}{h} + 1 \right] \quad \text{Equation (2.3e)}$$

Where;

E	Modulus of elasticity
$\mu$	Coefficient of friction
s	Deflection of diaphragm spring
t	Thickness of diaphragm spring
$K_1$	Constant dependant upon the ratio of $D_e / D_i$
$D_e$	Outer diameter of diaphragm spring
$h_o$	Free height of diaphragm spring
h	Thickness of diaphragm spring

As detailed by ZF Sachs [9], in 2004 launch control was banned in F1, having an effect upon clutch design. With launch control, the clutch disposes of surplus power as slip, resulting in extremely high loads for up to 2 seconds (or in exceptional circumstances, up to 10 seconds) and is heated to temperatures well in excess of 1000°C. Theoretically the change in regulations means that the clutch will not undergo such harsh conditions, because unlike a normal road car the paddle clutch in an F1 car doesn't experience a pressure point. Instead, the driver must remember in which paddle position the clutch is engaged. Even some of the world's best drivers can only slip the clutch for a maximum of half a second to help them pull away, which is only a quarter of the time that launch control would slip the clutch for. However, clutches are still as robust today as they were pre-launch control ban. This is due to the element of human error;

*“If a driver misses the pressure point and realises that the engine could stall, he disengages the clutch, lets the engine revs skyrocket and tries to re-engage the clutch again. Often the whole game is repeated several times. As a result even higher loads can arise than pulling away with launch control”* – Thomas Rudolf, Engineer for Clutch Systems; ZF Sachs Race Engineering.

Even if such mistakes are the exception, rather than the rule – most race clutch manufacturers have opted to make provision for them by refraining from utilising the reserves released by the banning (and subsequent reinstatement then re-banning) of launch control.

## **2.4 Control Systems**

The race start is controlled by a mathematical program (sometimes known as launch control) that has been written by the teams control systems engineers. This program uses a calculated friction co-efficient of the clutch, determined from the formation start to establish the required torque for an efficient and successful launch. However, the friction co-efficient can often be inconsistent, leading to poor calculations and in turn, a poor getaway.

Calculation of race start friction ( $\mu$ )

$$\mu = T / (n \times P \times r) \qquad \text{Equation (2.4a)}$$

Where: T = input torque to the clutch

n = number of working surfaces,

P = clamp load (using cylinder area, pressure and lever ratio)

r = mean effective friction radius

A typical race start (RS) coefficient of friction is calculated using a control system similar to that shown below in SimuLink.



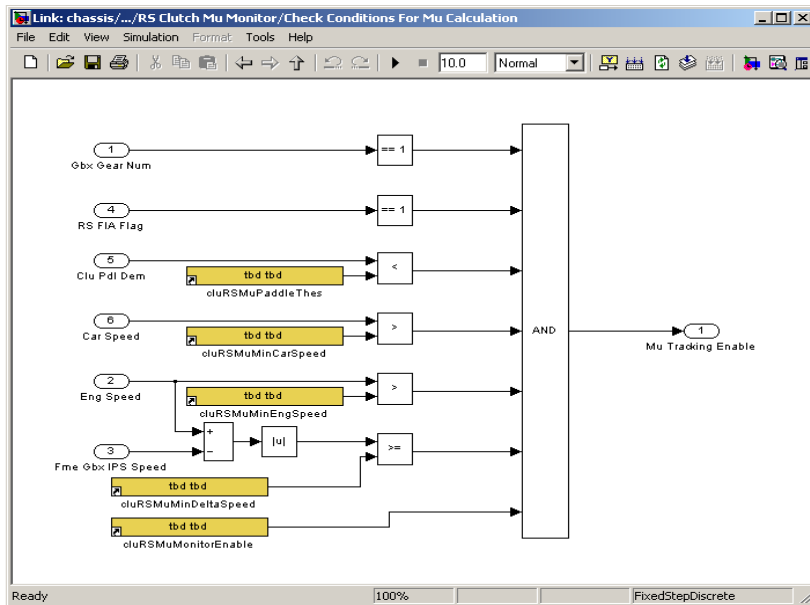


Figure 2.4b – A typical SimuLink model for F1 clutch Mu calculation [10]

The coefficient of friction is calculated only when all of the following criteria are met:

- First gear is selected
- RS flag is set to logical argument 1 (ie, the program knows that it is about to perform a race start)
- Clutch paddle demand is less than threshold value of 90%
- Car speed is greater than 3kph but less than 60kph
- Engine speed is greater than 6000rpm
- The difference in engine and gearbox input shaft speed is greater than 1500rpm (that is, the engine is running and under load, but the gear is not fully engaged)
- Monitoring subject to a debounce time of 0.2s (If improper debouncing is employed then the dirty input could cause an unwanted state change)

These criteria have been selected in order to state the conditions that define the race start and to eliminate any anomalous friction characteristics, particularly seen at the start and the end of the clutch engagement period.

The model uses the following conditions for  $\mu$  monitoring;

Name	Description	Max Value	Min Value	Value	Unit
cluRSMuCarSpdBeforeUpdate	The car speed required before the integrated mu is averaged	400	0	60.0000	kph
cluRSMuClutchSpec	Torque transfer characteristic of the clutch	100.0000	0.0010	0.24583	-
cluRSMuDebounceTime	Debounce time from conditions being met to start mu monitoring	10.0000	0.0000	0.20000	s
cluRSMuMinCarSpeed	Clutch RS mu monitoring enabled above this car speed	400	0	3.00000	kph
cluRSMuMinDeltaSpeed	Clutch RS mu monitoring enabled above this engine/IPS delta speed	25000	0	1500.00	rpm
cluRSMuMinEngSpeed	Clutch RS mu monitoring enabled above this engine speed	25000	0	6000.00	rpm
cluRSMuMonitorEnable	Enable RS Mu monitoring	1.00000	0.00000	Yes	-
cluRSMuPaddleThes	RS clutch mu monitoring enabled below this paddle demand	100.0000	0.0000	90.0000	%
cluRSMuPdlDemToReArm	The clutch paddle demand required to re-arm the system after a previous mu monitoring event	100.0000	0.0000	95.0000	%
cluRSMuTimeBeforeUpdate	The amount of time to expire before the a Mu update can happen	60.00000	0.00000	1.50000	s

Figure 2.4c – Mu calculation control conditions. [11]

The kinetic energy of the two faces rotating at different speeds is transformed into thermal energy, caused by the friction of the plates. Where the kinetic energy is represented by:

$$E = \frac{1}{2} mv^2 \quad \text{Equation (2.4d)}$$

Where: m = mass of the clutch plate

v= angular velocity of the plate

All of the kinetic energy within the clutch system needs to be dissipated by heat, which is a by-product of the friction of the plates, so the friction co-efficient of the plate plays a very important role.

The clutch mechanism works on two different levels of friction: static and sliding. Static friction co-efficient values are generally much higher than their sliding counterparts, and it is this type of friction that acts as the mechanism to ‘hold’ an object in place. The clutch clamp load also plays a large part in the static friction characteristic of the clutch, due to the fact that the friction force is calculated as;

$$F = \mu r \quad \text{Equation (2.4e)}$$

Where: F = force required to initiate sliding of the plates over each other

$\mu$  = static friction co-efficient

r = clamping force

Amonton’s 2<sup>nd</sup> Law states that the friction force is independent of the area of contact, and this is important to note. In multi-plate clutches, the main purpose

of the design is to increase the contact area between the driving and driven plates, and although this has little bearing in the friction of the clutch, it does have a bearing upon the ability of the clutch to transmit the high torque forces and dissipate the generated heat effectively whilst maintaining a low inertia.

The most important quality of the clutch design is that the clutch must effectively transmit the torque from the engine to the gearbox, and for this to happen the plates must not slide in relation to each other:

$$F < \mu r \qquad \text{Equation (2.4f)}$$

This is achieved by using high clamping loads. Sliding friction ( $\mu_k$ ) comes into effect when the two plates slide over each other (known as 'slipping the clutch') and it is this frictional characteristic that we are investigating in the following work. This type of friction occurs when two objects are moving relative to each other and rub together, in this case, the two friction plates within the clutch. According to Coulomb's Law of Friction; the sliding friction is independent of the velocity at which the faces pass over each other.

Fluid friction is also a sub-category of sliding friction and this plays an important role in the overall friction properties of the clutch. As the clutch wears, its dust creates a layer on the face of the clutch that acts very similarly to a fluid. Fluid friction is the interaction between a solid object and a fluid as an object moves in relation to that fluid, two examples of which are the skin friction of air on an planes wing or water over a dolphin. This type of friction is not only due to rubbing (which creates a force normal to the surface of the object: as seen in equation 2.4e) but it also creates forces that are orthogonal to the surface of the object, and it is these forces that significantly contribute to fluid friction.

It is universally acknowledged that the frictional characteristics are closely related to the temperature of the clutch, but this relationship has yet to be quantified. As the temperature of the clutch plates increase the friction co-efficient decreases. This is due to many factors, including the method of manufacture of the carbon, the bedding process and the material properties of the plates themselves.

Therefore, the main aim of this work is to create a mathematical model in Matlab and SimuLink that will be able to give a prediction of the friction coefficient of the clutch pack that will be able to be used and incorporated within the launch control program currently employed by F1 teams.

## **Chapter 3**

### **Literature Review**

This chapter looks at the works of others in the field of carbon-carbon composites. Clutch design and carbon-carbon manufacture are used as a starting point before taking a look at the microstructure and how this affects the material and surface properties. Factors affecting the wear and behaviour of the friction surface are also considered, before finally exploring surface treatments and what has been done in this field to improve the carbon-carbon material. Additionally, testing methodology and mathematical modelling are also reviewed in order to consider earlier work relevant to this thesis.

At initial the time of writing (2009), much research was on going into the tribological mechanisms and performance of carbon-carbon composites. It is clear from the large number of research papers available that a complete understanding is still being sought; however several fundamental theories appear to have been settled on by the tribological community. It is important to remember that the information presented within the investigated research papers is obtained from the testing of materials of a different specification, geometry and setup from those usually encountered in motorsport applications. Most of the existing research has been focussed on aircraft braking systems. Whilst the underlying principles can be assumed to be similar across all carbon-carbon composites, care must be taken when comparing numerical data.

This chapter finishes with an analysis of papers that have been published in the field between 2009 and 2013, including those which lie in a very similar field to the work undertake in this thesis.

#### **3.1 Clutch Design and Carbon-Carbon Manufacture**

On July 20<sup>th</sup> 1937 FC Stanley first patented the friction clutch [12], and although very primitive by today's standards this design began a long line of research and development into clutch mechanisms and friction materials. In 1991 patents were still being filed for clutch designs with items such as the groove patterns in the

plates. The work of Payver [13] highlighted a groove pattern for the friction facings of a wet clutch which was used to equalise the face temperature, thus increasing thermal capacity of the clutch. Following this in 1995 Sievers [14] submitted his design to the US patent office for a high performance clutch assembly with a refractory metal carbide thermal spray coating on the clutch disk engagement surfaces and the manufacturing.

The work of Tripathi and Agrowal [15] in 2007 looks at the design optimisation of the friction clutch; their paper claims that the friction clutch must be designed for minimal axial force between the pressure and clutch plates whilst satisfying the constraints of the peripheral velocity of the outer diameter of the friction surfaces. The parameters are grouped into : pre specified parameters (frictional torque and engine RPM), performance parameters (axial force and peripheral velocity), and design parameters (inside and outside diameters of friction plates, face width , normal pressure and co efficient of friction). A mathematical model which is very basic is proposed, and runs on the assumptions of constant axial force and clamp load. It does not account for any frictional variation within the clutch plate material. The 2005 work by Albers, Arsian and Mitariu [16] considers the use of engineering ceramics and carbons as friction materials. Although these offer dramatic improvements over traditional sintered metal facings, they bring about the difficulties of a varying coefficient of friction with temperature. This in turn means that the specific energy dissipation of the materials can vary significantly. Their work investigated the use of different friction pairs and looks at the friction coefficient as a function of sliding speed which they found to be inversely proportional to the friction co efficient.

In 2004 Christopher Byrne [17] began to investigate the use of lower cost precursor fibres and processing methodologies as a result of the increased use of carbon composite materials within the aerospace sector. However, after much investigation he determined that any changes in the current methods of carbon-carbon manufacture significantly affected the wear and friction mechanisms, causing mechanical and thermo chemical degradation and thermal gradients within the material. Earlier work was carried out by Gary Savage [18] of McLaren Racing, and published in 1992. This indicates that the level of material complexity

(and hence inconsistency) arises in the production of carbon-carbon composites in the variation of the structure of the matrix. The carbon matrix phase may consist of a glassy isotropic carbon through to a highly crystalline graphite with almost limitless variations in between, and the paper warns not to consider carbon-carbon as a single entity but rather as whole family of materials whose structure and properties maybe tailored to suit a large number of specialist applications. Savage outlines specific fabrication techniques regarding the densification of carbon-carbon, which involves filling the voids between the carbon fibres by either gas or liquid phase impregnation or a combination of both.

In his 1993 book, Carbon-Carbon Composites, Savage [19] outlines the commercial fibres used and processes, and states that all commercial carbon fibres are developed from one of three processes:

- Low Modulus Polyacrylonitrile (LM PAN);
- Cellulose Rayon; and
- Mesophase Petroleum Pitch.

LM PAN based fibres account for 90% of all commercial carbon fibres and are typically 93 – 95% acrylonitrile. Acrylonitrile is used principally as a monomer in the manufacture of synthetic polymers, especially polyacrylonitrile which comprises of acrylic fibres, which were a precursor of carbon fibres. True melt is not possible for PAN, as it decomposes below its melt temperature and this means that the PAN is instead extruded into filament form.

The LM PAN processing method begins with the copolymer that is first dissolved in a suitable solvent, for example dimethylacetamide, and will result in 15 -30% polymer by weight. This is then extruded through a spinneret with a large number of capillary holes, of approximately 100µm diameter, and followed by wet spinning in a coagulating bath with a hot gas environment, as shown in figure 3.1a. After this the fibres undergo one or two further stages of further stretching which aligns the polymer molecules parallel to the fibre axis and locks the molecular orientation into place; this will affect the final mechanical properties of the carbon fibre.

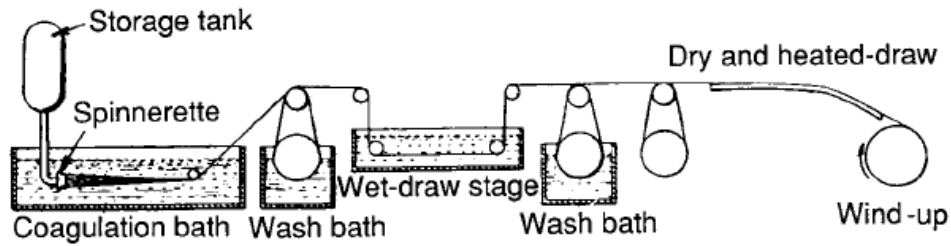


Figure 3.1a. The PAN Precursor Fibre Process [19]

The wet spinning stage of PAN has important considerations to take into account; this stage requires excessive amounts of solvent which necessitates its removal from the fibre. The solvent is very expensive and trace impurities in the solvent can limit the final mechanical properties of the fibres.

Cellulose rayon fibres have a typical low modulus of approximately  $4 \times 10^6$  psi. The first low-temperature treatment takes place at approximately  $300^\circ\text{C}$  and converts the structure of the rayon to a form that is more stable to higher processing temperatures. This process involves polymerization and the formation of cross-links. Before the first stage of oxidation exposure the rayon may be subjected to a chemical bath of either aqueous ammonium chloride solution or a dilute solution of phosphoric acid in a denatured ethanol, as seen in figure 3.1b. This chemical process reduces the time for the low temperature step from several hours to approximately 5 minutes. Of the fibre mass, approximately 50-60% is lost due to decomposition during oxidation.

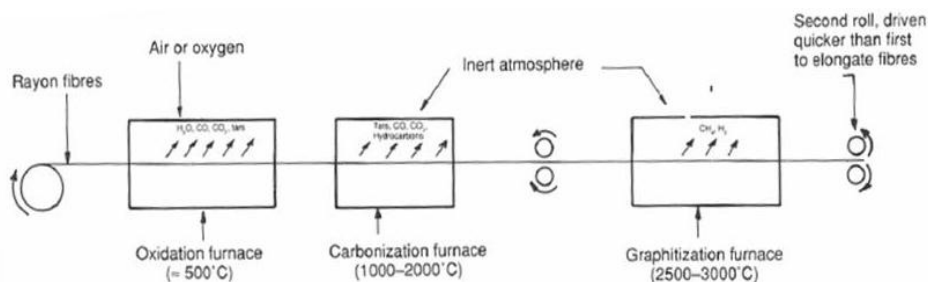


Figure 3.1b. Basic Elements Required to Produce Carbon Fibres from Rayon [19]

The mechanical properties of rayon are mediocre, due to the poor alignment of the graphene layers.



Isotropic pitch based fibres are manufactured from by products obtained in coal-tar and petroleum processing. They are relatively easy to spin into fibres from the melt but unfortunately, the way that they are formed also means that they have a low modulus and strength due to their isotropic structure. They are manufactured using the same general process as PAN, except that a melt spin is used, as unlike PAN, they do not decompose below their true melt temperature. As they are melt span, this also eliminates the requirement for the stretching process required in the PAN fibres to maintain the preferred alignment.

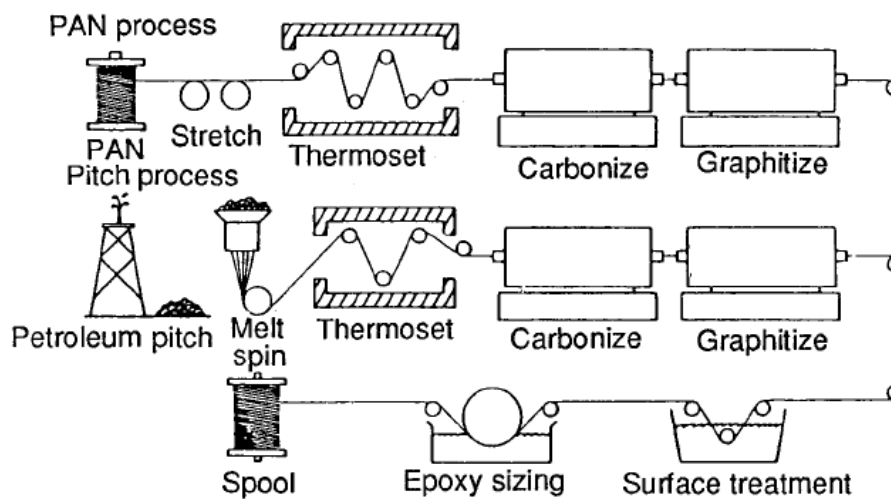


Figure 3.1c. The Processing Sequence for PAN and Mesophase Pitch-based Precursor Carbon Fibres [19]

Figure 3.1c shows the processing sequence for PAN and mesophase pitch-based precursor carbon fibres and the similarity of the two processes. The PAN process obtains highly orientated carbon chains by hot stretching of the polymer chains prior to carburation, while the high degree of orientation in pitch is a natural consequence of the mesophase (liquid crystal).

There are three main ways of processing carbon-carbon composites;

- Chemical vapour deposition (CVD)
- Multiple impregnation-pyrolysis using thermosets (eg. Phenolic)
- Multiple impregnation-pyrolysis using thermoplastics (eg. Pitch)

As outlined by Savage [19], the CVD (chemical vapour deposition) process is one in which a solid product nucleates and grows on a substrate, and this is where the

second carbon in 'carbon-carbon' comes from. This involves the heating of the matting to approximately 1200°C in a gaseous (usually methane) environment so that the carbon matrix is deposited from the gas phase into the matting. The rate of deposition is very slow and requires large material and energy inputs, which results in high production costs. For a strong dense composite to arise, the matrix must be deposited throughout the pore structure. Closed porosity is highly undesirable, as this means that 'pockets' of the matting go un-carburised, as seen in figure 3.1d

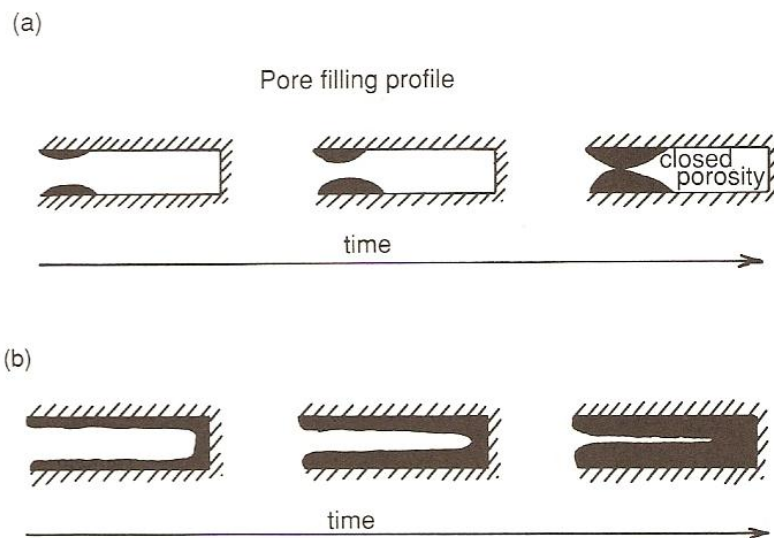


Figure 3.1d – The balance of diffusion and surface kinetics [19]: idealized depictions:  
 (a) surface reaction rate is greater than diffusion rate; (b) diffusion rate is greater than the reaction rate.

The reactants need to diffuse through the boundary layer of laminar flow, around the matting, diffuse into its pores, absorb and then react. The products from the reaction must then be released and diffuse back out along the same route. If the surface chemical reaction happens quickly in relation to the diffusion rate, then the deposition will occur near the mouth of the pore, and it will leave an empty un-reacted pocket further in. To combat this, the diffusion rate needs to be higher than that of the reaction rate – which will allow the pore to be filled in from the inside of the pore, outwards.

Honeywell International [20] have carried out further research into the area of carbon-carbon composite manufacture. They have patented a method which

involved a robotic selection of fibres that ensures that the shorter fibres are towards the exterior edges of the disc, while the longer fibres are towards the middle. This aids carburisation, and helps to ensure that no air pockets are left.

Thermosetting resins (such as phenolic) are used as matrix precursors in carbon-carbon composites because they are relatively easy to use to impregnate fibre. When selecting a thermosetting resin for densification processing of carbon-carbon, consideration needs to be paid to the following:

- Yields are in the range of 50 - 70% by weight. Experimental data indicates that carbon yields are not increased by the application of pressure during carbonisation;
- Carbon matrix structures are glassy, and do not graphitize at temperatures up to 3000°C;
- Stresses applied or induced during the heat treatment can lead to a graphitic microstructure; and
- In order to attain usable densities and properties, components formed by this route must be re-impregnated to minimise the porosity produced during the pyrolysis.

Along with a high carbon yield and ease of impregnation of the fibres, there are three further requirements for a suitable matrix precursor. Firstly the carbonisation shrinkage of the matrix should not damage the carbon and secondly, the porosity formed during the pyrolysis of the resin must be open and accessible for further impregnation.

Carbon-carbon composites formed by the thermoset resin technique are made by pyrolysing a laminated structure in an inert atmosphere to approximately 1000°C. The resulting carbon fibre reinforced isotropic carbon matrix composites may be subsequently heat treated to higher temperatures of approximately 2500°C in order to graphitize the matrix. This process is extremely inefficient as up to half of the matrix is lost during the carbonisation. However, this process is considerably quicker and cheaper than the CVD process. As this method is an ambient pressure fabrication method, the equipment required is not limited by size or a large capital investment, as it would be for the CVD process. Additionally, high quality

precursors may be produced by exploiting the technology developed for the 'conventional' composites industry.

In the liquid densification method, the component is generally vacuum impregnated with a resin or pitch and then re-carbonised. To aid penetration into the bulk of the sample, the resins are often diluted with a solvent to lower the viscosity but the solvent must be evaporated prior to curing and carbonisation.

The first stage of multiple impregnation-pyrolysis using thermoplastics is for the pitch to be converted to carbon by the process of pyrolysis. Pyrolysis is the chemical decomposition of organic materials by heating in the absence of oxygen or any other reagents. Extreme pyrolysis, which leaves only carbon as the residue is known as carbonisation. The carbon yield of the pitch depends very much on the composition of the precursor pitch and the conditions of the pyrolysis. Decreasing the heating rate, the application of pressure or the use of chemical additives prior to the thermal decomposition of the pitch will all increase its carbon yield.

Forest [20] claims that it has been shown that hot isostatic pressing (HIP) is capable of converting thermoplastic resin matrix composites to carbon-carbon. The HIP process uses high isostatic inert gas pressure to impregnate and densify carbon-carbon composites during the melting and carbonisation stages of the pyrolysis cycle.

Furthermore, the materials so formed have generally exhibited superior properties to those developed in phenolic precursors. Properties such as density, strength and stiffness are all increased by comparison with the phenolic precursors, as well as retaining a good deal of their polymeric characteristics, such as low porosity.

This work is reinforced by the earlier works of Marinkovic and Dimitrijevic [21] in their paper of 1985 which considers carbon-carbon composites prepared by chemical vapour deposition. This work is particularly relevant because of the size and shape of open pores within the substrate. It concludes that the kinetics of infiltration are highly dependant on the size and shape of open pores.

Consideration is also given to the effects of various post-formation heat treatment (HT) and geometric factors on the fundamental composite properties.

It is shown that the effects of heat treatment can be explained primarily by the structural changes in the substrate and the matrix as well as the relaxation of stresses existing within the composite. X-ray diffraction is used to show that HT composites display definite structural ordering of the substrate carbon. Substrates display a decrease in inter-layer spacing and an increase in crystallite dimensions although there is only a negligible three-dimensional ordering even at the highest HT used of 2400°C.

Increased HT of a c-c composite is accompanied by a decreased fibre strength and increased modulus. A certain effect of radial shrinkage is also observed. It is suggested by the authors that 1800°C is the optimum HT regarding material properties, as although the tensile strength of the fibres is reduced after treatment to this temperature, the reduction is significantly sizeable beyond this temperature. At 1800°C there is already a certain amount of radial shrinkage that is assumed by the author to be responsible in part for the separation of the fibres from the matrix. The HT weakens the strong bonds between the fibres and the matrix, making delamination possible and providing a subsequent increase in frictional performance. Heat treatment also provides a 'smoothing' of the surface, a consequence of two factors. Firstly, structural ordering means fewer crystallite edges on the surface owing to an increase in crystallite dimensions and preferred crystallite orientation. Secondly, there is a partial or complete removal of surface groups. It is stated that HT also provides an increased stability to air oxidation. In addition to crystallite growth and alignment, relaxation of stresses can be considered as a factor responsible for the observed dimensional changes of the composites upon HT.

Manocha [22] compares the carbon-carbon composites processes, as illustrated in Figure 3.1e

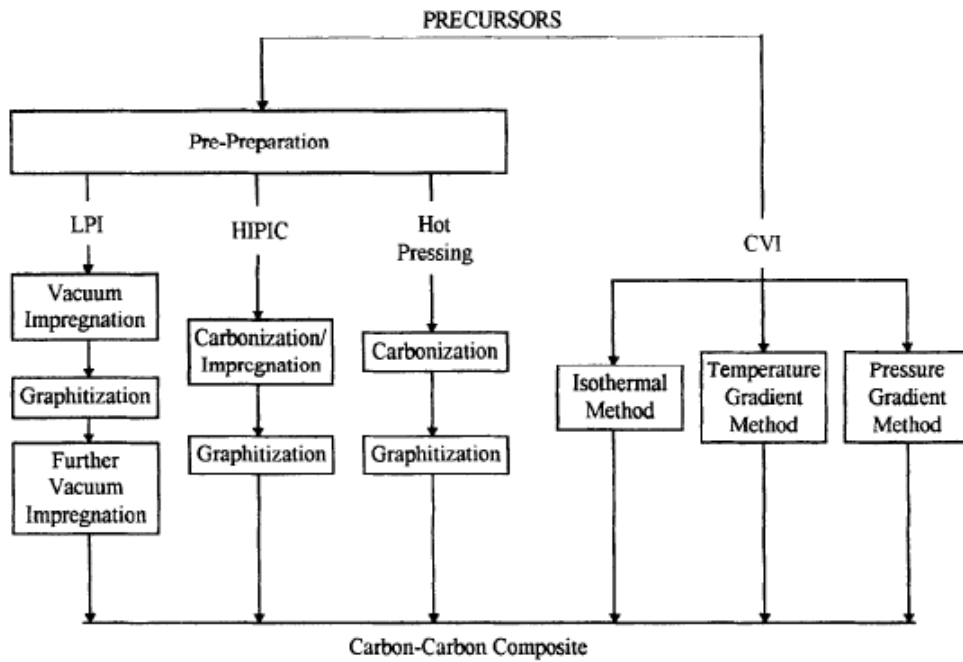


Figure 3.1e – The Carbon – Carbon Manufacturing Process [22]

Prime factors of importance in achieving tough and high thermal conductive carbon-carbon composites are proper choice of reinforcing carbon fibres carbon matrix microstructure density and macrostructure of the composites. Processing routes and choice of carbon precursor greatly influence the density macrostructure (type, size and quantities of defects such as pores and cracks) and matrix microstructure (orientation of carbon planes). The voids and macrocracks are normally fewer in carbon-carbon composites process through HIP route than those made by CVD. Manocha states that the strength and fracture of carbon-carbon composites are governed by the Cook -Gordon theory (23) of strengthening brittle solids. This states that;

*“If the ratio of the adhesive strength of the interface to the cohesive strength of the solid is in the right range, a large increase in strength and toughness of otherwise brittle material is achieved”.*

Composites with strong fibre – matrix bonding fail catastrophically without fibre pull-out while those with control interfaces fail in a mixed tensile combined shear mode exhibiting high strength [24], [25].

Keith Williams of Dunlop Aerospace [26] highlights that there is an approximately 6 week manufacturing lead time from when an aircraft brake disk begins manufacture as chopped carbon fibres through to their being woven into a carbon mat, being trimmed, and going through the CVD process through to final layup and the long pressure baking process. Although the manufacture of these parts must be as swift as possible every step in the process needs to be 100% accurate to ensure continuity of material properties, and as such a strict quality control program is imperative at each stage of manufacture.

Spokas [27] outlines test procedures for friction material evaluation as used by Rockford clutch component manufacturers. He describes four specific tests used in carbon-carbon materials: a burst test to determine the safe operating speed of the material, a wear test to determine the ability to withstand mating surface abrasion (data from this is also used to determine the engagement characteristics of the carbon clutch), a fade test to determine the effect of excessive heat, and a stick test to measure the tendency of the facing material to react to contaminants. Whilst basic in terms of the range of characteristics being scrutinised these tests are a satisfactory starting point in the quality control procedure and can be used as an initial overview of the material batch before deciding if more comprehensive testing is required.

Much work has been done to develop the processes used to ensure for more accurate and mechanically stable materials. In 1999, Walker et al. [28] filed for US Patent for an invention used to improve the Carbon – Carbon (C-C) material through the use of improved CVI techniques. These findings are reinforced by the later work of Gurin et al. [29], whose studies were aimed at developing carbon-carbon discs using thermal gradient gas phase methods for compaction. The paper proposes an equation to calculate the maximum final density of the carbon-carbon composite materials prepared by these methods in relation to the specific content and density of the filler. This equation is given as:

$$\rho_f^m = \left( 1 - \frac{C_f}{\rho_f} \right) P_{yc} \times \eta + C_f \quad \text{Equation 3.1f}$$

Where:

$\rho_f^m$  = theoretical final density in  $\text{g/cm}^3$

$C_f$  = specific content of perform filler in  $\text{g/cm}^3$

$\rho_f$  = pyncnometric density of the filler in  $\text{g/cm}^3$

$P_{yc}$  = pyncnometric density of the pyrocarbon matrix in  $\text{g/cm}^3$

By utilising this equation, it is possible to accurately predict the density of the laid up disc, on the assumption that there are no discrepancies within the manufacturing process. However, what this work does not predict is the microstructure of the resulting 'perfectly densified' carbon – carbon composite, and how predictable its thermal and mechanical properties are.

### 3.2 Microstructures of Carbon

The element Carbon can exist in many different states. These are called allotropes. Eight possible allotropes of Carbon are highlighted in Figure 3.2a [19].

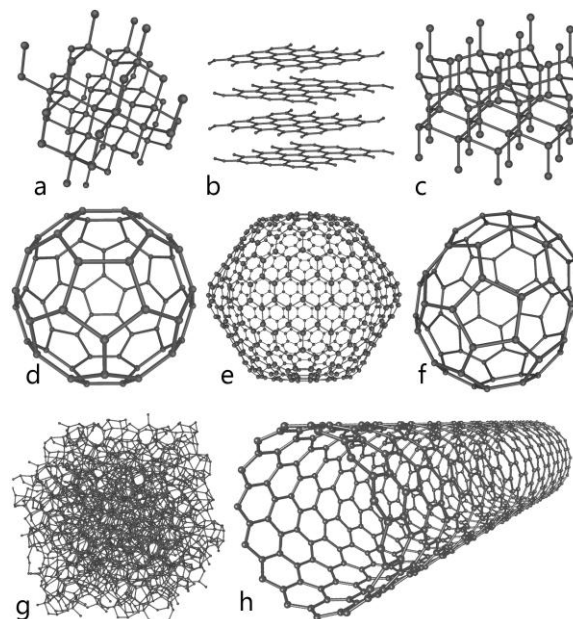


Figure 3.2a – Eight allotropes of Carbon [19]

Top, l-r: Diamond, graphite, Lonsdaleite

Middle l-r: Buckyball (spherical Fullerene), C540, C70

Bottom l-r: Amorphous Carbon, single walled Carbon nanotube (cylindrical Fullerene)



The allotropes important to the study of Carbon-Carbon morphology are amorphous carbon and graphite:

- Amorphous carbon is the state where short-range order is observed, but there is no long-range crystal structure. Amorphous carbon can contain graphite structures;
- Non-graphitic carbon is any variety of substance containing the element carbon with two-dimensional long-range order atoms in planar hexagonal networks but without any measurable order in the perpendicular direction.

A non-graphitic carbon can be transformed into graphitic carbon via thermal activation. This process is called graphitization. The degree of graphitization is dependent on the duration, pressure and temperature attained.

Kimura et al [30] investigated the friction and wear of carbon-carbon composites in 1983. Here they investigated six different carbon-carbon composites all with different microstructures; carbon fibres were woven in plane, specimens with tows woven in a satin structure and specimens made of random chopped carbon fibre. One of each of these different structures was heat treated at 1500 °C, while the other heat treated at 2500°C. Each new specimen, when added with thermo setting resin, saw the formation of a graphite structure after the heat treatment at above 2000°C, at approximately 2600°C the entire matrix transforms to graphite. The author compares his work to that of Weaver [31] who reported that the polycrystalline carbon showed an increase in torque at the initial period before attaining a stable state (this principle later became the basis for bedding as described in chapter 5).

Further extensive work into the microstructure of CVI carbon-carbon composites has been undertaken by Ju and Murdie [32]. The paper on the microstructure of pitch fibre-phenolic/CVI matrix carbon-carbon composites uses scan electron microscopy (SEM) transmission electron microscopy (TEM) and convectional light microscopy to examine the microstructure of a two D mesophase pitch fibre composite. Their work concludes that each individual fibre within a bundle is

surrounded by two distinctive CVI carbon layers and that a major portion of the interface between the fibre and the first CVI layer is physically separated, however, the interfaces between the two CVI layers are much better bonded as is the layers of the CVI and resin char, and that most resin char exists as pockets among fibre bundles.

The work of Luo and Li [33] looks into three different kinds of C-C composites, prepared using CVI and densified to the same density. The samples are; one of whose matrix carbon has a rough laminar microstructure heat-treated under 2300° C; one whose matrix carbon has a smooth laminar microstructure and heat treated at 2500°C and one whose matrix carbon has a rough laminar microstructure and is heat-treated to 2500°C. The relationship between brake moment and velocity, and the effects of factors on these relationships for the three materials were investigated and indicated that the micro structures of the matrix carbon heat treatment technology and braking conditions have a strong effect on both the initial braking moment heat values and the initial brake moment heat ratio values. These values can be reduced by increasing heat treatment temperatures and thus controlling the formation of the rough laminar matrix carbon in the preparation process. This is because there not only exists stronger bonds between the carbon fibres and matrix carbon but also the matrix carbon tends not to be prone to delamination. After braking starts, a large amount of powder debris with poor lubricating properties forms initially on the sliding surface, which is responsible for the biggest heat values. By analysing the same matrix carbons with the different treatment temperatures, it is indicated that that carbon with the increased treatment temperature has a decreased interlayer spacing of the matrix carbon and an increase in crystallite height leading to an increase of lubricating debris and thus a decrease in the peak values. This is particularly relevant to this thesis.

The works of Kimura [30] and Luo and Li [33], highlight the critical effects of heat treatment to the carbon-carbon material, and how it alters its chemical make-up and behaviour dramatically. The temperatures at which the carbon-carbon is heat treated to is in the same region as that predicted at the face of the clutch during a high energy slip. This heat treatment is essentially the same as putting the carbon-

carbon disks through the bedding process and, in particular, the work of Luo and Li offers evidence to support the scientific principles behind the bedding process.

### **3.3 Material Properties and Behaviour of Carbon-Carbon**

In 1989 Gibson and Taccini [6] of Hitco, California, presented a paper to the SAE on carbon-carbon friction materials for clutch applications. Hitco are an established carbon-carbon material supplier to the motorsport industry. This paper outlines general material practice of carbon-carbon in dry and wet brake and clutch applications. Wear characteristics have shown that c-c can last several times longer than conventional brake and clutch materials when properly designed. This is reinforced by the later work of Krenkel, Heidenreich and Renz [34] in their 2002 article. In this paper the authors outline the advanced structural properties of carbon-carbon silicon-carbide composites with specific focus on fibre content and density with relation to the thermal conductivity. The thermal conductivity greatly decreases by as much as 30% for a 50% increase in fibre content and on increase in density of 50% yields and almost 400% increase in thermal conductivity. This highlights the importance of consistent material manufacturing processes. Their paper also outlined the coefficient of friction and wear resistance of the carbon-carbon. Their paper indicates a loose inverse relationship between the average sliding speed (ranging between 0 and 15 m/s) and the coefficient of friction (ranging between 0.8 and 0.4).

The work of Luo et al [35] on the static friction properties of carbon-carbon composites looked at the influence of high temperature heat treatment and test temperatures with results showing that the high temperature heat treatment process plays an important factor of the static friction behaviour. With raising the treatment temperature, the interlayer spacing of the matrix carbon becomes small, and the crystallite width and height increases. Composites treated at 2000° owe their static friction coefficients to the absorption of less water and difficult delimitation of the matrix carbon.

In 2008 Krkosa and Filip [36] investigated the influence of humidity upon the frictional characteristics of aircraft brakes at low landing energy conditions. Disc-on-disc configurations are used to simulate several different energy braking events

(taxi and landing conditions for aeroplanes). A kinetic energy of 128.8kJ is taken as 100% normal landing energy (NLE) dissipation within the brake, although the mass of the specimen is unfortunately not given. However, the 2D c-c composite used is pitch fibre reinforced carbon with charred resin matrix, densified by carbon vapour infiltration. Experience suggests that this will typically have a density of approximately  $1.75\text{gcm}^{-3}$ .

Three relative humidity environments are used in the frictional tests – 2, 50 and 90% RH, controllable to within  $\pm 1\%$  of the desired value. Each testing sequence comprised 50 landings and 150 taxi stops (a taxi stop always being 4.5% NLE). After each sequence, the surface roughness of the friction surfaces was analysed to help evaluate evolution of roughness with energy and humidity.

It is shown that coefficient of friction is stable at all humidity levels for low energy input (12.5% NLE), with the average value being slightly higher for dry conditions than humid conditions. However, as the energy input is increased to 25% NLE, changes in the coefficient of friction are registered in humid conditions. The dry humidity still remained constant. The effects are exasperated as energy input increases further.

At 100% NLE, two friction transients (sudden changes) are observed, one at the beginning of the stop and one at the end of the stop. It is shown that the surface temperature of the discs increases rapidly at the time of the first transient.

It is shown that for 2D c-c composites (referring to the fibre orientation, as opposed to 3D), the thermal conductivity is low in the z-direction (perpendicular to the friction surface). Consequently, these composites have a higher surface temperature throughout the event than a 3D composite, and this higher temperature facilitates the release of chemisorbed and physisorbed species.

It is also shown that for 2D c-c composites, the average coefficient of friction detected at different landing conditions is very sensitive to the energy level applied during braking. There is a rapid reduction in friction coefficient as the energy increases from 50% towards 100% NLE. However, the coefficient of friction

for taxi stops after landings are similar for all energy levels from 12.5% to 200% NLE.

Krkosa and Filip note that all research on the subject of carbon-carbon friction is based fundamentally on the effects of frictional debris or a lubricating friction layer. In this study, friction layers were observed. The friction surfaces at low NLE have a darker appearance than those performed at high NLE. This is said to indicate that at low NLE, abrasive wear dominates. The scanned friction surfaces after high NLE friction are polished, indicating non-abrasive wear. Thus it is stated that at higher energy, a stable and sizable friction layer is generated and prevents the friction surface from wearing.

Krkosa and Filip attempt to correlate surface roughness with frictional performance, based upon fractal theory being used as a characterisation of the rubbed surfaces. This can be characterised by parameters D and G from the use of Hurst analysis (D = measure of the amount of roughness, G = measure of the surface waviness). However, this method did not yield any direct correlation.

Finally, TEM studies are performed on the friction surface [36]. TEM samples are taken at termination of braking for low energy, and at extreme  $\mu$  values for high energy. The microstructure of the friction layer at low energy exhibit amorphous nature. At high energy, when the first friction transition to high coefficient of friction is observed, the friction surface is found to be highly crystalline. The subsequent reduction in friction is due to the release of chemisorbed moisture. The second transition is the highest measured surface temperature and demonstrates amorphous characteristic. This surprised the authors as based on previous studies they anticipated high energy and high temperature would correspond to graphite carbon states.

Further to this last point, the observations of Krkosa and Filip could be explained by the fact that at the end of the stop, the sliding speeds are such that the highly compact lubricating friction film cannot be maintained, and is disrupted back into powdery debris. It is recognised from other studies that powdery debris (typical of Type II surface morphology) provides a high coefficient of friction. It is interesting

to note that the authors suggest neural network modelling to provide a better correlation. The paper is co-authored by Peter Filip, who was later part of the project “Neural network modelling of wear in Formula One race car brakes” for Toyota Motorsport Group in 2004.

Further works by Blanco et al [37] [38] present summaries of several previous carbon-carbon studies and to introduce the fundamental carbon science associated with carbon-carbon brake performance. Real life aircraft brake performance is then analysed with the results related to relevant chemical and physical properties of carbon materials.

It is stated that the friction coefficient of carbonaceous material does not increase linearly with increasing degree of graphitisation. As the heat treatment temperature of the carbon increases, so the surfaces become more graphitic and hence the friction properties of the surface improve. However, there is a maximum benefit as increased graphitisation brings easier surface disintegration as grapheme layers can be pulled out from the surface with greater ease.

The concept of surface oxygen complexes is introduced. Not all of the oxygen molecules approaching the carbon surface return to the gas phase as carbon dioxide or carbon monoxide. Some atoms remain chemically bonded to the carbon surface in a variety of bondings. These constitute surface oxygen complexes, and include for example Hydroxyls, Ethers and Lactones. Surface oxygen complexes can only occur at temperatures below 1000°C (above this, direct gasification only occurs).

It is stated that as the degree of graphitisation increases, the extent of surface oxygen complex formation decreases. The reasons for this are put forward by the authors as a decrease in surface area of the friction material, and secondly the graphene constituents become more perfect in terms of structure and planarity.

The clustering effect of water molecules on carbon surfaces is also discussed. Water isotherms indicate the variation in the amount of adsorbate (water vapour) on the surface of the adsorbent (in this case, the carbon-carbon friction surface).

Although initially water molecules are not attracted to the surface, the surface contains enough defective sites with sufficient energy to attract individual molecules. Once a molecule is attracted, the water molecule attracts other water molecules, and a clustering effect occurs seeing an almost exponential rise seen in the isotherm.

Finally, the role of wear dust during the braking operation is discussed. Fragments of carbon break away from the friction surfaces and remain between the surfaces in the irregularities and cavities or porosity of the surfaces. SEM and TEM studies of the wear particles indicate they are essentially lamellar, are very thin and are of size 100nm to 10µm. Examination of the edges indicates significant serration, indicative of gasification or ablation from the edges. This means adequate facility for formation of surface oxygen complexes, the relevance of which is highlighted above.

The friction and temperature characteristics for a wet clutch were studied and reported by Holgerson [39]. He concluded that dynamic friction decreased with velocity, torque and inertia possibly due to a rise in temperature. Zagrodski [40] investigated the temperatures and thermal stresses in multiple disk clutches and drew conclusions on how the normal pressure distributions on the friction surfaces were affected. When the pressure distributions were non uniform the distributions of heat flux was also non uniform resulting in high local temperatures and thermal stresses, known as hot spots.

### **3.4 Factors Affecting Carbon – Carbon Material Behaviour**

The work of Scott and Suntiawattana in 1995 [41] investigated the effects of extreme pressure and the use of lubricating oil additives to change viscosity indices on the frictional characteristics of the sintered frictional material. The lubricant additives tested showed that with the viscosity additive, there was an increased friction reduced lock up time and lowered static to dynamic coefficient of friction ratio. Wear of the friction material was also marginally less. This is interesting to note for future developments of this project.

Audebert, Barber and Zagrodzki [42] looked at the plates of an automatic transmission clutch and examined buckling due to thermo elastic/plastic residual stresses. Axisymmetric and non-axisymmetric modes resulted from in-plane axisymmetric residual bending moments and the critical value for each mode is found. Whilst this work focuses mainly upon metallic plates this work is of interest as it highlights the possibility that this may be occurring within the carbon-carbon multiplate clutch used within F1 systems. Susceptibility to buckling increases by a factor to the radial thickness of the clutch

In 1999 the effects of post curing on frictional behaviour of phenolic composites in clutches were investigated by Jafari et al [43]. Phenolic friction composite (PFC) was made from whole asbestos yarn by dipping in M-phenol based formaldehyde resin. When tested the PFC showed a decrease in friction coefficient between the third and fourth cycles and gravimetric analysis showed some weight loss when the un-post-cured PFC was exposed to 300°C. This was attributed to the presence of moisture and volatile materials formed from the decomposed ingredients. It was shown that extending the post curing time by 100% helped in the elimination of slipping behaviours and marginally improved many desirable properties as it was shown that the moisture increased the coefficient of friction where the volatiles decreased it, and even helped to prevent the effect of moisture. Later on in 2002 Venkataraman and Sundararajan [44] looked at the influence of sample geometry on friction behaviour of carbon-carbon composites. This work led on from that of Audebert and extended upon this by studying the influence of sample geometry on the transition value to dusting wear, and by characterising the transition from normal to dusting wear on the basis of interfacial temperature measurement by utilising an eroding thermocouple. This is a standard way of measuring interfacial temperature and has been implemented for many years on industrial test rigs. This work concluded that carbon-carbon composites undergo a transition from a low friction coefficient normal wear regime to a high friction coefficient dusting wear regime when the interface temperature exceeds a critical value (usually in the range of 330 - 400°C). It was also noted that the sample geometry had a dramatic influence to the critical value of the transition to normal dusting wear and is essentially due to the fact that the extent to which the heat generated at the sliding interface partitions to the stationary sample is dependent on the



sample geometry. However, this paper did not give many numerical values and did not provide any significant information regarding the thermal profile of the clutch in order to make such claims as to the effect of sample geometry.

The variation in nature of organic fibres was investigated in the 2004 works by Satapathy and Bijwe [45]. Their work looked at brake fade and recovery with regards to the influence of four selected organic fibres. What is of specific interest is that one of these fibres was CF (carbon fibre). It was observed that the carbon fibre showed the highest resistance to brake fading recovery and demonstrated more overall stable effectiveness. It also demonstrated the least wear under fade recovery conditions. Although values were given for the brake fade and recovery what was not explained in this paper was the reasoning behind this.

Works on the effects of densification cycles on continuous friction behaviour of carbon-carbon composites were published in 2004 by Lee et al [46] and studied the continuous friction behaviour of c-c. In the densification process different numbers of densification cycle were adopted to investigate the influence upon its properties and concluded that as the number of densification cycles increased the number of open pores within the structure decreased giving a dense and smooth surface morphology. In addition to this a smooth adherent lubricating film was formed on the sliding surface during wear tests and thus had lower wear rates and average friction coefficients. This work is of particular significance as it highlights the requirement for consistent and uniform materials, especially as the main mechanism of sliding friction is due to the lubricating film formed on the surface.

As an addition to the earlier 1999 works of Jafari [43] Yuan et al [47] investigated the influence of high temperature heat treatment on the friction properties of carbon-carbon composites under wet conditions.

Their results show that the frictional behaviours were strongly affected by environmental wetness and friction coefficients in the wet decreased with a brake pressure increase for all samples. Composites treated at 2000°C kept a high friction coefficient. This work is of interest because with over work of clutches within an F1 application the carbon-carbon material within the clutch stack would

quite possibly see these temperatures, thus changing the material properties of said stack.

Later that year J Li continued his work [47] by collaborating on a further paper into the friction behaviours of c-c composites with different pyrolytic carbon textures [48]. This work used a homemade dyno to simulate airplane landing conditions with the morphology of the worn surfaces for three different composite laminar textures. Using an SEM to observe the surface morphology and using the results from the dyno it was concluded that the c-c composites with a medium textured rough laminar makeup had nearly consistent friction coefficients and stable friction curves whilst its smooth laminate counterpart experienced intensely decreasing friction coefficients and high oxidation losses under medium to high energy conditions. This was due to the properties of the rough laminar structure which tends to lead to a uniform friction film forming on the friction surface. During an F1 launch, the clutch will see its highest energy loads and so the work of Li et al is useful in the context of this thesis, even though this is different material to that used in F1.

One of the most recent works on the subject of carbon-carbon material properties was written by Li and Crosky [49] and their work investigated the effect of carbon fabric treatment on the de-lamination of two dimensional carbon-carbon composites. The properties including inter laminar shear stress density and open porosity were tested and de-lamination effects were characterised and it was found that the concentration of surface oxygen decreases whilst the carbon increases after high temperature treatments. The c-c treated with carbon fabric are non-de-laminable whilst the non-treated carbon fibre reinforced composites are de-laminable during carbonisation which is largely attributed to interfacial strength of the polymer matrix composites.

### **3.5 Surface Properties of Carbon – Carbon**

Chen and Ju [50] in their paper outlining the effects of sliding speed on the tribological behaviour of a PAN-Pitch c-c composite report on the behaviour of a 2D matrix. When the composite was slid at 800 and 1100 rpm no transition was

observed and a thick smooth lubricative film was formed on the warmer surfaces with friction wear remaining relatively low. However, at 1400 rpm and higher the composite experienced simultaneous transitions in friction wear and surface morphology. When the frictional transition occurs the temperature rises abruptly and this was due to a debris film which became unstable and suddenly disrupted causing the friction and wear to rise abruptly.

In the further research paper written by Chen, Chern Lin and Ju [51] details an investigation into the effect of humidity on wear and frictional behaviour of certain types of c-c composite, namely 2D PAN/pitch, PAN/CVI and pitch/resin/CVI. The test setup was typical of tribological c-c studies, utilising disc-on-disc friction via means of a lab dynamometer operating at different sliding speeds for a fixed load. The influence of humidity was assessed by conducting the investigation within a sealed steel chamber. Three relative humidity levels were studied. High relative humidity levels (HRH, >90%) were attained through continuous evaporation of water within the chamber, medium relative humidity (MRH, 50-60%) was an unaltered internal environment, and low relative humidity (LRH, 20-30%) were obtained by blowing powdered dry air into the chamber through a silica glass tube, whilst operating an electric desiccator inside the chamber for further drying.

The authors detail the three types of debris morphology and their associated characteristics, both physical and tribological. These are denoted Type I, Type II and Type III as is widely accepted.

It was found that relative humidity had a strong effect on the tribological behaviour of all tested c-c composites. High humidity generally lowered the coefficient of friction and the wear rate, and delayed the transition from Type I to Type II debris morphology. It was also found that high humidity enhanced the formation of Type III debris, particularly at high speeds.

It is stated that the exact mechanisms for transitions, particularly Type I to Type II, are not understood at the time of writing. However, the authors suggest that discussion of water vapour theory may be helpful. Savage and Rowe both suggest

that a small amount of adsorbed water vapour is necessary for a bulk carbon-graphite material to exhibit good friction and wear properties when sliding against metals. Without this water vapour, a high friction and wear process (dusting) takes place. Earlier studies show that surface temperature increases with sliding distance and that temperature rise also exhibits transition. Small amounts of water vapour are generally adsorbed on c-c composite surfaces. As temperature rises with sliding speed/distance, water content decreases as a result of desorption. The authors assume, based upon this observation, that when surface temperature approaches some critical level, water content in the c-c surfaces becomes low enough for the dusting process (Type I to Type II) to begin. It is said that this may help to explain the obtained result showing that for all tests undertaken, transition occurred earlier at higher sliding speeds and/or in lower humidity environments.

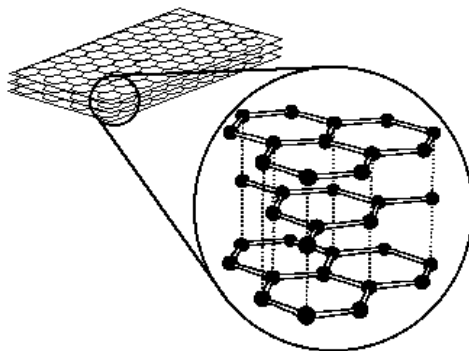


Figure 3.5a – Diagrammatic representation of graphene layers [19]

Figure 3.5a highlights the hexagonal structure of graphite, and the graphene layers. The black dots represent carbon atoms, the solid lines represent the covalent bond between atoms and the dashed lines represent the weak van der Waals bonds between layers.

Bond strength is very closely linked to bond length. In a graphite hexagonal ring, each C-C bond length is  $1.42 \text{ \AA}$ , whilst inter-layer C-C bond length is  $3.35 \text{ \AA}$ . This would indicate that the inter-planar bond strength is more than twice the strength of the inter-layer bond strength.

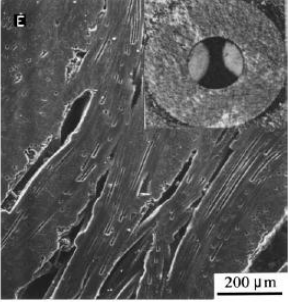
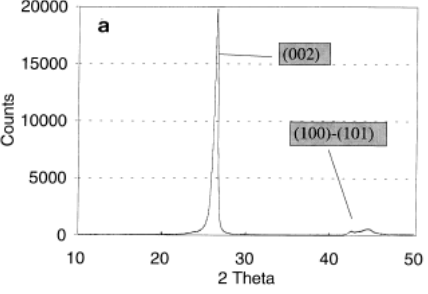
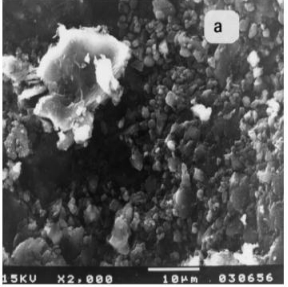
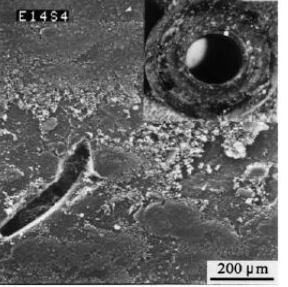
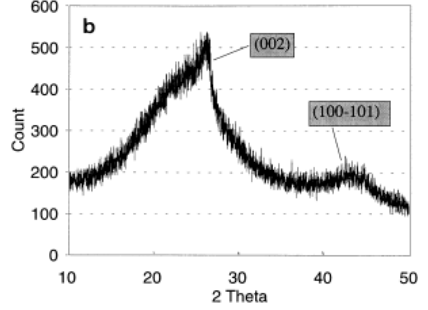
Applying this theory to the shearing of a graphite structure, it is clear that inter-layer bonds will be broken before the inter-planar bonds, and hence slip between the graphene layers is induced. This phenomenon provides an explanation for the widely observed self-lubricating properties of graphite.

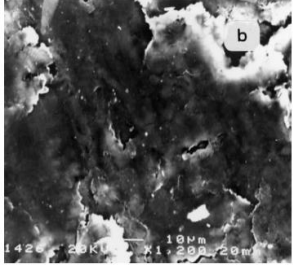
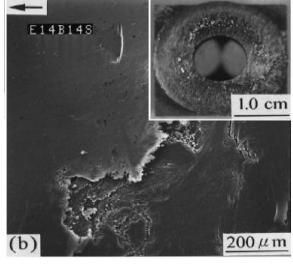
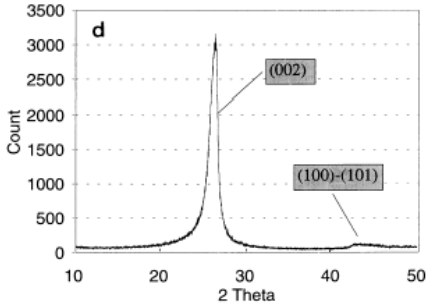
It should also be clear that the highly anisotropic thermal nature of graphitic carbon can now be explained, as phonons travel quickly across tightly bound planes. Hence, thermal conductivity parallel to the surface will be relatively high, however through-thickness thermal conductivity will be relatively low as phonons are slow to traverse the weakly bound planes from one graphene layer to the next.

The classification 'Type II' is given to the surface morphology consisting of thick, powdery debris of small dimensions. On a macroscopic level, this will appear dull and unpolished.

The classification 'Type III' is given to the surface morphology where there is a smooth compacted layer. High resolution analysis may show this to be consisted of extensive flat platelet (as opposed to the small particles seen in Type II). It appears as though the thick powdery debris has been transformed into this friction film as a result of high energy input.

Table 3.5b – Descriptions of the surface morphology classifications as suggested by Ju et al [51].

Classification	Macroscopic appearance	Description of wear debris or surface	$\mu$	High resolution SEM (illustrative purpose only)	Low resolution SEM (illustrative purpose only)	XRD spectra of wear debris (illustrative purpose only)
Type I	Machined and polished	Negligible amount of wear debris present on surface.  Surface has large pores present.	Low	n/a		
Type II	Dull, unpolished surface	Thick layer of powdery wear debris, loosely attached particles, all less than 5 $\mu$ m in dimension.  Many of the pores are filled in with debris.	High			

<p>Type III</p>	<p>Smooth, polished surface</p>	<p>Extensive flat platelets that are detached from the bulk surface. Surface wear debris has been transformed into a smooth friction film.</p>	<p>Low</p>	 <p>SEM image showing surface debris. A scale bar indicates 10 μm. A label 'b' is present in the top right corner.</p>	 <p>SEM image showing a circular feature. A scale bar indicates 200 μm. An inset shows a larger view of the feature with a 1.0 cm scale bar. A label '(b)' is in the bottom left corner.</p>	 <p>XRD pattern showing two peaks. The y-axis is labeled 'Count' (0 to 3500) and the x-axis is labeled '2 Theta' (10 to 50). The peaks are labeled '(002)' at approximately 26.5° and '(100)-(101)' at approximately 41.5°.</p>
-----------------	---------------------------------	--	------------	--	---	--

Further work by Chen, Chern Lin and Ju followed in 1996 with their work on the effect of load on the tribological behaviour of carbon-carbon [52]. This work was merely an extension of their previous work [50] and [51] and concluded that for all composites a higher load can accelerate the transition from type i to type ii but impedes the transition from type ii to type iii. This work was further continued by the trio in their investigation on the surface effects of braking behaviour [53] which concluded that specimens braked from higher speeds always suffered higher wear due to either higher friction coefficients or longer braking times. This led on to their works on the effects of surface condition on tribological behaviour [52]. Two specimen groups are used, defining the initial surface condition. AP specimens are mechanically polished at the friction surface to 1200 grit level, leaving an average surface roughness of  $1.8\mu\text{m}$ , whilst BI specimens are AP specimens that undergo subsequent break-in treatment (1.7MPa, 1800 cycles at 1400rpm) resulting in an average surface roughness of  $3.7\mu\text{m}$ .

For a braking test of initial speed 1400rpm, neither the AP or BI specimens underwent any tribological transition – the friction coefficient remained relatively consistent throughout at 0.22 and 0.25 respectively. However at a higher initial speed of 2000rpm, both specimens experienced tribological transition. For the AP sample, coefficient of friction started around 0.25, reduced to 0.13 and then immediately rose to 0.88. After this transition, the massive wear debris started to be compacted into a lubricating film, causing a reduction in coefficient of friction  $\mu$ . Around 15s,  $\mu$  began to increase again. A possible explanation put forward by the authors for this v-shaped  $\mu$  characteristic after transition is the repeated formation and disruption of the debris film. The BI sample at 200rpm initial speed displayed similar  $\mu$  characteristics, but with earlier transition.

Three types of surface film are introduced. Type I morphology is the initial smooth surface film seen pre-tribological transition. Type II morphology is a rough powdery layer of debris formed when Type I is suddenly disrupted at transition, accompanied by an increase in friction coefficient. Type III morphology is a smoother denser lubricative film formed when the powdery debris is compacted under certain conditions, causing a reduction in friction coefficient.



Surface morphology analysis shows that the post-transition BI 2000 sample displays mixed type II-III morphology, indicative of the repeated formation and disruption of the lubricating surface film.

Type III debris is stated to be more lubricative than type II, and with the former evolving from the powdery type II that was compacted and piled up layer by layer during sliding. However, as the mechanical bonding among these individual layers is weak, delamination occurs easily to the type III film, causing fragments to break off. These fragments are subsequently transformed back into type II powder. Whilst some debris escapes and some fills holes and pores within the structure, the remained is compacted back into type III debris. This continual formation-disruption cycle explains the undulating friction coefficient observed from after transition to just prior to the end of the braking manoeuvre. The final jump in  $\mu$  is because at low sliding speed (<500rpm), there was insufficient energy present to re-develop a stable lubricative debris film [53].

Although Chen, Churn Lin and Ju had produced significant works upon the tribological behaviour of carbon-carbon composites a paper written by Hou et al [54] on the internal friction behaviour of carbon-carbon composites expanded on this even further. This paper proposes two internal friction mechanisms; a thermo-elastic mechanism and a static hysteresis mechanism. It was concluded that as with graphite materials internal friction in carbon-carbon composites increases with increasing frequency and amplitude. More interestingly a unique internal friction phenomena was observed in the carbon-carbon composites as generally the internal friction decreases and the dynamic modulus increases with rising temperature. This can be attributed to the effects of the internal friction produced by the mismatching of the coefficient of thermal expansion at the fibre matrix interface.

These friction and wear mechanisms were investigated further in the paper by Gomes et al [55] whose work looks into the sliding speed and temperature on the tribological behaviour of carbon-carbon composites. Sliding experiments were performed in a pin-on-disc tribometer applying a 100N load in the temperature range of ambient temperature to 600°C at sliding speeds of 0.5 to 2.0 and 3.5m/s.

At room temperature and low sliding speed the wear coefficient was extremely low, however, the wear values increased by three orders of magnitude for the highest sliding speed tested. The same trend was observed when comparing results at RT and 300°C or above. Concluding that carbon-carbon composites show unique properties as wear resistant materials at RT and moderate sliding speeds. However direct or frictional heating may deteriorate the response of the materials. Although this work is well researched it does not offer any new information into the wear characteristics of c-c as its results had been previously reported in far more detail by many of the other researchers in this field, especially Chen, Churn Lin and Ju [50] [51] [52] [53].

In the paper “Effect of heat treatment on the tribological behaviour of 2D carbon/carbon composites” by Luo et al [56], it is stated that in ambient temperature conditions, water from the atmosphere is absorbed on the friction surfaces of specimens, forming the surface oxygen complex. Additionally, the presence of moisture lowers the shear resistance of the matrix carbon along the basal plane.

The authors suggest that specimens with higher interlayer spacing and smaller crystalline dimensions (i.e. the least perfect structure in terms of planarity and structure) will have the capability to absorb larger amounts of water and will have a greater extent of surface oxygen complex existing on the friction surfaces. This results in low static friction coefficient. It thus follows that those specimens with smaller interlayer spacing and larger crystalline dimensions will absorb less moisture. The result is that carbon/carbon composites that undergo high heat treatment temperature (HTT) will absorb little moisture over a given period of time.

It is also stated that a limit to the friction gain exists. Increasing HTT produces a corresponding delamination tendency at the friction surface, which reduces the static friction coefficient, indicating that a compromise between the two factors will yield the greatest friction benefits.

Static friction is found to reduce with increasing brake specific pressure regardless of the braking condition applied, which is attributed to increasing delamination. However, above a certain threshold, static friction is the same for all composite samples.

In a separate research project, Hutton et al. [57] performed microstructural studies of the wear debris generated from friction of carbon-carbon composite discs. One of the tests conducted was comparison of wear debris XRD spectra from events of different energies. The results are presented in Table 3.5c.

Material	$d_{002}/\text{\AA}$	$L_a/\text{\AA}$	$L_c/\text{\AA}$	$p$
Parent composite	3.38	247	208	0.12
Cold taxi wear debris	3.43	34	64	0.94
Landing wear debris, ordered component	3.38	–	200	0.12
Landing wear debris, disordered component	3.44	37	10	1.00
Rejected take-off wear debris	3.39	150	65	0.13

Table 3.5c – XRD analysis of wear debris by Hutton et al[57].

They concluded that after high energy events, a surface morphology indicative of Type III is formed, probably due to the combination of high interfacial temperatures and high power density. The Type II morphology of particulate powdered debris was observed after low power events. Samples of this wear debris were found to be of a very disordered carbon phase (i.e. amorphous), as a result of the shear deformation of the graphitic CVI matrix. The high energy friction film debris showed a more ordered state, indicating partial graphitization of the amorphous particulate wear debris. Increasing the energy further resulted in a XRD spectra similar to that of the parent material.

The authors begin with the introduction of the widely-acknowledged surface-morphology classifications, and a review of recent (at the time of writing) research relevant to tribological performance of c-c composites.

A study of the influence of carbon-fibre orientation at the wear face on the tribological behaviour of a carbon-carbon composite is reported. The samples are manufactured from polyacrylonitrile-based fibres (PAN) in a chemical vapour infiltrated (CVI) matrix derived from methane. The materials are cut to expose

four fibre orientations at the contact surface, these being top face, front face, side face and diagonal face. The normal orientation of the contact surface is the base composite, top face, with continuous fibres oriented parallel to the contact surface. The front face has alternate lamellae of the felt and fibres exposed, with the fibres oriented parallel to the contact surface. The side orientation is similar to the front, except that the continuous fibre bundles are perpendicular to the contact surface. The diagonal faces at the ends of the fibres intersect the contact surface face at 45°.

A typical disc-on-disc experimental procedure is carried out using a lab dynamometer. Testing takes place at speeds of 1800, 4200, 6000 and 8000rpm, with each test consisting of 20 cycles of 1 minute on and 1 minute off, making a total test time of 40 minutes. During the tests, pressure and bulk temperature are recorded with the former being used to calculate the coefficient of friction between rotor and stator.

SEM analysis of the base test composite shows that a friction film is absent for 1800rpm test speed. The surface finish of the tested composite is dull, and the surface contained fine particles signifying Type I debris. At 4200rpm, a mixture of Type I and Type II debris is observed. Low wear rates and friction are measured for high rotational speeds and are attributed to the formation of a bright reflective friction film (Type II debris), which partly covered the continuous fibre lamellae and to a lesser extent the felt lamellae. High wear rates are associated with abrasive wear by the particulate debris, and the use of differential interference contrast microscopy reveals wear tracks in the sliding direction, in the form of shallow grooves in the friction film.

The preferential formation of friction film in the continuous fibre regions may be due to the favourable orientation of the CVI carbon sheath around fibres at the wear face. The CVI carbon is highly graphitised and therefore easily deformed by shear forces, whilst the PAN fibres resist this shear.

At 1800rpm the author concluded that the shear forces and surface temperatures are too low to form the friction film, and that bulk temperatures in excess of 140°C are required before friction film can be generated.

Tests were carried out where stator and rotor both use the same orientation (e.g. Side-side, diagonal-diagonal), and also using different stators and rotors (e.g. Top-side, Side-Diagonal), in order to analyse the effect of orientation of tribological performance. Results more than two standard deviations larger and smaller than the mean base value are highlighted for investigation. It is shown that the different fibre orientations do not change the qualitative features of the wear mechanism, although they do affect the extent to which the friction film develops. Fibre orientations parallel to the wear face favour friction film formation through easier shear deformation of the graphitic CVI matrix formed around the fibres. The film also orientates preferentially around the fibres. Fibre orientations perpendicular to the wear surface inhibit friction film formation and results in high wear rates but low friction at low speed. Hutton suggests this is because microfracture of the fibre ends emerging at the wear surface creates Type I particulate debris, which would account for heavy wear, and also low friction specifically at low speed as the particulate debris rolls between the surfaces. At high speeds, temperatures and shear forces are great enough to overcome unfavourable fibre orientations and friction films are generated.

The process of transforming disordered (amorphous) carbon material into an ordered (graphitic) state is depicted in Figure 3. When starting with an initial disordered, isotropic carbon, it can be seen that as temperature increases, the disordered phase is gradually transformed into a more ordered, anisotropic state.

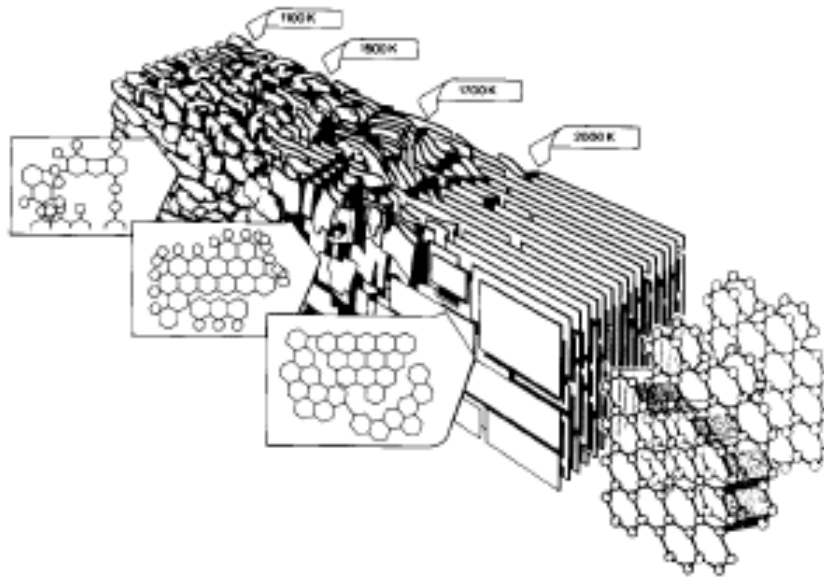


Figure 3.5d – Schematic diagram of changes in the lamellar structure of a graphitizing carbon with increasing HTT [19]

Luo et al. [58] conducted an investigation into the effect of heat treatment on the tribological behaviour of 2D c-c composites. Table 3.5e below presents the results of their XRD analysis.

Specimen	Interlayer spacing, $d_{(002)}$ (nm)	Crystallite height, $L_c$ (nm)	Crystallite width, $L_a$ (nm)
A	0.3429	5.3	16.6
B	0.3414	6.3	32.0
C	0.3424	6.4	25.2
D	0.3404	10.3	38.1

Table 3.5e – XRD analysis of HTT specimens by Luo et al [58].

*Specimen A = 1800°C at 1hr*

*Specimen B = 1800°C at 1hr, then 2000°C at 1hr*

*Specimen C = 2000°C at 1hr*

*Specimen D = 2300°C at 1hr*

Observation of specimen A, C and D shows that increased HTT yields smaller interlayer spacing and larger crystallite dimensions. This is characteristic of an increased degree of graphitization i.e. becoming more ordered.

A separate HTT study by Byrne [17] provides similar results to those obtained by Luo et al [59]. Figure 3.5f shows the XRD spectra of a c-c sample before and after high temperature heat treatment is applied. The sample after heat treatment shows a higher ordered crystal structure.

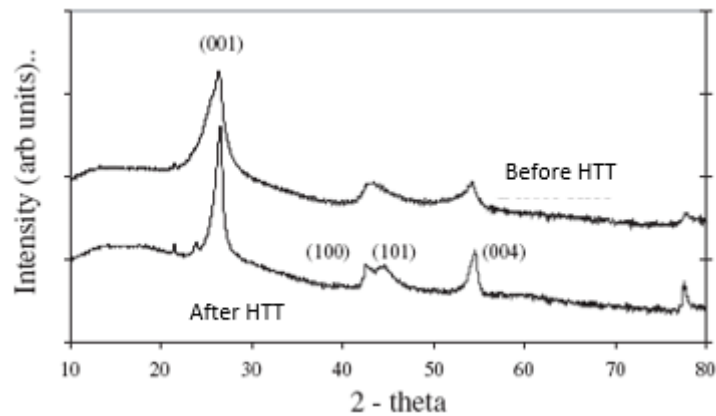


Figure 3.5f – XRD spectra of CVI-densified carbon-carbon composite before and after HTT (intensity on log scale) [59]

Table 3.5f shows the influence of HTT on the measured brake moment (torque) peak ratio value. Caution should be exercised when comparing this data to HRF/HGT data as the experimental setup is very different (plate-on-plate, different plate dimensions, long stopping duration, etc). However, the data shows that for higher energy events, increased HTT reduces the measured brake peak moment value. This would potentially indicate that if clutch plates undergo HTT prior to bedding, the number of events required for a consistent state to be attained will be reduced.

Linear sliding velocity ( $\text{m s}^{-1}$ )	Angular velocity (rpm)	Brake energy ( $\text{MJ m}^{-2}$ )	Moment inertia ( $\text{kg m}^2$ )	Brake moment peak ratio value			
				Specimen A	Specimen B	Specimen C	Specimen D
6.2	1800	1.9 (low energy)	0.25	1.1	1.2	1.4	1.1
8.6	2500	3.7	0.25	1.3	1.2	1.1	1.3
15.5	4500	12.0	0.25	1.3	1.4	1.4	1.1
20.7	6000	21.2	0.25	1.5	1.4	1.4	1.2
26.0	7500	33.1 (normal energy)	0.25	1.5	1.5	1.5	1.2
26.0	7500	39.8	0.29	1.8	1.5	1.4	1.3
26.0	7500	42.3 (high energy)	0.31	1.9	1.6	1.4	1.3

Table 3.5g – Experimental data from testing of HTT specimens by Luo et al [59].

The effects of material properties on the thermo elastic stability of sliding systems was investigated in 2001 by Decuzzi and Demelio [60]. They concluded that the influence of the material properties on the thermo elastic stability of a multi layered sliding system could easily be found via a relationship held between the sliding velocity or rotating critical speed and the arbitrary material parameter  $\xi$ . This can be employed in estimating the optimum set of material properties for sliding systems.

Xiong, Huang, Li and Xu [61] consequently investigated the friction and wear properties of c-c composites with different surface textures – smooth laminar structure (SL), rough laminar structure (RL), and a hybrid displaying a mixture of these two characteristics.

A home-made inertia-type laboratory dynamometer was used to simulate braking between a stator and rotor ring specimen, of inner and outer diameters 53mm and 75mm, thickness 15mm. The samples were CVI densified carbon-carbon, with final densities of 1.83-1.85g/cm<sup>3</sup>,  $V_f$  of 33-35% and were heat treated at 2300°C.

Three c-c samples are produced – A, B and C with degree of graphitisation 35.5, 49.0 and 87.2% respectively. Microstructure analysis shows sample A to be of SL characteristic, sample B to be hybrid SL-RL, and sample C to be RL. As has previously been stated, it is observed that increased graphitisation results in increased crystalline height ( $L_c$ ).

Three energy levels were selected for the investigation based upon aeronautical application – normal landing (NL), overload landing (OL) and rejected take-off (RTO) in ascending order of energy dissipation.

The experimental results show that the friction coefficients for the three specimens are almost the same at NL braking level (lowest energy). As the braking energy increases to OL and RTO, specimen A (SL) sees coefficient of friction values



drop to 0.25 and 0.19 respectively, whilst the  $\mu$  for samples B and C remains at the same level observed for low energy input.

SEM morphology of the worn surfaces for different energy levels shows that a uniform compacted film forms on the surface of B and C at different braking levels, whilst specimen A displays a coarser friction surface.

The Xiong et al conclude that the process of friction-film formation on specimens is a dynamic state of balance. Carbon layers at the friction surface deform at high temperature and pressure during a braking event. Specimens with high graphitisation will inherently be of low hardness characteristic, and hence the carbon layers in their friction surfaces are easy to deform. This allows the formation of the uniform compacted film. The compacted films will be smashed to wear debris driven by the frictional shear force in the following braking. Some wear debris will escape from the friction surface by eccentric force, while others will be compacted again to restore the film. This will reach a dynamic balance state until the braking energy is changed.

Concluding, c-c composites with a high and medium texture pyrolytic carbon have stable friction coefficients, friction curves and reasonable wear loss at various braking energy levels. These positive points are due to the characteristics of the RL, which leads to a uniform friction film formed on the friction surfaces.

### **3.6 Friction Film and Wear Mechanisms**

In the early 1990s, understanding of the surface degradation in carbon-carbon was still very limited,. However, work was continuing into the clutch wear mechanisms of its sintered plate predecessor and this led the way for later c-c testing. One such work was that carried out by Osnani et al [62] which details an experimental and theoretical analysis of the heat transfer at the sliding interface between a paper disc and a sapphire plate in oil, and by using these two methods, a degradation curve for the wet friction paper was proposed. Due to the early time of this paper, the modelling and testing methods are quite primitive, although the principles of the paper are useful to this thesis.

Another group of researchers who were investigating the carbon-carbon material in the early 1990's was Murdie, Ju, Don and Fotruno [63]. Friction and wear properties were tested under different energy conditions and using optical, scanning and scanning electron microscopy, the structure of the composites was characterised. Results agreed with the work of others in the field; that under low energy conditions, the type I wear debris predominates the friction surface, whilst at higher energies, the type II was predominant. Later work following on from this was presented by Hutton et al [57] in a paper presenting studies of the wear surfaces and the generated wear debris from a carbon-carbon composite under low energy, high energy and very high energy landing conditions. These energy parameters are defined as aircraft taxiing, aircraft landing and rejected take-off respectively. Data is provided from an unpublished study by the authors, estimating that rejected take-off generates a power density of  $2.0 \text{ MWm}^{-2}$  with interface temperatures within the range 1300 to 1500°C. Normal landing is said to generate  $1.0 \text{ MWm}^{-2}$  power density and circa 950°C interface temperatures, with cold taxiing generating  $0.2 \text{ MWm}^{-2}$  and 100°C.

The carbon-carbon composite was made from PAN fibres in a CVI matrix. Dynamometers are used to simulate the braking events, with full scale brakes used for the higher energy events. For low energy and high energy events, wear debris was collected underneath the dyno for analysis, whilst for the rejected take-off event wear debris had to be brushed off the surface for analysis, due to experimental setup constraints.

The wear surfaces and wear debris were analysed using a multitude of techniques - Scanning Electron Microscopy, X-Ray Diffraction, and density gradient separation. The results provided from the different analysis techniques showed consistent results throughout the test methods and hence the discrepancy introduced when collecting wear debris was not deemed to be significant.

The results show that under simulated cold-taxi conditions, particulate wear debris comprising of a disordered carbon phase containing fibre fragments is formed. This is provided mainly by the shear deformation of the graphitic CVI

matrix, whilst the fibre fragments are from small fractures of the PAN-fibres. The shear modulus of well-graphitised materials is low (a value of 4.5GPa is quoted) whilst PAN-based carbon fibre is quoted as having shear modulus in the range of 40-80GPa. Hence, the CVI matrix is more susceptible to shear deformation and thus contributes the majority of the wear debris. The fibres fracture in response to shear stresses generated during braking because they have a low transverse modulus (5-25GPa).

Under the estimated conditions for landing braking, the particulate debris described above is partly transformed by shear processes into a friction film. Although the platelet morphology is different to the particulate morphology of the taxiing wear debris, the microstructures are similar, comprising the disordered carbon phase incorporating fibre fragments.

Under extreme temperature and power density as witnessed in the simulated rejected take-off, the disordered friction film is partially re-ordered by shear-stress assisted graphitisation. It is possible that wear debris undergoes graphitisation if the interface surface temperature exceeds 1300°C.

A further paper, written by Filip, Weiss and Rafaja [64] concerns polymer matrix composites (PMCs) and hence the experimental data cannot be directly compared with c-c, but is directly relevant. In order to characterise the friction surface and developed friction layers, glancing angle X-Ray diffraction, scanning electron microscopy and transmission electron microscopy were used.

To investigate and characterise the friction layer in the perpendicular direction with respect to the friction surface, selected samples were nickel-plated, embedded in a moulding resin, cut using a diamond saw in the perpendicular direction, and finally ground and polished using standard materialographical procedures. Examples obtained using this method are presented below.

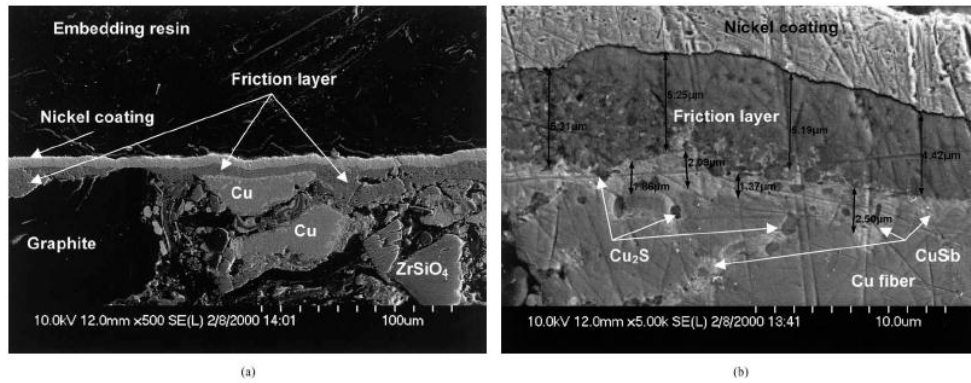


Figure 3.6a The SEM cross-sectional profile of carbon-carbon material. The scales are found at the bottom right hand corner of each figure [64].

Filip et al then proceed to analyse the thickness of friction film generated at different temperatures by taking measurements at 80 random locations across cross-sectional profiles of samples where friction commenced at various initial temperatures. It is shown that for higher initial temperatures, friction film thickness increases.

An equivalent testing situation is set up where an ‘equivalent’ apparent temperature and compressive loading is applied to a sample in order to investigate the effects of mechano-chemical interaction due to frictional operation, and it is shown that there is significant difference in phase stability and the kinetics of interactions for ‘friction’ and ‘equivalent non-friction’ operating conditions.

Further work on the interfacial morphologies of the c-c composite was undertaken by Lee [65]. His work used SEM, PLM (polarised light microscopy) and TEM techniques to characterise the microstructure of the CVI matrix C-C composite. SEM results indicated that the deposit consists of two structures; an isotropic phase is present in the fibre bundle junctions, and a highly orientated lamellar structure is present in the intra-bundle matrix. TEM shows that matrix platelets are highly parallel to the fibre axis and the crystallites of the matrix near the fibre exhibit better alignment than those farther away. This work is of particular significance as it provides theoretically sound evidence of how much the CVI process affects the material properties, especially at the surface.

It is well documented that in order to achieve and maintain the required friction within a clutch, the correct combination of surface properties and additives is required. In the paper written by Oldfield and Watts [66], the impact of different additive chemistries on the friction of carbon fibre clutch plates was investigated. When comparing three carbon fibre materials to Kevlar and cellulose based materials, it was observed that increases in dynamic friction of up to 40% could be observed via the addition of surface additives. This work is certainly of great interest to the project, as the effect of additives could be utilised within the F1 clutch for more stable and predictable friction characteristics.

Saito et al of Honda R&D [67] completed studies of the wear history of plate facings in multi plate clutches concluding correlations between the initial wear and disk contact pressure, and between steady wear and temperature, claiming that it was possible to determine the wear condition of the clutch independently of other components by determining the wear property of the facing material.

In 2005, Oczan and Filip continued their work in the field of Carbon-Carbon composites with a paper on microstructure and wear mechanisms [68]. In this paper, they proposed that as a result of different wear mechanisms, different friction layers are formed on the surface. This work supports the work by so many of the other authors discussed as part of this literature survey. However, what is different about this particular paper is that it also introduces the formation and propagation of microcracks. Results showed that intensive cracking occurred within the highly anisotropic material, with less frequent cracking seen in medium textured carbons. It was also concluded that whilst the mechanical properties of the carbon fibre do not have an effect on the micromechanisms of crack and wear, the deviation of the advancing crack lied mainly in the CVI carbon. They also stated that whilst the effects of Oxidation on the carbon-carbon were not investigated as part of their work, it was apparent that this had a major effect upon the materials at higher energies where the plate saw temperatures great than 1000°C

### 3.7 Surface Tribological Behaviour and Oxidation

Early works into the oxidation of clutch facing materials were carried out by Bunda et al [69] and Metricaru [70]. The papers written by both authors describe the wear and friction behaviour of pre carbon-carbon clutch materials with regards to clutch drag and judder. However, neither paper proves oxidation to be a contributing factor towards this. At the same time, similar works carried out by Chang [71] upon carbon-carbon composites indicated that wear rates in terms of weight loss are always greater than those in terms of thickness reduction over a wide range of braking conditions, and suggests that the reason for this is oxidative weight loss through the diffusion of oxygen through the pores. This work, although undertaken over 25 years ago is still considered to be relevant.

Yen and Ishihara [72] undertook work on the surface morphology and structure of carbon-carbon composites in high energy sliding contact in 1994 and concluded that there exist two types of surface morphology due to different energy events in the clutch. However, what Yen and Ishihara offer in regards to new information are results indicating non-uniform friction heat generation, which causes unequal thermal expansion of the contact surface, hinting at the existence of banding. Their paper also touches upon the subject of oxidation although this is only hinted at and not proven at this stage. A further paper by the same authors [73] does however research into the effects of nitrogen and air on the friction and wear mechanisms of c-c composites. The aim of this work was to establish and quantify the existence of oxidation using nitrogen as an 'inert' reference. During their experiments the specimen was allowed to reach 700°C by frictional heating and in line with the work of Murdi et al [63] demonstrated that c-c composite materials undergo an abrupt transition from normal wear to dusting wear regime as a result of the desorption of physisorbed water vapour from the rubbing surface. However, in nitrogen materials undergo dusting wear only owing to lack of lubrication vapour meaning that for the same applied loads a clutch in a nitrogen environment will have a higher coefficient of friction than for the same clutch in ambient air.

Further works by Yen and Ishihara [74] investigated the temperature dependent tribological regimes and oxidation of carbon-carbon composites up to 1800°C. This

was a follow on of their previous work and built upon it with the inclusion of wear loss at the rubbing surface and oxidation loss at the exterior of the specimen. The friction and wear of the carbon-carbon composite materials in ambient air up to 1800°C was characterised by three temperature dependant tribological regimes; normal wear, water- desorption dusting wear and oxygen – desorption dusting wear. In normal wear the friction is low because water vapour in the air acts like a lubricant to inhibit the dusting wear. Above 150-200°C the desorption of water vapour from the carbon surface initiates this dusting wear regime and an increase in friction can be seen. The next transition at 650-700°C corresponds to the desorption of chemisorbed oxygen on the carbon surface leading to this dusting wear regime. In addition the pair reported that the exterior of the specimen experience severe oxidation losses when the maximum temperature exceeded the failure temperature of the oxidation inhibitor at 1050°C hence they concluded that the maximum operation temperature of c-c is limited by oxidation. Further work upon oxidation inhibitors is discussed in section 3.8.

Weaver [75] performed a heat transfer analysis of a clutch plate in order to determine the transient response of a disk due to the time varying heat flux boundary condition. For two disks in sliding contact without cooling a measure of the fraction of the heat generated at the interface that transfers into each disk was determined and used in determining the maximum material temperature limits for disk of specific dimensions and material properties. He also proposed that the maximum and minimum cyclic temperatures could be useful in determining high cycle fatigue due to thermal stress. Chen and Ju [76] also imparted their continued research on carbon-carbon composites by publishing a paper on the low energy tribological behaviour of carbon-carbon composites. Referring back to the works of Murdie et al [63] and Ju et al [50] [53] the paper presents further information into type i and type ii wear and reported upon the fact that for a pitch resin CVI the friction coefficient slightly increased after an initial period of sliding but this increase was not reflected in the weight loss curve indicating that wear rate was consistent after a stable debris film was generated and began to lubricate the disks.

Following on from this paper, Ju collaborated with Lee and Chern Lin [77] to investigate the braking behaviour of carbon-carbon composites by performing simulated stops using a home-made disc-on-disc sliding wear tester. The specimen is a 2D pitch-resin CVI hybrid matrix, with density of  $1.74 \text{ gcm}^{-3}$  and  $V_f$  of approximately 50%.

Two sliding speeds are investigated, 1400rpm and 2000rpm, as well as two initial surface morphologies. The first group of specimens are designated AP (as-polished) with surface roughness  $0.9\mu\text{m}$ , whilst the second group are BI (broken-in) and have surface roughness  $2.0\mu\text{m}$ .

Testing of both surfaces was carried out at both initial sliding speeds. It was found that the initial surface condition had a significant influence on the braking performance of the sample, and the stopping time was more dependent on this than on initial speed. The polished sample at 1400rpm did not undergo a frictional transition, and examination of the surface morphology showed the surface was covered in a smooth thin debris film, which had filled small pores. Larger pores were still recognisable. Frictional transitions were shown by the authors to be a consequence of a change in the frictional film properties.

Under the same test conditions, broken-in (BI) specimens are shown to display higher friction coefficients than those of as-polished samples. The highest temperature rise (measured via a thermocouple inserted 1mm beneath the friction surface) was observed in the BI 2000rpm test.

V shape variations are observed in the post-transitional friction coefficients after Type I to Type II transition had occurred. It is suggested that severe structural damage during the final stage of the braking event (where differential speed is low) is responsible for this final increase, as the friction film delaminates and cannot be recovered.

This work is further expanded upon by Samah et al [78], whose work investigated the damage of carbon-carbon composites surfaces under high pressure and shear strain in 2D and 3D construction. Using SEM and EDS (energy, dispersive x-ray spectroscopy) the authors research the friction track properties and describe the



role of the transferred layers in friction and wear. Patches of scattered wear debris and worn fibres with longitudinally oriented structure were clearly visible on the contact surface of the 2D surfaces. The friction track of the 3D carbon-carbon is covered with a layer of film like structure debris leading to a lower wear rate.

Ju, Chern Lin, Lee and Kuo continued their extended carbon-carbon work in the investigation of the coefficient of friction between two c-c discs over repeated simulated braking manoeuvres [79]. A lab dynamometer is used to engage a rotor at 1400rpm with the stator, via a constant pressure of 1.7MPa until the rotor is completely stopped. This process is repeated 45 times. The discs are allowed to cool before each event is recommenced.

The coefficient of friction during each event is recorded, and a photograph of the rotor friction surface is taken after each event.

For PAN-CVI and PAN-pitch composite, it is shown that coefficient of friction varies significantly over the course of the 45 events. Definite transitions are observed, with pre-transitional coefficient of friction around 0.2, and post-transitional coefficient of friction in the region of 0.4 to 0.8. The corresponding worn surface morphology (from the photographs of the friction surfaces) shows that pre-transitional, low friction coefficients are associated with smooth uniform surfaces. Post-transitional coefficients usually corresponded to rough non-uniform morphology. When severe structural damage is observed, the coefficient of friction is upwards of 0.8. It is seen that as the surface morphology recovers from damaged and non-uniform back to smooth and uniform, the coefficient of friction also drops.

Pitch-resin-CVI composite is shown to perform differently in tribological terms, in that transition from low-friction to high-friction occurred very quickly. However, the coefficient of friction over the duration of the 40 events (by event 40, the surface had degraded so much that the experiment could not reach the 45 event conclusion) was still seen to fluctuate between those typical of Type II and Type III surface morphology. Whilst the speeds and pressures used in this investigation do not compare to those required by this work, the method and technique is

interesting and it would be of value to perform a similar study using typical RS operating conditions.

Shin et al followed on from this work with their paper on the tribological properties of 2D C-C composites [80]. They concluded that the exposure of the fabric filler at the friction surface was found to have a dominant effect on the increase of friction coefficient and wear rate, but also that the friction coefficient decreases and wear rate increases when the kinetic energy loading is increased.

A small amount of research was also done in this field by Mäki, who produced two papers on wet clutch tribology [81], and the influence of surface topography on the friction characteristics in wet clutch applications [82]. In these papers, he looks at sintered materials, and whilst not directly relevant to the work in this project, he outlines some interesting proposals regarding clutch wear. By using scanning interferometry, the topography can be measured, and results from this showed that the changes in the topography influence the friction characteristics of the clutch. So, this opens up the possibility of research upon this area within the field of C-C clutches. By looking at the worn clutch plates, it may be possible to determine what friction characteristics that stack of plates would have, and in turn, be able to more accurately predict the mu value for its future uses.

Another team to research into the surface roughness and topography was Yuan et al [83]. However, rather than carbon-carbon material, they looked into the wear conditions of general machinery, and so their findings were very generalised. By collecting and analysing the wear particles generated during the 'running in' and 'steady state' wear stages, the team enhanced the general understanding of wear mechanisms, and also used this data in the prediction of the future wear characteristics of the machinery in question. Currently this is done routinely with race clutches, with the stack analysed after each run.

In the paper 'Oxidation Kinetics and Mechanisms of 2D C-C Composites' [84] Guo, Xiao, Yasuda and Cheng tested a series of c-c samples under different energy conditions. Although actual energy values are presented, comparison with data presented within other scientific reports and with data possessed by ourselves is

difficult as specimen dimensions (such as mass and friction surface area) are not included. This is an annoying oversight, although the observed trends can be compared against those from other data.

Examination of the specimens by hand showed that the worn surfaces of the composite consisted of several bands with different reflectivities. In general, high energy dyno-test conditions resulted in a greater extent of bright bands on the wear surface. Those bright bands are believed by the author to represent areas of high contact during sliding.

Wear debris in dull bands is generally found to be particulate in nature, comprising particles of fibre, CVI and resin. The particulate type debris causes abrasive wear and increase both the friction coefficient and wear rate.

It was observed that a wear-induced amorphous film, around 1 $\mu$ m in size, was non-uniformly distributed across the entire friction surface. The high energy samples are found to yield lower friction coefficient than the low energy samples. This finding is linked by the author to the smooth friction film generated from ground and compacted wear debris. The effect of energy formation on the formation of a friction film is two-fold. Firstly, under a higher energy braking event, a higher pressure is applied to the friction surfaces, which can assist the deformation of wear particles to form a debris film. Secondly, a higher surface temperature is induced under high energy conditions, which enhances plastic deformation of the wear particles to form the film.

Under low energy conditions however, the particulate-type debris observed in this study dominates the worn surface. These worn particles may cause abrasive wear, which is the most damaging mode in terms of the wear of c-c brakes. This surface wear has been evidenced by the presence of surfaces scratches/grooves that run parallel to the sliding direction, as well as the fact that the majority of weight loss actually occurs during low energy braking. The author highlights that the temperature of rubbing surfaces can exceed 1000°C, which has significant consequences as oxidation can occur at these temperature levels.

The effects of Oxidation were further observed in the pin-on-disk experiments of Gouider et al [85]. The friction of the c-c was studied using a pin-on-disk tester equipped with a mass spectrometer, allowing for gas exchange analysis on the contact spot. Oxidation of regions or particles is detected by a release of CO<sub>2</sub>, and generally begins when the transmission from the low to high friction and dusting regime occurs, after this point, oxidation is maintained as long as friction and wear remain high.

### **3.8 Surface and Heat Treatments**

As stated in previous papers mentioned in this literature survey, clutch plate surface treatments have been investigated and reported upon favourably. Their use is based on the fact that the surface treatments alter the thermomechanical properties of the material by inhibiting factors such as oxidation. In 1992, work was published by Yesnik and Lam on surface treatments that would improve the frictional characteristics of the clutch [86]. Their paper outlines an experiment in which a separator plate with a titanium nitride coating was used in a sintered clutch to increase the friction of the plate, whilst not affecting the wear rate. The conclusions of the work were that friction coefficients were enhanced by up to 25%, and also remained at a stable level throughout the course of the event. Following on from this early work, Liu et al [87] investigated the relationship between graphitisation and frictional behaviour of DLC coatings. Although, like the work of Yesnik and Lam, their work was not directly related to C-C materials, the theories promoted in the paper were of interest. The authors state that the application of DLC (diamond like coatings) to various metallic substrates reduces the steady state friction coefficient due to the formation of a low friction tribolayer caused by the enhancement of shear deformation and transformation of the DLC structure into graphite at higher loading cases. In this case, it was not the surface treatment itself that was the friction modulator, it was the breakdown of the treatment.

Carbon-carbon was tested with an oxidation inhibitor at low energies by Park, Seo and Lee [88]. In this study, the C-C composites were impregnated with different amounts of MoSi<sub>2</sub>, which was used as an oxidation inhibitor. When compared to a

control plate with no oxidation inhibitors, the MoSi<sub>2</sub> plates showed an improvement in activation energies for wear resistance owing to the reduction of cracked interfaces and the formation of a lubricative powdery debris film and were less sensitive to the frictional transition at approximately 150 - 180°C that the non treated plates underwent. The author placed these findings down to the effect of the MoSi<sub>2</sub> filler, which increased the adherent surface areas between the fibres/matrix/inorganic powders and/or decreased the porosity between the fibre and matrix, leading to an increased abrasion resistance.

The effect of heat treatment was investigated by Luo et al [56] and in their investigation preforms are fabricated from layers of carbon cloth,  $V_f$  of 40%, and densified using the rapid directional diffusion chemical vapour infiltration (RDD CVI) process. The average density of the specimens was 1.75 g/cm<sup>3</sup>. The specimens are divided into groups A,B,C and D (each group having a stator and a rotor disc), with each group heat treated at 1800°C, 1800°C then 2000°C, 2000°C and 2300°C respectively. The maximum temperature was always reached at a time of 1 hour. The preforms are finally machined into discs of 8mm thickness, 55mm internal diameter and 77mm outer diameter.

The preforms are tested on a dynamometer in dry conditions and allowing specific pressure, angular velocity and brake moment inertia to be changed. For each tested condition, seven stops were performed to ensure the friction surface contact area exceeded 80%. Following satisfaction of this condition, no less than five stops were performed for each condition.

The results of x-ray diffraction analysis showed that increasing heat treatment temperature (HTT) led to an increase in crystallite height and width, and a reduction in the interlayer spacing of the matrix carbon and this results in less cross-linking coupled with a more preferential orientation of the infiltration carbon crystallites. A consequence of this is an increased delamination tendency of the matrix, forming a lubricating debris film on the friction surfaces which remained present throughout the entire braking process.

Increased HTT also causes a substantial weakening of the fibre/matrix bond and a relaxation of the stresses within the as-deposited composites, making delamination during braking easier. Friction surface temperature during a braking manoeuvre is reduced when the material has undergone higher HTT. This indicates that the thermal conductivity increases with HTT. The effect of specific pressure upon the friction surface temperature for constant energy dissipation was shown to be negligible. Increased pressure did not lead to an increased temperature.

It has been previously explained that higher HTT results in an increased delamination characteristic. For a specimen with high HTT, the initial plate contact generates powdery debris. It was found that for a low energy braking manoeuvre, the debris generated initially did not form a compact lubricating film. However, when the manoeuvre was of normal and high energy, the debris densifies into a lubricating debris film and hence the friction coefficient is lower.

Most recently, research into the durability prediction technology has been undertaken on behalf of Honda by Saito et al [89]. The team outlines a series of tests and measurements that confirm the correlation between initial wear and disc contact pressure when the clutch is engaged, and also between the steady wear and the plate temperature.

Enzl, a researcher working on behalf of Skoda under the supervision of Honner, undertook extensive research into the area of brake system coatings [90], [91]. By looking into the area of machine parts, Enzl researched into the possibility of using coatings on brake discs to alter their surface properties, whilst allowing the bulk requirements for strength, weight and costs to be chosen independently of their wear resistance or other surface properties. Although this paper was merely a research one, with no obvious conclusions, this work was of significance to the project, as it focused specifically on surface properties of a component and their interaction with the base material. Modelling techniques used and results analysis of thermal barrier coatings have highlighted that regardless of the desire to limit the analysis to the surface, its interaction with the bulk of the material will always determine the outcome of the analysis. With regards to the specific application of race clutch plates, this was particularly important as the plates use 'z fibres' which

transmit the energy through the thickness of the disc, away from the surface, which helps to eliminate saturation.

In a 2006 paper, Lam, Chavdar and Newcomb [92] describe new generation friction materials and technologies. Similar to the works of Enzl and Honner [93] [94], Lam et al investigate the desired characteristics for material facings with respect to high energy transfer, high coefficient of friction and durability. The paper draws together basic principles of clutch material manufacture and describes how the properties can be optimized to prevent the occurrence of 'hot spots' and clutch shudder in wet clutch applications. Clutch shudder in wet clutches is also addressed by Berglund et al [95] in their paper on clutch degradation monitored by lubricant analysis.

### **3.9 Heat Measurement Sensors**

Following on from the work of Enzl and Honner, much has been done on the field of high performance brakes by the University of West Bohemia's New Technologies Research Centre. A paper written by M Honner and J Kunes of the University [94] detailed the development of a system for fast non-contact measurement of temperature distribution on a brake disc surface during a braking event, which lead on to a further investigation of phenomena connected to extreme braking, including 'hot spots'. By using one channel two colour infrared, Honner had enabled an accurate representation of the brake disc to be mapped, with surprising results and has proved the existence of 'hotspots' on a cast iron brake disc, despite no apparent reason for them to be there. This work highlighted how infrared can be effectively used to draw an illustration of the heat variation over a complete disc, and also describes the methods used.

Honner has taken the work of this paper further in his paper entitled 'Origination and Consequences of Thermo-mechanical Instabilities in Brake Systems' [95]. The work focuses hot spots, their causes and effects. It is interesting to note that the hot spots result in frictional heating, thermo elastic distortion and elastic contact – which are experienced by the driver as brake judder. Thermal judder causing the hot spots can also cause permanent distortions and cracking to the disc as well as

brake fade and excessive wear. By looking at the macro and micro scale of the thermo-mechanical instabilities, Honner derived and verified experimental methods and instruments for the prediction, early diagnosis and control of the thermal instabilities. By measuring the temperatures and vibrations on brake dynamometers and on cars, and coupling this with computer simulation of the thermo elastic instability origination it was possible to characterise the effects, and to minimise them. This work was of particular interest to the work undertaken with the clutch, especially as it featured how to account for the hot spot phenomena when creating a mathematical model, indicating that if hot spotting was found within the clutch, then it would be possible to emulate the results within a mathematical model, using the brake data.

The nature of the environment in which the clutch plate is enclosed means that normal methods of temperature measurement are difficult to utilise. Not only are the plate faces entirely covered by other clutch components, but these components are also moving in relation to the plate. The plate is also susceptible to wear, which is a contributing difficulty with any possible temperature measurement methods.

Dr. Fritz Brunner [96] presented a paper to the construction industry, giving an overview of fibre optic sensors that could be used within the industry. His work highlights that the use of fibre optics can result in misleading outcomes when being used in environments where the optical fibre is likely to be susceptible to pressure and deformation, as these qualities result in a loss of intensity. The rest of his paper continues to discuss how fibre optics can be used to measure strain, a property that will have little effect upon the friction – temperature relationship of the clutch plate material. Because of his construction background, Brunner perhaps may not provide further useful direction to this work. However, his proof and quantification of the effects of pressure and deformation could prove useful.

Engine combustion chamber temperature measurement is a field very akin to the problem that is faced with the clutch plate temperature measurement. Infrared imaging has been utilised and in 1993, a high speed spectral imaging system was used by the Ford Motor Co, in association with Jiang, Kent, McComiskey, Qian and



Rhee [97] to create a thermal image within the combustion chamber of an engine. Poorman, Xia and Wlodarczyk of Optrand Inc [98] report upon the use of fibre optic combustion pressure sensors for engine control and monitoring. Again, like the Brunner paper, this work highlights how fibre optics can be used for pressure sensing. Although this may not appear to be of significant relevance to the field of clutch plate temperature measurement, the principles applied to getting the fibre optic cabling into the chamber can be transposed onto the same difficulties of getting a cable into the spinning clutch. Special measurement spark plugs were used, with an off axis, small diameter central electrode, and are a compromise of either durability or performance. This work could be applicable when it comes to considering the possibility of routing fibre optic cables into the clutch assembly.

The work of Poorman [98] et al was closely followed by research into measuring fuel film dynamics of a port injected engine using optical sensors by Timothy Coste of Control Devices Inc, and Lawrence Evers of the Michigan Technological University [99]. The measurement system presented was designed specifically to allow for the constraints of measuring fuel film in an intake port. The sensing face is small and mounted flush with the surface of the intake port. This concept could be very useful if there were a way to mount the sensing face flush with the edge of the clutch plate face. Depending on the wear, this concept could prove adaptable to the project, and further investigations into the wear characteristics of the plate were undertaken.

In 2000, Hall and Zuzek of the University of Texas [100] developed a fibre optic spectroscopic sensor to measure the time-resolved concentration of exhaust gas recirculated into an intake manifold of an engine. More relevant engine measurement work was published by the SAE in 2002. Wilson et al [101] reported upon the 'High Bandwidth Heat Transfer and Optical Measurements in an Instrumented Spark Ignition Internal Combustion Engine'. By using a combination of three different methods, combustion within a single cylinder four stroke engine was investigated. Thin film gauges, fibre optic instrumentation and high speed video were all used. The high speed video method is of particular interest to the project, as it is highly dependant upon the speed of the engine and the frame rate of the camera. In this instance, with an engine speed of 2000rpm and a frame rate

of 500 frames per second, it was possible to record one frame for every 24° of crank angle. This is an interesting concept to note, as the clutch will be spinning and the work of Wilson et al highlights the limitations of temperature recording at high speeds, and how little data is to be gained per revolution of the component. With reference to the clutch, which spins at up to 20,000rpm, the same frame rate would mean that only one recording is taken every 240° or 2/3<sup>rd</sup>s of a revolution.

Fibre optics were also used in conjunction with laser absorption thermometry by Levick and Edwards of the National Physical Laboratory in the UK [102]. Laser absorption radiation thermometry is a non contact technique based on photo thermal radiometry, which effectively allows the temperature to be measured regardless of the emissivity of the target, reflected background radiation, or absorptions from the atmosphere. However useful this technique may seem, it is of minor significance to the work of clutch plate temperature measurement, as the process requires modulation of the surface temperature. Due to this modulation, it is a comparatively slow process, and would be of very little use to the project.

A laser interferometry system was also utilised to measure the temperature of unburned gas in a spark ignition engine. The Yamaha Motor Company, in conjunction with Okayama University in Japan [103] used a polarization-preserving fibre and metal mirror to deliver the test beam into the engine, and to measure the temperature of the unburned gas before knocking [104]. This method is limited to only measuring within its line of sight due to the very restricted nature of the engine cylinder. Heterodyne interferometry was used due to its insensitivity to the fluctuations in signal intensity caused by mechanical vibration. This work is particularly applicable to clutch temperature measurement and the properties of the heterodyne interferometry may be of use further on in the investigation.

Possibly the most significant work is that of Litos, Lang and Kunes [105], who have used both fibre optic and infrared detectors in dynamic temperature field measurements. The paper discusses the limiting factors associated with using

infrared, and highlights that operating temperature is a paramount consideration, and cooling is required. Litos et al used a two colour infrared detector with an InSb layer to measure the shorter wavelengths and an HgCdTe detector to measure the longer ones, while using the fibre optics to conduct the light from the brake disc to the detector. The team concluded that by using the two colour detector, the emissivity problem is greatly reduced, which will be of high significance to the issue that carbon clutch discs are almost entirely absorbent to radiation. Two colour detection would allow for this absorbance and still give accurate results [106].

Jones, Gardiner and Richards identified a need for the measurement of aluminium whilst moving along on a conveyor belt during processing [107]. By using a two colour infrared system, with Ge and PbS and then using each band separately as a one colour brightness detector, a range of 250°C to 600°C was measured. The trio conclude that there is no significant advantage between the one colour or two colour method. Reynolds [108] suggests that by using a two colour ratio method, significantly lower errors than that of a brightness pyrometer would not be present. In fact, if the emissivity value was incorrectly measured, not obtainable or constantly changing (as with the carbon clutch face) then the ratio method would prove to be more accurate. Ratio infrared thermometry has also been used in the exhaust system in the works of Kong and Shih [109], who used the technique to measure the temperature distribution of diesel particulate filters. A two colour sensor using PbS and PbSe was used for this application and was used at temperatures ranging to 400°C. By 2005, two colour infrared was second only to pressure measurement in its use as an in-cylinder diagnostic tool. Associates of the Brigham Young University [110] have used the two colour infrared application to analyse the optical thickness of soot. Soot is of a very similar absorbance to carbon dust, and thus this work can be considered to be comparable. If it is possible to measure the thickness of such soot through infrared means, then it would also indicate that carbon dust could also be accounted for.

The European Space Agency [111] [112] has undertaken work on the development of infrared sensors for space applications which are to be used on future earth observation satellites. Using short wavelengths and a one colour application, the

aim is to observe very low frequencies of light which have travelled a long way. This calls for a photon amplifier which allows the signals to be multiplied and accurately read. This is a stark contrast to the application of clutch temperature measurement, as the light emitted is very bright and this could actually saturate a detector if it was not selected properly, rendering the results highly inaccurate. This highlights the need for the selection of the correct type of infrared detector, to allow for maximum accuracy.

Using two colour infrared, Howe [113] looks at the thermal imaging aspect of the infra red uses in respect to 'night vision'. Although still infra red, this uses a different wavelength of IR in its application when compared to sensors used for measuring the clutch temperature. This is because the temperatures being analysed are in a much lower range for the night vision application.

### **3.10 Experimental Testing**

In 2009, Ivanovic, Herold and Deur, in collaboration with Jaguar Cars Ltd. [114] experimentally characterised wet clutch friction using a rig. They concluded that it was possible to effectively use a quasi-static test procedure for identifying the coefficient of friction with respect to clutch slip speed, applied force and interface temperature. Following on from this in 2012, the same three authors, this time in collaboration with the Ford Motor Co. [115] describe the design of test rigs for a dry clutch and its electromechanical actuator. The first rig (the actuation system rig) being an actuation system test rig, provides identification of the actuation system parameters and characterises the overall system behavior, and includes a built in sensor for force measurement normal to the clutch plate faces. The second of these rigs (the transmission test rig) provides more comprehensive characterisation of the actuation system, and of the clutch torque transfer dynamics, as well as the friction coefficient, wear and thermal dynamic properties. The transmission test rig is very similar to that used by AP racing, except for the inclusion of a gearbox within the system. This is a standard set up for many gearbox test rigs used by many F1 teams including Lotus, McLaren and Mercedes.

The Ford Motor Co, along with LuK USA conducted a study into thermal properties and the development of a durability test profile in wet clutch launches, with a particular focus on shudder durability [116]. Using a configuration of clutch plates, including radial bands, the heat transfer was measured. Testing concluded that the radial plate was one of those with the better heat transfer characteristics, compared to waffle-parallel patterns.

Roger and Gregori [117] also investigated judder, using a methodology to determine the clutch facing sensitivity. A bench test was developed specifically to measure the judder sensitivity of various clutch materials, and this was split down into two parts; firstly a numerical simulation to narrow the test materials down to three main candidates, and then the second part, where the practical comparison was performed and used to validate the efficiency of the numerical simulations, as well as to classify the judder sensitivity of the three materials in question.

In 2013 Hoic, Herold, Kranjcevic and Duer, in association with Ivanovic of Ford Motor Co. [118] followed on from their 2012 work on the design of test rigs for a dry clutch and its electromechanical actuator [119] by experimentally characterising and modelling the thermal expansion effects of a dry dual clutch. With the earlier demonstration of the torque of a electromechanically actuated clutch depending largely on the temperature-dependence of the clutch friction coefficient and / or the thermal expansion of the clutch, the 2013 paper looks into this second element and presents results of experimental characterisation and mathematical modelling of the thermal effects on torque control accuracy.

Experimental characterisation was conducted by recording the torque vs temperature curves during the clutch cooling phase from 200 degrees celcius to 40 degrees, in steps of 10 degrees C. In each recording, the clutch was actuated in a sinusoidal manner for three periods, whilst the clutch was slipped at a constant speed. The results from this experimental element of the testing clearly concluded that there is considerable influence on both the clearance and torque transfer due to thermal expansion. The mathematical model was then developed to calculate the thermal clearance and this was then used to 'correct' the actuator position. This paper supports the theory put forward in this thesis in Chapter 14 – Further

work, where thermal expansion testing is outlined as the next logical step in this body of work.

### **3.11 Mathematical Modelling and Prediction**

Sacks and Joskowicz [119] present an analysis program for rigid part mechanisms, such as brakes using MATLAB [120]. The program performs a kinematic simulation of the driving motions and part contacts, with a very limited simulation of gravity, springs and friction. This is a very wide ranging model, as it claims that its algorithm captures the workings of up to 2500 mechanisms. This program is made up within a CAD package. MATLAB has been integrated into the McLaren Electronic Systems ATLAS (Advanced Telemetry Linked Acquisition System) software used in powertrain test cells, and this work highlights that it may be possible that a MATLAB model could be integrated within the software running the clutch dynamometer. This would save valuable time, and enable for more accurate results, as the process of data transfer between the two programs would no longer be of any issue. Blunsdon et al [121] used CFD to explore the suitability of infrared emission as a combustion diagnostic. This work could be applicable to the project, as a CFD model of the flow of the heat within the clutch would enable an accurate thermal map to be determined, and to investigate the areas where the heat dissipates faster.

In the works of J and P Padovan [122], the wear of intermittently slipping high speed interfaces was modelled using finite element analysis. The paper develops a methodology and associated algorithms to model the wearing process in areas of intermittent slipping in mechanical parts. This model included modelling material degradation and its effects on the progressive wear of the surface and was presented within the example of an aircraft tyre model. This model was of interest to the project as it was the first paper to mention the effects of the material degradation and its consequent effect upon the further wear. The wear model is self adaptive and has a 'death' option which kills the mesh nodes that have satisfied the wear criteria and an ongoing re-mesh and concomitant interpolation onto new nodes.

Lebedev and Belyaev [123] presented a paper in 1984 regarding the determination of the temperature field of a multidisc clutch. Although not carbon-carbon, this work was interesting due to the modelling of the temperature field during and after the slipping event. The initial / boundary value for the heat conduction is formulated for the model in terms of generalised functions, and offers only a weak solution to the problem. However, a year later, Zagrodzki [124] offered a further insight into this by using the finite element method to determine the temperature field in a similar steel / friction lining clutch, only this time, it was in wet conditions. In his paper, Zagrodzki uses an unsteady heat conduction model to account for the non homogeneity of the materials, states initial boundary conditions and derives the heat conduction equations. Thermal stresses are also modelled and calculations for these were performed under normal clutch loading conditions. The results from this paper mainly focused upon the determination of the factors permitting in a reduction of thermal stress. Yang et al [125] also studied this same line of work a year later after Zagrodzki published his paper. Their mathematical model also used FEA to describe the heat transfer during the engagement cycles of a wet clutch and their model was compared to experimental measurements. What this paper offers in addition to its predecessors is that it considers the effects of the fluid hydrodynamics and further heat transfer factors during the engagement period. The model proved to have a good level of accuracy when compared to the experimentally determined results, and gives guidelines regarding the important factors that need to be included when thermally modelling a clutch. These previous works, and especially this one [125] offer a unique starting point when considering a mathematical model for F1 applications.

Wet clutch thermal characteristics continued to be modelled throughout the late 1990s and early 2000s, with further papers being presented by Yang et al [126], Jang [127] [128], Tatara and Payvar [129], and Gao and Barber [1230]. However, none of these papers seemed to offer any new contributions to the field, and simply re-instated the theories and models put across by the earlier papers.

One of the first papers to model driveline systems without the use of FEA was Denery [131] who developed motion control in SimuLink [132]. Whilst using

SimuLink to primarily develop an embedded control system for a hovercraft, the author places significant emphasis upon the modelling of the powertrain and the clutch. This is done using SimDriveline [133], an add-on to the original SimuLink package. SimDriveline enables efficient modelling of 1 dimensional rotational mechanical systems, and includes block sets for all of the major driveline components. Denery [131] describes the advantages and disadvantages of using such a modelling package and concludes that the efficiency of the physics based methods used by SimDriveline in delivering a model makes the use of this method of modelling highly desirable when compared to traditional FEA methods for the majority of modelling tasks. He also notes that by including mathematical and data driven approaches (such as look up tables or using real data), it would be possible to deliver *'the most accurate, complete, computationally efficient and easily built models'*. An important factor to note regarding the author however is that he is an employee, and writing on behalf of, The Mathworks, who are the manufacturer of the SimuLink and SimDriveline products. This makes his conclusions seem a little biased towards the functionality and accuracy of the product in question.

Satapathy and Bijwe [134] used multiple criteria decision modelling (MCDM) to optimise several conflicting criteria dependent systems. Their paper outlines a model built around the performance defining attributes of mu fade, coefficient of friction recovery, performance mu, wear and temperature rise which was used to rank five non-asbestos fibre reinforced organic friction materials. By using an out-ranking matrix, triangularised to obtain an implicit ordering of options, a pair-wise comparison of the five options was used to determine the suitability of each material for certain applications. This work is more decision modelling than mathematical modelling, but its theories remain of interest to this project. Another paper with a non-direct mathematical modelling is the one presented by Zhang et al [1357]. Their paper outlines the modelling of the electronic systems used in the optimal control of automatic clutch systems. Again, although this is not of direct use to the project, the concept of optimising the clutch engagement through the electronic control system would be a logical next step after the thermal / friction model is created, and with this in mind, such a possibility should



be accounted for within any future mathematical model created for the F1 launch system.

In 2003, Khamlichi et al [136] presented their paper on optimising the thermal properties of clutch facings. Here they modelled the thermal properties of general organic clutch facings. Starting with the material formulation the team use the 'rule of mixtures' approach to determine the local thermal properties of the plate using the assumption that the material acts homogeneously. Although this paper omits any difference in surface states, it does mention spot temperature rises. This is the first paper to mention the possibility of non-complete and uniform contact between the two faces, but does not offer much information regarding the prediction and modelling of such an occurrence unless the spots are considered to be long term and stable.

In 2003, Kovrov, Koshkina and Moshev [137] presented an article outlining the study of interfacial friction in filled polymers. They undertook experiments on physical models which represented an elastic matrix contacting with the friction surface. The friction law obtained experimentally was then used to develop algorithms describing the processes of cyclic loading and relaxation in filled polymers in the event of permanent contact between the matrix and a hard inclusion. The problems of modelling in such a way is that any experimental errors that may have occurred, either through anomalous results, rounding errors or sensor discrepancies, will have been transferred through into the model.

Liu and Bamba [138] used an analytical model to obtain results of sliding friction in an overrunning CVT clutch. By beginning with the relatively simple equations for sliding friction of dry contacts, the pair then moved on to modelling the sliding friction of lubricated contacts by using the Reynolds equation in describing the lubrication. Elastic deformation of the lubricant was then modelled, along with the film thickness and density – pressure relationship. This was of future use when modelling the effects of the clutch wear particles, which have a lubrication effect upon the clutch, as described earlier in this literature survey

With more than half of the world's carbon-carbon material used in aircraft braking systems, this is an excellent source of carbon-carbon research information. Aircraft brakes are very much like a clutch, in that the friction faces are entirely covered. Therefore, the paper by Marx et al [139], entitled 'Measurement of Interfacial Temperatures during Testing of a Subscale Aircraft Brake' is of particular relevance to the project. The work focuses upon a dynamometer test using fibre optic inserts within the stationary brake ring, and highlights how the temperature distribution varies with the dynamometer test conditions. Although this work is very similar, it is a simplified example of the clutch, as one of the two components is stationary. On a clutch dynamometer both parts are spinning, which complicates the condition.

The work of Marx et al goes on to present a 2D axis-symmetric finite element model and incorporates the measured temperature dependence of the thermal diffusivity and specific heat capacity. The initial calculations are specifically relevant, as they provide some good grounding for a mathematical model for this type of configuration, so can be applied to a clutch model.

Similar to clutches in their mechanical requirements, Mace [14-] of AP Racing has done work in the area of thermally mapping the temperature profile of a brake disc using the Geostar COSMOS computer simulation package [141] [142]. The model was based on a lot of practical dynamometer work, which had measured the temperature of the brake disc directly, before then going on to be modelled. This sort of modelling is heavily reliant upon ensuring that the model is 100% representative of the practical situation which it is modelling, otherwise large errors could occur. This work can be directly compared to the modelling situation within the clutch plate stack due to similarities within the materials used and the nature of the heat kinetics. If the same methods were to be used, then a method of accurately measuring the temperature of the clutch whilst it is under load would need to be determined. Once again, however, this level of modelling is based on FEA.

Possibly the closest research found to the requirement of an F1 friction model is presented in a paper written by Zhao et al [143]. Their work outlines the

behaviour of a composite multidisc clutch subjected to a mechanically and frictionally excited thermal load. The team uses a 2D axisymmetric finite element model to simulate the thermo-mechanical behaviour of the clutch by using temperature – displacement coupled four node bilinear axisymmetric elements. Since the gradient of localised temperature near the friction surface was more prevalent, a finer mesh was applied here to better capture the thermo-mechanical behaviour. Using ABAQUS [144], contact pairs were set up between the friction surfaces. Within ABAQUS, a sub-routine was written in FORTRAN to define the frictional behaviour between the contacting surfaces, and this was only called upon when the clutch stack was clamped up. In this sub routine, the heat generated by friction was simply defined as:

$$\Delta q = \mu r \omega P \Delta t \quad \text{Equation 3.10a}$$

Where;

$\Delta q$  = the heat flux increment

$\mu$  = the friction coefficient

$r$  = mean effective radius

$\omega$  = angular velocity

$P$  = contact pressure

$\Delta t$  = the time increment

The team concluded that the friction surface closest to the back plate of the multi-plate clutch experiences the highest temperature (probably due to its location near the basket and incapability to easily disperse heat), and that the highest temperature was noted approximately 2s into a 4s slip event, under normal operating conditions. They also state that the large variation during operation induces high thermal stress in the system, and that the increase of clutch disk thickness decreases the peak temperatures. Although this model would not be suitable for use in the high energy F1 applications, due to its approximations and lack of surface type inclusions, this work could provide an excellent platform to work from in the development of a high energy, fast response, accurate mathematical model, which takes into account surface lubrication types.

Much work has been undertaken recently in the area of modelling the clutch itself, in respect to both the dynamics and the thermal properties. The works of Madhavan et al [145], Cameron et al [146] [147], and Duque and Augusto [148], all focus in on the clutch as a part of a driveline and use it in specific applications such as driveline damping and stability of limited slip differentials. Whilst all of these papers contain an element of modelling, none use carbon-carbon materials, and so the relevance to this work is limited only to the drive line system, and simple clutch mechanics.

A combined simulation approach for dry clutch systems was undertaken by Przybilla et al [149], and studies into the substitution of road and lab tests with analysis software. Using an iterative process for the model, the paper was inconclusive in its outcomes. A more conclusive paper on this subject was written by Liu et al [150] on clutch torque formulation and calibration for dry dual clutch transmissions. This model is based on constant friction and clutch actuator parameters and uses a wheel speed data input in an algorithm to create a correlation between the clutch torque and actuator. This is similar to the work undertaken in this thesis and described in Chapter 9 – Modelling the Rig.

Tarasow and Bohn of Clausthal University et al [151] developed a method for identifying the ‘kiss point’ (referred to in this work as the ‘bite point’) of a hydraulically actuated friction clutch. This method is developed for wet clutches and primarily developed for one system only, although it does have the potential to be expanded out into further clutch systems.

Cameron et al, following on from their earlier works [146] [147], produced a paper investigating the modelling of the flash temperature in clutches [152]. This is of particular relevance to this work as the flash temperature is one of the hardest to account for within the model. Two models were created; one for a large thermal mass with a good conduction path and the second for a small thermal mass without a good conduction path. The models were used to predict surface flash temperatures for specific experimental cases with model 1 predicting the lower boundary temperature, and model two predicting the upper boundary. The

limitations of this paper are that it only supplies a range within which the flash temperature occurs, and not a fixed value with a level of confidence or error.

Thermal analysis at a constant energy engagement was investigated by Jen and Nemecek [153], and used combined experimental and thermal analysis on one clutch engagement of a single sintered plate wet clutch arrangement. This model produced 'idealised' data, which did not replicate the non-linear variations of a clutch engagement, caused by factors such as non-uniform fluid flow and plate variations.

In 2012 Chen et al [154] defined a model for a rotating clutch temperature using rapid prototype controllers with the primary objective of detecting surface overheating and enhanced shift quality. The model was developed and compared to experimental data obtained on a rig. The authors employed the use of wireless sensors to detect the clutch temperature, but do not specifically give further information into this. The mathematical model was created in SimuLink and processed through a dSpace RPC box which was also used to process the data from the rig. The clutch is not carbon, and therefore the model is more simplistic, nevertheless, after optimization the model produced results with good correlation.

Two further papers have been written regarding modelling the clutch under launching conditions; the first by Duque, Barreto and Fleury in 2009 [155], who have created a model to simulate the energy during the vehicles launch. Based heavily on the works of Shaver [7], the authors use a simplified approach to modelling total clutch energy dissipation and assumptions of partial engine torque loading. This paper is more biased towards the automotive industry and states its application to be aimed at emissions and reliability. The modelling of the behavior of the clutch itself is only a very small element of the work in this paper and is based around the cushion spring force, with a clutch torque calculation being a product of the vehicle, transmission and driveline models and assumes that the clutch friction is constant. The second of these two papers, by Sun et al published in 2013 [156] studies the analysis of the thermal load for a dry clutch under frequent launch conditions. A dynamic model of the powertrain was created and friction work generated during the launch process was simulated and calculated.

Using a simple twin plate clutch and three different clutch materials (copper based powder metallurgy, paper based and resin based asbestos), ANSYS was used to draw temperature profiles of the clutch after 10 full load launch events. The initial findings report that the surface of the clutch remains the hottest and that this temperature 'steps' over the course of a number of slip events. Additionally, the investigations deduce that the resin based asbestos friction material (which is the one most similar to carbon-carbon material), had the lowest temperature profile for the same given inputs. Conclusions drawn are mainly limited to road car applications and include advice on the consequences of overloading, the importance of limited slip time, and methods of cooling which could be employed.

### **3.12 Control System Development**

In their two papers of 2009 and 2010, Nissan Motor Co Ltd., in collaboration with the National Defense Academy of Japan [157] and Utsunomiya University [158], developed a slip speed control system for a lock-up clutch. Part II focuses on anti stall, and the ability of using the control system to prevent the engine from stalling at a hard braking event on a low friction road, whilst Part III investigates using a control system to prevent unnecessary revving of the engine by controlling the slip speed of the clutch. In 2011, the Nissan Motor Co Ltd. [159] went on to develop a slip control system for rear wheel drive hybrid vehicles using integrated motor-clutch control. Bench and driving tests were conducted to evaluate the effectiveness of the control system, which used a feedback loop to estimate the driving torque.

In an application closer to motorsport, Adhitya et al of IAE, TU Braunschweig [160] developed a new control strategy of wet clutch dual transmission clutch and synchronizer for seamless gear preselect. As discussed in Chapter 2, seamless shift is now commonplace in F1 transmissions. Pre-selection of gears is the industry standard for shifting, known as Type III shifts, where the new gear is preselected before drive is disengaged from the old gear. In their 2013 paper the model that the authors are using is a dated version of that already in use in F1 where drivetrain models are compartmentalised into smaller models, such as a

synchroniser model and an electrohydraulic model, to optimize the trigger time and torque values.

### **3.13 Motorsport Applications**

Three confidential race reports written in 2012 by Lawrence [161] [162] [163] discuss the implementation of the clutch bite point learn procedure to preheat the clutch before the formation start; evoking similar clutch temperatures between formation and race launches. Tests were conducted over three race events (Silverstone 2012, Nurburgring 2012 and Budapest 2012) and conclusively highlight the benefits of running such a procedure with respect to selecting the final bite point for the race start. The benefits of this could be seen numerically through an increased distance travelled in the initial four seconds after the start in comparison to the 'control subject'. This work built directly upon the studies undertaken in this thesis.

### **3.14 Summary**

The literature review has considered the manufacture of carbon-carbon materials and its effects upon the material properties of the final product by looking at the microstructure of carbon-carbon materials and the material properties and behaviour and the factors affecting these.

The surface properties of carbon-carbon have been researched and investigated in depth in order to further understand the wear mechanisms involved. Friction film formation mechanisms have been researched experimentally by several collaborative teams, with standout research being conducted by Chen et al in their proposals of Type I, II and III wear mechanisms and the dynamic relationships between them.

Further surface properties have been investigated focusing on surface behaviours and oxidation, with a specific consideration for the temperatures for approximately 1000 degrees Celsius seen on a carbon-carbon clutch during a race

launch and as a result of this, heat treatment of the materials has also been thoroughly researched to determine any implications of this high instantaneous launch temperature.

Methods and sensors for heat measurement have been researched with the suitability of each one being assessed for its application for the measurement of the inter-facial temperatures of the clutch plates. Investigations into experimental testing methods followed on from this and critical analysis was undertaken regarding using elements of these works within the experimental testing of this project.

A large proportion of the research was done into the area of mathematical modelling, with works being highlighted by others as either bulk thermal property modelling, or surface thermal modelling. There were no papers in the public domain which combined the two models. From this it was clear that no model had been successfully created which was able to predict the dynamic changes of surface state and consequently the friction coefficient of the clutch surface for the  $n$ th time step of a clutch slip.

Following on from the modelling, clutch control systems were identified and reviewed. With the research being concluded with race reports from Marussia F1 Team highlighting procedures used to condition and create a 'base line' condition for the clutch to enable better prediction of clutch surface friction coefficient values at a Formula One race start.

### **3.15 Gaps Identified in Previous Research**

There is a great deal of work that has been undertaken on carbon-carbon materials, especially regarding its surface morphology. However, a lot of the work is replicated by others, whilst several papers are simply extensions of previous work. The literature survey has revealed that although extensive work has been done regarding the observation and recording of the surface changes, very limited mathematical modelling has been carried out to predict when critical surface



changes will occur. In order for the model in this project to be successful, it must be able to accurately predict when the surface changes happen, and on the basis of the existing literature this would provide an original contribution to the field.

Of all of the sensors and test methods researched, none of them offers a way of directly measuring the closed friction face of the clutch. Many used thermocouples, but none of the methods proposed were capable of being adapted for direct measurement of the surface temperature. Therefore, for the experimental testing of the clutch element of this work to be successful and offer direct results of the plate face temperature during a slip, a new measurement method is also required. Based on existing literature, this element of the work also involves a novel concept in the application of infrared thermometry to closed faces.

Although there has been a lot of work done in the area of modelling clutches, none of this considers applications which are as high energy and for as shorter period of time as is required for this project. The existing models also only consider temperature, and there is no consideration of the friction co-efficient or its dependency on type I, type II and type III wear modes. Also, there are no models which have the adaptability to be transferred from a simulated condition to a 'real life one' i.e. to work as part of a car model. Carbon-carbon is a complex material to model, due to its inherent unpredictability, and so far in literature, only a handful of papers have managed to successfully do this [131], [132], [133] [157], [159] and [160]. The work proposed here is to take elements from these models, to develop a more complex MATLAB model that is suitable for the high energy slip events of an F1 launch.

Overall the literature review has conclusively proven that there is a requirement for a new mathematical model to be developed which can accurately predict the temperature (and in turn, the friction) of a carbon-carbon composite whilst including the prediction of wear rates, failure modes and surface morphologies under high energy conditions.

## Chapter 4

### Race Start Analysis

This chapter explores race start analysis from a mathematical point of view, and examines the success of each race start from two cars over the 2006 Formula One season. Each start is analysed with respect to several different parameters and conclusions are drawn as to how this could be improved by mathematical modelling. Before analysing a number of race starts from the 2006 season, a sample race start is described and the parameters and variables that need to be considered are explained, along with their importance and how they are measured or estimated.

#### 4.1 Background

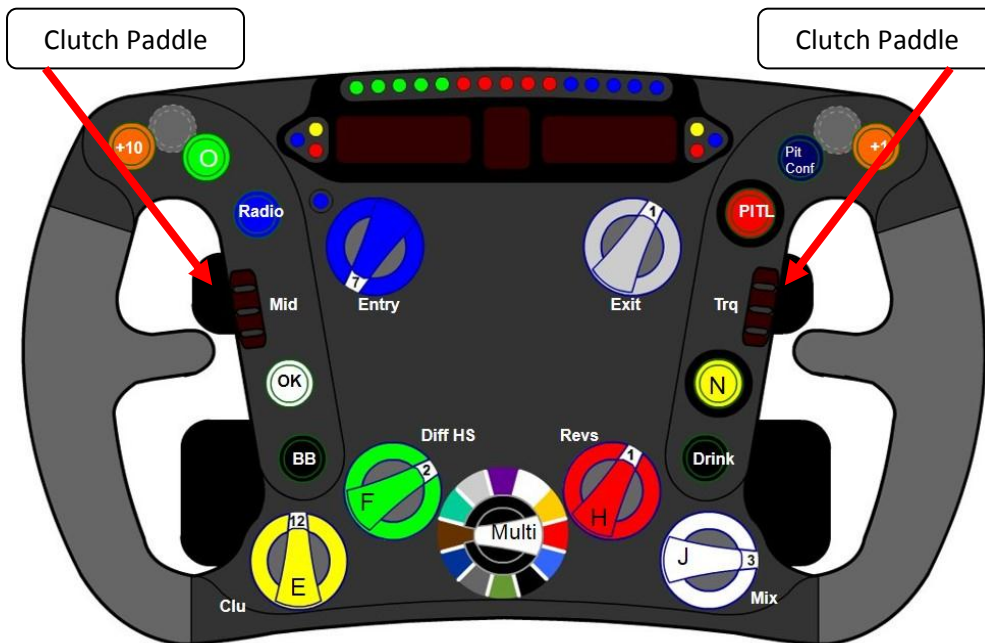


Figure 4.1a A Typical F1 Steering Wheel.

At a race start the driver is required to follow a set procedure (the relevant switches are illustrated in figure 4.1a above);

- Select the clutch trim as instructed by the Race Engineer using the 'CLU' rotary.

- Select the start torque map as instructed by the Race Engineer using the 'TRQ' rotary.
- Pull either clutch paddle fully, and hold in this position (this is referred to as the “first paddle”) and pull the upshift paddle to select 1st gear.
- Position the 2nd clutch paddle (referred to as the “second paddle”) to approximately 50% of its stroke.
- All of the green lights on the dash display will come on when you reach 50% and stay on for anything above 50%.
- Apply the throttle pedal until all of the red lights come on. If you go too far a blue light will come on.
- Hold this throttle position (it should be around 35-45%) the engine will now be held at the pre-start revs (~15,600rpm for a dry start. The throttle pedal position may be adjusted for a wet start; this will be discussed prior to attempting a wet start).
- To perform the start, release the first clutch paddle completely.
- After a period of approximately 1 second, a tone indicates when to release the second paddle. At the same time as releasing the second paddle, increase the throttle pedal to 75%, or more if there is no wheel slip.
- A second tone will indicate when to upshift to 2nd gear – it is important to react quickly to this in order to avoid time loss caused by running into the rev limiter.
- Once in 2nd gear, increase to full throttle.

A race start data trace will typically look like the one in figure 4.1b

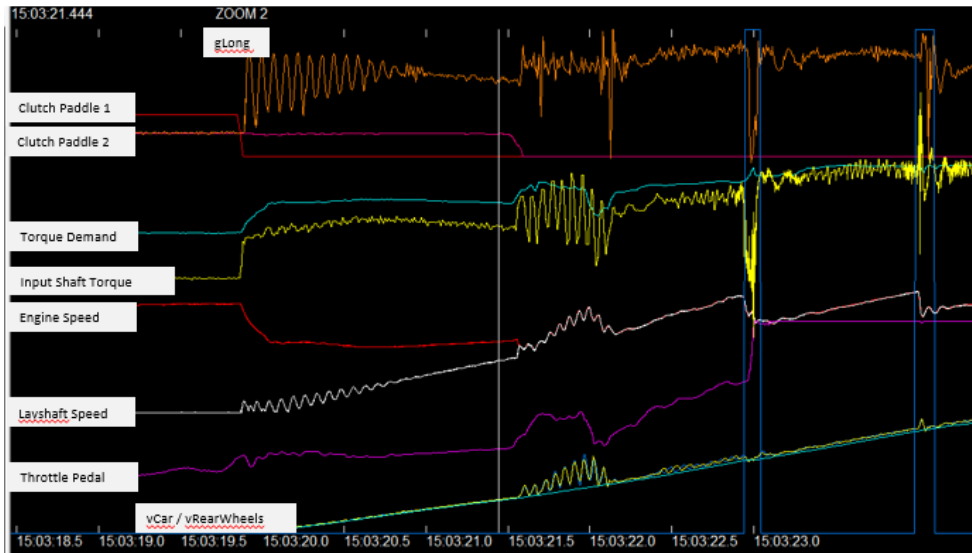


Figure 4.1b. Typical Race Start Trace (units removed for confidentiality)

It can be seen in figure 4.1b that as clutch paddle 1 is released, the input shaft torque sharply increases and the engine speed decreases. The layshaft speed begins to increase and this drives the wheels (seen at the bottom of the screen shot). During this initial phase the clutch is slipping and this can be seen by the difference in engine and layshaft speeds. After the 2<sup>nd</sup> paddle is released the clutch is fully engaged and transmits the full engine torque through the gearbox. At this time it can be seen that there is wheelspin, as the tyres break traction with the full torque of the engine being transmitted through them (this can be seen on the plot of vCar / vRearWheels, where the rear wheel speed is greater than that of the car speed),. This is not an optimal start and ideally the 2<sup>nd</sup> Paddle would have been released a little later so that the difference in engine and layshaft speeds did not create a torque spike through the input shaft.

When getting the power from the engine to the track, there is a path that it follows;

- Engine Output Shaft (including any internal frictions, oils etc)
- Clutch (what we are investigating)
- Gearbox (including any internal friction caused by oils, gear couplings etc)
- Driveshafts (including and torsional inefficiencies and losses in the CV joint bearings)
- Hubs (bearing losses can be accounted for here)

- Tyres (pressure, temperature, elastic deformation and friction coefficient)
- Track (temperature and friction coefficient)

When analysing a race start, it is very difficult to measure items such as the torsional inefficiency of the driveshafts or the losses in hub bearings and while sensors are available to monitor these parameters directly, running them during a race weekend is against the FIA regulations. The most important properties to record are the fuel load, clutch position, engine speed, gearbox input shaft speed, tyre temperatures, throttle position and car speed.

During any car running, the data acquisition system on the car will monitor and record a number of parameters for use in later analysis and development. As part of this wheel speed, air temperature and engine speed are all directly monitored. There are also other channels known as 'maths channels', which take the information supplied from sensors on the car and manipulate it in a way such that other properties can be determined. Examples of maths channels include oversteer/ understeer gradients (determined from steering angles and the g sensor along with chassis constants such as wheelbase), wheel spin (determined from gearbox output speed and wheel speed) and clutch friction (determined from gearbox input speed, engine output speed and clutch actuation pressure).

When looking at the data with regards to the start performance the main parameters for analysis are;

#### **4.1.1 Qualifying Position**

This is where the car qualified but is not always necessarily where the car starts the race from. This could be due to grid penalties taken by drivers for an engine change or unsporting driving during qualifying, meaning that the drivers behind them would move up the grid for the race.

#### **4.1.2 Grid Position (R/D)**

This is the grid position from where the car started the race. The 'R/D' denotes whether that grid position lies on the racing line of the track, or the dirty side. The 'clean' side is that which lies on the racing line, and the 'dirty' side of the grid is

not on this racing line, and is instead where much of the debris from the racing line gets swept to throughout running. Usually, the odd numbered grid slots are on the racing line, as pole position is placed so as to allow the car to be on the inside at the entry point to the first corner. However, there are some instances where this is not the case; for example in Monaco, where due to the layout of the track and the racing lines mean that although pole position is still placed for an inside line to the first corner it is actually on the dirty side of the track.

#### **4.1.3 0 – 100kph Time**

This is the time that it takes the car to accelerate from 0kph up to 100kph. It is important to note that this parameter, although used for determining the clutches performance, also needs to be used in conjunction with the throttle trace of the car. Traffic may cause the driver to lift off, and thus increase the 0-100kph time. On the surface this would appear as a 'bad' launch, but to assume this without careful inspection of other parameters would be a misleading assumption.

#### **4.1.4 Position Change**

This is the number of places that the driver gains or loses between leaving his grid slot, to entry into the first corner and is ultimately the only true parameter that the success of the start is based upon.

#### **4.1.5 Time on Grid**

This is the time from when the car arrives at its grid slot, to when it launches. The cars towards the front of the grid have a longer time on the grid, due to waiting for the cars at the rear to enter their grid slots and form up. This factor is important because it gives a good indication of general heat soak in the car, and especially the clutch (as it is located in a very warm area inside the gearbox, with little air flow around it).

#### **4.1.6 Race start (RS) Fuel**

This is the fuel on board the car at the time of the launch, and takes into account fuel that has been burnt during the journey to the grid and for the formation lap. This parameter is essential, as it allows an exact weight of the car to be given at the time of launch. The minimum weight of car plus a driver in 2006 was 605kg, so

with the knowledge of the fuel weight, it is simple to calculate how much mass was launched from the grid.

#### 4.1.7 Tyre Temperatures; Initial & Race Start

Although the tyres are preheated before they go on the car, they lose heat during the green flag (formation) lap as the tyres are not being worked to their optimum. Most teams will factor this into their race strategies and perform a number of short sharp 'burnouts' as the car approaches the grid slot. If the day is cool, this temperature loss will be greater than if on a warm day (as stated by the laws of thermal equilibrium) and due to the ideal gas law (equation 4.1a) this also means that the tyre pressure will also drop (as  $V$ ,  $n$  and  $R$  all remain constant).

$$pV = n R T \qquad \text{Equation (4.1b)}$$

Where:

$p$	Pressure (bar)
$V$	Volume in $\text{m}^3$
$n$	Number of moles of gas
$R$	Gas constant = $0.821 \text{ m}^3 \text{ bar mol}^{-1} \text{ K}^{-1}$
$T$	Temperature in $^{\circ}\text{K}$

The importance of tyre pressure on the race start is that if the tyre has less pressure, then it sits flatter on the ground, and thus has more contact area with the track than a tyre with higher pressure, theoretically meaning that more power can be transmitted through it. However, factors such as the increased elastic deformation along the longitudinal axis, mean that transmitting that power equally and smoothly is a complex issue. The tyre temperature is again one that affects the race start mode (clutch bite point) that is selected, and is occasionally the reason why the race start mode is altered between the formation and race starts.

#### 4.1.8 Clutch Mode; Formation Start and Race Start

The clutch modes are a simply the bite point which the clutch will drop to at the race start. This is determined from a mid-point, and then trimmed in and out using the clutch bite point map. This mode is determined by the controls engineer

before the formation and race starts and is based on the assumption that engine revs, clutch pressure and throttle position remain the same for each start. The formation RS mode number is determined from data accumulated from end of pit lane race starts, and pit box pull aways over the race weekend, with the race start clutch mode determined from data obtained at the formation start. If after the formation start, the engineers feel that the mode could be optimised, they radio instruction to the driver to change the mode for an optimised race start.

#### **4.1.9 Clutch Friction; Formation Start, Race Start and Delta**

This is determined from the energy dissipation, gearbox input, engine output and clutch actuation pressure at the race start and the formation start. The delta is also a very useful property to understand as it highlights the consistency / inconsistency of the clutch materials friction.

#### **4.1.10 Energy; Formation start, Formation Lap and Race Start**

This is the energy dissipated through the clutch during the launch at the formation start, during the formation lap and again at the race start, and is used as an indicator as to how hot the clutch is getting, and therefore, assists in determining the friction characteristics.

#### **4.1.11 Number of Clutch Events for Stack**

This is the number of launches that the clutch stack has undertaken since new, and includes formation starts, race starts, pit lane practice starts and pull aways from the pit box. It is used as a general indicator of wear, and how many heat cycles the clutch material has been through.

Other external factors that have been included in the clutch performance analysis are;

#### **4.1.12 Number of Race Starts**

Occasionally (and usually for reasons of safety) the race director deems it necessary to red flag the start of the race and restart the race. This could happen for many reasons, such as a dangerous first lap incident, which was the case in



Melbourne 2006. When this occurs then the data from the first start is the one that is recorded and analysed in this work.

#### **4.1.13 Weather**

Whether the car is starting the race on wet or slick tyres will have an effect upon the overall view of the race start. The reduced grip caused by the wet track requires the power from the engine to the tyres to have to be delivered more gently to limit wheelspin, and so a greater amount of clutch slip and a reduced initial engine revs input are required. If the clutch engaged immediately and the revs were too high, the result would simply be wheelspin. The weather factors are taken into account by utilising a different race start mode.

#### **4.1.14 Air Temperature**

This is used to assist with the tyre and general running properties of the car. If it's a cooler day, tyre pressures will take longer to raise, but the engine will be noticeably more powerful than on a warmer day.

#### **4.1.15 Track Temperature**

This is a tyre related property relating to the surface properties. The higher the track temperature, the quicker the surface of the tyre will heat up, and the stickier (higher coefficient of friction) that it will be, meaning the more power can be transmitted through it.

#### **4.1.16 Friction Co-efficient of the Grid**

This related to the track temperature, and is the other half of the friction couple between the 'sticky' tyre and the road and the friction co-efficient of the grid makes up the very last piece on the path of the power from the engine to the track.

## 4.2 Race Start Data<sup>1</sup>

A series of race start data collected by the Honda Racing F1 Team throughout the 2006 season was analysed with respect to the criteria listed in sections 4.1.1 to 4.1.16 above. All data plots can be found in Appendix A, with a selection shown here in the following sections. The race starts are graphically represented on the following pages, with figure 4.2a giving guideline to a typical race start plot from these events. All of the units for the starts are on the same axis, and are as listed in the key below:

### KEY

**Car Speed [m/s]**

**Clutch  $\mu$  x 10**

**Clutch Actuation Pressure [MPa]**

**Engine Speed [rpm]**

**Gbx IPS Speed [rpm]**

**Throttle Posn [%/10]**

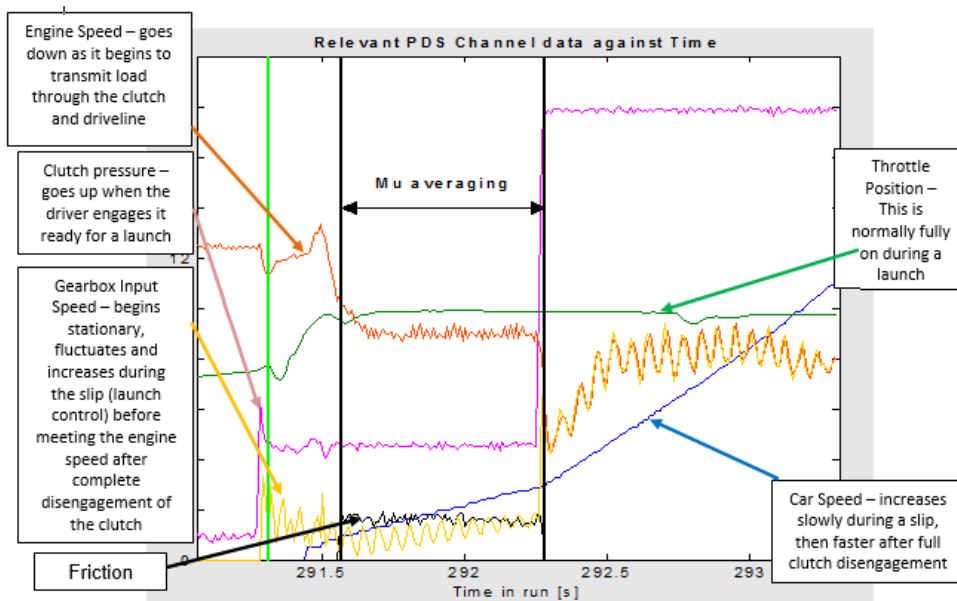


Figure 4.2a. Typical Race Start Graph with Plot Explanations

<sup>1</sup> Since this data has been analysed, the start procedure of an F1 car has significantly changed. Throttles are now required to be held at approximately 50% (as described in Chapter 4.1), whilst a two paddle system on the steering wheel means that the first paddle release will drop the clutch to its set bite point, whilst a gentle release of the 2<sup>nd</sup> paddle will then fully engage the clutch.

### 4.2.1 Melbourne

Date: 2<sup>nd</sup> April 2006

Circuit Length: 5.30km

Race Distance: 302.271km (57 laps)  
on first lap)

Number of Race Starts: 2 (red flag)

Weather: Dry

Air Temp: 17°C

Track Temp: 24°C

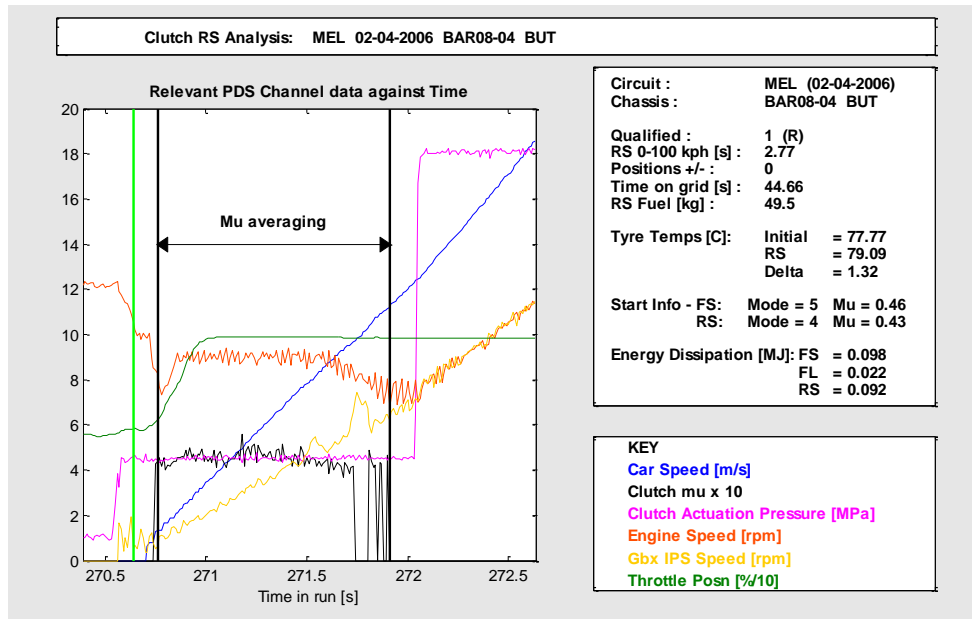


Figure 4.2.1a. Race Start, Car One, Melbourne Circuit

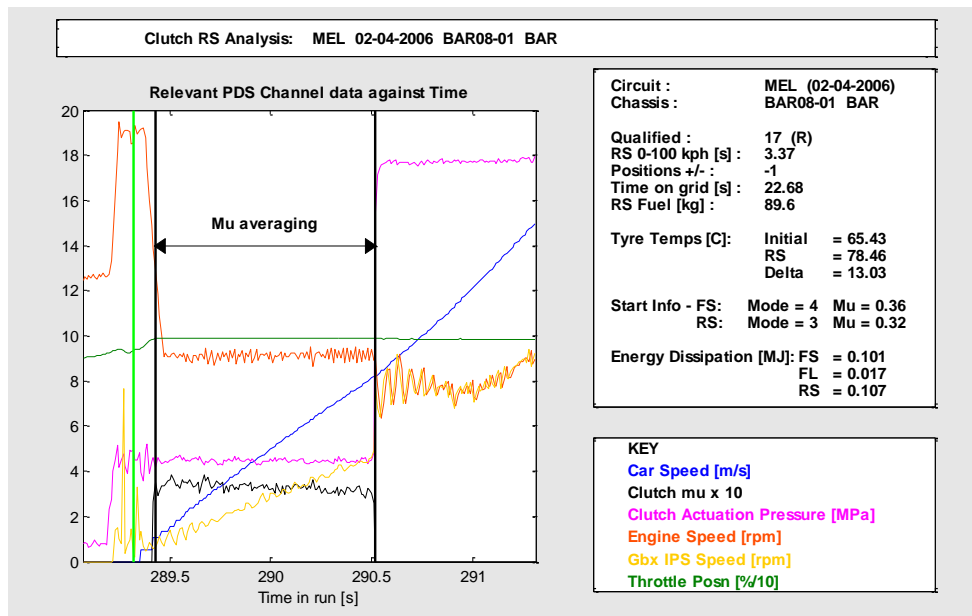


Figure 4.2.1b. Race Start, Car Two, Melbourne Circuit

### 4.2.2 Barcelona

Date: 14<sup>th</sup> May 2006

Circuit Length: 4.627km

Race Distance: 305.382km (66 laps)

Number of Race Starts: 1

Weather: Dry

Air Temp: 26°C

Track Temp: 37°C

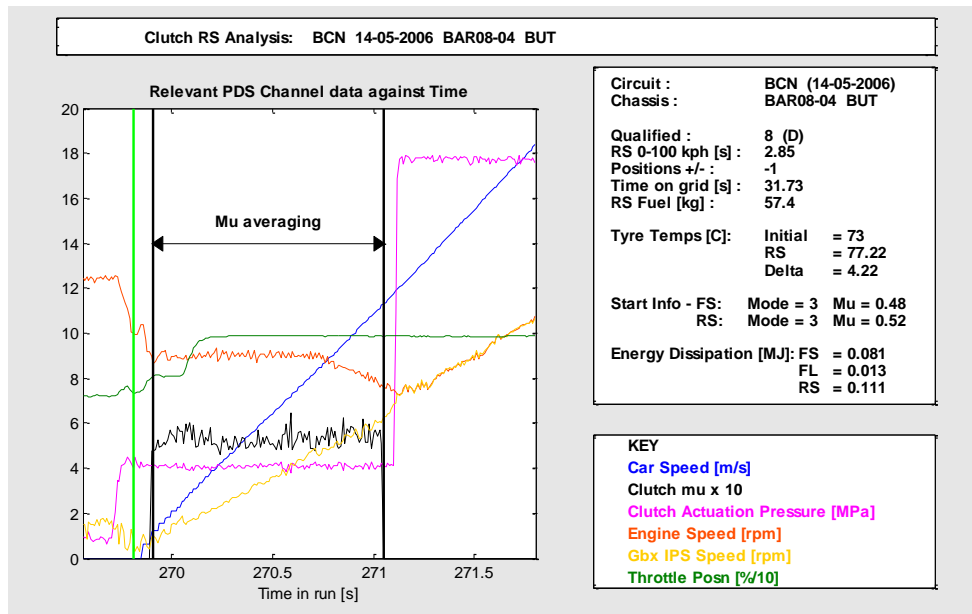


Figure 4.2.2a. Race Start, Car One, Catalunya Circuit

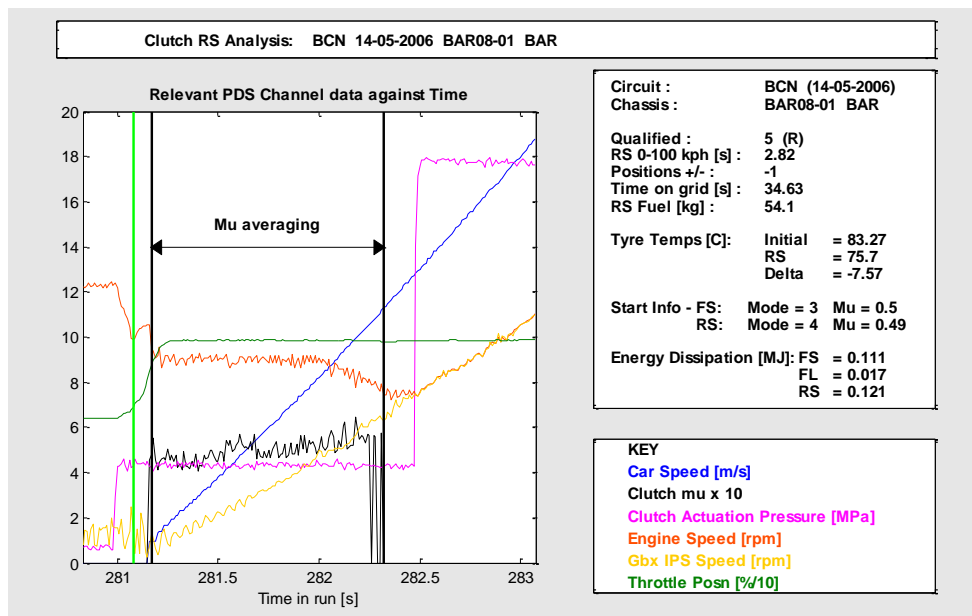


Figure 4.2.2b. Race Start, Car Two, Catalunya Circuit

### 4.2.3 Budapest

Date: 6<sup>th</sup> August 2006

Circuit Length: 4.381km

Race Distance: 306.67km (70 laps)

Number of Race Starts: 1

Weather: Wet

Air Temp: 18°C

Track Temp: 21°C

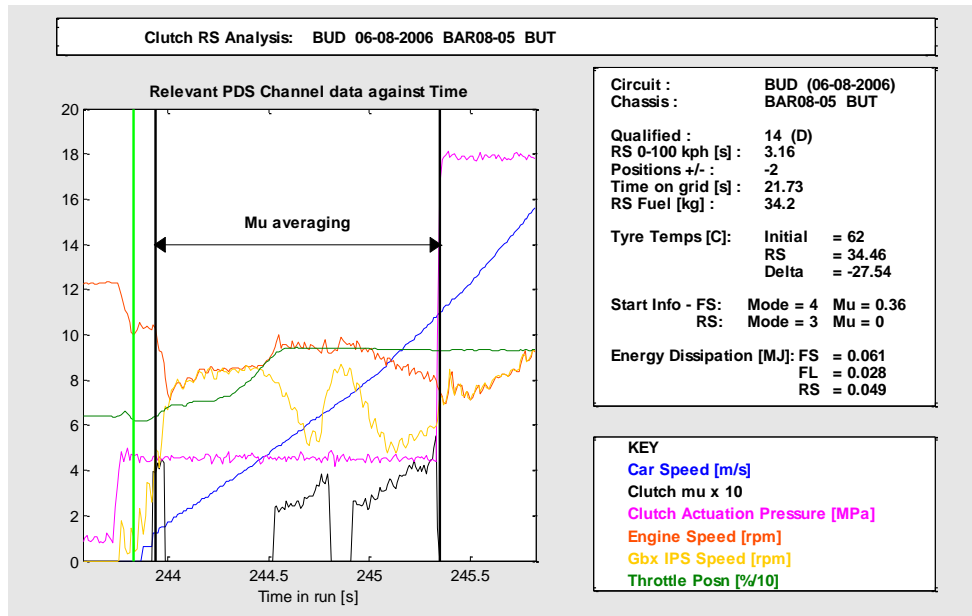


Figure 4.2.3a. Race Start, Car One, Hungaroring

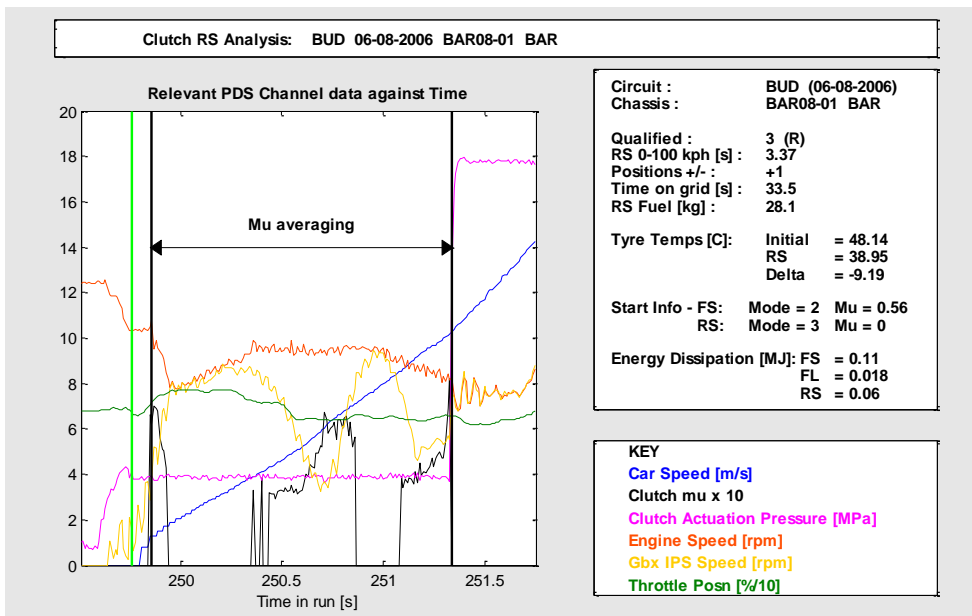


Figure 4.2.3b. Race Start, Car Two, Hungaroring

### 4.3 Analysis of Starts

The three starts of interest are those from Melbourne, Barcelona and Budapest; Melbourne as there were two race starts, as the initial start was red flagged due to an incident. Barcelona is of particular interest because despite the two cars starting on two sides of the grid (one dirty and one clean), both have a 0-100kph time within 0.03 seconds of each other. Budapest was a wet start and this can be seen by the sporadic clutch mu and input shaft speeds, where the drivers are struggling to control the wheel spin brought about by the low grip surface.

By looking at results from previous race starts shown in Appendix A, it is possible to build up a picture of how successfully the existing coefficient of friction ( $\mu$ ) calculation program works. This is done by correlating several of the key elements of the start with each other, and determining how much of an effect each element has upon the others.

The key areas of information are:

Qualifying Position; where the car qualified on the grid for the race. Not particularly useful by itself, but provides important information when provided with the (R/D) information and the position change.

Grid Position (R/D); if the car started the race from the racing line, or the 'dirty' side of the track where the dust settles and there is inherently less traction.

Position Change; how many places were made up or lost from the grid to the braking point for the first corner, this is one of the primary indicators of a successful launch.

0 – 100kph Time; this is the other primary indicator of a successful launch, a low times means a quick getaway.

Number of clutch events during the Formation Lap; this gives a general indication as to how much work the clutch has done between the formation start and the race start, and when combined with the property 'change in friction between starts' can be a useful indicator to the consistency of the carbon-carbon material.

Energy, Formation Start; this is the energy dissipated through the clutch on the formation start, and will not be as high as that dissipated during the actual launch, as the launch duration is much longer.

Energy Formation Lap; this is the energy dissipated over the duration of the formation lap, and will usually correlate closely to the number of clutch events during the formation lap, as more events will sum more energy.

Energy Race Start; this is the energy dissipated during the launch of the car at the start of the race.

Clutch Mode, Formation Start; this is simply a number stating which mode the clutch control program is running in, based on its mu calculation.

Clutch Mode, Race Start; this is again, simply a number stating the clutch control program mode, but it is very useful when compared to that of the mode used in the formation start, as this indicates that a change in mu has been detected, and so a mode change is required for a successful launch.

Clutch Friction, Formation Start; this is the calculated actual mu value of the friction plates of the clutch during the formation start.

Clutch Friction, Race Start; this is the calculated actual mu value of the friction plates of the clutch during the race start.

Change in Friction between Starts; this is an important factor to note, as the mu calculation program works by determining the clutches friction at the formation start. So if this value is high and the two mu values are dissimilar then the clutch mode will not be suited for the friction co-efficient that was actually being seen during the launch, and this will generally result in a poor start.

The comparisons between each of the parameters were done by using the correlation coefficient function within MATLAB [112]. This correlation coefficient calculates the Pearson correlation [164], and is defined as in equation 4.2a:

Equation 4.3a

$$r = \frac{\sum_{i=1}^n x_i y_i - \frac{1}{n} \sum_{i=1}^n x_i \sum_{i=1}^n y_i}{\sqrt{\sum_{i=1}^n x_i^2 - \frac{1}{n} \left( \sum_{i=1}^n x_i \right)^2} \sqrt{\sum_{i=1}^n y_i^2 - \frac{1}{n} \left( \sum_{i=1}^n y_i \right)^2}}$$

Where;

r = correlation co-efficient

x = time in seconds

y = temperature in degrees

Pearson's correlation reflects the degree of linear relationship between two sets of variables, ranging from -1 to +1. A correlation of +1 means that there is a perfect positive linear relationship, a correlation of -1 meaning that there is a perfect negative linear relationship, and a correlation of 0 meaning that there is no linear relationship at all. However, correlations are rarely -1 or +1 due to the fact that this would indicate a perfect relationship and such a perfect relationship is never obtainable in real life; even the smallest of outside influences will affect every test from which the data is acquisitioned. Equally a correlation of 0 is just as unobtainable; despite the fact that tests may render completely different sets of results, there is always a correlation between them, even if it is very small.

Whilst the Pearson correlation indicates the strength of a linear relationship between two variables, its value alone may not be sufficient enough to evaluate the relationship. For example, figure 4.3b [46] which shows scatter plots of 'Anscombes Quartet'; a collection of four different sets of variables created by Francis Anscombe [164] which have the same mean (7.5), standard deviation (4.12), correlation (0.81) and trend line ( $y = 3 + 0.5x$ ).



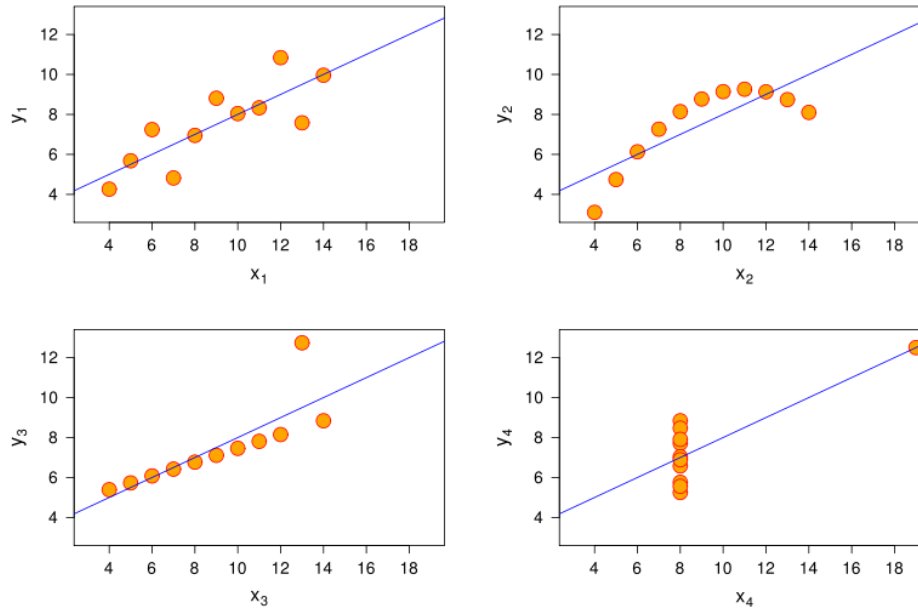


Figure 4.3b. Anscombes Quartet [164]

The first (top left) is normally distributed, the second (top right) is not normally distributed, although an obvious relationship can be observed. The third (bottom left) shows that the linear relationship is perfect, except for one anomaly which exerts enough influence to change the correlation coefficient from 1 to 0.81. The fourth example (bottom right) shows the opposite of the third case, where the variables are not linear at all, but the anomaly result is enough to produce the high correlation coefficient. These examples highlight that as a summary statistic, the correlation coefficient cannot replace the simple examination of data by eye. The MATLAB code that was written to extract and tabulate this data can be seen in appendix B.

#### 4.4 Results Analysis

Each race start presented in Appendix A is analysed in depth, and a summaries of each of the four key areas of investigation are drawn. These key areas of investigation are:

- Race Start 0-100kph
- Number of clutch events during the formation lap
- Race start energy
- Race start clutch coefficient of friction,  $\mu$

The 0-100kph race time is important because how quickly the car accelerates away from the start is the single thing that indicates the success of the launch. A high time will mean that the cars around will have passed into the first corner, whilst a low time will hopefully mean that a few places will be made up before the first corner.

The number of clutch events during the formation lap is an important factor to note, as theoretically the more of these events that occur, the more energy will have passed through the clutch during the formation lap, meaning the bulk temperature should be higher at the launch.

The race start energy is a principle factor in the analysis, as it is this that gives an indication of how much work the clutch is doing, how much slip is occurring and how effective the clutch material is at turning the excess kinetic energy (from the difference in engine input speed to the output speed to the gearbox) into thermal energy.

The race start  $\mu$  is an important factor to correlate with the race start energy, as it is this that forms the basis of the entire thesis work.

The tables are organised by the parameter that is being observed, and is ordered by the highest to the lowest. Within these tables, the 6 'best' occurrences of any particular parameter are highlighted green (for example the 6 best qualifying positions are those with the lowest numbers, but the 6 best energies are those with the highest values), whilst the 6 'worst' occurrences are highlighted red. This further aids a visual reference as to whether any parameters have an effect on each other.

#### 4.4.1 Race Start 0-100kph

Track/Driver	Energy Graph				Quali Posn	Grid Posn [R/D]	Posn Change	RS 0-100 kph [s]	Num Clutch Events	Energy FS [MJ]	Energy FL [MJ]	Energy RS [MJ]	Energy Total [MJ]	Clutch Mode FS	Clutch Mode RS	Clutch Mu FS	Clutch Mu RS	Delta Clutch Mu
	FS Energy Dissipation	FL Energy Dissipation	RS Energy Dissipation	Total Energy Dissipation														
MEL: BAR	17	R	-1	3.37	45	0.101	0.017	0.107	0.22431	4	3	0.36	0.32	-0.04				
BAH: BUT	3	R	-3	3.37	66	0.106	0.045	0.058	0.20922	8	3	0.2	0.16	-0.04				
SHA: BAR	3	R	0	3.13	49	0.099	0.019	0.113	0.23152	3	3	0.52	0.49	-0.03				
SHA: BUT	4	D	0	3.12	59	0.102	0.037	0.123	0.26243	3	3	0.54	0.52	-0.02				
HOK: BAR	6	D	-2	3.01	52	0.107	0.016	0.124	0.24721	5	6	0.76	0.39	-0.37				
IMO: BAR	3	R	-2	2.92	49	0.108	0.035	0.108	0.25178	5	4	0.48	0.47	-0.01				
MTL: BUT	8	D	-2	2.91	58	0.065	0.049	0.139	0.25317	4	4	0.36	0.46	0.1				
INT: BUT	14	D	0	2.89	56	0.047	0.023	0.064	0.13392	5	4	0.4	0.39	-0.01				
MTL: BAR	9	R	-1	2.87	58	0.066	0.019	0.11	0.19508	4	4	0.35	0.36	0.01				
MZA: BAR	8	D	-2	2.85	66	0.118	0.047	0.125	0.29026	3	3	0.49	0.45	-0.04				
BCN: BUT	8	D	-1	2.85	52	0.081	0.013	0.111	0.20425	3	3	0.48	0.52	0.04				
IST: BUT	6	D	0	2.84	64	0.107	0.029	0.113	0.24858	3	3	0.52	0.5	-0.02				
BCN: BAR	5	R	-1	2.82	50	0.111	0.017	0.121	0.24805	3	4	0.5	0.49	-0.01				
MCO: BUT	13	D	+1	2.81	56	0.118	0.034	0.118	0.26979	3	5	0.37	0.36	-0.01				
NUR: BAR	4	D	-2	2.81	62	0.071	0.022	0.108	0.20103	5	6	0.48	0.48	0				
MGC: BUT	17	R	+1	2.8	47	0.056	0.017	0.061	0.13476	5	5	0.44	0.41	-0.03				
IMO: BUT	2	D	+1	2.8	63	0.092	0.032	0.102	0.22562	5	5	0.27	0.56	0.29				
SEP: BUT	2	D	0	2.79	72	0.101	0.017	0.068	0.18697	4	2	0.47	0.46	-0.01				
BAH: BAR	6	D	+1	2.78	47	0.092	0.024	0.086	0.20218	8	4	0.43	0.41	-0.02				
MEL: BUT	1	R	0	2.77	60	0.098	0.022	0.092	0.21155	5	4	0.46	0.43	-0.03				
SEP: BAR	12	D	+2	2.77	49	0.113	0.01	0.077	0.1994	4	2	0.4	0.43	0.03				
MZA: BUT	5	R	-1	2.76	71	0.107	0.049	0.126	0.28148	3	3	0.46	0.45	-0.01				
MGC: BAR	13	R	+1	2.75	42	0.066	0.017	0.117	0.19898	5	5	0.41	0.42	0.01				
SIL: BAR	6	D	-1	2.75	37	0.124	0.01	0.133	0.26677	4	4	0.57	0.54	-0.03				
INT: BAR	5	R	0	2.71	44	0.068	0.02	0.109	0.1965	5	4	0.34	0.47	0.13				
IST: BAR	13	R	-1	2.71	51	0.074	0.056	0.115	0.24493	4	4	0.5	0.46	-0.04				
MCO: BAR	5	D	0	2.65	52	0.124	0.013	0.13	0.26693	3	5	0.44	0.42	-0.02				
SUZ: BAR	8	D	-1	2.64	54	0.083	0.022	0.111	0.21563	4	4	0.44	0.48	0.04				
NUR: BUT	6	D	+1	2.58	85	0.103	0.043	0.108	0.22379	5	5	0.55	0.61	0.06				
SUZ: BUT	7	R	+1	2.54	57	0.108	0.025	0.111	0.24444	4	4	0.45	0.49	0.04				
SIL: BUT	19	R	0	2.53	54	0.059	0.024	0.11	0.19327	4	4	0.38	0.51	0.13				
	-0.09			1	-0.08	0.19	0.08	-0.18	0.04	0.17	-0.29	-0.14	-0.59	-0.35				
	Correlation Coefficient																	

Figure 4.4.1a – Mu calculation control conditions - Race Start 0 – 100kph.

The 0-100kph comparison can often be a misleading one, as the driver occasionally needs to come off of the throttle in order to avoid an accident going down into the first corner. To combat this, the car speed was extrapolated along from the point where the driver lifts off of the throttle and this theoretical

acceleration was used to determine the time at which the car speed would have reached 100kph.

When comparing the 0-100kph time for each race, the number of formation lap slip events appears to have very little bearing and this is most likely due to the fact that the clutch stack wear is constantly monitored and the clutch stack is replaced before the race if needed, meaning that each carbon stack would easily have sufficient 'life' in it to perform an RS efficiently. Due to the nature of the carbon-carbon material, whilst the stack is within life, the material characteristics are very consistent.

The race start energy has a loose negative correlation when compared to the 0-100kph time; generally, the higher the energy, the faster the RS. This is an obvious correlation

Over the 2006 season, a strong negative correlation between  $\mu$  and 0-100kph time was observed. A higher RS  $\mu$  tends to give lower RS time. The higher friction coefficient means that less time is spent with the clutch slipping, and a higher percentage of the energy being transferred from the engine directly into the gearbox, rather than being lost through heat.

#### 4.4.2 Number of Clutch Events Performed during Formation Lap

Track/Driver	Energy Graph			Quali Posn	Grid Posn (R/D)	Posn Change	RS 0-100 kph [s]	Num Clutch Events	Energy FS [MJ]	Energy FL [MJ]	Energy RS [MJ]	Energy Total [MJ]	Clutch Mode FS	Clutch Mode RS	Clutch Mu FS	Clutch Mu RS	Delta Clutch Mu
	FS Energy Dissipation	FL Energy Dissipation	Total Energy Dissipation														
NUR: BUT	6	D	0	2.58	85	0.073	0.043	0.108	0.22379	5	5	0.55	0.61	0.06			
SEP: BUT	2	D	0	2.79	72	0.101	0.017	0.068	0.18697	4	2	0.47	0.46	-0.01			
MZA: BUT	5	R	-1	2.76	71	0.107	0.049	0.126	0.28148	3	3	0.46	0.45	-0.01			
MZA: BAR	8	D	-2	2.85	66	0.118	0.047	0.125	0.29026	3	3	0.49	0.45	-0.04			
BAH: BUT	3	R	-3	3.37	66	0.106	0.045	0.058	0.20922	8	3	0.2	0.16	-0.04			
IST: BUT	6	D	0	2.84	64	0.107	0.029	0.113	0.24858	3	3	0.52	0.5	-0.02			
IMO: BUT	2	D	+1	2.8	63	0.092	0.032	0.102	0.22562	5	5	0.27	0.56	0.29			
NUR: BAR	4	D	-2	2.81	62	0.071	0.022	0.108	0.20103	5	6	0.48	0.48	0			
MEL: BUT	1	R	0	2.77	60	0.098	0.022	0.092	0.21155	5	4	0.46	0.43	-0.03			
SHA: BUT	4	D	0	3.12	59	0.102	0.037	0.123	0.26243	3	3	0.54	0.52	-0.02			
MTL: BAR	9	R	-1	2.87	58	0.066	0.019	0.11	0.19508	4	4	0.35	0.36	0.01			
MTL: BUT	8	D	-2	2.91	58	0.065	0.049	0.139	0.25317	4	4	0.36	0.46	0.1			
SUZ: BUT	7	R	+1	2.54	57	0.108	0.025	0.111	0.24444	4	4	0.45	0.49	0.04			
INT: BUT	14	D	0	2.89	56	0.047	0.023	0.064	0.13392	5	4	0.4	0.39	-0.01			
MCO: BUT	13	D	+1	2.81	56	0.118	0.034	0.118	0.26979	3	5	0.37	0.36	-0.01			
SUZ: BAR	8	D	-1	2.64	54	0.083	0.022	0.111	0.21583	4	4	0.44	0.48	0.04			
SIL: BUT	19	R	0	2.53	54	0.059	0.024	0.11	0.19327	4	4	0.38	0.51	0.13			
HOK: BAR	6	D	-2	3.01	52	0.107	0.016	0.124	0.24721	5	6	0.76	0.39	-0.37			
MCO: BAR	5	D	0	2.65	52	0.124	0.013	0.13	0.26693	3	5	0.44	0.42	-0.02			
BCN: BUT	8	D	-1	2.85	52	0.081	0.013	0.111	0.20425	3	3	0.48	0.52	0.04			
IST: BAR	13	R	-1	2.71	51	0.074	0.056	0.115	0.24493	4	4	0.5	0.46	-0.04			
BCN: BAR	5	R	-1	2.82	50	0.111	0.017	0.121	0.24805	3	4	0.5	0.49	-0.01			
SHA: BAR	3	R	0	3.13	49	0.099	0.019	0.113	0.23152	3	3	0.52	0.49	-0.03			
IMO: BAR	3	R	-2	2.92	49	0.108	0.035	0.108	0.25178	5	4	0.48	0.47	-0.01			
SEP: BAR	12	D	+2	2.77	49	0.113	0.01	0.077	0.1994	4	2	0.4	0.43	0.03			
MSC: BUT	17	R	+1	2.8	47	0.056	0.017	0.061	0.13476	5	5	0.44	0.41	-0.03			
BAH: BAR	6	D	+1	2.78	47	0.092	0.024	0.086	0.20218	8	4	0.43	0.41	-0.02			
MEL: BAR	17	R	-1	3.37	45	0.101	0.017	0.107	0.22431	4	3	0.36	0.32	-0.04			
INT: BAR	5	R	0	2.71	44	0.068	0.02	0.109	0.1965	5	4	0.34	0.47	0.13			
MGC: BAR	13	R	+1	2.75	42	0.066	0.017	0.117	0.19898	5	5	0.41	0.42	0.01			
SIL: BAR	6	D	-1	2.75	37	0.124	0.01	0.133	0.26677	4	4	0.57	0.54	-0.03			
Correlation Coefficient	-0.35			-0.08	1	0.01	0.54	-0.12	0.12	-0.02	-0.1	-0.02	0.13	0.13			

Figure 4.4.2a – Mu calculation control conditions – Number of Events

The number of formation lap clutch events that take place appear to have absolutely no bearing upon the 0-100kph time, the race start energy or the race start friction. This indicates consistency of the clutch material to provide similar launches regardless of the number of events that it undertakes.

However, there is a loose connection between the number of events and formation lap energy, which would naturally be case as more individual events clutch event energies would naturally imply more total energy.

### 4.4.3 Race Start Energy

Track/Driver	Energy Graph				Qualif Posn	Grid Posn [R/D]	Posn Change	RS 0-100 kph [s]	Num Clutch Events	Energy FS [MJ]	Energy FL [MJ]	Energy RS [MJ]	Energy Total [MJ]	Clutch Mode FS	Clutch Mode RS	Clutch Mu FS	Clutch Mu RS	Delta Clutch Mu
MTL: BUT		8	D	-2	2.91	58	0.065	0.049	0.139	0.25317	4	4	0.36	0.46	0.1			
SIL: BAR		6	D	-1	2.75	37	0.124	0.01	0.133	0.26677	4	4	0.57	0.54	-0.03			
MCO: BAR		5	D	0	2.65	52	0.124	0.013	0.13	0.26693	3	3	0.44	0.42	-0.02			
MZA: BUT		5	R	-1	2.76	71	0.107	0.049	0.126	0.28148	3	3	0.46	0.45	-0.01			
MZA: BAR		8	D	-2	2.85	66	0.118	0.047	0.125	0.29026	3	3	0.49	0.45	-0.04			
HOK: BAR		6	D	-2	3.01	52	0.107	0.016	0.124	0.24721	5	6	0.76	0.39	-0.37			
SHA: BUT		4	D	0	3.12	59	0.102	0.037	0.123	0.26243	3	3	0.54	0.52	-0.02			
BCN: BAR		5	R	-1	2.82	56	0.111	0.017	0.121	0.24805	3	4	0.5	0.49	-0.01			
MCO: BUT		13	D	+1	2.81	56	0.118	0.034	0.118	0.26979	3	5	0.37	0.36	-0.01			
MGC: BAR		13	R	+1	2.75	42	0.066	0.017	0.117	0.19898	5	5	0.41	0.42	0.01			
IST: BAR		13	R	-1	2.71	51	0.074	0.056	0.115	0.24493	4	4	0.5	0.46	-0.04			
SHA: BAR		3	R	0	3.13	49	0.099	0.019	0.113	0.23152	3	3	0.52	0.49	-0.03			
IST: BUT		6	D	0	2.84	64	0.107	0.029	0.113	0.24658	3	3	0.52	0.5	-0.02			
SUZ: BAR		8	D	-1	2.64	54	0.083	0.022	0.111	0.21583	4	4	0.44	0.48	0.04			
SUZ: BUT		7	R	+1	2.54	57	0.108	0.025	0.111	0.24444	4	4	0.45	0.49	0.04			
BCN: BUT		8	D	-1	2.85	52	0.081	0.013	0.111	0.20425	3	3	0.48	0.52	0.04			
MTL: BAR		9	R	-1	2.87	58	0.066	0.019	0.11	0.19508	4	4	0.35	0.36	0.01			
SIL: BUT		19	R	0	2.53	54	0.059	0.024	0.11	0.19327	4	4	0.38	0.51	0.13			
INT: BAR		5	R	0	2.71	44	0.088	0.02	0.109	0.1965	5	4	0.34	0.47	0.13			
NUR: BAR		4	D	-2	2.81	62	0.071	0.022	0.108	0.20103	5	6	0.48	0.48	0			
NUR: BUT		6	D	+1	2.58	85	0.073	0.043	0.108	0.22379	5	5	0.55	0.61	0.06			
IMO: BAR		3	R	-2	2.92	49	0.108	0.035	0.108	0.25178	5	4	0.48	0.47	-0.01			
MEL: BAR		17	R	-1	3.37	45	0.101	0.017	0.107	0.22431	4	3	0.36	0.32	-0.04			
IMO: BUT		2	D	+1	2.8	63	0.092	0.032	0.102	0.22562	5	5	0.27	0.56	0.29			
MEL: BUT		1	R	0	2.77	60	0.098	0.022	0.092	0.21155	5	4	0.46	0.43	-0.03			
BAH: BAR		6	D	+1	2.78	47	0.092	0.024	0.096	0.20218	8	4	0.43	0.41	-0.02			
SEP: BAR		12	D	+2	2.77	49	0.113	0.01	0.077	0.1994	4	2	0.4	0.43	0.03			
SEP: BUT		2	D	0	2.79	72	0.101	0.017	0.068	0.18697	4	2	0.47	0.46	-0.01			
INT: BUT		14	D	0	2.89	56	0.047	0.023	0.064	0.13392	5	4	0.4	0.39	-0.01			
MGC: BUT		17	R	+1	2.8	47	0.056	0.017	0.061	0.13476	5	5	0.44	0.41	-0.03			
BAH: BUT		3	R	-3	3.37	66	0.106	0.045	0.058	0.20922	8	3	0.2	0.16	-0.04			
	Correlation Coefficient	-0.11			-0.18	-0.12	0.27	0.17	1	0.78	-0.58	0.23	0.38	0.42	-0.04			

Figure 4.4.3a – Mu calculation control conditions - Race Start Energy.

By analysing the race start energy, very few of the obvious correlations have been seen. The amount of dissipated energy at the race start has a very loose correlation with the clutch's mu value, despite the implication that one should go in hand with the other, due to the energy being a function of the clutch temperature, which is a function of the friction. However, this also highlights the

requirement for further investigation into this area through experimentation and modelling.

There is a strong correlation between the race start energy dissipation and the total energy dissipation, but this is due to the fact that the race start actually accounts for most of the value of the total energy dissipation.

Other factors including the race start time and the number of clutch events appear to have little bearing on the race start dissipated energy.



#### 4.4.4 Race Start Coefficient of Friction

Track/Driver	FS Energy Dissipation	FL Energy Dissipation	RS Energy Dissipation	Total Energy Dissipation	Quali Posn	Grid Posn [R/D]	Posn Change	RS 0-100 kph [s]	Num Clutch Events	Energy FS [MJ]	Energy FL [MJ]	Energy RS [MJ]	Energy Total [MJ]	Clutch Mode FS	Clutch Mode RS	Clutch Mu FS	Clutch Mu RS	Delta Clutch Mu
NUR: BUT	0.043	0.073	0.108	0.22379	6	D	+1	2.58	85	0.073	0.043	0.108	0.22379	5	5	0.55	0.61	0.06
IMO: BUT	0.032	0.092	0.102	0.22562	2	D	+1	2.8	63	0.092	0.032	0.102	0.22562	5	5	0.27	0.56	0.29
SIL: BAR	0.01	0.124	0.133	0.26777	6	D	-1	2.75	37	0.124	0.01	0.133	0.26777	4	4	0.57	0.54	-0.03
SHA: BUT	0.037	0.102	0.123	0.26243	4	D	0	3.12	59	0.102	0.037	0.123	0.26243	3	3	0.54	0.52	-0.02
BCN: BUT	0.013	0.081	0.111	0.20425	8	D	-1	2.85	52	0.081	0.013	0.111	0.20425	3	3	0.48	0.52	0.04
SIL: BUT	0.024	0.059	0.11	0.19327	19	R	0	2.53	54	0.059	0.024	0.11	0.19327	4	4	0.38	0.51	0.13
IST: BUT	0.029	0.107	0.113	0.24858	6	D	0	2.84	64	0.107	0.029	0.113	0.24858	3	3	0.52	0.5	-0.02
SUZ: BAR	0.025	0.108	0.111	0.24444	7	R	+1	2.54	57	0.108	0.025	0.111	0.24444	4	4	0.45	0.49	0.04
SHA: BAR	0.019	0.099	0.113	0.23152	3	R	0	3.13	49	0.099	0.019	0.113	0.23152	3	3	0.52	0.49	-0.03
BCN: BAR	0.017	0.111	0.121	0.24805	5	R	-1	2.82	50	0.111	0.017	0.121	0.24805	3	4	0.5	0.49	-0.01
SUZ: BAR	0.022	0.083	0.111	0.21583	8	D	-1	2.64	54	0.083	0.022	0.111	0.21583	4	4	0.44	0.48	0.04
NUR: BAR	0.022	0.071	0.108	0.20103	4	D	-2	2.81	62	0.071	0.022	0.108	0.20103	5	6	0.48	0.48	0
INT: BAR	0.02	0.068	0.109	0.1965	5	R	0	2.71	44	0.068	0.02	0.109	0.1965	5	4	0.34	0.47	0.13
IMO: BAR	0.035	0.108	0.108	0.25178	3	R	-2	2.92	49	0.108	0.035	0.108	0.25178	5	4	0.48	0.47	-0.01
IST: BAR	0.056	0.074	0.115	0.24483	8	D	-1	2.71	51	0.074	0.056	0.115	0.24483	4	4	0.5	0.46	-0.04
MTL: BUT	0.049	0.065	0.139	0.25317	8	D	-2	2.91	58	0.065	0.049	0.139	0.25317	4	4	0.36	0.46	0.1
SEP: BUT	0.017	0.101	0.068	0.18697	2	D	0	2.79	72	0.101	0.017	0.068	0.18697	4	2	0.47	0.46	-0.01
MZA: BAR	0.047	0.118	0.125	0.29026	8	D	-2	2.85	66	0.118	0.047	0.125	0.29026	3	3	0.49	0.45	-0.04
MZA: BUT	0.049	0.107	0.126	0.28148	5	R	-1	2.76	71	0.107	0.049	0.126	0.28148	3	3	0.46	0.45	-0.01
MEL: BUT	0.022	0.098	0.092	0.21155	1	R	0	2.77	60	0.098	0.022	0.092	0.21155	5	4	0.46	0.43	-0.03
SEP: BAR	0.01	0.113	0.077	0.1994	12	D	+2	2.77	49	0.113	0.01	0.077	0.1994	4	2	0.4	0.43	0.03
MGC: BAR	0.017	0.066	0.117	0.19898	13	R	+1	2.75	42	0.066	0.017	0.117	0.19898	5	5	0.41	0.42	0.01
MCO: BAR	0.013	0.124	0.13	0.26693	5	D	0	2.65	52	0.124	0.013	0.13	0.26693	3	5	0.44	0.42	-0.02
MGC: BUT	0.017	0.056	0.061	0.13476	17	R	+1	2.8	47	0.056	0.017	0.061	0.13476	5	5	0.44	0.41	-0.03
BAH: BAR	0.024	0.092	0.086	0.20218	6	D	+1	2.78	47	0.092	0.024	0.086	0.20218	8	4	0.43	0.41	-0.02
INT: BUT	0.047	0.047	0.064	0.13392	14	D	0	2.89	56	0.047	0.047	0.064	0.13392	5	4	0.4	0.39	-0.01
HOK: BAR	0.016	0.107	0.124	0.24721	6	D	-2	3.01	52	0.107	0.016	0.124	0.24721	5	6	0.76	0.39	-0.37
MTL: BAR	0.019	0.066	0.11	0.19508	9	R	-1	2.87	58	0.066	0.019	0.11	0.19508	4	4	0.35	0.36	0.01
MCO: BUT	0.034	0.118	0.118	0.26979	13	D	+1	2.81	56	0.118	0.034	0.118	0.26979	3	5	0.37	0.36	-0.01
MEL: BAR	0.017	0.101	0.107	0.22431	17	R	-1	3.37	45	0.101	0.017	0.107	0.22431	4	3	0.36	0.32	-0.04
BAH: BUT	0.045	0.106	0.058	0.20922	3	R	-3	3.37	66	0.106	0.045	0.058	0.20922	8	3	0.2	0.16	-0.04
	Correlation Coefficient																	
	-0.2																	
	-0.59																	
	-0.07																	
	0.13																	
	0.42																	
	0.19																	
	-0.43																	
	0.09																	
	0.44																	
	1																	
	0.39																	

Figure 4.4.4a – Mu calculation control conditions - Race Start Friction.

Relating clutch friction co-efficient ( $\mu$ ) to total energy dissipation over entire formation period does not yield any conclusive information as results do not appear to follow and type of pattern. However, during the race start there is a rather strong correlation between the dissipated energy and the clutch mu but interestingly, this relationship does not hold true for the formation start. This

could be explained by the fact that the formation start is only a fraction of the race start; that is, in the race start, the driver is going as fast as he can all the way down to the first corner, however, in the formation start, the driver is only trying to do the first few seconds of the practice launch and so a complete launch from 0-100kph is not completed. This will imply that the energy dissipation will be lower than that for an actual race start.

The 0 – 100 time is inversely proportional to the clutch  $\mu$ ; the higher the  $\mu$ , the quicker the car will accelerate from 0-100kph. This is quite an obvious statement to make as the increased friction will naturally lead to a better 'bite' in the clutch and therefore better traction through the drive train. There is the obvious danger that the friction could be so high that the engine would stall, but the drivers and software account for this and adjust accordingly.

When looking at the number of clutch events that the stack has undergone during the formation lap, there is no real and clear relationship. This is once again due to the fact that the carbon stacks are closely monitored for wear and are replaced if deemed to be near to out of life. This should mean that each and every start is exactly the same throughout the duration of the carbon stacks lifetime.

The change in clutch  $\mu$  between the formation and race starts does not appear to be affected by the clutch friction at the race start. If the  $\mu$  is higher during the race start that does not necessarily mean that there is a large difference between the race start  $\mu$  and the formation start  $\mu$ .

It is interesting to note that differences in clutch  $\mu$  between the formation and race starts are usually in the region of 10%, but by looking at the values highlighted in green, it is also possible to see that on occasion, they can fluctuate by up to 30 – 50%. Although, interestingly, the three main occasions when the variation is high (Car One, BUT in Imola, Car One, BUT at Silverstone, and Car Two, BAR in Interlagos) the cars have not lost any places from their grid positions and in the case of Car One in Imola, a place is actually gained.

#### 4.5 Conclusions from the Race Start Analysis

This race start analysis has shown;

- A strong negative correlation observed between the clutch friction coefficient ( $\mu$ ) and 0-100kph time where a higher  $\mu$  tends to give lower race start time.
- The race start  $\mu$  is independent of the number of starts (and the life) of the carbon clutch stack.
- Relating clutch  $\mu$  to total energy dissipation over entire formation period does not yield the strong results expected at the outset of this investigation.

The analysis has also shown the requirement for a better method for friction prediction than was currently available, this would give the launch control system a capability for more accurate  $\mu$  calculations, which could translate into better race starts.

The follow on step from this work was to look at the dynamics of the friction / heat properties within a carbon-carbon race clutch to further understand the heating mechanisms, and to determine whether it was possible to experimentally obtain realistic data that is comparable to that seen on the race track.

## Chapter 5

### Clutch Bedding

This chapter looks at bedding of race clutches; what it is, why it's important and how it is done. This is important to understand before the undertaking of any experimental or mathematical work, as bedding can completely change the characteristics of the carbon-carbon material. If bedding is incomplete or executed incorrectly, then the predictability of the material rapidly decreases, meaning reduced probability of gaining meaningful results from modelling and experimentation. The importance of bedding is presented by explanation of techniques employed by teams and manufacturers and detailed mathematically and graphically in this chapter. This is fundamental in underpinning some of the pre-requisites and assumptions that were made during the experimentation and modelling section of the work.

#### 5.1 What is Clutch Bedding?

Bedding is the single most important factor in establishing a stable friction coefficient between any two carbon-carbon material faces. With a correct bedding procedure in place, it is possible to narrow the friction co-efficient range and thus assist the predictability of the clutch unit.

Advantages of bedding in are that it:

- Gradually heat treats the clutch plates and eliminates any thermal shock in the rotor;
- Burns off volatiles and moisture from the resin that is near the surface. This will eliminate "green fade"(where the friction characteristics of the clutch appear to change dramatically as the volatiles burn off);
- Mates the two surfaces to a near perfect geometrical match, so that the contact area is optimum and therefore the torque that can be transmitted over the surface is maximised;

- Establishes a layer of transfer film about a few microns thick on the plate surface. Shearing of the film during friction is an effective source of friction force. Otherwise, when using a freshly ground rotor without the transfer film, the main friction force would come from cutting, ploughing, or scoring the asperities on the clutch plate surface. This leads to inconsistent clutch-clutch slip characteristics and overall effectiveness.

If the bedding in procedure is not applied, a stable transfer film may not be established for a long time. In other words, the rotor surface would have to be constantly regenerating a film that is not stable for a prolonged period of time. This effect would reduce the performance and increase the wear.

For optimal use of any given clutch system, the clutch plate faces have to be compatible with each other and the bedding-in procedure establishes that compatibility between them. This is achieved by a combination of rubbing speed, temperature, line pressure, and inertia. Bedding-in is also influenced by the material chemistries of the carbon-carbon clutch material.

#### **5.1.1 Friction Mechanism During Bedding**

To understand the bedding-in process more clearly, it is important to consider the friction mechanism in operation. There are two basic types of clutch plate friction mechanisms: abrasive friction and adherent friction. Typically the abrasive mechanisms predominantly act within the lower temperature ranges while adherent mechanisms are more prevalent at higher surface temperatures. Both mechanisms allow for friction or the conversion of kinetic energy to thermal energy by the breaking of molecular bonds, but this occurs in two very different ways:

- a) The abrasive mechanism generates friction or energy conversion by the mechanical rubbing of the material of the clutch plates over each other. This causes the weaker of the bonds in the material to become broken down and results in mechanical wear of the clutch stack;
- b) In an adherent system, a thin layer of clutch plate material actually transfers and sticks (adheres) on the opposite face. This layer of carbon-carbon material, once evenly established on the plate, is what actually rubs between the two mating faces of the clutch. The bonds that are broken, for the conversion of

kinetic to thermal energy, are formed instantaneously before being broken again. It is this 'clutch plate-on-transferred clutch plate' material interaction at a molecular level that yields the conversion process. Wear is significantly reduced in comparison to the abrasive mechanism.

### **5.1.2 Problems Created by Little or No Bedding in**

Uneven deposits of carbon material dust on the clutch face are the primary cause of 'snatching' or vibration. It only takes a small amount of thickness (a few microns) variation in the transfer layer to initiate clutch vibration. The problem starts very small and is un-noticeable at first, but as the clutch plates begin to ride the high and low spots, more and more material is generated until the vibration begins to become noticeable. With prolonged exposure, the high spots can become hot spots and can actually change the metallurgy of the plate in those areas, creating "hard" spots on face that are virtually impossible to remove. This significantly limits the torque that can be transmitted.

### **5.1.3 Effect of Bedding Process on Actual Clutch Behaviour.**

The target of a clutch bedding process is for the coefficient of clutch friction ( $\mu$ ) to become more stable whereby the coefficient of friction is repeatable to a set tolerance over a series of clutch events. This is illustrated by Figure 5.1.3a [164] which plots data taken from the bedding rig at Honda for the coefficient of friction as the clutch goes through a number of bedding cycles (illustrated on the X-axis of the plot). The coefficient of friction was measured as a function of output torque. The points shown as blue circles represent the coefficient of friction just after engagement at the start of a clutch event, the points shown as red triangles represent the coefficient of friction at the end of a clutch event, just before the clutch is disengaged, and the points shown as black spots represent the average coefficient of clutch friction during that clutch event.

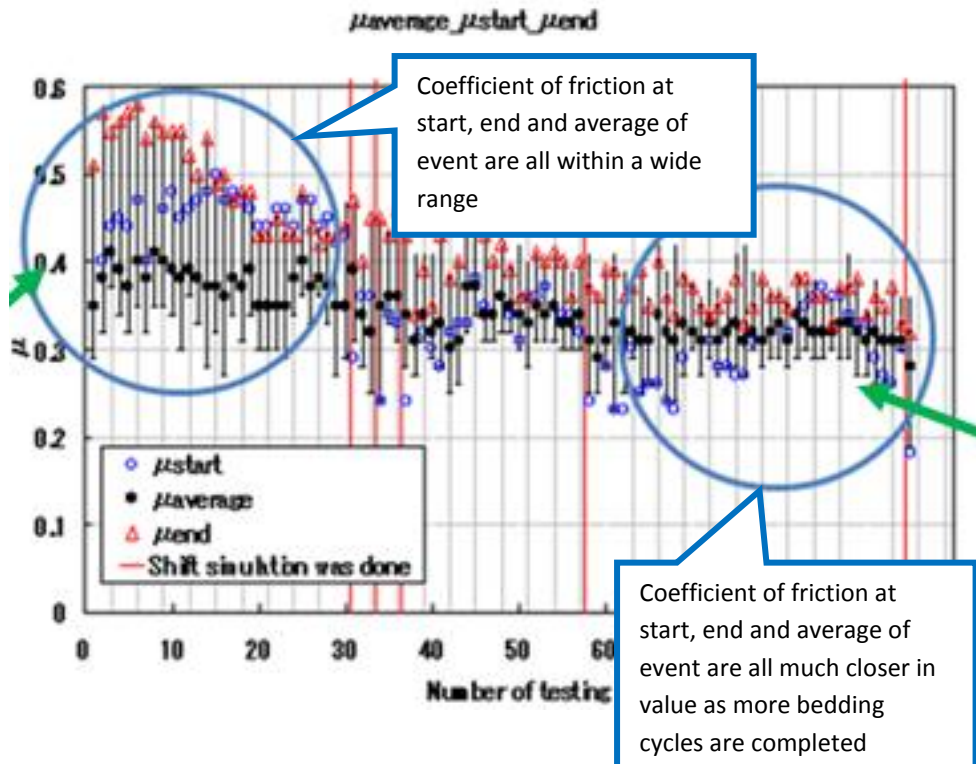


Figure 5.1.3a – Peak coefficient of friction values for a typical new F1 clutch at the start and end of clutch engagement [164].

As seen in figure 5.1.3a, the initial, final and average coefficient of friction are all very different values during the early stages of bedding, as can be seen in the left hand blue circle at the early number of cycles. This is due to the insufficient build up of a transfer layer, causing the two plates to ‘grab’ and ‘snatch’ each time that they come into contact with each other. If the clutch were to be used during a race start in this condition the resulting torque trace of such an event would be similar to that seen in Figure 5.1.3b [164] where the green trace is clutch friction, seen here as a function of torque (blue) at the input shaft to the gearbox.

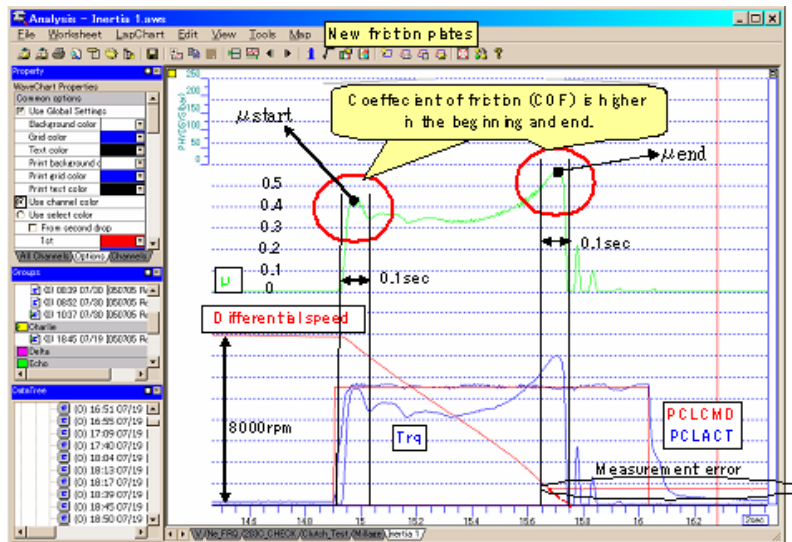


Figure 5.1.3b – Peak coefficient of friction values at the start and end of a clamping event after approximately 20 bedding cycles [164]

As the bedding cycle progresses, the coefficient of friction becomes more stable throughout the clutch slip event, with much smaller peaks (green), signifying less ‘grabbing’ of the clutch and giving a much smoother and more predictable torque transfer and hence feel, as seen on the blue trace. This is illustrated in Figure 5.1.3c [164],

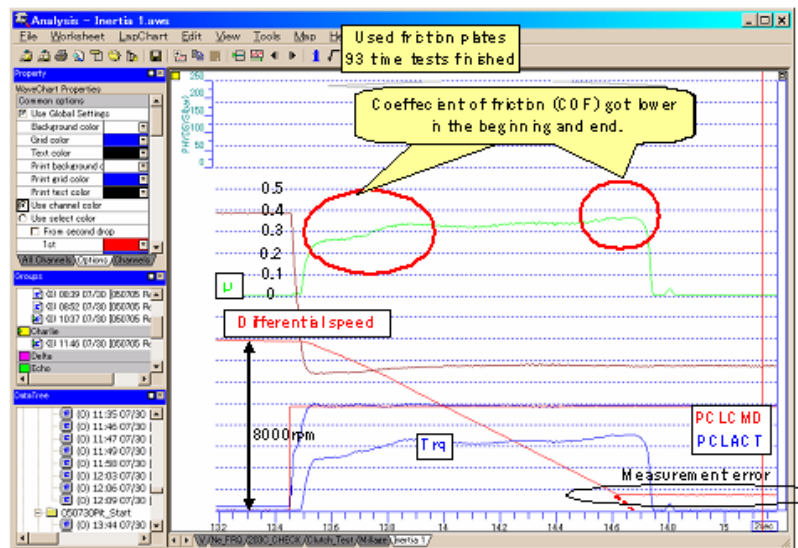


Figure 5.1.3c – Peak coefficient of friction values at the start and end of a clamping event after approximately 70 bedding cycles[164].

This is a clear illustration of how important it is that a clutch is properly bedded-in before use. Without proper bedding-in, the unpredictable coefficient of friction



causing 'grabbing' and slip of the clutch does not provide a smooth torque transfer to the input shaft and this would consequently cause the car to either jump the start or stall – both of which would be catastrophic to the driver and team in terms of race progress.

## **5.2 How are Clutches Bedded?**

In general, bedding-in in practice is carried out by heating the system to its adherent temperature to allow the formation of a transfer layer. The 'adherent' temperature is the one at which the bonds of the structure break down and permit type III wear. In carbon-carbon this is typically around 600 °C. The clutch is then allowed to cool whilst still rotating and without coming to rest, resulting in an even transfer layer deposition around the plate face. This procedure is typically repeated two or three times in order to ensure that the entire rotor face is evenly covered with clutch plate material. Too little heat during bedding-in stops the material from transferring to the plate face, while overheating the system can generate uneven deposits due to the material breaking down and depositing randomly on to the plate face.

The bedding-in process of a race clutch is a highly accurate process that has been refined over years of development. Each team has their own way of bedding in a clutch, and sometimes, even between the team and engine supplier, variations on the process can be found. Generally, a clutch pack is said to be 'consistent' when the change in torque transfer through the clutch over a slip event is less than 120Nm (a good race start typically yields a torque transmission of 120-140Nm). This condition is usually reached between the 60<sup>th</sup> and 70<sup>th</sup> event.

The bedding program used for race clutches has the following main steps:

1. Disk baking / heating (to eliminate any surface volatiles): 300 °C for 1 hour in a baking oven.
2. On the clutch dynamometer, with initial delta speed (the difference in speed between the engine and the gearbox, through the unclamped clutch): 8000(rpm), and disk temperature, approximately 200 °C

3. Clutch pressure: 40→70→50→70→60→70(bar) is one cycle. It is repeated 10 to 12 times which gives a total of 60 to 72 clutch slips. This is known as one event (as seen on the x-axis of Figure 5.1.3a).
4. This is repeated 64 times. Interval between repetitions: 6 minutes (6 minutes is a time interval determined by pre-testing to keep the clutch disk temperature condition stabilized around 200 degrees).

Figure 5.2a [164] shows a typical dynamometer bedding cycle for the Sachs 3297 clutch and it can be seen that even after the 64<sup>th</sup> event, the average coefficient of friction appears to still have some variation, but upon closer inspection, it can be observed that the peak initial and peak final values are actually within a closer range to the average value over the whole event, meaning less ‘grabbing’ and a smoother clutch slip and subsequent transfer of torque. The values also demonstrate the cyclic variation characteristics of the bedding cycle, with the lower energy slips (at the lower clutch pressures during the initial part of the event) consistently returning lower values for the coefficient of friction.

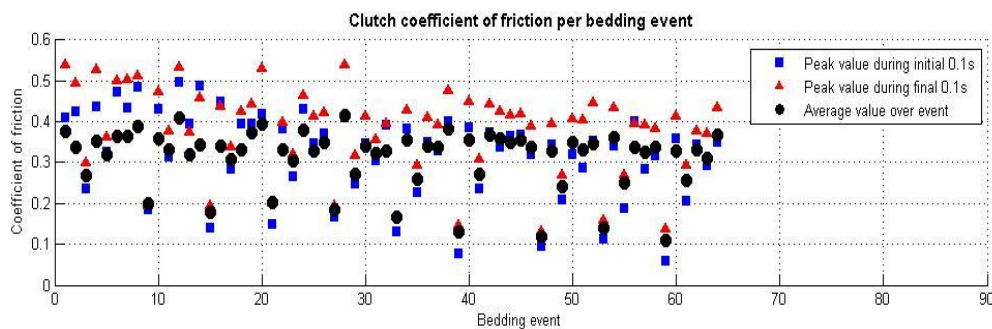


Figure 5.2a. Bedding cycle for Sachs 3209 clutch: Friction Co-Efficient [164]

The peak values for friction are calculated as the peak friction value during the first 0.1s of the event, and the last 0.1s of the event, as highlighted in the red circles in Figure 5.2b [164].

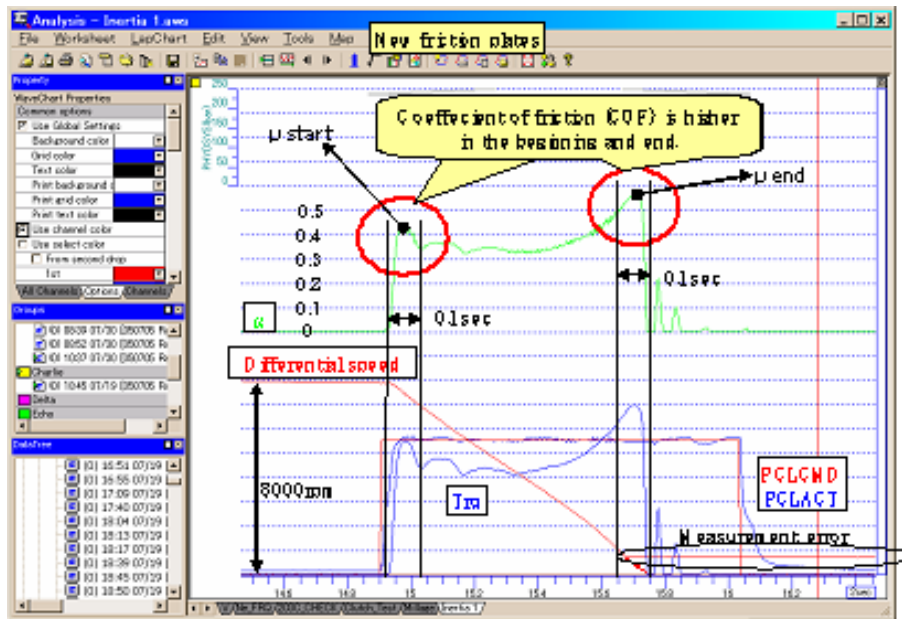


Figure 5.2b. Calculation of Peak Friction Values [164]

With the peak friction coefficients in mind, the following equation is used to calculate the instantaneous coefficient of friction:

$$\mu = \frac{T}{n \times r_e \times P \times L} \quad \text{Equation 5.2c}$$

Where  $n$  = number of working surfaces = 6

$r_e$  = mean effective radius of the clutch plates [m]

$P$  = clamp load [N] (the load that is used to clamp the driving and driven faces of the clutch)

$T$  = Torque [Nm]

$\mu$  = Coefficient of friction

$L$  = Lever ratio = 4.73 (for this test rig)(This is clutch design dependant, and is the ratio of the distance from the fulcrum to the actuation point of the force from the dynamometer or car to the distance of the fulcrum to the point at which the force is applied to the clutch plates)

There are three methods to calculate the mean effective radius (the distance from the theoretical centre of the friction plate to the centre of the friction face).

With  $r_o$  = Outer radius of friction surface = 48.5mm

$r_i$  = Inner radius of friction surface = 32.5mm;

Constant Wear Method  $r_e = \frac{1}{2}(r_o + r_i) = 40.5 \text{ mm}$

Equation 5.2d

Constant Pressure Method  $r_e = \frac{2}{3} \frac{(r_o^3 - r_i^3)}{(r_o^2 - r_i^2)} = 41.03 \text{ mm}$

Equation 5.2e

Equal Area Method  $r_e = \sqrt{\frac{R_o^2 + R_i^2}{2}} = 41.28 \text{ mm}$

Equation 5.2f

The generally accepted industry method for this calculation is the constant pressure method, which gives  $r_e = 41.03\text{mm}$  in this case. This is adopted due to the fact that the clutch dynamometer is able to maintain a constant pressure on the clutch.

### 5.2.1 Variation of Kinetic Energy through the Bedding Process

The initial kinetic energy is calculated for each event and is a direct function of the engagement speed. Due to the conservation of energy, where energy in = energy out, the only energy source into the clutch is the rotational speed delta and so when the clutch is engaged, the initial kinetic energy is a function of this with respect to the coefficient of friction of the clutch. The maximum kinetic energy is found to be 78kJ and the minimum kinetic energy is found to be 74kJ, calculated to be a difference of 5.3%. This range of difference is due to the inconsistent coefficient of friction characteristic of the clutch disc but is considered to be well within acceptable limits. After approximately 28 slips, the kinetic energy value becomes higher and more consistent, and it is here that the effects of bedding can begin to be observed. Kinetic energy is a good indication of the degree of bedding due to the consistency of the coefficient of friction that it highlights. For the average energy input (initial speed of engagement) the only factor that can affect the initial kinetic energy of the clutch is the coefficient of friction and therefore a stable initial kinetic energy indicates a stable initial coefficient of friction. With a better bedding cycle and good mathematical modelling it would be possible to

reduce the range of values even further, and to obtain more accurate figures for the friction coefficient of the clutches and hence perform more predictable torque transmissions at race starts.

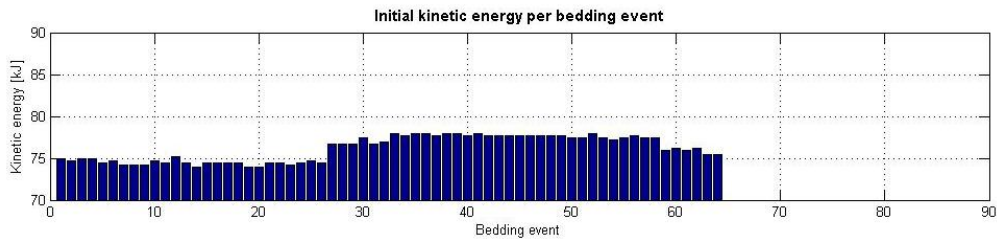


Figure 5.2.1a. Bedding cycle for Sachs 3207 clutch – Initial Kinetic Energy [164]

### 5.2.2 Variation of Bedding across Different Clutch Packs

It is useful to consider the variation of friction characteristics between clutch packs of the same material specification and bedding process. Figure 5.2.2ai below shows a range of clutch friction values obtained from dynamometer testing of 6 post-bedding slip events for each of 12 different clutch packs.

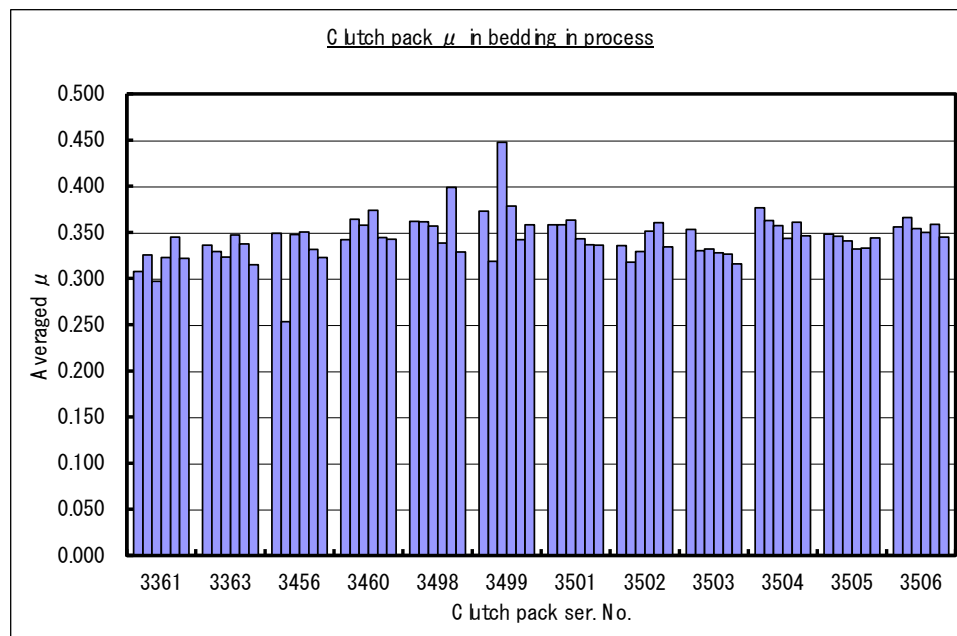


Figure 5.2.2a – Measured friction coefficient for 12 selected clutch packs over 6 post bedding clutch slips [164]

It can be observed that the coefficient of friction for the clutch packs after bedding is in the range 0.30 to 0.35 for the majority of cases. This indicates a consistency in the clutch friction, which is the definitive reason for bedding. But this value was also a cause of interest, as good clutch performance at a race start generally results from a measured/desired coefficient of friction in the range of 0.40 to 0.45 (as described in Chapter 4.3). The reason for this discrepancy will be investigated later in the thesis.

### **5.2.3 Clutch Bedding and Bite Point Learns at the Track**

At the track, a method is used to calibrate the clutch to determine the clutch trim position (also known as RS mode) that should be used at the start of the formation lap. The RS mode is also known as the clutch mode and is a set of parameters, including engine rotational speed, clutch pressure and throttle position which are set for a launch event. Each group of parameters is assigned to an RS mode number, and from data accumulated over the race weekend, an initial RS mode is chosen for the formation start. The actual race start clutch mode is determined from the formation start clutch mode. If after the formation start, the engineers feel that the mode could be optimised further, they radio instruction to the driver to change the mode for an optimised race start.

Within the ECU there is a set program for procedures such as launch control, sensor calibration and clutch calibration, these programs vary from team to team but most are very similar. The clutch calibration is carried out while the car is on the stands in the garage before the race, using a set program known as a 'bite point learn'. This consists of three cycles, lasting a total of just 2 seconds. The engine is started and ran to approximately 12,000rpm (nominal pre start revs determined by the engine torque map) before the clutch is engaged. Once a certain torque transmission is achieved (nominally 80Nm, which is an aggressive enough torque to give a representative value for the bite point, and yet not so aggressive that the car falls off its stands when performing this procedure in the garage) or the engine revs drop to a certain level (usually approximately 8,000 rpm), the clutch releases and then the cycle begins again. After the three repetitions, the average clutch engagement in mm is determined to meet this

80Nm torque transmission demand, and it determines the RS mode for the formation start.

Another clutch program within the ECU is for a 'clutch scrub'. This is a very simple program designed to clean the surface of the clutch from moisture and volatiles by slipping the clutch at a set torque transmission for approximately one second. It is important to do this before the clutch calibration program is undertaken, as if surface impurities are present during this calibration, the characteristics could change, and the clutch trim position calculation will be incorrect.

Even though bedding takes place on the dyno before installation in the car, there are occasions when the clutch friction coefficient behaves irregularly. Figure 5.2.3a taken from the Honda Bedding procedure [164] illustrates this:

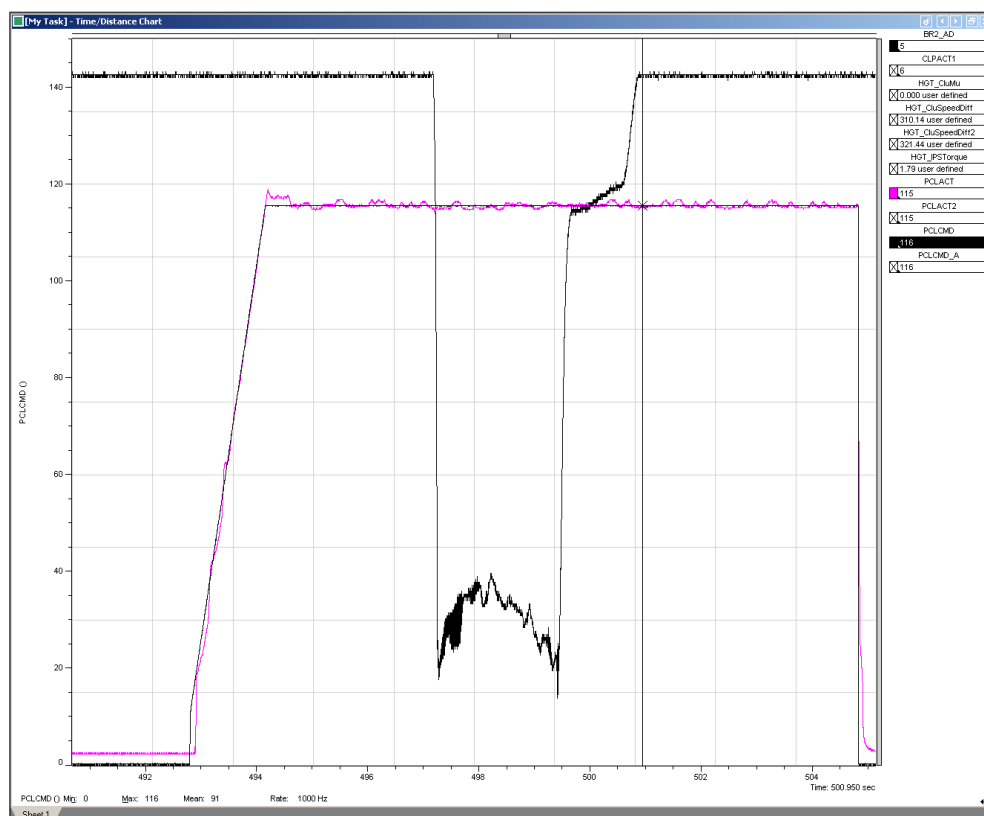


Figure 5.2.3a – Pi Toolbox screen grab highlighting the varying clutch friction (black) despite constant torque input (pink) of single event from a bedded Sachs 3556 clutch [164]

The clutch is subject to constant clamp load (seen in pink) during the running in process, but clutch friction coefficient (shown in black) does not follow the same

characteristic. This anomaly could be put down to many factors, including a 'bad spot' in the clutch material or a surface impurity caused by external contamination such as a hydraulic fluid leak, or mishandling of the clutch plates during installation onto the car.. This highlights that although bedding aids the consistency of the clutch, it cannot guarantee it and as such, there will always be an element of uncertainty when predicting the friction characteristic of the carbon-carbon material for any given clutch slip event.



## Chapter 6

### Design of Experiments and Instrumentation

This chapter explores the initial design of experiments and instrumentation for the testing that was to be used for the creation of a mathematical model. This section covers an introduction into the test dynamometer, the sensor selection process, rig adaptation and validation through FEA modelling, along with test planning through to results analysis and recommendations for changes prior to the final test. This stage of the work was particularly important in the understanding the friction versus temperature relationship for the clutch material as it allowed external factors (such as residual heat from the engine / gearbox) to be quantified and for the further tests to be conducted with this knowledge.

The specific aims of the initial test work were to explore the various options with regards to the suitability of sensors, rig construction and apparatus and to validate these choices before moving on to use them within a more extensive and comprehensive test plan.

#### 6.1 Overview of the Clutch Dynamometer and Current Test

##### Procedures

The clutch dynamometer is a device that is designed to be as accurately representative of real life conditions for a race clutch as possible. Each part of the dynamometer corresponds to a part of the car. The drive motor represents the engine with the clutch between it and the gearbox, which is represented as a load applied onto a disc by a brake caliper. Between the motor and the clutch are several gears which increase the speed and inertia of the load that is to be applied to the clutch. A schematic of the dynamometer used in this work is shown in Figure 6.1a, with a photograph of the actual rig used in Figure 6.1b...

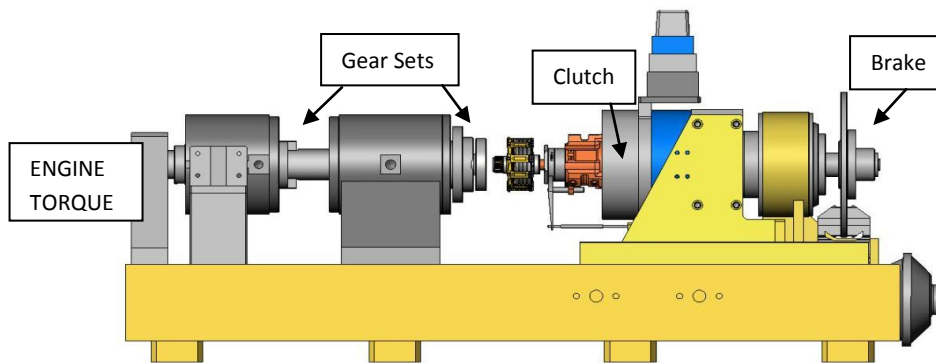


Figure 6.1a – Representation of the Clutch Dynamometer at AP Racing

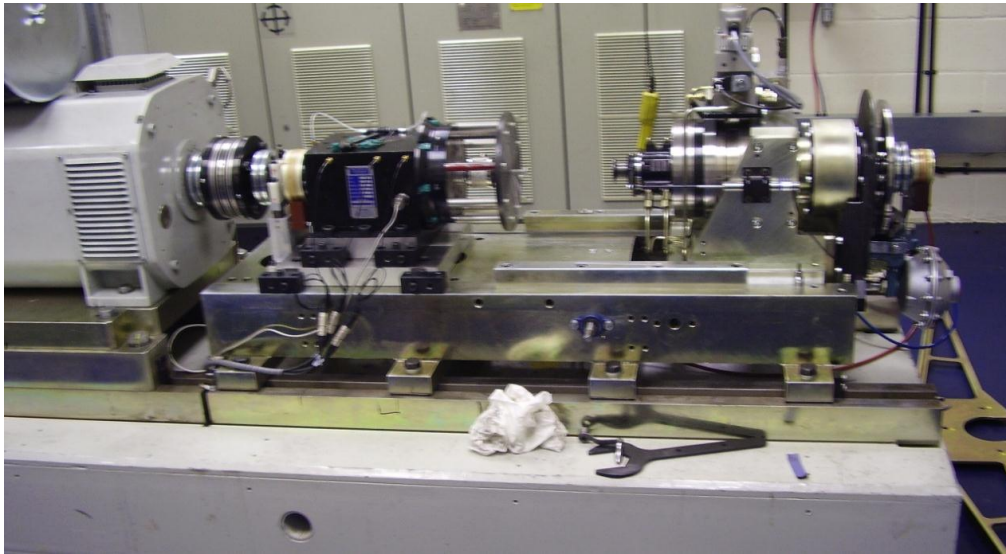


Figure 6.1b. The Clutch Dynamometer at AP Racing, Coventry

### 6.1.1 Temperature Measurement of the Clutch on the Dynamometer

To measure the temperature of the clutch whilst it is being tested on the dynamometer, a thermocouple is placed inside each clutch drive plate, inside a drilled hole at approximately halfway through its thickness, as shown in figure 6.6.1a. All of the thermocouples are plugged into a permanent fixture on the rotating head of the clutch dynamometer. The danger of this arrangement is that the centrifugal force acting upon the thermocouple connectors often means that they come flying off at high speed – which could be hazardous.

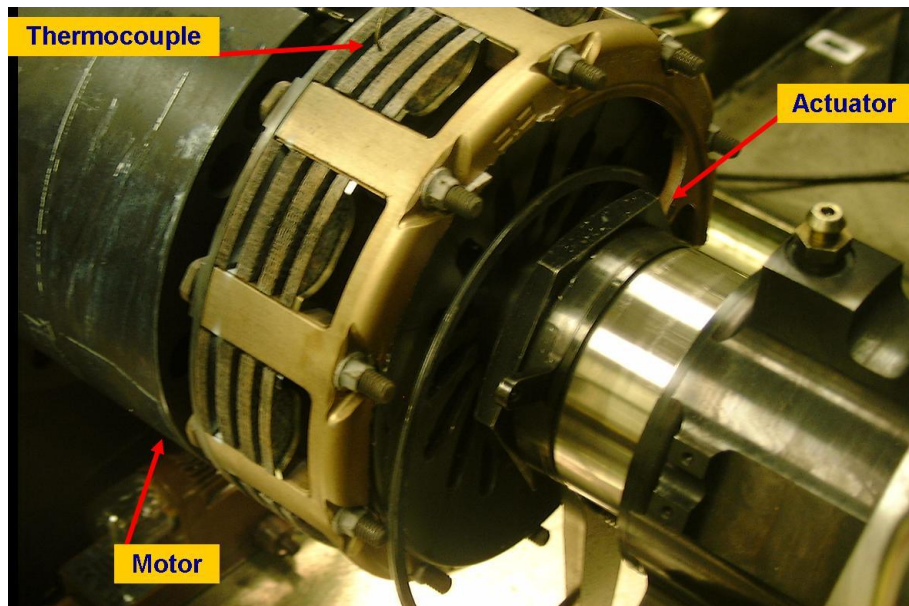


Figure 6.1.1a. Thermocouple Mountings on the clutch in the dynamometer

This method does not accurately measure interfacial temperature, but instead measures the bulk temperature of the clutch plate. Due to dissipation throughout the material and thermal energy losses to the surrounding atmosphere, and hence time taken for heat transfer, the temperature readings are delayed and significantly lower than the interface would be experiencing. Although this can be compensated for by using the thermal properties of the carbon clutch plate material, there is inaccuracy in being unable to measure the temperature directly. Because of this it is also difficult to observe how the temperature changes with the friction of the clutch plate. The interfacial temperature actually increases at a very high rate, which means that calculation of the interface temperature at any given point in time would be highly inaccurate, as even the slightest inconsistencies in material would mean that any temperature were to be extrapolated from the thermocouple to the interface using the material properties could contain a large margin of error.

Another method that has been used to measure the temperature of the clutch plates is to place an infra red temperature sensing gun at the edge of the clutch plate interface and measuring the heat by the infra red energy that is being emitted from the face (see figure 6.1.1b). The nature of the clutch means that the faces that get the hottest are in constant contact with each other implicating that

a simple infra red sensor will not suffice as it cannot measure the temperature at these close faces. The temperature on the faces of the clutch needs to be measured precisely and by using an IR detector at the edge of the clutch heat that has already been dissipated into the bulk of the plates or the surrounding assembly has been lost.



Figure 6.1.1b Heat Dissipated by a Clutch Whilst Slipping (taken during initial clutch testing)

## 6.2 IR versus Fibre Optic Measurement of Temperature

From the literature review it became apparent that for direct thermal energy measurement there were two clear choices: fibre optic measurement and infra red. This section compares both methods for their suitability for directly measuring the temperature of the closed faces of the clutch.

Fibre optics work by transmitting the light signal (in this instance the infrared light emitted by the clutch during a slip) along its length to a converter which is used, along with look up tables, to determine the temperature of the specimen at this hard to access area of the clutch stack.

For the use of fibre optics, one of the biggest problems in the installation is how to convert the signal received from the plate face. There are two ways to do this:

by converting the signal at the clutch end of the fibre optic cable or to convert the signal remotely from the clutch. The advantage of converting the signal at the clutch means that an electrical signal can then be sent from the signal converter via a slip ring, which is already in use by AP Racing. The signal converters (approximately 0.5kg) are bulky and if attached at the clutch would be spinning at up to 20,000 rpm, which would add a large eccentric load, and could be very hazardous.

By installing the system so that the signal is converted away from the clutch there are still problems because the fibre optic cable will be spinning at up to 20,000 rpm, whilst the converter remains stationary. One way of tackling this may be to design a signal converter head that would replace the current slip ring arrangement on the clutch dynamometer as shown in Figure 6.2a.

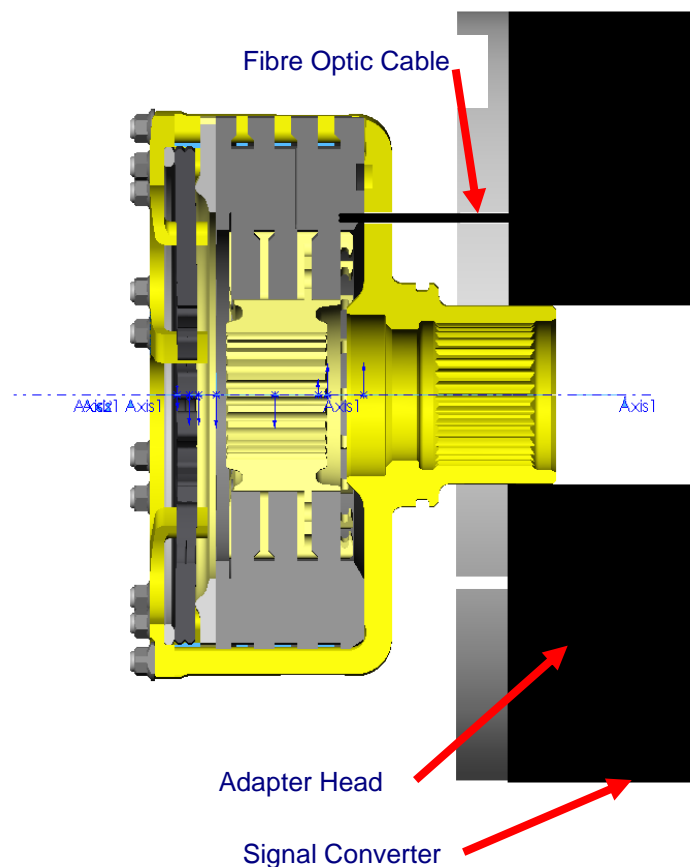


Figure 6.2a Possible Fibre Optic Signal Converter Mounting Point

As the clutch spins, the head and converter would remain stationary. Although this idea is feasible in theory, in practice, it would be very difficult to use effectively due to the fact that outside light radiation could permeate the converter through the cut-out in the head. With such high speeds, it would be impossible to ensure that the only radiation received by the signal converter is from the clutch face, and this would make the results unrepresentative of the actual situation.

When determining the location of the sensor head there are many considerations to take into account. It is easily possible to position many sensors which will be able to read the plate face nearest to the basket end of the clutch. This can be done by drilling a hole straight through the basket and the bottom 'stationary' plate (this is one of the plates which does not move in relation to the basket) – see figure 6.2b.

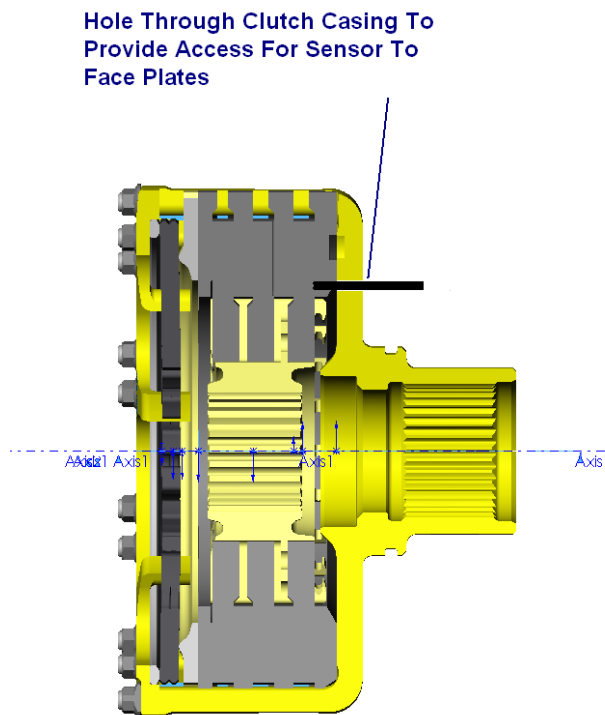


Figure 6.2b. Proposed Sensor Exit Location.

With a small amount of adaptation of the basket, it is also possible to use this method for the top stationary plate to read the temperature at interface 6 (where the Interface numbers are measured at the point where a stationary plate mates

to a spinning plate, and are numbered from the basket end of the clutch). However, due to the movement of the spinning plates, it is not possible to measure the temperature at interfaces 2, 3, 4 and 5.

The method of drilling holes can also be used in the application of infrared to the clutch arrangement. By drilling a series of holes at the bottom of the clutch basket and through the first stationary plate to interface number 1 it is possible to aim the IR beam so that it can read the temperature at interface 1. It would also be possible to connect the data processor for the IR beam so that data is acquired at the same frequency as the clutch rotation, so that the IR beam would sample only when the viewing hole is in line with it. This would mean that the IR beam would only ever acquire the temperature data when it was aiming at the interface and not when it is aimed at the spinning basket.

Due to the data accuracy, ease of transferability and ease of installation, it was decided that the initial practical testing should use the method of IR detection for the measurement of inter-facial clutch temperature on the dynamometer. The sensor, produced as a special order from Raytek (a subsidiary of Radir in Milton Keynes, UK) was a result of a working relationship between Radir and the author, and was configured with this specific purpose in mind. The sensor is designed to read temperatures within the range of 200 °C to 1200 °C with a response time of 150ms. This working range was determined through previous thermocouple measurements obtained with the dynamometer running, with the response time chosen to be the lowest possible for the temperature and price range constraints. Figures 6.2c, 6.2d and 6.2e below shows the selected sensor and its technical specifications.



Figure 6.2c. The infrared sensor, as used in the dynamometer testing

**Right Angle Mirror** for Air Cooling Jacket and Air Purge Jacket only (XXXMIACRAJ)

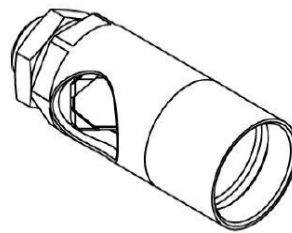
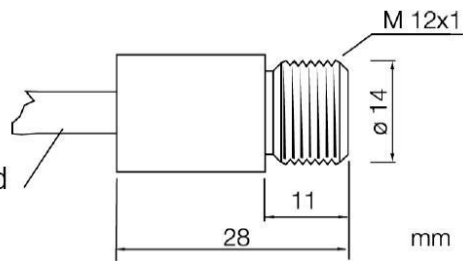


Figure 6.2d. The mirrored head, used in the infrared sensor

**Sensing Head**

Preinstalled cable, standard cable length 1 m



**Electronics Housing**

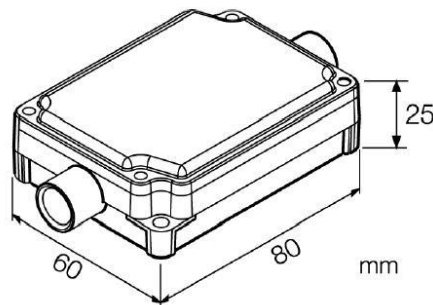


Figure 6.2e. The Infrared sensor dimensions, as supplied by Radir.



### **6.3 Determination of the Emissivity of the Carbon Material**

The radiated Infrared energy of the clutch is a function of temperatures multiplied by the emissivity of the sample, and so to utilise the IR equipment to its full ability, the emissivity of the carbon – carbon material needed to be accurately determined. Emissivity is the ratio of the radiation intensity of a non-black body to the radiation intensity of a black body and characterises the radiation or absorption quality of non-black bodies. The ratio is always less than, or equal to one, with only true black bodies having an emissivity of 1. A spectral emissivity of zero means that the heat radiator emits no radiation at this wavelength.

The emissivity depends on factors such as temperature, emission angle, and energy wavelength. Emissivity testing was undertaken over a 3.5 – 4.0  $\mu\text{m}$  range, to coincide with the wavelength range of the infrared detector that was being used.

#### **6.3.1 Emissivity Materials Testing**

The leading standard regarding emissivity testing is ASTM E-423-71 (2002) [165] (*Standard Test Method for Normal Spectral Emittance at Elevated Temperatures of Nonconducting Specimens*). This test method describes an accurate technique for measuring the normal spectral emittance of electrically conducting materials or materials with electrically conducting substrates, in the temperature range from 600 to 1400K, and at wavelengths from 1 to 35 $\mu\text{m}$ . The method produces data that are accurate to within a few percent. It is suitable for research laboratories where the highest precision and accuracy are desired, but because of cost, it is not recommended for routine production or acceptance testing. However, because of its high accuracy this test method can be used as a reference for other methods for production and acceptance testing.

Using the methods stated in ASTM E-423-71 [165] a sample of used carbon-carbon clutch material from an F1 clutch was tested for its emissivity at the National Physical Laboratory facilities in Teddington, London, UK. The procedure was undertaken using the NPL absolute emissometer shown in Figure 6.3.1a.

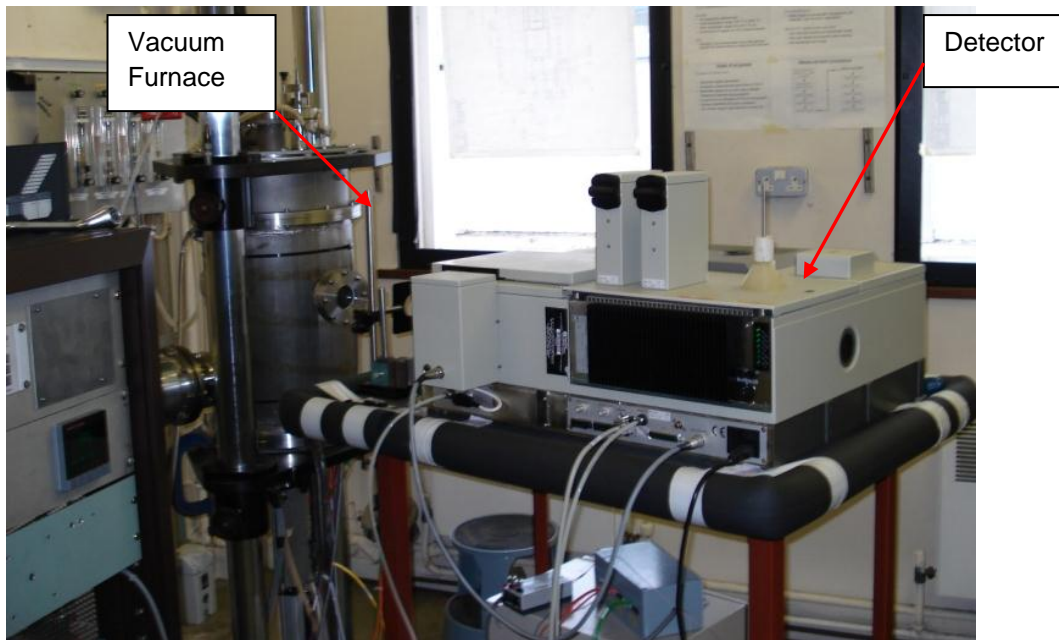


Figure 6.3.1a. Emissivity Test Apparatus at the National Physical Laboratory Teddington UK

The main component of the emissometer consists of an electronically heated tantalum furnace with a graphite block mounted in the central region, as observed in figure 6.3.1b This graphite block has two holes on its upper face; one is 6mm diameter by 30mm deep and forms a blackbody cavity, the other hole is 10mm diameter by 10mm deep and houses the specimen.



Figure 6.3.1b. Close up of the Graphite Block Used to Hold the Sample (taken at the National Physical Laboratory – Teddington)

A specimen of nominal dimensions of 10.0mm diameter and 6.00mm thickness was taken from a used, bedded clutch plate (this is because new plate material has a 'shiny' appearance which would affect the emissive values obtained) and placed into the specimen cavity. Tantalum radiation shields are used at either end of the furnace and help to produce an approximately isothermal condition in the central region of the furnace, meaning that the blackbody and specimen samples are assumed identical in temperature. The radiation shields above the graphite block are supported on a shutter mechanism that moves via the use of a stepper motor. This stepper motor means that the shutter can move very quickly, to allow for it to be pulled away from the sample and measurements to be taken as soon as possible to ensure that the reading is as accurate as possible by reducing the time for heat loss to occur. A periscope, comprising of a parabolic mirror and two flat mirrors, is used to accumulate and direct radiation from the target area towards the detection system.

The whole assembly is enclosed in a vacuum chamber with a calcium fluoride window in its side through which the thermal radiation is detected and this is shown in Figure 6.3.1c.

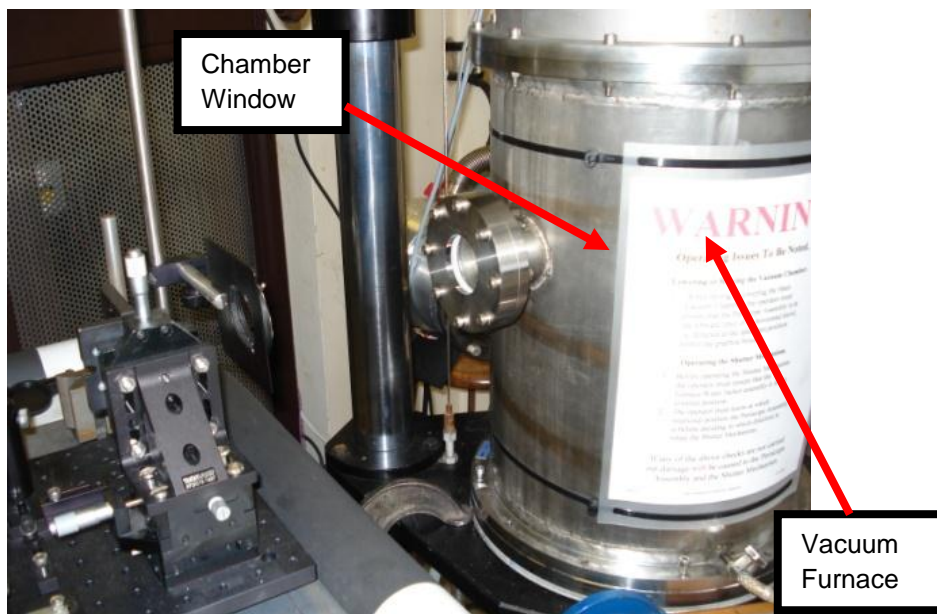


Figure 6.3.1c. The Emissivity Vacuum Chamber and Window (taken at the National Physical Laboratory – Teddington)

A Fourier-transform spectrometer (shown in Figure 6.3.1d) with a photovoltaic mercury indium antimonide (InSb) detector is used to measure radiation over the wavelength  $5.5\ \mu\text{m}$  with a spectral resolution of  $16\text{cm}^{-1}$ .

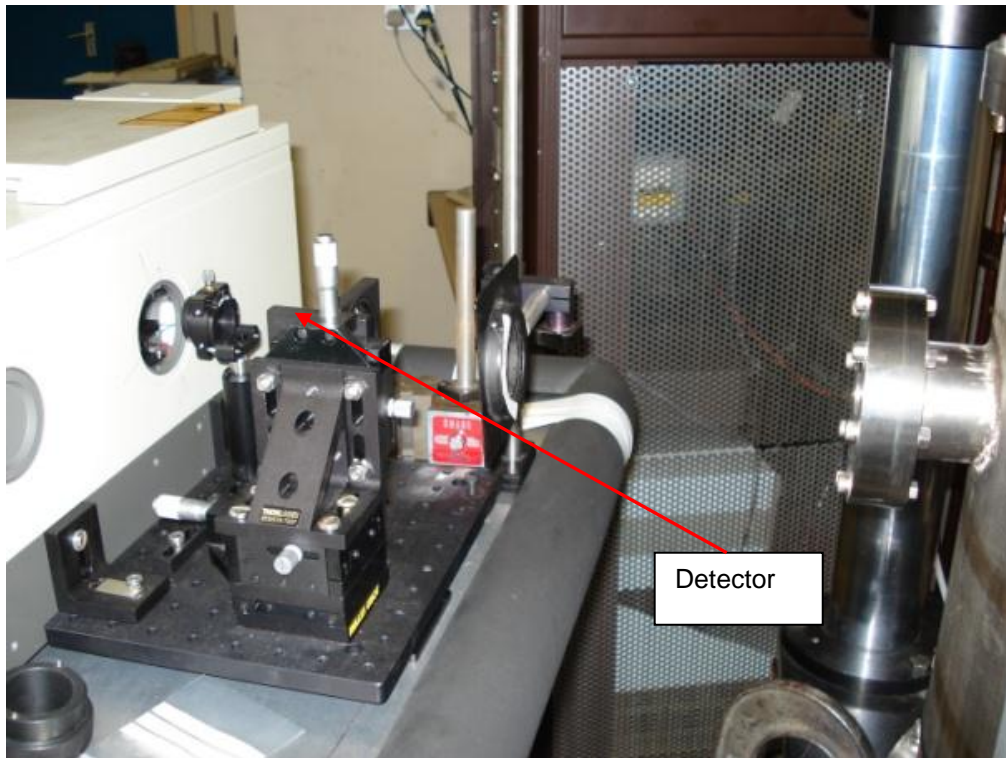


Figure 6.3.1d. The Emissivity Spectrometer / Detector (taken at the National Physical Laboratory – Teddington)

During an emissivity measurement, a zero value reading of emissivity ( $I_0$ ) is required to determine signal values and for this purpose initial readings are recorded with a white card placed over the vacuum chamber window. After the card is removed, the shutter signal is recorded while the furnace is lowered, before the shutter withdraws at speed to expose the sample surface for measurements. For measuring the blackbody hole, the procedure is similar, except that the periscope is re-aligned to target the blackbody cavity.

At each wavelength the signal versus time data can be fitted by a polynomial equation to find the signal  $I(\lambda, t)$  at  $t = 0$ , corresponding to the moment immediately before the removal of the shutter when the target was isothermal and at a known temperature,  $T_0$ , as measured by thermocouples planted inside

the graphite block. The spectral emissivity value is then given by the ratio of specimen signal,  $I_s(\lambda, 0)$  to a blackbody signal,  $I_B(\lambda, 0)$  by;

$$\epsilon(\lambda) = \frac{I_s(\lambda, 0) - I_0}{I_B(\lambda, 0) - I_0} \quad \text{Equation 6.3.1e}$$

Where;

$\epsilon(\lambda)$  Emissivity (at wavelength)

$I_s$  Specimen signal

$I_B$  Blackbody signal

$I_0$  Signal at  $T_0$

$T_0$  Known temperature

Using Planck's Law, the calculated emissivity can be adjusted as necessary to compensate for any initial temperature difference between the specimen and blackbody.

Emissivity tests were undertaken at a range of temperatures from 300°C to 1200°C, at 150°C intervals. This range and these interval steps were chosen because of the operating range of the carbon determined through the literature review and the previous testing knowledge of AP Racing.

### 6.3.2 Results from Emissivity Materials Testing

The results from the emissivity testing of the F1 carbon-carbon clutch material sample are summarized as follows:

Wavelength / μm	Temperature / °C						
	300	450	600	750	900	1050	1200
3.3	0.842	0.837	0.841	0.840	0.846	0.840	0.835
3.4	0.827	0.835	0.840	0.839	0.845	0.839	0.833
3.5	0.834	0.836	0.838	0.838	0.844	0.837	0.832
3.6	0.832	0.835	0.838	0.838	0.843	0.837	0.830
3.7	0.825	0.833	0.834	0.838	0.842	0.836	0.829
3.8	0.825	0.833	0.833	0.837	0.841	0.836	0.828
3.9	0.829	0.832	0.832	0.836	0.840	0.834	0.826
4.0	0.828	0.830	0.829	0.835	0.839	0.834	0.825
4.1	0.826	0.828	0.827	0.835	0.838	0.833	0.824
4.2	0.820	0.830	0.840	0.816	0.836	0.833	0.819

Table 6.3.2a. Normal Spectral Emissivity Results Obtained from Emissivity Testing at NPL, Teddington UK

As the emissometer operated through its range, the percentage uncertainty of the results obtained fluctuated. This is a calculated value from a look up table determined by the NPL at calibration of the emissometer, and is summarised in table 6.3.2b

Wavelength / μm	Temperature / °C						
	300	450	600	750	900	1050	1200
3.3	4.2	4.5	4.1	3.6	3.1	3.1	3.4
3.4	4.2	4.5	4.0	3.6	3.1	3.1	3.4
3.5	4.1	4.4	4.0	3.6	3.1	3.1	3.4
3.6	4.1	4.3	3.9	3.6	3.1	3.1	3.4
3.7	4.0	4.3	3.9	3.5	3.1	3.1	3.4
3.8	4.0	4.2	3.8	3.5	3.1	3.1	3.4
3.9	3.9	4.2	3.8	3.5	3.1	3.1	3.3
4.0	3.9	4.1	3.8	3.5	3.1	3.1	3.3
4.1	3.8	4.1	3.7	3.4	3.1	3.1	3.3
4.2	3.8	4.0	3.7	3.4	3.1	3.1	3.3

Table 6.3.2b Emissivity Measurement Uncertainty (Percent)

Usually the Radir IR sensor selected for the application of measuring the clutch temperature on the dynamometer is set up to provide results for perfect black bodies with an emissive value of 1. Even though carbon is considered to be very emissive, it is not perfectly so. From the emissivity test undertaken at the NPL at a range of temperatures from 300°C to 1200°C at 150°C intervals, it was determined that for these low temperature applications, an average emissivity was calculated to be 0.85 and using this value would allow the sensor to deliver accurate results for the face temperature of the plate.

#### **6.4 Dynamometer Adaptation for Accommodation of the Infrared Sensor**

The clutch dynamometer is usually used with both the driving and driven assemblies being free to rotate about their axis. The basket is mounted to the clutch motor and is driven at speeds which simulate actual engine speed. The actuation spring is engaged and disengaged using a pusher connected to the

braking assembly of the clutch, which calculates the output torque by measuring the resistance to the braking.

To enable the infrared sensor access to the plate faces, the two options were:

- Drill a hole through the clutch assembly to the face that is required to be measured.
- Using a variable acquisition detector and timing it to sample data when a set of holes are all aligned it would be possible to allow the temperature to be read on every set of interfaces.

Using the first method, it would only allow for the first interface from the basket end to be analysed. Due to the complexity of correlating the dynamometer speed with the data acquisition speed, and given the errors involved, it was decided to use the drilling method for the initial testing.

The method of drilling a hole in the back of the clutch has difficulties which needed to be overcome. Due to cabling issues and the relatively large size of the detector when compared to a thermocouple, it is required that the detector remains stationary. Previously there had been problems with small thermocouples becoming detached from the rig at high velocity. It was imperative that the infrared detector (which weighs and costs a lot more than a small thermocouple) was not allowed to come loose from its fixings and be able to cause damage to surrounding components.

For the sensor to remain stationary, there were two options:

- The sensor would capture clutch data at set intervals, where the acquisition rate is correlated with the speed of the clutch rotation.
- The basket of the clutch would also remain stationary.

The first option only allows for one clutch speed to be used due to the fixed acquisition speed sensor, so the option of holding the basket stationary became the best choice if a full range of delta speed results were to be obtained. As a result of these requirements the clutch dynamometer had to undergo adaptations



including the re-designing of fixtures, alternative modes of operation and the modification of the clutch itself. Each of these items is now explained in turn.

## 6.5 Dynamometer Rig Modifications

As discussed earlier in this chapter, the clutch rig works by spinning the basket end to the required speed, applying a load to the spring via an actuator, clamping up the stack of carbon and transmitting a load from the driven to the driving plates. This method of clutch actuation means that the basket is spinning, and the internal drive plates are stationary until slip begins between the two sets of plates. By inverting the clutch on the rig, and mounting the basket so that it is stationary, it is possible to drill a slot in the back of the basket and the first pressure plate to provide an optical route through onto the first plate interface, as shown in figure 6.5a.

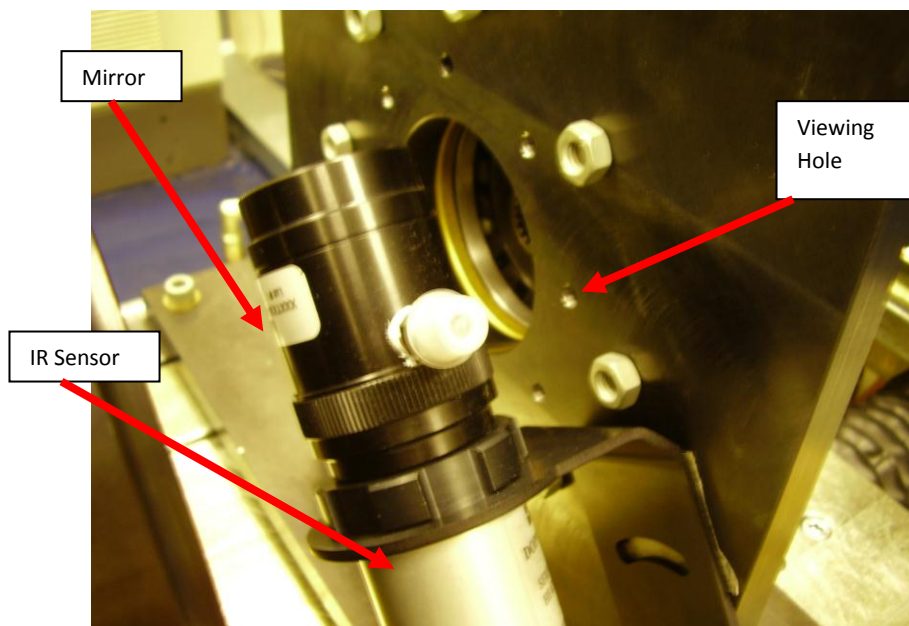


Figure 6.5a. Infrared sensor configuration on the adaptor plate for the clutch on the dynamometer (taken during initial testing)

An overall view of the final adapted test configuration is shown in figure 6.5b. In normal test conditions, the clutch (c) is mounted directly onto the drive torque motor (a), and spins with it. The intermediate plates (those which are driven by the lugs of the clutch) remain stationary in relation to the drive plates, with the

actuator (d) engaging and disengaging the clutch by pulling and pushing on an actuating spring. The output torque is measured using the resistance to a brake connected to an output shaft mounted on the drive hub. As the clutch begins to engage, the intermediate plates move, and a torque is transmitted and measured at the brake.

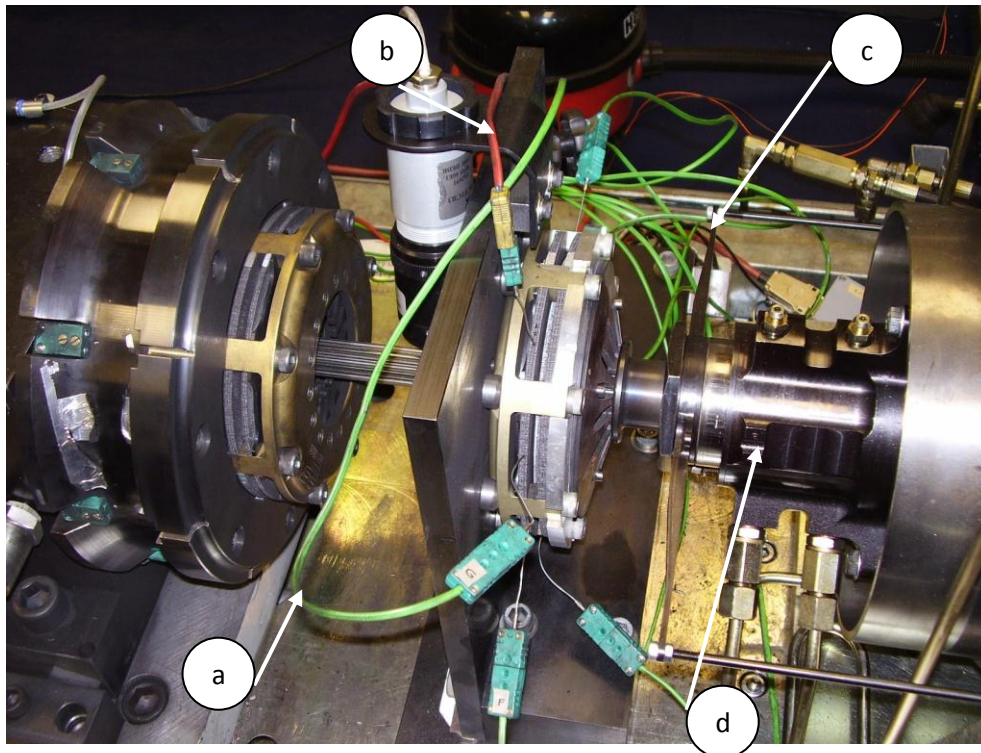


Figure 6.5b. a. Drive torque motor, b. Body of infrared sensor, with right angled mirror attached, c. Clutch assembly, d. Actuator (taken during initial testing).

In the adapted test, the basket and drive plates remained stationary and the intermediate plates were driven, using an output shaft driven by the drive torque motor. The clutch was actuated using the actuator (d) acting upon a plate (seen on the right hand side of the clutch (c) in figure 6.5b), which compressed the carbon stack together, and eliminated the use for the traditional use for the actuating spring and fulcrum ring on which it can pivot.

However, the actuating spring was used in a different manner; this was placed between the actuator plate and actuator (as seen in figures 6.5c and 6.5d), and a small level of cushioning between the plate and the actuator was provided. Without the spring, when the actuator was used to clamp up the carbon stack it

moved and came to an instant halt when the stack clamped up. The sensor and software feedback loop is programmed to protect the equipment, so when a solid resistance is met the actuator will automatically back away as it believes that it has hit a solid object and that continuing with the force will only cause damage. This could have been overcome by changing the protection parameters within the rig software, but the addition of a spring meant that resistance was gradually met as the actuator moved and the clamp load was applied.

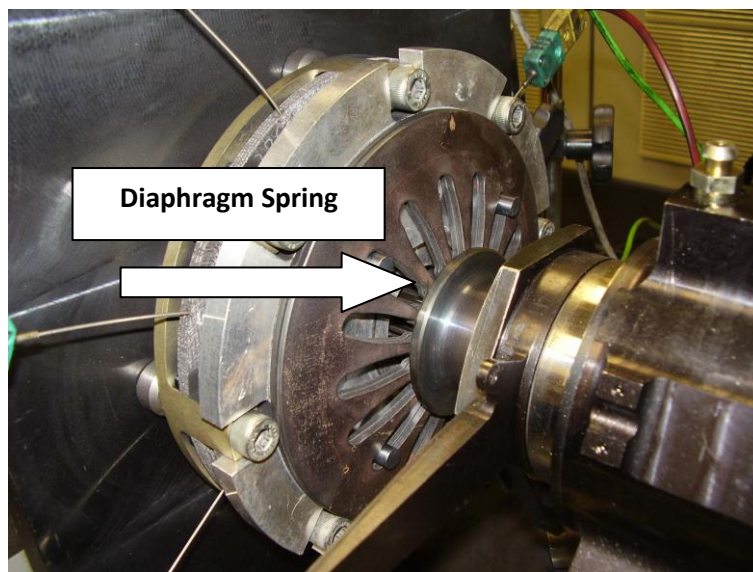


Figure 6.5c. Spring Cushioning between Actuator Plate and Actuator

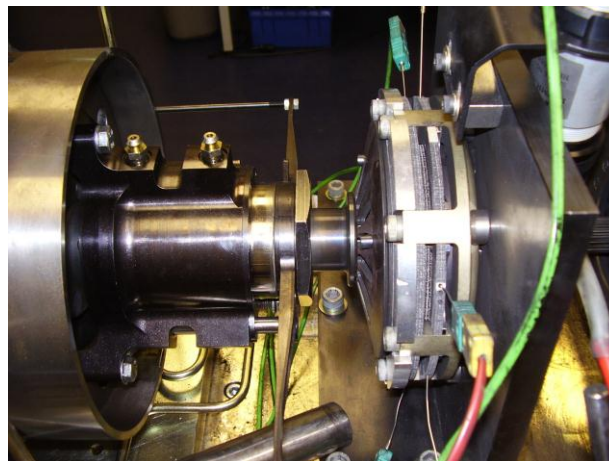


Figure 6.5d. Overview of Spring Cushioning between Actuator Plate and Actuator

By using the fulcrum spring to cushion the pressure, it allowed the clutch to be gradually clamped up, and with the majority of the clutch assembly held

stationary it was imperative that the clutch did not completely lock up and transmit the full torque, as this could have resulted in a catastrophic failure.

To allow thermocouple data and IR data to be captured at the same rate, the IR sensor was connected to the dynamometer using K-type thermocouple fittings. K-Type thermocouples are a standard type of thermocouple, and have a range of -200°C to 1250°C with a 0.75% or 2.2°C error (whichever is the greater of the two). This allowed the data from the IR to be seen by the dynamometer software package as though it were a thermocouple.

A selection of drawings for the test apparatus and parts can be found in Appendix C.

## **6.6 Structural FEA modelling of the adapted dynamometer test rig**

To ensure that the adapted parts were of a safe and durable standard, FEA analysis of these parts was undertaken. Structural modelling was carried out because it was important to validate the design of the rig adaptation components. By using FEA, it was possible to check that the designs were going to withstand the loads that it would be exposed to. Applied loads are illustrated by the purple arrows, while the constraints are indicated by the green arrows, as seen in Figures 6.6a to 6.6e.

The main test plate was analysed using the FEA package Cosmos in SolidWorks. The material properties for the aluminium were set from the database within the package. The base was fixed, as illustrated by the green arrows in figure 6.6a, and a rotational force was applied to the bolt holes where the clutch would affix to the plate. The magnitude of the force was calculated by using the 'worst case' scenario of complete lock up at 20,000 rpm with a clamp load of 3,500N.

A range of FEA analysis was undertaken to ensure that the proposed plate design was capable of safely constraining the clutch under the test conditions. These analyses included;

- Test plate deformation
- Test plate displacement,

- Factor of safety.
- Von Mises Stress

This series of FEA analyses gave confidence that the design of the adapted rig components was adequate, with maximum displacement of 0.5mm, a minimum factor of safety of 5 and maximum Von Mises Stress of 112 MPa. In the event that the worst should have happened and total lock up and torque transfer occur at the highest speed and clamp load, then the component would have been able to withstand this event and protect the clutch and clutch dynamometer.

## 6.7 Clutch Adaptation

This section focuses on the adaption of the clutch itself for the purposes of the experimentation. An F1 clutch is very small, and contains several interfaces, and it is impossible to measure the face temperatures on all of the faces simultaneously. Due to this, the clutch to be measured and the rig on which it was measured had to be significantly modified in order to gain access to the plate faces for the infrared detector to take readings.

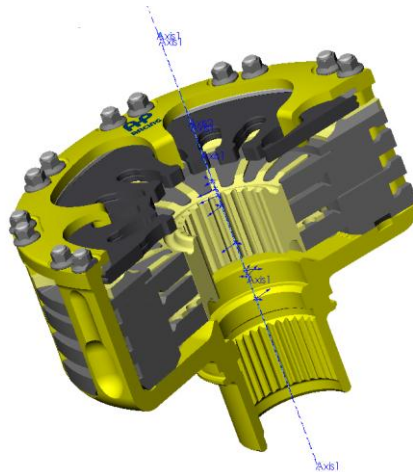


Figure 6.7a. A typical AP Racing multi plate clutch arrangement (Solidworks screen grab) .

For the initial testing, a larger 140mm diameter, clutch with the same friction material as the F1 clutch was used. Technical information on this clutch is given in Appendix D. The purpose of this was to allow for a bigger radius over which a

temperature could be observed in order to obtain more radial data, to enable a more accurate heat profile to be determined. This increased diameter also allowed for more flexible designs for rig adaptation, and an increase in surface area of the clutch. This enabled expansion of the available surrounding area allowing for more sensors and components to be utilised.

Due to the unique method of drive and actuation, the clutch assembly itself had to be adapted. The new clutch required spacers between the clutch basket bolting points (as shown in Figure 6.7c) and the backing plate of the clutch installation assembly to allow for a completely flat contact between the clutch and the rig. The springs and fulcrum ring were also removed and replaced with a spacer. These components were no longer needed as the new configuration clutch was to be actuated away from the basket end. Figure 6.7b and figure 6.7c show exploded diagrams of how the clutch was adapted. In figure 6.7b, it can be seen that most of the components rotate (as indicated by the red dot), but the modifications to the clutch configuration seen in clutch 6,7c mean that far less of the components rotate, therefore allowing the basket to be held stationary.

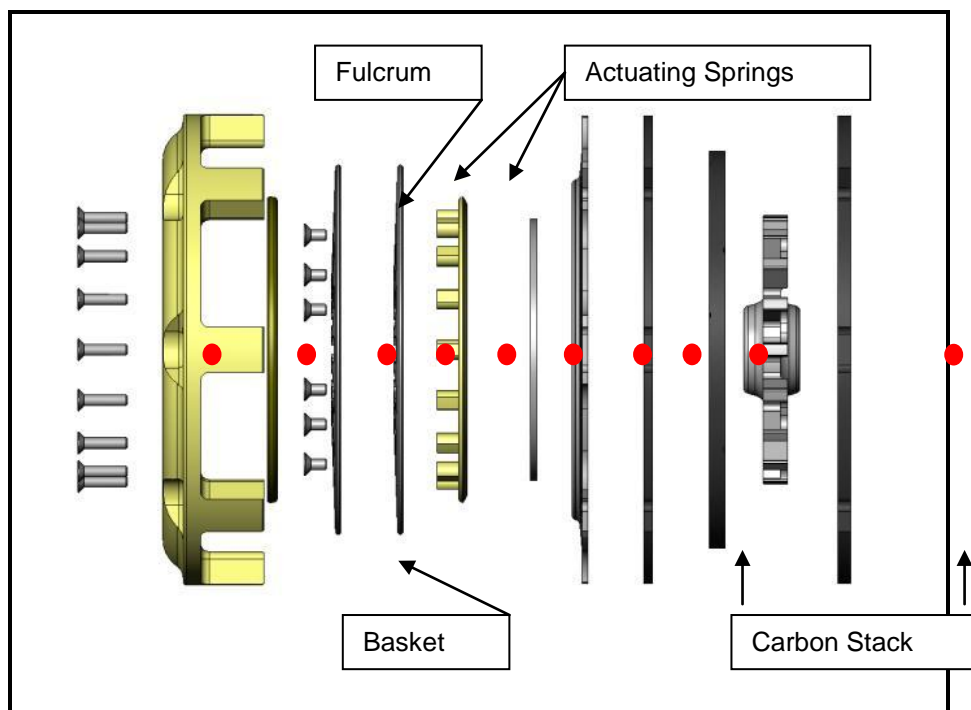


Figure 6.7b. The Old Clutch Configuration prior to modification (parts with a red dot rotate)

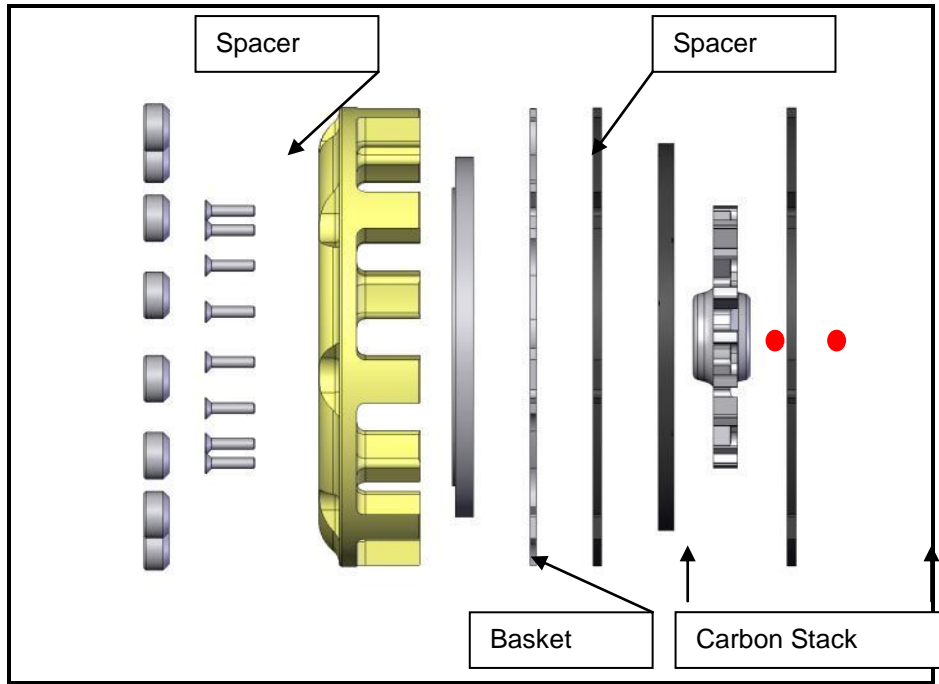


Figure 6.7c. The New Clutch Configuration after modification (parts with a red dot rotate)

## 6.8 Experimental Validation of Initial Set Up

One of the biggest difficulties of testing the clutch ‘back-to-front’ was to determine whether it would be possible to accurately determine the torque output, as this is normally measured using the resistance against a braking device. As the output shaft would not be spinning with the revised clutch arrangement, there would be no resistance and effectively no torque output.

To overcome this, a torque sensor was mounted on the input shaft. To test this, the input torque was measured along with the output torque during a range of dynamometer tests. The results showed that the two data traces were comparable and that the input torque trace was suitably accurate to use in testing.

### 6.8.1 Analysis of Validation Test Data

Using the proposed test configuration, a graph (figure 6.8.1a) was plotted of the drive torque compared with the output torque against time. From this graph, a number of observations can be made:

1. The output torque does not commence zero at the beginning of the test – this implies that there is a small error in the sensor calibration.
2. Once the clamping load has been set, the two data traces follow the same path, although the output torque trace was very noisy.

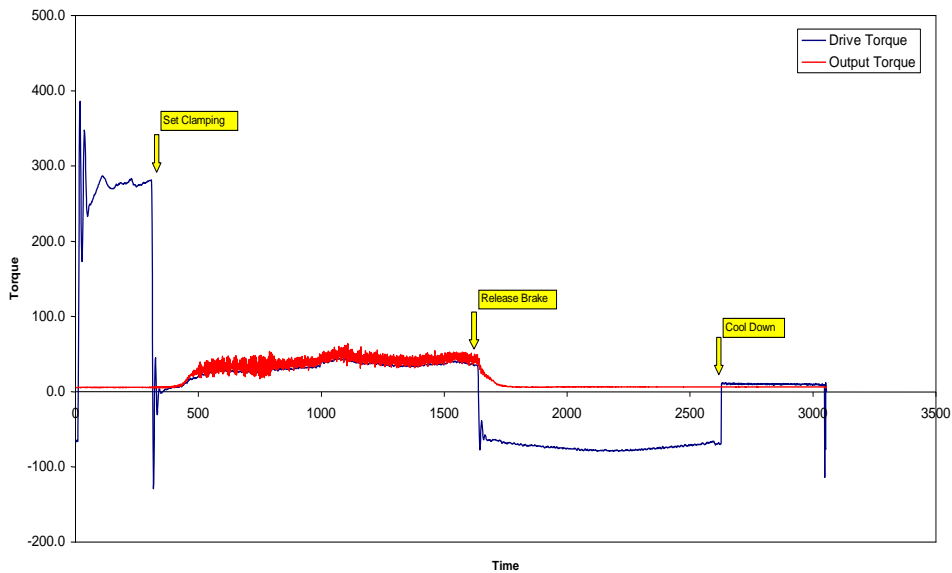


Figure 6.8.1a. Drive Torque Vs. Output Torque.

A closer inspection of the clamping event from graph shown in Figure 6.8.1a showed that the noisy output torque trace follows that same path as the drive torque trace, apart from that it is offset, as seen in Figure 6.8.1b. This implied that the output torque is higher than the input torque, which is not possible in the configuration that is being tested. This can be explained by inaccurate calibration, a theory which is reinforced by the first graph, which showed that the output torque sensor did not appear to have been set to zero before the test. By offsetting the input graph by the torque value at  $T=0$ , the two graphs then matched. This also highlighted the importance of calibrating and zero-ing the sensors before each test run.



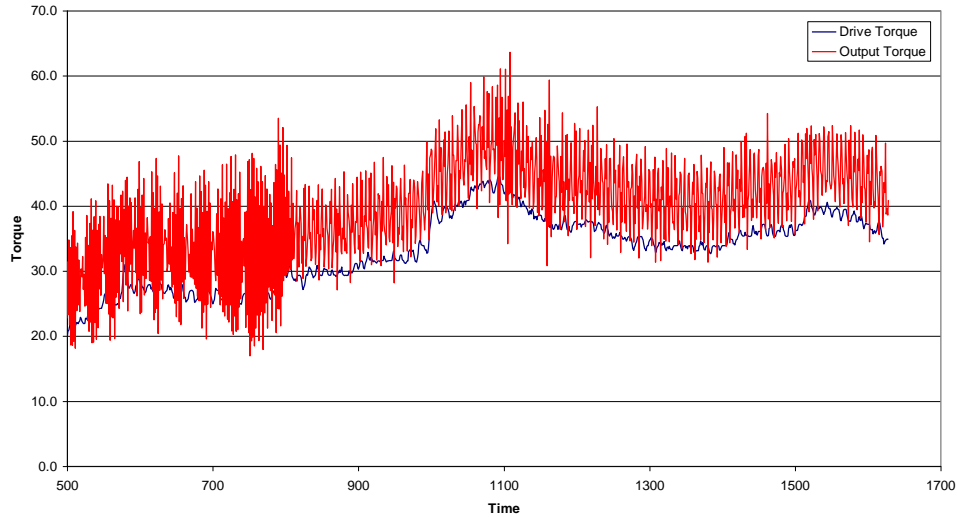


Figure 6.8.1b. Drive Torque Vs. Output Torque During Clamping.

Initially there were a few installation problems with the two torque devices, and the output torque was reading marginally higher than the input torque, and was also very 'noisy'. By back-checking the instrumentation, and through observation of the red trace on Figure 6.8.1a (which reads an offset before the clutch is even clamped) it was possible to observe that the output sensor had not been properly calibrated, and was reading an offset value of 6Nm. The noisy data was filtered using averaging over ten data points, representing 0.1 seconds, and once this had taken place the two data traces were similar enough to construe that the output torque trace could be used in place of the input torque trace.

A particular hazard of filtering is that certain samples are effectively 'wiped out' in a phenomenon known as 'aliasing'. This is where the filter applied is a multiple of a frequency of occurrence within the data, and thus the samples are either always only seen, always never seen, or seen at a rate of multiples of its true existence. This was accounted for in this particular application by the comparison of the original data to the filtered data, but can never be ruled out from the initial data sampling from the sensor itself.

## 6.9 Test Plan

The aim of this initial test was to gain a profile of how the infrared sensor compared to the thermocouple over a range of temperatures, clamp loads and input speeds, as well as to gain data of how the surface temperature changes. This could then be compared to the output torque and a relationship between the two can be determined.

During the tests, the initial temperature soaking of clutch plates allowed for rate of thermal conductivity to be observed and gave an insight into the rate of change of the surface temperature with relation to the core temperature. The energy rate was varied by changing the torque, so that its effects could be determined. The test matrix used for this can be observed in Table 6.9a.

Clamp Load ►			
Temp ▼	1500N	2500N	3500N
100°C	3000rpm	3000rpm	3000rpm
	7000rpm	7000rpm	7000rpm
200°C	3000rpm	3000rpm	3000rpm
	7000rpm	7000rpm	7000rpm

Table 6.9a. Test Plan for varying initial temperatures, clamp loads and input speeds

A range of slips at a constant torque and speed deltas were completed from a range of initial temperatures. Torque, input speed, release bearing position, thermocouple temperature and IR sensor temperature were to be recorded. Each test was terminated by temperature trip at a 500 °C thermocouple reading. Thermocouple temperatures were used as 'trip' temperatures as it was uncertain what surface temperatures would be seen during the test situation. A 500°C thermocouple trip temperature was known from historical clutch data to be a 'safe' temperature which would have not allow the clutch to overheat, but still permitted a wide range of data to be accumulated.

Using varying thermocouple radii on the pressure plate allowed for the effects of heat travel to be observed through the carbon radius and for its effects to be

logged. Thermocouples were embedded at radii of 54mm (thermocouple 1), 56mm (thermocouple 2), 58mm (thermocouple 3), 60mm (thermocouple 4), 62mm (thermocouple 5), 64mm (thermocouple 6) and 66mm (thermocouple 7) (figure 6.9b).

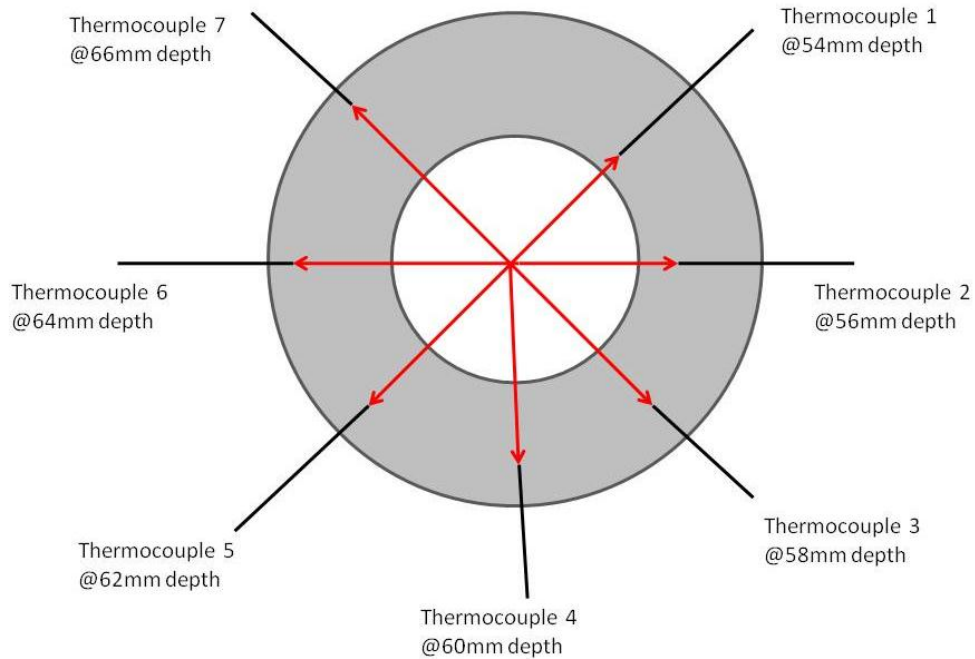


Figure 6.9b. Thermocouple Radial Depth Locations

The infrared camera was initially placed at the minimum radius of 54mm and a slot was drilled so that the infrared camera could read a range of radii up to 66mm in preparation for the next round of testing.

## 6.10 Results

Graphs from all initial test runs can be seen in appendix E.

The purpose of the initial test work was to determine the equipment and test method, and so the results of this initial work were used to ensure that all the equipment was functioning as expected. There were still problems which had to be solved in terms of both the temperature and torque analysis and each turnoff these will be considered in turn.

### 6.10.1 Temperature Analysis

During the tests, thermocouple two malfunctioned and did not give any readings. However, the remainder of the thermocouples yielded some interesting results. Thermocouple 4, which was at the mid radii of the plate, consistently experienced the highest temperatures, with thermocouples 3 and 5 showing the next highest temperatures, with 1 and 7 showing the lowest readings. It is also suspected that thermocouple 6 was defective, as it consistently exhibited substantially lower temperatures than the others. Graph 6.10.1a is taken from a 7000rpm test with a soaked temperature of 200°C and applied force of 3500N. This graph highlights the patterns of heat flow throughout the radius of the clutch plate as it undergoes a slip.

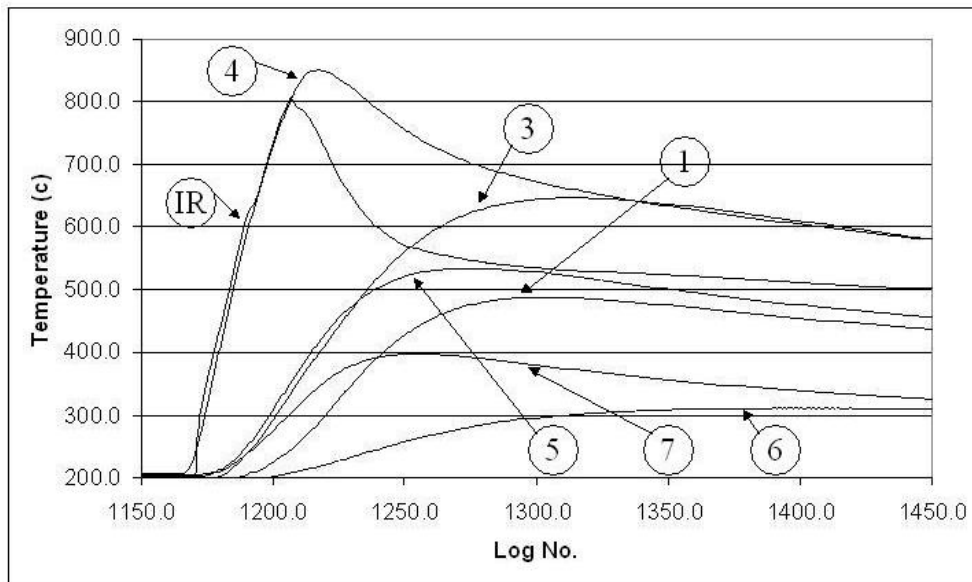


Figure 6.10.1a. Thermocouple Profile

It is also interesting to note from graph 6.10.1a that the infrared camera does not yield results of temperatures higher than those for thermocouple 4. This was not necessarily the case for all of the slips and graphs 6.10.1b and 6.10.1c show how the infrared readings compare to the highest thermocouple readings at 100°C and 200°C respectively. Starting from the left, the bars represent the following conditions:

- 1500N applied force, 3000rpm (red)
- 1500N applied force, 7000rpm (orange)

- 2500N applied force, 3000rpm (yellow)
- 2500N applied force, 7000rpm (green)
- 3500N applied force, 3000rpm (blue)
- 3500N applied force, 7000rpm (purple)

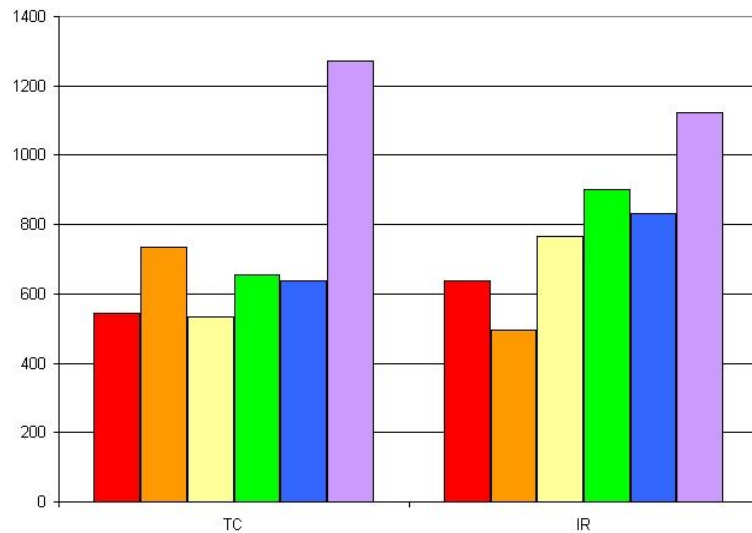


Figure 6.10.1b. Infrared vs. Thermocouples at initial temperature of 100°C

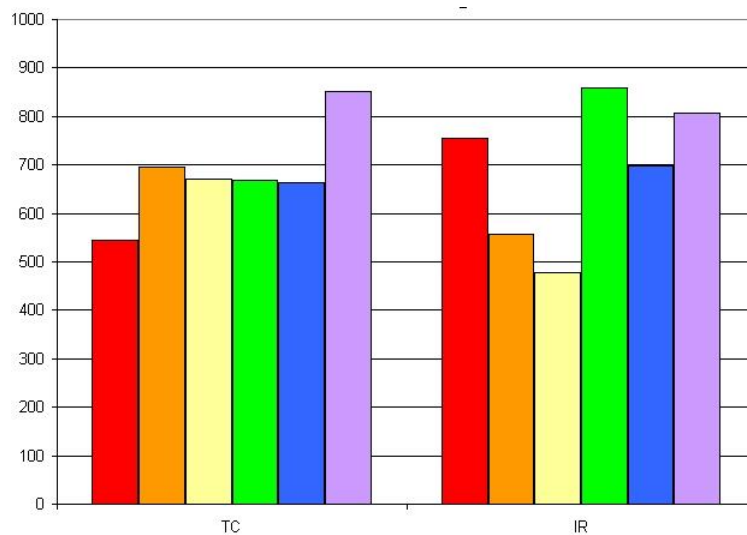


Figure 6.10c. Infrared vs. Thermocouples at initial temperature of 200°C

The infrared camera works by taking an average temperature over a spot. This spot converges to 2.5mm at a distance of 76mm, before increasing to 4.6m at 92mm, and beyond. These results infer that the sensor may have been taking an average of the carbon temperature and the temperature of any tooling upon

which the beam came into contact with. This would have simply caused the infrared camera to read lower temperatures than the carbon was experiencing, but it would have affected all of the infrared results in the same manner which, as shown by figures 6.10.1b and 6.10.1c, is clearly seen to not be true.

Conversely, the apparent 'randomness' in the differences in the readings between the highest thermocouple reading and the infrared camera could be explained by the occurrence of banding. As banding itself is a randomly occurring act, it is impossible to predict at what radius it will occur next, and how thick the band will be. If the IR camera were pointing at a hot band, then the temperature reading would be significantly higher than the reading for the thermocouple. When the IR sensor was directed far away from a band, the IR temperature would appear lower than that for a thermocouple; especially if the thermocouple was located directly underneath the band.

Banding is a known phenomenon that occurs on the surface of a brake disc, during a braking event. This happens due to the fact that the discs and the pads are never 100% flat and have slightly raised areas which stand proud from the surface. At the first braking event (stop one) these areas will make contact first and so will get hotter than the rest of the disc, causing the banding effect seen in figure 6.10.1d. As the material gets hotter, it expands and so these areas will continue to take the full energy loading during this braking event. After the first stop when these areas are allowed to cool, they contract and cause a valley on the surface of the disc as the loading of this initial event has worn away some of the disc material. This means that at the next stop the material that was in the hot band at the first stop is now in the cool band in the second braking event, because it sits lower than material which was in the cool band during the first stop.

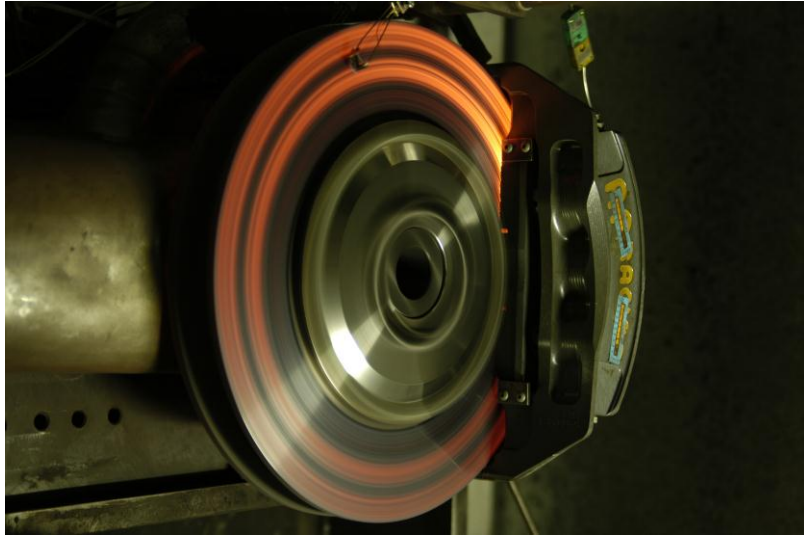


Figure 6.10.1d. Brake Banding Taken on the brakes dynamometer. (Courtesy of AP Racing)

It has been suggested that banding occurs on the surface of a clutch plate, in a very similar way to how it occurs on a brake disc, and this may go part way into explaining the apparent ‘random’ characteristics that are seen when comparing the IR temperatures to those of the thermocouples.

### 6.10.2 Torque Analysis

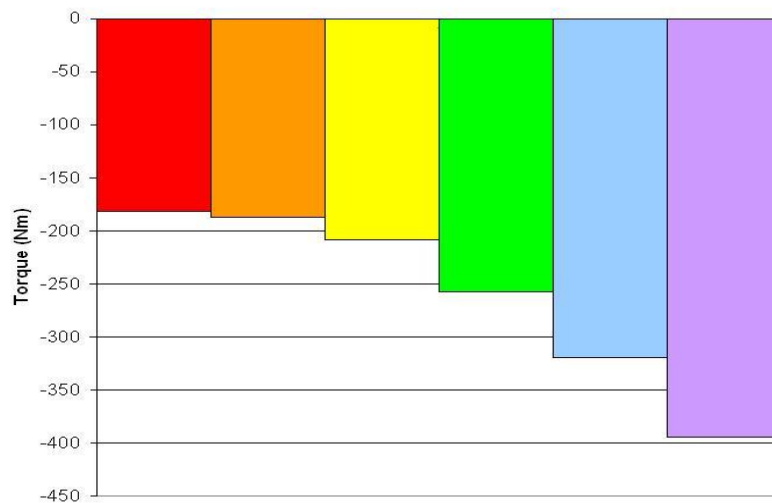


Figure 6.10.2a. Torque analysis at initial temperature of 100°C

Figure 6.10e shows how the maximum torque output varied for each condition of a 100°C start temperature slip. Starting from the left, the bars represent the following conditions:

- 1500N applied force, 3000rpm (red)

- 1500N applied force, 7000rpm (orange)
- 2500N applied force, 3000rpm (yellow)
- 2500N applied force, 7000rpm (green)
- 3500N applied force, 3000rpm (blue)
- 3500N applied force, 7000rpm (purple)

The torque values appear as a negative, due to the reversed configuration of the clutch on the rig, as described earlier.

The torque output increases with the applied load, at 3000rpm, a 75.7% increase in transmitted torque was observed when increasing the applied force from 1500N to 3500N. At 7000rpm, this was much higher, with an increase of 110.5% between the two applied loads.

What is also interesting to note is how much the torque varies with the increased speed. For the 1500N applied force, this difference is only 3%, but for the higher loads the difference caused by the 133% increase in speed is a 19% increase in torque.

The torque was observed to 'spike' upon initiation, which is a natural effect of the initial bite of the clutch material. This 'bite' varies from clutch to clutch and relies heavily on the material and method of load initiation.

### **6.10.3 Torque vs. Temperature Analysis**

Using data from a variety of test parameters and plotting the temperature against the torque, it is possible to observe the relationship between the two. Data from the highest reading thermocouple (4) was compared to torque data gained from the motor.

Figure 6.10.3a shows how the torque varies with the temperature over a range of slips from a start temperature of 100°C. The numbers on the graph indicate the slips as follows:

- 1 = 1500N applied force, 3000rpm
- 2 = 1500N applied force, 7000rpm



- 3 = 2500N applied force, 3000rpm
- 4 = 2500N applied force, 7000rpm
- 5 = 3500N applied force, 3000rpm
- 6 = 3500N applied force, 7000rpm

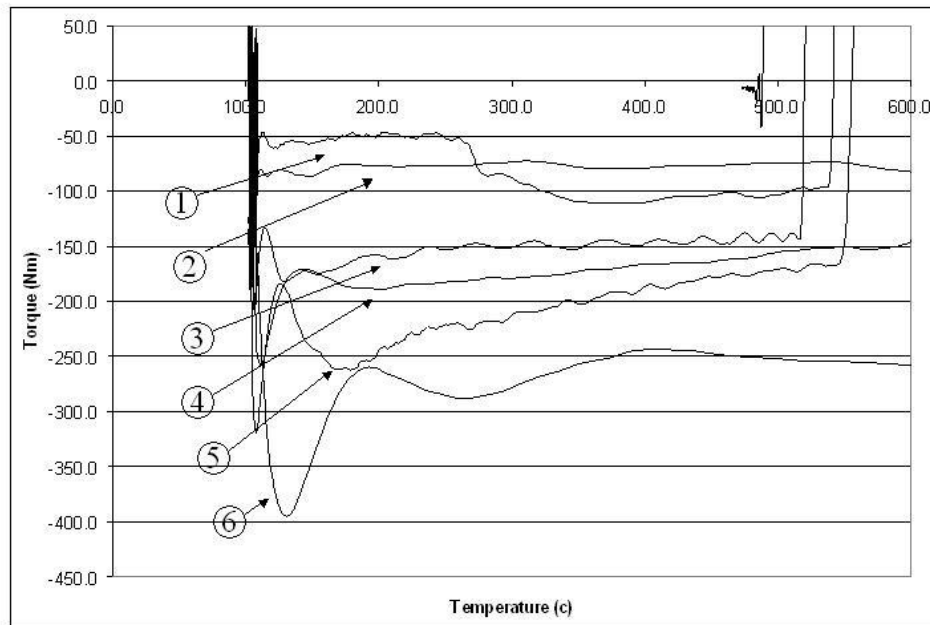


Figure 6.10.3a. Torque vs. temperature analysis from initial temperature of 100°C

For the period of the slip, it can be observed that both the applied force and the clutch speed have an effect upon how much torque is transmitted at what temperature. It is not easily observed if there are any effects upon the torque that are as a result of this rapid increase in temperature.

On the cool down period after the slip has taken place, the relationship becomes clearer. Figure 6.10.3b indicates the presence of the effects of temperature upon the output torque in the cool down period from a slip at 7000 rpm, with an applied load of 3500N and initial soak temperature of 100°C. As the heat within the clutch plate dissipates from approximately 850°C to 180°C, it can be observed that the output torque reduces from 340 Nm to 300 Nm.

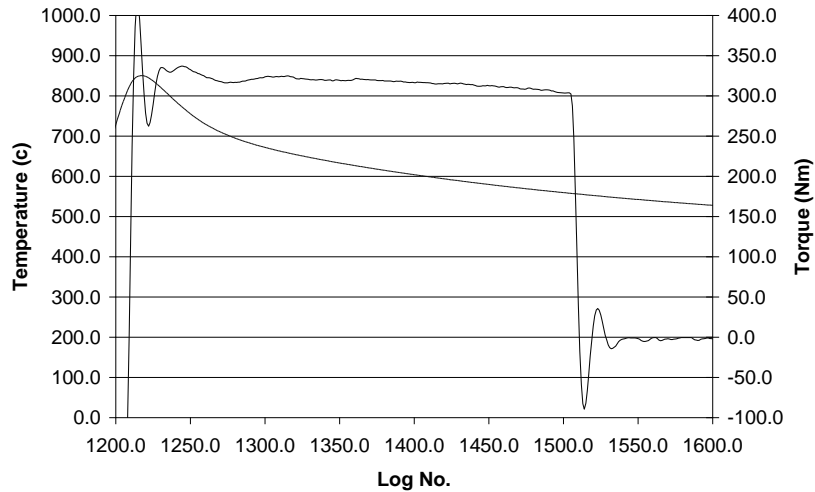


Figure 6.10.3b. Torque vs. temperature analysis during the 'cool down' phase from a 7000rpm, 3500N slip with initial soak of 100°C

This trend continues throughout the data sets for all speeds giving an average of an 11.45% decline in torque for a 39.19% decline in temperature, and can be seen in table 6.10.3c, which illustrates how the torque was affected with the heat decline for the runs performed in the initial testing.

	High Temp	High Torque	Low Temp	Low Torque	% heat diff	% torque diff
1500N_3000rpm	535.8	128.6	372.9	111.6	-43.68463	-15.232975
1500N_7000rpm	710.6	330.3	504.5	318	-40.85233	-3.8679245
2500N_3000rpm	523.4	125.8	501.9	103.3	-4.283722	-21.78122
2500N_7000rpm	636.48	324.7	457.2	304.9	-39.2126	-6.4939324
3500N_3000rpm	657	132.7	532.5	119.4	-23.38028	-11.139028
3500N_7000rpm	1119.6	337	609.3	305.8	-83.75185	-10.202747

Table 6.10.3c. Percentage heat reduction and its effects on the reduction in torque from initial testing.

#### **6.10.4 Infrared Sensor Alignment**

During the initial testing the IR readings were observed to be sporadic and inconsistent. After further investigation it was understood that the IR beam was misaligned and too far away from the clutch plate area that it was trying to measure. This meant that the target spot emitted by the IR wasn't only 'seeing' carbon but also had some of the (relatively cold) mild steel bracket in its field of view. As the IR detector takes an average reading of the temperature seen in its field of view, the increased distance meant that this field of view was larger than it should have been and was also including areas of mild steel causing the average IR readings to be lower than expected.

The IR detector used was of a converging / diverging type, meaning that it focused to a spot size of 3.5mm at a distance of 76mm from the sensor lens. This 76mm path length did not necessarily need to be in one straight line and mirrors could be used to reflect the beam at an angle so the IR sensor did not necessarily need to be in the direct line of sight from the target. The bracket that held the IR sensor was modified as a result of the first round of testing with more secure fixing points and was made to tighter tolerances to ensure that the sensor remained aligned throughout testing. This ensured that the target spot was exactly the correct distance from the sensor to allow for only carbon to be seen in the sensors field of view.

Once the distance was correctly set, the beam was then aligned using a mirror, a laser pen and a smoke machine. The smoke machine generated smoke so that once the laser pen was switched on the laser path could clearly be seen. Using a mirror positioned at 90 degrees to the clutch mounting plate to reflect the beam back on itself, the sensor was aligned. To ensure that the sensor stayed correctly aligned, score marks were placed on the sensor and bracket, for a quick visual reference to ensure that the sensor had not been knocked or moved and so that it could be accurately realigned very quickly.

## **6.11 Conclusions and Recommendations for Further Experimental Work**

In the middle of the plate, there is more radial distance for the heat to dissipate through. When comparing thermocouple pairs, for instance 7 and 1 - which are at equal distances from the outer and inner radii respectively, temperatures always showed that the thermocouple that is on the outer radius is lower in temperature. This is partly due to the inclusion of the titanium spline hub, which is located at the inner radius of the plate. This hub retains heat, and also blocks the airflow to the inner radius, meaning that heat build-up occurs.

Testing also hinted that banding does occur within the clutch, due to the unpredictability of the relationship between the maximum thermocouple temperature and the infrared temperature readings despite the consistent positioning of both the IR sensor and the thermocouples. This strongly suggests that banding is occurring, although at this point further testing was required to determine the extent to which this happens. IR sensor alignment appeared to be inaccurate due to inconsistent readings from the infrared sensor. It is imperative that the infrared beam is at the optimal distance and can read the plate temperature clearly. The initial testing highlighted the requirement for an accurate method of alignment which could be relied upon to give an accurate result

The initial soak temperature did not appear to have an effect upon the output torque of the clutch, and in turn, the friction. At low energy slips, there was approximately 0.294 percent change in the torque for every percent change in temperature. It must not be assumed that this relationship is completely linear and this was explored further in the next stage of testing. Further investigations into high energy slips would add supplementary clarification to the relationship. More testing need was needed to determine further effects of increasing the clutch speed as F1 engines can rotate at up to 20,000rpm, it is critical that this effect is understood.

Although it is acknowledged throughout the industry that the temperature does have an effect upon the output torque (and hence the friction) of a carbon clutch, it is hard to put an exact figure on how much this occurs. Phenomena such as banding and material wear characteristics will always have an influence upon how the carbon heats and cools and will consequently also have an effect upon the overall friction co-efficient.

By collecting and using the thermocouple readings in addition to the infrared camera during the experiment meant that it was possible to relate the thermocouple data back comparing it to archived results and looking up its respective surface temperature. In theory, this allows a very broad collection of historical data to also be used for analysis, should a predictable relationship between the thermocouple and surface temperatures be determined in the next round of testing.

## **Chapter 7**

### **Experimental Testing**

This chapter discusses the experimental work and conclusions upon the effectiveness of the solution and results obtained.

The objective of this experimental work was to build upon the information gathered from the initial testing, and to develop the results so that they could be used, along with the material properties, as a starting point for developing and then validating the mathematical model. During the initial testing it was also hinted that banding may have played a part in the unusual results pattern and so an experiment to account for this was also introduced with the intention of using the information to gain a greater understanding of how much of an effect that banding really plays within the clutch, and its role within the friction / temperature relationship.

#### **7.1 Adaptations from the Initial Testing**

N.B All part drawings can be found in Appendix C.

##### **7.1.1 Experimental Investigation into the Effects of Banding**

During the initial testing it was hinted that banding may have played a part in the unusual results pattern and so an experiment to account for this was also introduced. By using 'enforced banding' through a series of machined plates, it was possible to ensure that the contact between plates was in this enforced banded area only. With this addition of 'banding' analysis to the testing, it was required that a quick and repeatable way be designed so that when the infrared sensor was moved radially, it was accurately aligned with the band which it was trying to measure. Using a nominal band width of 4mm (the IR detector spot size) band radii were selected, with reference to the bands inner radius (IR) and outer radius (OR) being 2mm either side of the mid radius. A series of marks was scored onto the back of the plate (see part number ct1207-101 in Appendix B) to measure predetermined mid-point radial locations of:

Plate	Internal Radius	Mid Radius	Outside Radius
A	52mm	54mm	56mm
B	54mm	56mm	58mm
C	56mm	58mm	60mm
D	58mm	60mm	62mm
E	60mm	62mm	64mm
F	62mm	64mm	66mm
G	64mm	66mm	68mm

Table 7.1.1a. Radial locations of the enforced bands

These radial locations were determined by the inside and outside radii of the friction surface of each plate, coupled with the 4mm wide band (determined from the focal spot size given by the IR sensor). By simply putting the inner radius of one band immediately next to the outer radius of the previous band would have given only 4 different band widths. However, by using a 2mm overlap seven band radii were established, which would give a larger spread of results. By machining 4mm wide bands onto the face of the plate at different diameters, it was possible to observe the effects of banding. An example of a plate with enforced banding is shown in figures 7.1.1b and 7.1.1b.

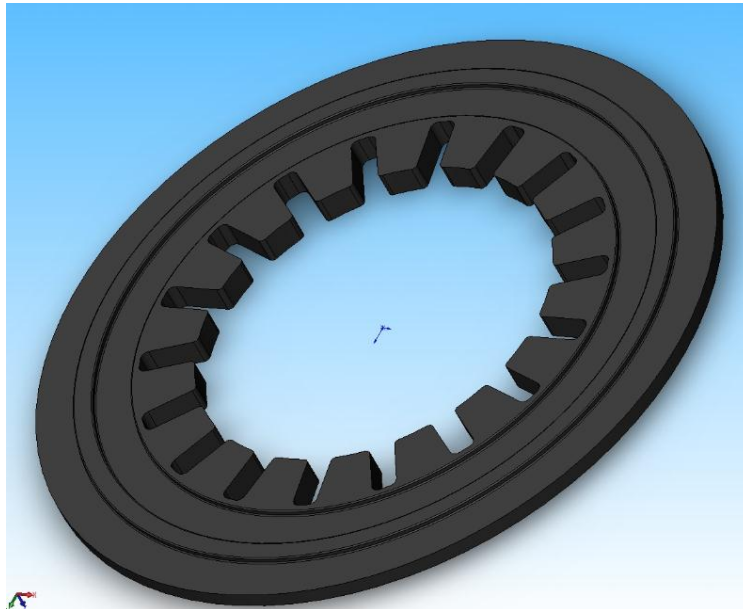


Figure 7.1.1b. SolidWorks Model of a Typical Banded Plate

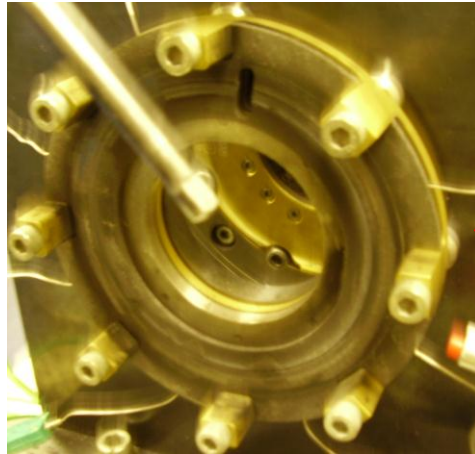
As each band was located at a different effective radius, it was hoped that it would be possible to analyse the results from each banded test to give a profile of where banding was occurring in the 'normal' flat plate of a race clutch, as used for the initial testing.



Figure 7.1.1c. A Typical Plate with enforced banding as used in testing

An extensive installation run was undertaken with one sample of the banded plate and this highlighted a minor design problem; initially the banding was only enforced on one side of the plate, and this had detrimental effects. Due to the elasticity of the plates and the pressure that was being applied to the carbon stack, the 1mm raised band cut away a groove in the carbon on the drive plate with a mirrored profile of that seen on the driven plate, as seen in figure 7.1.1d. This then meant that the temperature measured by the IR sensor was not representative of that observed on the band alone, because a) the band was cut out anyway, causing all of the plate area to remain in contact and b) the non-banded face (i.e. on the back) of the driven plate was still experiencing 'random banding', as would be seen on a standard driven plate, so effectively the banding was not being controlled in any way.





Worn Band in  
Drive Plate

Figure 7.1.1d. Damage Caused by the Cutting out of the Material by the Enforced Banding Plate

As a result of this more drive plates were ordered to allow for replacement should any possible grooves be worn into them during the slipping process. Using three different sets of drive plates, the banded areas which would be in contact with them were staggered so that they did not interfere with each other. This was considered to be sufficient for the tests as the reduced amount of time that each banded driven plate would come into contact with the drive plate in comparison to the installation run meant that minimal (if any) grooves would be worn into the drive plate. Drive plate set 1 was used for plates with band radii of 54mm 60mm and 66mm, set 2 was used for band radii 56mm and 64mm, and set 3 was used for band radii 58mm and 66mm.

Only the drive plates at the basket end interface (interface 1) were banded, with the rest of the clutch remaining in a standard configuration. To combat the random banding effect on the other side of the driven plate, the drive plates were sent away for the re-machining of an additional corresponding band on the back. This was to further force the banding on both sides, to allow for further predictability of the system, and to aid in the clarity of results and possible trends.

## 7.2 Test Plan

The data set range was extended from the initial testing to include a wider range of variables for the input speed, clamp load and initial soak temperature in order to capture a wider range of information and for more conclusive trends to be

observed. The input speed is the speed at which the dynamometer spins the driven plates before the clutch is engaged, the clamp load is the load which is applied by the dynamometer to engage the clutch and the initial soak temperature is the temperature at which the test begins, which is set to emulate different ambient operating conditions of the clutch.

The initial temperature soaking of clutch plates allowed for the effects of the different rates of thermal conductivity to be explored through the data obtained from the thermocouples and gave an insight into the rate of change of the face temperature with relation to the core temperature. The energy rate that was input into the clutch was varied by changing both the speed and clamp load so that the effects of this could be determined.

Table 7.2a give the values of the clamp load, input speed and initial soak temperature at which the various tests were carried out.

<b>Clamp Load ►</b>	<b>1500N</b>	<b>2500N</b>	<b>3500N</b>
<b>Initial Soak Temp ▼</b>			
<b>100°C</b>	3000rpm	3000rpm	3000rpm
	5000rpm	5000rpm	5000rpm
	7000rpm	7000rpm	7000rpm
<b>200°C</b>	3000rpm	3000rpm	3000rpm
	5000rpm	5000rpm	5000rpm
	7000rpm	7000rpm	7000rpm
<b>300°C</b>	3000rpm	3000rpm	3000rpm
	5000rpm	5000rpm	5000rpm
	7000rpm	7000rpm	7000rpm

Table 7.2a. Variables Showing the Clamp Load, Input Speed and Initial Soak Temperature for all tests

For the plates with enforced banding, seven different 4mm thick by 2mm high bands arranged at the following mid band radii; 54mm (plate A), 56mm (plate B), 58mm (plate C), 60mm (plate D), 62mm (plate E), 64mm (plate F) and 66mm (plate G), along with a standard non-banded plate as previously mentioned in section 7.1.1

This meant that a total of 216 tests (three temperatures x three input torques x three input speeds x eight plates) were required. Each test was predicted to take anywhere from 3 to 8 minutes each, and allowing for swap over times and reinstallation for each new set of plates, a period of 7 days was allocated for dynamometer testing. However, this time allocation meant that each test could be run only once (unless there was deemed to have been an issue with the dynamometer). As the clutch dynamometer is extensively used for customer tests and gets booked up well ahead of time, this, coupled with the fact that the clutch dyno was already running behind on its schedule due to software updates and hardware maintenance, meant that time allocation was restricted. As a result of this, it was only possible to get one data set, as opposed to the seven sets that the

author would have ideally like to have obtained, which would have allowed for more conclusive results.

By using varying thermocouple radii on the pressure plate, it allowed for the effects of heat travel to be observed through the carbon and for its effects to be logged. Thermocouples were embedded at the mid band radius of plates A to G, as described in table 7.1.1a and this can be seen in figures 7.2c and 7.2d. These thermocouple radii were set to correlate with the outside radius, mid radius and inside radius of the enforced bands, to allow for the heat profile of the effects of the band to be observed. Thermocouple port 8 was used to take data from the infrared sensor into the dynamometer interface. This enabled the IR data and the thermocouple data to be sampled at the same rate, eliminating the need to splice data files at a later stage.

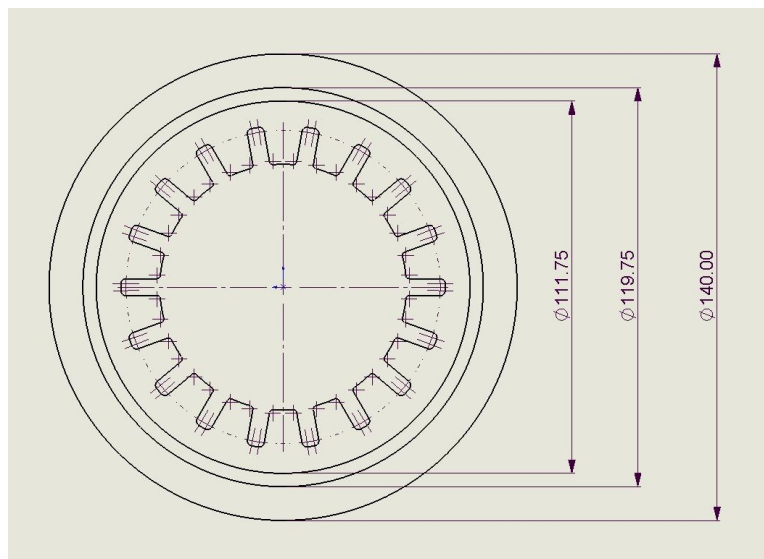


Figure 7.2c. The Configuration of enforced banding plate D

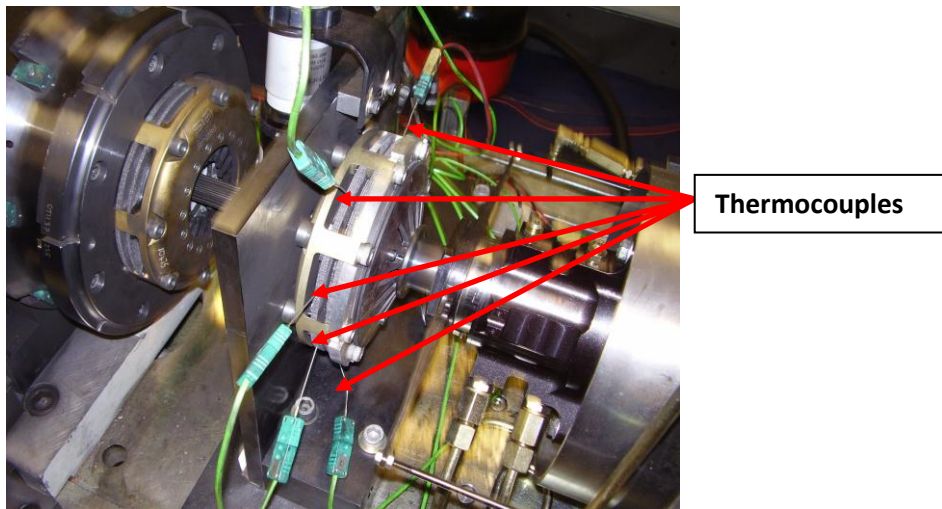


Figure 7.2d. Thermocouple Arrangements on Driving Plate

Testing was conducted using both the enforced banding plates A to G and a standard flat non banded plate. As with the initial testing; torque, input speed, release bearing position, thermocouple temperature and IR sensor temperature were to be recorded, with the test being terminated by a temperature limit at 800°C from the first thermocouple reading to reach this temperature. This figure of 800°C was revised as a result of the initial experimental design where a termination temperature of 500°C was used. This was considered at the time to be a conservative termination temperature estimate and analysis of the data from these validation runs highlighted that an increased termination temperature of 800 °C was still within the boundaries of safety, and also allowed for more data to be collected at the higher energy end of the slip.

### 7.3 Initial Result Observations

During the testing, initial observation requirements were done to check the quality of the data to ensure that the thermocouples were giving readings that were within expected limits and to observe the alignment of the infrared detector. This was done immediately after testing whilst the apparatus was still set up on the dynamometer, so that any repeat experiments could have been easily conducted if required. However as all data files were observed to have good temperature data readings with no thermocouple dropouts or signal losses, this was not necessary.

However, the temperature curves at lower clamp loads were inconsistent. They demonstrated quite severe fluctuations and this could be observed particularly clearly on the thermocouple 8 (infrared) trace at a low start temperature (as this slip takes longer to reach 800°C) and low speeds (again, this slip takes the longest to reach 800°C). This could be explained by the fact that there may be insufficient applied clamp load to maintain a constant clamp load. This effect is illustrated in figures 7.3a and 7.3b, where the thermocouple traces (shown in the solid plots) are fluctuating in the lower energy slip configuration shown in figure 7.3a, and are more consistent in figure 7.3b, where more clamp load has been applied.

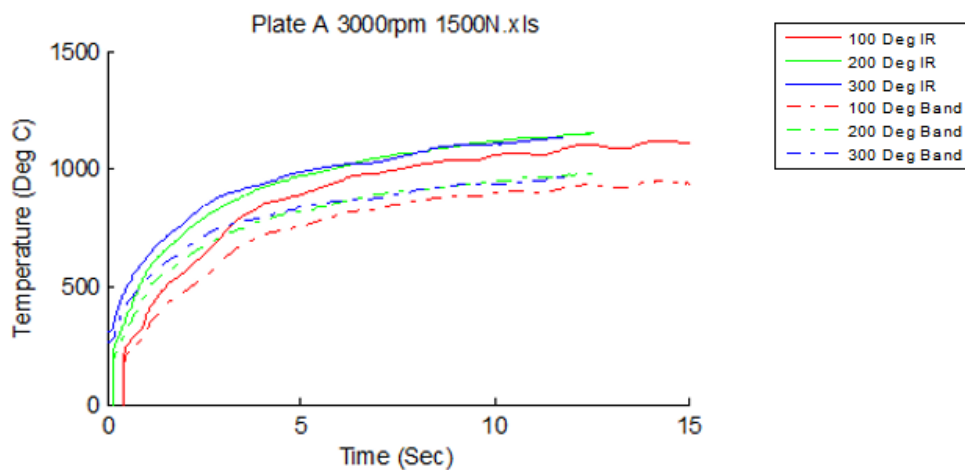


Figure 7.3a. Plate A at 3000rpm, 1500N Clamp Load at 100°C (red), 200°C (green) and 300°C (blue) soak temperatures

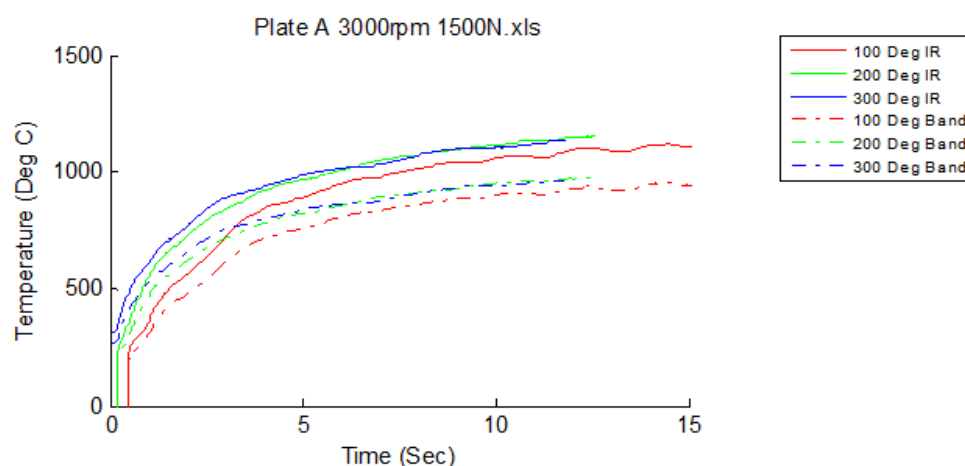


Figure 7.3b Plate A at 5000rpm, 3500N Clamp Load at 100°C (red), 200°C (green) and 300°C (blue) soak temperatures

Generally the values of thermocouple port 8 (which was where the infrared sensor was wired into) are significantly higher than those of the other thermocouples, indicating good alignment of the infrared sensor. When analysed, the thermocouples consistently gave higher readings at the internal diameter of the clutch bands, than at the outside diameter of the clutch bands.

As a way to quickly view any obvious trends, each output value was plotted across all the bands, and these are shown in illustrative graphs (figures 7.3.1 to 7.3.8 for each banded plate are given for the following variables: mid speed (5000rpm), mid start temperature (200°C) and mid input torque (2500Nm) in figure 7.3d, to 7.3k respectively. Each graph is a plot of drive speed against input torque, temperature °C and coefficient of friction. Each trace is colour coded as described in table 5.4c

Thermocouple Number	Loaction	Mid Band Radius	Colour on Plot
Thermocouple 1	(under band A)	54mm	
Thermocouple 2	(under band B)	56mm	
Thermocouple 3	(under band C)	58mm	
Thermocouple 4	(under band D)	60mm	
Thermocouple 5	(under band E)	62mm	
Thermocouple 6	(under band F)	64mm	
Thermocouple 7	(under band G)	66mm	
Thermocouple 8	(Infrared)	68mm	

Table 7.3c Thermocouple Legend for use in Graphs in Section 7.3

All graphs in section 7.3 can also be found on a larger scale in Appendix F.

### 7.3.1 Results for Enforced Banding Plate A

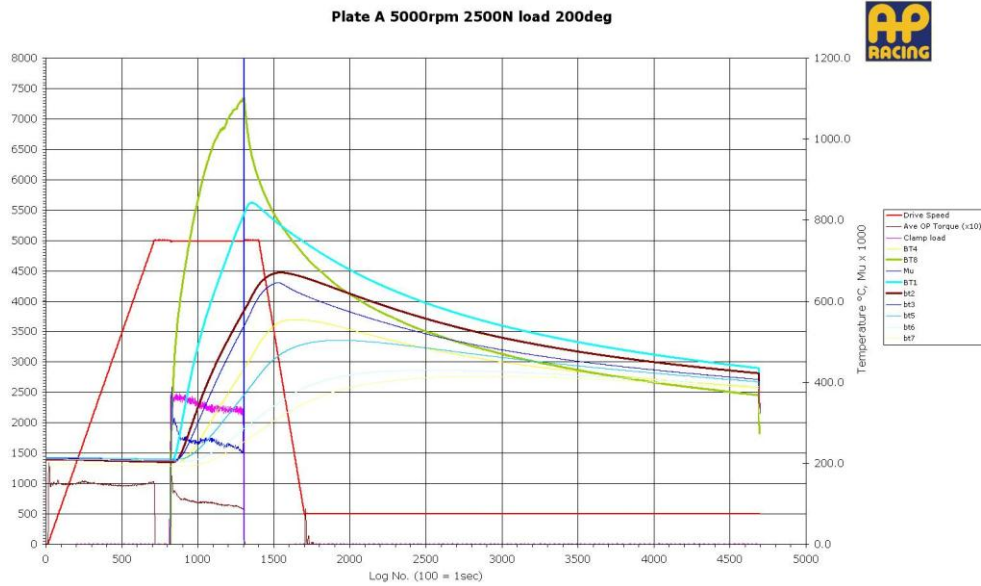
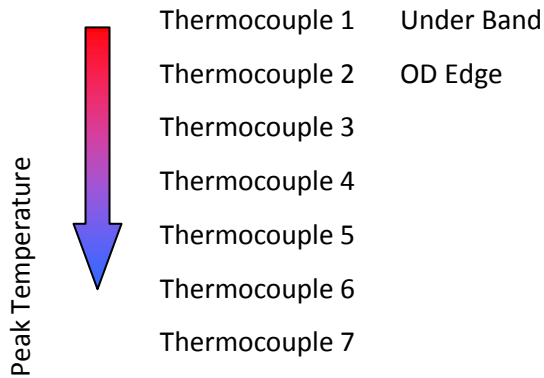


Figure 7.3.1a. Graph of drive speed (rpm) against input torque (Nm), temperature (°C), and coefficient of friction for Plate A at an input speed of 5000rpm, clamp load of 2500N and an initial soak temperature of 200°C

Thermocouple 1 was located directly under the band, with thermocouple 2 on the outside diameter. Infrared readings were consistently higher than all of the thermocouple readings – indicating good alignment. When observing the temperature against time traces for plate A, thermocouple 1 was always the highest reading, with thermocouples 2, 3, 4, 5, 6 and 7 in descending order. This follows the predicted trend that the temperature would be higher in the locality of the band.

Thermocouple peak temperature order (hottest to coldest);





### 7.3.2 Results for Enforced Banding Plate B

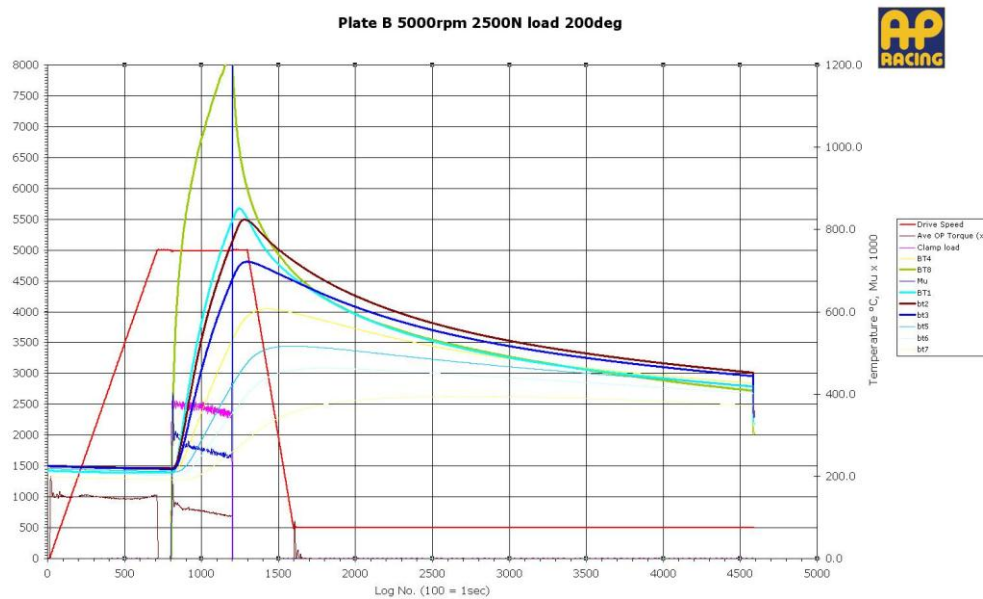
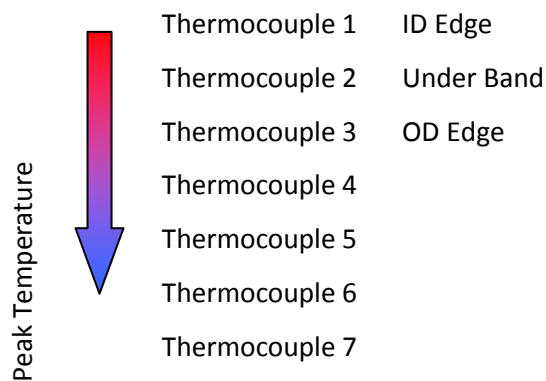


Figure 7.3.2a. Graph of drive speed (rpm) against input torque (Nm), temperature (°C), and coefficient of friction for Plate B at an input speed of 5000rpm, clamp load of 2500N and an initial soak temperature of 200°C

Thermocouple 2 was directly under the band, with thermocouple 3 on the outside diameter and thermocouple 1 on its inside diameter. Infrared readings were slightly higher than the thermocouple readings, suggesting that the alignment is good, but could perhaps be better. When observing the temperature vs. time plot, thermocouple 1 was consistently the highest reading, with thermocouples 2, 3, 4, 5, 6 and 7 following in descending order. This follows the predicted trend.

Thermocouple peak temperature order (hottest to coldest);



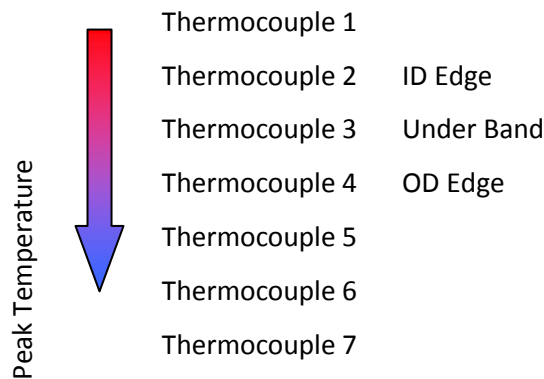
### 7.3.3 Results for Enforced Banding Plate C



Figure 7.3.3a. Graph of drive speed (rpm) against input torque (Nm), temperature (°C), and coefficient of friction for Plate C at an input speed of 5000rpm, clamp load of 2500N and an initial soak temperature of 200°C

Thermocouple 3 was directly under the band, with thermocouple 2 on its inside diameter edge, and thermocouple 4 on the outside diameter edge. Infrared readings were consistently higher than all thermocouple readings – indicating good alignment. Thermocouple 1 was generally the highest of the thermocouple values, with thermocouple 2 reading only slightly lower values. However, as the input load got higher, the tendency was for thermocouple 2 to read higher values than thermocouple 1. Thermocouples 3 and 4 appeared to be reading consistently similar temperatures, with thermocouple 3 tending to read hotter.

Thermocouple peak temperature order (hottest to coldest);



### 7.3.4 Results for Enforced Banding Plate D

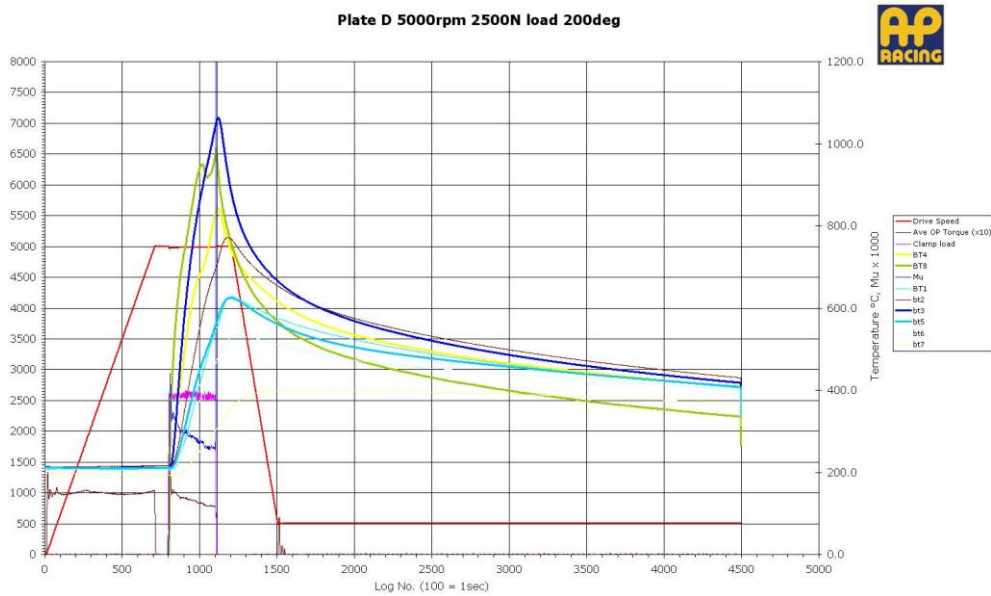
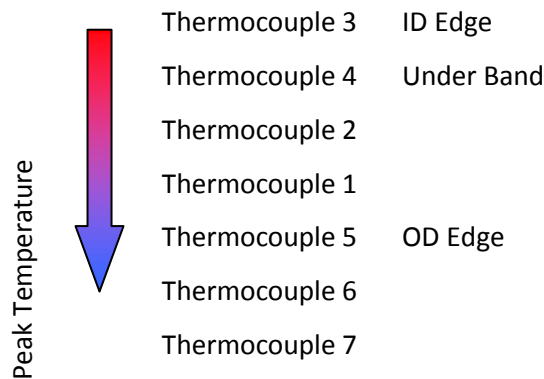


Figure 7.3.4a. Graph of drive speed (rpm) against input torque (Nm), temperature (°C), and coefficient of friction for Plate D at an input speed of 5000rpm, clamp load of 2500N and an initial soak temperature of 200°C

Thermocouple 4 was directly under the band, with thermocouple 3 on its internal diameter edge, and thermocouple 5 on the outside diameter edge. Infrared readings seemed particularly low throughout the testing of this plate, suggesting that perhaps the sensor may have been misaligned. This is also supported by the inconsistencies in the curve of the graph from approximately midway through the slip event. Thermocouple 3 was consistently higher than all other thermocouples, with thermocouple 2 consistently seeing the second highest readings. Thermocouple 4 was reading slightly lower than thermocouple 2, followed by thermocouples 1, 5, 6 and 7.

Thermocouple peak temperature order (hottest to coldest);



### 7.3.5 Results for Enforced Banding Plate E

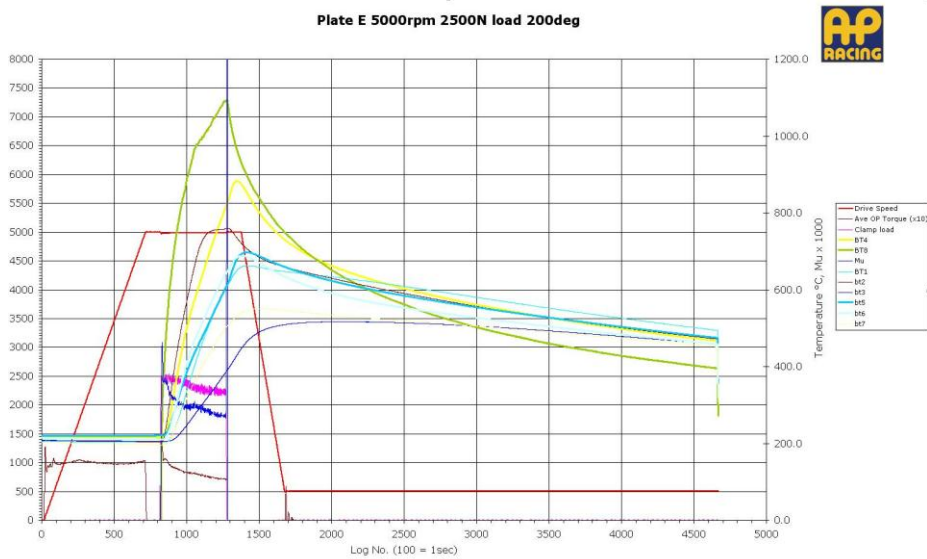
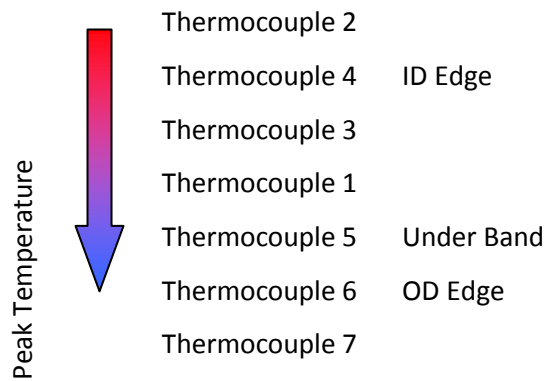


Figure 7.3.5a. Graph of drive speed (rpm) against input torque (Nm), temperature (°C), and coefficient of friction for Plate E at an input speed of 5000rpm, clamp load of 2500N and an initial soak temperature of 200°C

Thermocouple 5 was directly under the band, with thermocouple 4 on its internal diameter edge, and thermocouple 6 on the outside diameter edge. Infrared readings were consistently higher than all IR readings – indicating good alignment. Thermocouple 2 was consistently higher than all other thermocouples, with thermocouple 4 consistently seeing the second highest readings. Thermocouples 1, 3, 5 and 6 were all reading the third highest values throughout the varying slips on plate E. At the highest speeds and loads thermocouple 3 showed comparatively high values, whereas at the lower energy slips thermocouple 1 showed the highest values of the four.

Thermocouple Peak Temperature Order;



### 7.3.6 Results for Enforced Banding Plate F

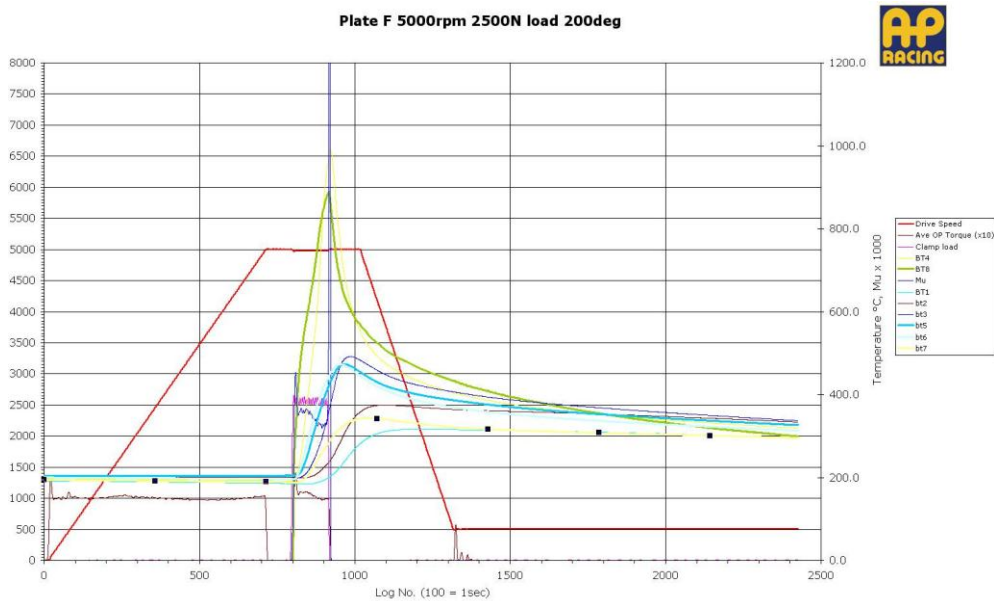
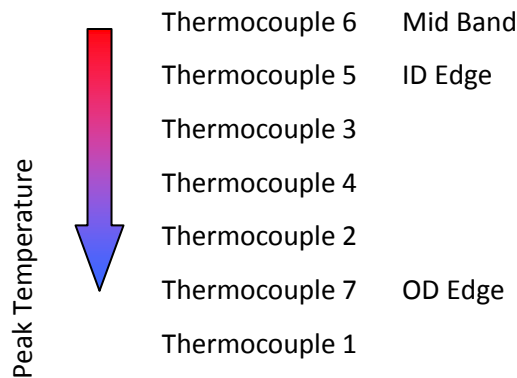


Figure 7.3.6a. Graph of drive speed (rpm) against input torque (Nm), temperature (°C), and coefficient of friction for Plate F at an input speed of 5000rpm, clamp load of 2500N and an initial soak temperature of 200°C

Thermocouple 6 was directly under the band, with thermocouple 5 on its internal diameter edge, and thermocouple 7 on the outside diameter edge. Infrared readings seemed particularly low throughout the testing of this plate, indicating perhaps some misalignment. This theory is also supported by the inconsistencies in the curve of the graph from approximately midway through the slip. Thermocouple 4 is consistently higher than all other thermocouples, followed by thermocouples 6, 5, 3, 2, 7 and 1.

Thermocouple peak temperature order (hottest to coolest);



### 7.3.7 Results for Enforced Banding Plate G

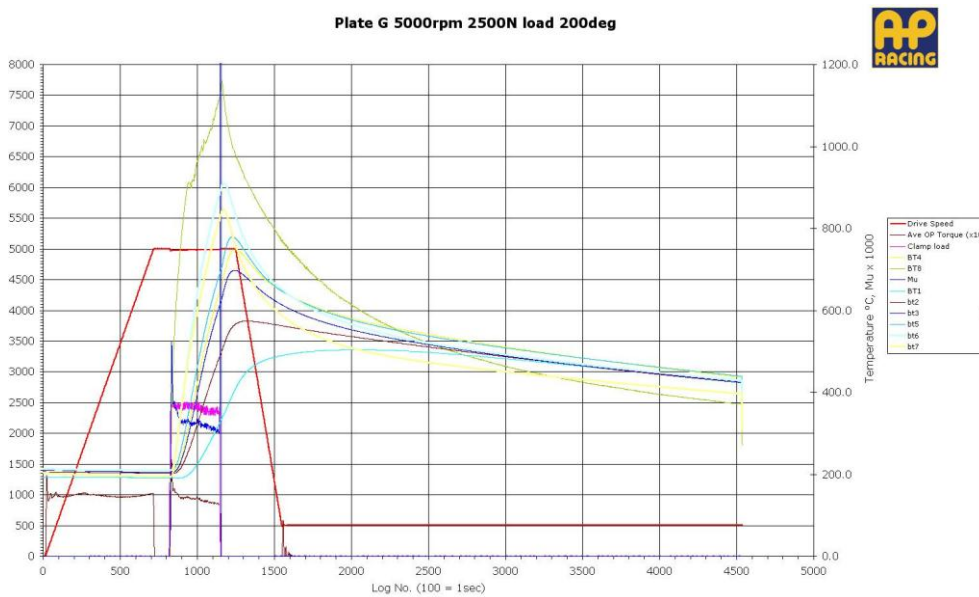
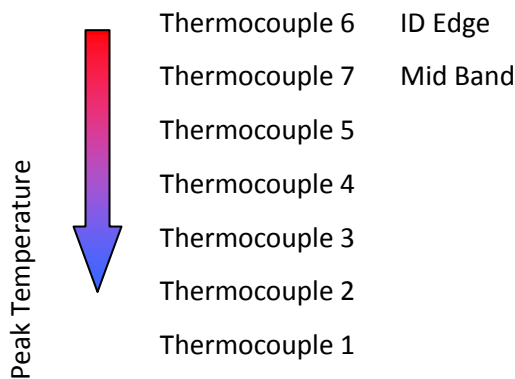


Figure 7.3.7a. Graph of drive speed (rpm) against input torque (Nm), temperature (°C), and coefficient of friction for Plate G at an input speed of 5000rpm, clamp load of 2500N and an initial soak temperature of 200°C

Thermocouple 7 was located directly under the band, with thermocouple 6 on its internal diameter edge. Infrared readings were observed to be consistently higher than all thermocouple readings, indicating good alignment of the sensor. Thermocouple 6 is consistently higher, followed by thermocouple 7, and then thermocouples 5, 4, 3, 2 and 1 respectively

Thermocouple Peak temperature order (hottest to coolest);



### 7.3.8 Results for Standard Plate with no Enforced Banding

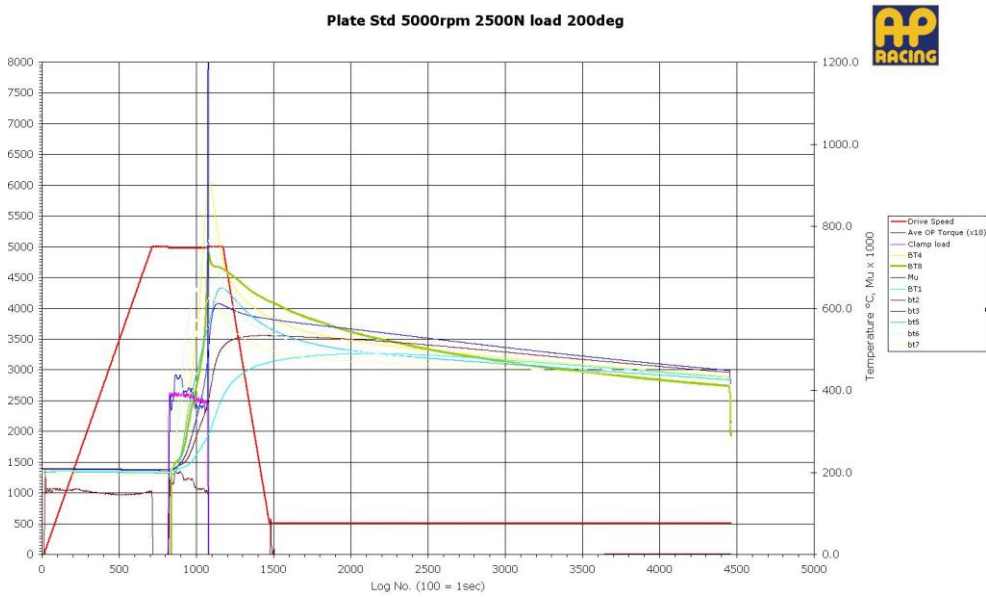


Figure 7.3.8a. Graph of drive speed (rpm) against input torque (Nm), temperature (°C), and coefficient of friction for a Standard Clutch Plate with no enforced banding at an input speed of 5000rpm, clamp load of 2500N and an initial soak temperature of 200°C

The infrared readings on the standard plate were rather unpredictable. This perhaps indicates the presence of banding produced by the clutch event, as at times the infrared sensor readings are higher than those of the thermocouple, but at others the sensor is reading significantly lower than thermocouple readings. This fluctuation of readings indicates that the sensor is not always aligned with the hottest part of the clutch plate. The thermocouple readings also followed no logical pattern in their order, and this also supports the suggestion that banding was occurring on the flat plate.

## Chapter 8

### Experimental Results Analysis

During testing the variables of input speed, clamp load and initial temperature soak were investigated for a series of clutch plates in both the standard flat configuration and with enforced banding. Due to the number of variables being investigated, the final testing produced a large volume of data. This was analysed to determine the effects that initial temperature, clamp load and input speed all had upon the temperature and the friction of the plate. Using MATLAB® the data was extracted and plotted. This chapter will cover the assessment of the data for accuracy, with experimental errors evaluated, and relationships analysed with respect to the effects of input speed, clamp load and start temperature on the overall friction versus temperature relationship.

Further analysis into the occurrence of banding was undertaken and conclusions as to the reliability of the data and subsequent possible theories were made.

#### 8.1 Constraints of the Experimental Programme

The clutch dynamometer operates within a commercial environment with each day of testing costing approximately £1000. An ideal scenario would have been to repeat each set of data tests 7 times to ensure repeatability and to consolidate any trends but this would have amounted to 10 weeks of testing at a cost of £50,000, making it uneconomical for both the project and the sponsoring company.

As a result of this a reduced programme of testing was constructed. By using the design of experiments and required mathematical model inputs, the testing was prioritised and streamlined to enable the required outcomes of the testing to be effectively met.



## 8.2 Estimation of Experimental Error

There were a number of experimental errors to account for in this work and they fell into three main categories; sensors, test apparatus and post-processing. These are now taken in turn and explained further.

### 8.2.1 Sensor Errors

Sensor errors are generated by errors in: the sensors themselves (thermocouple, IR, torque sensor and speed sensor), the sensor connections (wires and hardware connections), and sensor set up parameters (PC setup of the sensors on the rig, which include sampling rates and calibration tables).

#### Thermocouple Accuracy:

K-type thermocouples offer a wide temperature range of  $-200^{\circ}\text{C}$  to  $1250^{\circ}\text{C}$  and a relatively low error value compared to other thermocouple types. The sensitivity of the thermocouples used in this work is approximately  $41\mu\text{V}/^{\circ}\text{C}$  and typically, errors are within the range of  $\pm 1.5^{\circ}\text{C}$  at temperatures up to  $250^{\circ}\text{C}$  and  $\pm 2.2^{\circ}\text{C}$  at temperatures higher than this. Thermal shunting is often a cause of error with thermocouples. This is because thermocouples have mass and heating that mass takes energy. In addition, in this application, the thermocouple was protruding from the top of the clutch plate and so energy from the heated wire was being dissipated to the atmosphere, and so it is hard to quantify an absolute value for this heat loss.

#### IR Accuracy:

The temperature reading can be affected by the atmosphere and surrounding objects, such as reflected temperature from ambient surroundings and dust / steam and particles. Whilst the greatest care was taken to avoid these types of atmospheric inaccuracies, one factor that could not be eliminated was carbon dust. The presence of carbon dust in the air between the specimen and the sensor will have undoubtedly had some effect upon the results but this is very hard to quantify. The specified percentage error for the IR sensor in 'perfect' conditions is said to be  $\pm 1\%$ , but the manufacturer has suggested that perhaps a value of  $\pm 2\%$ , would be more applicable in the 'dirty' surroundings of the clutch dyno lab.

Torque Sensor:

The sensor is made up of two main components: A stainless steel shaft, dimensioned for the appropriate torque, and a second metal ring, which fits tightly on the shaft (see figure 8.2.1a), manufactured of titanium-nickel material, which has the property of being magneto-elastic.

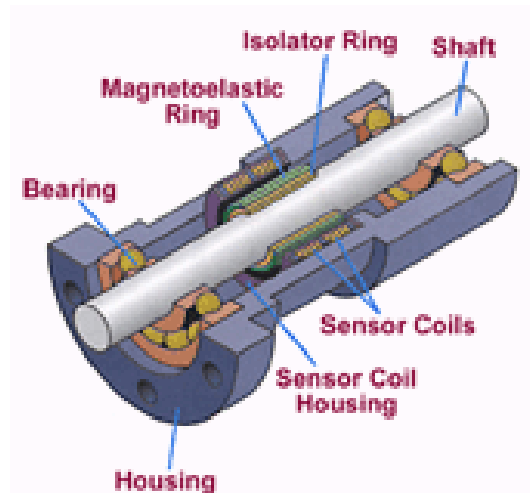


Figure 8.2.1a Torque Sensor (Courtesy of Variohm Sensors – Daventry UK)

Magneto-elastic materials are commonly known as ‘pseudo magnets’. When at rest, they produce no external magnetic fields, but as soon as their form experiences a change in shape through applied stress, their magnetic characteristics change to give a field whose strength is directly proportional to the applied stress. The ring of magneto-elastic material is magnetized circumferentially. Without an applied torque, the magnetic field is contained wholly within the ring. However, as torque is applied to the shaft, the magnetic field twists within the ring and field lines intersect with the surface of the ring in proportion to the amount of torque applied.

This type of sensor typically has a  $\pm 1\%$  accuracy in torque, due to the fact that it is calculated directly from a current. The torque has a consequential effect on the results though, as it is directly used to calculate the friction, using equation 8.2.1b

$$\text{Friction} = -1 \frac{(\text{ Output Torque } )}{( \text{ Clamp force } \times 0.05925 \times 2 )} \quad \text{Equation 8.2.1b}$$

Where  $0.05925m$  is the mean effective radius of the test piece and 2 is the number of interfaces (the whole equation is multiplied by -1 because the direction in which the force is acting is opposite to the input torque, which is a preset positive number within the dynamometer's configuration). This means that a  $\pm 1\%$  accuracy in torque, will not offer a large variance to the value of friction, as it is divided through by the clamp force (in the magnitude of a 1000N) multiplied by two relatively small constants.

#### Speed Sensor:

The speed of the rotation is based upon the speed of the dyno head, which is detected by a Hall Effect sensor. This is a simple transducer that varies its output voltage in response to changes in the magnetic field. By using a series of small metal teeth on the rotating input shaft, combined with a Hall Effect sensor, it is possible to predict the speed (and the rate of change of speed) by counting the number of times that the teeth pass through the sensor in a given time. This type of sensor generally has an accuracy of approximately 1%.

#### Sensor Connections:

Lead resistance is a common problem when using thermocouples and occurs when an extension lead is constructed of a different material to the thermocouple. This causes a change in the voltage resistance with the sensing software translating this resisted voltage to determine a temperature value that is not representative of that indicated by the voltage seen at the sensor. Lead resistance was overcome by using the appropriate extension cables specifically designed for the k-type thermocouple that was being used. This is also applicable for the IR sensor, but again, the appropriate manufacturer supplied lead was used and so any error caused by this can be negated.

#### Hardware Setup:

Data was set up to be captured at a rate of 10Hz – that is, 10 samples per second are collected. The calibration tables used for the IR and thermocouples are usually given as a list of set points (with the value obtained from the experiment extrapolated along lines drawn between these set points), not as an equation

(which would be far more accurate in any type of calibration curve beyond that of a 1<sup>st</sup> order relationship). However, these calibration curves (and the errors caused by them) are accounted for in the declared error values for the sensor itself and so the hardware aspect of this error can be negated.

### **8.2.2 Apparatus Errors**

Test apparatus errors were the physical anomalies that could occur within the test, such as slight misalignment of the clutch (which would cause eccentricity and 'hot spots'), changes in airflow or ambient temperature around the rig, surface contaminants that may have come into contact with the clutch or any other simple 'human error' factor. Whilst these were obviously taken into consideration, apparatus errors are the hardest to quantify.

### **8.2.3 Post Processing Errors**

#### Rounding Errors in Data Analysis

This is caused by data in the Excel spreadsheet being rounded up or down to the nearest 0.01 and was simply overcome by expanding the rounding error from 0.01 to 0.0001, giving very minor errors in respect to the other possible sources of error.

#### IR Emissivity Value Accuracy

Normally this would come within 'sensor errors', however, the factor of emissivity (determined through testing at NPL and described in Chapter 6) was applied to the raw data during the post processing stage of the results and played no part in the data collected from the sensor. Emissivity is not simply a linear relationship that is followed; it is actually a curve. By using an approximation for emissivity of 0.85, data at the extremes of the temperature range is less accurate than that obtained from the middle of the range. Figure 8.2.3a shows the typical temperature errors due to uncertainty of the emissivity.

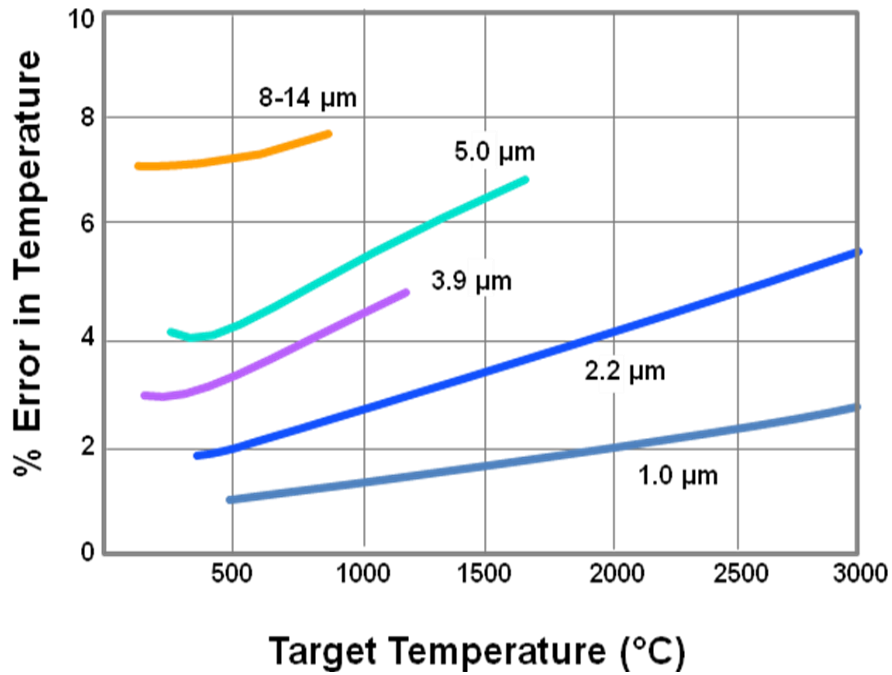


Figure 8.2.3a. Temperatures due to Emissivity Uncertainty [166]

The obvious solution was to use the shortest wavelength IR for the application, however, there were many factors governing wavelength selection, such as material type and transmission. Generally the shortest wavelength at which transmission is close to zero is the best one to use for infra red, as this is this wavelength at which low emissivity or low background radiation are best compensated for. Figure 8.2.3b shows the typical transmittance plot for polyethylene. Here, it is possible to observe that in this case the most appropriate wavelength to use would be 3 microns.

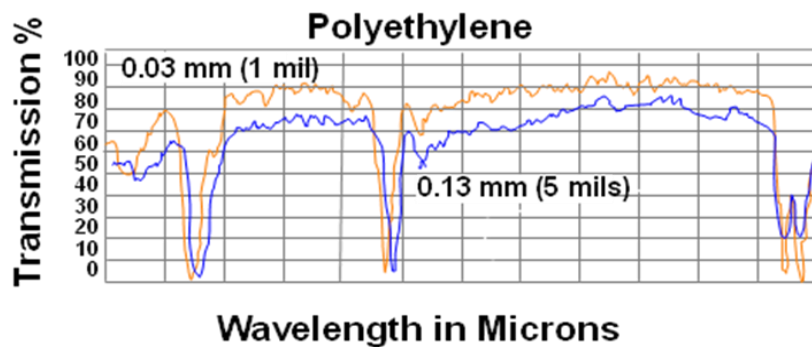


Figure 8.2.3b. IR Transmission Spectra of Polyethylene [166]

It was suggested by the manufacturers of the IR sensor, that a typical value of 10% error in emissivity be used for this application.

### **8.3 Processing of Raw Experimental Data**

When analysing the results for the friction vs. temperature relationship, the infrared temperature was the only temperature used. This is because the thermocouples were embedded and not at the surface where the friction was acting, whereas the infrared sensor gives a reading of on the face of the friction surface .

The MATLAB® was used for the data extraction, and the code for this can be found in Appendix F. Each main test variable will now be considered in turn and analysed with respect to other variables.

### **8.4 Experimental Data Results**

#### **8.4.1 Experimental results for the Effects of Initial Heat Soak**

All of the processed data and results generated by the MATLAB® code can be found in Appendix H, which contains a series of graphs for each plate. Each sub graph plots the different initial soak temperatures on axes of temperature versus time for set clamp loads and input speeds.

As the clamp load was released at a thermocouple temperature trip of 800°C, it was possible to use the time which the clamp load was applied to determine the amount of time that it took for the plates to heat up to 800°C. After this point, once the load had been released, the temperature began to decrease. As it was only the heating phase that was of interest then clamp load trip was assumed to be a good value to use as it was at this point when at least one point within the plate had reached the 800°C trip value. As used later in the mathematical modelling, the cut off value for the clamp force was 50N. This meant that whenever the clamp force value rose above 50N the clamp force was considered

to be on and once it dropped below the 50N threshold again then the clamping event was deemed to have ceased.

Run	Time above 50N (s)							
	Plate Standard	Plate A	Plate B	Plate C	Plate D	Plate E	Plate F	Plate G
3000rpm1500NData 100	17.3	17.85	12.35	14.69	8.72	16.91	8.8	16.16
3000rpm1500NData 200	9.38	12.6	11.24	9.74	8.41	12.43	8.33	14
3000rpm1500NData 300	8.04	11.8	9.21	8.89	6.43	11.83	7.33	13.09
3000rpm2500NData 100	7.99	10.34	7.68	8.82	7.14	12.83	2.93	8.29
3000rpm2500NData 200	5.81	9.31	6.63	6.3	6.02	9.48	2.35	8.08
3000rpm2500NData 300	4.4	7.96	5.51	5.31	5.33	7.94	1.57	6.68
3000rpm3500NData 100	8.6	6.94	5.37	6.72	6.87	8.26	1.83	6.8
3000rpm3500NData 200	4.72	6.22	5.17	5.83	5.93	6.34	1.69	5.25
3000rpm3500NData 300	6.82	5.43	4.32	4.87	5.42	5.44	1.23	4.31
5000rpm1500NData 100	4.15	8.23	5.9	6.65	4.41	8.12	2.93	6.56
5000rpm1500NData 200	3.31	7.24	5.83	4.87	4.35	11.66	2.23	5
5000rpm1500NData 300	4.11	7.14	5.21	7.81	3.72	5.03	1.51	10.71
5000rpm2500NData 100	2.86	5.55	4.08	4.13	4.12	5.31	1.44	3.42
5000rpm2500NData 200	2.6	4.89	4.01	3.58	3.13	4.62	1.24	3.32
5000rpm2500NData 300	3.89	4.19	3.52	2.92	3.31	4.26	1.2	3.02
5000rpm3500NData 100	4.81	4.11	3.25	3.23	3.52	3.64	0.83	3.12
5000rpm3500NData 200	4.18	3.74	2.99	3.03	3.41	3.43	0.96	2.73
5000rpm3500NData 300	2.12	3.24	2.72	2.64	2.93	3.01	0.94	2.52
7000rpm1500NData 100	4.53	6.61	4.1	4.08	3.83	5.82	1.41	3.02
7000rpm1500NData 200	7.1	5.05	5.2	3.92	3.77	4.43	1	7.48
7000rpm1500NData 300	3.53	5.68	3.13	4.49	3.21	4.9	1.11	3.09
7000rpm2500NData 100	2.41	3.51	3.13	2.84	2.09	3.12	0.92	2.52
7000rpm2500NData 200	6.83	3.54	2.9	2.93	2.8	3.11	0.71	2.62

7000rpm2500NData 300	2.5	2.93	2.61	2.4	2.74	3	0.74	2.4
7000rpm3500NData 100	3.81	2.92	2.43	3.23	2.33	2.43	1.03	2.34
7000rpm3500NData 200	4.33	2.52	2.23	3.03	2.44	2.51	1.23	1.93
7000rpm3500NData 300	3.61	2.33	2.03	2.64	2.03	2.15	0.99	1.88

Table 8.4.1a. Clamp Load Duration for all Variable Plates at Temperatures of 100°C, 200°C and 300°C, Grouped by Input Speed and Clamp Load

Table 8.4.1a shows the clamping period in seconds for each different temperature for a set of different speeds and clamp loads. When plotting the data, as seen in figure 8.4.1b (also in Appendix H), on the large scale the clamp load was on the x-axis and the decreasing speed was on the y-axis, with each smaller graph having a scale of temperature vs. clamp load application time.

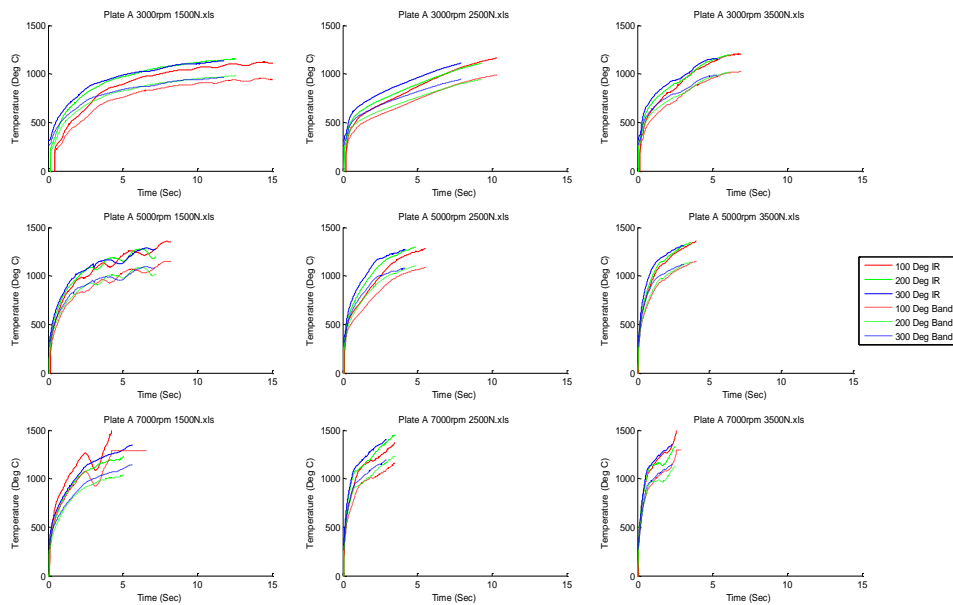


Figure 8.4.1b. Example of plots created for different initial soak temperatures with respect to time versus temperature on a scale of initial speed versus clamp load for enforced banding Plate A

To determine the effect of the initial soak temperature upon the slip period (the time that the clamp loads were over 50Nm until the thermocouple limit value of 800\_°C ), start temperature was plotted against slip period for enforced banding plates B, D and F, along with the standard flat non banded plate as seen in figure 8.4.1c



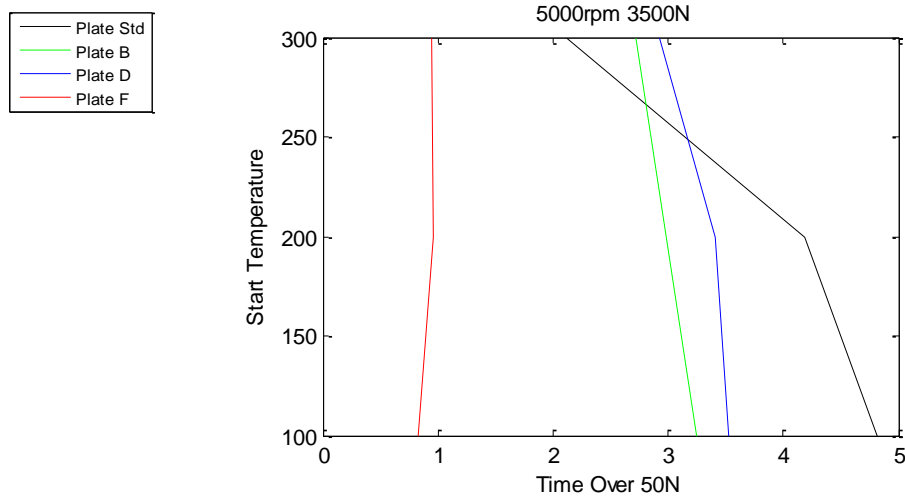


Figure 8.4.1c. Graph of Initial Soak Temperature against Time to reach 800°C (temperature limit for the slip period) for the Standard Plate, Plate B, Plate D and Plate F

As seen from figure 8.4.1c, although the plots loosely follow the general trend that higher initial soak temperatures imply shorter heating times, it is difficult to predict the extent of this relationship, as the rates of change are not clearly defined due to the lack of data points. The standard plate graphs did not show a consistent relationship between the initial soak temperatures and slip duration, while the banded plate plots were far more predictable and more likely to follow the rule that the higher initial soak temperature implies a shorter heating time. This may be due to the concentrated nature of the heat acting upon the banded area.

Appendix I is a collection of further plots for the same data, illustrating the friction properties for each plate, organised in a matrix of input speed by clamp load. Each sub graph plots the different initial soak temperatures on a friction vs. temperature axis for a set clamp load and input speed, as seen in Figure 8.4.1d.

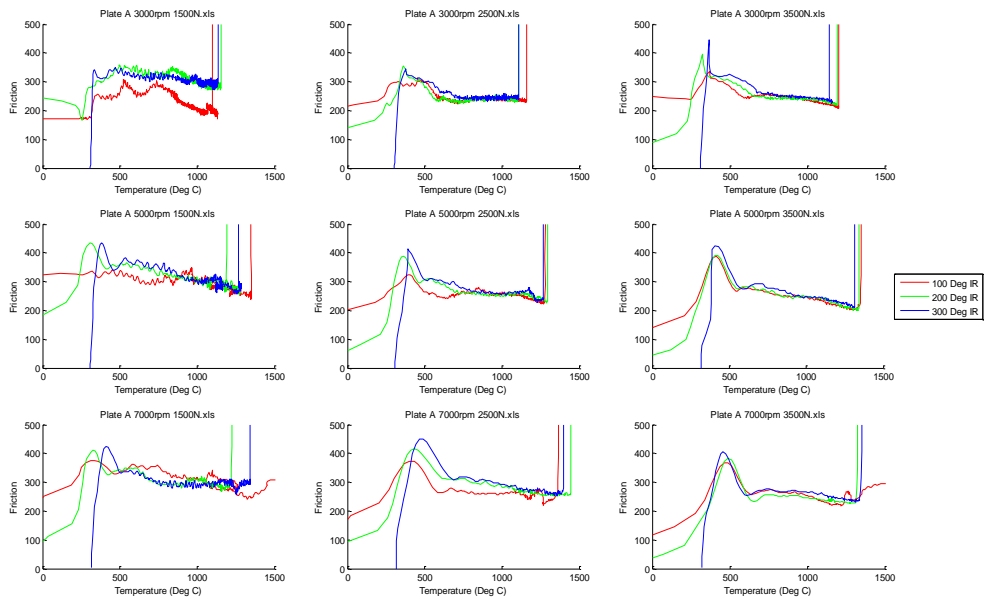


Figure 8.4.1d. Example of plots created for different initial soak temperatures with respect to coefficient of friction versus temperature on a scale of initial speed versus clamp load for forced banding Plate A

As the friction is a surface property the IR data was used for the temperature variable as this reading gives the surface temperature which is a snapshot of exactly what is occurring on the surface at any given time.

#### 8.4.2 Experimental results for the Effects of Clamp Load

Data and result plots for the effect of the clamp load, input speeds and initial soak temperatures on the slip duration can be found in Appendix J, which contains a series of graphs plotting time versus temperature on a scale of initial speed versus clamp load for each plate, along with a matrix of input speed against initial soak temperature. Each sub plot shows the different clamp loads on temperature vs. time axes for a set of initial soak temperature and input speed.

The slip period over 50Nm data was once again used with time data for each set of conditions grouped by different speeds and initial heat soaks, and then ordered by clamp load to judge the effect of these variables upon the slip period .

Run	Time above 50N (s)							
	Plate Std	Plate A	Plate B	Plate C	Plate D	Plate E	Plate F	Plate G
3000rpm1500NData 100	17.3	17.85	12.35	14.69	8.72	16.91	8.8	16.16
3000rpm2500NData 100	7.99	10.34	7.68	8.82	7.14	12.83	2.93	8.29
3000rpm3500NData 100	8.6	6.94	5.37	6.72	6.87	8.26	1.83	6.8
3000rpm1500NData 200	9.38	12.6	11.24	9.74	8.41	12.43	8.33	14
3000rpm2500NData 200	5.81	9.31	6.63	6.3	6.02	9.48	2.35	8.08
3000rpm3500NData 200	4.72	6.22	5.17	5.83	5.93	6.34	1.69	5.25
3000rpm1500NData 300	8.04	11.8	9.21	8.89	6.43	11.83	7.33	13.09
3000rpm2500NData 300	4.4	7.96	5.51	5.31	5.33	7.94	1.57	6.68
3000rpm3500NData 300	6.82	5.43	4.32	4.87	5.42	5.44	1.23	4.31
5000rpm1500NData 100	4.15	8.23	5.9	6.65	4.41	8.12	2.93	6.56
5000rpm2500NData 100	2.86	5.55	4.08	4.13	4.12	5.31	1.44	3.42
5000rpm3500NData 100	4.81	4.11	3.25	3.23	3.52	3.64	0.83	3.12
5000rpm1500NData 200	3.31	7.24	5.83	4.87	4.35	11.66	2.23	5
5000rpm2500NData 200	2.6	4.89	4.01	3.58	3.13	4.62	1.24	3.32
5000rpm3500NData 200	4.18	3.74	2.99	3.03	3.41	3.43	0.96	2.73
5000rpm1500NData 300	4.11	7.14	5.21	7.81	3.72	5.03	1.51	10.71
5000rpm2500NData 300	3.89	4.19	3.52	2.92	3.31	4.26	1.2	3.02
5000rpm3500NData 300	2.12	3.24	2.72	2.64	2.93	3.01	0.94	2.52
7000rpm1500NData 100	4.53	6.61	4.1	4.08	3.83	5.82	1.41	3.02
7000rpm2500NData 100	2.41	3.51	3.13	2.84	2.09	3.12	0.92	2.52
7000rpm3500NData 100	3.81	2.92	2.43	3.23	2.33	2.43	1.03	2.34
7000rpm1500NData 200	7.1	5.05	5.2	3.92	3.77	4.43	1	7.48
7000rpm2500NData 200	6.83	3.54	2.9	2.93	2.8	3.11	0.71	2.62
7000rpm3500NData 200	4.33	2.52	2.23	3.03	2.44	2.51	1.23	1.93

7000rpm1500NData 300	3.53	5.68	3.13	4.49	3.21	4.9	1.11	3.09
7000rpm2500NData 300	2.5	2.93	2.61	2.4	2.74	3	0.74	2.4
7000rpm3500NData 300	3.61	2.33	2.03	2.64	2.03	2.15	0.99	1.88

8.4.2a. Clamp Load Time for all Variable Plates for Clamp Loads of 1500N, 2500N and 3500N,  
Grouped by Input Speed and Temperature

The information displayed in table 8.4.2a gives the clamping period in seconds for each different temperature grouped by a single set of input speeds and clamp loads. MATLAB® was used to create a graph from this data, consisting of three further graphs as seen in Figure 8.4.2b (further plots for all plates can be seen in Appendix J).

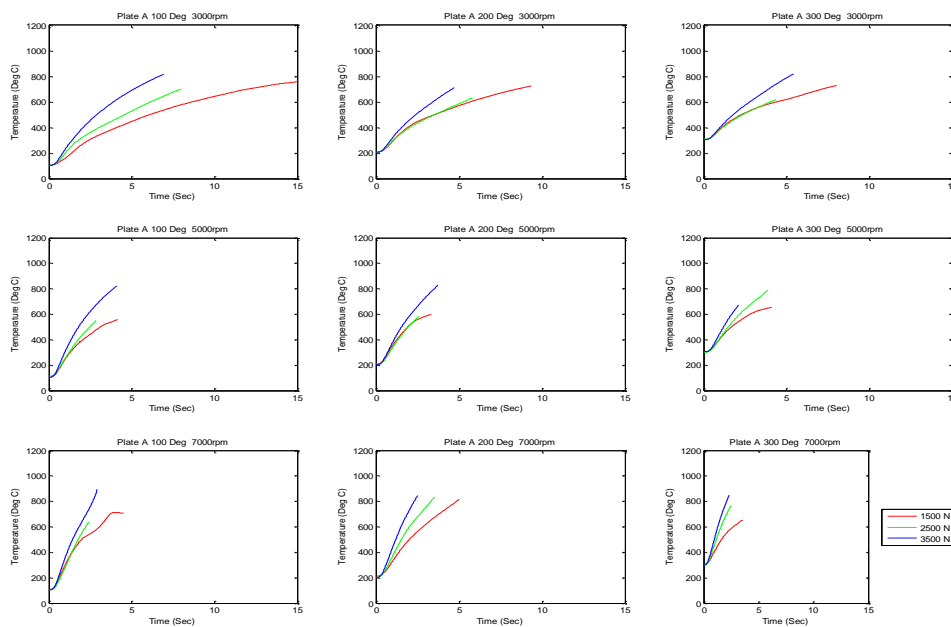


Figure 8.4.2b. Example of plots created for different clamp loads with respect to temperature versus time on a scale of initial speed versus initial soak temperature for forced banding Plate A

Plotting the temperature versus clamp load in respect to clamp load against speed. Points for the values for the standard plate and banded plates B, D and F are plotted, in Figure 8.4.2c

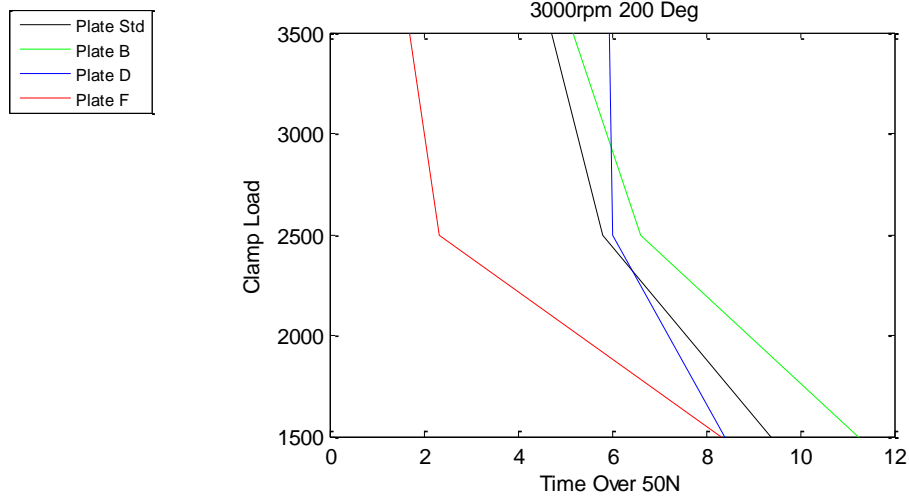


Figure 8.4.2c. Graph of Initial Clamp Load against Time to reach 800°C (temperature limit for the slip period) for the Standard Plate, Plate B, Plate D and Plate F

Appendix K is a further series of graphs illustrating the friction properties for each plate, organised in a matrix of input speed by initial soak temperature. Each sub graph plots the different initial soak temperatures on a friction vs. temperature axis for a initial soak temperature and input speed, as seen in Figure 8.4.2d.

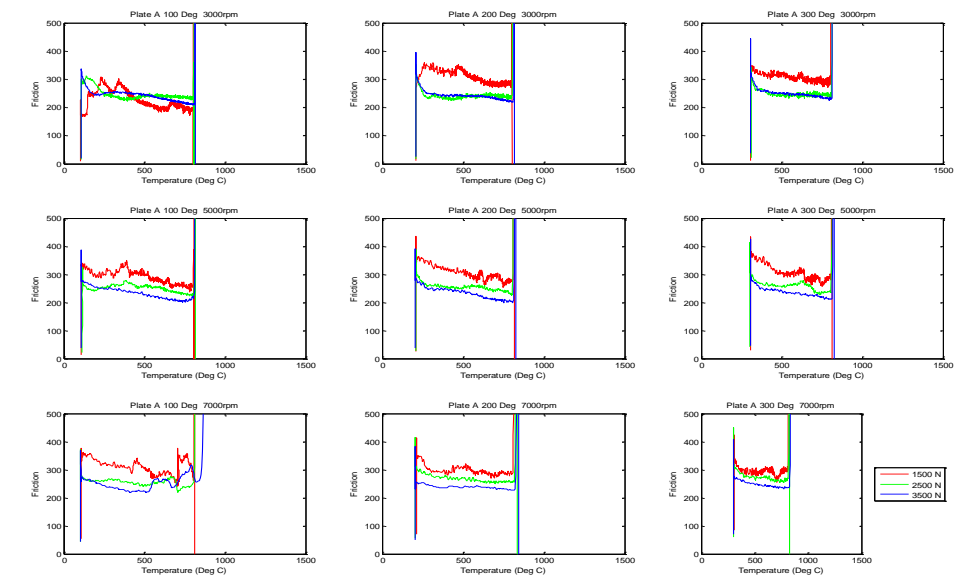


Figure 8.4.2d. Example of plots created for clamp load with respect to coefficient of friction versus temperature on a scale of initial speed versus initial soak temperature for forced banding Plate A

Each sub graph plots the different clamp loads on a friction vs. temperature axis for a set initial soak temperature and input speed. As the friction is a surface property, the IR data was used for the temperature variable, as this also gave a surface property reading.

#### 8.4.3 Experimental results for the Effects of Initial Speed

Data and results generated by the MATLAB® code can be found in Appendix K, which contains a series of graphs for each plate, organised in a matrix of clamp load by initial soak temperature. Each sub plot illustrate the different input speeds on a temperature vs. time axis for a set clamp load and initial soak temperature.

Run	Time Above 50N (s)							
	Plate Std	Plate A	Plate B	Plate C	Plate D	Plate E	Plate F	Plate G
3000rpm1500NData 100	17.3	17.85	12.35	14.69	8.72	16.91	8.8	16.16
5000rpm1500NData 100	4.15	8.23	5.9	6.65	4.41	8.12	2.93	6.56
7000rpm1500NData 100	4.53	6.61	4.1	4.08	3.83	5.82	1.41	3.02
3000rpm2500NData 100	7.99	10.34	7.68	8.82	7.14	12.83	2.93	8.29
5000rpm2500NData 100	2.86	5.55	4.08	4.13	4.12	5.31	1.44	3.42
7000rpm2500NData 100	2.41	3.51	3.13	2.84	2.09	3.12	0.92	2.52
3000rpm3500NData 100	8.6	6.94	5.37	6.72	6.87	8.26	1.83	6.8
5000rpm3500NData 100	4.81	4.11	3.25	3.23	3.52	3.64	0.83	3.12
7000rpm3500NData 100	3.81	2.92	2.43	3.23	2.33	2.43	1.03	2.34
3000rpm1500NData 200	9.38	12.6	11.24	9.74	8.41	12.43	8.33	14
5000rpm1500NData 200	3.31	7.24	5.83	4.87	4.35	11.66	2.23	5
7000rpm1500NData 200	7.1	5.05	5.2	3.92	3.77	4.43	1	7.48
3000rpm2500NData 200	5.81	9.31	6.63	6.3	6.02	9.48	2.35	8.08
5000rpm2500NData 200	2.6	4.89	4.01	3.58	3.13	4.62	1.24	3.32
7000rpm2500NData 200	6.83	3.54	2.9	2.93	2.8	3.11	0.71	2.62

3000rpm2500NData 300	4.4	7.96	5.51	5.31	5.33	7.94	1.57	6.68
5000rpm2500NData 300	3.89	4.19	3.52	2.92	3.31	4.26	1.2	3.02
7000rpm2500NData 300	2.5	2.93	2.61	2.4	2.74	3	0.74	2.4
3000rpm3500NData 100	8.6	6.94	5.37	6.72	6.87	8.26	1.83	6.8
5000rpm3500NData 100	4.81	4.11	3.25	3.23	3.52	3.64	0.83	3.12
7000rpm3500NData 100	3.81	2.92	2.43	3.23	2.33	2.43	1.03	2.34
3000rpm3500NData 200	4.72	6.22	5.17	5.83	5.93	6.34	1.69	5.25
5000rpm3500NData 200	4.18	3.74	2.99	3.03	3.41	3.43	0.96	2.73
7000rpm3500NData 200	4.33	2.52	2.23	3.03	2.44	2.51	1.23	1.93
3000rpm3500NData 300	6.82	5.43	4.32	4.87	5.42	5.44	1.23	4.31
5000rpm3500NData 300	2.12	3.24	2.72	2.64	2.93	3.01	0.94	2.52
7000rpm3500NData 300	3.61	2.33	2.03	2.64	2.03	2.15	0.99	1.88

Table 8.4.3a. Clamp Load Time for all Variable Plates for Speeds of 3000rpm, 5000rpm and 7000rpm,  
Grouped by Temperature and Clamp Load

The information displayed in Table 8.4.3a shows the clamping period in seconds for each different temperature grouped by a single set of input speeds and clamp loads. Data and result plots for the effect of the clamp load, slip duration and initial soak temperatures on the slip duration can be found in Appendix L, which contains a series of graphs plotting time versus temperature on a scale of initial speed versus clamp load for each plate, along with a matrix of input speed against initial soak temperature, an example of which can be seen in Figure 8.4.3b

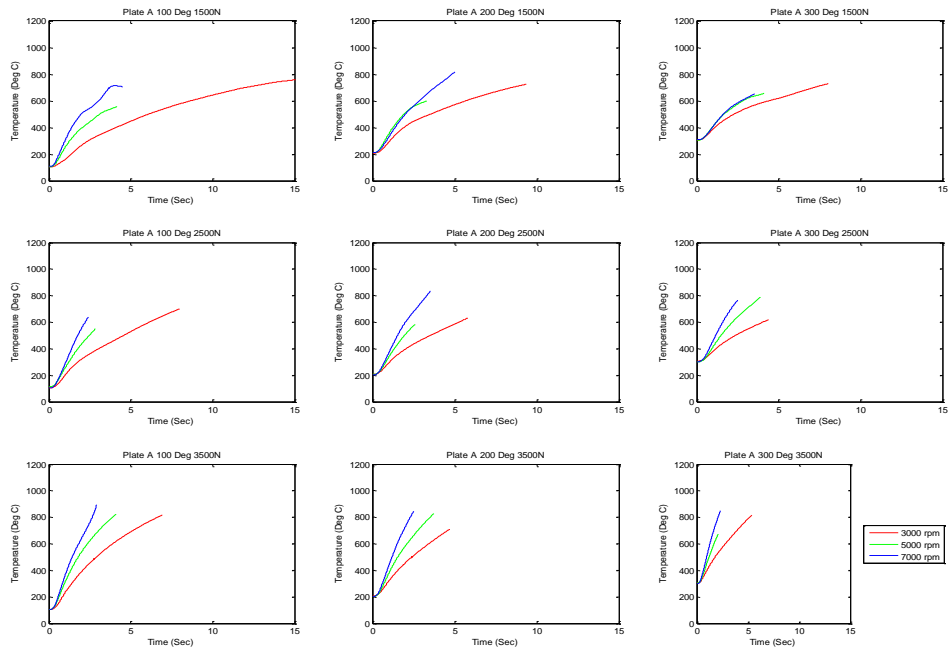


Figure 8.4.3b. Example of plots created for different initial input speeds with respect to temperature versus time on a scale of initial clamp load versus soak temperature for forced banding Plate A

Plotting the initial input speed versus clamp load in respect to clamp load against speed. Points for the values for the standard plate and banded plates B, D and F were all plotted, and were as seen in figure 8.4.3c

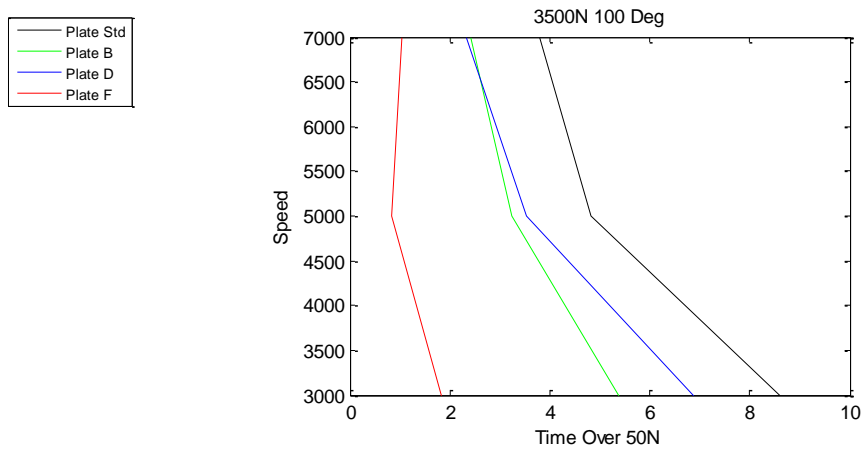


Figure 8.4.3c. Graph of Input Speed against Time to reach 800°C (temperature limit for the slip period) for the Standard Plate, Plate B, Plate D and Plate F

Figure 8.4.3d illustrates a further series of graphs illustrating the friction coefficient variation for each plate, organised in a matrix of clamp load by initial



soak temperature. Each sub graph plots the different clamp loads on a friction vs. temperature axis for a set clamp load and initial soak temperature. Full sets of graphs for all plates can be found in Appendix M

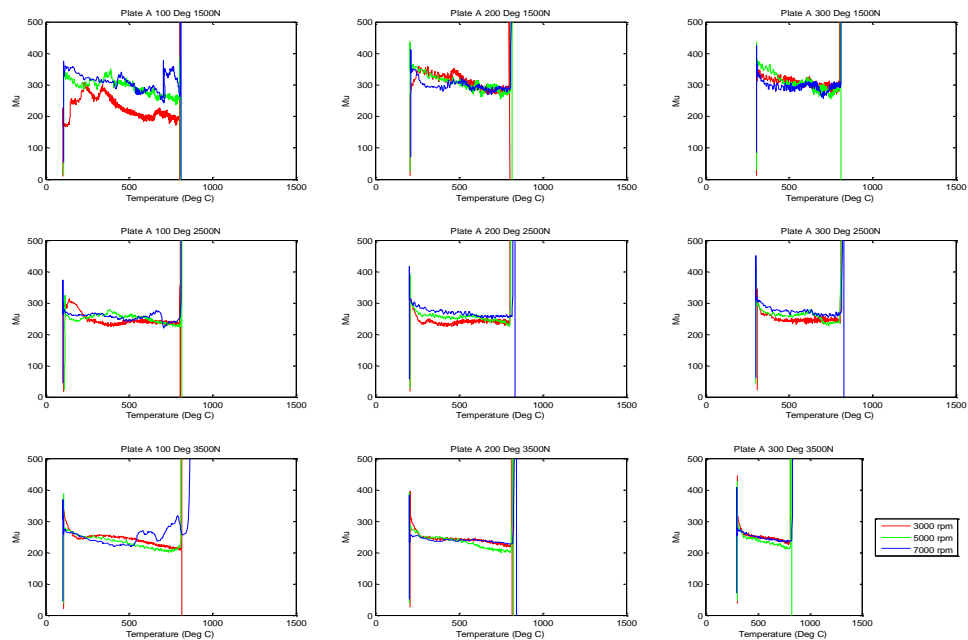


Figure 8.4.3d. Example of plots created for initial input speeds with respect to coefficient of friction versus temperature on a scale of clamp load versus initial soak temperature for forced banding Plate

A

## 8.5 Discussion of Results Obtained from Experimental Testing

The graphs shown in section 8.3 (and in appendices I, K and M) imply that friction is decreasing with the increase in temperature after 500°C (figure 8.4a). Conventional carbon-carbon understanding contradicts this theory and so further investigation was required to understand this occurrence.

As the friction is a function of the output torque, further investigations into the torque curve data showed that this was also experiencing a reduction in value. The torque value is in relation to the clamp load and when this was investigated, it too was shown to decrease slightly over the duration of the slip. This happened through all slips and an example plot can be seen in figure 8.5a.

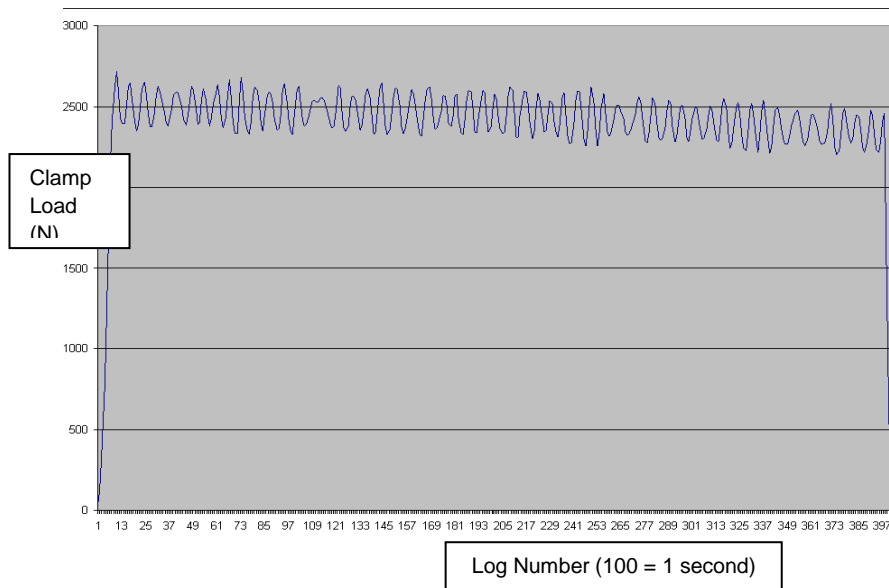


Figure 8.5a. Graph of Clamp Load vs. Log Number (time) for Plate B at 5000rpm, 2500N and 200°C

During the dyno testing, the hydraulic system was malfunctioning. The hydraulic system was leaking slightly and losing pressure, and at the time of the testing it was considered to have been rectified, but because the clamp load can be seen to be decreasing, rather than remaining constant, this implies that it is not the case.

Ideally, the clutch dynamometer would have been pressure controlled (as used on most race cars), as this would have compensated for the hydraulic malfunction. The combination of the loss of hydraulic pressure and the fact that the clamp load was controlled by a position sensor, and not a pressure sensor, it can be concluded that this is the reason that the drop in clamp load arose. Despite the clamp load decreasing, because this fault remained throughout the duration of the testing, the results still provide a valid set of data.

The region of 0 - 500°C was of particular interest when looking at the friction vs. temperature relationship, because the prediction is that the friction coefficient increases with the temperature. Figures 8.5b & 8.5c illustrate the friction coefficient properties for each plate against temperature, with individual curves for the different temperatures for a set clamp load and initial speed.

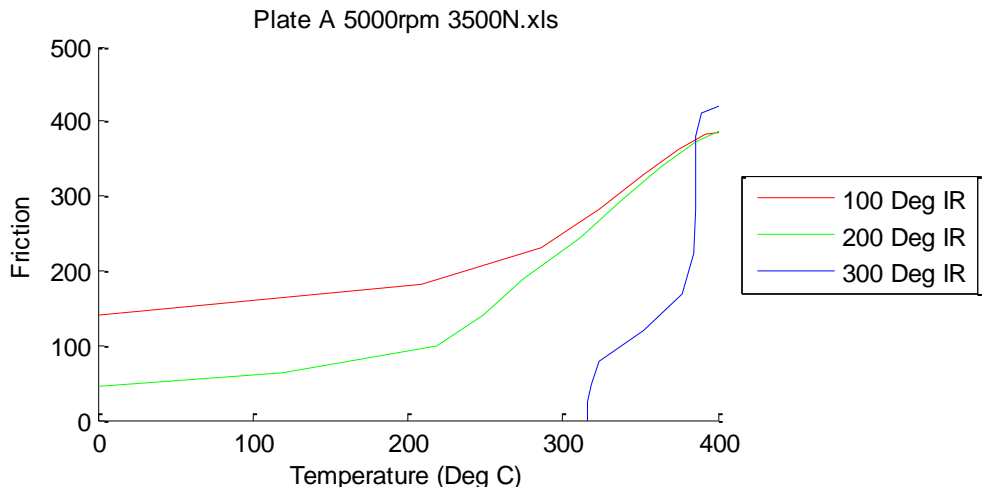


Figure 8.5b. Graph of Friction Coefficient vs. Temperature up to 400°C for Plate A at 5000rpm and 3500N Clamp Load

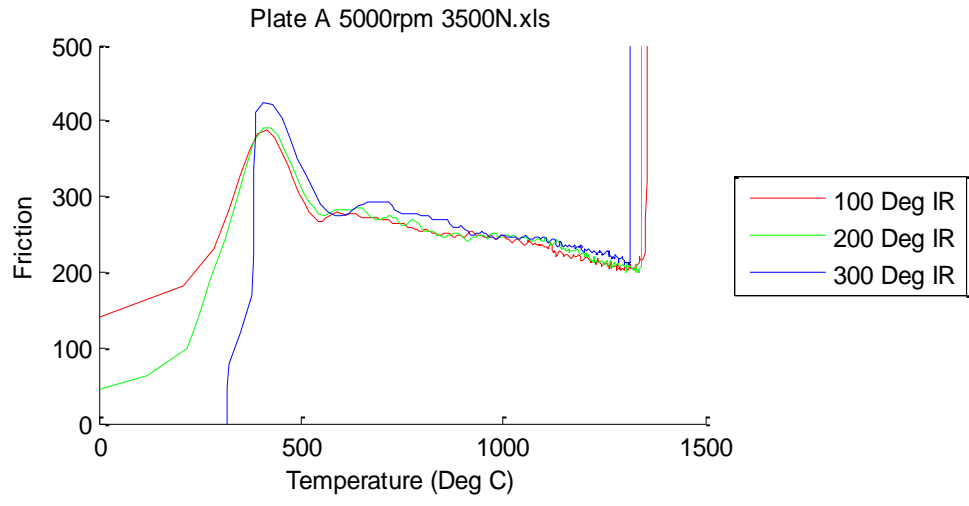


Figure 8.5c. Graph of Friction Coefficient vs. Temperature up to 1500°C for Plate A at 5000rpm and 3500N Clamp Load

As seen by the non linear relationship followed by the 300°C soak IR trace up to the 400°C generated by the plate slip in figure 8.5d above, at surface temperatures in excess of 300°C (as measured using the IR sensor) there is no clear relationship between the friction and the temperature. However, once the surface temperature increases past this 400°C, as seen in figure 8.5c, the three initial soak temperatures all follow the same linear trend. This observation could be due to thermal saturation; in the thermal decomposition testing (outlined in Chapter 14), the onset of the decomposition was at approximately 500°C.

By conducting further tests, it would be possible to determine whether the thermal decomposition was a contributing factor to the decline of the friction at temperatures about that of the thermal decomposition and beyond. To observe this experimentally, a clutch plate could be heated (via thermal energy generated by slipping the clutch plates over each other) to surface temperatures of 250°C (below the thermal decomposition temperature), 300°C and 600°C and observe the curves for each. Assuming that the oxidation is a surface property and that the oxidised part of the clutch face caused by the previous slip is worn away during the early part of the following slip, it would be possible to observe the effects of whether the clutch plate face is thermally decomposing at 300°C. By comparing the friction vs. temperature plots of all three plates, the effects of the oxidation could be determined.

#### **8.5.1 The Use of Scanning Electron Microscopy to Determine Oxidisation**

The use of a scanning electron microscope (SEM) may also offer some illustrative picture of the change in the surface properties of the different plates. Figures 8.5.1a, 8.5.1b and 8.5.1c give an illustrative overview of the surface state of the carbon clutches using SEM images.

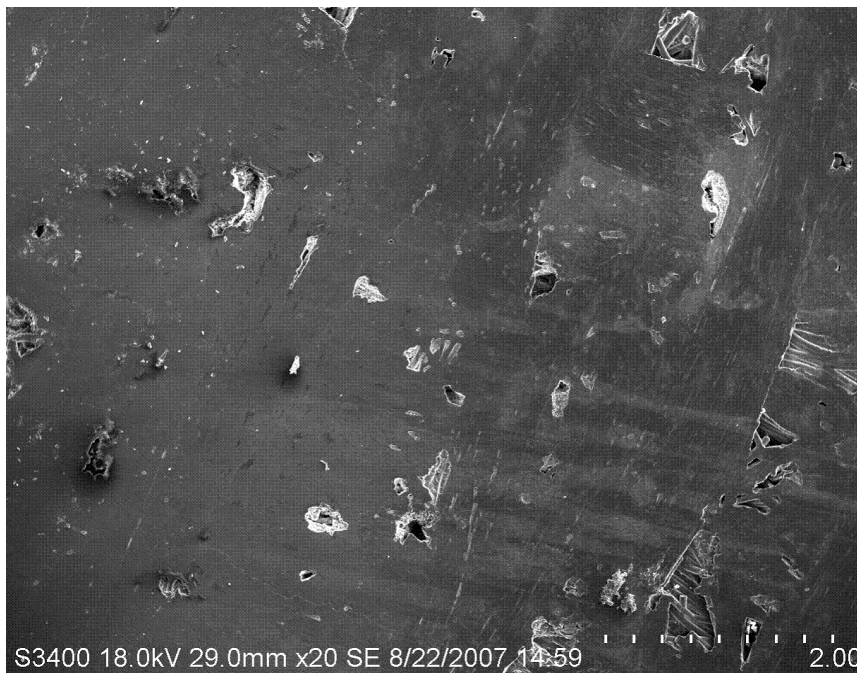


Figure 8.5.1a. SEM Photo Showing a Dull Banded, Oxidised Area, Moving Into an Un-oxidised Area of a Carbon-Carbon Clutch Disc (taken using the SEM at Honda Racing F1)

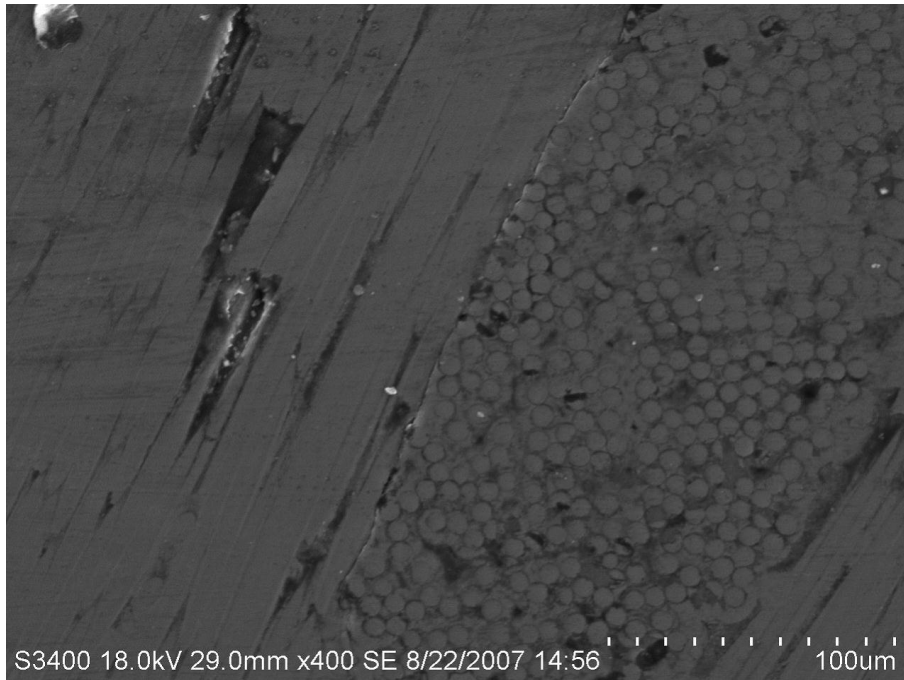


Figure 8.5.1b. SEM Photo of an Oxidised Area of a Carbon-Carbon Clutch Disc (taken using the SEM at Honda Racing F1)

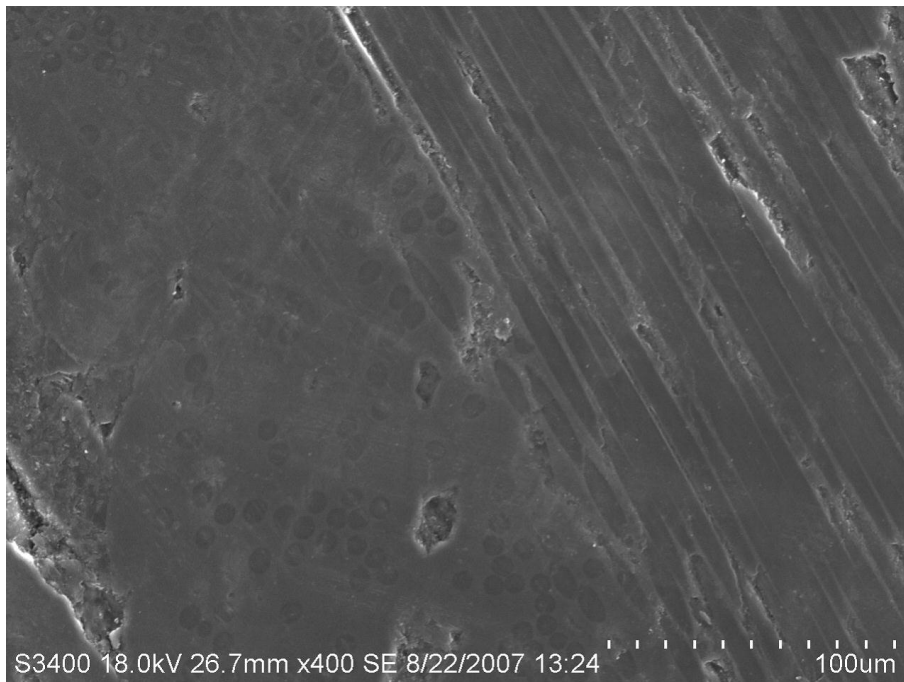


Figure 8.5.1c. SEM Photo of an Un-oxidised Area of a Carbon-Carbon Clutch Disc (taken using the SEM at Honda Racing F1)

Figure 8.5.1d is an SEM scan of a pore in a carbon-carbon clutch. The oxidation can clearly be seen in the white areas around the pore. This type of graphical

analysis would conclusively determine the presence of oxidation, which may be leading to the decrease in the friction coefficient above 500°C.

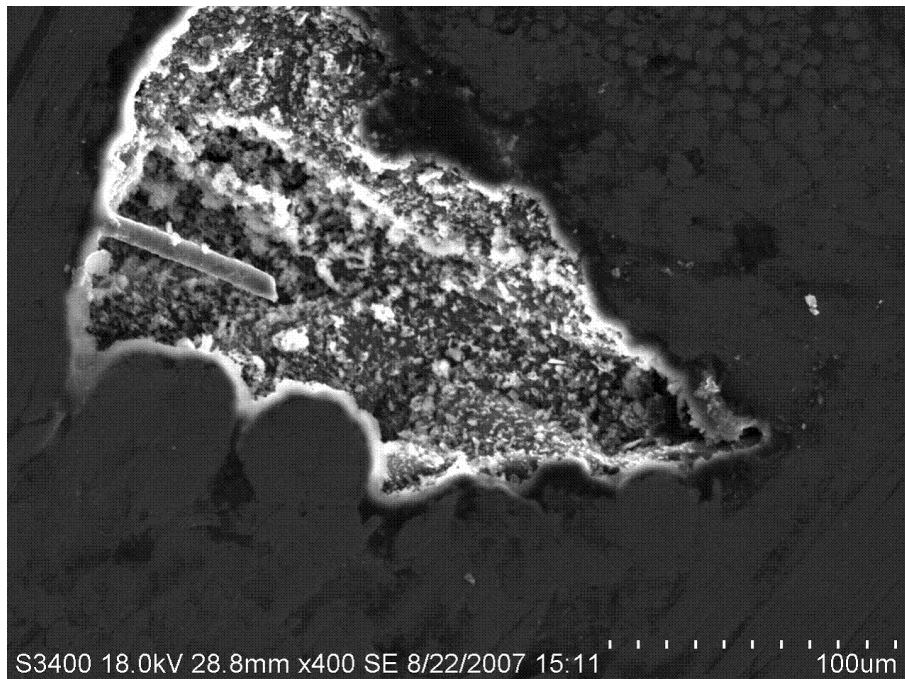


Figure 8.5.1d. SEM Photo of a Pore in an Oxidised Area of a Carbon-Carbon Clutch Disc (taken using the SEM at Honda Racing F1)

It could also be possible to see the effects of oxidation by conducting tests at the three temperatures (pre oxidation, oxidation and post oxidation) on the clutch dynamometer, whilst in an inert environment. If an air-tight chamber were constructed that could contain the clutch, this could be filled with an inert gas, such as argon or helium. From slipping the clutch in this environment, it would be possible to see whether the downwards friction vs. temperature relationship was due to oxidation or not. Argon and helium are inert gases, and so this would mean that oxidation would not take place. Conversely, the air-tight chamber could also be filled with oxygen to determine further the effects of oxidation, and to observe whether the onset temperature of this is reduced in a more oxygen-rich environment.

## 8.6 Processing of 'Banding' Raw Data

As the presence of banding was implied during the initial design of experiments, the experimental testing was designed to investigate this further.

A MATLAB script was required to compare the temperature of the non-banded plate to that of the corresponding slip for the banded plates. The aim of this script was to calculate a correlation coefficient to be used to determine which bands are acting upon the standard plate for any given slip and was done using the temperature versus time curve produced during the slip period for each banded and the standard flat plate, as described in section 8.4 The slip period is defined as the time during which the clutch is subjected to a clamp load and has the two sets of faces engaged.

Using the plots obtained in section 8.4 a comparison of the traces from the standard plate with those produced by the banded plates, led to observations as to how closely these curves matched, and from this it was possible to infer whether that particular band was active on the face of the plate for that particular slip. For example, if the temperature against time plots for the same input conditions between the standard plate and Plate A for thermocouple 1 (underneath band A at a radius of 54mm on the banded plate, and at a radius of 54mm on the flat plate) were identical, it could be inferred that this radius on the flat plate was experiencing the same energy input as the deliberately banded plate A, and so this band was also acting upon the flat plate during this slip.

These curve comparisons were done by using the correlation coefficient function within MATLAB. This correlation coefficient calculates the Pearson [166] correlation, and is defined as in equation 8.6a:

$$r = \frac{\sum_{i=1}^n x_i y_i - \frac{1}{n} \sum_{i=1}^n x_i \sum_{i=1}^n y_i}{\sqrt{\sum_{i=1}^n x_i^2 - \frac{1}{n} \left( \sum_{i=1}^n x_i \right)^2} \sqrt{\sum_{i=1}^n y_i^2 - \frac{1}{n} \left( \sum_{i=1}^n y_i \right)^2}} \quad \text{Equation 8.6a}$$

Where;

r = correlation co-efficient

x = time in seconds

y = temperature in degrees

Pearson's correlation reflects the degree of linear relationship between two sets of variables, ranging from -1 to +1.

Within MATLAB, there are two ways to measure the correlation coefficient, using the functions corr(x) and corrcoef. The difference between the two functions is that while the corrcoef function calculates the Pearson's correlation alone, the corr(x) function calculates the Pearson's correlation and the corresponding p-value

By using this function, it also greatly sped up the calculation time by reducing the processing capacity required by the model to determine the results.

The correlation coefficient results were returned from the MATLAB® script in a tabulated form and were displayed in the table format and illustrated in Table 8.6b.

	Plate A	Plate B	.....
3000rpm_1500N_100degrees	xx	xx	xx
3000rpm_1500N_200degrees	Xx	xx	Xx
.....	xx	Xx	xx

Table 8.6b. Table illustrating the correlation coefficients required for each set of test parameters and each banded test plate

The thermocouple temperatures were used as opposed to the infrared temperatures as the infrared sensor was placed at the mid radius of the standard flat plate, meaning that the sensor was not necessarily always viewing the hottest part of the friction surface. When comparing the temperatures of those seen on the plate and those seen in the bands, the most accurate temperature to use was



that of the corresponding thermocouple which lies underneath the particular band, a list of which is shown in table 8.6c:

<u>Plate Number</u>	<u>Thermocouple under Band</u>
A	1
B	2
C	3
D	4
E	5
F	6
G	7

Table 8.6c. Banded Plates and Their Corresponding Thermocouples

Before the script was created, it was important to ensure that all of the data was of a good quality with regards to noise, robustness and the general trends displayed, and also that there were no thermocouple drop outs (where the thermocouple ceases reading temperature) or other anomalies in the data. The data cut off points were at the beginning and end of the clamp loading stage. This was because the banding effect only occurs when the clutch is engaged and subject to loading.

Using the thermocouple that is under the band which is being correlated (e.g. thermocouple 1 for plate A correlation), and comparing it to the same thermocouple in the standard plate, it was possible to get a comparison between the two curves and the coefficient of how closely they compare. This co-efficient was then used in a table to determine which bands were acting upon the flat plate by looking at the correlation values.

When comparing the data from the banded plate to that from the standard plate it was essential that the data traces were of the same length, as any over run in one trace compared to the other would mean that the correlation would be inaccurate, as there would be no data to compare after the plate with the shortest vector had ceased to plot a trace. As each data trace was a different length, the MATLAB® script was programmed to set to cut the data down so that

the time trace began when the clamp load reached 50N, whilst it was increasing; and the time trace ended when clamp load again reached 50N, but this time, whilst it was decreasing. The shortest time trace of the two plates that were being compared was used as t=end. The larger of the data traces was cropped rather than stretching the shorter of the traces as this would have distorted the rate of change the temperature data.

Some data traces were observed to have ‘noisy’ temperature plots, but this was generally found at lower clamp loads, an issue that has been described in Chapter 6. As these ‘noisy’ traces are parts of the data, and are not thermocouple anomalies, the data could be used in the correlation script without any modification. If any thermocouple dropouts were found, the plan to overcome this would have been to extrapolate the results either side of the drop out, to make the data spike ‘disappear’.

The script was then set to determine a correlation coefficient based upon the two equal data traces from the standard flat plate and the enforced banding plate to which it was being compared and to tabulate these results for each given set of slip parameters, comparing the standard non-banded plate to each different banded plate in turn.

### 8.7 ‘Banding’ Data Results

Table 8.7a shows the results for the correlation coefficients, as determined by the MATLAB® script. Each value given in the cells is the correlation coefficient of the standard plate to the plate, and hence the band, which is identified as column headings in table 8.5d, at the test conditions listed in the row headings in the table.

	Plate A	Plate B	Plate C	Plate D	Plate E	Plate F	Plate G
<b>3000rpm1500NData</b>							
<b>100</b>	0.883827	0.959786	0.949134	0.989659	0.983143	0.9982	0.961879
<b>3000rpm1500NData</b>	0.889939	0.940862	0.937457	0.962105	0.982817	0.986834	0.969948

<b>200</b>							
<b>3000rpm1500NData</b>							
<b>300</b>	0.866131	0.917749	0.892479	0.92164	0.966917	0.97897	0.964982
<b>3000rpm2500NData</b>							
<b>100</b>	0.933144	0.931681	0.953955	0.961687	0.992527	0.957868	0.992136
<b>3000rpm2500NData</b>							
<b>200</b>	0.889033	0.919629	0.919538	0.929631	0.9953	0.971834	0.995489
<b>3000rpm2500NData</b>							
<b>300</b>	0.890265	0.930719	0.927703	0.9258	0.995718	0.995952	0.992053
<b>3000rpm3500NData</b>							
<b>100</b>	0.954003	0.976926	0.990015	0.987195	0.993493	0.9954	0.998611
<b>3000rpm3500NData</b>							
<b>200</b>	0.897858	0.937071	0.939699	0.929175	0.986129	0.947222	0.994236
<b>3000rpm3500NData</b>							
<b>300</b>	0.920968	0.938076	0.959049	0.953613	0.991065	0.985404	0.997981
<b>5000rpm1500NData</b>							
<b>100</b>	0.860004	0.942118	0.951496	0.96299	0.995177	0.992897	0.99737
<b>5000rpm1500NData</b>							
<b>200</b>	0.914264	0.967523	0.949446	0.873994	0.974908	0.993927	0.996441
<b>5000rpm1500NData</b>							
<b>300</b>	0.777278	0.865694	0.811647	0.930373	0.985965	0.967096	0.9926
<b>5000rpm2500NData</b>							
<b>100</b>	0.888319	0.934123	0.941149	0.945702	0.993871	0.995993	0.991549
<b>5000rpm2500NData</b>							
<b>200</b>	0.92576	0.951902	0.944946	0.892664	0.998576	0.994872	0.993933
<b>5000rpm2500NData</b>							
<b>300</b>	0.90438	0.959581	0.939703	0.929084	0.986389	0.985818	0.996196
<b>5000rpm3500NData</b>							
<b>100</b>	0.886809	0.935324	0.953536	0.949153	0.998503	0.981573	0.996762
<b>5000rpm3500NData</b>							
<b>200</b>	0.876015	0.933111	0.964587	0.909092	0.988369	0.97685	0.997843
<b>5000rpm3500NData</b>							
<b>300</b>	0.944535	0.988642	0.994746	0.818361	0.980065	0.978301	0.994979
<b>7000rpm1500NData</b>							
<b>100</b>	0.864969	0.889796	0.950718	0.963886	0.993993	0.987568	0.99275
<b>7000rpm1500NData</b>							
<b>200</b>	0.899091	0.915562	0.839547	0.961765	0.997905	0.96025	0.979732

<b>200</b>							
<b>7000rpm1500NData</b>							
<b>300</b>	0.841909	0.8859	0.950866	0.925379	0.998133	0.959907	0.987594
<b>7000rpm2500NData</b>							
<b>100</b>	0.924317	0.959985	0.984174	0.947304	0.982454	0.997276	0.997778
<b>7000rpm2500NData</b>							
<b>200</b>	0.843506	0.904917	0.935151	0.920949	0.99249	0.965315	0.999626
<b>7000rpm2500NData</b>							
<b>300</b>	0.846863	0.919706	0.957024	0.967253	0.992223	0.965531	0.977246
<b>7000rpm3500NData</b>							
<b>100</b>	0.883295	0.951199	0.965086	0.934778	0.995417	0.99858	0.990834
<b>7000rpm3500NData</b>							
<b>200</b>	0.815167	0.892158	0.94333	0.930475	0.985814	0.999182	0.998868
<b>7000rpm3500NData</b>							
<b>300</b>	0.739099	0.735176	0.916329	0.940436	0.98264	0.999634	0.997706

Table 8.7a. Correlation Coefficients of the Banded Plates Compared to the Standard Flat Plate

After the correlation between the flat plate and the banded plates had been tabulated, the highest correlating figure for each slip was transposed into a bar graph, with the order in which the slips took place along the X axis and the correlation factor on the Y axis in order to provide a simple visual comparison. Each plate was colour coded so that the bars in the graph could easily illustrate if any relationships were occurring with regards to the order in which the bands activate.

The graph was created as follows;

- The data was imported into MATLAB in array form from its excel spreadsheet (which was automatically generated by the clutch dynamometer control software)
- Give each slip a unique ID number (as shown in table 8.7b)
- Plot a bar chart for each set of slip parameters, for each plate on the x axis, against the correlation coefficient on the y-axis.

<b>Run Number</b>	<b>Run Details</b>
1	3000rpm1500NData 100
2	3000rpm1500NData 200
3	3000rpm1500NData 300
4	3000rpm2500NData 100
5	3000rpm2500NData 200
6	3000rpm2500NData 300
7	3000rpm3500NData 100
8	3000rpm3500NData 200
9	3000rpm3500NData 300
0	5000rpm1500NData 100
11	5000rpm1500NData 200
12	5000rpm1500NData 300
13	5000rpm2500NData 100
14	5000rpm2500NData 200
15	5000rpm2500NData 300
16	5000rpm3500NData 100
17	5000rpm3500NData 200
18	5000rpm3500NData 300
19	7000rpm1500NData 100
20	7000rpm1500NData 200
21	7000rpm1500NData 300
22	7000rpm2500NData 100
23	7000rpm2500NData 200
24	7000rpm2500NData 300
25	7000rpm3500NData 100
26	7000rpm3500NData 200
27	7000rpm3500NData 300

Table 8.7b. Slip ID Numbers, as used by the MATLAB® Model.

After the correlation between the flat plate and the banded plates had been tabulated, the correlation values for each slip were transposed into a bar graph (also seen in Appendix P), with the order in which the slips took place, i.e. the run number (see table 8.7b) along the X axis and the correlation factor on the Y axis.

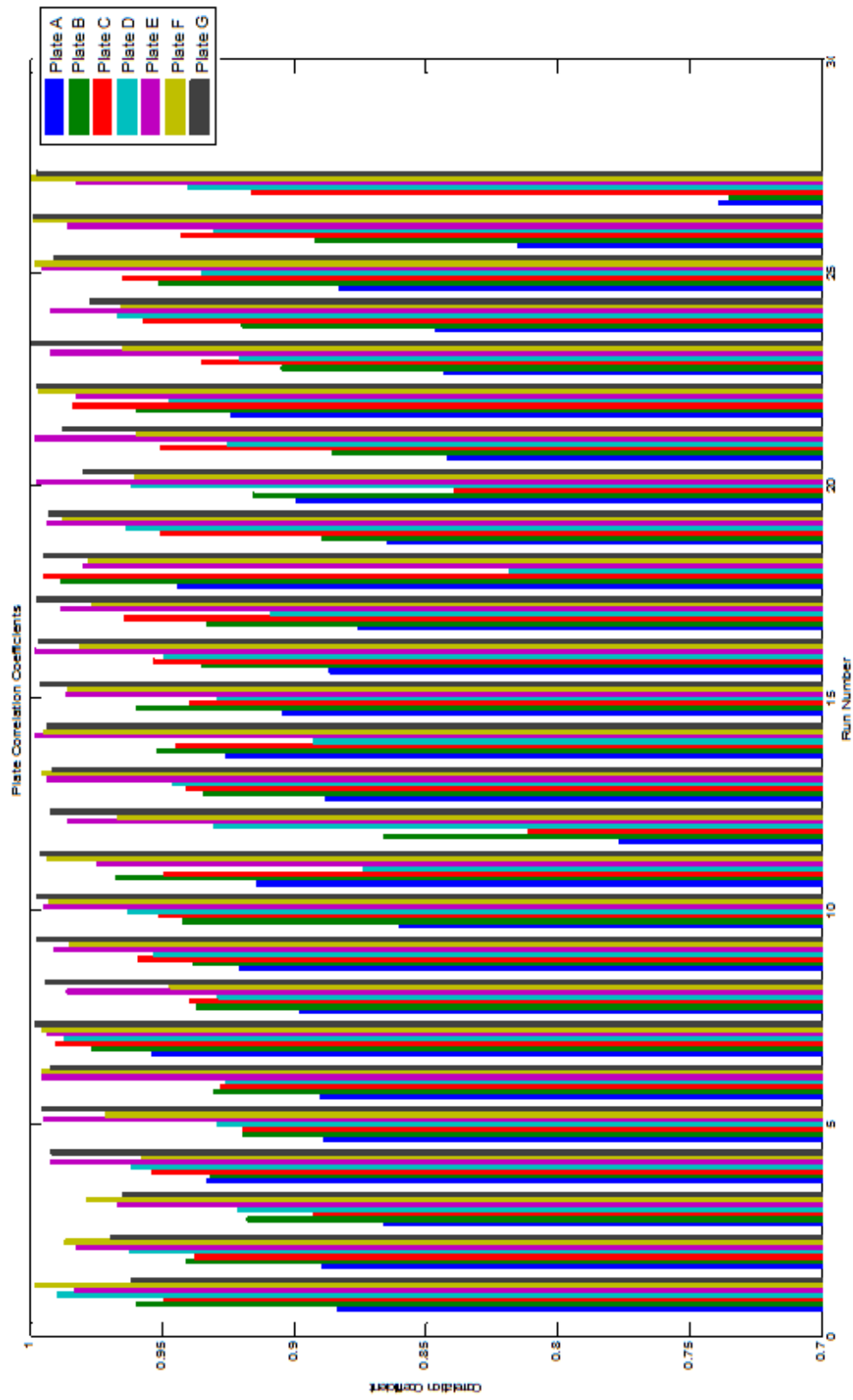


Figure 8.7c. Bar Chart Illustrating the Correlation Coefficients of All Banded Plates

Considering again the correlation coefficients given in table 8.7a, these have a very small range over which they acted, with the maximum correlation coefficient

being 0.999626 (Plate G) and the minimum being 0.735176 (Plate B). Table 8.7e illustrates the maximum (red) and minimum (green) correlation coefficients for each given set of slip conditions and is listed by run number as declared in Table 8.7b.

	Plate A	Plate B	Plate C	Plate D	Plate E	Plate F	Plate G
3000rpm1500NData 100	0.883827	0.959786	0.949134	0.989659	0.983143	0.9982	0.961879
3000rpm1500NData 200	0.889939	0.940862	0.937457	0.962105	0.982817	0.986834	0.969948
3000rpm1500NData 300	0.866131	0.917749	0.892479	0.92164	0.966917	0.97897	0.964982
3000rpm2500NData 100	0.933144	0.931681	0.953955	0.961687	0.992527	0.957868	0.992136
3000rpm2500NData 200	0.889033	0.919629	0.919538	0.929631	0.9953	0.971834	0.995489
3000rpm2500NData 300	0.890265	0.930719	0.927703	0.9258	0.995718	0.995952	0.992053
3000rpm3500NData 100	0.954003	0.976926	0.990015	0.987195	0.993493	0.9954	0.998611
3000rpm3500NData 200	0.897858	0.937071	0.939699	0.929175	0.986129	0.947222	0.994236
3000rpm3500NData 300	0.920968	0.938076	0.959049	0.953613	0.991065	0.985404	0.997981
5000rpm1500NData 100	0.860004	0.942118	0.951496	0.96299	0.995177	0.992897	0.99737
5000rpm1500NData 200	0.914264	0.967523	0.949446	0.873994	0.974908	0.993927	0.996441
5000rpm1500NData 300	0.777278	0.865694	0.811647	0.930373	0.985965	0.967096	0.9926
5000rpm2500NData 100	0.888319	0.934123	0.941149	0.945702	0.993871	0.995993	0.991549
5000rpm2500NData 200	0.92576	0.951902	0.944946	0.892664	0.998576	0.994872	0.993933
5000rpm2500NData 300	0.90438	0.959581	0.939703	0.929084	0.986389	0.985818	0.996196
5000rpm3500NData 100	0.886809	0.935324	0.953536	0.949153	0.998503	0.981573	0.996762
5000rpm3500NData 200	0.876015	0.933111	0.964587	0.909092	0.988369	0.97685	0.997843
5000rpm3500NData 300	0.944535	0.988642	0.994746	0.818361	0.980065	0.978301	0.994979
7000rpm1500NData 100	0.864969	0.889796	0.950718	0.963886	0.993993	0.987568	0.99275
7000rpm1500NData 200	0.899091	0.915562	0.839547	0.961765	0.997905	0.96025	0.979732
7000rpm1500NData 300	0.841909	0.8859	0.950866	0.925379	0.998133	0.959907	0.987594
7000rpm2500NData 100	0.924317	0.959985	0.984174	0.947304	0.982454	0.997276	0.997778
7000rpm2500NData 200	0.843506	0.904917	0.935151	0.920949	0.99249	0.965315	0.999626
7000rpm2500NData 300	0.846863	0.919706	0.957024	0.967253	0.992223	0.965531	0.977246
7000rpm3500NData 100	0.883295	0.951199	0.965086	0.934778	0.995417	0.99858	0.990834
7000rpm3500NData 200	0.815167	0.892158	0.94333	0.930475	0.985814	0.999182	0.998868
7000rpm3500NData 300	0.739099	0.735176	0.916329	0.940436	0.98264	0.999634	0.997706

Table 8.7d. Correlation Coefficients of the Banded Plates Compared to the Standard Flat Plate



Each maximum and minimum correlating plate was taken for each run and tabulated.

	Maximum Correlating Plate	Minimum Correlating Plate
3000rpm1500NData 100	A	F
3000rpm1500NData 200	A	F
3000rpm1500NData 300	A	F
3000rpm2500NData 100	B	E
3000rpm2500NData 200	A	G
3000rpm2500NData 300	A	F
3000rpm3500NData 100	A	G
3000rpm3500NData 200	A	G
3000rpm3500NData 300	A	G
5000rpm1500NData 100	A	G
5000rpm1500NData 200	D	G
5000rpm1500NData 300	A	G
5000rpm2500NData 100	A	F
5000rpm2500NData 200	D	E
5000rpm2500NData 300	A	G
5000rpm3500NData 100	A	E
5000rpm3500NData 200	A	G
5000rpm3500NData 300	D	G
7000rpm1500NData 100	A	E
7000rpm1500NData 200	C	E
7000rpm1500NData 300	A	E
7000rpm2500NData 100	A	G
7000rpm2500NData 200	A	G
7000rpm2500NData 300	A	E
7000rpm3500NData 100	A	F
7000rpm3500NData 200	A	F
7000rpm3500NData 300	B	F

Table 8.7e. Maximum and Minimum Correlation Coefficients of the Banded Plates Compared to the Standard Plate

Table 8.7b illustrates the order in which the test slips took place. This was imperative to understand, as the order in which the tests were run may have held some information regarding the pattern of the banding occurrence. Table 8.7b

was used in conjunction with figure 8.7f, in order to provide a clearer visualisation of the banding occurrence.

The graphical representation figure 8.7c gave the correlation coefficient for all plates and all variable slips. However, for clarity, in figure 8.7f, the graph was reduced to only include just the two highest correlation coefficients for each plate and was colour coded to aid clarity. Figure 8.5m shows the correlation coefficients of the two highest correlations for the slips in a run. All graphs are reproduced in Appendix Q as full sized versions.

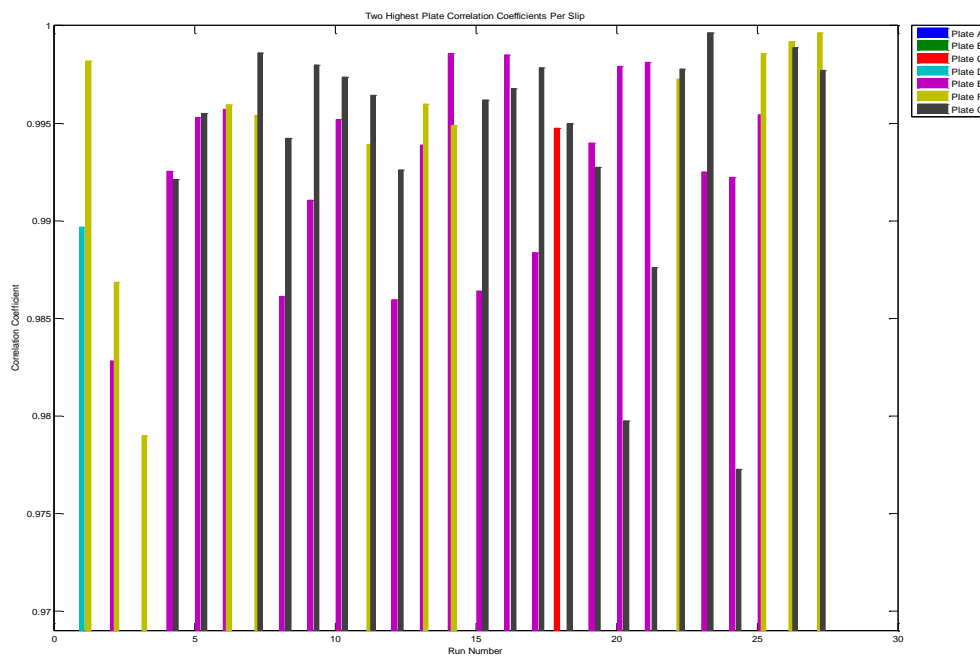


Figure 8.7f. Bar Chart illustrating the two Highest Correlation Coefficients of Standard Plate Compared to the Banded Plates

As seen in figure 8.7f, the two highest acting bands usually come from the outer radii of the clutch plate. By observing only the highest correlation coefficient (figure 8.7g), it was possible to further observe this effect. The closest correlation coefficient was the band that was on the outside radius of the plate.

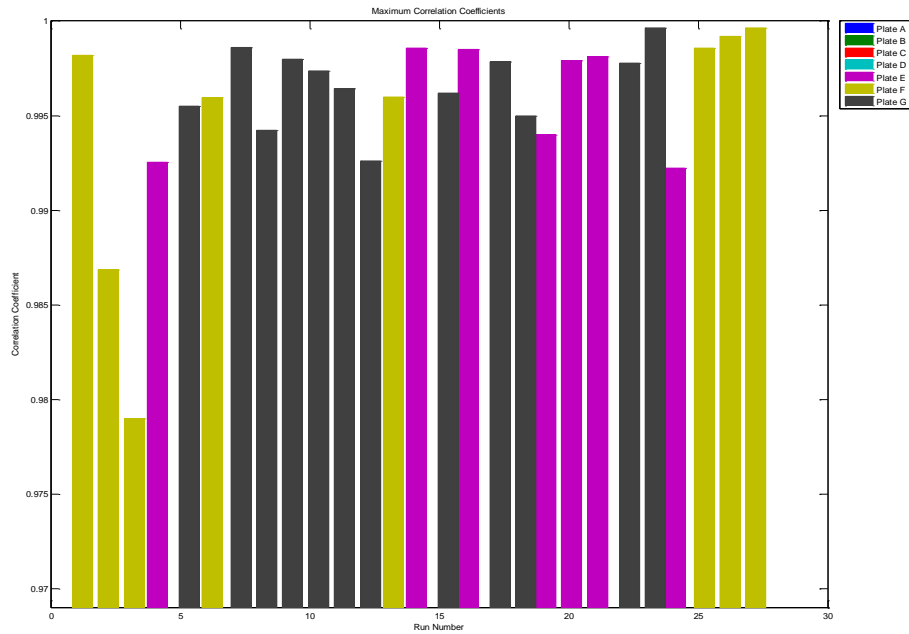


Figure 8.7g. Bar Chart Illustrating the Highest Correlation Coefficients of Standard Plate Compared to the Banded Plates

An important factor to note is that the friction coefficient of the carbon-carbon material is unpredictable. Due to the variability of the material the value for the friction / temperature relationship tends to vary. As Carbon-Carbon is a statistically complex material, it is vital to use a number of slips for the same set of variables, and to take an average, maximum, minimum and standard deviation of the data obtained, and to use this in calculations to obtain a range of values for which the friction temperature relationship is predictable.

Observing the two plates with the highest correlation coefficient it became apparent that the two highest correlations tend to appear on adjacent banded plates. This could suggest that perhaps the naturally occurring band is wider than the 4mm induced band that was used in the dynamometer tests.

The most important fact to note as a result of the 'banding analysis' is simply that the amount of information gained, the lack of repeatability and the similarity of the results from each set of banded plates mean that the application of the experimental errors from the thermocouples, infra red, rig and spreadsheet rounding would quite easily turn any hypothesis round. If the results had been

demonstrated an obvious trend, then a more detailed banding analysis with errors included could have been taken into account. However, as a clear banding theory could not be determined using the results obtained, this element of the work was abandoned at this point, with focus shifting to the mathematical model, based on the assumption of full face contact between the faces of the clutch plates.

## **8.8 Conclusions from Experimental Testing**

In retrospect it would have been more beneficial to have sacrificed some of the testing of the banded plates in order to obtain more repeated data sets. At the time of developing the testing, the initial experimentation had hinted at the possibility of banding as an important behaviour to investigate, and it was felt by both the author and the industrial partner that this should have been explored in depth. But with the hindsight the presence, predictability and effects of banding were all inconclusive in the tests undertaken.

In conclusion, the experimental element of the work did provide an important understanding of the frictional and temperature behaviour of the carbon-carbon material within the clutch.

## Chapter 9

### Input Modelling

This chapter outlines the three main components of the mathematical model, and describes in detail the first of these three: the input model of the clutch dynamometer.

From the experimental element of the testing, it was determined that the mathematical model account for complete face-to-face contact, and discount any banding theories. To accurately replicate a 'real life' situation, the model was split down into three logical elements (seen in Figure 9a; surface modelling, thermal modelling and modelling of the test rig, and was done this way for two reasons;

- 1) To allow for greater future flexibility for model development
- 2) To split up the two main thermodynamic heat transfer mechanisms (surface and thermal heat transfer) and the input parameters of the rig.

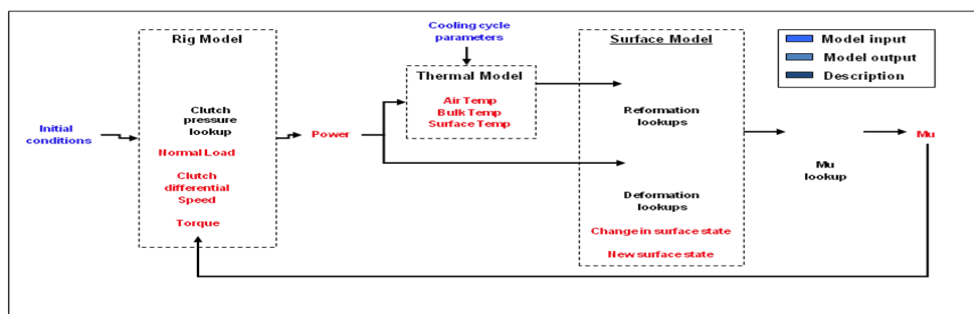


Figure 9a. Initial Schematic of the Mathematical Model.

Each element was considered in turn and independently modelled, before being put together into one final model that was used to determine the clutch friction for any given race start. The rig model was modelled to obtain profiles equivalent to those of a bedding cycle (to ensure its accuracy), the thermal model was used to generate surface temperature, whilst the friction model converts power and temperature profiles into deformation and reformation of the surface friction film, then using this current surface state to obtain the instantaneous value of the coefficient of friction.

A free body diagram of the system is shown below in figure 9b.

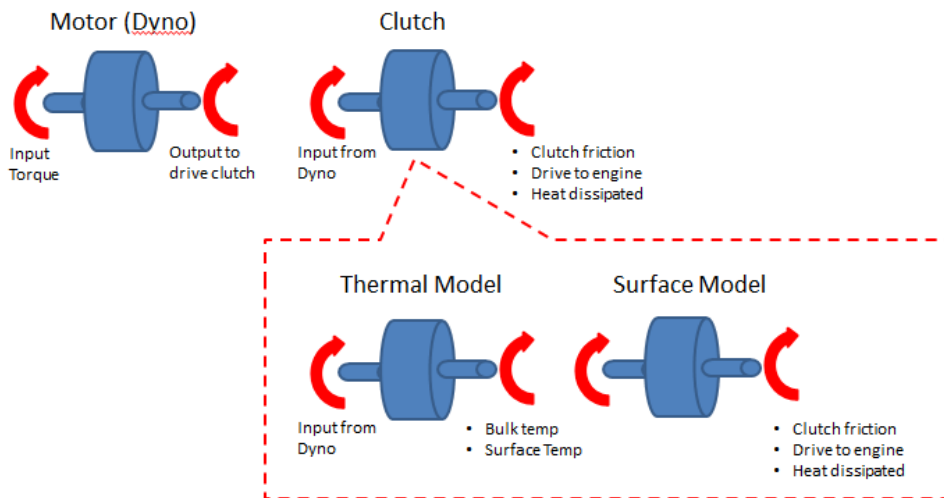


Figure 9b Free body diagram of the system to be mathematically modelled.

In this chapter, an overview of clutch dynamometers is given as background, and then the clutch dynamometer is split down into its component parts with the modelling process described in relation to these parts.

## 9.1 Rig Model Overview

Figure 9.1a highlights the rig model and where it resides in relation to the overall mathematical model.

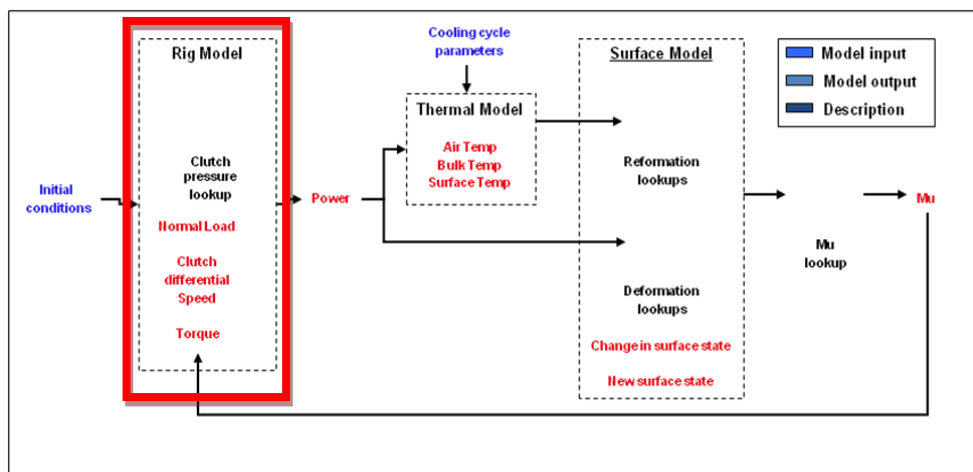


Figure 9.1a. The model schematic and where the rig model fits into it.

An important factor to note is that although the rig model is used to establish the power that will be transmitted through the clutch on the rig, this model could be adapted to be more generic, and could simply be an engine power input model. However, as data from the clutch dynamometer rig was used to validate the final model, it was essential that the model be as accurate and representative of the validation data as possible. More information on how this model could be changed to account for an on-car situation can be found in Chapter 13 – Critical Assessment.

## 9.2 Clutch Dynamometers: Overview

The clutch dynamometer is a device that is designed to simulate as closely as possible the real life conditions experienced by a clutch in all aspects of its operation. Each part of the dynamometer corresponds to a part of the car; the drive motor represents the engine, and provides the engine torque. In a car, the clutch is positioned between the drive motor and the gearbox, in the application on the rig the gearbox is represented as a load applied by the brake. Between the motor and the clutch are several gears which increase the speed and inertia of the load that is to be applied to the clutch.

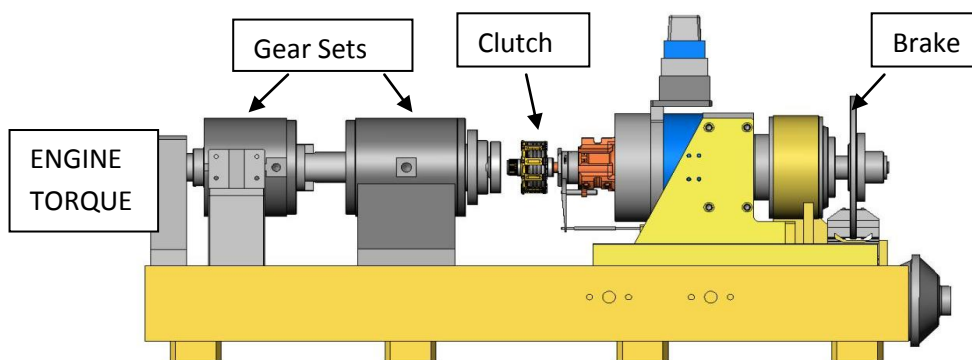


Figure 9.2a – Diagrammatic Representation of the Clutch Dynamometer at AP Racing

Figure 9.2b shows a clutch dynamometer used by HGT (a division of Honda Motorsport)

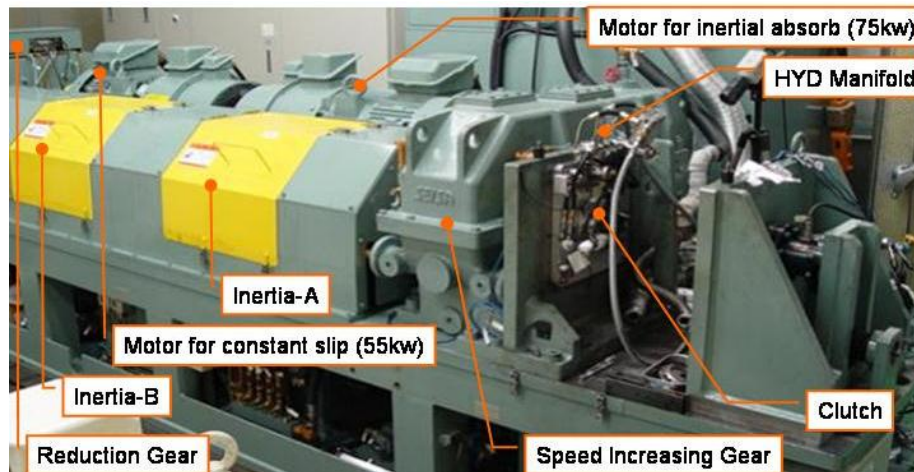


Figure 9.2b – The Clutch Dynamometer at HGT (Japan) [164]

There are two motors on the dyno at HGT; a 75kW motor, which is primarily used for inertial absorption tests, and a smaller 55kW motor, which is used for constant slip tests. Whilst the 75kW motor is capable of the higher input speeds, which are in the region of those typically seen on an F1 car during launch, the 55kW motor is capable of a higher input torque, as given in Table 9.2c and so is more suited for analysing the constant slip phase of the clutch by applying a constant torque to it.

Motor	75kW		55Kw	
	Input Speed	~25,000rpm	5000~15,000rpm	1~150rpm
Input Torque	-	-	~3,000Nm	~1,600Nm

Total Inertia = 0.2362~1.0629kgm<sup>2</sup> (Variable some level)

Table 9.2c – Motor specifications for the clutch dynamometer at HGT (Japan) [164]

### 9.3 Schematic of the Clutch Dynamometer

In order to accurately model the dynamometer, it was split up into its main parts of: motor, reduction gear, flywheel, speed increasing gears and finally the clutch (which will be further split down into a surface model and a bulk material model in Chapter 10 – Thermal Modelling and Chapter 11 – Surface Modelling).



Figure 9.3a shows a schematic of the clutch dynamometer at HGT, and how it is split down into its base components. Gears are highlighted in pink, motors in blue, fly wheels in yellow and the clutch specimen in purple.

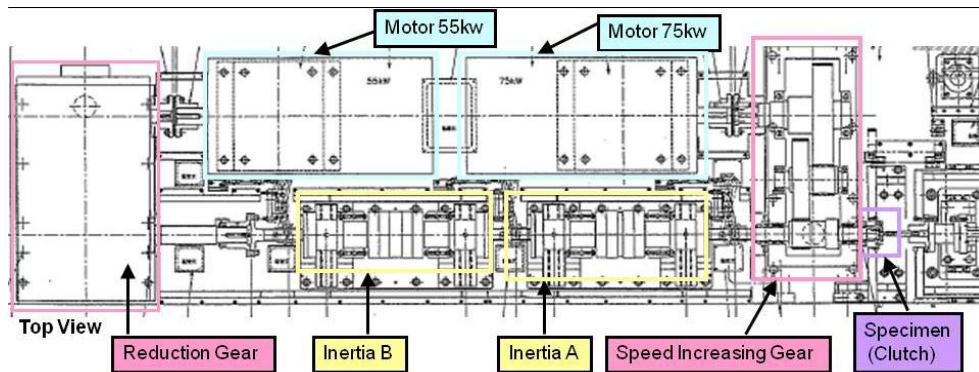


Figure 9.3a – Schematic diagram of the HGT Clutch Dynamometer [164]

A more detailed drawing of the dynamometer in figure 9.3a, and individual component drawings, can be found in Appendix R.

Figure 9.3b shows this in a more simplified manner;

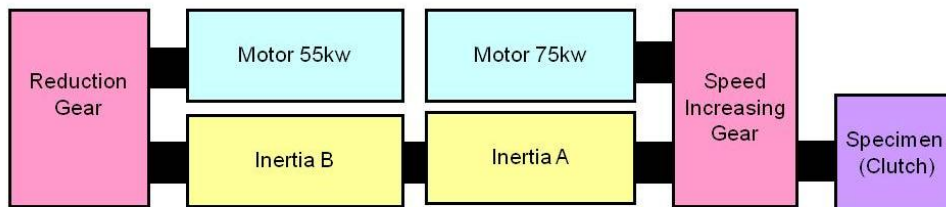


Figure 9.3b – Block Diagram of the Clutch Dynamometer at HGT

There are two main methods of operation for the clutch dynamometer; inertial absorption and constant slip. Inertial absorption is where the dynamometer is sped up to a set speed and inertia (as set by the motor and flywheels), and then the clutch is engaged either partially or fully (this can be set using the clamp load). The output signal of temperature and torque are observed as the clutch absorbs the inertia and transmits this energy into heat through friction. This method is of particular use when characterising a set amount of power that needs to be dissipated through the clutch in a set time, and can also help characterise the initial 'bite' of the clutch when it is first engaged. Figure 9.3c illustrates how the

power and inertia transmit through the dynamometer in the inertial absorption scenario. As in Figures 9.2a and 9.2b, gears are highlighted in pink, motors in blue, fly wheels in yellow and the clutch specimen in purple, with the orange lines indicating the transmission of power.

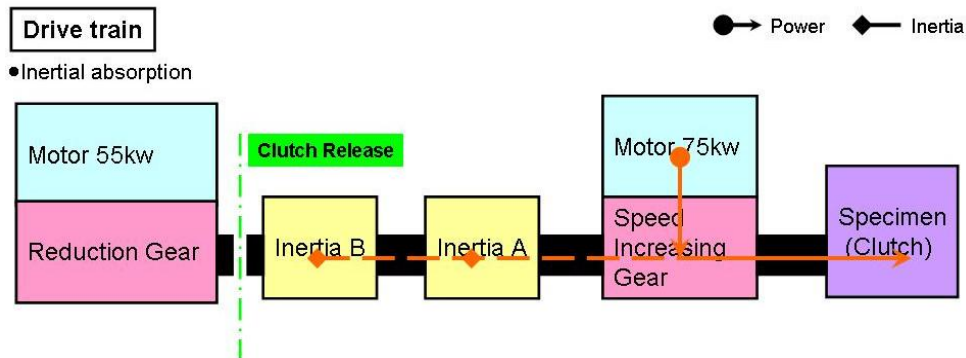


Figure 9.3c – Block diagram of the clutch dynamometer at HGT in inertial absorption configuration

Constant slip is different; here the motor is used to slip the clutch, much as an engine would do during a race start. The clutch is subject to a constant slip, the severity of which would be determined by the clamp load and the input torque of the motor. This method is used when trying to emulate the conditions of a clutch under launch conditions, as a constant power is being supplied to it and the clutch is required to slip until a set time when the clamp load would be increased and the clutch becomes fully engaged. This is the method of operation that is defined exclusively in the modelling in this project, due to its similarities to the ‘real life’ situation on the track. Figure 9.2d illustrates how the power and inertia transmit through the dynamometer in this scenario.

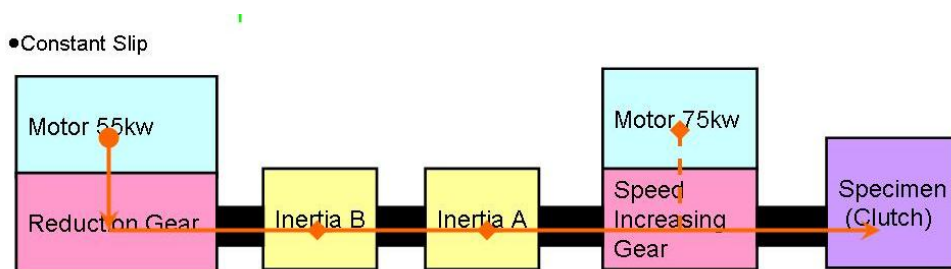
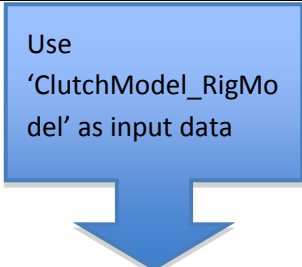
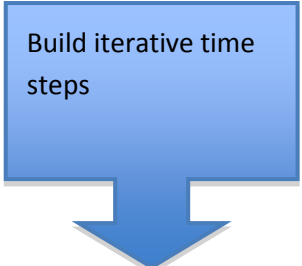
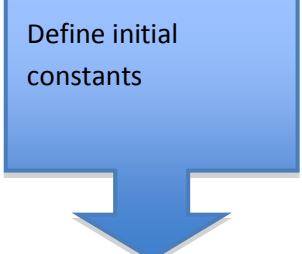
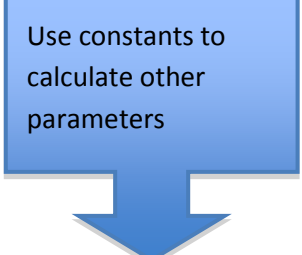








Figure 9.3d – Block diagram of the clutch dynamometer at HGT in constant slip configuration

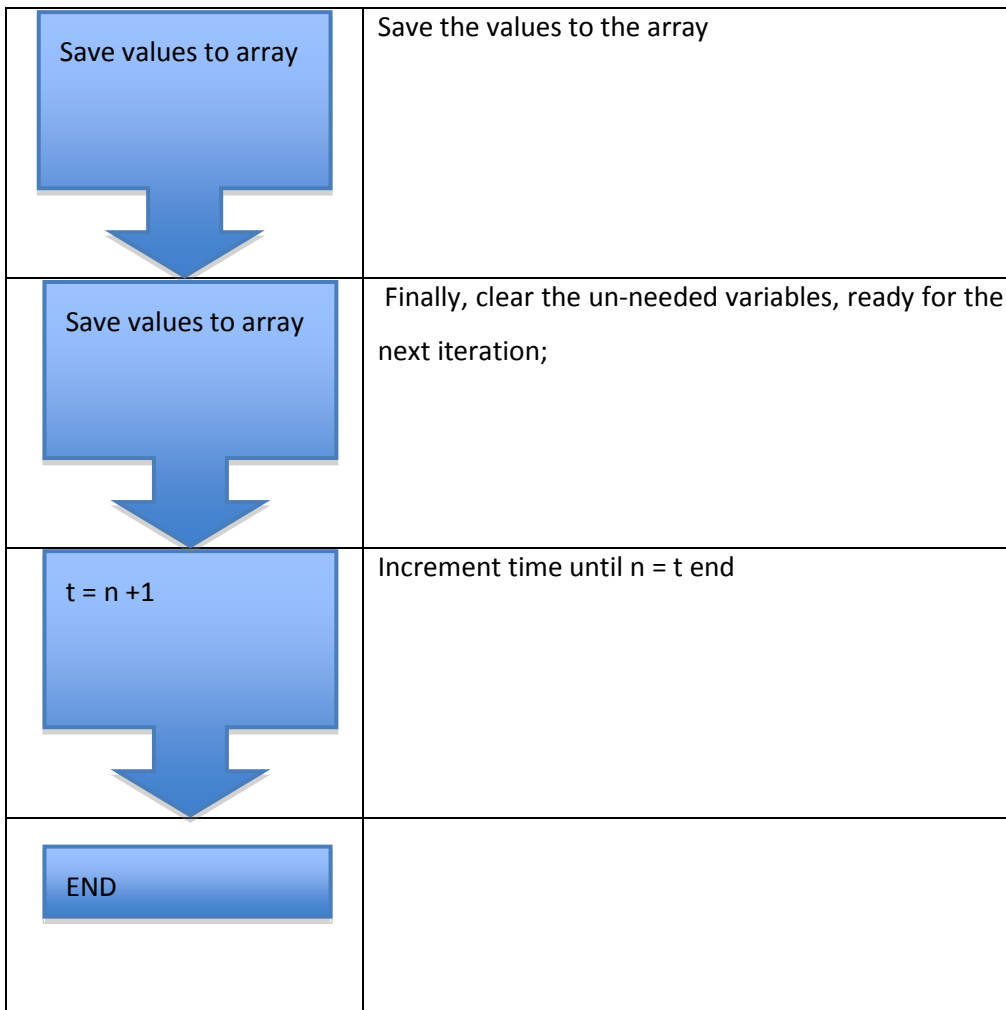
## 9.4 Clutch Dynamometer Modelling

Using the blocks in section 9.3 as the main starting point for building the code in MATLAB. Initial constants were first to be defined; first for the clutch itself, and then for the dynamometer.

A flow outline of the code is shown in this section and full code can be found in Appendix S

Flow Steps	Description
 <p>Use 'ClutchModel_RigModel' as input data</p>	<p>Define 'ClutchModel_RigModel' (where input data from the actual clutch rig is stored, and used as an input to the model)</p>
 <p>Build iterative time steps</p>	<p>Iterative time steps were built and populated with input values of time (Time_s), clutch evaluation data (sCluData), Time differential (dt_s), initial friction co-efficient (CluMuPrev), and the speed differential of the clutch plates (CluSpeedDiffPrev_rpm).</p>
 <p>Define initial constants</p>	<p>Define Clutch Constants, rig constants and initial condition (including ambient) constants</p>
 <p>Use constants to calculate other parameters</p>	<p>Calculate further information from the initial constants</p>

<p>Create functions for inputs clutch pressure and clamp load,</p> 	<p>Using the data from 'ClutchModel_RigModel', functions were created for the initial clutch pressure (CluPressurePrev_bar) and clamp load (CluClampLoadPrev_N)</p>
<p>Create functions for outputs of torque, speed and power</p> 	<p>Using the data from 'ClutchModel_RigModel', the functions were created for output torque (CluTorqueNew_Nm), speed differential of the clutch plates (CluSpeedDiffNew_rpm) and power output (CluPowerNew_W);</p>
<p>Is the clutch clamped or not?</p> 	<p>The evaluation of each time step was initiated, starting with an 'if' statement to determine if the clutch was clamped, or in the process of being clamped.</p>
<p>Calculate clamp load, transmitted torque and delta speed</p> 	<p>Clutch clamp loads, torques and speed differences were then calculated;</p>
<p>Determine new clutch speed</p> 	<p>Using the speed difference in RPM and function for the new torque, along with the value for the rigs inertia the new clutch speed was defined;</p>
<p>Calculate power dissipation</p> 	<p>Then the power dissipation was calculated using the torque and angular velocity and the speed difference was converted back to rpm;</p>



### 9.5 Model Code Validation

To validate the method used and the system being modelled, a measured torque trace from the actual dyno was input into the simulation in order to predict the clutch speed difference (the difference between the driving and driven plates) profile as an output. This simulation output was compared against the actual measured speed profile from the dynamometer at different actuation pressure profiles of 40, 50, 60 and 70 bar. The results are displayed in Figure 9.5a.

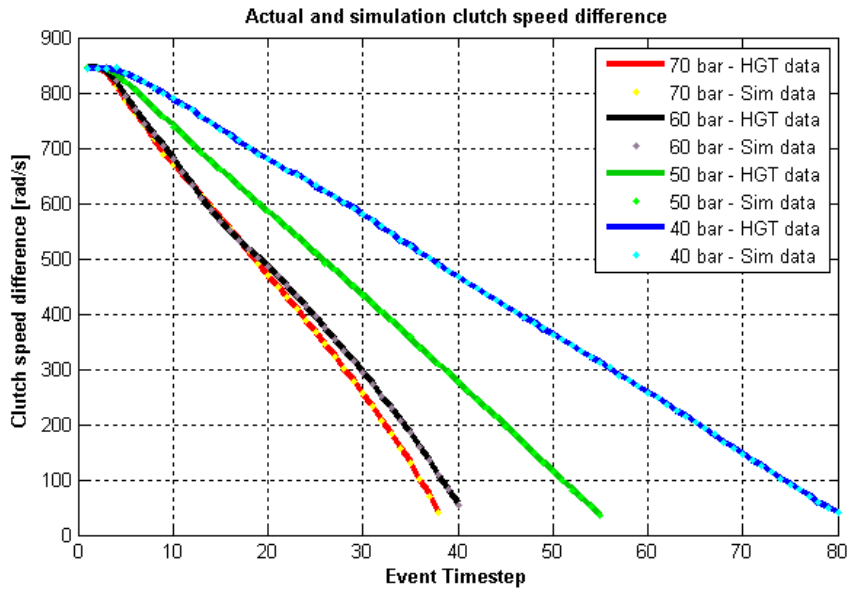


Figure 9.5a Dynamometer data versus. Modelled data for clutch speed difference for different values of clutch actuation pressure

From Figure 9.5a it can be seen that for all pressure profiles, the simulation output matches the measured profiles to an acceptable level of accuracy. Using a sample of 5 independent runs at constant speed input and a variation of clamp loads, each consisting of 500 – 800 data points (obtained from the testing outlined in Chapter 7). Using the speed (or velocity) data output from both the rig and the model and assuming that the mass of the clutch is equal in both representations, it was established that the model had an approximate kinetic energy accuracy of 2 – 5 %. This was done using equation 9.5b

$$\text{Kinetic Energy (KE)} = \frac{1}{2} * m v^2 \quad \text{Equation 9.5b}$$

Where:

m = mass of the clutch that is moving

v = speed (in this instance it is the speed delta from maximum to minimum to obtain the KE delta)

This simple validation of the rig modelling code gave confidence that the values obtained as an output of this model would be accurately represented as input data when being carried forward into the clutch thermal and surface models.

## Chapter 10

### Thermal Modelling

This chapter focuses on the modelling of thermal behaviour within the final model (Figure 10a below) and the incorporation of bulk material characteristics of the carbon – carbon material. A range of material characteristics are identified and quantified, along with the output values for speed and torque from the rig model to determine the bulk and theoretical surface temperatures. Due to the complexity of the surface morphology of the clutch material, further work is undertaken on the surface characteristics using the theoretical surface temperature outlined in this chapter.

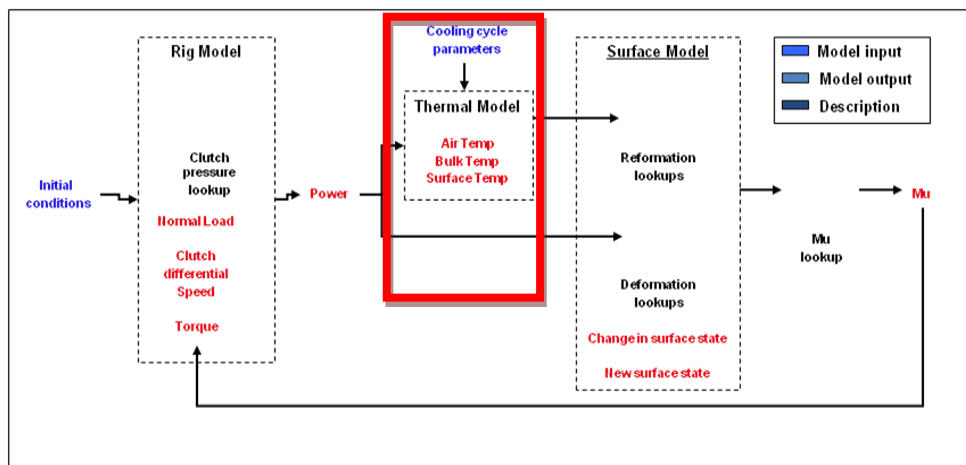


Figure 10a. The model schematic and where the thermal model fits into it.

This section of the work begins by focusing on the main material properties required for thermal modelling, and the determination of these through materials testing. The model is then described in terms of these characteristics and built up from thermal equations and known values.

#### 10.1 Thermal Modelling Background

As described in Chapter 3: Literature Review, there has been extensive work done in the area of thermal profiling of carbon-carbon. However the reliability of achieving the thermal profiling relies heavily upon the quality control procedure within the manufacture of the carbon-carbon plates. The thermal model

presented here is based on the main assumption that the material used within the clutch stack has been manufactured to a high quality, and has consistent material properties, as obtained from the samples used in materials testing. It is also assumed that the mechanical and thermal values will remain the same.

## **10.2 Materials Characterisation**

To understand how heat travels through the clutch plate, it was essential to know which thermal properties have an effect upon the dimensional and frictional properties of the clutch and to what extent this occurs. The most important of these in relation to the bulk thermal properties and the thermal behaviour of the carbon-carbon material are:

- Thermal conductivity,
- Specific heat at constant pressure, and
- Density.

One approach to obtain these values was to approach manufacturers themselves. The two main carbon friction material suppliers, Carbone Industrie and Hitco, are very reluctant to give detailed information on the exact material properties due to the highly competitive nature of their industry, and values vary at each time of enquiry. Dunlop Aerospace, a manufacturer of aircraft brakes, have also supplied information regarding the thermal properties of carbon plates, but this information is not specific to the carbon material being used in F1 clutch applications, so although this information can be used as a reference point, it cannot be relied upon for the thermal model of the clutch.

An alternative would be to use a generic property value made up from values given by various sources ranging from the internet to values supplied by the manufacturers themselves, but this would only provide an approximation. It was therefore decided that the best approach, to ensure that the material properties represented in the model were as representative as possible, was that samples of carbon from the same batch as the plates used in the testing on the dynamometer were independently tested by a specialist materials analysis lab.



Each of these material properties and their subsequent testing will now be described in turn.

### **10.2.1 Specific Heat**

Specific heat of a substance is the amount of energy required to raise 1 unit of mass of that substance by 1°C, and is more commonly described as the ability to absorb and communicate large quantities of heat. This thermal property is very important factor in the design and optimisation of a carbon clutch. The speed at which heat is lost from the plates to their surroundings is one of the key factors in the performance of a clutch, as it is by this mechanism that the kinetic energy arising from the speed difference between the driving and driven plates of the clutch is lost during slipping.

Using ASTM E 1269-05 (2005) *Standard Test Method Determining Specific Heat Capacity by Differential Scanning Calorimetry* [167]. This test method standard covers the determination of specific heat capacity by differential scanning calorimetry and is generally applicable to thermally stable solids and liquids. A differential scanning calorimeter (or DSC) measures the amount of energy (heat) absorbed or released by a sample as it is heated cooled or held at a constant (isothermal) temperature. Two samples are heated; one with a known specific heat capacity, and the unknown sample. By measuring the difference in required energy to heat the samples to the same temperature, the DSC calculates the differences between the two samples and hence gives the value for the specific heat capacity of the unknown sample.

A specimen of 6mm diameter by 1.4mm thick was used for the specific heat measurement testing. This measurement were taken over a temperature range of 50°C to 1000°C using a Netzsch DSC404 high temperature heat flux calorimeter. The temperature measurements were taken using 10% RhPt/Pt (Rhodium, Platinum / Platinum) (type S) thermocouples. These thermocouples are capable of reading temperatures within the range of 0°C to 1450°C to an accuracy of ±0.5°C to 1100°C and ±3.0°C to 1450°C. The test specimen was measured whilst heating at 10°C a minute from 50°C to 1000°C under an argon purge flowing at approximately 60ml per minute to prevent oxidation.

Two specific heat measurements were made on the carbon-carbon clutch material and the data from both runs is very similar and suggests that the material had not been changed by being heated up to 1000°C on the first run.

A cubic polynomial was fitted to the measured data and was then used to interpolate the specific heat values given in Appendix T.

### 10.2.2 Thermal Diffusivity / Conductivity

Thermal conductivity is defined as the quantity of heat transmitted in a unit of time through one unit of thickness in a direction that is normal to the surface, due to the temperature difference.

Thermal conductivity is impossible to measure by itself, however, thermal diffusivity is straightforward to measure and can be used to determine thermal conductivity using the relationship described in the equation below;

$$K = h_d \rho C_p \quad \text{Equation 10.2.2a}$$

Where;

K	Thermal conductivity
$h_d$	Thermal diffusivity
$\rho$	Density
$C_p$	Specific heat

The following standards outline the test procedure for thermal diffusivity to ensure accurate and repeatable tests;

- BS EN821-2:1997 *Advanced Technical Ceramics – Monolithic Ceramics – Thermo-physical Properties – part 2: determination of thermal diffusivity by the laser flash (or heat pulse) method [168]*.. This part of the standard specifies the method for the determination of thermal diffusivity of advanced monolithic technical ceramics, to an accuracy of approximately  $\pm 5\%$ . It is suitable for the range  $0.1\text{mm}^2/\text{s}$  to  $1000\text{mm}^2/\text{s}$  at temperatures greater than  $-180^\circ\text{C}$ .

- BS EN1159-2:2003 *Advanced Technical Ceramics – Ceramic Composites – Thermo-physical Properties – part 2: determination of thermal diffusivity* [169]. This part of the standard describes the laser flash method for determination of thermal diffusivity of ceramic matrix composites with continuous fibre reinforcement. The experimental conditions are such that the material behaves in a homogeneous manner for each of its axes of anisotropy and that the heat transfer occurs only by thermal conduction. The method is applicable to materials which are physically and chemically stable during the measurement, and covers the range of temperature between 100K and 2800K. It is suitable for the measurement of thermal diffusivity values in the range between  $10^{-4}\text{m}^2\text{s}^{-1}$  and  $10^{-7}\text{m}^2\text{s}^{-1}$ .

One side of a plane and parallel test piece is exposed to a uniformly distributed energy laser pulse emitted from a controlled source that is of very short duration (approximately 0.1s) in comparison to the transient half time. The transient temperature on the opposite face is recorded as a function of time, as shown in figure 10.2.2b.

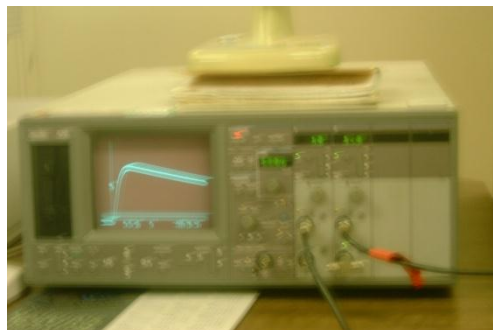


Figure 10.2.2b Thermal Diffusivity Test Signal

The difference between these two values, along with the material density and thickness are used to calculate how quickly the thermal energy has travelled through the specimen, and hence to calculate the thermal conductivity. Following the testing of the carbon-carbon specimen, a control specimen with a known thermal conductivity was tested to enable the conductivity of the specimen holder to be eliminated. The specimen is placed in a holder (figure 10.2.2cd) and then placed in the vacuum chamber. This is done so as to eliminate the thermal

conductivity of the air around the specimen, which would carry heat away from it and not give true values.



Figure 10.2.2c Thermal Diffusivity Sample Holder

The energy source is a laser built specifically to heat the surface of the specimen in a uniform manner. A photograph of the apparatus is given in figure 10.2.2d.

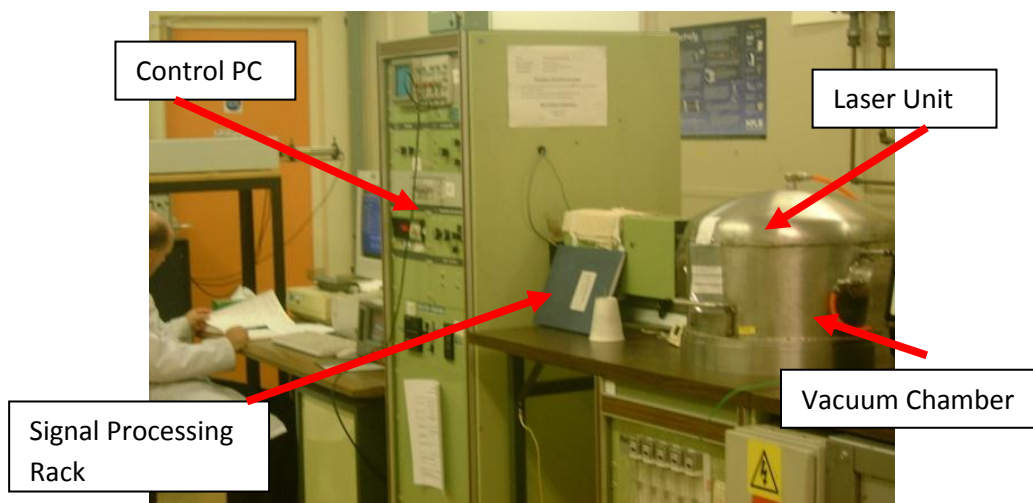


Figure 10.2.2d Thermal Diffusivity Test Apparatus

Two measurements were made on the material and the data from both tests were very similar, which again suggests that the material has not been changed by being heated up to 1000°C in the first test. Raw data obtained from the thermal diffusivity and thermal conductivity testing is given in the table in Appendix T.

Figure 10.2.2e shows a plot of the thermal diffusivity against temperature for the clutch plate material during the heating and cooling phases.

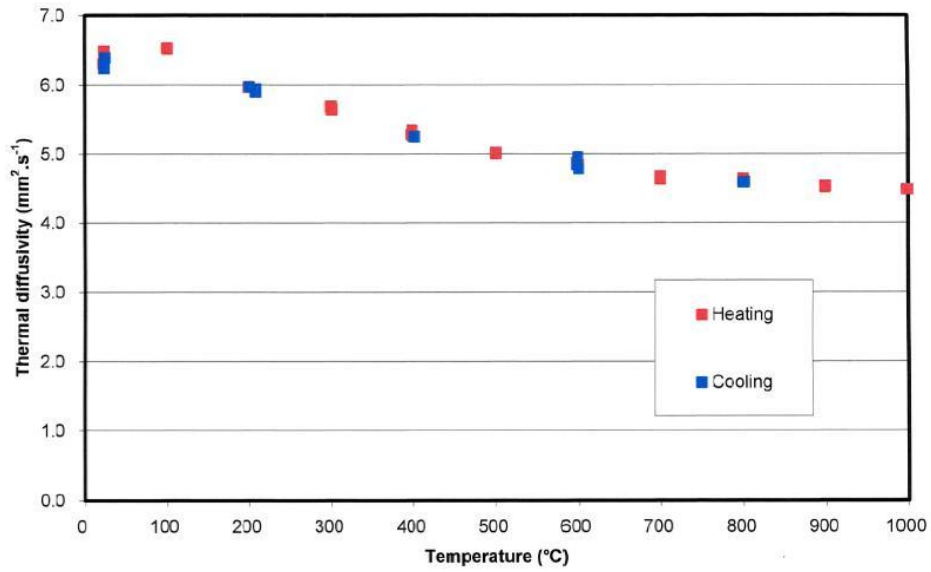


Figure 10.2.2e. Thermal Diffusivity of a Carbon Clutch Plate Material

Figure 10.2f shows the thermal conductivity of the clutch plate material at the different temperatures tested.

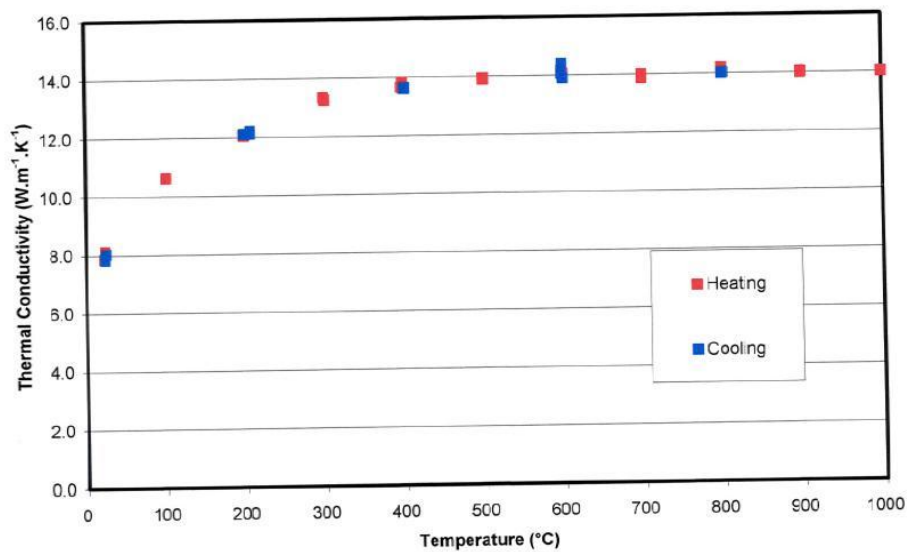
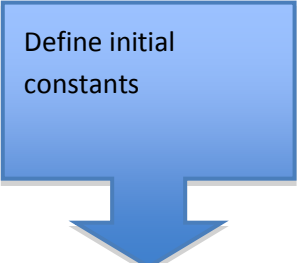
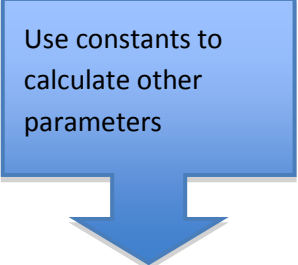
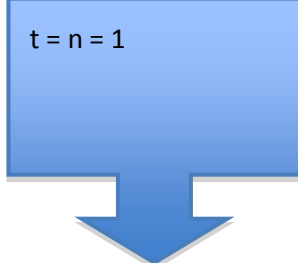
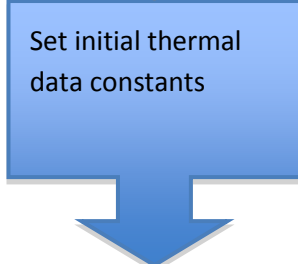


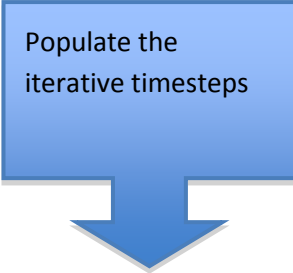
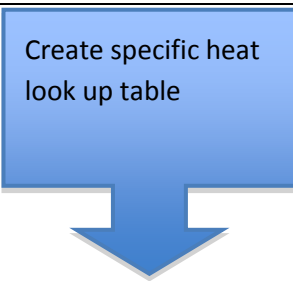
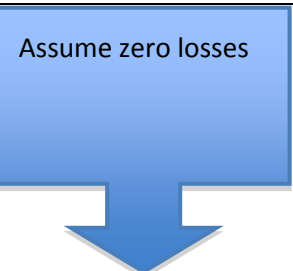
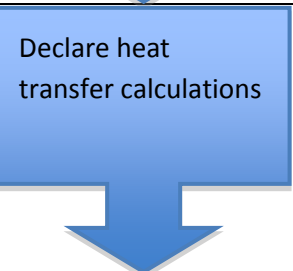
Figure 10.2f. Thermal Conductivity of a Carbon Clutch Plate Material

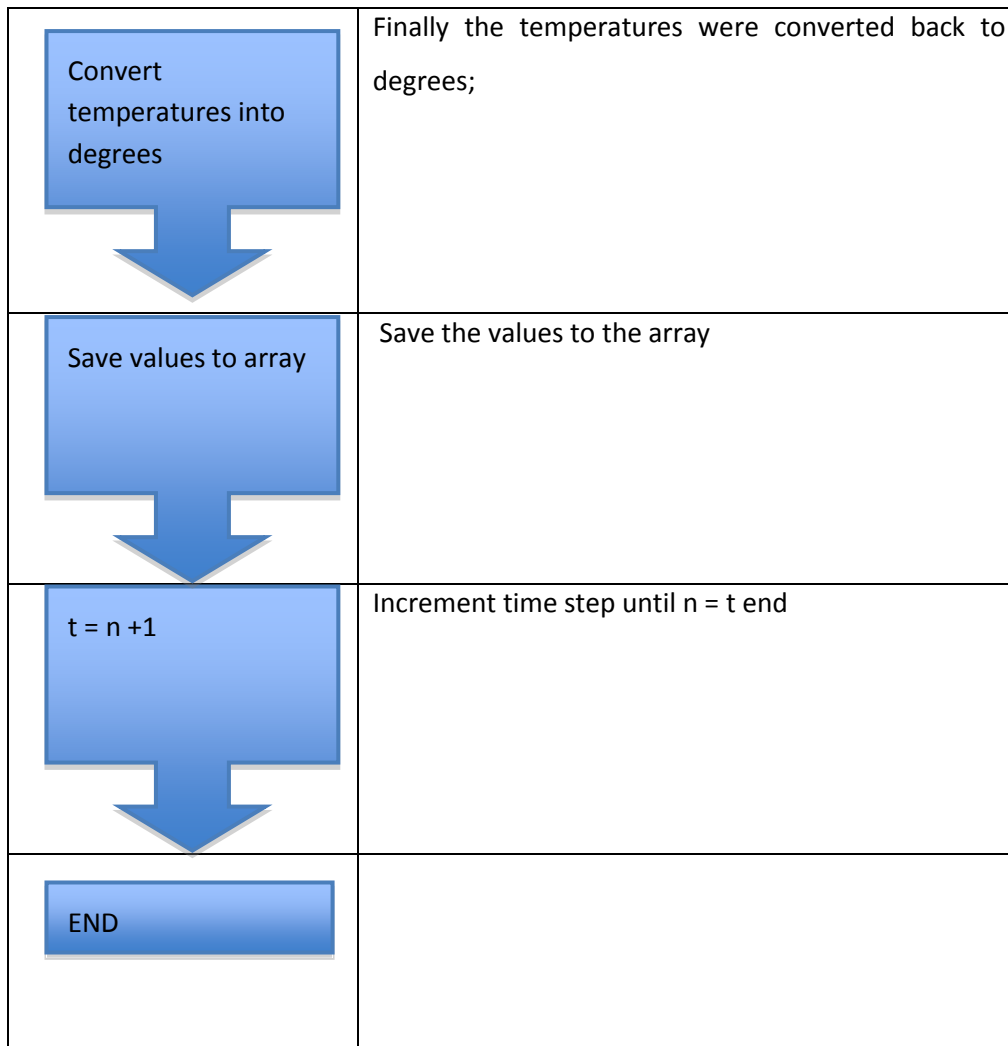
Data from the thermal conductivity / diffusivity and the specific heat experiments were placed into Excel look up tables, to be used in the MATLAB model.

### 10.3 Thermal Model Code Generation and Structure

A flow outline of the code is shown in this section and full code can be found in Appendix U

Flow Steps	Description
 <p>Define initial constants</p>	<p>Initial constants were named and defined;</p> <p>Ambient conditions were also defined</p>
 <p>Use constants to calculate other parameters</p>	<p>Constants were used to determine further parameters, such as area and total volume of material.</p>
 <p>t = n = 1</p>	<p>Time step was set to 1 for the first data pass.</p>
 <p>Set initial thermal data constants</p>	<p>The initial conditions were specified for the thermal data obtained from the materials testing for;</p> <p><i>Density of material [kg/m<sup>3</sup>]</i></p> <p><i>Emissivity of c-c</i></p> <p><i>Specific Heat Capacity at 27degC [J/kg*K]</i></p> <p><i>Specific Heat Capacity at 1000degC [J/kg*K]</i></p> <p><i>Thermal conductivity perpendicular to friction surface at room temp [W/m.K]</i></p>

 <p>Populate the iterative timesteps</p>	<p>Populated iterative timesteps using functions and created using data from the program, 'ClutchModel_ThermalModelSimple' with input values of clutch evaluation data (sCluData), Air temperature (TempAirPrev_degC), bulk temperature (TempBulkPrev_degC), surface temperature TempSurfacePrev_degC, clutch power determined from the rig model (CluPowerNew_W) and time incrementation (dt_s). And this was written in the code as;</p>
 <p>Create specific heat look up table</p>	<p>Next the specific heat capacity lookup was created for both the bulk and surface, using the materials testing data and a series of 'if' functions:</p> <p>If the previous surface temperature is less than 27 degrees, then assume that the heat capacity is equal to the heat capacity at 27 degrees.</p> <p>If it's more than 1000 degrees, then assume the specific heat to be equal to that at 1000 degrees.</p> <p>If between 27 and 1000 degrees then perform a linear interpolation of the results obtained from the materials testing.</p>
 <p>Assume zero losses</p>	<p>An assumption was written that the entire energy dissipated is absorbed into the friction surface as heat and that there are zero losses.</p>
 <p>Declare heat transfer calculations</p>	<p>Next the heat transfer calculations were written for;</p> <ul style="list-style-type: none"> <li>• Heat flux from surface to bulk conduction</li> <li>• Heat flux from surface to bulk convection</li> <li>• Heat flux due to radiation</li> <li>• Total flux for surface, bulk and ambient</li> </ul>



The subsequent output data of this model is the temperature of the clutch for the power output given by the model created in Chapter 9, at any defined time-step during its engagement. However, despite the model also giving a value for the temperature of the surface of the clutch, this is an approximation . Hence the model is developed further in Chapter 11, where surface characteristics such as different wear modes and different surface roughness values are accounted for.

#### 10.4 Validation of the Thermal Model

When creating the thermal model code, it was written in such a way as to minimise the required changes to the code to be able to adapt it for representation of the car data. This was specifically done because the overall aim



of the project was to obtain a model that can be used to determine the coefficient of friction of the clutch on the car during the formation lap.

Due to the difficulty of measuring this thermal effect part of the process experimentally, it was impossible to devise a method to accurately determine the validity of this thermal component of the model alone. One suggestion would have been to use the thermocouple values from the experimental dynamometer testing carried out in Chapter 7, and the input power from the rig. There are inaccuracies in the model at this stage, because the effects upon the coefficient of friction due to the surface characteristics of the carbon-carbon material have not been included in the model. These would have a significant effect on the temperature gradient of the clutch plates.. Because the model presented in this chapter was to be part of a much larger overall model, as will be described in Chapters 12, it was decided to leave the validations which took into account surface characteristics until the validation of the final model

## Chapter 11

### Surface Modelling

When modelling the clutch as a whole the surface sub- model is undoubtedly the one that requires the most accuracy, as it is this that predicts the contact characteristics between the two material faces. The surface model is also the most complicated model to create due to the complexities of the surface wear mechanisms. The model requires factors for the surface morphology, the chemical bonding of the carbon-carbon material and the dust produced by the material contact (which acts as a lubricant for subsequent slip events). This chapter goes into depth regarding the background to surface modelling, the surface characteristics of the carbon-carbon material and how these characteristics are modelled within the model, along with the modelling of other affecting factors. Thermal decomposition testing is also undertaken to obtain material specific information for the lookup table used in the model.

The surface model is structured into three sub models, as shown in Figure 11a.

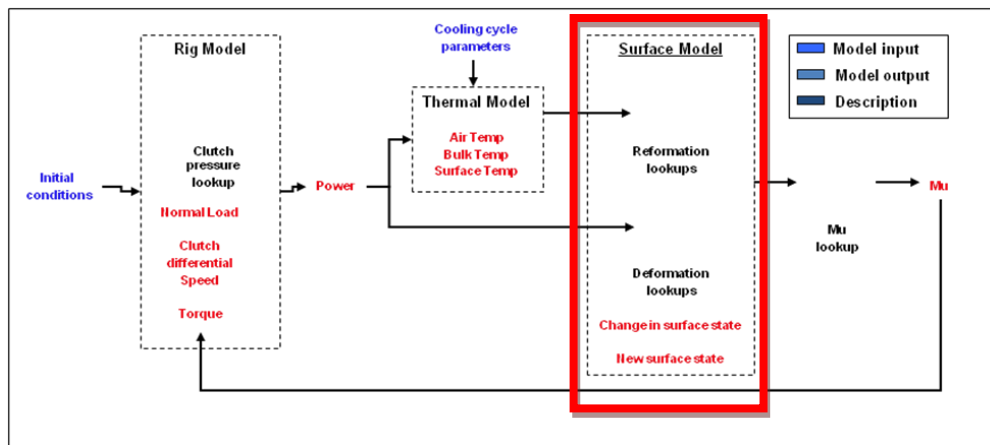


Figure 11a. The model schematic and where the surface model fits into it.

## 11.1 Surface Characteristics

As discussed in the literature review, there are three types of carbon-carbon surface morphology [50]:

- Type I, which has a machined or polished appearance and a negligible amount of surface debris. This has a low coefficient of friction.
- Type II, which has a dull unpolished surface and a thick layer of powdery wear debris with particles all less than 5 microns in diameter. This has a high friction coefficient.
- Type III, which has a smooth polished surface with surface wear debris that has been transformed into a smooth friction film. This has a low coefficient of friction.

Figures 11.1 a, b and c show SEM photos of carbon – carbon discs with each of the three morphologies.

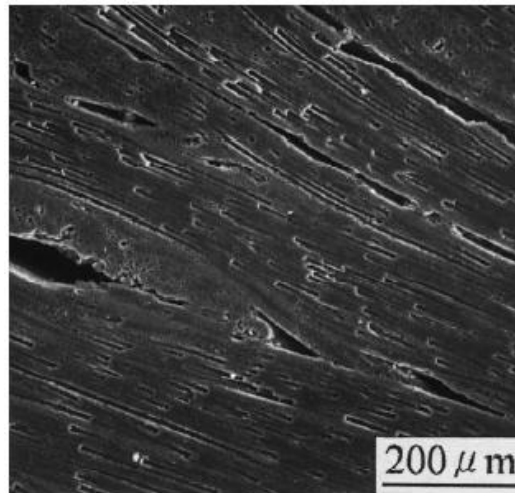


Figure 11.1a. SEM highlighting the surface morphology of as-polished disc (Type I) [50]

Type I. This type of wear happens at low energy conditions. At these conditions, particulate powdery wear debris is formed. The worn particles cause abrasive wear which is the most damaging mode in terms of carbon-carbon wear, very much like applying a sand paper over the surface of the clutch plate. These particles are mostly formed by carbon matrix, not carbon fibres.

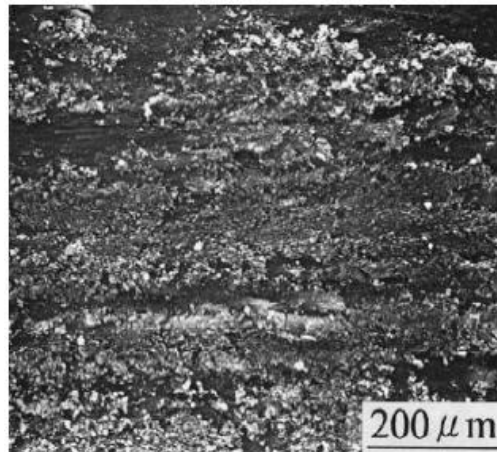


Figure 11.1b. SEM highlighting the surface morphology of bedded material (Type II/Type III transition) [51]

Type II. This type of wear happens at high energy conditions. The difference between this and type I is that at these conditions, a smooth friction film is formed on the surface of the clutch which serves as a solid self-lubricant. This film protects the material, therefore it wears less. This is because under higher braking energy conditions, higher pressure and temperature assist deformation of wear particles to form a debris film. The particles do not melt though, but plastically deform. However, this 'lubricant' means that the efficiency of the clutch suffers as the friction coefficient is lower once the material has formed such a film.

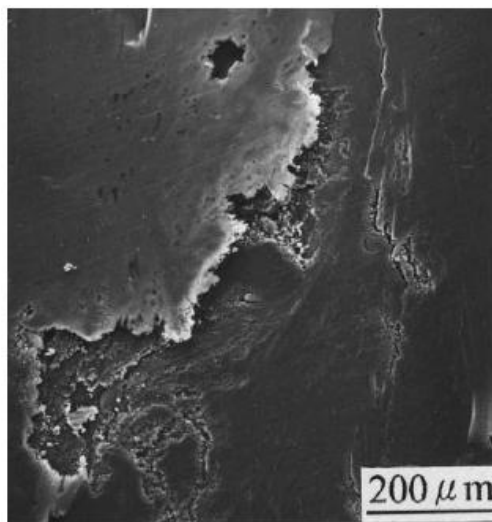


Figure 11.1c. SEM highlighting Type III surface morphology (lubricating friction film) [50]

Type III. If temperature and braking energy rise even higher, the friction film would break into chunks due to shear stresses and the wear rate would increase

244

again. The other undesirable thing that could happen at extremely high energy clutch slips is oxidation of the materials.

Proper carbon-carbon tribological performance is highly dependent on the formation and destruction of the friction layer. Under certain conditions the high coefficient of friction, type II morphology is worked into a smooth and dense compacted layer of carbon that acts as a lubricating film; this yields low coefficient of friction type III morphology. The disruption and reformation of this layer is a continual dynamic process: disruption of the film being driven by shearing due to high power dissipation, with reformation tending to occur at higher temperatures in the materials working range.

## **11.2 Materials Characterisation**

As described in the literature review, oxidation is a process of thermal decomposition that greatly affects the surface properties of the carbon-carbon material. It is important to understand where the carbon clutch plate material begins to decompose by oxidation, as this has a large effect upon the frictional properties of the clutch plate materials. This was investigated experimentally by using a Thermo-Gravimetric Analysis (TGA) machine which can be used to measure the rate of thermal decomposition of a small sample.

To determine the rate of thermal decomposition profile of the carbon-carbon clutch material, 4 small samples of approximately 20mg of the carbon clutch plate material were decomposed through heating at a rate of 200°C per minute from 100°C to 400°C and then holding isothermally at 400°C for 2 minutes, then heating from 400°C to 800°C at 10°C per minute. The weight of the platinum crucible was recorded beforehand, the sample was then added and the temperature taken to 100°C. The weight was then sampled and recorded throughout the test. The test chamber was purged with compressed atmospherically composed air at a rate of 30ml per minute in order to aid the oxidation process.

To ensure complete accuracy and reliability of results, the following standards were adhered to;

- ISO 11358 (1997). *Plastics – Thermogravimetry (TG) of Polymers – General Principles* [170]. This standard specifies a method for the determination of the activation energy in the Arrhenius equation for the decomposition of polymers using a thermogravimetric technique. This method is applicable only if the reaction proceeds by a single mechanism. It is applicable to multistage reactions if they consist of clearly separated single stage steps.
- ISO 11288-2 (2005). *Plastics – Thermogravimetry (TG) of Polymers – Part 2: Determination of Activation Energy* [171]. This part of the standard specifies a method for the determination of the activation energy,  $E_a$ , in the Arrhenius equation for the decomposition of polymers using a thermogravimetric technique. The method is applicable only if the reaction proceeds by a single mechanism. It is applicable to multistage reactions only if they consist of clearly separated single stage steps.

A plot of sample weight against temperature is shown in Figure 11.2a. This shows that thermal decomposition of the samples began at approximately 400°C, with the full effects being seen after 550°C – 600°C. By approximately 850°C, thermal decomposition had a clear effect on the weight of the sample, and there is then a rapidly decreasing sample weight after this temperature. This oxidation changes the surface properties of the carbon-carbon and so these results were used to create a look up table for use within the model, to account for the effects of the thermal decomposition.

Individual sample graphs can be found in Appendix V

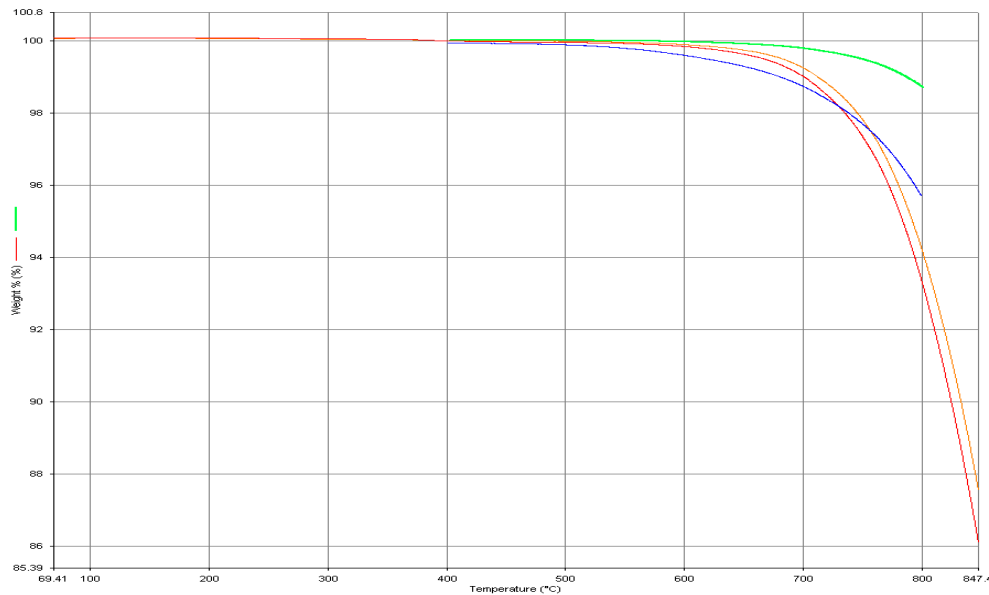


Figure 11.2a. Sample Decomposition Summary

Although this testing was effective in understanding the thermal decomposition, and was used to account for this within the mathematical model, further investigations into the effects on the linear thermal expansion at very fast temperature ramp rates could have provided more accurate representations of the behaviour during a clutch slip event. The temperature ramp rate of 1°C per minute used by the thermo gravimetric analyser is very low and allows for heat soak to occur, giving a steady and uniform relationship between the decomposition of the material and the increase in the temperature. A very fast rate of temperature increase, of approximately 18,000°C per minute (which comes from the suspected approximate plate face temperature of 1500°C is seen to occur within 0.5 seconds of slip for a typical F1 race clutch) would yield results more applicable to the project; however, test apparatus that would be able to do this is not available at the present time.

### 11.3 Modelling of the Surface

The first part of the surface model needed to determine which state the surface is in at any given point in time ie , and therefore a surface state model was first to be constructed. The purpose of the surface state model was to determine which surface state mode the friction face was experiencing at that given time and to generate the coefficient of friction values for the surface.

Deformation / reformation / ability to deform / reform and the friction coefficient curves (determined later in the program, but set to an initial value at the start of the iterative process), coordinates were defined.

- xDeformation1 - x co-ordinate of knee in deformation coefficient curve
- yDeformation2 - y co-ordinate of final point of deformation coefficient curve
- yDeformation1 - y co-ordinate of knee in deformation coefficient curve
- xReformation1 - x co-ordinate of knee in reformation coefficient curve
- yReformation2 - y co-ordinate of final point of reformation coefficient curve
- yReformation1 - y co-ordinate of knee in reformation coefficient curve
- xAbilityDeform1 - x co-ordinate of knee in deformation ability curve
- xAbilityReform1 - x co-ordinate of knee in reformation ability curve
- xFriction1 - x co-ordinate of first knee in coefficient of friction curve
- xFriction2 - x co-ordinate of second knee in coefficient of friction curve

The power lookup table was used to determine the power at which deformation and reformation of the surface layers occurred. Originally all of these variables were set to 1 but after several runs the following values were decided upon as more suitable starting points.

#### *% POWER LOOKUP TABLE*

*xDeformation1 = 1    % x co-ordinate of the deformation knee*  
*yDeformation1 = 0.5    % y co-ordinate of the deformation knee*  
*xReformation1 = 1.4    % x co-ordinate of the reformation knee*  
*yReformation1 = 0.6    % y co-ordinate of the reformation knee*

A graph was then plotted of the power against the coefficient of deformation / reformation and an ability to deform / reform lookup table was generated. This was used to determine the ability of the surface to deform / reform, that is, whether the surface was likely to deform or reform its bonds and change state types.



*% ABILITY LOOKUP TABLE*

*xAbilityDeform1 = 0.1*

*yAbilityDeform1 = 0.95*

*xAbilityReform1 = 0.9*

*yAbilityReform1 = 0.95*

A graph was then plotted of the surface state against the ability to deform / reform the surface and friction lookup table was generated.

*xFriction1 = 0.4;*

*xFriction2 = 0.6;*

*yFriction1 = 0.55;*

*yFriction2 = 0.35;*

*aLookup\_xFriction = [0,xFriction1,xFriction2,1];*

*aLookup\_yFriction = [0.6,0.6,0.3,0.3];*

Structures were created for the cycle values of cycle deformation, reformation, deformation ability, reformation ability, surface state change and surface state. The cycle friction co-efficient was determined through linear interpolation of the XFriction (x), and YFriction (y) at the point's Cycle.SurfaceState.

The outputs of this model are the array of average coefficient of friction for each event, and the array of the coefficient of friction for the first time-step of each event (in this case, 0.1s).

#### **11.4 Surface State Look Up Table Generation**

Before the main model could be created, the deformation and reformation of the surface lubricating film had to also be defined in a look up table. Along with this, a look up table for the friction values and normalising values was required.

To enable the simulation of clutch frictional performance, the surface morphology at any given instant has to be defined as a function of power density and interfacial temperature. The coefficient of friction is a function of the surface

state. At each discrete time step the model calculates a new surface state based upon the net change from reformation and deformation of the friction layer.

- Reformation is driven by interfacial temperature, and causes a shift towards Type III
- Deformation is driven by power density, and causes a shift towards Type II

Using Chen's type I, II and III surface states [50], the clutch plate was modelled using the following assumptions:

- Reformation is driven by interfacial temperature, and causes a shift towards Type III
- Deformation is driven by power density, and causes a shift towards Type II
- The surface state coefficient is used to characterise the state of the friction layer at any given time step
- Surface state coefficient = 0: purely type II (high-friction characteristic, with thick layer of powdery wear debris)
- Surface state coefficient = 1: purely type III (low-friction characteristic, with smooth friction film)

Between 0 and 1 indicates a mixture of type II and type III

- Surface deformation = 0; Type III and equates to zero deformation of surface
- Surface deformation = 1; Type II but at end of time step all friction layer reverts to purely type II

Deformation: Type III -> Type II

- Surface reformation = 0; Type II and equates to zero reformation of surface
- Surface reformation = 1; Type III but at end of time step all friction layer reverts to purely type III

Reformation: Type II -> Type III

The following symbols have been assigned to the following parameters. The extreme limits of the parameters are also presented.

$\alpha$	= Coefficient of surface deformation	$0 \leq \alpha \leq 1$
$\beta$	= Coefficient of surface reformation	$0 \leq \beta \leq 1$
$\zeta$	= Coefficient of surface state	$0 \leq \zeta \leq 1$
$P/P_{\max}$	= Normalised power	$0 \leq P/P_{\max} \leq 1$
$T/T_{\max}$	= Normalised temperature	$0 \leq T/T_{\max} \leq 1$

The model oscillates between type I and type II surface states; with the lower surface state coefficient (more type II) indicating a higher coefficient of friction (as the type II morphology has a higher friction coefficient than type III) and the boundaries of the look up table were set using these known fixed values.

Using data obtained from dynamometer testing, the values of coefficient of friction were populated within the look up table, and then interpolated to create a 3D look-up table.

The 3D lookup table of coefficient of deformation versus surface state versus normalised power is illustrated by plot shown in Figure 11.4b and is used to calculate the surface state coefficient based on the interfacial temperature and power density where:

$$P/A = T\omega/A. \quad (\text{Equation 11.4a})$$

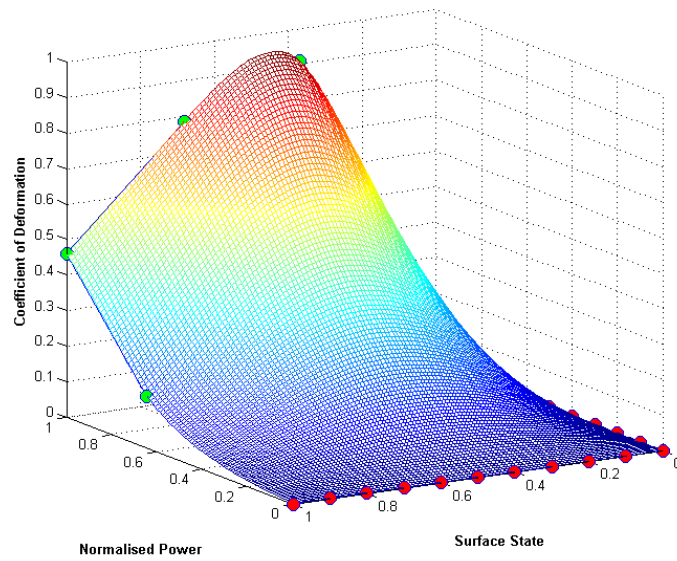


Figure 11.4b – Generation of 3D lookup table with defined points highlighted (known = red, generated = green)

The deformation lookup table in Figure 11.4c was generated by the routine, however it clearly will produce a flawed result as the relationships it describes are not logical.

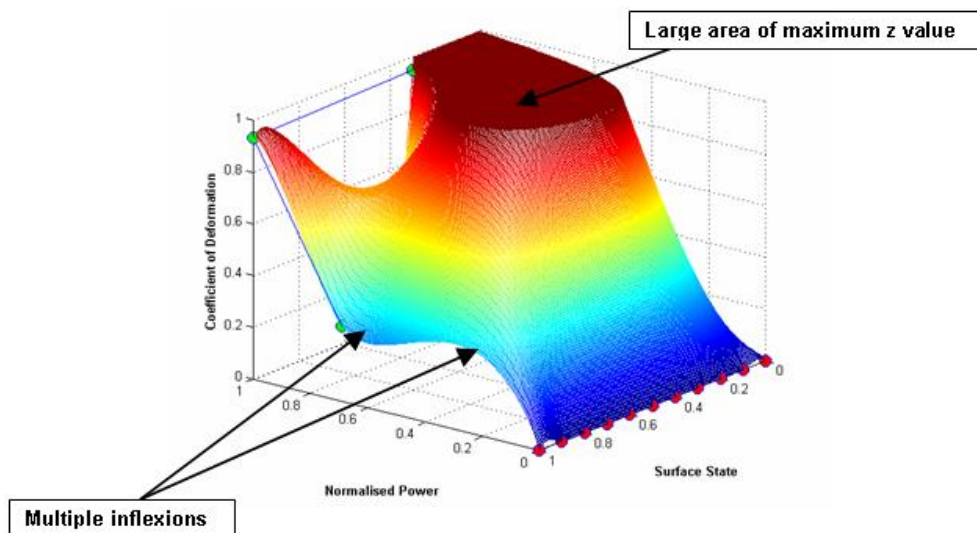


Figure 11.4c – Example of a poorly generated lookup table

- Multiple inflexions in the power axis; despite the defined points adhering to the statements defined previously the interpolation does not. The

gradient of this section should never be negative. A zero gradient and thus single inflexion may be possible.

Solution: check z values at discrete points, if gradient is negative the reject entire dataset.

- Large area of maximum z value; despite the defined points all lying within the limits defined previously, the interpolation generates areas of the curve lying outside the limits. Whilst these can be set equal to the maximum/minimum value, it clearly will generate a poor result.

Solution: find number of z values equal to max and min values, if either greater than a specified threshold then reject entire dataset.

Routines were included in the lookup table generator that ensures that the defined statements and relationships mentioned above are adhered to at all discrete points.

A graphical representation of the lookup table for changes in surface state coefficient versus normalised temperature versus normalised power can be seen below in figure 11.4d

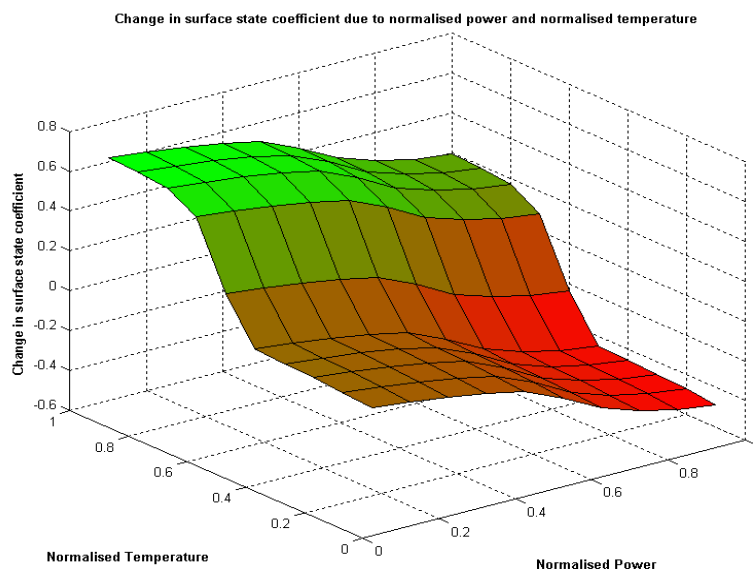
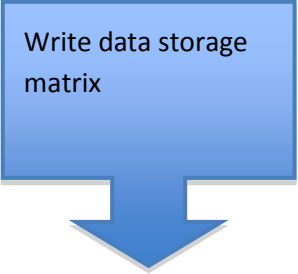
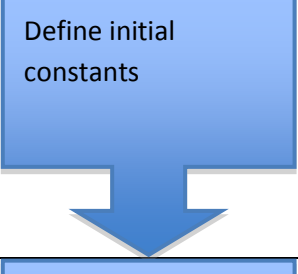
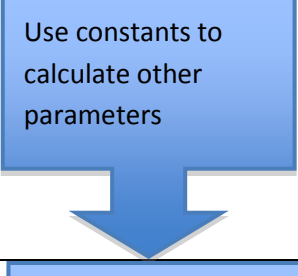
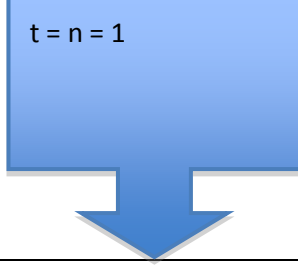












Figure 11.4d Change in Surface State Coefficient Due to Normalised Power and Normalised Temperature

## 11.5 Surface Model Code Generation

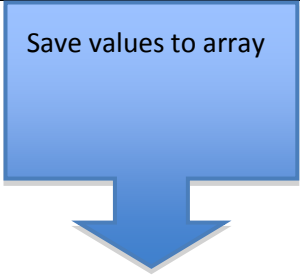
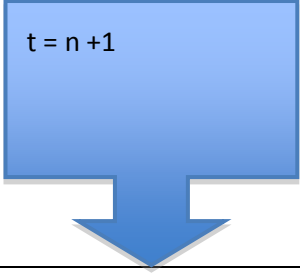
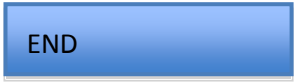
A flow outline of the code is shown in this section and full code can be found in Appendix W

Flow Steps	Description
 <p>Write data storage matrix</p>	<p>Write a matrix to store the data in as it is calculated; All of the functions created are determined through the program ClutchModel_SurfaceModel, with input values of input generation (iGen), clutch evaluation data (sCluData), clutch power was determined from the rig model (CluPowerNew_W), surface temperature determined by the thermal model (TempSurfaceNew_degC), co-efficient of surface state; whether it is a type I, II or II (CoefSurfaceStatePre) and the structure co-ordinates for the current iteration (sCoordsCurrent).</p>
 <p>Define initial constants</p>	<p>Initial constants were named and defined for geometric, thermal and ambient conditions.</p>
 <p>Use constants to calculate other parameters</p>	<p>The initial calculations were performed in terms of the constants and known inputs. For example, inner diameter, outer diameter and number of plates was used to calculate the total working area of carbon within the clutch.</p>
 <p>t = n = 1</p>	<p>Create first timestep t= n = 1</p>

<p>Determine power density at initial conditions from look up table</p> 	<p>The power density (power per square metre of carbon surface) was defined using the sCoordsCurrent function. An 'if' function was also created to say that if the calculation for the power density co-efficient was more than 1, then make the power density equal to one.</p>
<p>Determine surface temperature from look up table</p> 	<p>Surface temperature was defined using the look-up table.</p>
<p>Co-efficient of power density = % age of max power density</p> 	<p>The coefficient of power density was defined (that is, what percentage of the maximum power density the clutch is experiencing in relation to the maximum power density at that particular time step);</p>
<p>Co-efficient of temperature = % age of max surface temp</p> 	<p>Temperatures were converted to degrees into Kelvin (the standard SI unit) and the coefficient of temperature was defined (that is, what percentage of the maximum temperature the clutch is experiencing in relation to the maximum temperature at that particular time step);</p>
<p>Determine co-efficients of deformation and reformation</p> 	<p>The coefficients of deformation and reformation were determined by bicubic interpolation, using the known points in the look up table and the input parameter points at which the deformation / reformation needed to be determined.</p>

<p>Determine co-efficients of ability to deform and reform</p> 	<p>The coefficients of the ability of the deformation and reformation were determined by 'pchip' interpolation, using the known values and the values of coefficient of deformation which the deformation / reformation needed to be determined. Pchip interpolation is a third-degree spline with each polynomial of the spline in Hermite form. The Hermite form consists of two control points and two control tangents for each polynomial.</p>
<p>Determine surface state characteristics</p> 	<p>The difference in surface state was then determined (using the coefficients of reformation and deformation) and the new coefficient of surface state was also determined.</p>
<p>IF co_surf_stat &gt; 1 then co_surf_state =1 IF co_surf_state &lt;0 then co_surf_state =0</p> 	<p>An 'if' statement was then written stating the if the coefficient of surface state was above 1, then it should be made equal to 1, and if it were below 0, then it should be made to zero. This was done because the coefficient of surface state is a percentage value of the surface state therefore was a value between 0 and 1.</p>
<p>Determine friction co-efficient</p> 	<p>The new clutch friction coefficient was determined by cubic interpolation, using the known values of coefficient of surface state and the values of coefficient of deformation at which the deformation / reformation needed to be determined</p>
<p>IF <math>\mu &gt; 1</math> then <math>\mu = 0</math></p> 	<p>Finally, an 'if' function was also created to say that if the calculation for the friction co-efficient was more than 1, then make it equal to one. This was done so as to stop any errors occurring from the program in the event that anomalous data was</p>



	present.
	<p>Save values to the array and carry calculate;  <i>(iGen)</i>, clutch evaluation data  <i>(sCluData)</i>, clutch power determined from the rig model  <i>(CluPowerNew_W)</i>, surface temperature determined by the thermal model  <i>(TempSurfaceNew_degC)</i>, co-efficient of surface state;  <i>(CoefSurfaceStatePre)</i> whether it is a type I, II or III  <i>(sCoordsCurrent)</i>. the structure co-ordinates for the current iteration</p>
	<p>Increment time step and begin again until <math>t = \text{total time steps}</math> determined by initial conditions.</p>
	<p>The end result of this model is at each time step, a new clutch surface state and a new clutch co-efficient of friction is given.</p>

### 11.6 Model Validation

Due to the difficulty of operating this section of the model in isolation, it was impossible to devise a method to experimentally determine the validity of the model to any degree of accuracy. One suggestion would have been to use the thermocouple and infra-red values from the experimental testing, and the input power from the rig, but due to the experimental errors seen within the rig testing it was decided that the values would not have offered enough accuracy to determine a level of confidence with the model.

## Chapter 12

### Final Model

This chapter outlines the final model created through the rig model, thermal model and surface models outlined in Chapters 9, 10 and 11 respectively., as shown in Figure 12a

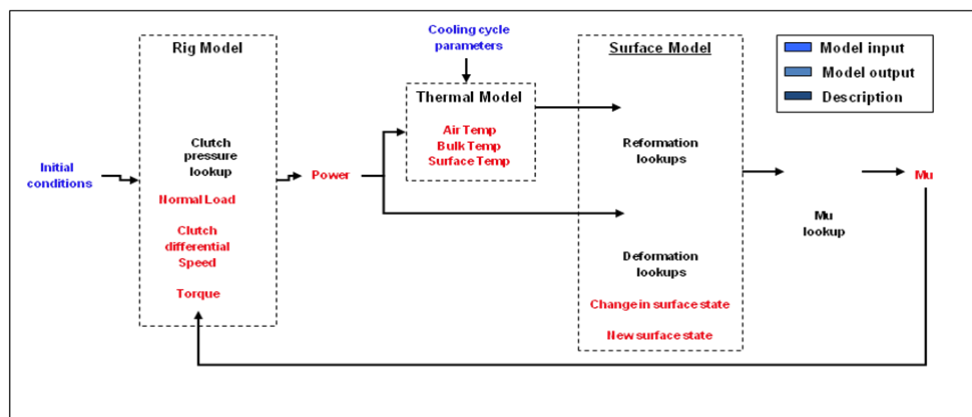


Figure 12a - The overall model schematic

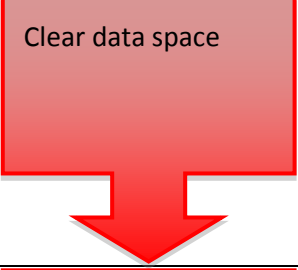
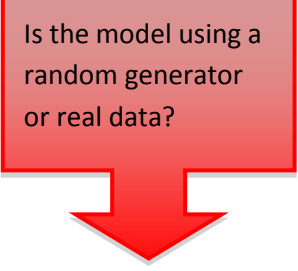
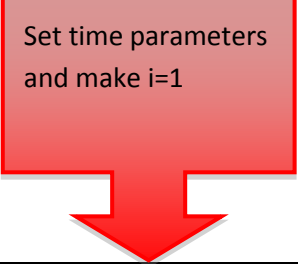
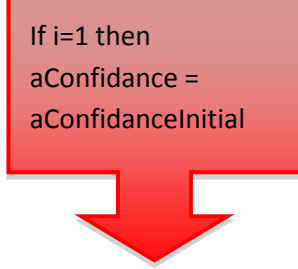
### 12.1 Final Model Overview





The final model was split into 9 parts;

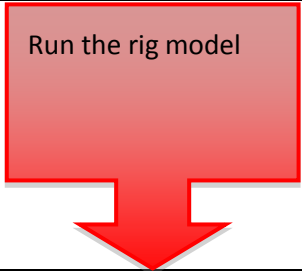
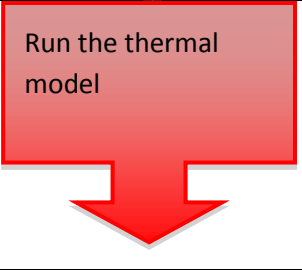
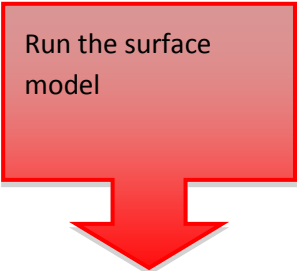
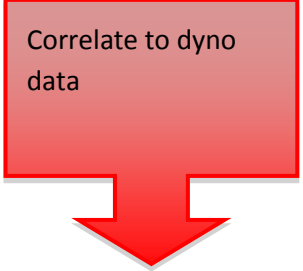

- Initial Conditions Program
- Random Number Generator
- Surface State Model
- Look up Table Generator
- Confidence Update Program
- Current Data Storage Array
- Input Model
- Thermal Model
- Surface Model


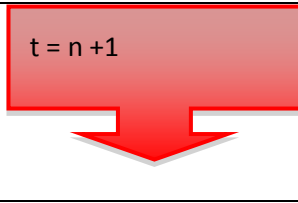
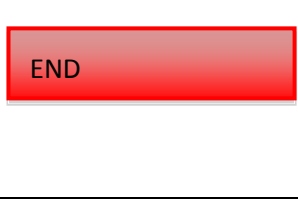
## 12.2 Final Model Code for Thermal Characteristic Generation

The final code is illustrated and described here, but due to its length, can be found in full in Appendix X.

Flow Steps	Description
 <p>Clear data space</p>	First general clearing and re-population of the workspace took place, before loading the required data.
 <p>Is the model using a random generator or real data?</p>	An 'if' statement was then introduced so that if the random number generator was being used (i.e. if the program was being used for iterative purposes) then the program was required to load the lookup table and define how many runs were to be performed from by the length of the sCoordsLoad structure.
 <p>Set time parameters and make i=1</p>	Next parameters were set for the time parameters and lookup table datasets to test, then the numbers were set to i=1 (the first set of data).
 <p>If i=1 then aConfidance = aConfidanceInitial</p>	The lookup table was then specified and an if statement was written to say that if the program was going through the first iteration then all variable confidence values were set to be equal to aConfidanceInitial and stored in the array sConfidence.

<p>Use CoordGen to look up variable location then store coordinates</p> 	<p>The function CoordGen was used to return the lookup table coordinate matrices for each of the variables for this iteration of the look up tables. The generated co-ordinates were then stored into the structure sCoords.</p>
<p>Generate structure to store current coordinates</p> 	<p>A further structure was then generated, known as sCoordsCurrent where the current coordinates of the matrices for each variable could be stored. This was done to make it easier to pass the coordinates of the matrices forward to future functions.</p>
<p>Is optimisation being used? If no, coordinates from sCoordsCurrent</p> 	<p>A function was created declaring that if the lookup table optimisation is not being used (for instance, in car data once the model has been proven), then load the lookup table coordinates from the structure sCoordsCurrent.</p>
<p>Determine the clutch pressure</p> 	<p>With i still set to 1 (the first set of event data), for iEvent = 1:nEvents (for each event from the first to the last), the clutch pressure needed to be determined. As the clutch pressure was not consistent throughout the bedding process (and it was this that was being used to validate the data), the data had to be filtered to account for this, so that for each event the correct pressure was used. A failsafe was written in, for the event that no actuation data was provided, and this was set to be 150bar. A small value would have tended the clutch event to last longer, so by using a high value subsequent events are sped up. Time steps were written and set to 1 (first data set) and the clutch speed was set to equal the initial conditions, and while above a lower limit of 300rpm, the time steps would continue to carry on at a rate of dt_s (as</p>

	defined in the initial conditions).
 <p>Run the rig model</p>	For the rig model, at each time step the model was written to calculate the new rig clamp pressure, the new clutch differential speed, the new clutch torque and the power dissipated over the time step.
 <p>Run the thermal model</p>	The thermal model was written so that at each time step, the new clutch surface temperature, then new clutch bulk temperature and the new ambient temperature were calculated.
 <p>Run the surface model</p>	And for the surface model, at each time step, the new clutch surface state and coefficient of friction were to be calculated. At the first time step, all known values were set to their initial values as defined in the initial conditions model.
 <p>Correlate to dyno data</p>	The measurements were obtained for the purposes of correlation to check the accuracy of the simulation output against the measured output. The total event duration was determined, and the mu was checked at set intervals of 10, 30, 50, 70 and 90% of the way through the simulation. The peak and mean friction co-efficients were determined for the event, and also checked with the dyno data.
 <p>nAnalyseBestPercentage = 5</p>	nAnalyseBestPercentage was then set to a nominal value of 5, meaning that the best 5% of the results were analysed (meaning that any results generated during the early stages of the iterative process were not included in the final analysis).

 <p>Define plotting settings</p>	<p>Plot settings were then defined for the model.</p>
 <p><math>t = n + 1</math></p>	<p>The timestep was moved on and the iterative process re-cycled</p>
 <p>END</p>	

## **Chapter 13**

### **Model Results and Discussion**

After the mathematical model had been created, it was validated against a specific set of validation data from the clutch bedding process performed on the clutch dynamometer. When being analysed, the model was split down into two parts; the input model of the rig, and the final model as a whole. This chapter presents the final results of this validation, and provides a discussion of these results, and the robustness of the model that has been generated.

#### **13.1 Input Model Results**

For the purposes of analysing the validity of the data the model was split down into its three main components; the input model, the look up tables and the final model as a whole. The input model was analysed separately due to the fact that it was an 'add on' model that could be removed, and replaced with an adapted version of the program that would instead, simulate the running of the clutch on the car.

Using a sample of historic bedding data from the HGT clutch dynamometer [172], the simulation output was compared against the measured speed profile for the actuation pressure profiles for the 40, 50, 70 and 70 bar bedding procedures. Figure 13.1a illustrates the results from this analysis.

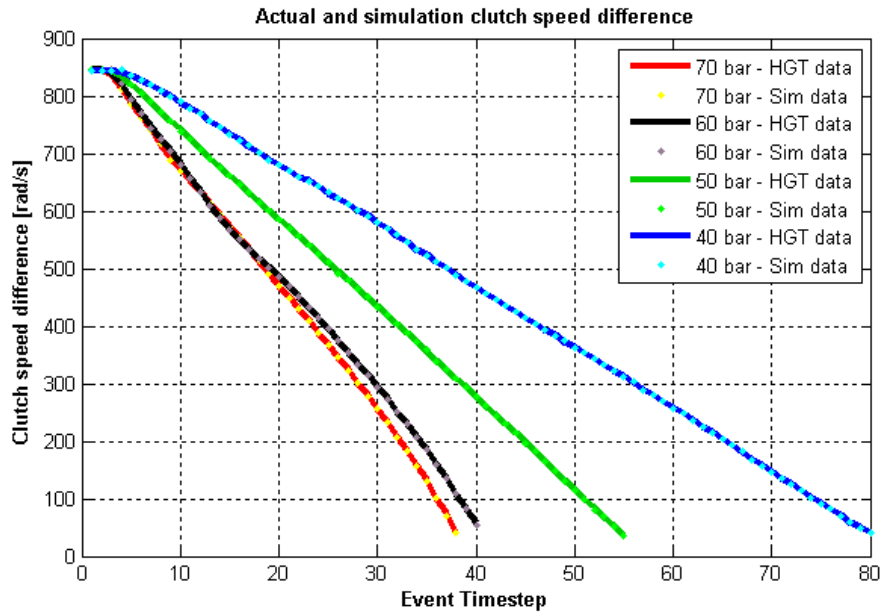


Figure 13.1a – Actual and Simulation Clutch Speed Difference for various Bedding Pressures

### 13.1.1 Input Model Results Discussion

As can be clearly seen, for all pressure profiles the simulation output matches the measured profiles. This is a good indication to the validity of the model; with the input parameters of the model being set to the same as those on the rig, the model accurately replicates the data trace that is observed from the rig when the clutch is actuated from a speed of approximately 850 rad/s (8000rpm) at the different clamping pressures used in the bedding process.

Following this, the model was used to generate a plot for a clamping event from 8000rpm to stopping. This can be observed in figure 13.1.1a.



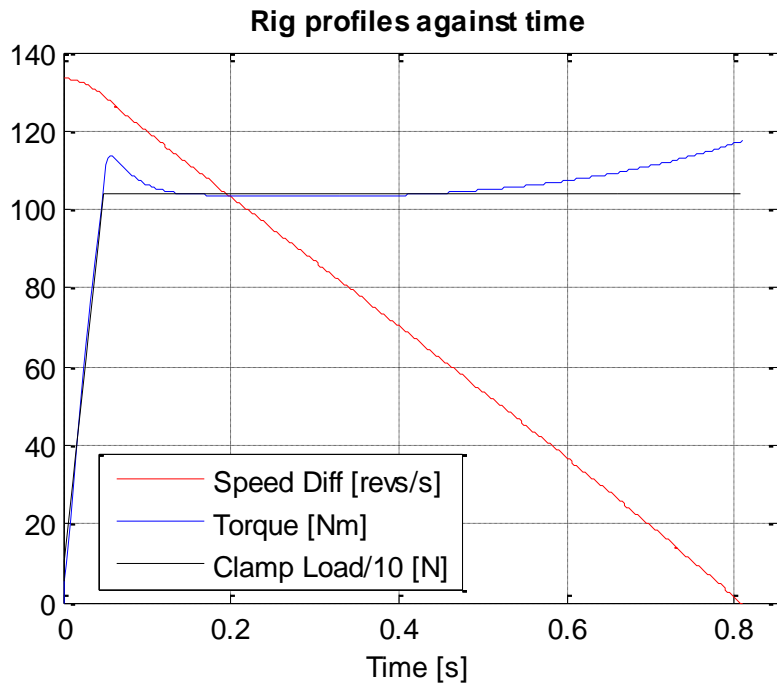


Figure 13.1.1a – Simulated Rig Speed / Torque curves

When compared to the torque and speed profile for the actual clutch dynamometer (figure 13.1c), it can be observed that the profile of the simulation matches that of the clutch dynamometer almost perfectly, with the characteristic torque spikes at the start and end of the clamping period (torque not shown in figure 13.1.1b).

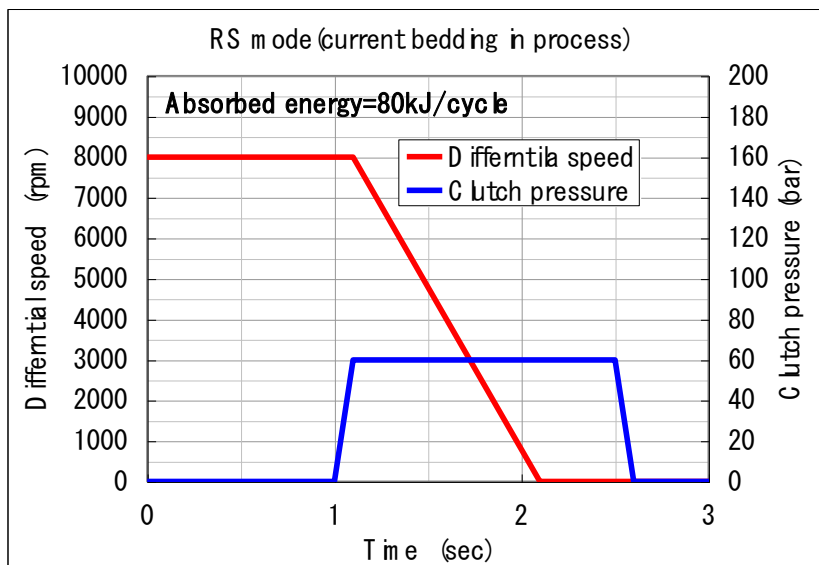


Figure 13.1.1b – Actual Rig Speed / Clamp Load Profile

## 13.2 Final Model Results and Assessment

The main validation was of the complete model. To do this a comparison was ran between the model, and a version of itself where the look up table was removed from the model and all profiles were generated from the measured clutch coefficient of friction input. This is how the model would work if it were used as a car based model. Figure 13.2a illustrates the results of the actual and simulated clutch speed difference for the four different pressures used in the bedding process.

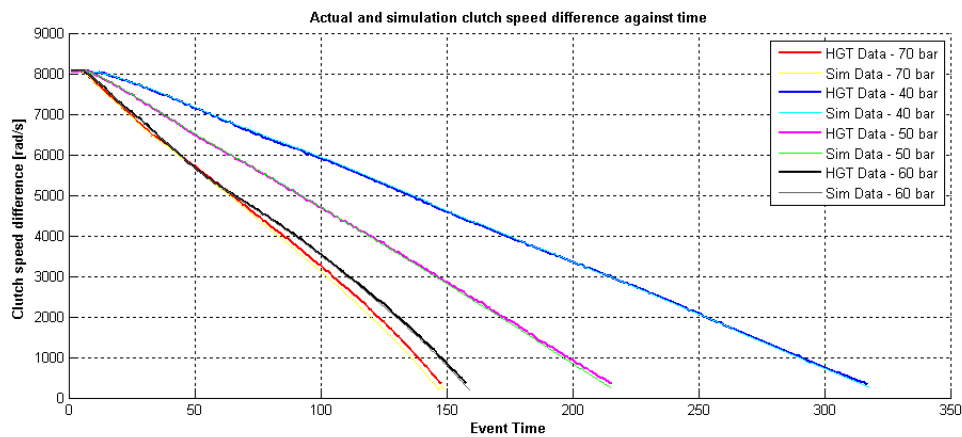


Figure 13.2a – Actual and Simulation Clutch Speed Differences during a clamping event from 8000rpm at varying clamp loads.

These simulated results were obtained through a rolling iterative process, which was set to stop iterating once 1000 results had been obtained which fell within a set range for the error in the average, start and end coefficient of friction, and these 1000 data points were obtained after approximately 44,000 look up table iterations. Figure 13.2b shows a scatter plot of the errors in coefficient of friction for each of the iterations. The s1 axis is for the coefficient of friction average value, s2 for the start coefficient of friction and s3 for the end coefficient of friction values seen over the simulated slip., The 1000 results which fell into the set values required between these three coefficient of friction results are highlighted in green.

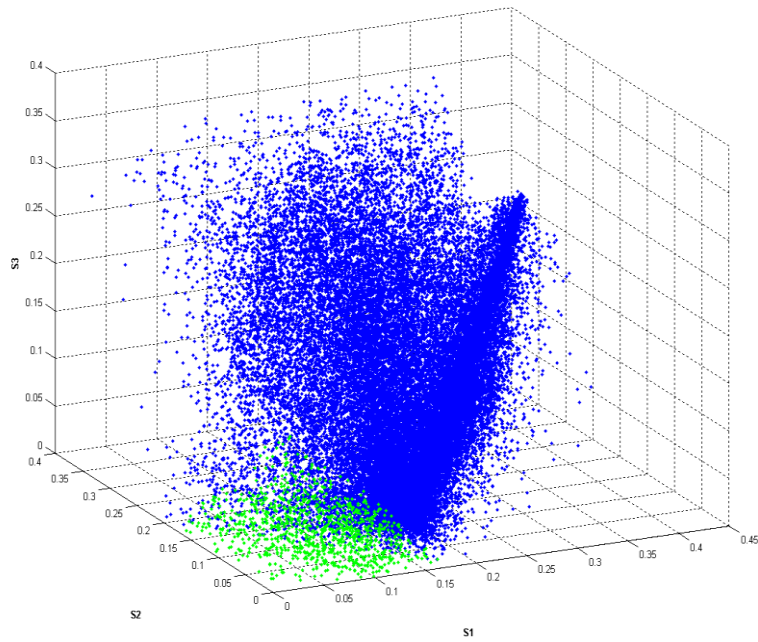


Figure 13.2b – Error in average coefficient of friction (s1), Start coefficient of friction (s2) and End coefficient of friction (s3) for a Single Event Using 44,000 different look up table iterations.

When compared with a rig profile from the clutch dynamometer (figure 13.2d), it can be clearly observed that the predicted co-efficient of friction plot (figure 13.2c) from the model closely matches this, including the initial ‘snatching’ of the clutch, where the peak coefficient of friction can be seen.

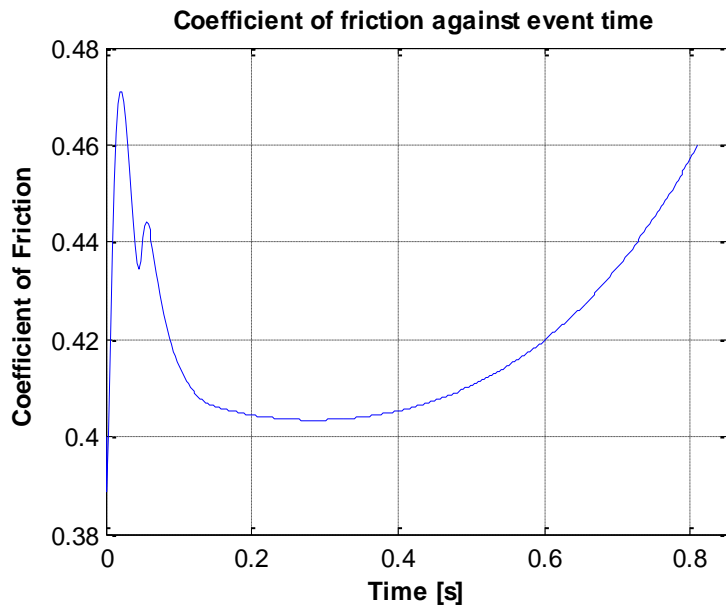


Figure 13.2c – A Simulation Result for Clutch Friction from the full model

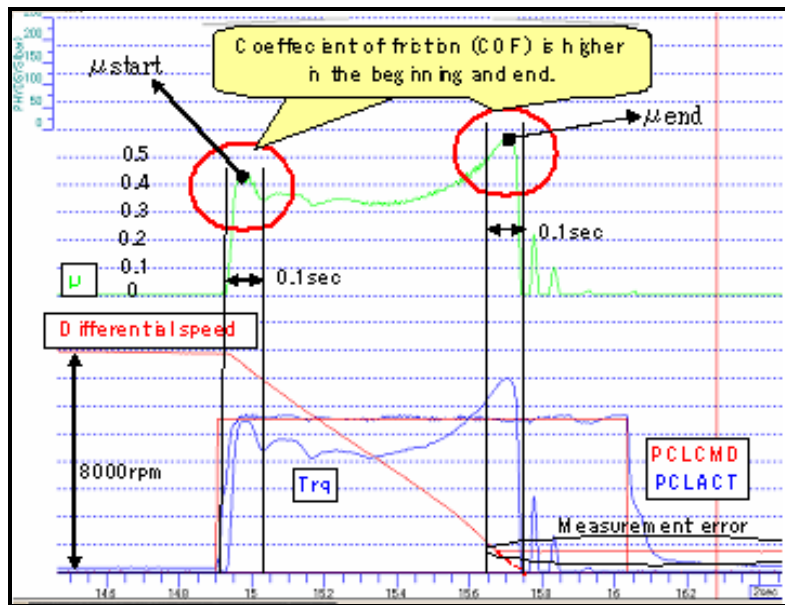


Figure 13.2d – Rig Data for Clutch Friction

### 13.3 Discussion, Discrepancies and Errors

There were a number of assumptions made in the model, namely the changes in the coefficient of clutch surface friction due to the surface morphology, which was obtained by guessing the interaction of the power dissipation with the deformation and reformation. This could be improved by further experimental analysis

Further categorisation could be by performing extensive SEM analysis of race clutches that have undergone differing conditions. By doing this it may be possible to create a classification scheme, based on Chen's [50] type I, type II classification. This would enable definition of the approximate initial coefficient of surface state, prior to bedding, mid bedding, prior to instillation on the car and at set points after this. This would enable a comparison of current surface state, event history and the measured coefficient of friction. A further aid to this characterisation would be to perform an XRD analysis on the wear debris created to determine the degree of graphitisation that has taken place, as (according to the works of Chen) this can also be used as a determination of surface state and future wear and friction properties.

Presently, the interfacial flash (that is, the initial flash of light that can be observed at the instant that the two surfaces come into contact) temperature of the clutch at the beginning of the slip is not modelled. This fundamental aspect would be important in future models as this sudden rise in heat causes thermal stresses, instant changes in surface morphologies and temperature gradients throughout the clutch stack. This would permit for a more accurate thermal model, and could be achieved through further experimental testing on the clutch dynamometer with the infra red sensor.

The model is currently limited in its capacity as it is only set to perform analysis for a single clutch event, due to time constraints and computational power.

## Chapter 14

### Further Work

This work has opened up the possibility of many other research opportunities. The first and most significant of which is; the effects of an electric current on the carbon-carbon material. When undertaking research for the literature review, this topic continually came up in searches. When looking further into this, it was highlighted that by passing a current through the plates, significant changes could be observed in both the friction and wear properties. This could open up research into the field of electromagnetically actuated carbon-carbon clutches.

Further research opportunities arising as a result of the work carried out in this project, include further investigations into the carbon-carbon manufacturing process, the dimensions of the clutch and oxidation temperatures, as well as follow on work from the mathematical model.

#### 14.1 Follow-On Work as a Result of the Literature Review

Whilst undertaking the literature survey, many of the papers reviewed highlighted that if a small electrical current (in the region of  $10\text{A}/\text{cm}^2$ ) is passed through the carbon-carbon material, its friction characteristics change dramatically. Carbon is an electrical conductor and when passing a charge through it the friction coefficient increases.

Work has been undertaken in the main following areas:

- Thermal properties on friction performance of carbon composites
- Effects of current on the friction coefficient of composites
- Effects of current on the wear volume of composites
- Contact voltage drop of composites
- Effect of carbon nanotubes on the friction and wear properties of composites

General trends show that the wear volume loss of composites with current was greater than that without current, caused the increase in the roughness and intensification. Because of oxidation reaction and weakening of the bonds a continuous lubrication film was formed, and so giving samples with the current passed through them, a higher friction coefficient.

This would be an area of interest when looking forward to development of clutch systems and could possibly be integrated as part of the KERS package that has been running on F1 cars in 2009 – 2010 and again since 2012.

## **14.2 Recommendations for Further Experimental Work**

### **14.2.1 Plate Profile**

In conducting dynamometer testing, and observing the order that the plates heat up, it may be possible to see if a pattern occurs through a testing a number of slips with the same parameters, and then conducting the same number of slips with slightly altered parameters. This may give an insight into the apparent 'randomness' of the order in which the plates heat up.

It may also be of note to undertake further studies into the concept that perhaps the first driven plate to bite actually takes most of the load. The theory behind this works on the principle that the biting driven plate transmits the load through into the hub, on which all of the driven plates are located. This means that as the biting driven plate transmits the load into the hub, the hub then transmits the load into the non biting plates and essentially 'drags' them round.

### **14.2.2 Saturation and Oxidation Temperature Investigation**

By conducting further tests into the saturation and oxidation properties of the material, it would be possible to determine whether this was a contributing factor to the decline in friction at temperatures where thermal decomposition was present. To do this, a clutch plate could be heated (and also slipped) up to 400°C (below the thermal decomposition temperature), 500°C and 600°C and observe

the curves for each. The use of a scanning electron microscope may also render offer some illustrative picture of the change in the surface properties

Although the materials testing was useful in understanding the effects of thermal decomposition, and was accounted for within the mathematical model, further investigations into the effects on the linear thermal expansion at very fast ramp rates could be undertaken. At present a ramp rate of 1°C per minute, as measured, is very low. A very fast rate of temperature increase, that is at a rate of approximately 18,000°C per minute (which comes from the suspected approximate plate face temperature of 1500°C seen to occur within 0.5 seconds of slip) would provide results more applicable to this work but test apparatus that would be able to do this is not available at the present time.

### **14.3 Recommendations for Further Modelling Work**

#### **14.3.1 Improvements that could be made to the Existing Model**

During the material properties experimental work, an additional test was undertaken for the linear co-efficient of thermal expansion. This was originally hoped to be used within the mathematical model, but its addition proved complicated when in conjunction with the clamping load acting upon the carbon stack. The coefficient of linear thermal expansion is ratio of change in length per degree K to the length at 273K (0°C).

$$\alpha = \frac{1\delta L}{L\delta T} \quad \text{Equation 14.3.1a}$$

Where;

- $\alpha$             Thermal expansion
- $\delta L$            Change in length
- $\delta T$            Change in temperature
- $L$              Initial length

ISO 11359-1 (1999). *Plastics – Thermomechanical Analysis (TMA). Part 1 – General Principles* [168]. This part specifies the general conditions for the



thermomechanical analysis of thermoplastics and thermosetting materials, filled or unfilled, in the form of sheet or moulded parts.

ISO 11359-2 (1999). *Plastics – Thermomechanical Analysis (TMA), Part 2 – Determination of Coefficient of Linear Thermal Expansion and Glass Transition Temperature* [169]. This part specifies a test method using thermodilatometry, for the determination of the coefficient of linear thermal expansion of plastics in a solid state by thermomechanical analysis (TMA). This part of the standard also specifies the determination of the glass transition temperature using TMA.

A Perkin Elmer DMA (Dynamic Mechanical Analysis) machine was used for the testing. The displacement of the sample is measured as it expands or contracts as a function of temperature. By plotting the displacement against the temperature, the expansion coefficient can be calculated. The machine is used for measuring several thermal dynamic properties, and for thermal expansion, the sample is placed on a quartz plate with a quartz probe sat on top of it. The fact that the plate and the probe are both quartz is very important, as quartz is considered to not expand or contract and this means that only the expansion or contraction of the samples alone will be seen and not a combination of the sample and the surrounding apparatus. As the sample expands and contracts, the probe sensor determines how much it has moved, and from this, gives the thermal expansion.

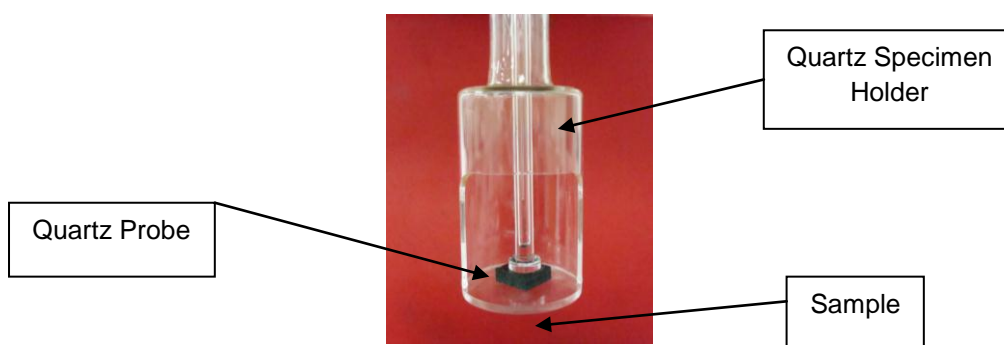


Figure 14.3.1b. DMA Sample and Sample Holder



Figure 14.3.1c. Perkin Elmer DMA Machine

Tests were carried out from 0°C to 500°C at a rate of 1°C per minute with a hold for ten minutes at 0°C and again at 500°C. This was to allow for a heat soak and to ensure that the specimen was uniformly heated before the heat ramps took place. A static force of 10mN was applied by the probe to keep it in contact with the sample without putting on too much force and pushing it down, and hence, restricting its expansion.

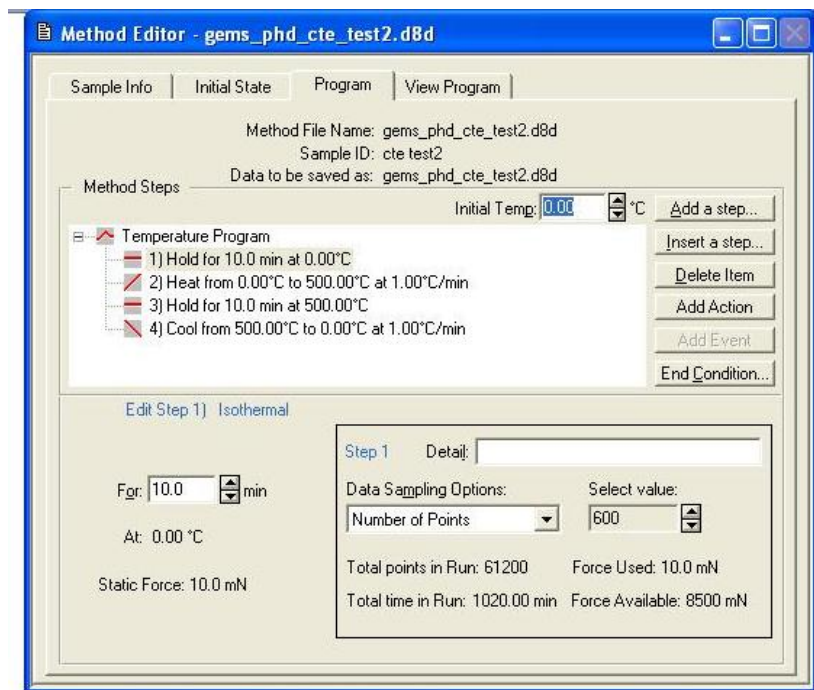


Figure 14.3.1d. Perkin Elmer DMA Test Program

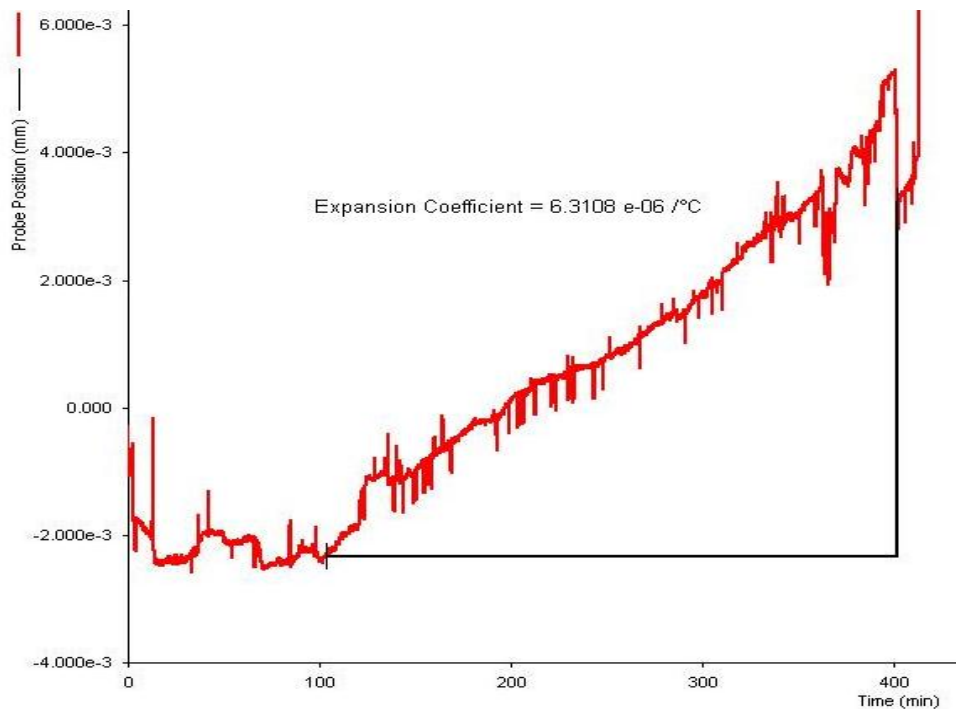


Figure 14.3.1e. Thermal Expansion Graph

### 14.3.2 Further Investigation of Surface Behaviour

Further categorisation could be done by using race clutches, and performing extensive SEM analysis of clutches that have undergone differing conditions. By doing this, it may be possible for the team to create their own classification scheme, based on Chen's type I, type II classification. This would enable definition of the approximate initial coefficient of surface state, prior to bedding, midway bedding, and prior to instillation on the car and at set points after this. This would enable a comparison of current surface state, event history and the measured coefficient of friction. A further aid to this characterisation would be to perform an XRD analysis on the wear debris created to determine the degree of graphitisation that has taken place, as (according to the works of Chen) this can also be used as a determination of surface state and future wear and friction properties.

## Chapter 15

### Conclusions

A novel method for measuring the interfacial temperatures within a race clutch was developed. By using the reversed layout on the clutch dynamometer it was possible to use the infrared detector to view the thermal profile of the surfaces. This method of clutch temperature measurement has not been recorded in literature prior to the work of the SAE paper published by Lawrence et al in 2006 [173], This method of temperature measurement could be developed further and used on an engine with a gearbox dynamometer, and the car. This could lead to the possibility of even more accurate predictions of the friction coefficient in the future.

Because the model was created and built upon in a methodical manner, it went through several stages before becoming the final model that is presented here in this document. Due to this, extra items were added, tolerances tightened and the introduction of new equations, laws and theories were added at every stage of development. When the model became the final version that is presented here, the use of confidence and error values meant that the model would continue with the iterative process until it reached a set level of accuracy, ensuring that the model could be as exact as possible.

Three main original contributions have been established as a result of this work with an addition to the general understanding of carbon-carbon behaviour within the scientific and engineering community. The work has investigated and put across theories regarding the destruction and formation of transfer films that act between the two mating carbon-carbon clutch faces, as well as investigating and experimentally determining and mathematically modelling the effects of thermal decomposition within the clutch.

The first main contribution is the thermal testing of the carbon-carbon material. Due to the sensitive and competitive nature of the race clutch designs, properties for the materials used are not available in the public domain. A suite of materials testing was undertaken and has experimentally determined values for a variety of

thermal properties of carbon-carbon clutch material using industry standard and independent test laboratories. The properties obtained are for the thermal decomposition, specific heat, thermal diffusivity, emissivity and thermal expansion for the S6 carbon-carbon clutch material used in race clutches.

In addition to the general understanding and materials testing, a more motorsport specific contribution has been ascertained; that is a method of accurately predicting the clutch's frictional  $\mu$  value at the instant before a race start, and to use that prediction within a launch control program to ensure a successful race start. This work has conclusively and unquestionably provided a significant piece of the jigsaw needed to obtain the best start strategy in F1.

This project has not only developed a proven method of optimising a race start, but in achieving this, a consistent and reliable method for direct clutch plate surface temperature measurements has also been developed. This could be further adapted for installation on a race car for testing purposes or even for more accurate temperature readings, which would allow for even more accurate friction calculations and even better race starts. Presently, there is no other method of clutch plate surface temperature measurement that has the capability to be developed in this way.

In addition to these original contributions, this work has also delved a little deeper into existing theories and contributions made by others; the presence of banding within a race clutch has been suggested by the results of the experimental work carried out by the collaborating establishment, AP Racing, but as explained in Chapter 3 (Literature Review) banding has already been investigated extensively in carbon brakes, and touched upon in carbon clutches. The experimental results have taken this work on a step further by using an infra red sensor in conjunction with embedded thermocouples to obtain a thermal profile from the surface, through the thickness of the clutch. However, further work needs to be undertaken on this to make conclusions regarding the size, location, any radial patterns of the bands and how the bands interact with each other in the multi-plate clutch arrangement.

## References

- [1] VARIOUS (2006). *Oxford English Dictionary*. Oxford, United Kingdom: Oxford University Press.
- [2] AP RACING (2006). *The History of AP Racing*.  
<http://www.apracing.com/info/history.htm> [accessed 23 April 2006]
- [3] AKEHURST, S (2007). *Lean Powertrain Development*.  
<http://staff.bath.ac.uk/enssa/LPDev.htm> [accessed 14th September 2007]
- [4] ZEROSHIFT (2007). *Zeroshift System Animation*  
<http://www.zeroshift.com/animation.html> [accessed 14th September 2007]
- [5] TILTON DRIVELINE COMPONENTS (2007). Carbon Clutches.  
<http://www.tiltonracing.com/content.php?page=list2&id=354&m=d>  
[accessed 18th May 2007].
- [6] GIBSON, D.W; TACCINI, G.J (1989). Carbon/Carbon Friction Materials for Dry and Wet Brake and Clutch Applications. (890950) Warrendale, PA: Society of Automotive Engineers.
- [7] RACE CAR ENGINEERING (2004). Insight – Engineering in Miniature. London: Racecar Graphic Ltd. (Volume 2, Issue 1 – Summer 2004)
- [8] SHAVER, R (1997). *Manual Transmission and Clutch Systems*. Warrendale, PA, USA: Society of Automotive Engineers International pp 1–12, 65-70
- [9] ZF SACHS (2007). Formula One Clutch.  
[http://www.sachs racing.com/direkt.php?link=owx\\_76\\_89618\\_2\\_6\\_0\\_e7047385394f52.html](http://www.sachs racing.com/direkt.php?link=owx_76_89618_2_6_0_e7047385394f52.html) [accessed 18th May 2007].
- [10] MCLAREN ELECTRONIC SYSTEMS. *SECU Chassis App Simulink Code: Check Conditions for Mu Calculation* (2007). McLaren. Woking UK
- [11] MCLAREN ELECTRONIC SYSTEMS. *System Monitor Chassis Parameters* (2007). McLaren. Woking UK
- [12] STANLEY, F.C (1937). *US Patent 2087488; Friction Clutch*. Alexandria, Virginia: United States Patent Office.
- [13] PAYVAR (1991). *US Patent 4995500; Groove Pattern for High Thermal Capacity Wet Clutch*. Alexandria, Virginia: United States Patent Office.

- [14] SIEVERS (1995). *US Patent 5407048; High Performance Automotive Clutch Assembly*. Alexandria, Virginia: United States Patent Office.
- [15] TRIPATHI, K. AGRAWAL, M.D. (2007) *Design Optimisation of Friction Clutch*. Journal of the Institution of Engineers (India): Mechanical Engineering Division. (Volume 88, pp29-33).
- [16] ALBERS, A. ARSLAN, A. MITARIU, M. (2005). *Clutches Using Engineering Ceramics as Friction Material*. Materialwissenschaft und Werkstofftechnik (Volume 36, Issue 3-4, pp102-107). Weinheim, Germany: Wiley-VCH.
- [17] BYRNE, C. (2004) *Modern Carbon Composite Brake Materials*. Journal of Composite Materials (Volume 38, No. 21, pp1837-1850) Oxford: Elsevier Science.
- [18] SAVAGE, G (1992). *Carbon – Carbon Composites*. Chemistry & Industry Journal 20<sup>th</sup> July 1992.
- [19] SAVAGE, G (1993) *Carbon – Carbon Composites* London: Chapman & Hall.
- [20] FOREST, M. *US Patent 7063870: Manufacture of functionally graded carbon – carbon composites*. Honeywell International Inc. Available from <http://www.patentstorm.us/patents/7063870-claims.html> [accessed 9th June 2006]
- [21] MARINKOVIC, S. DIMITRIJEVIC, S. (unknown) *Carbon/Carbon Composites as Prepared by Chemical Vapour Deposition*. Carbon Journal (Volume 23, No. 6, pp691-699). Oxford: Elsevier Science.
- [22] MANOCHA, L.M. (2003). *High Performance Carbon – Carbon Composites*. Sadhana Journal (Volume 28, Parts 1&2, pp349-358). India.
- [23] COOK, J. GORDON, J. (1964). *Proc. R. Soc. London A2:508*
- [24] MANOCHA, L.M. (1988). *Carbon – Carbon Composites*. Carbon Journal (Volume 26, pp333). India.
- [25] MANOCHA, L.M. (1994). *Carbon – Carbon Composites*. Carbon Journal (Volume 32, pp213). India.
- [26] WILLIAMS, KEITH (2006) *Carbon Disc Manufacture* Presentation given at Dunlop Aerospace, Coventry, United Kingdom.
- [27] SPOKAS, R.B. (1984). *Clutch Friction Material Evaluation Procedures*. (841066) Warrendale, PA: Society of Automotive Engineers.

- [28] WALKER (1999). *US Patent 5962135; Carbon / Carbon Friction Material*. Alexandria, Virginia: United States Patent Office.
- [29] FURSOV, S.G. GURIN, I.V. GURIN, V.A. NEKLYUDOV, I.M (2001). *Carbon – Carbon Composite Materials for Friction Purposes*. The Journal of Powder and Metallurgy and Metal Ceramics (Volume 40, No. 3-4, pp97 – 102). Plenum Publishing Company.
- [30] KIMURA, S. NARITA, N. YASUDA, E (1984) *Friction and Wear of Carbon / Carbon Composite*. Japanese Society of Lubrication Engineers – Journal (Volume 5, pp 11-16).
- [31] WEAVER, J.V. (1972). *Carbon Aeronautical Journal* (Volume 695).
- [32] JU, C.P. MURDIE, N. (1992). *Microstructure of Pitch Fiber-Phenolic/CVI Matrix Carbon-Carbon Composite*. Journal of Materials Chemistry and Physics (Volume 34, pp244-250). Oxford: Elsevier Science.
- [33] LUO, R. LI, Q (2003). *Brake Characteristics of 2D Carbon/Carbon Composites Prepared by Rapid Direction Diffused CVI Technology*. Journal of Materials Science and Engineering (Volume 379, pp33-38). Lausanne, Switzerland; Elsevier.
- [34] HEIDENREICH, B. KRENKEL, W. RENZ, R (2002). *C/C-SiC Composites for Advanced Friction Systems*. Advanced Engineering Materials (Volume 4, No. 7, pp427- 436). Weinheim: Wiley-VCH Verlag GmbH
- [35] DING, H. LUO, R. QU, J. XU, S (2004). *Static Friction Properties of Carbon / Carbon Composites*. Materials Letters (Volume 58, pp 1251 – 1254). Oxford: Elsevier Science
- [36] KRKOSA, M. FILIP, P. (2008). *Humidity and Frictional Performance of C/C Composites*. Developments in Advanced Ceramics and Composites: Ceramic Engineering and Science Proceedings (Volume 26, No.8). Carbondale: American Ceramic Society.
- [37] BLANCO, C. BEREMJO, J. MARSH, H. MERNENDEZ, R. (1997). *Chemical and Physical Properties of Carbon as Relating to Brake Performance*. Journal of the European Ceramic Society (Volume 23, pp2857-2866). Oxford: Elsevier Science
- [38] BLANCO, C. CASAL, E. GRANDA, M. MERNENDEZ, R. (2003). *Influence of Fibre-Matrix Interface on the Fracture Behaviour of Carbon-Carbon Composites*. Journal of the European Ceramic Society (Volume 23,



- pp2857-2866). Oxford: Elsevier Science.
- [39] HOLGERSON, M. (2000). *Influence of Operating Conditions on Friction and Temperature Characteristics of a Wet Clutch Engagement*. Tribotest Journal (Volume 7, Dec 2000) Deal, UK:Leaf Coffin
- [40] ZAGRODSKI, P. (1991). *Influence of Design and Material Factors in Thermal Stresses in Multiple Disc Wet Clutches and Brakes*. (911883) Warrendale, PA: Society of Automotive Engineers.
- [41] SCOTT, W. SUNTIWATTANA, P. (1995). *Effect of Oil Additives on the Performance of a Wet Friction Clutch Material*. Wear Journal (Volume 181-183, No. 2 pp850-855). Lausanne, Switzerland; Elsevier.
- [42] AUDEBERT, N. BARBER, J.R. ZAGRODZKI, P. (1998) *Buckling of Automatic Transmission Clutch Plates due to Thermoelastic / Plastic Residual Stresses*. Journal of Thermal Stresses (Volume 21, No. 3 – 4, pp 309 – 326). Taylor and Francis
- [43] JAFARI, S.H. FALLAHZADEH, F. RANA, S.K. (1999). *Effect of Post-Curing on Frictional Behaviour of Non-Woven Phenolic Composite in Automobile Clutch Facing*. Iranian Polymer Journal (Volume 8, No. 3, pp143-148).
- [44] SUNDARARAJAN, G. VENKATARAMAN, B. (2002). *The Influence of Sample Geometry on the Friction Behaviour of Carbon – Carbon Composites*. Acta Materiali Journal (Volume 50, Issue 5, pp1153 – 1163). Oxford: Elsevier Science
- [45] SATAPATHY, B.K. BIJWE, J. (2004). *Performance of Friction Materials Based on Variation in Nature of Organic Fibres – Part I; Fade and Recovery Behaviour*. Wear Journal (Volume 257, No. 5-6 pp573-584). Lausanne, Switzerland; Elsevier.
- [46] LEE, K.J. CHENG, H.Z. CHEN, J.S (2006). *Effect of Densification Cycles on Continuous Friction Behaviour of Carbon – Carbon Composites*. Wear Journal (Volume 260, pp99-108). Lausanne, Switzerland; Elsevier.
- [47] YUAN, Y. LUO, R. ZHANG, F. LI, J. LIU, T. ZHOU, W. (2005). *Influence of High Temperature Heat Treatment on the Friction Properties of Carbon / Carbon Composites Under Wet Conditions*. Journal of Materials Science and Engineering (Volume 402, pp203-207). Lausanne, Switzerland; Elsevier.

- [48] XIONG, X. HUANG, B. LI, J. XU, H. (2004). *Friction Behaviours of Carbon/Carbon Composites with Different Pyrolytic Carbon Textures*. Carbon Journal (Volume 44, pp463-467). Oxford: Elsevier Science.
- [49] LI, C. CROSKY, A (2006). *The Effect of Carbon Fabric Treatment on Delamination of 2D-C/C Composites*. Journal of Composites Science and Technology (Volume 66, pp2633-2638). Oxford: Elsevier Science.
- [50] CHEN, J.D, JU, C.P (1995). *Effect of Sliding Speed on the Tribological Behaviour of a PAN-Pitch Carbon-Carbon Composite*. Journal of Materials, Chemistry and Physics (Volume 39, pp174-179). Oxford: Elsevier Science concurrent
- [51] CHEN, J. CHERN-LIN, J. JU, C. (1995). *Effect of Humidity on the Tribological Behaviour of Carbon/Carbon Composites*. Wear Journal (Volume 193, No. 1, pp38-47). Lausanne, Switzerland; Elsevier.
- [52] CHEN, J.D, CHERN LIN, J.H. JU, C.P. (1996). *Effect of Load on Tribological Behaviour of Carbon-Carbon Composites*. Journal of Materials Science (Volume 31, pp 1221 – 1229). London: Chapman and Hall,
- [53] CHEN, J.D, JU, C.P. LEE, K.J. (1996). *Surface Effect on Braking Behaviour of PAN-Pitch Carbon-Carbon Composite*. Wear Journal (Volume 199, pp228 - 236) Oxford: Elsevier
- [54] HOU, X. LI, H. WANG, C. ZHU, Z. SHEN, J. (2000). *Internal Friction Behaviour of Carbon-Carbon Composites*. Carbon Journal (Volume 38, pp2095 – 2101). Oxford: Elsevier Science
- [55] GOMES, J.R. PARDINI, L.C. SILVA, C.M, SILVA, O.M, SILVA, R.F (2001). *The Effect of Sliding Speed and Temperature on the Tribological Behaviour of Carbon – Carbon Composites*. Wear Journal (Volume 249, pp240 - 245) Oxford: Elsevier.
- [56] LUO, R. HUAI, X. QU, J. DING, H. XU, S. (2003). *Effect of Heat Treatment on the Tribological Behaviour of 2D Carbon/Carbon Composites*. Carbon Journal (Volume 41, No. 14, pp2693-2701). Oxford: Elsevier Science.
- [57] HUTTON, T. JOHNSON, D. Mc.ENANEY, B. (1998). *Structural Studies of Wear Debris from Carbon/ Carbon Composite Aircraft Brakes*. Carbon Journal (Volume 37, No. 6, pp 907-916). Oxford: Elsevier Science.
- [58] LUO, R. QU, J. DING, H. XU, S. (2003). *Static Friction Properties of Carbon/Carbon Composites*. Materials Letters (Volume 58, Issues 7-8,

- pp1251-1254). Oxford: Elsevier Science.
- [59] DING, H. LUO, R. QU, J. XU, S (2004). *Static Friction Properties of Carbon / Carbon Composites*. Materials Letters (Volume 58, pp 1251 – 1254). Oxford: Elsevier Science
- [60] DECUZZI, P. DEMELIO, G. (2002). *The Effect of Material Properties on the Thermoelastic Stability of Sliding Systems*. Wear Journal (Volume 252, pp311-321). Lausanne, Switzerland; Elsevier.
- [61] XIONG, X. HUANG, B. LI, J. XU, H. (2004). *Friction Behaviours of Carbon/Carbon Composites with Different Pyrolytic Carbon Textures*. Carbon Journal (Volume 44, pp463-467). Oxford: Elsevier Science.
- [62] OSANAI, H. IKEDA, K. KATO, K. (1990). *Relations Between Temperature in Friction Surface and Degradation of Friction Materials During Engaging of Wet Friction Paper*. (900553). Warrendale, PA: Society of Automotive Engineers
- [63] MURDIE, N. JU, C.P. DON, J. FORTUNATO, F.A. (1990). *Microstructure of Worn Pitch/Resin/CVI C-C Composites*. Carbon Journal (Volume 29, No. 3 pp335-342). Oxford: Elsevier Science.
- [64] FILIP, P. WEISS, Z. RAFAJA, D. (2001). *On Friction Layer Formation in Polymer Matrix Composite Materials for Brake Applications*. Wear Journal (Volume 252, No. 3-4, pp189-198). Oxford: Elsevier Science.
- [65] LEE, K.J. (2003). *Surface and Interfacial Morphologies of PAN-CVI Carbon – Carbon Composite*. Composite Interfaces (Volume 11, No. 5-6, pp347-359). Netherlands: VSP
- [66] OLDFIELD, R.C. WATTS, R.F. (2006) *Impact of Lubricant Formulation on the Friction Properties of Carbon Fibre Clutch Plates*. Lubrication Science Journal (Volume 18, pp37-48). Oxford: Wiley InterScience
- [67] SAITO, T. KOTEGAWA, T. MATSURA, Y. TANAKA, S. OHTSUKI, K. (2007). *Study of Durability Prediction with Focus on Wear Properties for Multiple Plate Clutches*. (2007-01-0240). Warrendale, PA; Society of Automotive Engineers.
- [68] OZCAN, S. FILIP, P. (2005). *Microstructure and Wear Mechanisms in C/C Composites*. Wear Journal (Volume 259, pp642-650). Lausanne, Switzerland; Elsevier.
- [69] BUNDA, T. FUJIKAWA, A. YOKOI, K (1975). *Friction Behaviour of Clutch-*

- Facing Materials: Friction Characteristics in Low-Velocity Slippage.* (750522) Warrendale, PA: Society of Automotive Engineers.
- [70] METRICARU, V. (1982) *Results Concerning the Friction and Wear Behaviour of Some Materials For Brake and Clutch Facings.* EuroTrib: 3<sup>rd</sup> International Tribology Congress Proceedings (Volume 3, pp266-274). Oxford: Elsevier Science.
- [71] CHANG, H.W. (1982). *Correlation of Wear with Oxidation of Carbon – Carbon Composites.* Wear Journal (Volume 80, pp7-14) Oxford: Elsevier Science
- [72] YEN, B.K. ISHIHARA, T (1994). *The Surface Morphology and Structure of Carbon-Carbon Composites in High Energy Sliding Contact.* Wear Journal (Volume 174 pp111-117). Lausanne, Switzerland; Elsevier.
- [73] ISHIHARA, T. YEN, B.K (1995). *An Investigation of Friction and Wear Mechanisms of Carbon – Carbon Composites in Nitrogen and Air at Elevated Temperatures.* Carbon Journal (Volume 34, No. 4 pp489 – 498). Oxford: Elsevier Science / American Carbon Committee.
- [74] ISHIHARA, T. YEN, B.K. (1996). *On Temperature Dependent Tribological Regimes and Oxidation of Carbon-Carbon Composites up to 1800°C.* Wear Journal (Volume 196, pp254 – 262) Oxford: Elsevier Science
- [75] WEAVER, J.A. (1994). *Heat Transfer Analysis of the Ungrooved Disk of a Cooled, Multi-plate Clutch.* Journal of Thermophysics and Heat Transfer (Volume 8, No. 1 pp152-158) Reston, USA: American Institute of Aeronautics and Astronautics.
- [76] CHEN, J.D. JU, C.P. (1995). *Low Energy Tribological Behaviour of Carbon – Carbon Composites.* Carbon Journal (Volume 33, No.1, pp57 – 62). Oxford: Elsevier Science
- [77] LEE, K.J. CHERN LIN, J.H. JU, C.P (1996). *Simulated Stop Tribological Behaviour of Pitch Resin CVI Carbon-Carbon Composite.* Journal of Materials Chemistry and Physics (Volume 49, pp217-224). Oxford: Elsevier Science.
- [78] EL MANSORI, M. PAULMIER, D. SAMAH, A. (1999). *Damage of Carbon – Carbon Composite Surfaces Under High Pressure and Shear Strain.* Surface and Coatings Technology (No. 120-121, pp636 – 640). Oxford: Elsevier.

- [79] JU, C. CHERN-LIN, J. LEE, K. KUO, H (1999). *Multi-Braking Tribological Behaviour of PAN-pitch, PAN-CVI and Pitch-Resin-CVI Carbon/Carbon Composites*. Materials Chemistry and Physics Journal (Volume 64, No.3, pp196-214). Lausanne, Switzerland; Elsevier
- [80] SHIN, H,K. LEE, H.B. KIM, K.S. (2001). *Tribological Properties of Pitch Based 2-D Carbon – Carbon Composites*. Carbon Journal (Volume 39, pp959 – 970). Oxford: Elsevier Science
- [81] MAKI, R. (2003). *Wet Clutch Tribology – Friction Characteristics in All Wheel Drive Differentials*. Tribologia; Finnish Journal of Tribology (Volume 22, pp5-16).
- [82] NYMAN, P. MAKI, R. OLSSON, R. GANEMI, B. (2006). *Influence of Surface Topography on Friction Characteristics in Wet Clutch Applications*. Wear Journal (Volume 261, pp46-52). Lausanne, Switzerland; Elsevier.
- [83] PENG, Z. YAN, X.P. YUAN, C.Q. ZHOU, X.C (2005). *The Surface Roughness Evolutions of Wear Particles and Wear Components Under Lubricated Rolling Wear Condition*. Wear Journal (Volume 259, pp512 – 518). Oxford: Elsevier Science
- [84] GUO, W. XIAO, H. YASUDA, E. CHENG, Y. (2006). *Oxidation Kinetics and Mechanisms of a 2D C/C Composite*. Carbon Journal (Volume 44, No. 15 pp3269-3276). Oxford: Elsevier Science.
- [85] GOUIDER, M. BERTHIER, Y. JACQUEMARD, P. ROSSEAU, B. BONNAMY, S. ESTRADÉ-SZWARCKOPF, H. (2004). *Mass Spectrometry During C/C Composite Friction; Carbon Oxidation Associated with High Friction Coefficient and High Wear Rate*. Wear Journal (Volume 256, pp1082-1087). Lausanne, Switzerland; Elsevier.
- [86] YESNIK, M. LAM, R.C (1992). *Clutch Plate Surface Treatment for Improved Frictional Characteristics*. (922099) Warrendale, PA: Society of Automotive Engineers.
- [87] ERDEMIR, A. LIU, Y, MELETIS, E.I. (1996). *An Investigation of the Relationship Between Graphitization and Frictional Behaviour of DLC Coatings*. Surface and Coatings Technology (No. 86-87, pp564 – 568). Oxford: Elsevier.
- [88] PARK, S.J. SEO, M.K. LEE, J.R. (2002). *Effect of Oxidation on the Low Energy Tribological Behaviour of Carbon-Carbon Composites*. Carbon

- Journal (Volume 40, pp835-843). Oxford: Elsevier Science.
- [89] SAITO, T. KOTEGAWA, T. MATSUURA, Y. TANAKA, S. OHTSUKI, K. (2007) *Research into Durability Prediction Technology Taking into Account Multiple Plate Clutch Wear Properties*. Proceedings of 2007 ASME International Engineering Congress and Exposition. ASME.
- [90] HONNER, M. (2005). *Thermo-Mechanical Instabilities – Project Proposal*. Paper presented at a meeting between the University of West Bohemia and AP Racing, Pilsen, Czech Republic
- [91] ENZL, R (2004). *Technology and Material for High Thermal Conductivity Coating for Brake Systems*. Paper presented at a meeting between the University of West Bohemia and AP Racing, Pilsen, Czech Republic.
- [92] LAM, R.C. CHAVDAR, B. NEWCOMB, T. (2006). *New Generation Friction Materials and Technologies*. (2006-01-0150). Warrendale, PA; Society of Automotive Engineers.
- [93] HONNER, M (2004). *Brake Disc Thermal Mapping System* University of West Bohemia. Available from <http://www.ttp.zcu.cz/en/publikace> [Accessed 23rd February 2005]
- [94] HONNER, M (2004). *Origination and Consequences of Thermo-mechanical Instabilities in Brake Systems*. Paper presented at a meeting between the University of West Bohemia and AP Racing, Pilsen, Czech Republic.
- [95] BERGLAND, K. MARKLUND, P. LARSSON, R. PACH, M. OLSSON, R. (2010). *We Degradation Monitored by Lubricant Analysis*. (2010-01-2232). Warrendale, PA; Society of Automotive Engineers.
- [96] BRUNNER, FRITZ K (2004). *Fibre Optic Sensors – An Overview*. Paper presented at the FIG International Symposium on Engineering Surveys for Construction Works and Structural Engineering. Nottingham, United Kingdom, June
- [97] JIANG, H; KENT, J.C; MCCOMISKEY, T; QIAN, Y; RHEE, K.T (1993). *High Speed Spectral Infrared Imaging of Spark Ignition Engine Combustion*. (930865) Warrendale, PA: Society of Automotive Engineers.
- [98] POORMAN, THOMAS. J; WLODARCZYK, MAREK. T; XIA, LIANGDAO (1997). *Ignition System-Embedded Fiber-Optic Combustion Pressure Sensor for Engine Control and Monitoring*. (979845) Warrendale, PA: Society of Automotive Engineers.

- [99] COSTE, TIMOTHY. L; EVERS, LAWRENCE.W (1997). *An Optical Sensor for Measuring Fuel Film Dynamics of a Port-Injected Engine*. (970869) Warrendale, PA: Society of Automotive Engineers.
- [100] HALL, MATTHEW. J; ZUZEK, PATRICK (2000). *Fiber Optic Sensor for Time-Resolved Measurements of Exhaust Gas Recirculation in Engines*. (2000-01-2865) Warrendale, PA: Society of Automotive Engineers.
- [101] BRYANSTON-CROSS, P.J; CHANA, K.S; DUNKLEY, P; HANNAH, P; JONES, T.V; WILSON, T.S (2002). *High Bandwidth Heat Transfer and Optical Measurements in an Instrumented Spark Ignition Combustion Engine*. (2002-01-0747) Warrendale, PA: Society of Automotive Engineers.
- [102] EDWARDS, GORDON; LEVICK, ANDREW (Undated). *A Fibre-Optic Based Laser Absorption Radiation Thermometry (LART) Instrument for Surface Temperature Measurement*. [online]., Middlesex: National Physical Laboratory. Available from [http://www.npl.co.uk/thermal/publications/andrew\\_levick/fiber\\_optic.pdf](http://www.npl.co.uk/thermal/publications/andrew_levick/fiber_optic.pdf) [4th June 2005]
- [103] GOTO, KAZUHIRO; KAWAHARA, NOBUYKI; OHNISHI, KENJI; TOMITA, EIJI (2005). *In-situ Unburned Gas Temperature Measurement in a Spark Ignition Engine Using Laser Interferometry*. (2005-01-0646) Warrendale, PA: Society of Automotive Engineers.
- [104] TOMITA E, HANAMOTO, Y, JIANG, D: (1994) *Temperature and Pressure Histories of End Gas Under Knocking Condition in an SI Engine*. Proc. Of International Symposium on COMODIA 94.
- [105] KUNES, J; LANG, V; LITOS, P (2004). *Optic Fibres and Infrared Detectors in Dynamic Temperature Field Measurements*. Paper presented at a meeting between the University of West Bohemia and AP Racing. Pilsen, Czech Republic.
- [106] BRIARS, RON (2007). *When to Use a Two-Colour Infrared Thermometer*. Ircon Inc. [http://www.coleparmer.com/techinfo/techinfo.asp?htmlfile=When\\_IRTherm.htm&ID=82](http://www.coleparmer.com/techinfo/techinfo.asp?htmlfile=When_IRTherm.htm&ID=82)
- [107] GARDNER, J. L. JONES, T. P. RICHARDS, A. J. (1987). *Radiation Pyrometers for Temperature Measurement During Aluminium Processing*. Sydney, Australia. Institute of Physics.

- [108] REYNOLDS P.M; (1964) *A Review of Multi Colour Pyrometry for Temperatures Below 1500°C*. Journal of Applied Physics 15 p579.
- [109] KONG, JIAN; SHIH, ALBERT. J (2004). *Infrared Thermometry for Diesel Exhaust After Treatment Temperature Measurement*. (2004-01-0962) Warrendale, PA: Society of Automotive Engineers.
- [110] MACKRORY, ANDREW. J; RICHARDS, MICHAEL. J; SVENSSON, KENTH. I; TREE, DALE. R (2005). *Calibration of an RGB, CCD Camera and Interpretation of its Two-Color Images for KL and Temperature*. (2005-01-0648) Warrendale, PA: Society of Automotive Engineers.
- [111] KLEBBA, ROBERT. E; LOWRY, STEPHEN. R; TIMMERMAN, GEORGE (1995). *A Comparison of Fourier Transform Infrared Spectroscopy with Traditional Analyzers for Enhanced Inspection and Maintenance Testing*. (950219) Warrendale, PA: Society of Automotive Engineers.
- [112] CHORIER, P. TRIBOLET, P (2001). *High Performance HgCdTe Detectors for Hyperspectral Instruments*. Proceedings of SPIE – International Society for Optical Engineering (Volume 4540, pp.328-341).
- [113] HOWE, J.D. (1999) *Two-Color Infrared Full-Strokes Imaging Polarimeter Development*. Aerospace Conference Proceedings. (Volume 4, pp. 79-85).
- [114] IVANOVIC, V. HEROLD, Z. DEUR, J. HANCOCK, M. ASSADIAN, F. (2009). *Experimental Characterization of Wet Clutch Friction Behaviors Including Thermal Dynamics*: 01-1360). Warrendale, PA; Society of Automotive Engineers.
- [115] IVANOVIC, V. HOIC, M. DEUR, J. HEROLD, Z. TSENG, E. (2012). *Design of Test Rigs for a Dry Dual Clutch and its Electromechanical Actuator*. (2012-01-0807). Warrendale, PA; Society of Automotive Engineers.
- [116] JAFRI, F.A. FUSS, M. BAILEY, G. KAO, C.K. RAZZACKI, S.T. ANVY, E (2009). *Shudder Durability of a Wet Launch Clutch Part I – Thermal Study and Development of Durability Test Profile*. (2009-01-0329). Warrendale, PA; Society of Automotive Engineers.
- [117] ROGER, I. GREGORI, S. (2010). *Methodology to Determine the Clutch Facing Sensitivity Regarding Judder in the Vehicle*. (2010-36-0501). Warrendale, PA; Society of Automotive Engineers.
- [118] HOIC, M. HEROLD, Z. KRANJCEVIC, N. DEUR, J. IVANOVIC, V. (2013). *Experimental Characterization and Modeling of Dry Dual Clutch Thermal Expansion Effects*. (2013-01-0818). Warrendale, PA; Society of



Automotive Engineers.

- [119] JOSKOWICZ, L. SACKS. E (1993) *Automated Modelling and Kinematic Simulation of Mechanisms*. Journal of Computer Aided Design (Volume 25 No. 2 pp106 – 118) Oxford: Elsevier Science
- [120] MATLAB Software. Available from [www.mathworks.com](http://www.mathworks.com) [24th November 2013]
- [121] BLUNSDON, C.A; DENT, J,C; MALALASEKERA, W,M,G; (1993). *Modelling Infrared Radiation from the Combustion Products in a Spark Ignition Engine*. (932699). Warrendale, PA; Society of Automotive Engineers.
- [122] PADOVAN, J. PADOVAN, P. (1994). *Modelling Wear at Intermittently Slipping High Speed Interfaces*. Computers & Structures Journal (Volume 52, No. 4, pp795-812) Oxford: Elsevier Science.
- [123] LEBEDEV, P.A. BELYAEEV, A.N. (1984). *Determination of Multidisc Friction Clutch Temperature Field*. Soviet Journal of Friction and Wear; English Version (Volume 5, No. 4, pp15-21).
- [124] ZAGRODZKI, P. (1985). *Numerical Analysis of Temperature Fields and Thermal Stresses in the Friction Discs of a Multidisc Wet Clutch*. Wear Journal (Volume 101, pp255-271) Elsevier Sequoia, Netherlands.
- [125] CHEN, Y.F. LAM, R. YANG, Y. (1995). *Modelling of Heat Transfer and Fluid Hydrodynamics for a Multidisc Wet Clutch*. (950898) Warrendale, PA: Society of Automotive Engineers.
- [126] FUJII, T. LAM, R.C. YANG, Y. (1998). *Prediction of Torque Response During Engagement of Wet Friction Clutch*. (981097) Warrendale, PA: Society of Automotive Engineers.
- [127] JANG, J.Y. KHONSARI, M.M (1999). *Thermal Characteristics of a Wet Clutch*. Journal of Tribology; Transactions of the ASME (Volume 121, No.3, pp610-617) Lausanne, Switzerland; Elsevier.
- [128] JANG, J.Y. KHONSARI, M.M (2002). *On the Formation of Hot Spots in Wet Clutch Systems*. Journal of Tribology; Transactions of the ASME (Volume 124, No.2, pp336-345) Lausanne, Switzerland; Elsevier.
- [129] TATARA, R.A. PAYVAR, P. (2002). *Multiple Engagement Wet Clutch Heat Transfer Model*. Numerical Heat Transfer Journal (Volume 42, Part A, pp215-231). London: Taylor & Francis
- [130] GAO, H. BARBER, G. (2002). *Engagement of a Rough, Lubricated and*

*Grooved Disk Clutch with a Porous Deformable Paper-Based Friction Material*. Tribology: Transactions (Volume 45, No. 4, pp464-470)..

- [131] DENERY, T: (2005). *Multi-Domain Modelling of the Dynamics of a Hovercraft for Controller Development*. Natick, MA; The Mathworks & American Institute of Aeronautics and Astronautics
- [132] SimuLink Software. Available from [www.mathworks.com](http://www.mathworks.com) [24<sup>th</sup> November 2013]
- [133] SimDriveline Software. Available from [www.mathworks.com](http://www.mathworks.com) [24<sup>th</sup> November 2013]
- [134] SATAPATHY, B.K. BIJWE, J. (2004). *Performance of Friction Materials Based on Variation in Nature of Organic Fibres – Part II; Optimisation by Balancing and Ranking Using Multiple Criteria Decision Model (MCDM)*. Wear Journal (Volume 257, No. 5-6 pp585-589). Lausanne, Switzerland; Elsevier.
- [135] CHEN, L. XI, G. ZHANG, J. (2002) *System Dynamic Modelling and Adaptive Optimal Control for Automatic Clutch Engagement of Vehicles*. IMech E Conference Proceedings / Journal of Automobile Engineering (Volume 216, Part D pp983 – 991). London: IMechE.
- [136] KHAMLICHI, A. BEZZAZI, M. PARRON-VERA, M.A. (2003). *Optimizing the Thermal Properties of Clutch Facings*. Journal of Materials Processing Technology (Volume 142, pp634-642). Lausanne, Switzerland; Elsevier.
- [137] KOSHKINA, T.B, KOVROV, V.N, MOSHEV, V.V (2003). *Research on the Interfacial Friction in Filled Polymers*. Mechanics of Composite Materials Journal. (Volume 39, Issue 3, pp.301-310 - June 2003)
- [138] BAMBA, E. LIU, K. (2005). *Analytical Model of Sliding Friction in an Overrunning Clutch*. Tribology International (Volume 38, pp. 187-194)
- [139] DINWIDDLE, RALPH B; MARX, DAVID T; POLICANDTIOTES, TOD; SCOTT, JEREMY; WANG HSIN; ZHANG, SU (2001). *Measurement of Interfacial Temperatures During Testing of a Subscale Aircraft Brake* [online] Southern Illinois University, Carbondale, United States: Institute of Physics Publishing Ltd. Available from <http://iop.org> [18<sup>th</sup> July 2005]
- [140] MACE,G (2004) *Innovative Brake Disc Design Through Research*. AP Racing, Coventry.
- [141] MACE, G (2004) *Guidelines for Modelling Brake Discs in Geostar Cosmos*.

Internal Procedure, AP Racing, Coventry

- [142] Geostar Cosmos. Computer Software available from [www.solidworks.com](http://www.solidworks.com) [24<sup>th</sup> November 2013]
- [143] DHARANI, L.R. HILMAS, G.E. ZHAO, S. (2007). *Behaviour of a Composite Multidisc Clutch Subjected to Mechanical and Frictionally Excited Thermal Load*. Wear Journal (Volume 264, Issues 11-12, pp1059-1068) Oxford: Elsevier Science
- [144] Abaqus Software. Computer Software available from [www.3ds.com](http://www.3ds.com) [24<sup>th</sup> November 2013]
- [145] MADHAVAN, J. PANDIT, G. BARNHOLT, M. SUPPIGER, R. (2012). *Application of Simulation Based Methods in Development of Wet Clutch System*. (2012-28-0022). Warrendale, PA; Society of Automotive Engineers.
- [146] CAMERON, T.M. HEWETTE, C. MCCOMBS, T. DEGONIA, D. JAO, T.C. (2007). *Traction and Clutch Effects on the Natural Frequency and Vibration Stability of Limited Slip Differential Axles*. (2007-01-2295). Warrendale, PA; Society of Automotive Engineers.
- [147] CAMERON, T.M. JAO, T.C. HEWETTE, C. MCCOMBS, T. DEGONIA, D. (2008). *Effect of Limited Slip Clutch Friction on the Driveline Dynamics of a Rear Wheel Drive Vehicle Coasting in a Turn*. (2008-01-1582). Warrendale, PA; Society of Automotive Engineers.
- [148] DUQUE, E.L. AUGUSTO. R.A. (2012). *Mathematical Formulation of Dynamic Automotive Clutch Damper*. (2012-36-0454). Warrendale, PA; Society of Automotive Engineers.
- [149] PRZYBILLA, M. KUNZE, C. CELIK, S. DONGAONKAR, S. (2011). *Combined Simulation Approach for Dry Clutch Systems*. (2011-01-1232). Warrendale, PA; Society of Automotive Engineers.
- [150] LIU, Y. QUI, D. JIANG, H. LIU, C. ZHANG, Y. (2011). *Clutch Torque Formulation and Calibration for Dry Dual Clutch Transmissions*. Mechanism and Machine Theory (Volume 46, pp.218-227 ).
- [151] TARASOW, A. BOHN, C. WACHSMITH, G. SERWAY, R. EISBACH, M. ZHAO, Q. BAUER, G. (2012). *Method of Identification of the Kiss Point as well as Takeoff Point of a Hydraulically Actuated Friction Clutch*. (2012-01-0112). Warrendale, PA; Society of Automotive Engineers.

- [152] CAMERON, T.M. MCCOMBS, T. TERSIGNI, S. JAO, T.C. (2005). *Flash Temperature in Clutches*. . (2005-01-3890). Warrendale, PA; Society of Automotive Engineers.
- [153] JEN, T.C. NEMECEK, D.J. (2008). *Thermal Analysis of a Wet-disk Clutch Subjected to a Constant Energy Engagement*. International Journal of Heat and Mass Transfer (volume 51, pp.1757-1769).
- [154] CHEN, G. DOURRA, H. SHAH, D. (2012). *Rotating Clutch Temperature Model Development Using Rapid Prototype Controllers*. (2012-01-0625). Warrendale, PA; Society of Automotive Engineers.
- [155] DURQE, E.L. BARRETO, M.A. FLEURY, A. (2009). *Math Model to Simulate Clutch Energy During Vehicle Launch*. (2009-36-0401). Warrendale, PA; Society of Automotive Engineers.
- [156] SUN, S. LEI, Y. FU, Y. YANG, C. LI. S.B. (2013). *Analysis of Thermal Load for Dry Clutch Under the Frequent Launching Condition*. (2013-01-0814). Warrendale, PA; Society of Automotive Engineers.
- [157] KATSUMATA, Y. SEGAWA, S. ADACHI, K, HIGASHIMATA, A. OCHI, Y. (2008). *Development of a Slip Speed Control System for a Lock-Up Clutch (Part II)*. (2008-01-0001). Warrendale, PA; Society of Automotive Engineers.
- [158] KANEKO, Y. ADACHI, K. IINO, F. HIRATA, M. (2009). *Development of a Slip Speed Control System for a Lock-Up Clutch (Part III)*. (2009-01-0955). Warrendale, PA; Society of Automotive Engineers.
- [159] MOTOSUGI, J. ADACHI, K. ASHIZAWA, H. FUJIMOTO, S. OCHI, Y. (2011). *Development of a Slip Control System for RWD Hybrid Vehicles using Integrated Motor-Clutch Control*. (2011-01-0945). Warrendale, PA; Society of Automotive Engineers.
- [160] ADHITYA, M. MUSTAFA, R. PLOTNER, A. KUCUKAY, F. (2013). *A New Control Strategy of Wet Dual Clutch Seamless Transmission (DCT) Clutch and Synchronizer for Seamless Gear Preselect*. (2013-01-0340). Warrendale, PA; Society of Automotive Engineers..
- [161] LAWRENCE, G. (2012). *Control System Event Report 07\_10Sil MVR02-03*. (internal Report) Marussia Virgin Racing. Banbury, UK.
- [162] LAWRENCE, G. (2012). *Control System Event Report 07\_24Nur MVR02-03*. (internal Report) Marussia Virgin Racing. Banbury, UK.

- [163] LAWRENCE, G. (2012). *Control System Event Report 07\_31 Bud MVR02-03*. (internal Report) Marussia Virgin Racing. Banbury, UK.
- [164] HONDA RACING F1 (2006). *Clutch Bedding Process Report*. (Internal Report). Honda Racing F1. Brackley UK,
- [165] ASTM E-423-71 (2002) (Standard Test Method for Normal Spectral Emittance at Elevated Temperatures of Nonconducting Specimens)
- [166] UNKNOWN (2007). Correlation. Accessed 20th November 2007  
<http://en.wikipedia.org/wiki/correlation>
- [167] ASTM E 1269-05 (2005) Standard Test Method Determining Specific Heat Capacity by Differential Scanning Calorimetry
- [168] BS EN821-2:1997 *Advanced Technical Ceramics – Monolithic Ceramics – Thermo-physical Properties – part 2: determination of thermal diffusivity by the laser flash (or heat pulse) method*.
- [169] BS EN1159-2:2003 *Advanced Technical Ceramics – Ceramic Composites – Thermo-physical Properties – part 2: determination of thermal diffusivity*
- [170] ISO 11359-1 (1999). *Plastics – Thermomechanical Analysis (TMA). Part 1 – General Principles*.
- [171] ISO 11359-2 (1999). *Plastics – Thermomechanical Analysis (TMA), Part 2 – Determination of Coefficient of Linear Thermal Expansion and Glass Transition Temperature*.
- [172] HONDA RACING DEVELOPMENTS (2005). Bedding Data from Clutch Dyno.
- [173] LAWRENCE, G; MACE, G; BOWLER, N; GODDARD, G; MORREY, D: (2006). Measurement of the Interfacial Plate Temperatures within a Carbon Clutch, and Determination of Effects upon its Friction Characteristics. (2006-01-3634) Warrendale, PA: Society of Automotive Engineers.

## Copies of Published Materials

- [A] LAWRENCE, G; MACE, G; BOWLER, N; GODDARD, G; MORREY, D: (2006). *Measurement of the Interfacial Plate Temperatures within a Carbon Clutch, and Determination of Effects upon its Friction Characteristics*. (2006-01-3634) Warrendale, PA: Society of Automotive Engineers.

This paper may be accessed via the following link: <http://papers.sae.org/2006-01-3634/>

# Appendix A - 2006 Race Starts Data Plots

## Bahrain International Circuit

Date: 12<sup>th</sup> March 2006

Circuit Length: 5.411km

Race Distance: 308.238km (57 laps)

Number of Race Starts: 1

Weather: Dry

Air Temp: 22°C

Track

Temp: 34°C

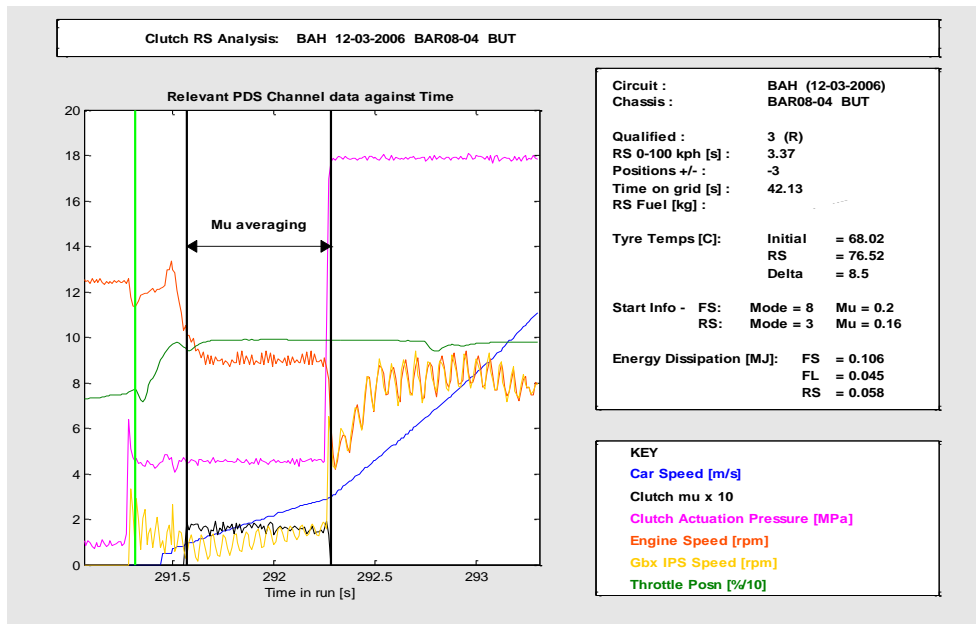


Figure 4.1a-i. Race Start, Car One, Bahrain Circuit

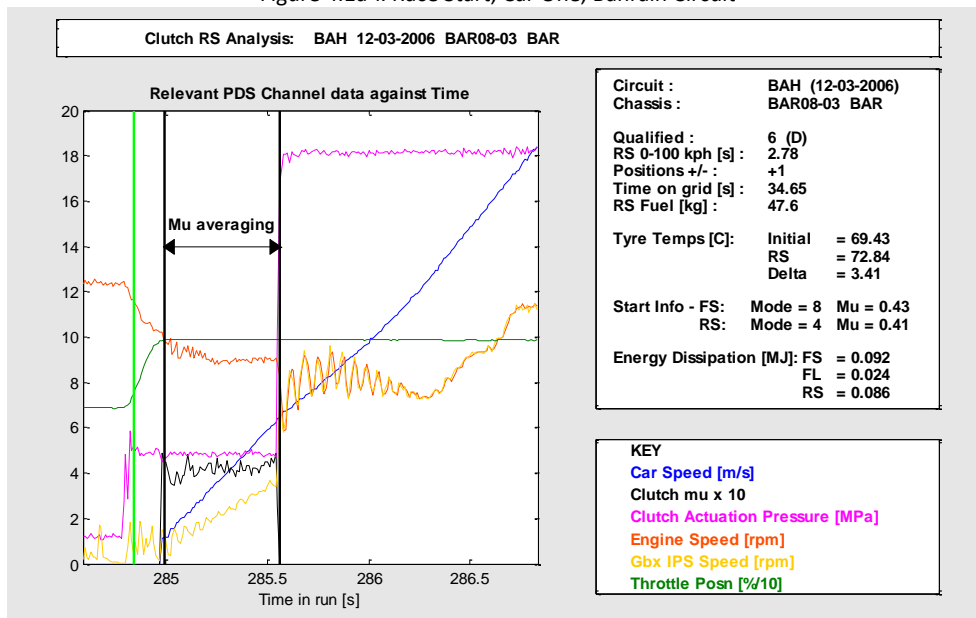


Figure 4.1a-ii. Race Start, Car Two, Bahrain Circuit

## Sepang International Circuit

Date: 19<sup>th</sup> March 2006

Race Distance: 310.408km (56 laps)

Weather: Dry

Track Temp: 39°C

Circuit Length: 5.54km

Number of Race Starts: 1

Air Temp: 32°C

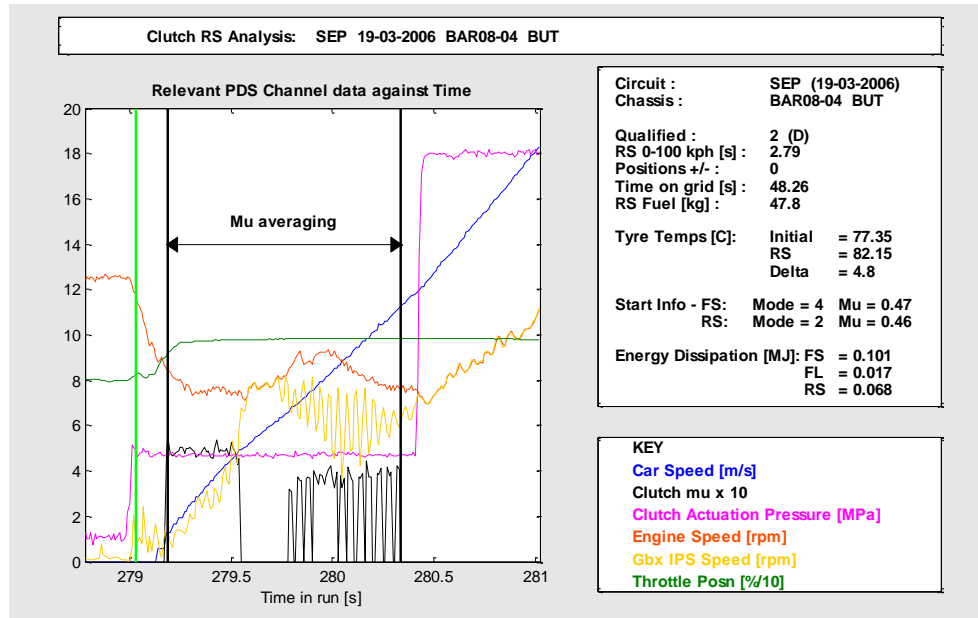


Figure 4.1b-i. Race Start, Car One, Sepang Circuit

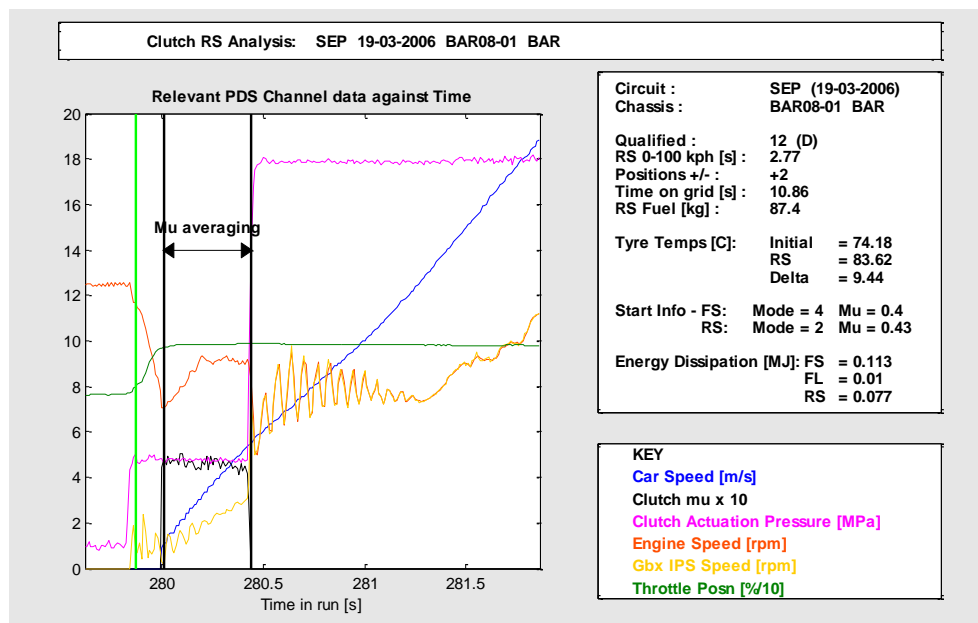


Figure 4.1b-ii. Race Start, Car Two, Sepang Circuit



## Melbourne Grand Prix Circuit

Date: 2<sup>nd</sup> April 2006

Circuit Length: 5.30km

Race Distance: 302.271km (57 laps)  
on first lap)

Number of Race Starts: 2 (red flag

Weather: Dry

Air Temp: 17°C

Track

Temp: 24°C

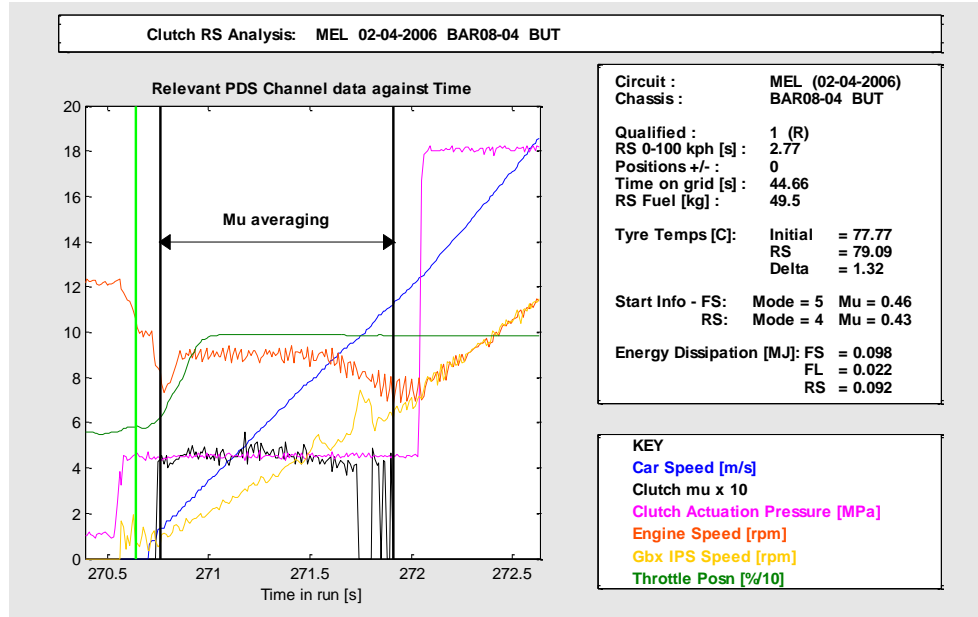


Figure 4.1c-i. Race Start, Car One, Melbourne Circuit

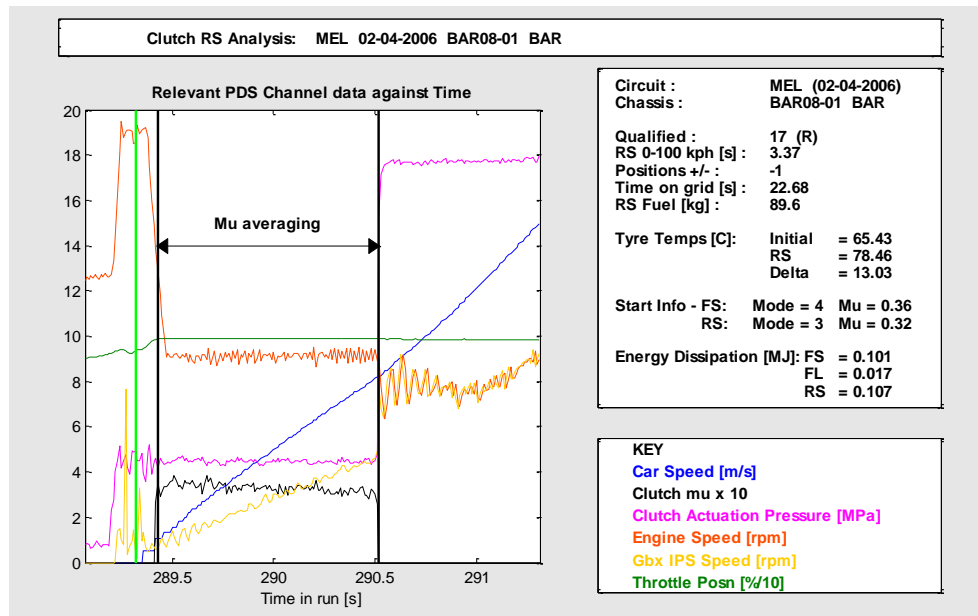


Figure 4.1c-ii. Race Start, Car Two, Melbourne Circuit

## Autodromo Enzo e Dino Ferrari, Imola Circuit

Date: 23<sup>rd</sup> April 2006

Circuit Length: 4.933km

Race Distance: 305.609km (62 laps)

Number of Race Starts: 1

Weather: Dry

Air Temp: 26°C

Track

Temp: 37°C

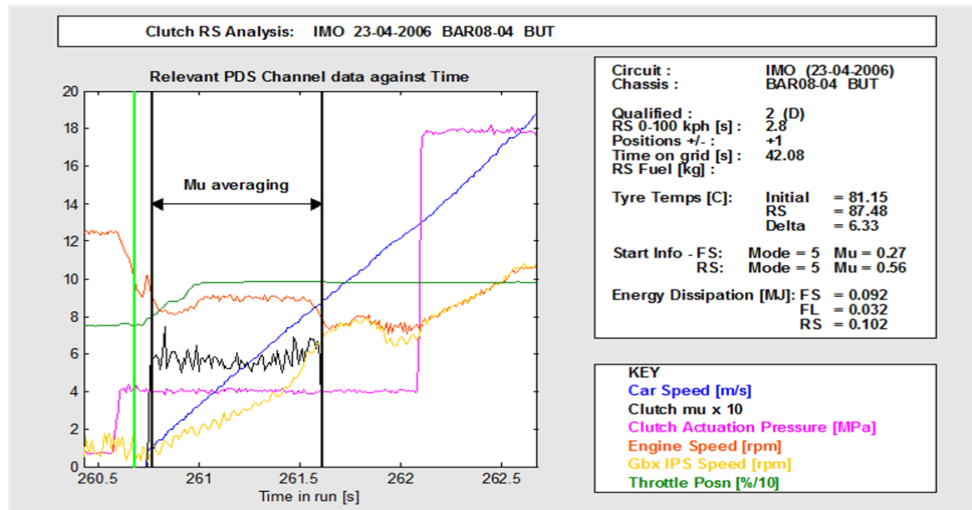


Figure 4.1d-i. Race Start, Car One, Imola Circuit

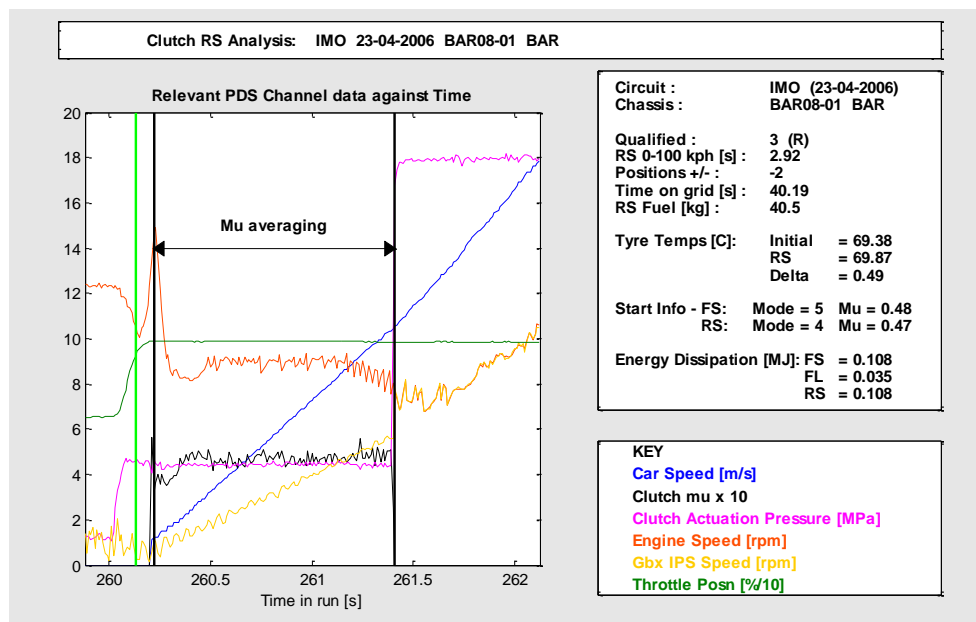


Figure 4.1d-ii. Race Start, Car Two, Imola Circuit

## Nurburging Circuit

Date: 7<sup>th</sup> May 2006

Circuit Length: 5.148km

Race Distance: 308.88km (60 laps)

Number of Race Starts: 1

Weather: Dry

Air Temp: 20°C

Track

Temp: 30°C

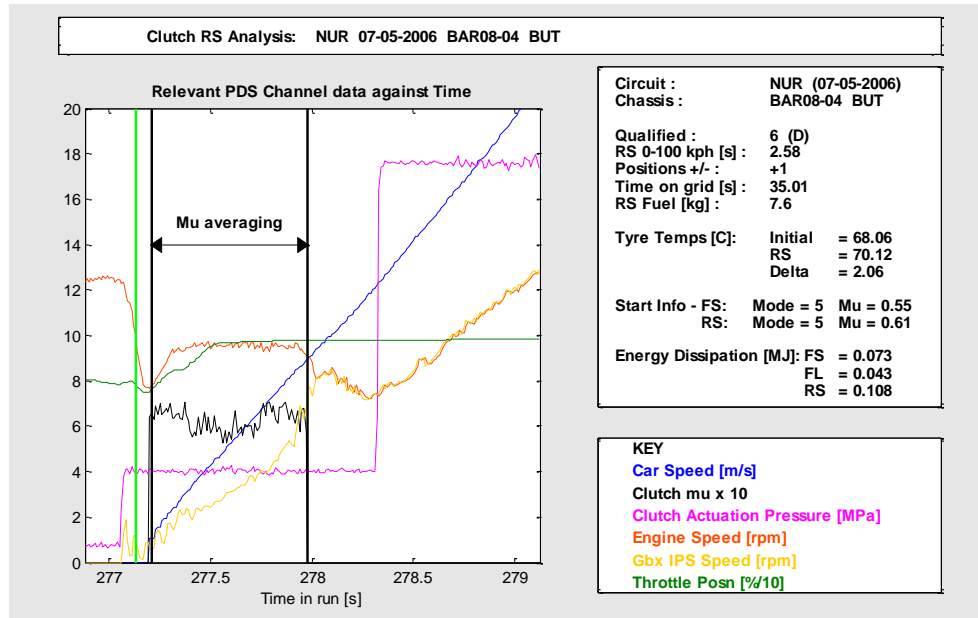


Figure 4.1e-i. Race Start, Car One, Nurburging Circuit

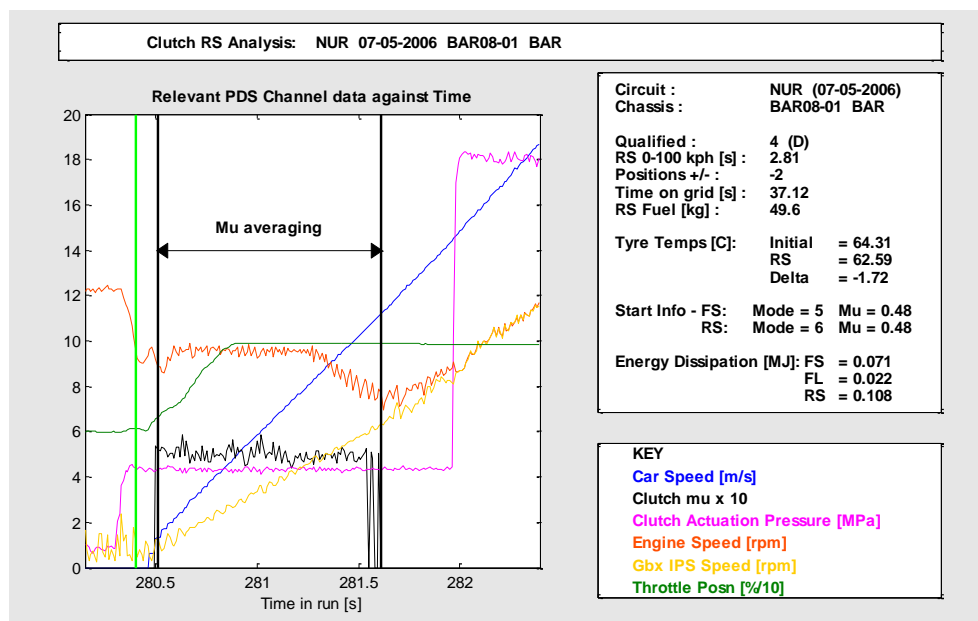


Figure 4.1e-ii. Race Start, Car Two, Nurburging Circuit

## Circuit de Catalunya

Date: 14<sup>th</sup> May 2006

Circuit Length: 4.627km

Race Distance: 305.382km (66 laps)

Number of Race Starts: 1

Weather: Dry

Air Temp: 26°C

Track

Temp: 37°C

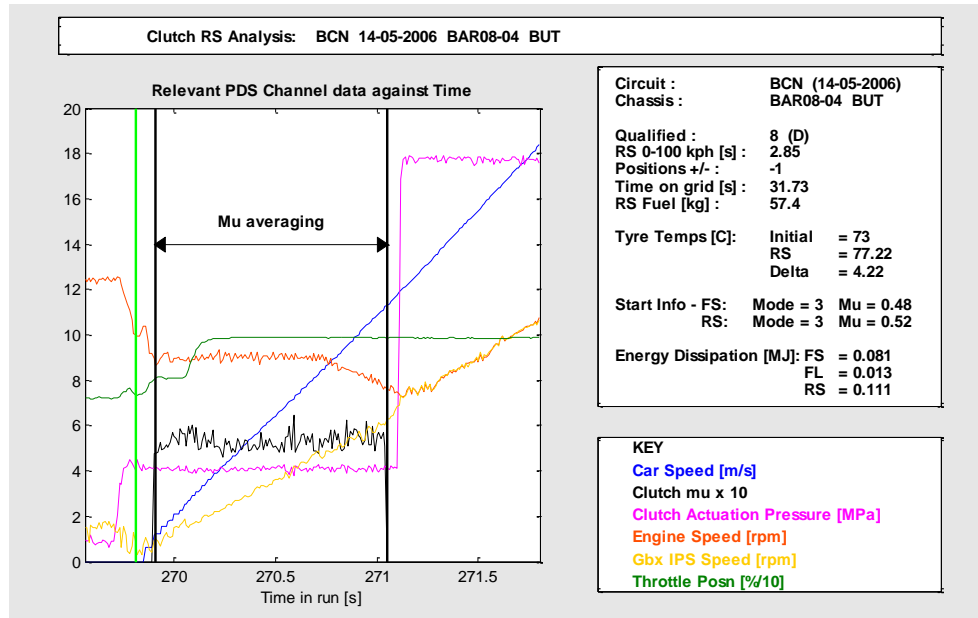


Figure 4.1f-i. Race Start, Car One, Catalunya Circuit

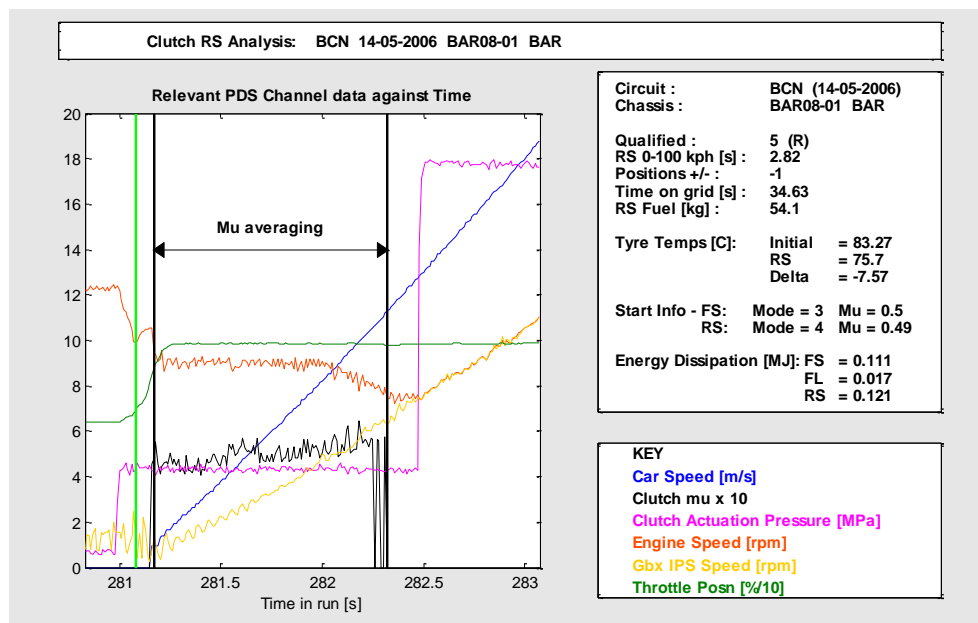


Figure 4.1f-ii. Race Start, Car Two, Catalunya Circuit

## Circuit de Monaco

Date: 28<sup>th</sup> May 2006

Circuit Length: 4.627km

Race Distance: 260.52km (70 laps)

Number of Race Starts: 1

Weather: Dry

Air Temp: 24°C

Track

Temp: 41°C

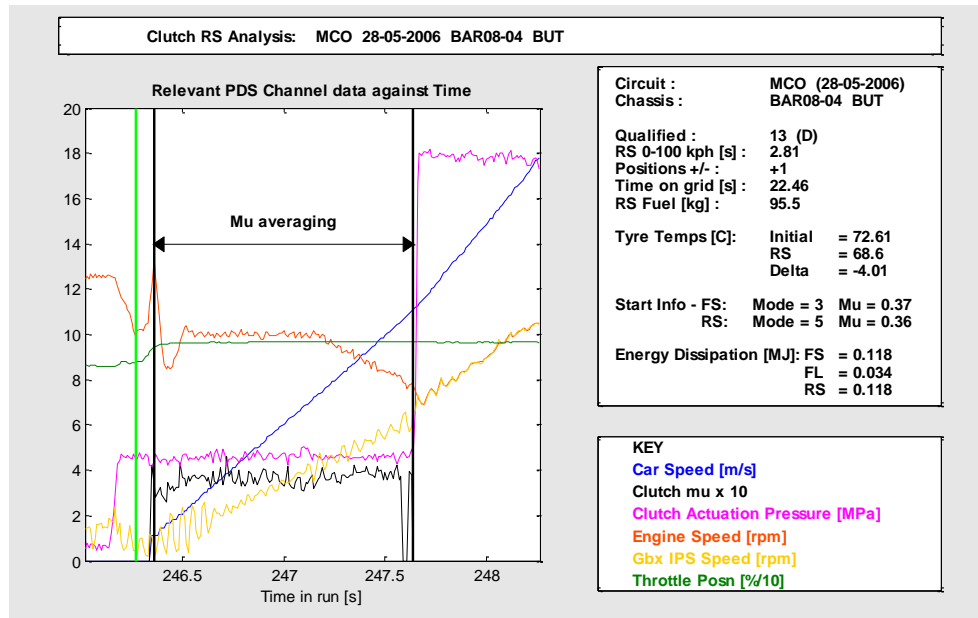


Figure 4.1g-i. Race Start, Car One, Monaco Circuit

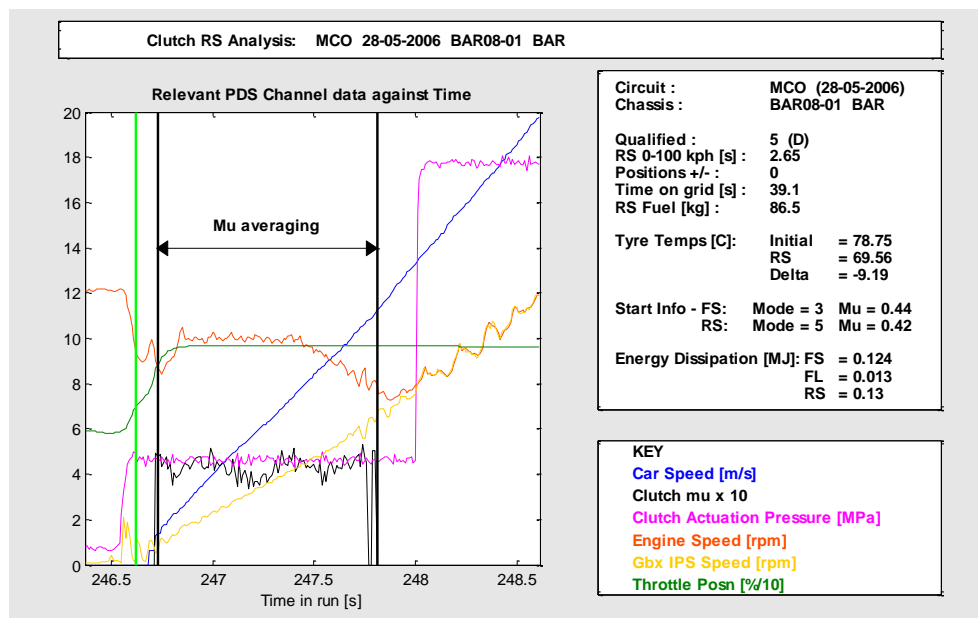


Figure 4.1g-ii. Race Start, Car Two, Monaco Circuit

## Silverstone Circuit

Date: 11<sup>th</sup> June 2006

Circuit Length: 5.141km

Race Distance: 308.355km (60 laps)

Number of Race Starts: 1

Weather: Dry

Air Temp: 26°C

Track

Temp: 36°C

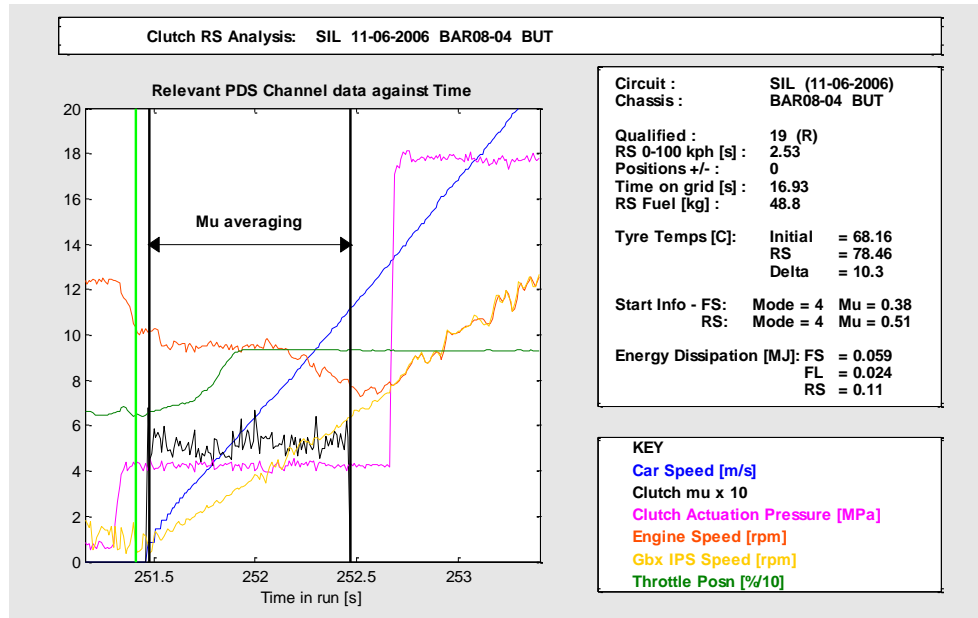


Figure 4.1h-i. Race Start, Car One, Silverstone Circuit

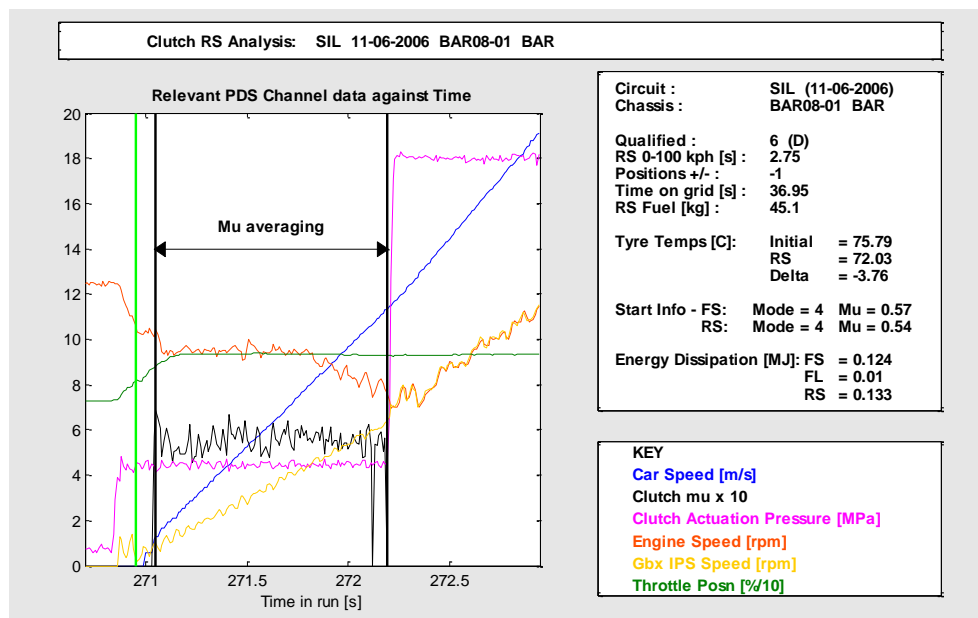


Figure 4.1h-ii. Race Start, Car Two, Silverstone Circuit

**Circuit Gilles Villeneuve, Montreal**

Date: 25<sup>th</sup> June 2006

Race Distance: 305.27km (70 laps)

Weather: Dry

Track Temp: 43°C

Circuit Length: 4.361km

Number of Race Starts: 1

Air Temp: 28°C

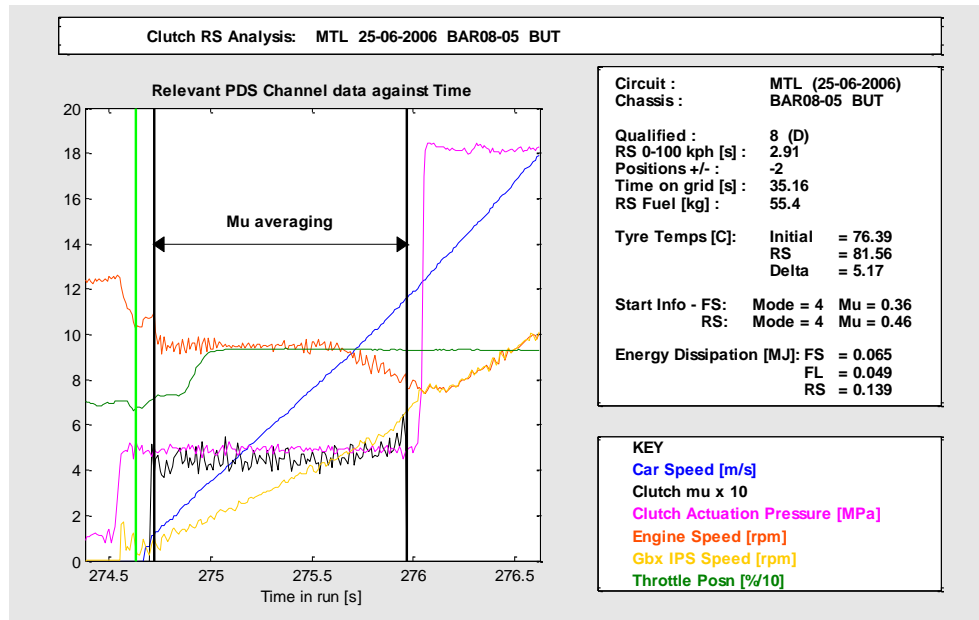


Figure 4.1i-i. Race Start, Car One, Montreal Circuit

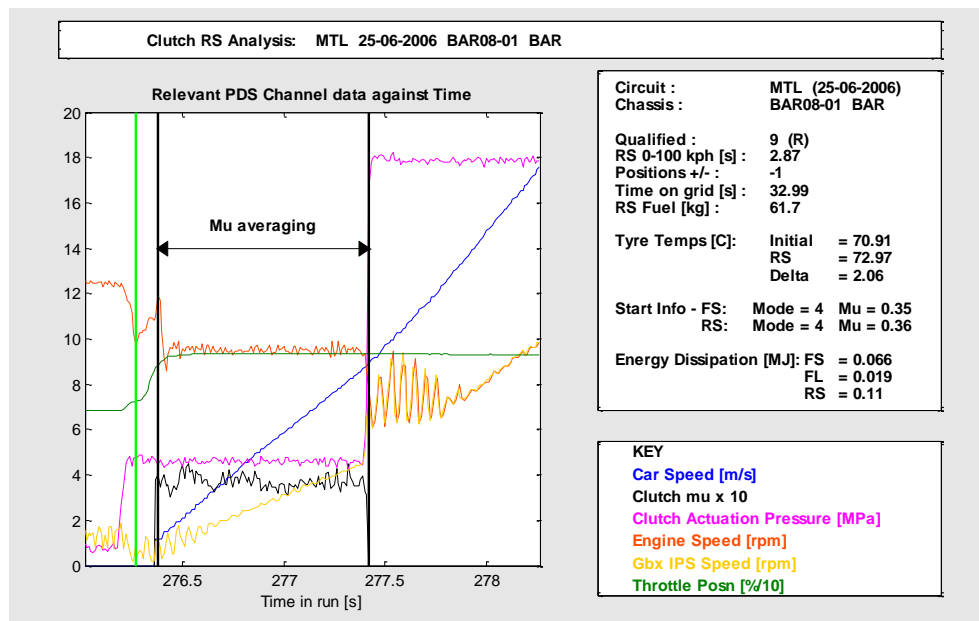


Figure 4.1i-ii. Race Start, Car Two, Montreal Circuit

## Indianapolis Motor Speedway

Date: 2<sup>nd</sup> July 2006

Race Distance: 306.016km (73 laps)

Weather: Dry

Track Temp: 46°C

Circuit Length: 4.195km

Number of Race Starts: 1

Air Temp: 35°C

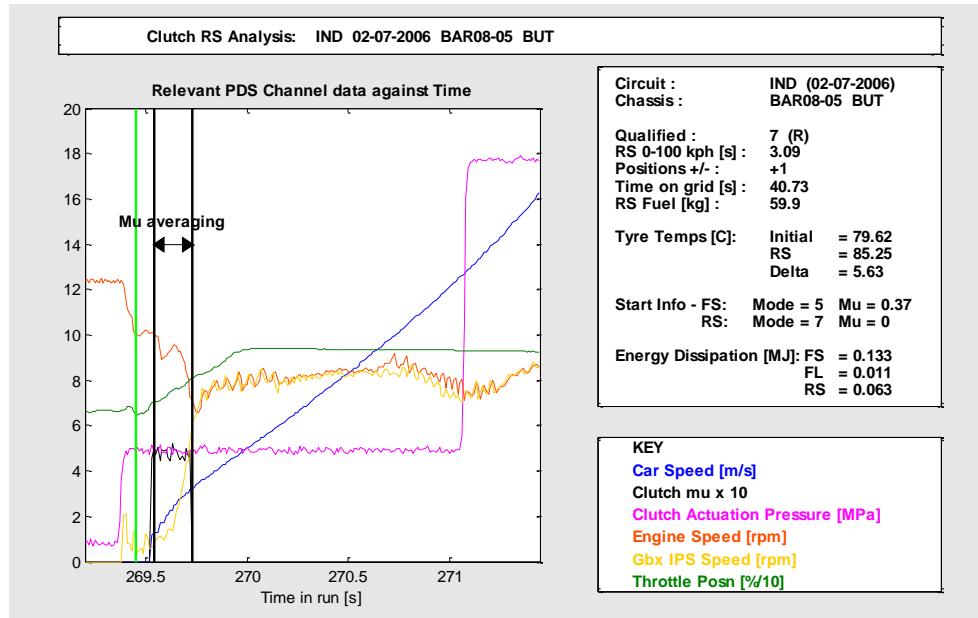


Figure 4.1j-i. Race Start, Car One, Indianapolis Motor Speedway

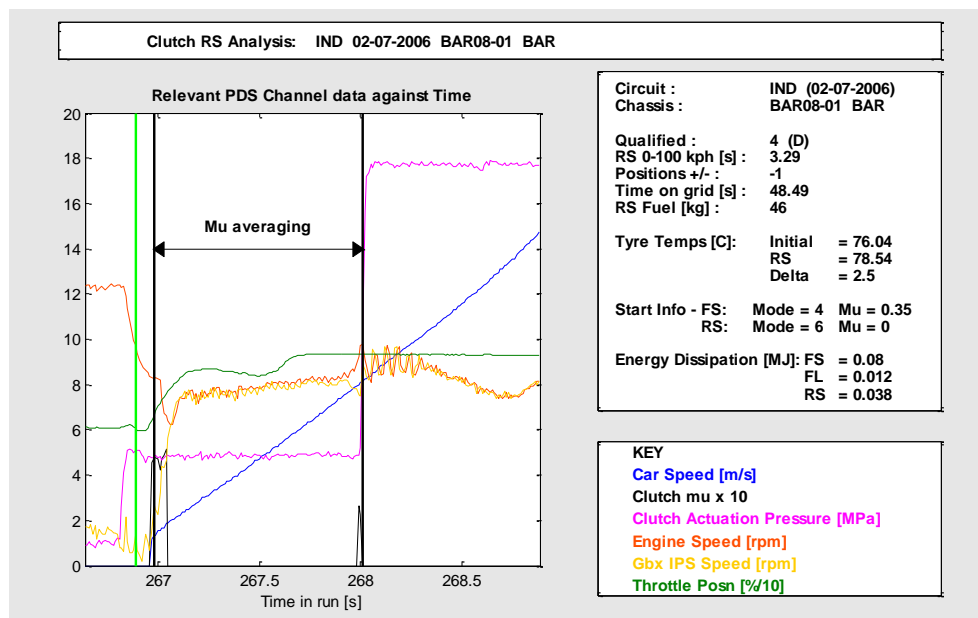


Figure 4.1j-ii. Race Start, Car Two, Indianapolis Motor Speedway



## Circuit de Nevers Magny-Cours

Date: 16<sup>th</sup> July 2006

Race Distance: 308.77km (70 laps)

Weather: Dry

Track Temp: 48°C

Circuit Length: 4.411km

Number of Race Starts: 1

Air Temp: 34°C

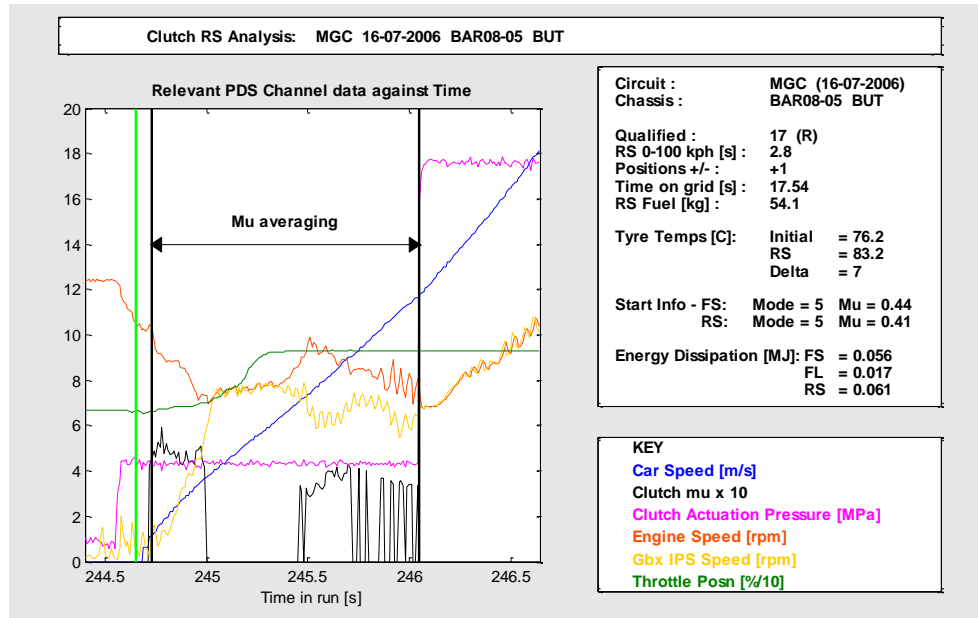


Figure 4.1k-i. Race Start, Car One, Magny-Cours Circuit

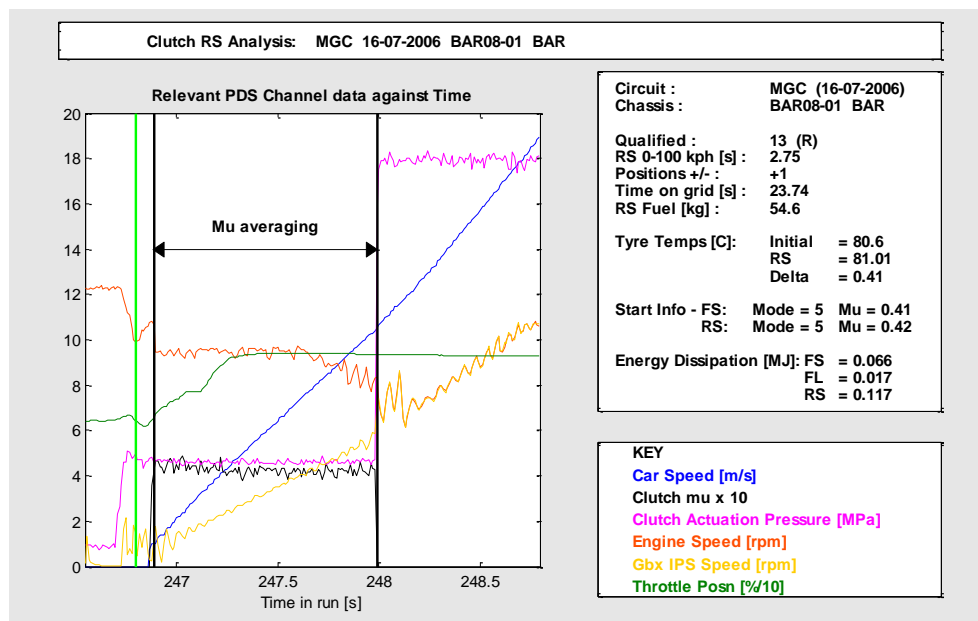


Figure 4.1k-ii. Race Start, Car Two, Magny-Cours Circuit

# Hockenheimring

Date: 30<sup>th</sup> July 2006

Race Distance: 306.458km (67 laps)

Weather: Dry

Track Temp: 45°C

Circuit Length: 4.574km

Number of Race Starts: 1

Air Temp: 32°C

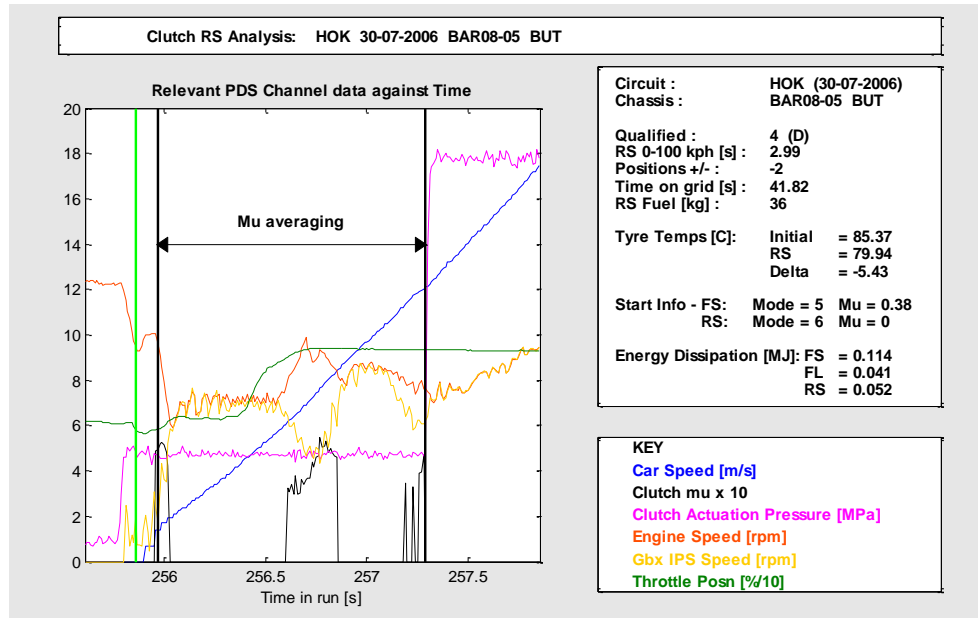


Figure 4.11-i. Race Start, Car One, Hockenheimring

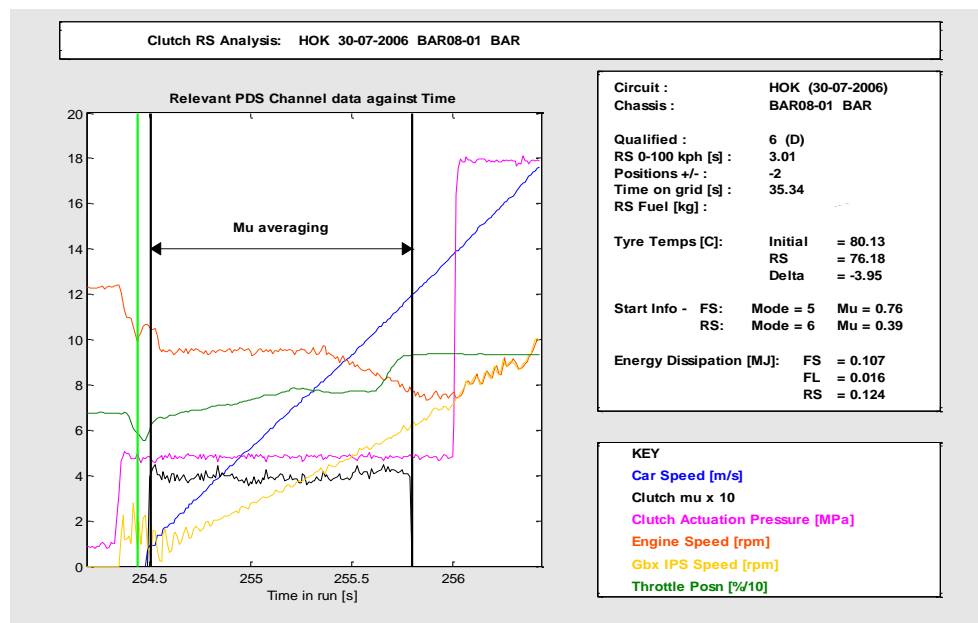


Figure 4.11-ii. Race Start, Car Two, Hockenheimring

## Hungaroring

Date: 6<sup>th</sup> August 2006

Race Distance: 306.67km (70 laps)

Weather: Wet

Track Temp: 21°C

Circuit Length: 4.381km

Number of Race Starts: 1

Air Temp: 18°C

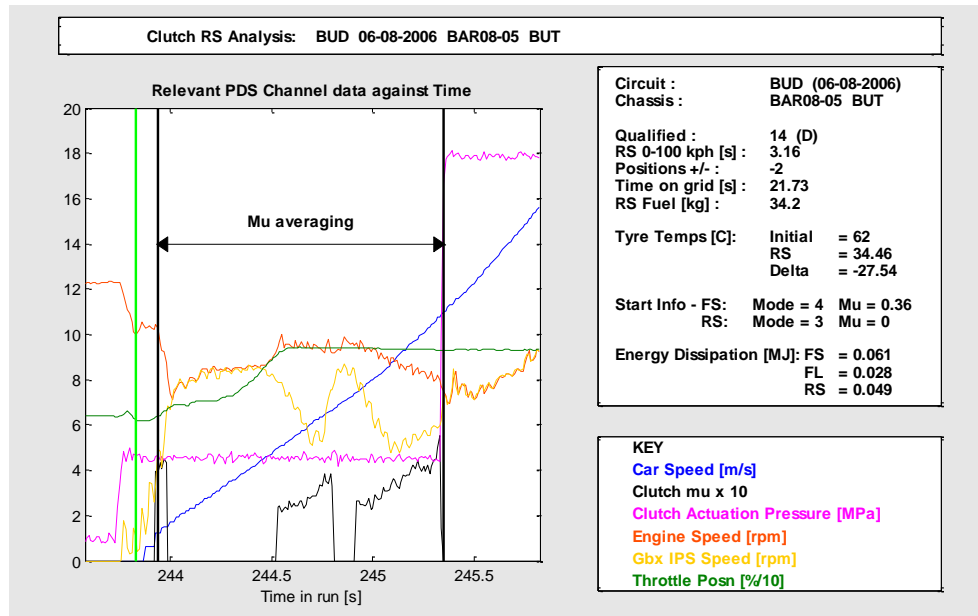


Figure 4.1m-i. Race Start, Car One, Hungaroring

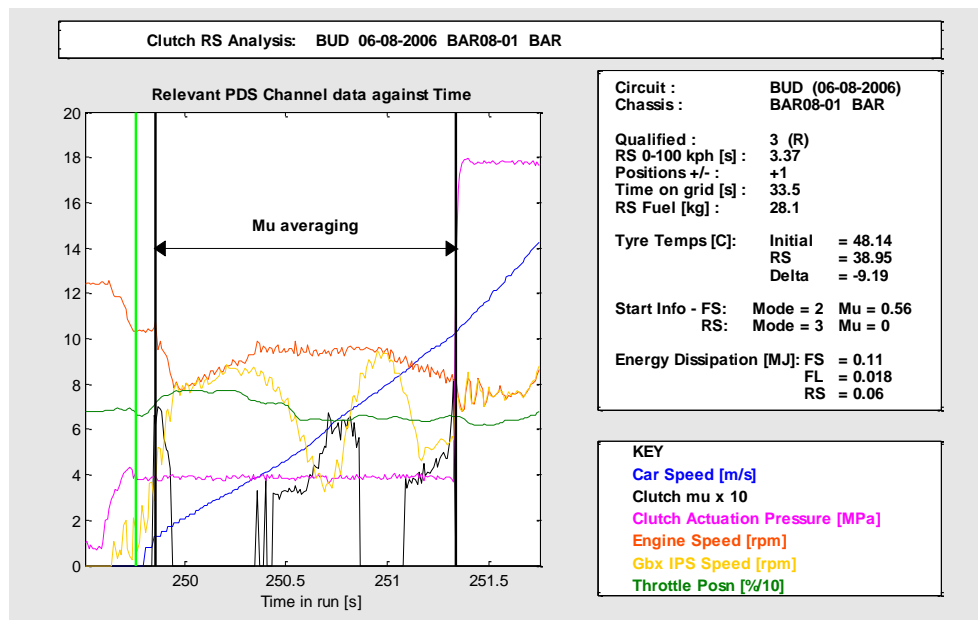


Figure 4.1m-ii. Race Start, Car Two, Hungaroring

## Istanbul Circuit

Date: 27<sup>th</sup> August 2006

Race Distance: 309.72km (58 laps)

Weather: Dry

Track Temp: 50°C

Circuit Length: 5.34km

Number of Race Starts: 1

Air Temp: 35°C

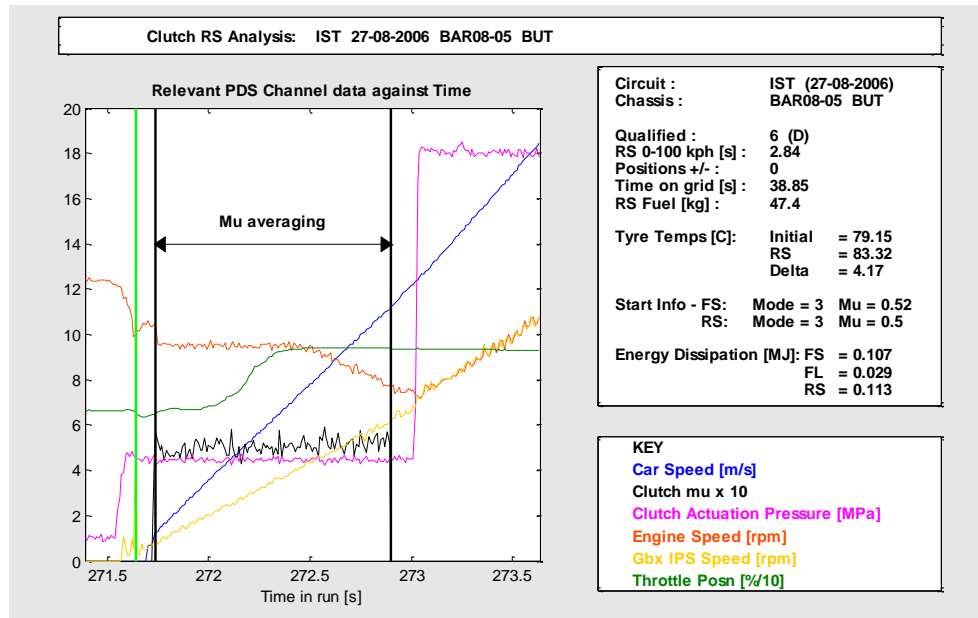


Figure 4.1n-i. Race Start, Car One, Istanbul Circuit

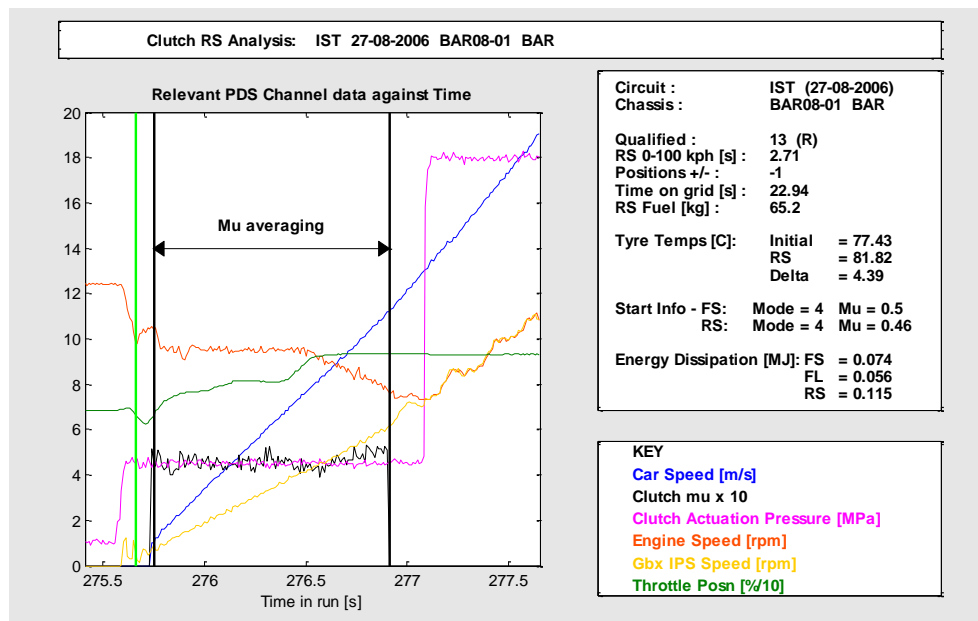


Figure 4.1n-ii. Race Start, Car Two, Istanbul Circuit

# Autodromo Nazionale Monza

Date: 10<sup>th</sup> September 2006  
 Race Distance: 309.029km (53 laps)  
 Weather: Dry

Circuit Length: 5.793km  
 Number of Race Starts: 1  
 Air Temp: 27°C

Track Temp: 40°C

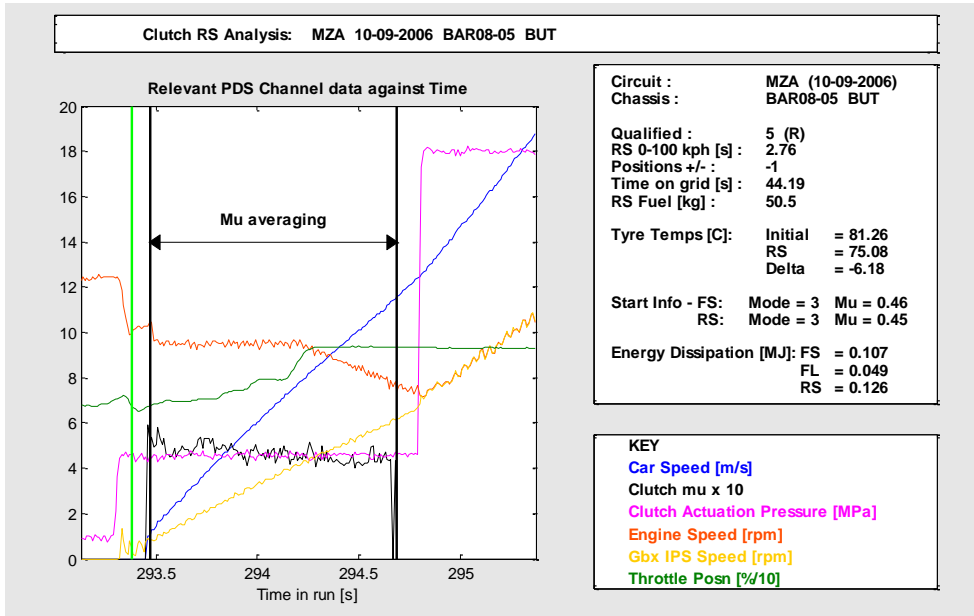


Figure 4.1o-i. Race Start, Car One, Monza Circuit

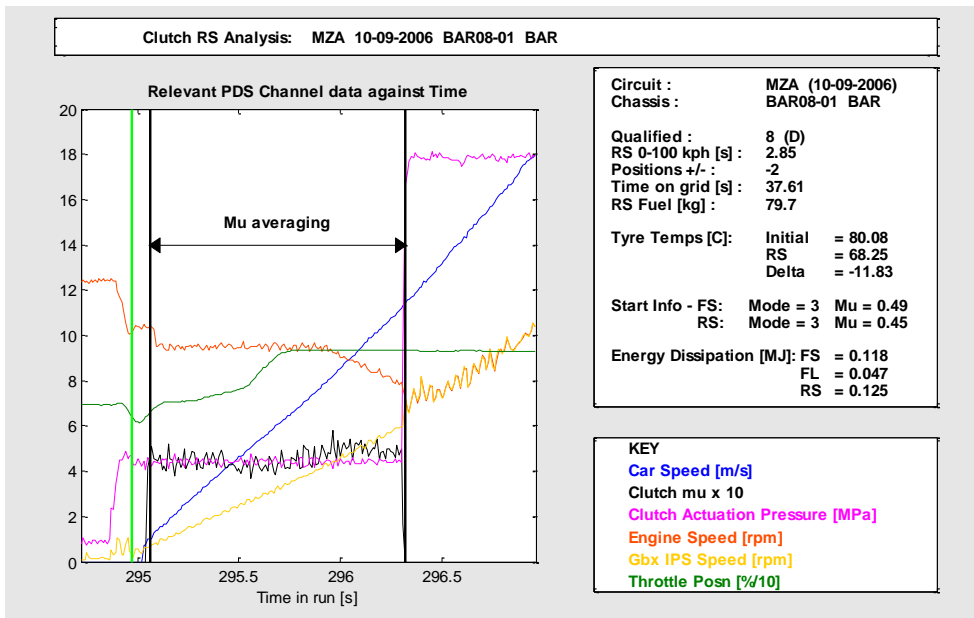


Figure 4.1o-ii. Race Start, Car Two, Monza Circuit

## Shanghai International Circuit

Date: 1<sup>st</sup> October 2006

Circuit Length: 5.451km

Race Distance: 305.066km (56 laps)

Number of Race Starts: 1

Weather: Rain at start for 60mins, then drying

Air Temp: 21°C

Track Temp: 22°C

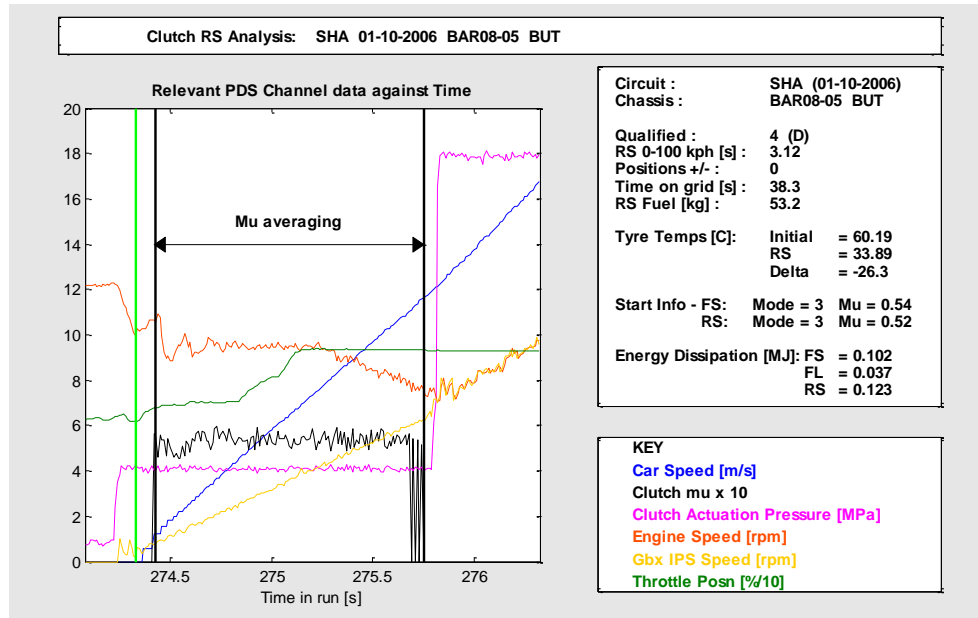


Figure 4.1p-i. Race Start, Car One, Shanghai Circuit

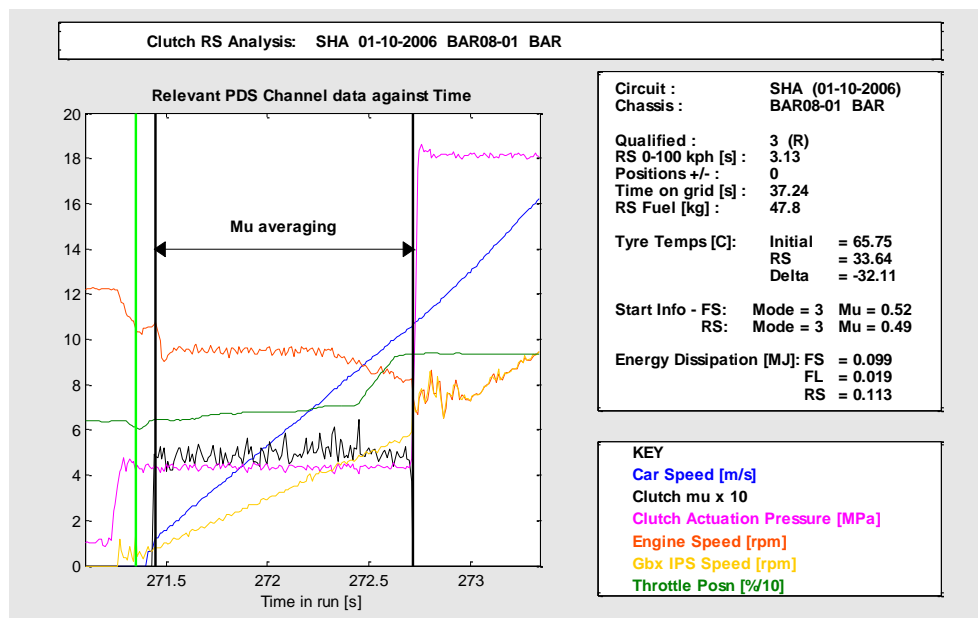


Figure 4.1p-ii. Race Start, Car Two, Shanghai Circuit

## Suzuka Circuit

Date: 8<sup>th</sup> October 2006

Circuit Length: 5.807km

Race Distance: 307.573km (53 laps)

Number of Race Starts: 1

Weather: Dry

Air Temp: 24°C

Track Temp: 31°C

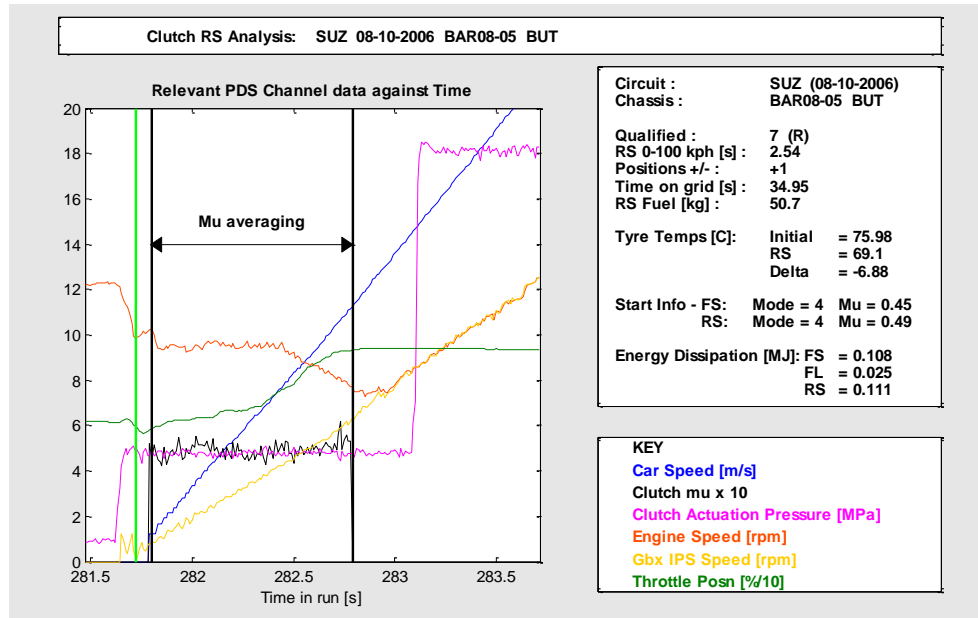


Figure 4.1.q-i. Race Start, Car One, Suzuka Circuit

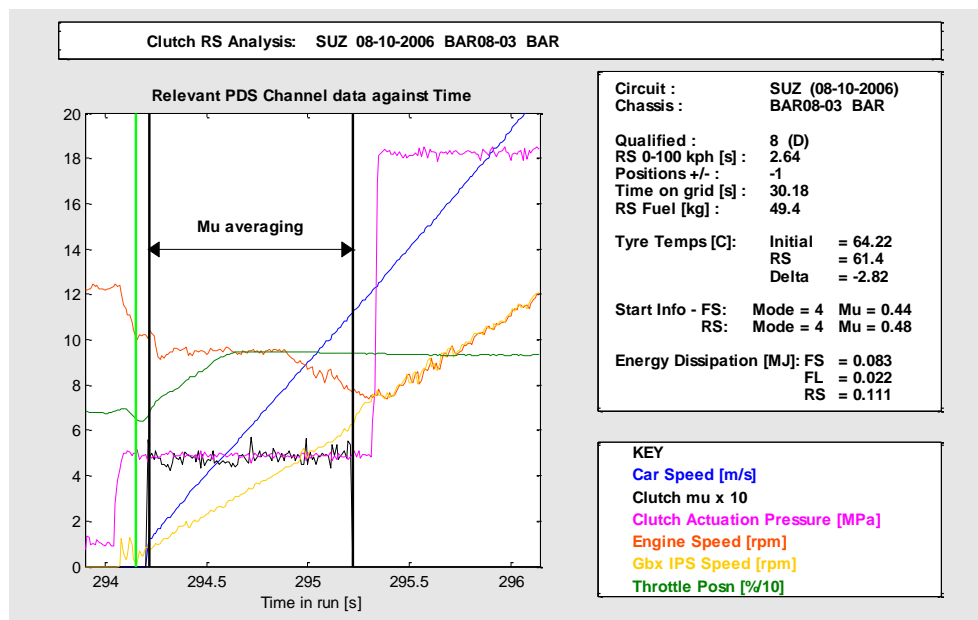


Figure 4.1q-ii. Race Start, Car Two, Suzuka Circuit

### Sao Paulo Circuit

Date: 22<sup>nd</sup> October 2006

Race Distance: 305.909km (71 laps)

Weather: Dry

Track Temp: 42°C

Circuit Length: 4.309km

Number of Race Starts: 1

Air Temp: 25°C

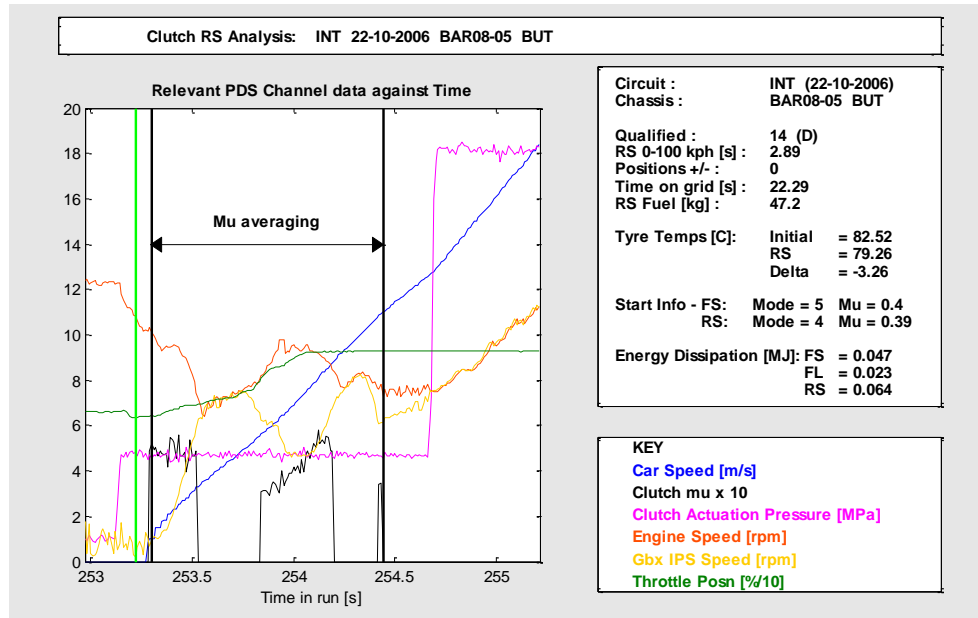


Figure 4.1r-i. Race Start, Car One, Sao Paulo Circuit

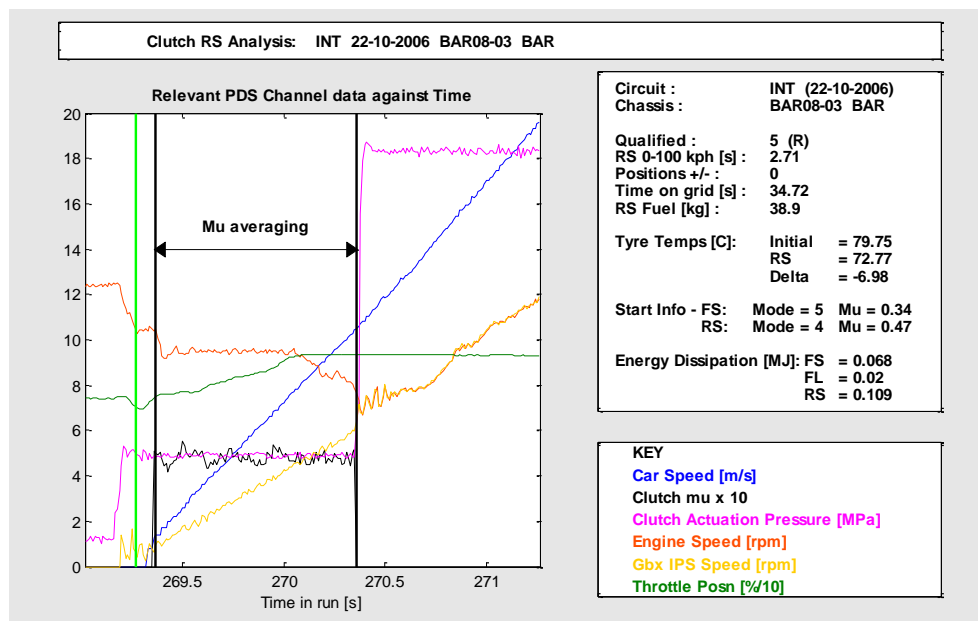


Figure 4.1r-ii. Race Start, Car Two, Sao Paulo Circuit



## Appendix B - Race Start Analysis MATLAB Code

```
% ~~~~~  
% CLUTCHSTARTANALYSIS_2006  
% ~~~~~  
  
clear all;  
close all;  
  
% Define set of global constants  
% Sets order in which parameters are saved into sData file  
scriptSetGlobalConstants;  
  
strDisplayLap = '1'; % Lap number or fastest  
strDisplayCorner = '1';  
  
% Define file path for storage of run history  
strSavePath = C:\Users\Gem\Documents\PhD  
  
% Define current version of script  
% If no match or old version, V6load will be run  
% If match found, .mat file loaded directly to save time  
CurrentDataVersionNo = 1.26;  
  
% Set data collation freq (Hz)  
iSampleRate_Hz = 100;  
  
% ~~~~~  
% PLOT SETUP  
% Boolean operators: 0 = NO, 1 = YES  
%  
bIndivRSPlot = 1; % PLOT TELEMTRY FOR EACH INDIVIDUAL RS  
bCorrelationPlot = 0; % PLOT A TABLE OF RESULTS WITH CORRELATIONS  
% ~~~~~  
  
% sJenson and sRubens structure  
% - All externally looked-up data for drivers stored in this structure  
% - i.e. data in here hasnt come from a .pds file  
% - Data here is stored in event order e.g. Mco = 7th entry, Ist = 14th entry  
% sJenson  
sJenson.Round = [1,2,3,4,5,6,7,8,9,10,11,12,13,14,15,16,17,18];  
sJenson.FuelFS_kg =  
[0,50,51.7,0,10,59.5,97,51,57.6,61.5,56,38,36.3,49.5,53.3,55.7,53.2,49.2];  
sJenson.QualPosn = [3,2,1,2,6,8,13,19,8,7,17,4,14,6,5,4,7,14];  
sJenson.QualSide = ['R','D','R','D','D','D','R','D','R','R','D','D','D','R','D','R','D'];  
sJenson.PosnChange = [-3,0,0,+1,+1,-1,+1,0,-2,1,1,-2,-2,0,-1,0,1,0];  
% sRubens  
sRubens.Round = [1,2,3,4,5,6,7,8,9,10,11,12,13,14,15,16,17,18];  
sRubens.FuelFS_kg =  
[49.8,89.6,92,42.4,51.8,56,88.1,47,63.6,47.6,56.3,0,30,67.5,82.4,50.1,52.1,41.0];  
sRubens.QualPosn = [6,20,16,3,4,5,5,6,9,4,13,6,3,13,8,3,8,5];  
sRubens.QualSide = ['D','D','R','R','D','R','D','D','R','D','R','D','R','R','D','R','D','R'];  
sRubens.PosnChange = [+1,+3,0,-2,-2,-1,0,-1,-1,-1,1,-2,1,-1,-2,0,-1,0];  
  
% 2006 FIA Formula One World Championship Race Calendar  
% - Round numbers stored in structure sRound
```

% - This will allow import of quali data etc regardless of the order the .pds files are imported

% - e.g. Import 05\_07Nur BAR08-01-BAR first, we can see this is Rubens at Nurburgring (Round 5) so it will import the 5th column of all relevant data from sRubens

sRound.BAH = 1;  
sRound.SEP = 2;  
sRound.MEL = 3;  
sRound.IMO = 4;  
sRound.NUR = 5;  
sRound.BCN = 6;  
sRound.MCO = 7;  
sRound.SIL = 8;  
sRound.MTL = 9;  
sRound.IND = 10;  
sRound.MGC = 11;  
sRound.HOK = 12;  
sRound.BUD = 13;  
sRound.IST = 14;  
sRound.MZA = 15;  
sRound.SHA = 16;  
sRound.SUZ = 17;  
sRound.INT = 18;

% ~~~~~  
% LIST OF .PDS FILES FOR ANALYSIS

% ~~~~~  
% .pds files are described by two cell string arrays  
% - acstrDataPath = the folder location of the file  
% - acstrFilenames = the name of the specific file within the folder  
% From these the full filepath is constructed

acstrDataPath{1} = 'R:\Race\2006\03\_12Bah\BAR08-04\Data\'; % Bahrain: Jenson Race  
acstrDataPath{2} = 'R:\Race\2006\03\_12Bah\BAR08-03\Data\'; % Bahrain: Rubens Race  
acstrDataPath{3} = 'R:\Race\2006\03\_19Sep\BAR08-04\Data\'; % Sepang: Jenson Race  
acstrDataPath{4} = 'R:\Race\2006\03\_19Sep\BAR08-01\Data\'; % Sepang: Rubens Race  
acstrDataPath{5} = 'R:\Race\2006\04\_02Mel\BAR08-04\Data\'; % Melbourne: Jenson Race  
acstrDataPath{6} = 'R:\Race\2006\04\_02Mel\BAR08-01\Data\'; % Melbourne: Rubens Race  
acstrDataPath{7} = 'R:\Race\2006\04\_23Imo\BAR08-04\Data\'; % Imola: Jenson Race  
acstrDataPath{8} = 'R:\Race\2006\04\_23Imo\BAR08-01\Data\'; % Imola: Rubens Race  
acstrDataPath{9} = 'R:\Race\2006\05\_07Nur\BAR08-04\Data\'; % Nurburgring: Jenson Race  
acstrDataPath{10} = 'R:\Race\2006\05\_07Nur\BAR08-01\Data\'; % Nurburgring: Rubens Race  
acstrDataPath{11} = 'R:\Race\2006\05\_14Bcn\BAR08-04\Data\'; % Barcelona: Jenson Race  
acstrDataPath{12} = 'R:\Race\2006\05\_14Bcn\BAR08-01\Data\'; % Barcelona: Rubens Race  
acstrDataPath{13} = 'R:\Race\2006\05\_28Mco\BAR08-04\Data\'; % Monaco: Jenson Race

acstrDataPath{14} = 'R:\Race\2006\05\_28Mco\BAR08-01\Data\'; % Monaco: Rubens Race  
 acstrDataPath{15} = 'R:\Race\2006\06\_11Sil\BAR08-04\Data\'; % Silverstone: Jenson Race  
 acstrDataPath{16} = 'R:\Race\2006\06\_11Sil\BAR08-01\Data\'; % Silverstone: Rubens Race  
 acstrDataPath{17} = 'R:\Race\2006\06\_25Mtl\BAR08-05\Data\'; % Montreal: Jenson Race  
 acstrDataPath{18} = 'R:\Race\2006\06\_25Mtl\BAR08-01\Data\'; % Montreal: Rubens Race  
 acstrDataPath{19} = 'R:\Race\2006\07\_02Ind\BAR08-05\Data\'; % Indy: Jenson Race  
 acstrDataPath{20} = 'R:\Race\2006\07\_02Ind\BAR08-01\Data\'; % Indy: Rubens Race  
 acstrDataPath{21} = 'R:\Race\2006\07\_16Mgc\BAR08-05\Data\'; % Magny Cours: Jenson Race  
 acstrDataPath{22} = 'R:\Race\2006\07\_16Mgc\BAR08-01\Data\'; % Magny Cours: Rubens Race  
 acstrDataPath{23} = 'R:\Race\2006\07\_30Hok\BAR08-05\Data\'; % Hockenheim: Jenson Race  
 acstrDataPath{24} = 'R:\Race\2006\07\_30Hok\BAR08-01\Data\'; % Hockenheim: Rubens Race  
 acstrDataPath{25} = 'R:\Race\2006\08\_06Bud\BAR08-05\Data\'; % Budapest: Jenson Race  
 acstrDataPath{26} = 'R:\Race\2006\08\_06Bud\BAR08-01\Data\'; % Budapest: Rubens Race  
 acstrDataPath{27} = 'R:\Race\2006\08\_27Ist\BAR08-05\Data\'; % Istanbul: Jenson Race  
 acstrDataPath{28} = 'R:\Race\2006\08\_27Ist\BAR08-01\Data\'; % Istanbul: Rubens Race  
 acstrDataPath{29} = 'R:\Race\2006\09\_10Mza\BAR08-05\Data\'; % Monza: Jenson Race  
 acstrDataPath{30} = 'R:\Race\2006\09\_10Mza\BAR08-01\Data\'; % Monza: Rubens Race  
 acstrDataPath{31} = 'R:\Race\2006\10\_01Sha\BAR08-05\Data\'; % Shanghai: Jenson Race  
 acstrDataPath{32} = 'R:\Race\2006\10\_01Sha\BAR08-01\Data\'; % Shanghai: Rubens Race  
 acstrDataPath{33} = 'R:\Race\2006\10\_08Suz\BAR08-05\Data\'; % Suzuka: Jenson Race  
 acstrDataPath{34} = 'R:\Race\2006\10\_08Suz\BAR08-03\Data\'; % Suzuka: Rubens Race  
 acstrDataPath{35} = 'R:\Race\2006\10\_22Int\BAR08-05\Data\'; % Interlagos: Jenson Race  
 acstrDataPath{36} = 'R:\Race\2006\10\_22Int\BAR08-03\Data\'; % Interlagos: Rubens Race

% End time selected to be prior to braking into the first corner after RS

acstrFileNames{1} = 'BAR08-04-BUT.03-12.19-34.pds'; afEndTime(1) = 299.800;  
 acstrFileNames{2} = 'BAR08-03-BAR.03-12.19-27.pds'; afEndTime(2) = 299.800;  
 acstrFileNames{3} = 'BAR08-04-BUT.03-19.20-22.pds'; afEndTime(3) = 289.100;  
 acstrFileNames{4} = 'BAR08-01-BAR.03-19.20-05.pds'; afEndTime(4) = 291.269;  
 acstrFileNames{5} = 'BAR08-04-BUT.04-02.18-41.pds'; afEndTime(5) = 274.899;  
 acstrFileNames{6} = 'BAR08-01-BAR.04-02.16-53.pds'; afEndTime(6) = 294.930;  
 acstrFileNames{7} = 'BAR08-04-BUT.04-23.18-12.pds'; afEndTime(7) = 268.614;  
 acstrFileNames{8} = 'BAR08-01-BAR.04-23.18-08.pds'; afEndTime(8) = 268.007;  
 acstrFileNames{9} = 'BAR08-04-BUT.05-07.16-15.pds'; afEndTime(9) = 287.640;  
 acstrFileNames{10} = 'BAR08-01-BAR.05-07.18-10.pds'; afEndTime(10) = 290.730;  
 acstrFileNames{11} = 'BAR08-04-BUT.05-14.18-10.pds'; afEndTime(11) = 280.850;

```

acstrFileNames{12} = 'BAR08-01-BAR.05-14.18-04.pds'; afEndTime(12) = 292.350;
acstrFileNames{13} = 'BAR08-04-BUT.05-28.18-23.pds'; afEndTime(13) = 251.700;
acstrFileNames{14} = 'BAR08-01-BAR.05-28.18-26.pds'; afEndTime(14) = 251.840;
acstrFileNames{15} = 'BAR08-04-BUT.06-11.14-33.pds'; afEndTime(15) = 258.100;
acstrFileNames{16} = 'BAR08-01-BAR.06-11.16-12.pds'; afEndTime(16) = 277.190;
acstrFileNames{17} = 'BAR08-05-BUT.06-25.16-47.pds'; afEndTime(17) = 280.490;
acstrFileNames{18} = 'BAR08-01-BAR.06-25.13-23.pds'; afEndTime(18) = 282.450;
acstrFileNames{19} = 'BAR08-05-BUT.07-02.13-14.pds'; afEndTime(19) = 280.410;
acstrFileNames{20} = 'BAR08-01-BAR.07-02.16-44.pds'; afEndTime(20) = 278.100;
acstrFileNames{21} = 'BAR08-05-BUT.07-16.15-27.pds'; afEndTime(21) = 251.410;
acstrFileNames{22} = 'BAR08-01-BAR.07-16.16-02.pds'; afEndTime(22) = 253.680;
acstrFileNames{23} = 'BAR08-05-BUT.07-30.18-23.pds'; afEndTime(23) = 261.910;
acstrFileNames{24} = 'BAR08-01-BAR.07-30.16-37.pds'; afEndTime(24) = 261.110;
acstrFileNames{25} = 'BAR08-05-BUT.08-08.19-11.pds'; afEndTime(25) = 250.000;
acstrFileNames{26} = 'BAR08-01-BAR.08-08.20-13.pds'; afEndTime(26) = 260.205;
acstrFileNames{27} = 'BAR08-05-BUT.08-27.18-41.pds'; afEndTime(27) = 277.688;
acstrFileNames{28} = 'BAR08-01-BAR.08-27.18-42.pds'; afEndTime(28) = 281.740;
acstrFileNames{29} = 'BAR08-05-BUT.09-10.17-57.pds'; afEndTime(29) = 301.010;
acstrFileNames{30} = 'BAR08-01-BAR.09-10.18-01.pds'; afEndTime(30) = 304.010;
acstrFileNames{31} = 'BAR08-05-BUT.10-01.18-23.pds'; afEndTime(31) = 281.600;
acstrFileNames{32} = 'BAR08-01-BAR.10-01.18-08.pds'; afEndTime(32) = 278.600;
acstrFileNames{33} = 'BAR08-05-BUT.10-08.18-02.pds'; afEndTime(33) = 288.700;
acstrFileNames{34} = 'BAR08-03-BAR.10-08.17-58.pds'; afEndTime(34) = 301.600;
acstrFileNames{35} = 'BAR08-05-BUT.10-22.17-53.pds'; afEndTime(35) = 260.200;
acstrFileNames{36} = 'BAR08-03-BAR.10-22.17-49.pds'; afEndTime(36) = 275.300;

```

```

for iRunCnt = 1:length(acstrFileNames)
    strDataPath = acstrDataPath{iRunCnt};
    % Build full file path of .pds file to be accessed
    acstrFullFileNames{iRunCnt} = [strDataPath char(acstrFileNames{iRunCnt})];
end

```

```

% ~~~~~
% LIST OF .PDS CHANNELS TO BE IMPORTED
% ~~~~~
% Channel names to be imported will be held in an array of cell strings
acstrV6ChannelList = [...
    {'LapDistance'} {'Lap Number'} {'Distance'} ...
    {'Pit Limit Armed'} {'Fuel Flap Active'}...
    {'Clu Act Pres'} {'Clu BP Wear Comp'} {'Drv RS Mode'}...
    {'Eng Speed'} {'Gbx IPS Speed'} ...
    {'Eng Thr Trq Max'} {'Eng Thr Trq'} {'Gbx IPS Trq'} {'Gbx IPS Trq Gain'} {'Gbx IPS
Trq Offset'}...
    {'Gbx Position'} {'Eng Thr Pos'} {'Eng Fuel Total'}...
    {'Car Speed'} {'Speed FL'} {'Speed FR'} {'Speed RL'} {'Speed RR'}...
    {'Car Accel Long'} {'Car Drag Force'} ...
    {'Tyre Temp RL1'} {'Tyre Temp RL2'} {'Tyre Temp RL3'} {'Tyre Temp RL4'} {'Tyre
Temp RL5'} {'Tyre Temp RL6'}...
    {'Tyre Temp RR1'} {'Tyre Temp RR2'} {'Tyre Temp RR3'} {'Tyre Temp RR4'} {'Tyre
Temp RR5'} {'Tyre Temp RR6'} ...
    {'Gbx Teeth Input 1'} {'Gbx Teeth Input 2'} {'Gbx Teeth Input 3'} {'Gbx Teeth Input
4'} {'Gbx Teeth Input 5'} {'Gbx Teeth Input 6'} {'Gbx Teeth Input 7'} {'Gbx Teeth Input
Bevel'} {'Gbx Teeth Input Diff'} ...
    {'Gbx Teeth Output 1'} {'Gbx Teeth Output 2'} {'Gbx Teeth Output 3'} {'Gbx Teeth
Output 4'} {'Gbx Teeth Output 5'} {'Gbx Teeth Output 6'} {'Gbx Teeth Output 7'} {'Gbx
Teeth Output Bevel'} {'Gbx Teeth Output Diff'} ...

```

```

{'Car Tyre Radius R'} {'Tyre Pres FL'} {'Tyre Pres RL'} ...
];

[sData] = GetFileData_V5(acstrFullFileNames...
    , 'SavePath', strSavePath...
    , 'currentdataversionno', CurrentDataVersionNo...
    , 'v6channellist', acstrV6ChannelList...
    , 'samplerate', iSampleRate_Hz...
    , 'end_time', afEndTime...
    , 'alllaps'...
);

sData = rmfield(sData,'aTime');

% Add the driver-specific information to relevant structure entry
for iCnt = 1:length(acstrFileNames)
    % Find the driver name
    DriverName = upper(sData(iCnt).CarName(10:12));
    Race = ['sRound.',upper(sData(iCnt).Track(6:8))];

    % SWITCH - used because file import order might not be consistent
    % - if driver = BUT, load info from sJenson
    % - if driver = BAR, load info from sRubens
    switch DriverName

        case 'BUT'
            sData(iCnt).FuelFS_kg = sJenson.FuelFS_kg(eval(Race));
            sData(iCnt).QualPosn = sJenson.QualPosn(eval(Race));
            sData(iCnt).QualSide = sJenson.QualSide(eval(Race));
            sData(iCnt).PosnChange = sJenson.PosnChange(eval(Race));
        case 'BAR'
            sData(iCnt).FuelFS_kg = sRubens.FuelFS_kg(eval(Race));
            sData(iCnt).QualPosn = sRubens.QualPosn(eval(Race));
            sData(iCnt).QualSide = sRubens.QualSide(eval(Race));
            sData(iCnt).PosnChange = sRubens.PosnChange(eval(Race));
        otherwise
            error('Unknown Driver and/or Event')
            break
    end
end

clear sJenson sRubens sRound strSavePath strDisplayLap strDisplayCorner
strDataPath acstrFullFileNames acstrDataPath acstrV6ChannelList
CurrentDataVersionNo DriverName Race afEndTime

for iRunCnt = 1:length(acstrFileNames)

% ~~~~~
% CLUTCH DATA

```

```

% ~~~~~
% Define clutch data (RA106 data)
CluSinglePistonDiameter_mm = 10.5;
CluSinglePistonArea_mm2 = 0.25*pi*CluSinglePistonDiameter_mm^2;
CluNumberOfPistons = 2;
CluTotalPistonArea_mm2 = CluNumberOfPistons * CluSinglePistonArea_mm2;
CluDiamInner_mm = 65;
CluDiamOuter_mm = 97;
Clu_NumWorkingSurfaces = 6;
Clu_LeverRatio = 3.46;
% Calculate clutch mean friction diameter
CluMeanFrictionRad_mm = (2/3)*(((0.5*CluDiamOuter_mm)^3)-
((0.5*CluDiamInner_mm)^3)) / (((0.5*CluDiamOuter_mm)^2)-
((0.5*CluDiamInner_mm)^2));
CluDebounceTime_s = 0.2;

% -----
% CLUTCH CALCUATIONS

% Define threshold for a clutch event assuming DPC
% A clutch event is said to occur when clutch actuation pressure drops below
nCluEventThreshold_bar
% - Nb. This value is just based on past experience to capture the required clutch
events
nCluEventThreshold_bar = 150;

% Find the clutch disengagement points
% - DPC is disengaged when the actuation pressure drops below the threshold
aCluDisengaged = find((sData(iRunCnt).Clu_Act_Pres) < nCluEventThreshold_bar);

% A new clutch event can start when the threshold engagement pressure has been
exceeded for more than 0.05s
aBelowCluThresholdStarts = [aCluDisengaged(1);
aCluDisengaged(find(aCluDisengaged(2:end)-aCluDisengaged(1:end-1) > 5)+1)];
% Locate the associated times
aCluEventStartTime = sData(iRunCnt).Time(aBelowCluThresholdStarts);

% Clutch event end points are where the next disengagement point is more than 5
time steps ahead
% - Nb. Again, this value is used simply to capture the required events
aBelowCluThresholdEnds = [aCluDisengaged(find(aCluDisengaged(2:end)-
aCluDisengaged(1:end-1) > 5)); aCluDisengaged(end)];
% Locate the associated times
aCluEventEndTime = sData(iRunCnt).Time(aBelowCluThresholdEnds);

sData(iRunCnt).aBelowCluThresholdStarts = aBelowCluThresholdStarts;
sData(iRunCnt).aBelowCluThresholdEnds = aBelowCluThresholdEnds;

clear aCluDisengaged

% Number of times clutch manouvers occur throughout duration of data in question
% - Number of times used = number of times an event starts
sData(iRunCnt).iNumUse = length(aBelowCluThresholdStarts);

% Clutch speed difference = input speed - output speed
% = engine speed - gearbox input shaft speed

```

```

sData(iRunCnt).aCluSpeedDiff_rpm = (sData(iRunCnt).Eng_Speed -
sData(iRunCnt).Gbx_IPS_Speed);
sData(iRunCnt).aCluSpeedDiff_radpers = sData(iRunCnt).aCluSpeedDiff_rpm *
(2*pi/60);

% Force acting on clutch i.e. Clamp Force
% -  $P = F / A$  hence  $F = P \times A$ 
% - SI units preferable hence conversion from mm and bar
Clu_Act_Pres_Pa = sData(iRunCnt).Clu_Act_Pres.*100000;
Clu_BP_Wear_Comp_Pa = sData(iRunCnt).Clu_BP_Wear_Comp.*100000;
Clu_Pres_Effective_Pa = (Clu_Act_Pres_Pa - Clu_BP_Wear_Comp_Pa);
Clu_TotalPistonArea_m2 = CluTotalPistonArea_mm2./1000000;
% - Final force must account for the lever ratio
sData(iRunCnt).aCluForce_N = Clu_Pres_Effective_Pa .* Clu_TotalPistonArea_m2
.*Clu_LeverRatio;

clear Clu_TotalPistonArea_m2 Clu_Pres_Effective_Pa Clu_BP_Wear_Comp_Pa
Clu_Act_Pres_Pa

% Clutch power
% - Power = Torque x Angular Velocity
sData(iRunCnt).aCluPower_W = abs((sData(iRunCnt).Gbx_IPS_Trq) .*
sData(iRunCnt).aCluSpeedDiff_radpers);

% Clutch Energy Dissipated
% - Energy = Power x Time
dt = 1/sData(iRunCnt).iScanRate_pers;
sData(iRunCnt).TotalKEClu_J = cumsum(abs(sData(iRunCnt).aCluPower_W).*dt);

% Find the maximum clutch power for the set of events on the run
sData(iRunCnt).CluPower_MW_max =
(max(sData(iRunCnt).aCluPower_W))./1000000;
% Find the maximum clutch energy for the set of events on the run
sData(iRunCnt).TotalKEClu_MJ_max =
(max(sData(iRunCnt).TotalKEClu_J))./1000000;

% Clutch Mu Calculation
% - Coefficient of friction = Torque / (num working surfaces x Force x mean friction
rad)
% - Nb. Mu calculated for entire dataset - relevant range will be calculated later

aCluMuValid =
find((sData(iRunCnt).aCluSpeedDiff_rpm>1500)&(sData(iRunCnt).Eng_Speed>6000)
&(sData(iRunCnt).Car_Speed>3)&(sData(iRunCnt).Car_Speed<60));

sData(iRunCnt).aCluMu = zeros(1,length(sData(iRunCnt).Time));
sData(iRunCnt).aCluMu(aCluMuValid) = abs(
(sData(iRunCnt).Gbx_IPS_Trq(aCluMuValid))./ (Clu_NumWorkingSurfaces *
sData(iRunCnt).aCluForce_N(aCluMuValid) * (CluMeanFrictionRad_mm*(1/1000))));

% Determine start locations
aStarts = find((sData(iRunCnt).Car_Speed(2:end-
199))>=2)&(sData(iRunCnt).Car_Speed(1:end-
200)<2)&(sData(iRunCnt).Car_Speed(201:end)>10));

```

```

sData(iRunCnt).FormationStart = aStarts(1);

RaceStart = aStarts(end);

RaceStart2 = find((sData(iRunCnt).Car_Accel_Long(RaceStart-
199:RaceStart)>=0.50)&(sData(iRunCnt).Car_Accel_Long(RaceStart-200:RaceStart-
1)<0.50));
sData(iRunCnt).RaceStart = RaceStart2(1)+RaceStart-201;

clear aStarts RaceStart2 RaceStart

sData(iRunCnt).TimeOnGrid_s =
length(find(sData(iRunCnt).Car_Speed(sData(iRunCnt).RaceStart-
6000:sData(iRunCnt).RaceStart+100)<2))./iSampleRate_Hz;

% Find the 0 to 100 kph time for the RS
sData(iRunCnt).f100kphTime_s =
(min(find(sData(iRunCnt).Car_Speed(sData(iRunCnt).RaceStart:end) >= 100))-2)*dt;

for iCluEvent = 1:1:sData(iRunCnt).iNumUse

% Use all the clutch event data by looking at the data before the event for the last
time the pressure was above the lower threshold
CluOff = aBelowCluThresholdStarts(iCluEvent);
sData(iRunCnt).aCluEvent(iCluEvent,EVENTSTARTTIME) = CluOff;
% Use all the brake event data by looking at the data after the event for the first
time the pressure was above the lower threshold
CluOn = aBelowCluThresholdEnds(iCluEvent);
sData(iRunCnt).aCluEvent(iCluEvent,EVENTENDTIME) = CluOn;

% Duration of clutch event
sData(iRunCnt).aCluEvent(iCluEvent,CLUTCHDURATION) = (CluOn - CluOff)*dt;

% Save clutch start and end times
sData(iRunCnt).aCluEvent(iCluEvent,CLUTCHSTART) =
aCluEventStartTime(iCluEvent);
sData(iRunCnt).aCluEvent(iCluEvent,CLUTCHEND) =
aCluEventEndTime(iCluEvent);

% Max clutch power in event is largest clutch power value between start and end
of clutch event
sData(iRunCnt).aCluEvent(iCluEvent,MAXPOWER) =
max(sData(iRunCnt).aCluPower_W(CluOff:CluOn));

% Energy = Power x Time
sData(iRunCnt).aCluEvent(iCluEvent,EVENTENERGY) =
sum(sData(iRunCnt).aCluPower_W(CluOff:CluOn)*dt);

aCluEventEnergy =
sData(iRunCnt).aCluPower_W(CluOff:CluOn)./iSampleRate_Hz;

```



```

    sData(iRunCnt).aCluEventTotalEnergy(iCluEvent,:) =
max(cumsum(aCluEventEnergy));

    % Determine the instantaneous time at which the clutch event can be said to
occur
    sData(iRunCnt).aCluEvent(iCluEvent,EVENTMEANTIME) =
0.5*(sData(iRunCnt).aCluEvent(iCluEvent,EVENTSTARTTIME) +
sData(iRunCnt).aCluEvent(iCluEvent,EVENTENDTIME));

    %sData(iRunCnt).aCluEvent(iCluEvent,CLUMUVALID) =
find((sData(iRunCnt).aCluSpeedDiff_rpm(CluOn:CluOff)>1500)&(sData(iRunCnt).Eng_
Speed(CluOn:CluOff)>6000)&(sData(iRunCnt).Car_Speed(CluOn:CluOff)>3)&(sData(iR
unCnt).Car_Speed(CluOn:CluOff)<60))

    % Clear un-needed variables
clear CluOff CluOn iCluEvent

end

clear aBelowCluThresholdStarts aBelowCluThresholdEnds dt
nCluEventThreshold_bar aCluEventEndTime aCluEventStartTime aCluEventEnergy

    % Find the clutch event corresponding to the race start

RaceStartEvent=find(((sData(iRunCnt).aCluEvent(:,EVENTENDTIME))>sData(iRunCnt
).RaceStart) &
((sData(iRunCnt).aCluEvent(:,EVENTSTARTTIME))<sData(iRunCnt).RaceStart));

    % Find the maximum power at the race start
sData(iRunCnt).RaceStartPowerMax_MW =
sData(iRunCnt).aCluEvent(RaceStartEvent,MAXPOWER)/1000000;
sData(iRunCnt).CluEnergyRS_MJ =
sData(iRunCnt).aCluEvent(RaceStartEvent,EVENTENERGY)./1000000;

    % Find the clutch event corresponding to the formation start

FormationStartEvent=find(((sData(iRunCnt).aCluEvent(:,EVENTENDTIME))>sData(iR
unCnt).FormationStart) &
((sData(iRunCnt).aCluEvent(:,EVENTSTARTTIME))<sData(iRunCnt).FormationStart));
    % Find the maximum power at the formation start
sData(iRunCnt).FormationStartPowerMax_MW =
sData(iRunCnt).aCluEvent(FormationStartEvent,MAXPOWER)/1000000;
sData(iRunCnt).CluEnergyFS_MJ =
sData(iRunCnt).aCluEvent(FormationStartEvent,EVENTENERGY)./1000000;

    % Clutch energy on formation lap is sum of energies for all events between FS and
RS
sData(iRunCnt).CluEnergyFL_MJ =
sum(sData(iRunCnt).aCluEvent(FormationStartEvent+1:RaceStartEvent-
1,EVENTENERGY))/1000000;

    % Total energy of interest = Energy at FS + Energy over FL + Energy at RS
    % i.e. we are not interested in the energy dissipated during gear changes up to the
first corner
sData(iRunCnt).CluEnergyFSFLRS_MJ = sum(sData(iRunCnt).CluEnergyFL_MJ +
sData(iRunCnt).CluEnergyFS_MJ + sData(iRunCnt).CluEnergyRS_MJ);

```

```

    % FS Clutch Mode
    DrvRSMoDeFS =
round(mean(sData(iRunCnt).Drv_RS_Mode(sData(iRunCnt).FormationStart-
200:sData(iRunCnt).FormationStart)));
    % RS Clutch Mode
    DrvRSMoDeRS =
round(mean(sData(iRunCnt).Drv_RS_Mode(sData(iRunCnt).RaceStart-
200:sData(iRunCnt).RaceStart)));

    sData(iRunCnt).DrvRSModes = [DrvRSMoDeFS,DrvRSMoDeRS];

clear DrvRSMoDeFS DrvRSMoDeRS

FuelUsedFL_kg = (mean(sData(iRunCnt).Eng_Fuel_Total(sData(iRunCnt).RaceStart-
100:sData(iRunCnt).RaceStart))-mean(sData(iRunCnt).Eng_Fuel_Total(100:200)));
sData(iRunCnt).FuelRS_kg = sData(iRunCnt).FuelFS_kg - FuelUsedFL_kg;
clear FuelUsedFL_kg

if sData(iRunCnt).FuelRS_kg <= 0
    sData(iRunCnt).FuelRS_kg = 'n/a';
end

sData(iRunCnt).iNumUse_FSFLRS = (RaceStartEvent - FormationStartEvent) +1;

sData(iRunCnt).FSTyreTemp_R =
mean(sData(iRunCnt).Tyre_Temp_R(sData(iRunCnt).FormationStart-
300:sData(iRunCnt).FormationStart-250));
sData(iRunCnt).RSTyreTemp_R =
mean(sData(iRunCnt).Tyre_Temp_R(sData(iRunCnt).RaceStart-
50:sData(iRunCnt).RaceStart));
sData(iRunCnt).DeltaTyreTemp_R = sData(iRunCnt).RSTyreTemp_R-
sData(iRunCnt).FSTyreTemp_R;

    % Eng_Fuel_Total no longer required - remove from loop until structure can be
cleared
sData(iRunCnt).Eng_Fuel_Total = {'Cleared'};

RSStart = sData(iRunCnt).aCluEvent(RaceStartEvent,9);
RSEnd = sData(iRunCnt).aCluEvent(RaceStartEvent,10);

aCluMuValidRS =
RSStart+find((sData(iRunCnt).aCluSpeedDiff_rpm(RSStart:RSEnd)>1500)&(sData(iRu
nCnt).Eng_Speed(RSStart:RSEnd)>6000)&(sData(iRunCnt).Car_Speed(RSStart:RSEnd)
>3)&(sData(iRunCnt).Car_Speed(RSStart:RSEnd)<60));

    % Check that the slip is not broken, i.e. we only want the first engagement slip
    % Check that there is no gap greater than 10 timesteps (0.1s) between valid
timesteps
aCluMuValidContinuous = find((aCluMuValidRS(2:end)-aCluMuValidRS(1:end-
1))>10);

    % If aCluMuValidContinuous is not empty, then there is a break
if isempty(aCluMuValidContinuous) == 0

```

```

    aCluMuValidRS = aCluMuValidRS(1:aCluMuValidContinuous(1));
end

% Add the debounce time to the calculation
aCluMuValidRS = aCluMuValidRS(CluDebounceTime_s*iSampleRate_Hz:end);

% Clutch mu at RS is the mean of all valid mu values
sData(iRunCnt).CluMuRS = mean(sData(iRunCnt).aCluMu(aCluMuValidRS));

FSStart = sData(iRunCnt).aCluEvent(FormationStartEvent,9);
FSEnd = sData(iRunCnt).aCluEvent(FormationStartEvent,10);

sData(iRunCnt).FSStart = FSStart;
sData(iRunCnt).FSEnd = FSEnd;
sData(iRunCnt).aCluMuValidFS = FSStart +
find((sData(iRunCnt).aCluSpeedDiff_rpm(FSStart:FSEnd)>1500)&(sData(iRunCnt).Eng_Speed(FSStart:FSEnd)>6000)&(sData(iRunCnt).Car_Speed(FSStart:FSEnd)>3)&(sData(iRunCnt).Car_Speed(FSStart:FSEnd)<60));
sData(iRunCnt).aCluMuValidFS =
sData(iRunCnt).aCluMuValidFS(CluDebounceTime_s*iSampleRate_Hz:end);
sData(iRunCnt).CluMuFS =
mean(sData(iRunCnt).aCluMu(sData(iRunCnt).aCluMuValidFS));

% Find location of clutch plate speed matching
sData(iRunCnt).CluSpeedMatched =
RSStart+min(find((sData(iRunCnt).Eng_Speed(RSStart:RSEnd)-
sData(iRunCnt).Gbx_IPS_Speed(RSStart:RSEnd))<100));

clear aCluMuValid aCluMuValidContinuous FSStart FSEnd aCluMuValidRS
RaceStartEvent FormationStartEvent

end

acstrIndividualChannels =
{'Drv_RS_Mode','aCluSpeedDiff_radpers','aCluForce_N','aCluSpeedDiff_rpm','aBelowCluThresholdStarts','aBelowCluThresholdEnds','iNumUse','FuelFS_kg','Eng_Fuel_Total','Track','Driver','CarName'};
sData = rmfield(sData,acstrIndividualChannels);
clear acstrIndividualChannels

%acstrNewOrder =
{'Date','Circuit','Chassis','Drv','OriginalFilePath','OriginalFileName','iScanRate_pers','Time','LapDistance','Lap_Number','Distance','Pit_Limit_Armed','Fuel_Flap_Active','Clu_Act_Pres','Clu_BP_Wear_Comp','Eng_Speed','Gbx_IPS_Speed','Eng_Thr_Trq','Gbx_IPS_Trq','Gbx_IPS_Trq_Gain','Gbx_IPS_Trq_Offset','Gbx_Position','Eng_Thr_Pos','Car_Speed','Speed_FL','Speed_FR','Speed_RL','Speed_RR','Accel_Long_R','Car_Drag_Force','Tyre_Pres_FL','Tyre_Pres_RL','Tyre_Temp_R','aCluMu','QualPosn','QualSide','PosnChange','GbxRatios','GbxRatioBevel','GbxRatioDiff','GbxOverallRatioSelected','TyreRollingRadiusR_m','FormationStart','RaceStart','FSTyreTemp_R','RSTyreTemp_R','DeltaTyreTemp_R','aClu

```

```

Power_W','TotalKEClu_J','CluPower_MW_max','TotalKEClu_MJ_max','TimeOnGrid_s','f1
00kphTime_s','aCluEvent','aCluEventTotalEnergy','RaceStartPowerMax_MW','CluEner
gyRS_MJ','FormationStartPowerMax_MW','CluEnergyFS_MJ','CluEnergyFL_MJ','CluEne
rgyFSFLRS_MJ','DrvRSModes','FuelRS_kg','iNumUse_FSFLRS','CluMuRS'}
%sData = orderfields(sData,acstrNewOrder)

```

```

for iRunCnt = 1:length(acstrFileNames)
    sData(iRunCnt).CluMuRS = (round((sData(iRunCnt).CluMuRS)*100))/100;
    sData(iRunCnt).CluMuFS = (round((sData(iRunCnt).CluMuFS)*100))/100;
    sData(iRunCnt).RSTyreTemp_R =
(round((sData(iRunCnt).RSTyreTemp_R)*100))/100;
    sData(iRunCnt).FSTyreTemp_R =
(round((sData(iRunCnt).FSTyreTemp_R)*100))/100;
    sData(iRunCnt).FuelRS_kg = (round((sData(iRunCnt).FuelRS_kg)*10))/10;

```

```

    sData(iRunCnt).DeltaTyreTemp_R = sData(iRunCnt).RSTyreTemp_R-
sData(iRunCnt).FSTyreTemp_R;

```

```

    sData(iRunCnt).CluEnergyFS_MJ =
(round(sData(iRunCnt).CluEnergyFS_MJ*1000))/1000;
    sData(iRunCnt).CluEnergyFL_MJ =
(round(sData(iRunCnt).CluEnergyFL_MJ*1000))/1000;
    sData(iRunCnt).CluEnergyRS_MJ =
(round(sData(iRunCnt).CluEnergyRS_MJ*1000))/1000;

```

```

    PosnChange = num2str(sData(iRunCnt).PosnChange);
    if PosnChange(1) == '-'
        sData(iRunCnt).PosnChange = PosnChange;
    elseif PosnChange(1) == '0'
        sData(iRunCnt).PosnChange = PosnChange;
    elseif PosnChange(1) == '+'
        sData(iRunCnt).PosnChange = PosnChange;
    else
        sData(iRunCnt).PosnChange = ['+',PosnChange];
    end

```

```

end

```

```

close all

```

```

% ~~~~~
% PLOT INDIVIDUAL RS TELEMETRY TRACES
%

```

```

if bIndivRSPlot == 1
    for iRunCnt = 1:length(acstrFileNames)

        if isnan(sData(iRunCnt).CluMuRS) == 1
            sData(iRunCnt).CluMuRS = 0;
        end
    end

```

```

RSStart = sData(iRunCnt).RaceStart-25;
REnd = sData(iRunCnt).RaceStart+200;
a = RSStart+find(sData(iRunCnt).aCluMu(RSStart:REnd)>0.05);
CluMuStart = (a(1)-1)/100;
CluMuEnd = (a(end)-1)/100;
figure
set(gcf,'Position',[500 500 800 500]);
h4 = axes('position',[0.05,0.05,0.5,0.85],'OuterPosition',[0,0,0.6,0.9]);

%plot(sData(iRunCnt).Time(RSStart:REnd),sData(iRunCnt).Car_Speed(RSStart:REnd)./3.6);

plot(sData(iRunCnt).Time(RSStart:REnd),sData(iRunCnt).Speed_FL(RSStart:REnd)./3.6,'color',[0.2,0.35,1]);
hold on

plot(sData(iRunCnt).Time(RSStart:REnd),sData(iRunCnt).Speed_FR(RSStart:REnd)./3.6,'color',[0.2,0.35,1]);

plot(sData(iRunCnt).Time(RSStart:REnd),sData(iRunCnt).Speed_RL(RSStart:REnd)./3.6,'color',[0,0.1,1]);

plot(sData(iRunCnt).Time(RSStart:REnd),sData(iRunCnt).Speed_RR(RSStart:REnd)./3.6,'color',[0,0.1,1]);

plot(sData(iRunCnt).Time(RSStart:REnd),sData(iRunCnt).aCluMu(RSStart:REnd)*10,'color','k');

plot(sData(iRunCnt).Time(RSStart:REnd),sData(iRunCnt).Clu_Act_Pres(RSStart:REnd)./10,'color','m');

plot(sData(iRunCnt).Time(RSStart:REnd),sData(iRunCnt).Eng_Speed(RSStart:REnd)./1000,'color',[1,0.3,0]);

plot(sData(iRunCnt).Time(RSStart:REnd),sData(iRunCnt).Gbx_IPS_Speed(RSStart:REnd)./1000,'color',[1,0.8,0]);

plot(sData(iRunCnt).Time(RSStart:REnd),sData(iRunCnt).Eng_Thr_Pos(RSStart:REnd)/10,'color',[0,0.5,0]);

line([sData(iRunCnt).RaceStart/100,sData(iRunCnt).RaceStart/100],[0,20],'LineWidth',2,'Color','g')
line([CluMuStart,CluMuStart],[0,20],'LineWidth',2,'Color','k')
line([CluMuEnd,CluMuEnd],[0,20],'LineWidth',2,'Color','k')
line([CluMuStart,CluMuEnd],[14,14],'LineWidth',1,'Color','k')

plot(CluMuStart+0.03,14,'Marker','<','MarkerFaceColor','k','markerEdgeColor','k','MarkerSize',8)
plot(CluMuEnd-0.032,14,'Marker','>','MarkerFaceColor','k','markerEdgeColor','k','MarkerSize',8)
text((CluMuStart+CluMuEnd)/2,15,'Mu averaging','FontWeight','Bold','FontName','Arial','HorizontalAlignment','center')
axis([RSStart/100 REnd/100 0 20])
set(h4,'color',[1,1,1])
title('Relevant PDS Channel data against Time','FontWeight','Bold');
xlabel('Time in run [s]')

```

```
%legend('Car Speed [m/s]',Clutch Mu x 10',Clutch Act Pres [MPa'],'Engine Speed
[1000rpm]','Gbx IPS Speed [1000rpm]','Location','NorthWest')
```

```
h1 =
axes('Position',[0.6,0.05,0.35,0.25],'Visible','on','XLim',[0,1],'YLim',[0,10],'color',[1,1,1]
,'YTick',[0,10],'YTickLabel',[''],'XTick',[0,1],'XTickLabel',[''],'Box','On');
axes(h1);
```

```
set(gca,'color',[1,1,1],'YTick',[0,10],'YTickLabel',[''],'XTick',[0,1],'XTickLabel',
[''],'Box','On','XLim',[0,1],'YLim',[0,7]);
set(gcf,'color',[0.9,0.9,0.9]);
text(0.1,6.5,'KEY','FontWeight','Bold');
```

```
%plot(0.1,7,'Marker','s','MarkerFaceColor','r','MarkerEdgeColor','k','MarkerSize',10)
```

```
%plot(0.1,6,'Marker','s','MarkerFaceColor','r','MarkerEdgeColor','k','MarkerSize',10)
```

```
text(0.1,0.5,'Throttle Posn [%/10]','FontWeight','Bold','Color',[0,0.5,0]);
text(0.1,1.5,'Gbx IPS Speed [rpm]','FontWeight','Bold','Color',[1,0.8,0]);
text(0.1,2.5,'Engine Speed [rpm]','FontWeight','Bold','Color',[1,0.3,0]);
text(0.1,3.5,'Clutch Actuation Pressure [MPa]','FontWeight','Bold','Color','m');
text(0.1,4.5,'Clutch mu x 10','FontWeight','Bold','Color','k');
text(0.1,5.5,'Wheel Speeds [m/s]','FontWeight','Bold','Color','b');
```

```
%axis([0,1,0,10]);
%set(h1,'XLim',[0,1],'YLim',[0,10],'color',[1,1,1],'YTick',[0,10],'YTickLabel',[''],'
XTick',[0,1],'XTickLabel',[''],'Box','On')
set(gcf,'color',[0.9,0.9,0.9]);
```

```
h2 = axes('Position',[0.6,0.35,0.35,0.55],'Visible','on');
axes(h2);
set(gca,'color',[1,1,1],'YTick',[0,10],'YTickLabel',[''],'XTick',[0,1],'XTickLabel',
[''],'Box','On');
set(gcf,'color',[0.9,0.9,0.9]);
axis([0,1,0,10]);
```

```
text(0.05,9.5,'Circuit : ','FontWeight','Bold')
text(0.5,9.5,[sData(iRunCnt).Circuit,' (',sData(iRunCnt).Date,')'],
'FontWeight','Bold');
text(0.05,9.0,'Chassis : ','FontWeight','Bold')
text(0.5,9.0,[sData(iRunCnt).Chassis,' ',sData(iRunCnt).Drv], 'FontWeight','Bold')
text(0.05,8.0,'Qualified : ','FontWeight','Bold')
text(0.5,8.0,[num2str(sData(iRunCnt).QualPosn),
(' ',sData(iRunCnt).QualSide,')'], 'FontWeight','Bold');
text(0.05,7.5,'RS 0-100 kph [s] : ','FontWeight','Bold')
text(0.5,7.5,[num2str(sData(iRunCnt).f100kphTime_s)], 'FontWeight','Bold');
text(0.05,7.0,'Positions +/- : ','FontWeight','Bold')
text(0.5,7.0,[num2str(sData(iRunCnt).PosnChange)], 'FontWeight','Bold');
text(0.05,6.5,['Time on grid [s] : ','FontWeight','Bold');
text(0.5,6.5,[num2str(sData(iRunCnt).TimeOnGrid_s)], 'FontWeight','Bold');
text(0.05,6.0,['RS Fuel [kg] : ','FontWeight','Bold');
text(0.5,6.0,[num2str(sData(iRunCnt).FuelRS_kg)], 'FontWeight','Bold');
```

```

text(0.05,5.0,'Tyre Temps [C]: ', 'FontWeight','Bold')
text(0.5,5.0,['Initial ', 'FontWeight','Bold']);
text(0.5,4.5,['RS   ', 'FontWeight','Bold'];
text(0.5,4.0,['Delta ', 'FontWeight','Bold'];
text(0.7,5.0,['= ',num2str(sData(iRunCnt).FSTyreTemp_R)], 'FontWeight','Bold');
text(0.7,4.5,['= ',num2str(sData(iRunCnt).RSTyreTemp_R)], 'FontWeight','Bold');
text(0.7,4.0,['=
,num2str(sData(iRunCnt).DeltaTyreTemp_R)], 'FontWeight','Bold');

```

```

text(0.05,3.0,['Start Info - ', 'FontWeight','Bold']);
text(0.3,3.0,['FS: ', 'FontWeight','Bold'];
text(0.3,2.5,['RS: ', 'FontWeight','Bold'];
text(0.45,3.0,['Mode =
,num2str(sData(iRunCnt).DrvRSModes(1))], 'FontWeight','Bold');
text(0.45,2.5,['Mode =
,num2str(sData(iRunCnt).DrvRSModes(end))], 'FontWeight','Bold');
text(0.7,3.0,['Mu = ',num2str(sData(iRunCnt).CluMuFS)], 'FontWeight','Bold');
text(0.7,2.5,['Mu = ',num2str(sData(iRunCnt).CluMuRS)], 'FontWeight','Bold');

```

```

text(0.05,1.5,['Energy Dissipation [MJ]:'], 'FontWeight','Bold');
text(0.6,1.5,['FS'], 'FontWeight','Bold');
text(0.6,1.0,['FL'], 'FontWeight','Bold');
text(0.6,0.5,['RS'], 'FontWeight','Bold');
text(0.7,1.5,['= ',num2str(sData(iRunCnt).CluEnergyFS_MJ)], 'FontWeight','Bold');
text(0.7,1.0,['= ',num2str(sData(iRunCnt).CluEnergyFL_MJ)], 'FontWeight','Bold');
text(0.7,0.5,['= ',num2str(sData(iRunCnt).CluEnergyRS_MJ)], 'FontWeight','Bold');

```

```

h3 = axes('Position',[0.05,0.92,0.9,0.06], 'Visible','on');
axes(h3);
set(gca,'color',[1,1,1], 'YTick', [0,10], 'YTickLabel', ['', ''], 'XTick', [0,1], 'XTickLabel',
['', ''], 'Box', 'On', 'XLim',[0,1], 'YLim',[0,1]);
text(0.1,0.5,['Clutch RS Analysis: ',sData(iRunCnt).Circuit,
'sData(iRunCnt).Date, ' ,sData(iRunCnt).Chassis,
'sData(iRunCnt).Drv], 'FontWeight','Bold');

```

```

end
end

```

```

% ~~~~~
% PLOT TABLE OF RESULTS
% Will plot a table with all results in
% Sorts data according to input parameter
% Calculates correlations between all fields and sort parameter

```

```

if bCorrelationPlot == 1
    nSortParameter = input('-----\nParameter to sort data by? \n---
-----\nQualifying Position: 1\nQualifying Side [R/D]: 2\nPositions
+/- off grid: 3\nRS 0-100kph time: 4\nClutch Mu FS: 12\nClutch Mu FS:
13\nDelta Clutch Mu (RS-FS): 14\n-----');
    if nSortParameter == 0
        else

```

```

nSortParameter = nSortParameter+2;
end

sTable.Width_px = 1200;
sTable.Height_px = 800;
sTable.RowHeaderHeight_px = 150;
sTable.RowGenericHeight_rows = 1;
sTable.RowFooterHeight_px = 50;
sTable.NumRows = 1+length(acstrFileNames)*sTable.RowGenericHeight_rows+1;
sTable.Headers = {'Track/Driver','Energy Graph', 'Quali Posn', 'Grid Posn [R/D]',
'Posn Change', 'RS 0-100 kph [s]', 'Num Clutch Events','Energy FS [MJ]','Energy FL
[MJ]','Energy RS [MJ]','Energy Total [MJ]','Clutch Mode FS','Clutch Mode RS','Clutch Mu
FS','Clutch Mu RS','Delta Clutch Mu'};
sTable.NumCols = length(sTable.Headers);

sTable.ColWidth1_px = 100;
sTable.ColWidth2_px = 200;
sTable.ColWidthGeneric_px = (sTable.Width_px-sTable.ColWidth1_px-
sTable.ColWidth2_px)/(sTable.NumCols-2);

sTable.RowHeightGeneric_px = (sTable.Height_px-sTable.RowHeaderHeight_px-
sTable.RowFooterHeight_px)/length(acstrFileNames);

sTable.RowPosnTop =
[sTable.RowFooterHeight_px,sTable.RowFooterHeight_px+([1:sTable.NumRows-
2].*sTable.RowHeightGeneric_px),sTable.Height_px];
sTable.RowPosnMid =
[sTable.RowFooterHeight_px*0.5,sTable.RowFooterHeight_px+([(1:length(acstrFileNa
mes)]-0.5).*sTable.RowHeightGeneric_px),sTable.Height_px-
0.5*sTable.RowHeaderHeight_px];

sTable.aColPosnRight_px =
[sTable.ColWidth1_px,(sTable.ColWidth1_px+sTable.ColWidth2_px),(sTable.ColWidth
1_px+sTable.ColWidth2_px)+[1:sTable.NumCols-2].*sTable.ColWidthGeneric_px];
sTable.aColPosnMid_px =
[sTable.ColWidth1_px*0.5,(sTable.ColWidth1_px+sTable.ColWidth2_px*0.5),(sTable.C
olWidth1_px+sTable.ColWidth2_px)+[1:sTable.NumCols-2]-
0.5).*sTable.ColWidthGeneric_px];

aData = zeros(length(acstrFileNames),length(sTable.Headers));

for iRunCnt = 1:length(acstrFileNames);
    aData(iRunCnt,3) = sData(iRunCnt).QualPosn;

    aData(iRunCnt,6) = sData(iRunCnt).f100kphTime_s;
    aData(iRunCnt,7) = sData(iRunCnt).iNumUse_FSFLRS;
    aData(iRunCnt,8) = sData(iRunCnt).CluEnergyFS_MJ;
    aData(iRunCnt,9) = sData(iRunCnt).CluEnergyFL_MJ;
    aData(iRunCnt,10) = sData(iRunCnt).CluEnergyRS_MJ;
    aData(iRunCnt,11) = sData(iRunCnt).CluEnergyFSFLRS_MJ;

```



```

aData(iRunCnt,12) = sData(iRunCnt).DrvRSModes(1);
aData(iRunCnt,13) = sData(iRunCnt).DrvRSModes(2);
aData(iRunCnt,14) = sData(iRunCnt).CluMuFS;
aData(iRunCnt,15) = sData(iRunCnt).CluMuRS;
aData(iRunCnt,16) = sData(iRunCnt).CluMuRS-sData(iRunCnt).CluMuFS;

acstrTableData{iRunCnt,1} = [sData(iRunCnt).Circuit,' ',sData(iRunCnt).Drv];
acstrTableData{iRunCnt,2} = sData(iRunCnt).QualSide;
acstrTableData{iRunCnt,3} = sData(iRunCnt).PosnChange;
end

[aDataSortResult_Indiv(:,3),aDataSortIndex_Indiv(:,3)] = sort(aData(:,3),'descend');
[aDataSortResult_Indiv(:,6),aDataSortIndex_Indiv(:,6)] = sort(aData(:,6),'descend');
[aDataSortResult_Indiv(:,7),aDataSortIndex_Indiv(:,7)] = sort(aData(:,7),'descend');
[aDataSortResult_Indiv(:,8),aDataSortIndex_Indiv(:,8)] = sort(aData(:,8),'descend');
[aDataSortResult_Indiv(:,9),aDataSortIndex_Indiv(:,9)] = sort(aData(:,9),'descend');
[aDataSortResult_Indiv(:,10),aDataSortIndex_Indiv(:,10)] =
sort(aData(:,10),'descend');
[aDataSortResult_Indiv(:,11),aDataSortIndex_Indiv(:,11)] =
sort(aData(:,11),'descend');
[aDataSortResult_Indiv(:,12),aDataSortIndex_Indiv(:,12)] =
sort(aData(:,12),'descend');
[aDataSortResult_Indiv(:,13),aDataSortIndex_Indiv(:,13)] =
sort(aData(:,13),'descend');
[aDataSortResult_Indiv(:,14),aDataSortIndex_Indiv(:,14)] =
sort(aData(:,14),'descend');
[aDataSortResult_Indiv(:,15),aDataSortIndex_Indiv(:,15)] =
sort(aData(:,15),'descend');
[aDataSortResult_Indiv(:,16),aDataSortIndex_Indiv(:,16)] =
sort(aData(:,16),'descend');

aDataSortResult_Indiv(:,3) = flipud(aDataSortResult_Indiv(:,3));
aDataSortIndex_Indiv(:,3) = flipud(aDataSortIndex_Indiv(:,3));
aDataSortResult_Indiv(:,6) = flipud(aDataSortResult_Indiv(:,6));
aDataSortIndex_Indiv(:,6) = flipud(aDataSortIndex_Indiv(:,6));

nSortThreshold = 9; % Highlight the five best and five worst results

for iSortLimit = [3,6:16]
    aDataSortLimits(1,iSortLimit) =
aData(aDataSortIndex_Indiv(nSortThreshold,iSortLimit),iSortLimit);
    aDataSortLimits(2,iSortLimit) =
aData(aDataSortIndex_Indiv(length(acstrFileNames)-
nSortThreshold+1,iSortLimit),iSortLimit);
end

if nSortParameter ~= 0
    [aDataSortResult_Param,aDataSortIndex_Param] =
sort(aData(:,nSortParameter),'ascend');
end

for iDataSort = 1:length(sTable.Headers)
    if nSortParameter == 0
        aDataSorted_Param(:,iDataSort) = aData(:,iDataSort);
    else
        aDataSorted_Param(:,iDataSort) = aData(aDataSortIndex_Param,iDataSort);
    end
end
end

```

```

% -----
% CORRELATION COEFFICIENT CALCULATION
% r is a matrix of correlation coefficients
% p is a matrix of p-values for testing the hypothesis of no correlation
[r,p] = corrcoef(aDataSorted_Param);

% We are interested in the correlation between the sorted parameter and all the
other parameters
aCorrelation(1,:) = r(nSortParameter,:);
aCorrelation(2,:) = p(nSortParameter,:);

aCorrelation = (round(aCorrelation.*100))./100;

% Clear un-needed variables
clear r p

%line([0,sTable.Width_px],[0.5*sTable.RowFooterHeight_px,0.5*sTable.RowFooterHeight_px],
'Color','k','LineWidth',1);

line([0,sTable.Width_px],[sTable.RowFooterHeight_px,sTable.RowFooterHeight_px],
'Color','k','LineWidth',2);
text(sTable.aColPosnRight_px(2)-10,0.5*sTable.RowFooterHeight_px,'Correlation
Coefficient: ','HorizontalAlignment','right','FontWeight','bold');

hTable1 =
figure('Color',[1,1,1],'Position',[100,100,100+sTable.Width_px+10,100+sTable.Height_
px+10]);
hTable1Axes = axes('position',[0.025,0.025,0.95,0.95],'Visible','off');
set(gca,'color',[1,1,1],'YTick', [0,10], 'YTickLabel', ['', '10'], 'XTick', [0,1], 'XTickLabel',
['', '1'], 'Box', 'On');

rectangle('Position',[sTable.aColPosnRight_px(nSortParameter-
1),0,sTable.ColWidthGeneric_px,sTable.Height_px],'FaceColor',[0.75,0.75,1],'EdgeColor',
'[0,0,0]);

line([0,sTable.Width_px],[0,0],'color','k','LineWidth',2);
for iDrawRow = 1:sTable.NumRows-1

line([0,sTable.Width_px],[sTable.RowPosnTop(iDrawRow),sTable.RowPosnTop(iDra
wRow)],'color','k','LineWidth',1);
end

line([0,sTable.Width_px],[sTable.RowPosnTop(end),sTable.RowPosnTop(end)],'color',
'k','LineWidth',2);
line([0,sTable.Width_px],[sTable.RowPosnTop(end-1),sTable.RowPosnTop(end-
1)],'color','k','LineWidth',2);

line([0,0],[0,sTable.Height_px],'color','k','LineWidth',2);

line([sTable.aColPosnRight_px(1),sTable.aColPosnRight_px(1)],[0,sTable.Height_px],
'color','k','LineWidth',1);

```

```

line([sTable.aColPosnRight_px(2),sTable.aColPosnRight_px(2)],[0,sTable.Height_px],'c
olor','k','LineWidth',1);
    for iDrawCol = 2:sTable.NumCols

line([sTable.aColPosnRight_px(iDrawCol),sTable.aColPosnRight_px(iDrawCol)],[0,sTa
ble.Height_px],'color','k','LineWidth',1);
    end

line([sTable.aColPosnRight_px(end),sTable.aColPosnRight_px(end)],[0,sTable.Height_
px],'color','k','LineWidth',2);

line([sTable.aColPosnRight_px(1),sTable.aColPosnRight_px(1)],[0,sTable.Height_px],'c
olor','k','LineWidth',2);

line([sTable.aColPosnRight_px(2),sTable.aColPosnRight_px(2)],[0,sTable.Height_px],'c
olor','k','LineWidth',2);

line([sTable.aColPosnRight_px(6),sTable.aColPosnRight_px(6)],[0,sTable.Height_px],'c
olor','k','LineWidth',2);

line([sTable.aColPosnRight_px(11),sTable.aColPosnRight_px(11)],[0,sTable.Height_px
'],'color','k','LineWidth',2);

line([sTable.aColPosnRight_px(13),sTable.aColPosnRight_px(13)],[0,sTable.Height_px
'],'color','k','LineWidth',2);

    for iWriteHeaders = 1:sTable.NumCols

text(sTable.aColPosnMid_px(iWriteHeaders),sTable.RowPosnMid(end),sTable.Header
s(iWriteHeaders),'Rotation',[90],'HorizontalAlignment','center','VerticalAlignment','m
iddle','FontWeight','Bold','FontSize',[12]);
    end

    GraphNormalise = max(aDataSorted_Param(:,11));

    text(sTable.aColPosnRight_px(2)-10,sTable.RowFooterHeight_px*0.5,'Correlation
Coefficient','HorizontalAlignment','right','FontWeight','bold')
    for iWriteDataCol = [3,6:length(sTable.Headers)];

text(sTable.aColPosnMid_px(iWriteDataCol),0.5*sTable.RowFooterHeight_px,num2str
(aCorrelation(1,iWriteDataCol)),'FontWeight','bold','HorizontalAlignment','center');
    end

    for iWriteDataRow = 2:sTable.NumRows-1
        iGetData = iWriteDataRow-1;

        CluEnergyFSFLRS = aDataSorted_Param(iGetData,11);
        CluEnergyRS = aDataSorted_Param(iGetData,10);
        CluEnergyFL = aDataSorted_Param(iGetData,9);
        CluEnergyFS = aDataSorted_Param(iGetData,8);
        aCluEnergy = [CluEnergyFS,CluEnergyFL,CluEnergyRS,CluEnergyFSFLRS];
        [aCluEnergySort,aCluEnergyIndex] = sort(aCluEnergy,'descend');
        acstrCluEnergyColors = {[1,0.55,0],[1,1,0],[1,0,0],[0.2,0.2,0.2]};

        % Plot energy bar graphs for FS,FL,RS and FSFLRS
        % - Rectangles, length is normalised against max encountered value over season

```

```
rectangle('Position',[sTable.aColPosnRight_px(1)+0.05*sTable.ColWidth2_px,sTable.R
owPosnTop(iGetData)+0.1*sTable.RowHeightGeneric_px,0.9*sTable.ColWidth2_px*(a
CluEnergy(aCluEnergyIndex(1))/GraphNormalise),0.5*sTable.RowHeightGeneric_px],
'FaceColor','acstrCluEnergyColors{aCluEnergyIndex(1)}','EdgeColor','k');
```

```
rectangle('Position',[sTable.aColPosnRight_px(1)+0.05*sTable.ColWidth2_px,sTable.R
owPosnTop(iGetData)+0.2*sTable.RowHeightGeneric_px,0.9*sTable.ColWidth2_px*(a
CluEnergy(aCluEnergyIndex(2))/GraphNormalise),0.5*sTable.RowHeightGeneric_px],
'FaceColor','acstrCluEnergyColors{aCluEnergyIndex(2)}','EdgeColor','k');
```

```
rectangle('Position',[sTable.aColPosnRight_px(1)+0.05*sTable.ColWidth2_px,sTable.R
owPosnTop(iGetData)+0.3*sTable.RowHeightGeneric_px,0.9*sTable.ColWidth2_px*(a
CluEnergy(aCluEnergyIndex(3))/GraphNormalise),0.5*sTable.RowHeightGeneric_px],
'FaceColor','acstrCluEnergyColors{aCluEnergyIndex(3)}','EdgeColor','k');
```

```
rectangle('Position',[sTable.aColPosnRight_px(1)+0.05*sTable.ColWidth2_px,sTable.R
owPosnTop(iGetData)+0.4*sTable.RowHeightGeneric_px,0.9*sTable.ColWidth2_px*(a
CluEnergy(aCluEnergyIndex(4))/GraphNormalise),0.5*sTable.RowHeightGeneric_px],
'FaceColor','acstrCluEnergyColors{aCluEnergyIndex(4)}','EdgeColor','k');
```

```
for iWriteDataCol = 1:length(sTable.Headers)
    %[iGetData,iWriteDataCol]
    if iWriteDataCol == 1
```

```
text(sTable.aColPosnMid_px(iWriteDataCol),sTable.RowPosnMid(iWriteDataRow),acs
trTableData{aDataSortIndex_Param(iGetData),1},'HorizontalAlignment','center','Font
Weight','bold');
    elseif iWriteDataCol == 2
        % Do nothing
    elseif iWriteDataCol == 4
```

```
text(sTable.aColPosnMid_px(iWriteDataCol),sTable.RowPosnMid(iWriteDataRow),acs
trTableData{aDataSortIndex_Param(iGetData),2},'HorizontalAlignment','center','Font
Weight','bold');
    elseif iWriteDataCol == 5
```

```
text(sTable.aColPosnMid_px(iWriteDataCol),sTable.RowPosnMid(iWriteDataRow),acs
trTableData{aDataSortIndex_Param(iGetData),3},'HorizontalAlignment','center','Font
Weight','bold');
    else
        data = aDataSorted_Param(iGetData,iWriteDataCol);
        aColor = [0,0,0];
        if iWriteDataCol > 6 & iWriteDataCol~=12 & iWriteDataCol~=13

            %data = aData(iGetData,iWriteDataCol);
            if data > aDataSortLimits(1,iWriteDataCol);
                aColor = [0,0.75,0];
            elseif data < aDataSortLimits(2,iWriteDataCol)
                aColor = [1,0,0];
            else
                aColor = [0,0,0];
            end
        end
```

```
elseif iWriteDataCol == 3 | iWriteDataCol == 6
```

```
    if data <= aDataSortLimits(1,iWriteDataCol);
        aColor = [0,0.75,0];
```

```
elseif data >= aDataSortLimits(2,iWriteDataCol)
    aColor = [1,0,0];
else
    aColor = [0,0,0];
end

end

text(sTable.aColPosnMid_px(iWriteDataCol),sTable.RowPosnMid(iWriteDataRow),num2str(data),'HorizontalAlignment','center','color',aColor,'FontWeight','bold');
end

end
end
clear PosnChange
end
```



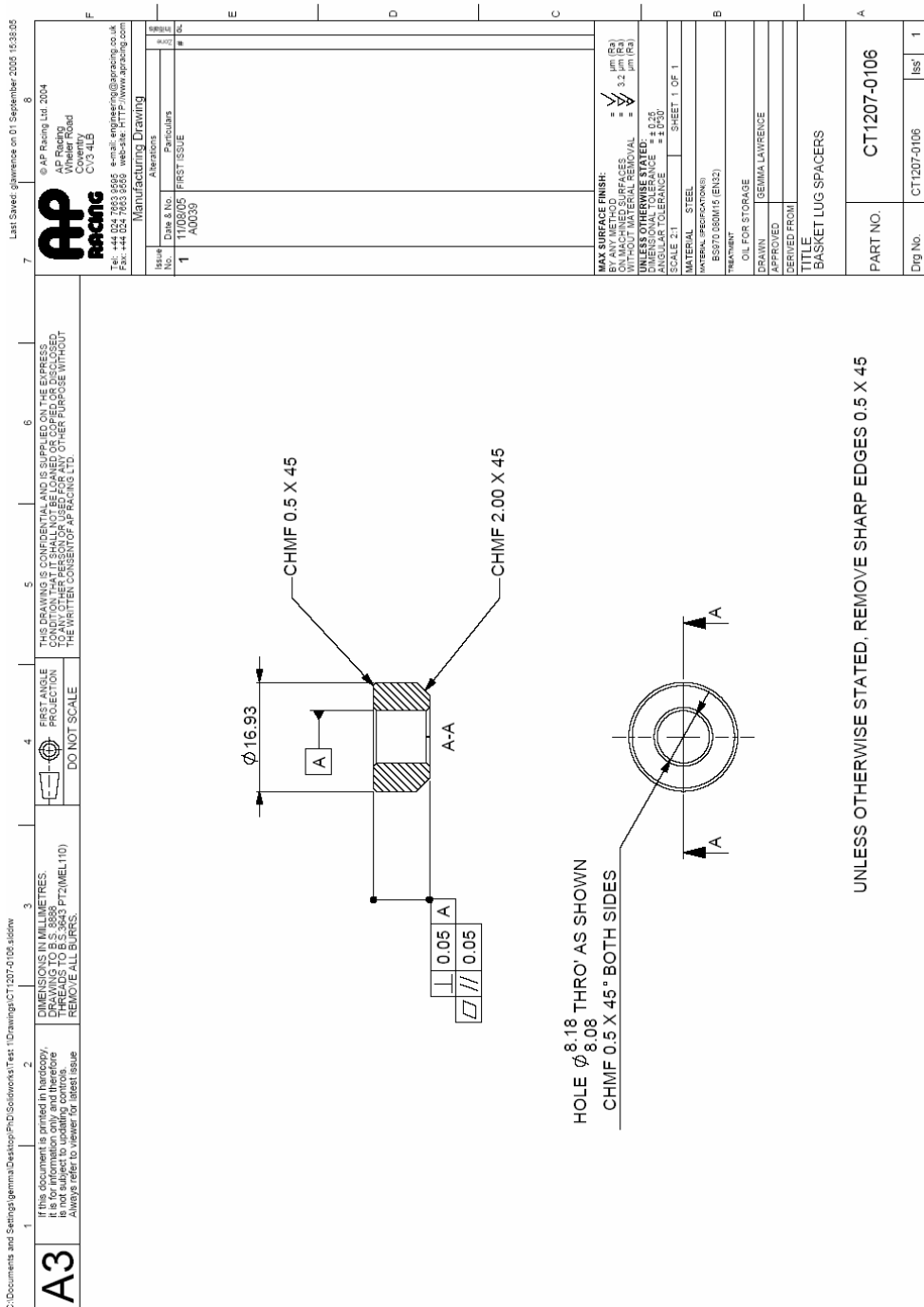












UNLESS OTHERWISE STATED, REMOVE SHARP EDGES 0.5 X 45

**A2** If this document is printed in landscape, it is for information use only and therefore should not be used for manufacturing. Always refer to viewer for latest issue.

DIMENSIONS IN MILLIMETRES. DRAWING TO U.S. STANDARD PRACTICES. REMOVE ALL BURS.

**DO NOT SCALE**

THIS DRAWING IS CONFIDENTIAL AND IS SUPPLIED ON THE EXPRESS CONDITION THAT IT SHALL NOT BE COPIED OR REPRODUCED OR DISCLOSED TO ANY OTHER PERSON OR USED FOR ANY OTHER PURPOSE WITHOUT THE WRITTEN CONSENT OF AP RACING LTD.

AP RACING LTD.  
 AP Racing  
 10000  
 44-024 795 5955  
 44-024 795 5955  
 44-024 795 5955

MANUFACTURING DRAWING

1 1207-0107 FIRST ISSUE

MAX SURFACE FINISH:  
 BY ANY METHOD: 3.2 µm (125 µin) Ra  
 WITHOUT MATERIAL REMOVAL: 3.2 µm (125 µin) Ra  
 UNLESS OTHERWISE STATED:  
 SURFACE TOLERANCE: ±0.05  
 ANGULAR TOLERANCE: ±0.5°

SCALE: 1:1 SHEET 1 OF 1

WORKING DIMENSIONS: 80975.00MM (RND)

TREATMENT: OIL FOR STORAGE

DRAWN: SEMMA LAWRENCE

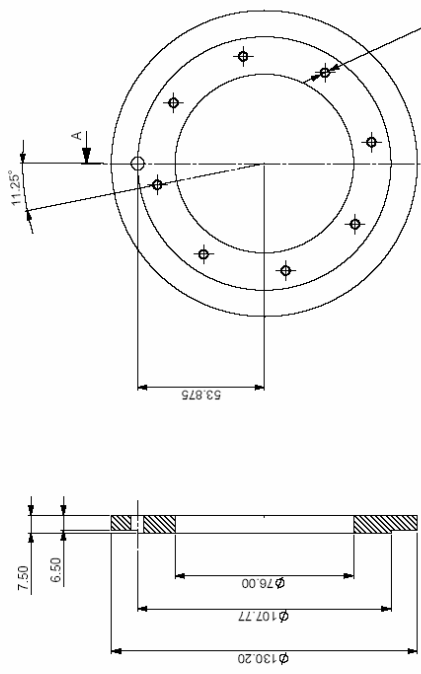
APPROVED:

TITLE: SPACER

PART NO.: CT1207-0107

DRG NO.: CT1207-0107

1



8 HOLES M4 X 0.7-6H THRO EQUISPACED  
 ON A  $\phi$  53.875 PCD  
 CHMF 1ST THREAD X .45°  
 $\phi$  0.05

UNLESS OTHERWISE STATED, REMOVE SHARP EDGES 0.5 X .45

**A1** THIS DOCUMENT IS UNCONTROLLED UNLESS SPECIFICALLY IDENTIFIED AS SUCH. IF YOU REQUIRE CONTROLLED DOCUMENTATION, PLEASE CONTACT THE AP RACING DESIGN OFFICE.  
 IF THIS DOCUMENT IS UNCONTROLLED, IT MAY BE DIFFERENT TO THE LATEST REVISION. REFER TO THE DRAWING NUMBER FOR LATEST ISSUE.

THIS DRAWING IS CONFIDENTIAL AND IS SUPPLIED ON THE EXPRESS CONDITION THAT IT SHALL NOT BE LOANED, COPIED OR DISCLOSED TO ANY OTHER PERSON OR USED FOR ANY OTHER PURPOSE WITHOUT THE WRITTEN CONSENT OF AP RACING LTD.

DO NOT SCALE  
 FIRST ANGLE PROJECTION

MANUFACTURING DRAWING

AP RACING LTD.  
 Wheeler Road  
 C13 1LE

Part Name: RETAINER SPACERS  
 Issue: 1  
 Issue Date: 15/05/02

Scale: 1:1  
 Material: 316L SS  
 Drawing No: CT1207-0108

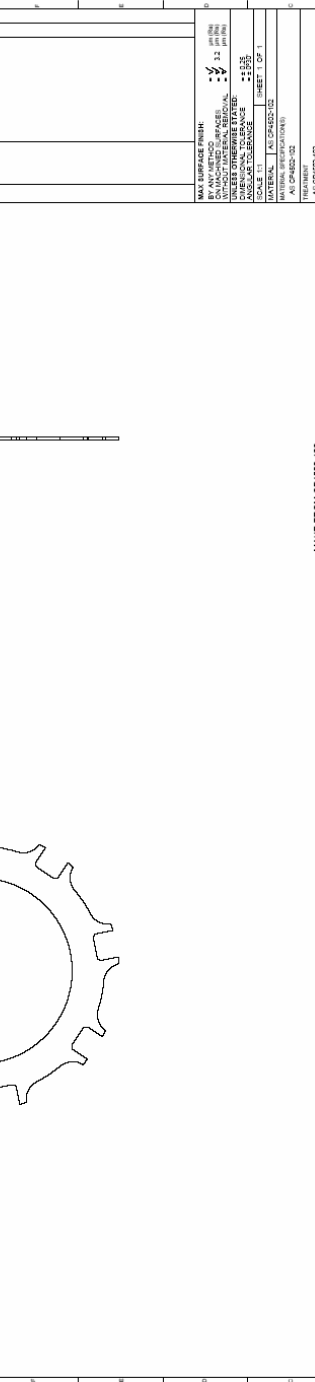
Max Surface Finish: 3.2  
 Max Chamfer: 1.5  
 Max Fillet: 1.5  
 Unless Otherwise Stated, Retain Sharp Edges 0.5 x 45°  
 Unless Otherwise Stated, Retain Sharp Edges 0.5 x 45°

Scale: 1:1  
 Material: 316L SS  
 Drawing No: CT1207-0108

Drawn: J. Lawrence  
 Approved: J. Lawrence  
 Title: RETAINER SPACER

Part No: CT1207-0108  
 Draw No: CT1207-0108

Sheet 1 of 1



MAKE FROM CT4602-102  
 UNLESS OTHERWISE STATED, REMOVE SHARP EDGES 0.5 X 45

A2

If this document is printed in landscape, it is for information use only and therefore not subject to our standard terms. Always refer to terms and conditions.

DIMENSIONS IN MILLIMETRES.  
DRAWING TO BS 5458 - DIMENSIONAL TOLERANCES ON DRAWINGS.  
REMOVE ALL DIMENSIONS.

FIRST ANGLE PROJECTION

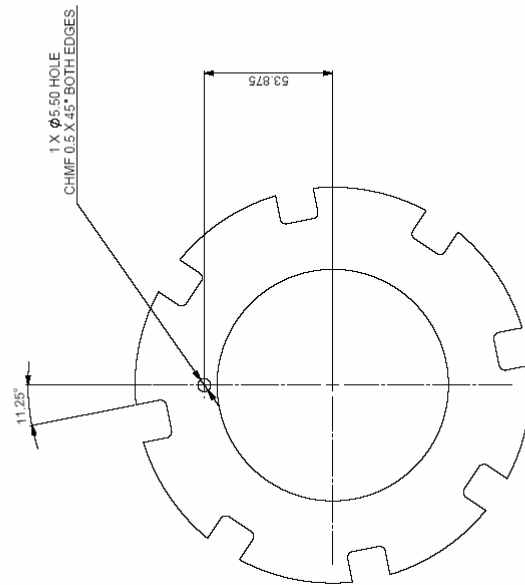
DO NOT SCALE

THIS DRAWING IS CONFIDENTIAL AND SHALL BE KEPT IN THE EXPRESS CONDITION THAT IT SHALL NOT BE LOANED OR COPIED OR DISCLOSED TO ANY OTHER PERSON OR USED FOR ANY OTHER PURPOSE WITHOUT THE WRITTEN CONSENT OF AP RACING LTD.

© AP Racing Ltd 2004  
AP Racing Ltd  
AP Racing Ltd  
Covering  
Tel: +44 (0) 1933 6585 8338 Fax: +44 (0) 1933 6585 8339  
E: [ap@apracetrack.com](mailto:ap@apracetrack.com)  
Web: <http://www.apracetrack.com>

MANUFACTURING DRAWING

REV	DATE & NO.	REVISION	BY
1	1/2005	FIRST ISSUE	AL



MAKE FROM CP4823-103S1

UNLESS OTHERWISE STATED, REMOVE SHARP EDGES 0.5 X 45

MAX SURFACE FINISH	3.2 µm (Ra)
ON MACHINED SURFACES	3.2 µm (Ra)
WITHOUT MATERIAL REMOVAL	12.5 µm (Ra)
UNLESS OTHERWISE SPECIFIED	± 0.25
DIMENSIONAL TOLERANCE	± 0.25
UNLESS OTHERWISE SPECIFIED	± 0.25
MATERIAL	AS CP4823-103S1
TREATMENT	AS CP4823-103S1
APPROVED	AS CP4823-103S1
DESIGNED BY	CP4823-103S1
CHECKED BY	CP4823-103S1
TITLE	INSPIRED CLUTCH-PLATE
PART NO.	CT1207-0109
DRG. NO.	CT1207-0109
REV	1

## Appendix D - 140mm Clutch Technical Information

the SCIENCE of FRICTION

ABOUT THE COMPANY    CAR PRODUCTS    MOTORCYCLE PRODUCTS

**AP RACING**

Competition Products

**Carbon Clutch Catalogue**

**CP7142-CM01-SN**

**140mm 2 Plate Carbon Clutch**

AIRJACKS

BRAKE CALIPERS

BRAKE DISCS

BRAKE KITS

BRAKE PADS

BRAKE FLUID

CARBON BRAKE DISCS

CARBON CLUTCHES

METALLIC CLUTCHES

MASTER CYLINDERS

PEDAL BOXES


RELEASE BEARINGS

RESERVOIRS

SLAVE CYLINDERS

Formula Student SAE

SOURCE PRODUCT



<b>Features</b>	Flat and Stepped Flywheel Fixing available, including Cushion Flywheel System (CFS), One Piece Lug Drive Cover, Lightweight, Low Inertia, Long Life, Durable & Abuse Resistant, <a href="#">Clutch Mounting Studs Available</a> , and Factory Reconditioning Service Available.		
	Clutch Installation drawing <a href="#">CP7142cd</a>		
<b>Typical Applications</b>	General Use, F3, Touring Car.		
<b>Torque Capacity</b>	741Nm (547lb/ft)	<b>"Wear In" between P/Plate Changes</b>	0.5mm
<b>Release Load Max peak worn</b>	4500 N	<b>Release Load At travel</b>	3000 N
<b>Set up height New</b>	31.54mm *measured from flywheel friction face*	<b>Set up height Max worn</b>	34.58mm *measured from flywheel friction face*
<b>Total allowable carbon stack wear</b>	4.0mm	<b>Main pressure plate material</b>	Kits CP4502-13S 0.5 - 3.5mm 0.5 steps, CP4502-14S 0.25 - 3.25mm 0.5 steps. Material - steel. <a href="#">Pressure Plate Fitment Guide</a>
<b>Weight</b>	1.92Kg	<b>Release Bearing</b>	CP3457-1, -9 or -11
<b>Complete assy inertia</b>	0.00646Kgm <sup>2</sup>	<b>D/Plate &amp; hub inertia</b>	0.00089Kgm <sup>2</sup>
<b>Ratio</b>	M.H.R	<b>Hub Family</b>	CP5142 Steel See installation drawing for details.

the SCIENCE of FRICTION

AP  
RACING

ABOUT THE  
COMPANY

CAR  
PRODUCTS

MOTORCYCLE  
PRODUCTS



AIRJACKS

BRAKE  
CALIPERS

BRAKE  
DISCS

BRAKE  
KITS

BRAKE  
PADS

BRAKE  
FLUID

CARBON  
BRAKE DISCS

CARBON  
CLUTCHES

METALLIC  
CLUTCHES

MASTER  
CYLINDERS

PEDAL  
BOXES

RELEASE  
BEARINGS

RESERVOIRS

SLAVE  
CYLINDERS

Formula  
Student/SAE

SOURCE  
PRODUCT

## Carbon/Carbon Clutches

Section Information:- [Introduction](#) | [Carbon Material](#) | [Overheating & Abuse](#) | [Release Bearings](#) | [Slave Cylinders](#) | [Maintenance & Repair](#) | [Flywheel](#) | [Clutch Mounting](#) | [New Clutch Numbering](#) | [Clutch Selection](#)

### Carbon Material

AP Racing policy is to use the best materials available. Two alternative materials are currently offered:-

- **S3** Material has a good wear rate and high strength and impact resistance. It is particularly suitable for very high speed engines (over 12 000 rpm) such as F1.
- **S1** Material has an exceptionally low wear rate and a lower cost than D2 material, but has a lower strength. This material is the usual choice for all lower speed engines (under 10 000 rpm).

AP Racing can advise on the most suitable Carbon / Carbon material required. This will normally be dependant on application.

**The full range of AP Racing products is available through our Official Distributors and Authorised Dealers. Once You have decided what product you wish to purchase please go to 'Source product' on the left sidebar to find details of our Distributors/Dealers.**

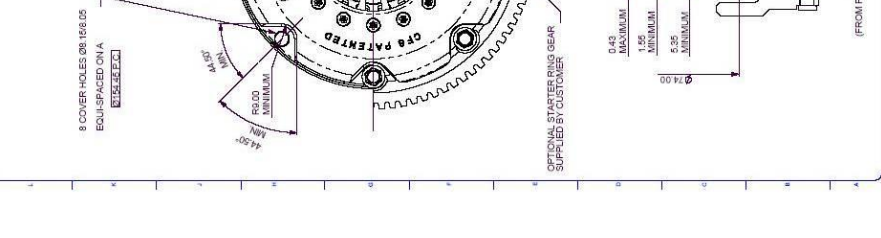
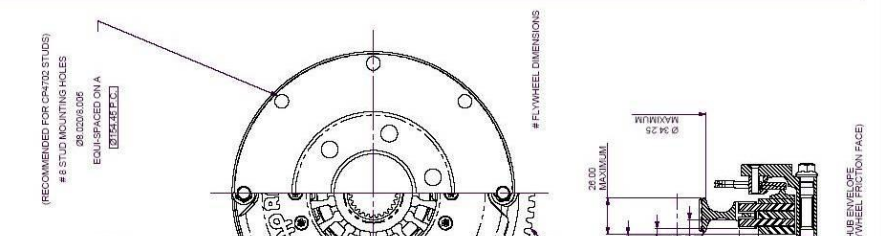
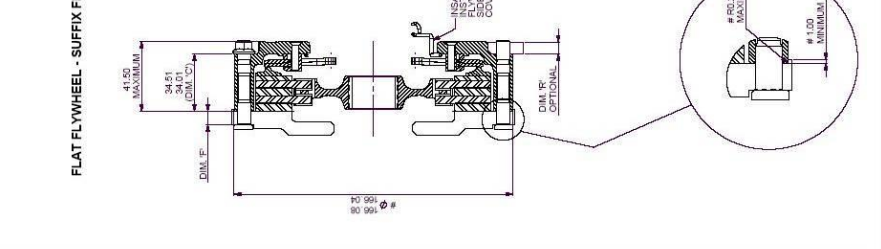
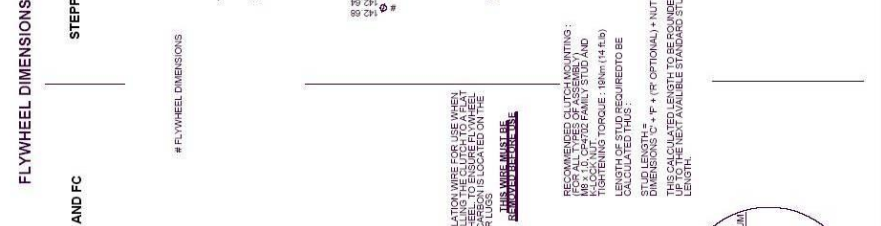
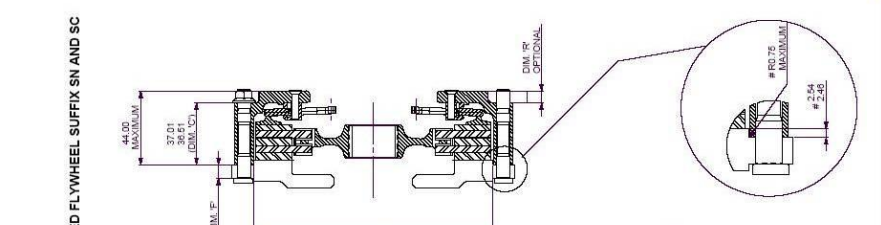
[home](#) | [history](#) | [technology](#) | [car](#) | [motorcycle](#) | [performance road car](#) | [USA stock car](#)

Created by **Spiderscope**  
new media Copyright 1999, All rights reserved





NO.	REV.	DESCRIPTION	DATE	BY	CHKD.
1	001	ISSUE FOR PRODUCTION	12/01/02	AP	AP
2	002	ISSUE FOR PRODUCTION	12/01/02	AP	AP
3	003	ISSUE FOR PRODUCTION	12/01/02	AP	AP
4	004	ISSUE FOR PRODUCTION	12/01/02	AP	AP
5	005	ISSUE FOR PRODUCTION	12/01/02	AP	AP
6	006	ISSUE FOR PRODUCTION	12/01/02	AP	AP



FLYWHEEL DIMENSIONS

STEPPED FLYWHEEL SUFFIX SN AND SC

FLAT FLYWHEEL - SUFFIX FN AND FC

FLYWHEEL DIMENSIONS

FLYWHEEL DIMENSIONS

FLYWHEEL DIMENSIONS

FLYWHEEL DIMENSIONS

FLYWHEEL DIMENSIONS

INSULATION WIRE FOR USE WHEN INSTALLING THE CLUTCH TO A FLAT SUFFIX CLUTCH LOCATED ON THE COVER LUGS

RECOMMENDED CLUTCH INSTALLATION FOR ALL TYPES OF ASSEMBLY: MS 10.0, CPT2 FAMILY STUD AND TIGHTENING TORQUE: 18Nm (14 lbf-ft) LENGTH OF STUD REQUIRED TO BE CALCULATED USING DIMENSIONS 'C' + 'F' (IF OPTIONAL) + NUT DIMENSIONS 'G' + 'H' (IF OPTIONAL) + NUT LENGTH. THIS CALCULATED LENGTH TO BE ROUNDED UP TO THE NEXT AVAILABLE STANDARD STUD LENGTH.

RECOMMENDED FOR CPT2 STUDS  
# 8 STUD MOUNTING HOLES  
Ø 28.028.006  
EQUI-SPACED ON A  
Ø 128.00

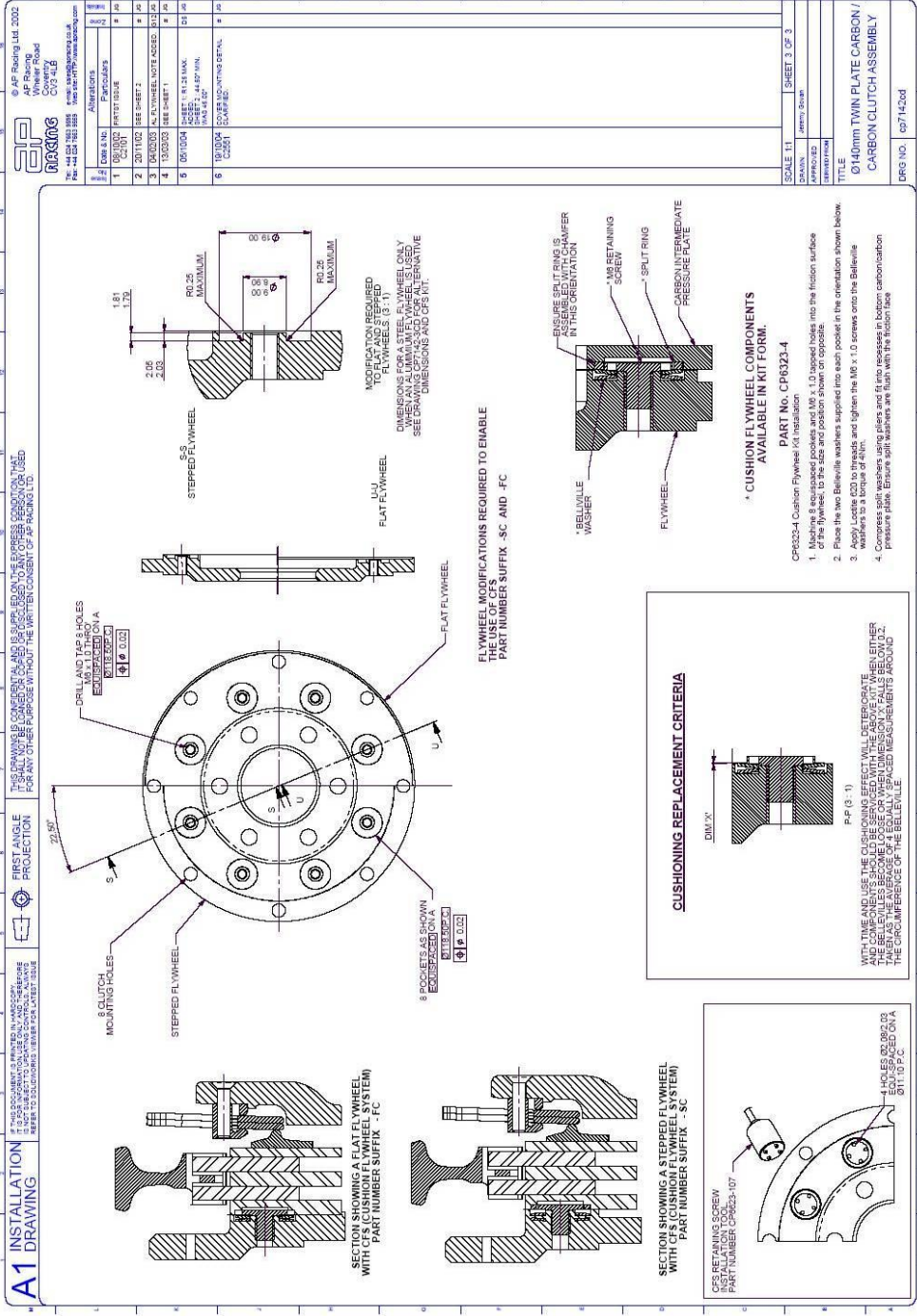
8 COVER HOLES Ø 148.05  
EQUI-SPACED ON A  
Ø 148.05

OPTIONAL SPACER RING GEAR  
SUPPLIED BY CUSTOMER

HUB ENVELOPE  
(FROM FLYWHEEL FRICTION FACE)

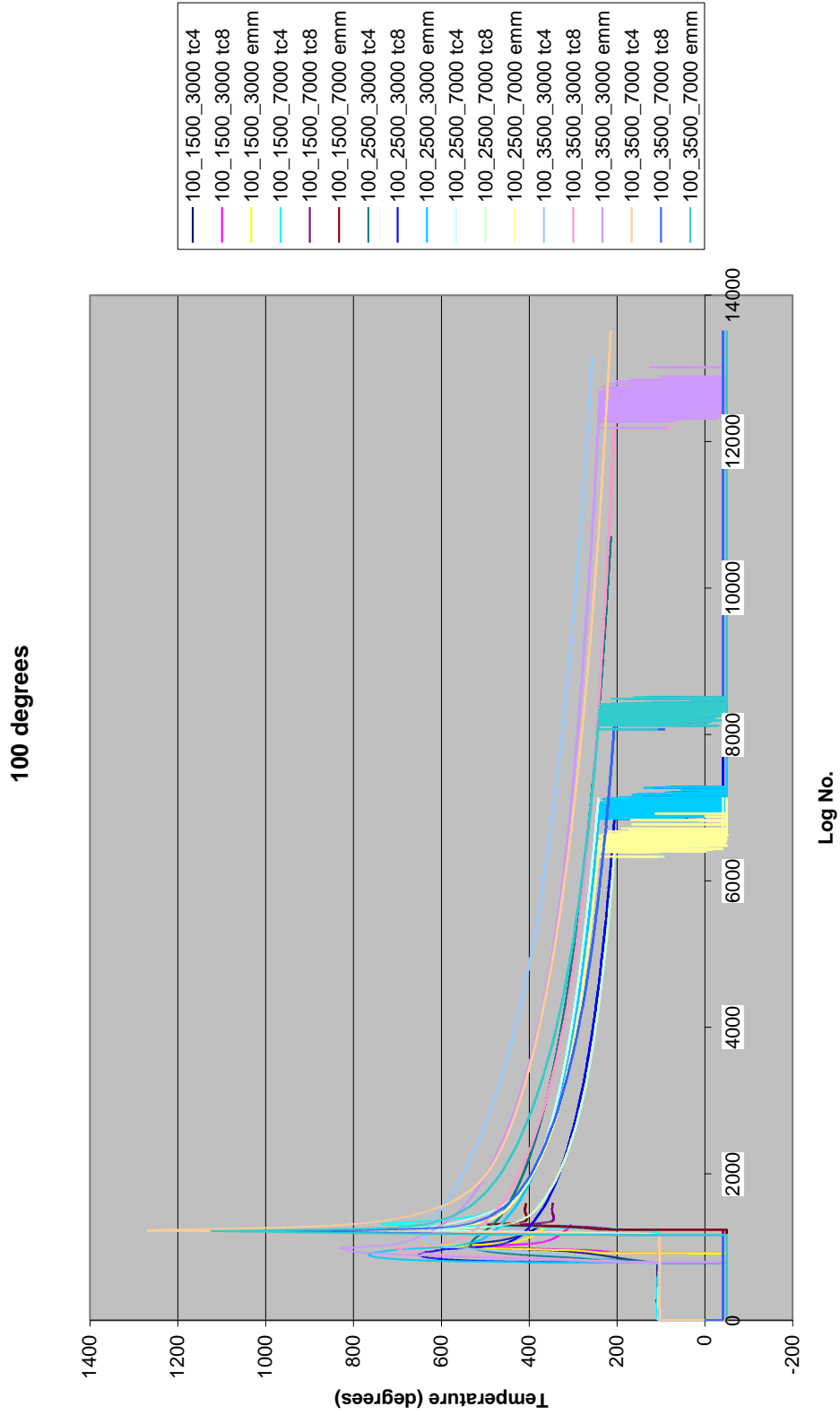
HUB ENVELOPE  
(FROM FLYWHEEL FRICTION FACE)

SCALE	1:1	SHEET	2 OF 3
DRAWN	AP	DATE	12/01/02
APPROVED	AP		
TITLE	Ø140mm TWIN PLATE CARBON / CARBON CLUTCH ASSEMBLY		
DRG NO.	69714261		

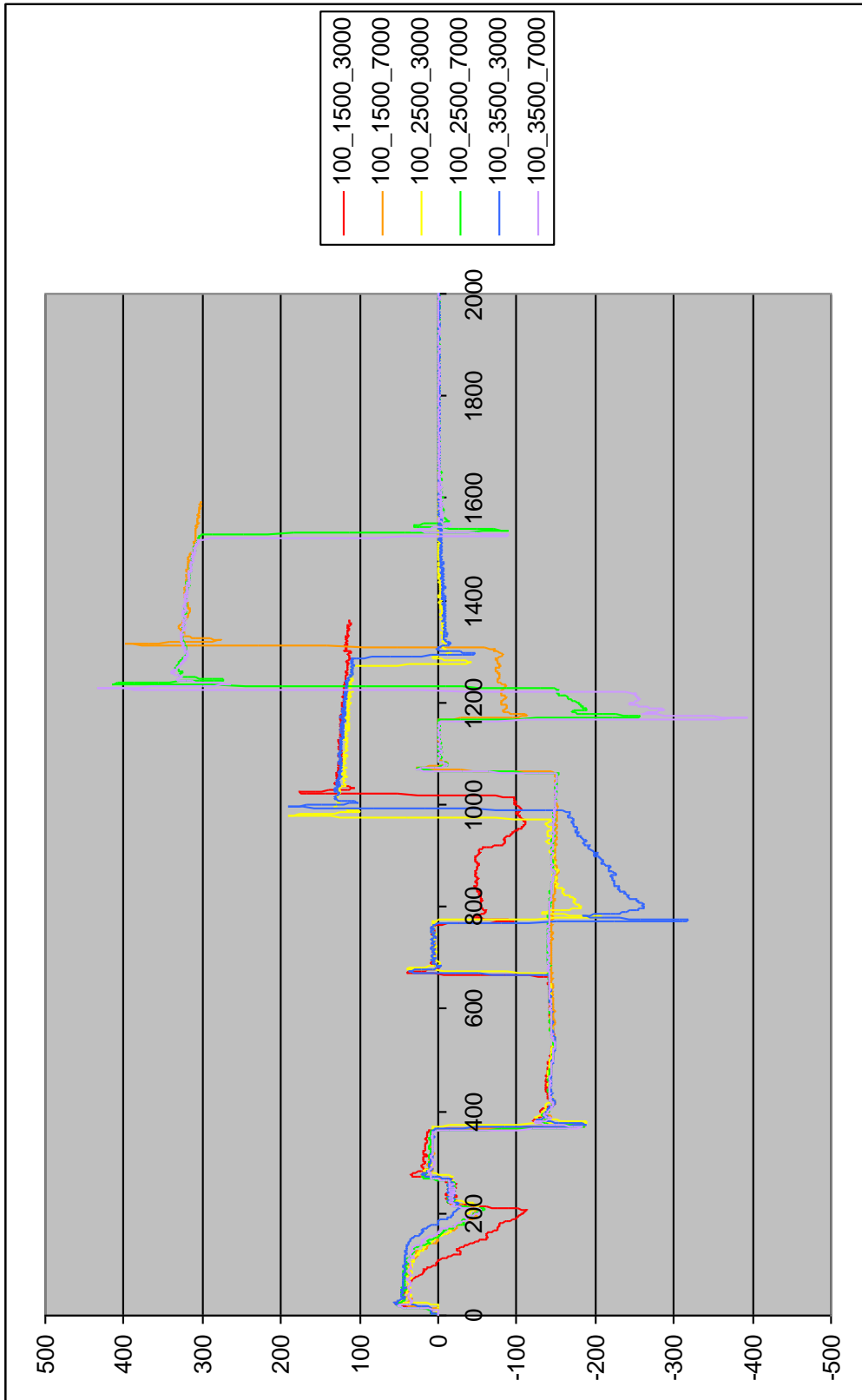


# Appendix E - Initial Testing Graphs.

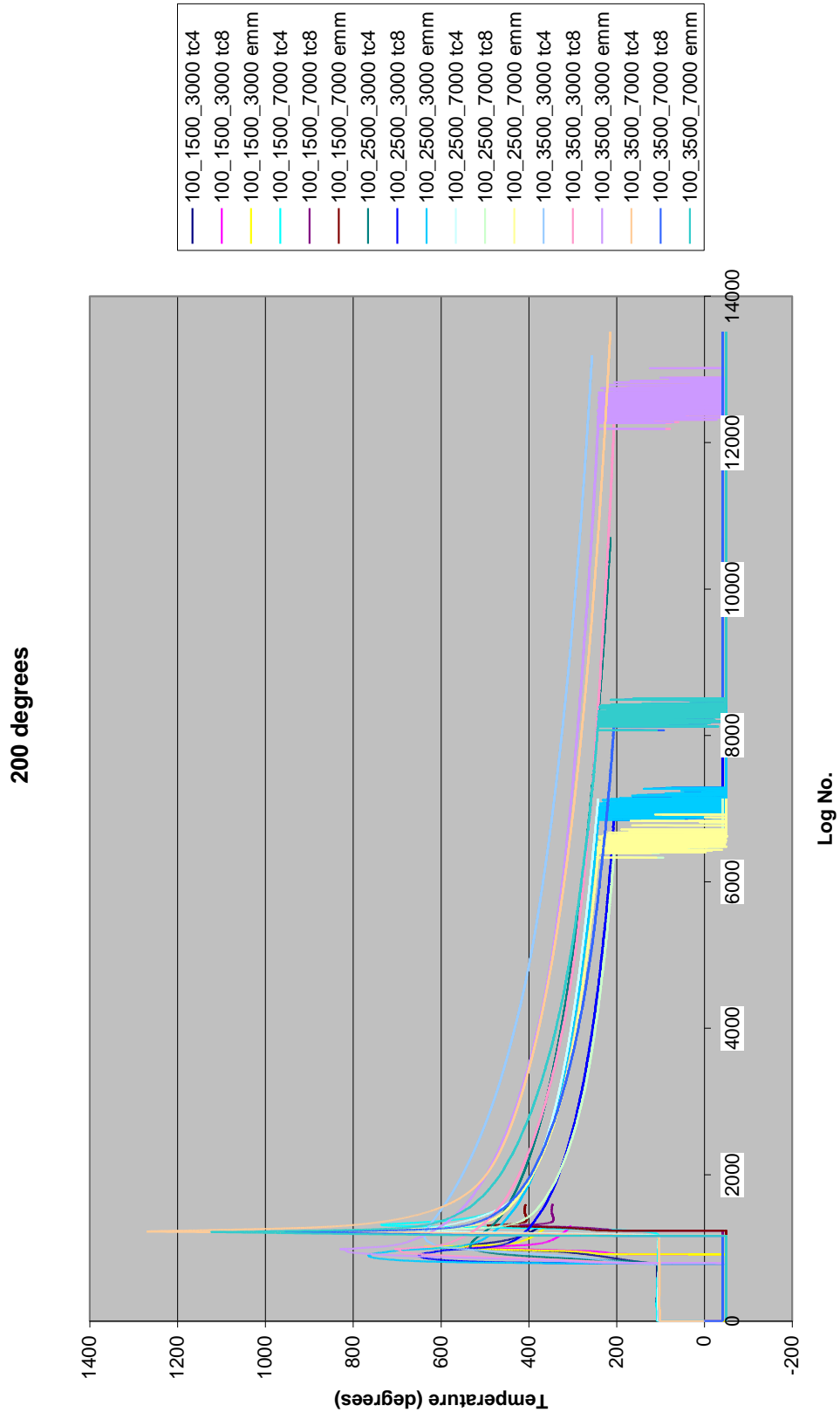
## Sensor Comparisons at 100°C



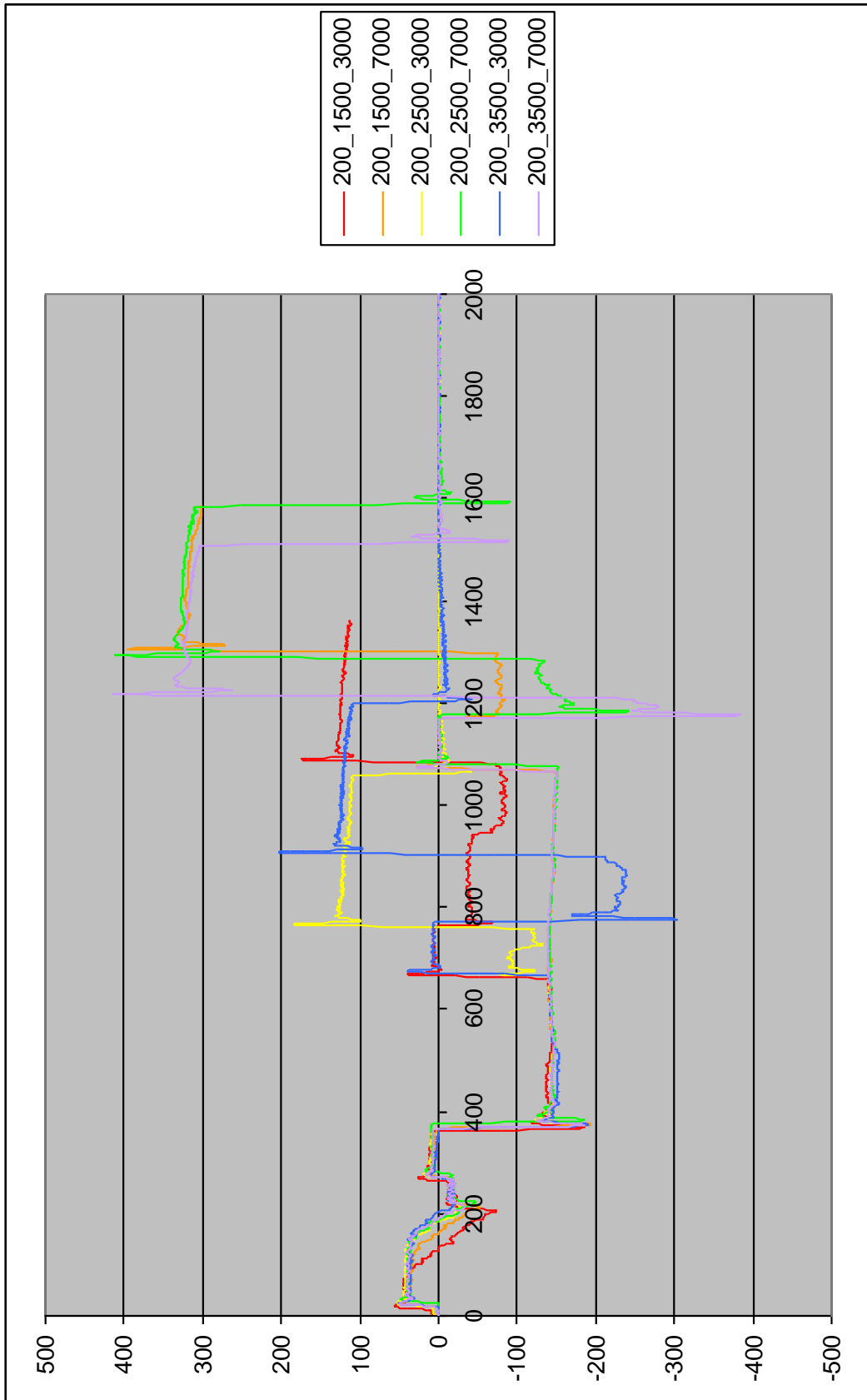
# Torque Comparisons at 100°C



# Sensor Comparisons at 200°C



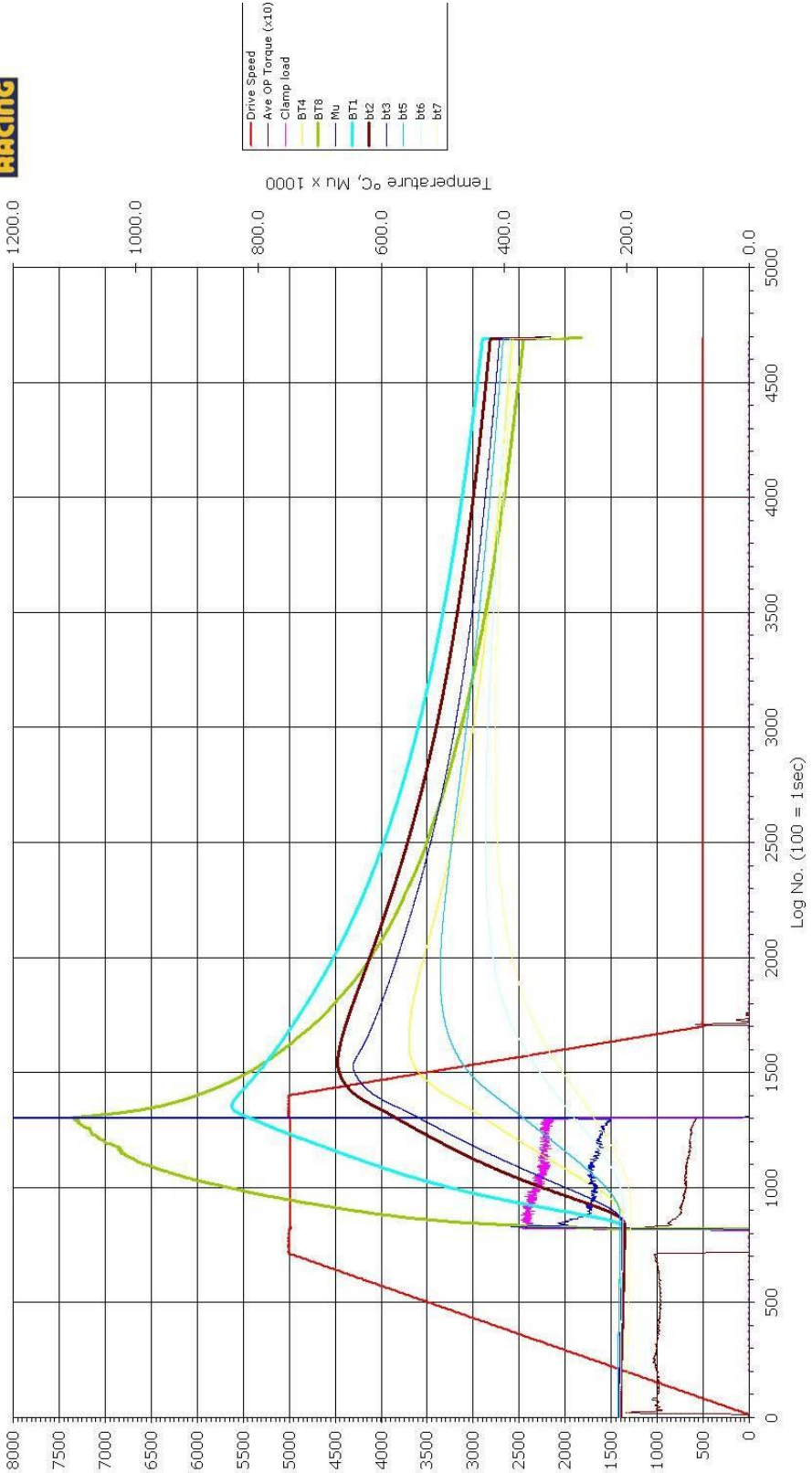
# Torque Comparisons at 200°C



# Appendix F - Initial Testing Graphs



Plate A 5000rpm 2500N load 200deg







**Plate B 5000rpm 2500N load 200deg**

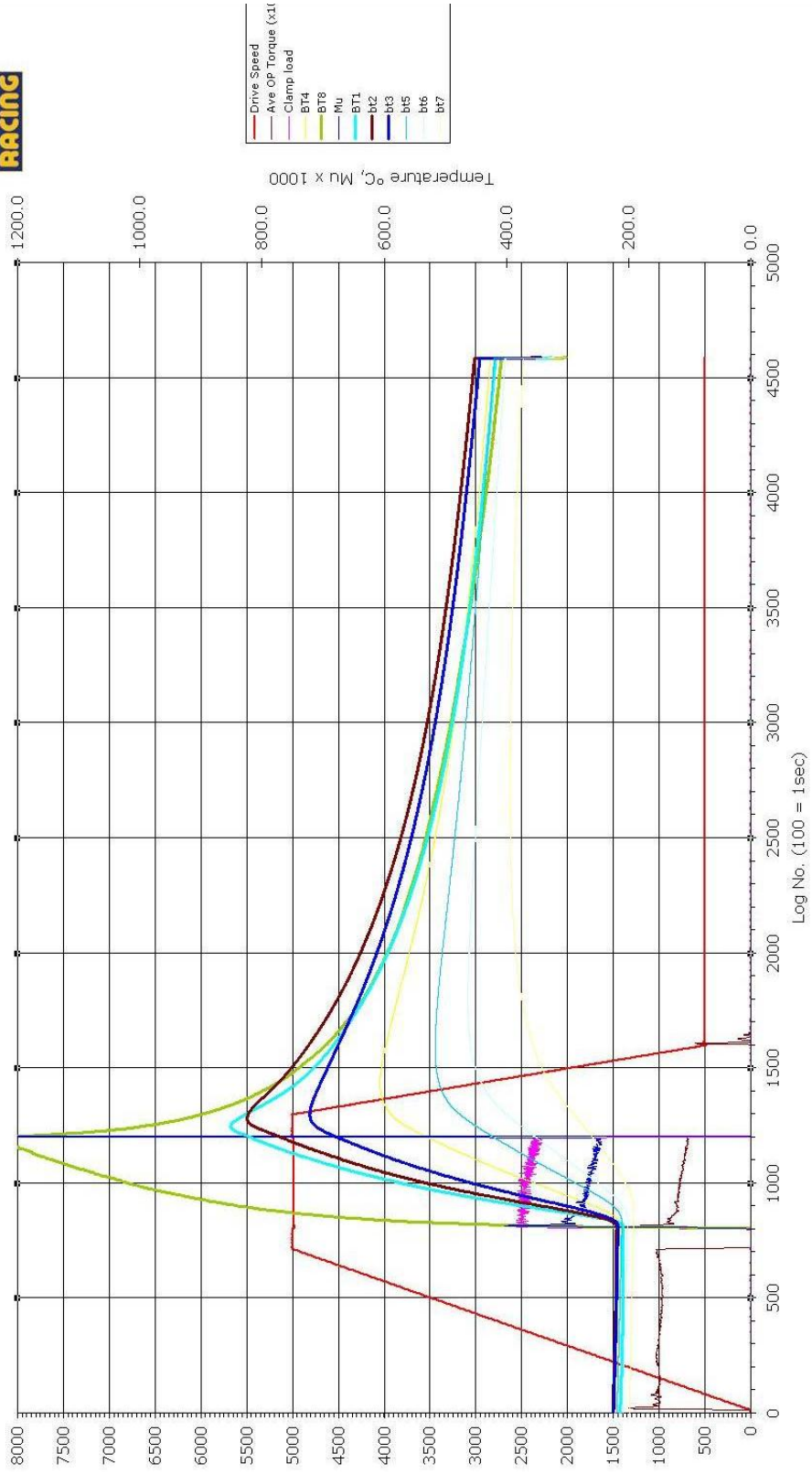




Plate C 5000rpm 2500N load 200deg

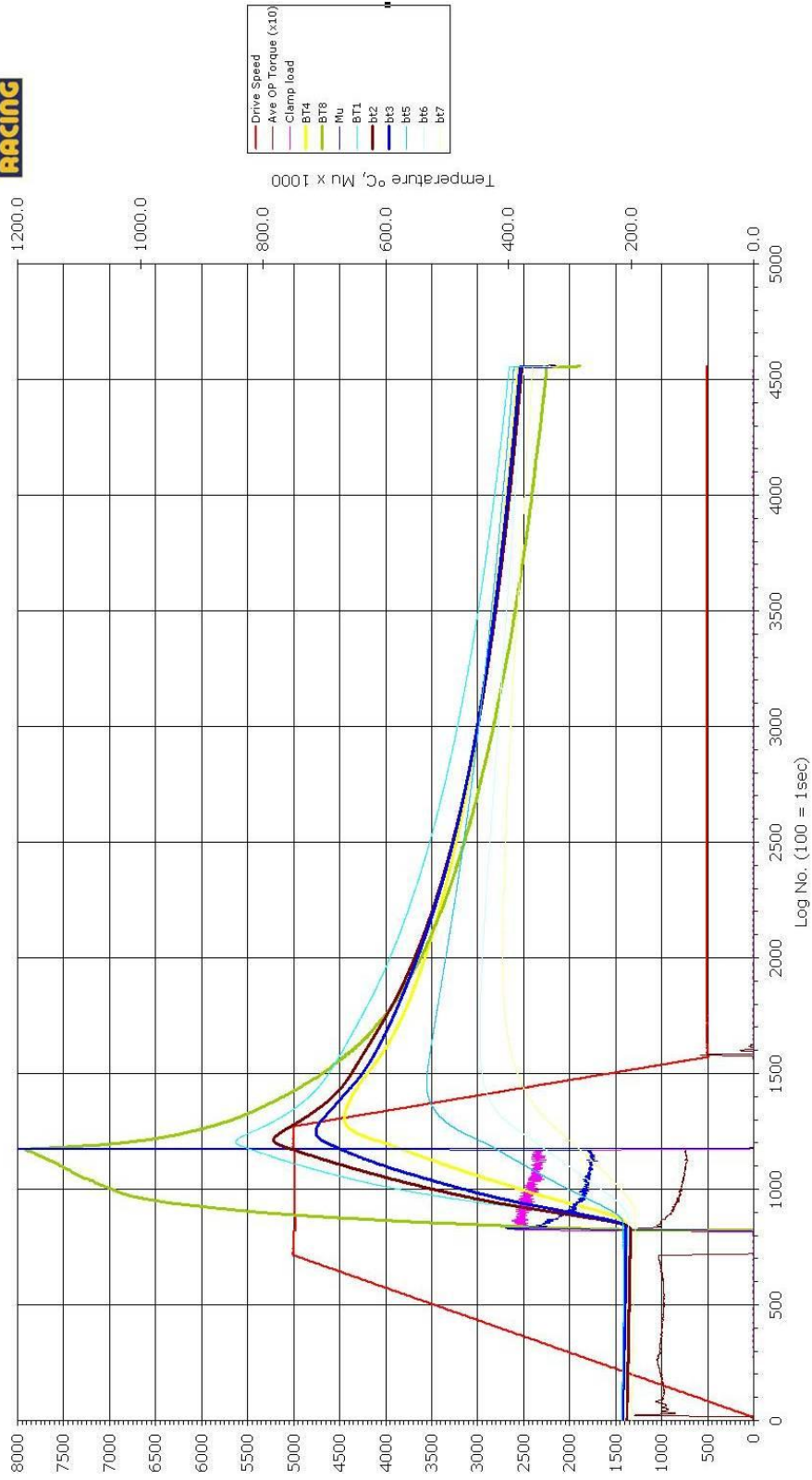




Plate D 5000rpm 2500N load 200deg

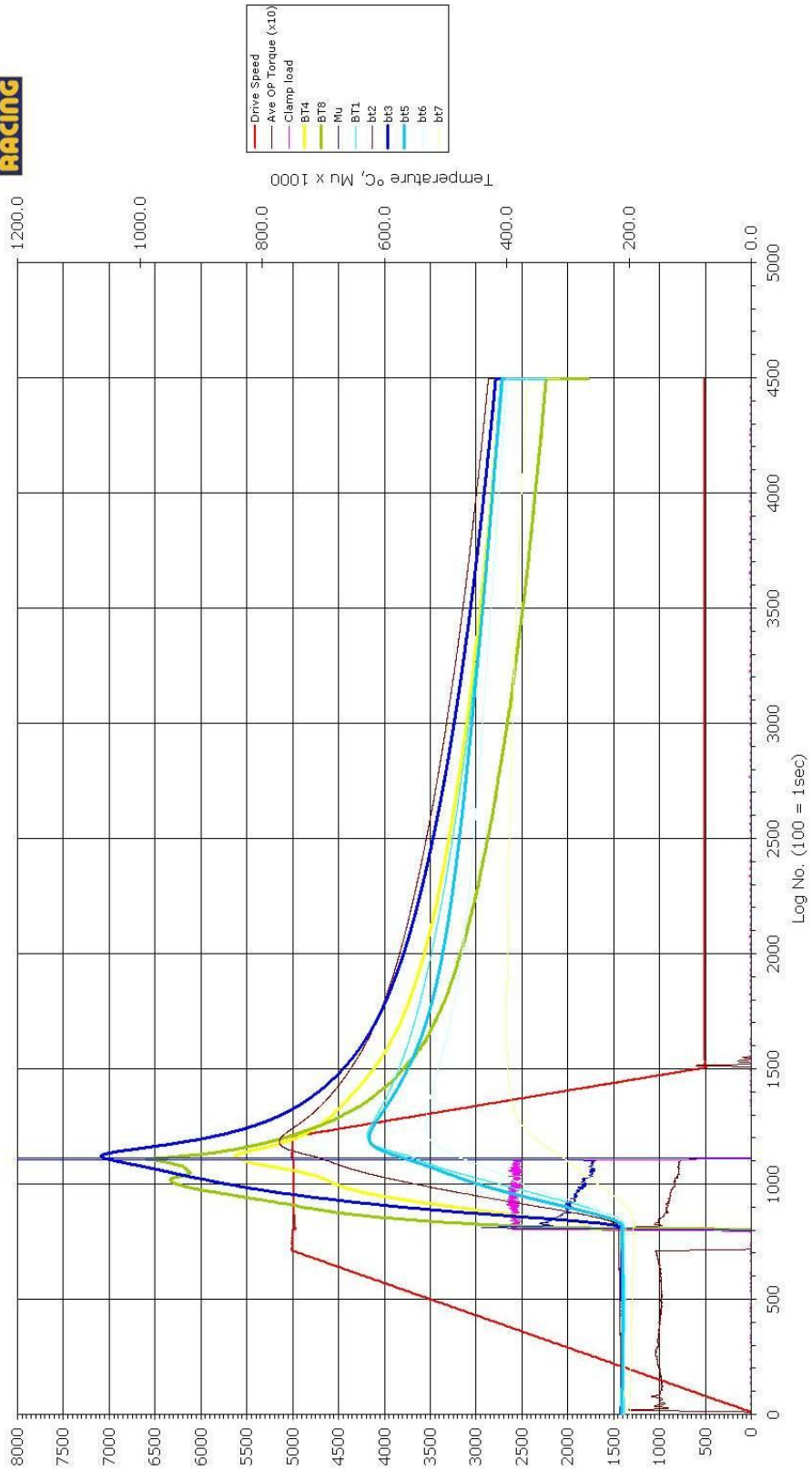




Plate E 5000rpm 2500N load 200deg

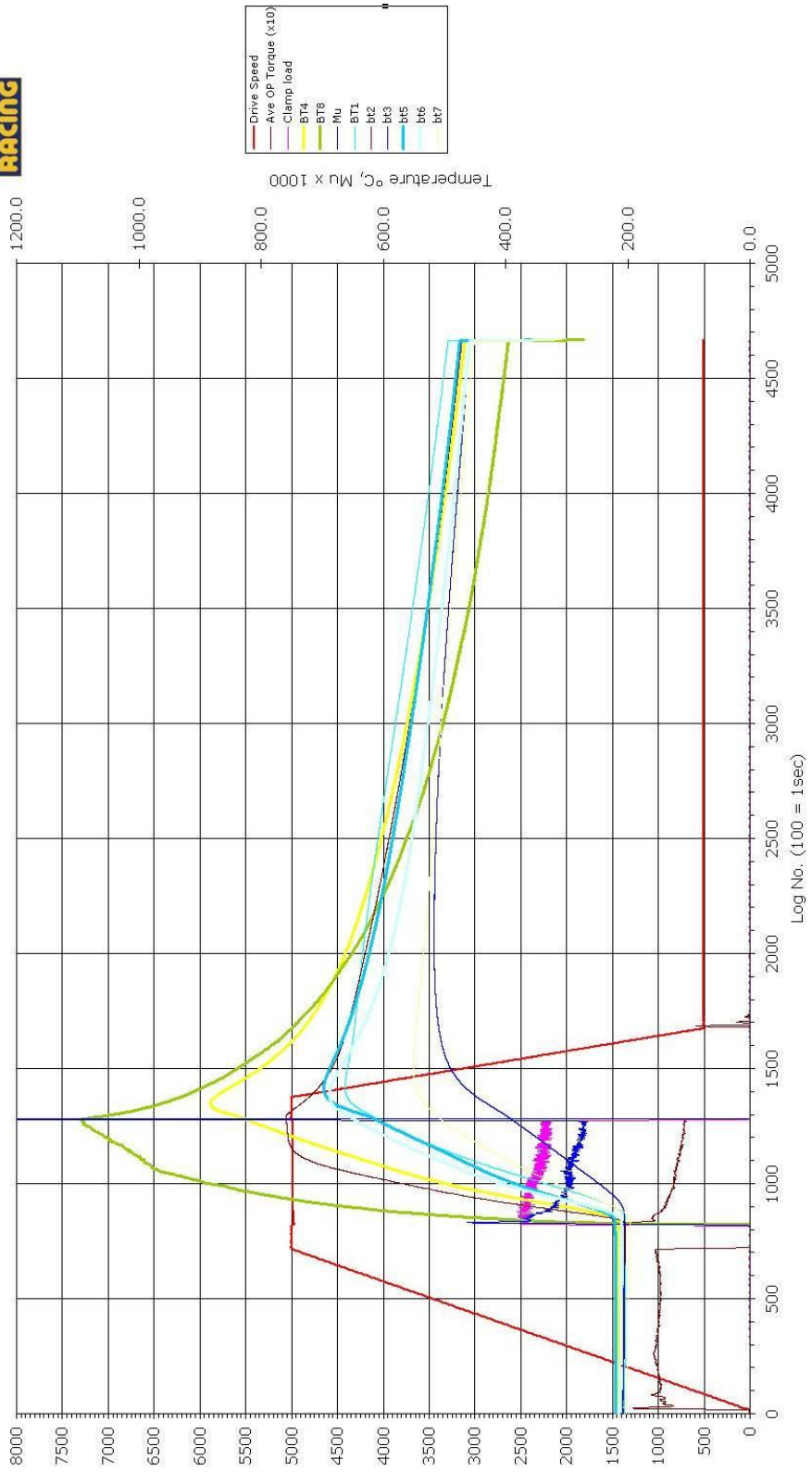
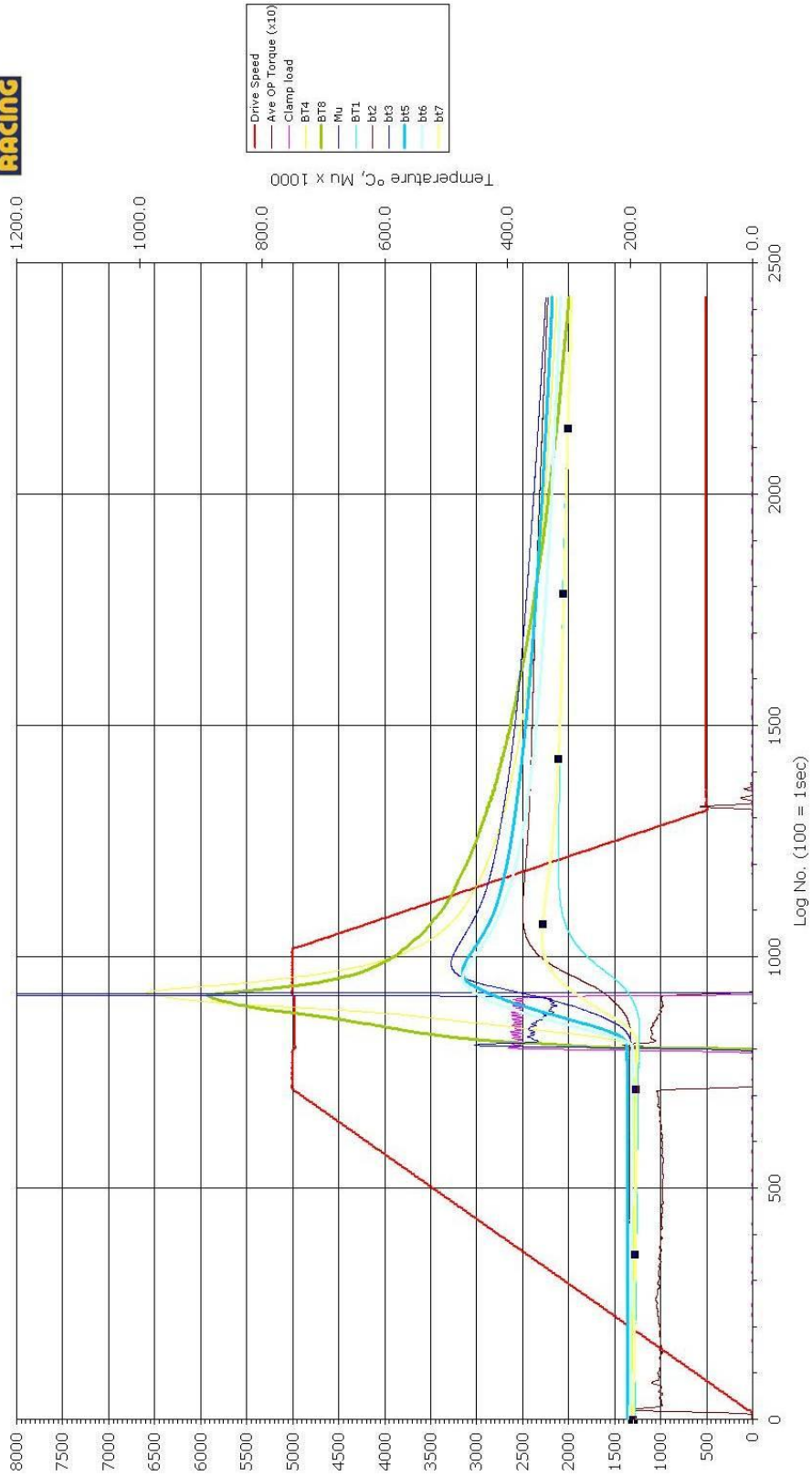
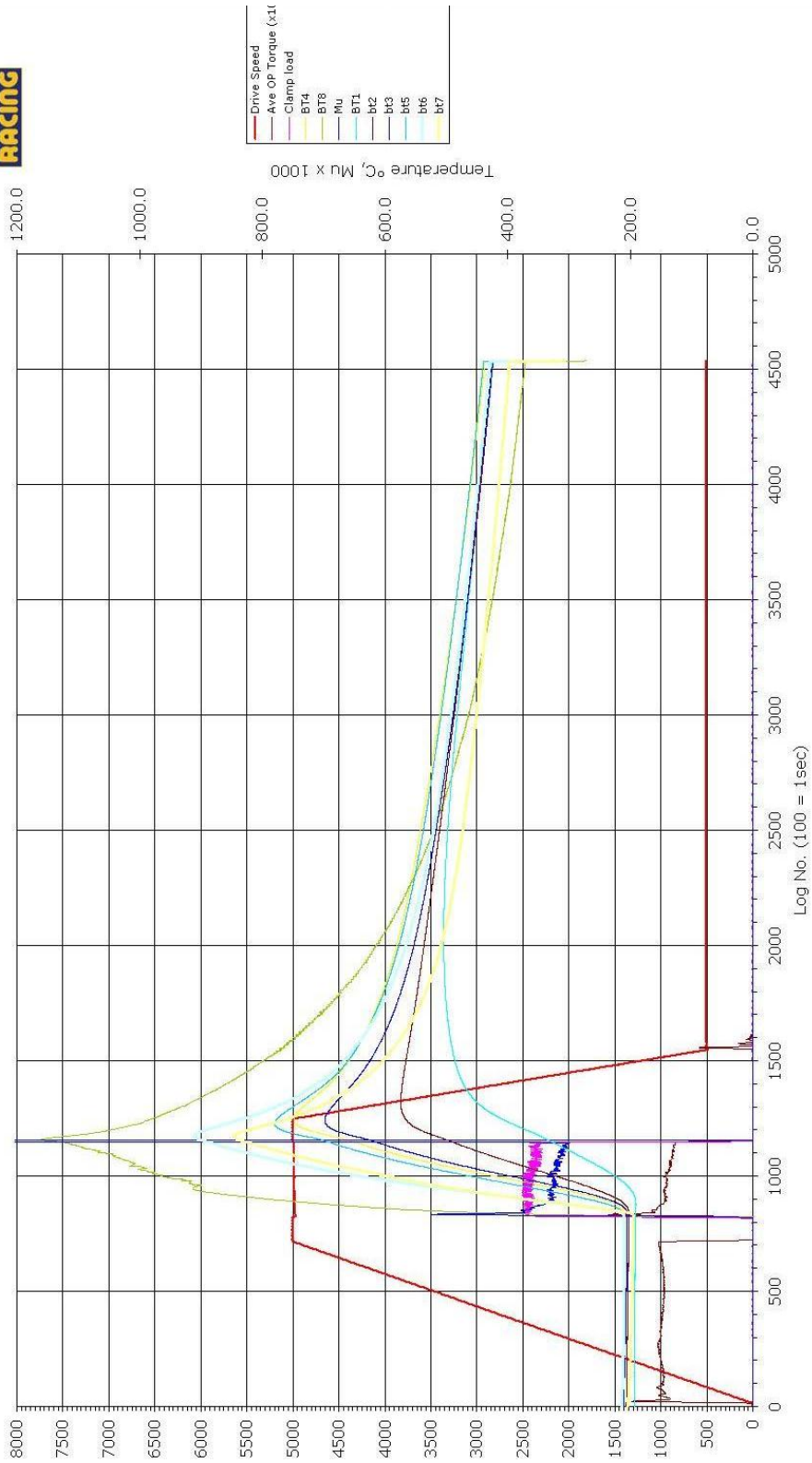


Plate F 5000rpm 2500N load 200deg



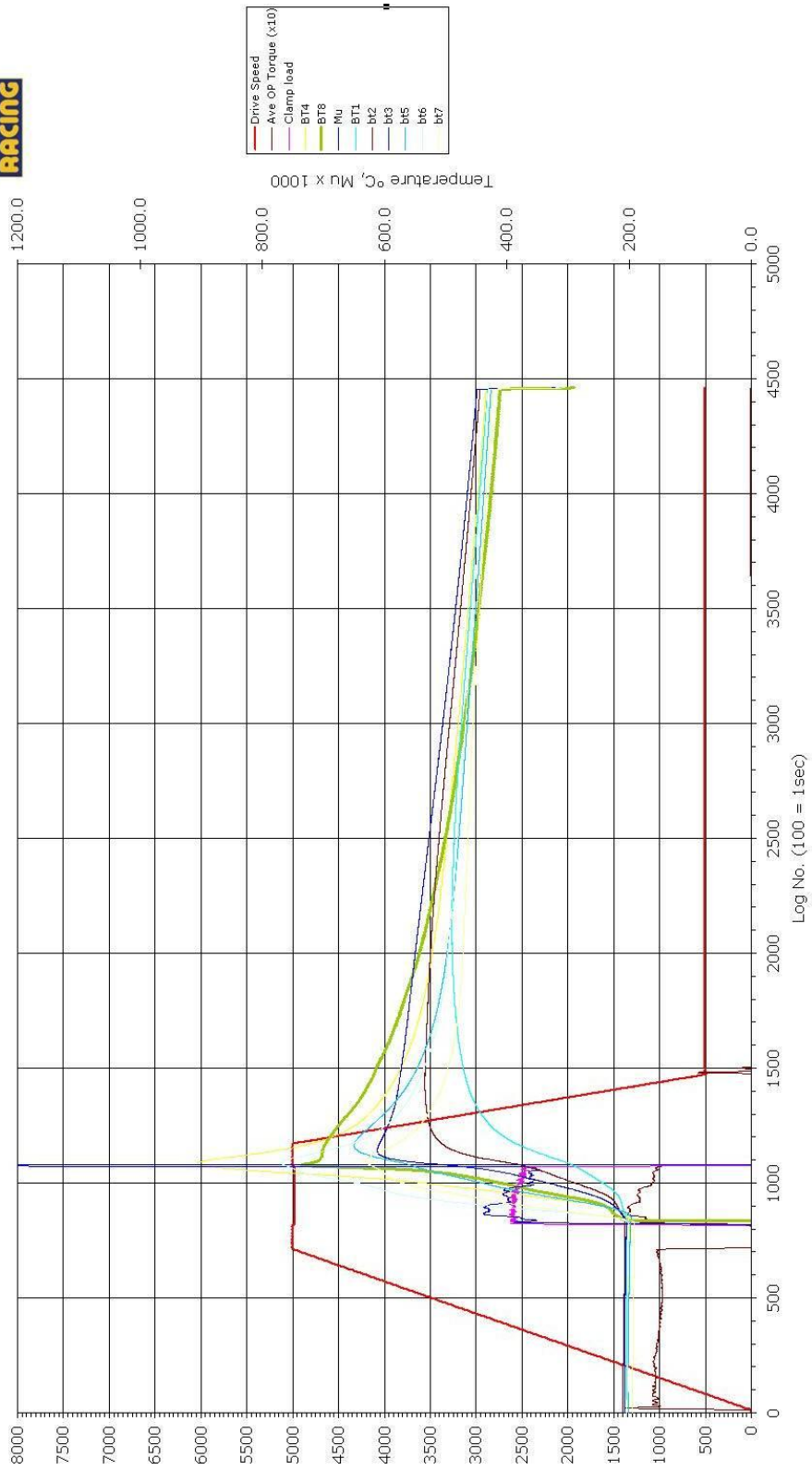


### Plate G 5000rpm 2500N load 200deg





### Plate Std 5000rpm 2500N load 200deg



## Appendix G - MATLAB® Code for Data Extraction

**For plotting the clamp loads on the temperature vs time axis**

```
tic
RowNum = 0;

%% IMPORT FROM EXCEL

PlateIndex = [{'Plate Std'} {'Plate A'} {'Plate B'} {'Plate
C'} {'Plate D'} {'Plate E'} {'Plate F'} {'Plate G'}];
ExcelIndex = [{'Q3:Q30000'} {'J3:J30000'} {'K3:K30000'}
{'L3:L30000'} {'M3:M30000'} {'N3:N30000'} {'O3:O30000'}
{'P3:P30000'}];

%% FOR EACH PLATE A - G:

for iPlateNum = 1:length(PlateIndex);

    RowNum = 0

    CurrentExcelColumn = ExcelIndex{iPlateNum};
    CurrentPlateID = PlateIndex{iPlateNum};
    CurrentPlateIDNoSpaces = CurrentPlateID(1:5);
    CurrentPlateIDNoSpaces(6) = CurrentPlateID(7);

    display(['Processing ' CurrentPlateID])

    SpeedList = [{' 3000rpm'},{' 5000rpm'},{' 7000rpm'}];
    SpeedListNoSpaces =
[{'3000rpm'},{'5000rpm'},{'7000rpm'}];

    ClampList = [{'1500N'},{'2500N'},{'3500N'}];

    workSheetList = [{'Data 100'},{'Data 200'},{'Data 300'}];

    scrsz = get(0,'ScreenSize');
    figure('Position',[1 scrsz(4) scrsz(3) scrsz(4)])

%% FOR EACH SPEED:

for iSpeedNum = 1:3

    CurrentSpeed = SpeedList{iSpeedNum};
    SpeedNoSpaces = 'RPM';
```



```

SpeedNoSpaces(4:7) = CurrentSpeed(2:5);
SpeedNoSpacesTime = SpeedNoSpaces;
SpeedNoSpacesTime(8) = 'T'; %RPM3000T

%% FOR EACH START TEMP:

    for iStartTemp = 1:3

        workSheet = workSheetList{iStartTemp};
        TempNoSpaces = strcat('Deg',workSheet(6:8));
        TempNameForPlot = workSheet(6:8);
        TempNameForPlot(4:7) = ' Deg';

%% FOR EACH CLAMP FORCE:

    for iClampNum = 1:3
        CurrentClamp = ClampList{iClampNum};
        ClampNoSpaces = 'N';
        ClampNoSpaces(2:5) = CurrentClamp(1:4); %e.g
N1500

        ClampNoSpacesTime = ClampNoSpaces;
        ClampNoSpacesTime(6) = 'T'; %e.g. N1500T

        StructureName = strcat(TempNoSpaces,SpeedNoSpaces);

        BandedFilePath =
        strcat('G:\R_D\Public\Gem\Tests\Test 2\DC0024
Gem\',CurrentPlateID,'\ ',CurrentPlateID,'
',CurrentSpeed,'_ ',CurrentClamp,'.xls');
        MasterFilePath =
        strcat('G:\R_D\Public\Gem\Tests\Test 2\DC0024 Gem\Plate
Std\Plate Std',' ',CurrentSpeed,'_ ',CurrentClamp,'.xls');
%           StartTemp = workSheet(1:4);
%           StartTemp(5:7) = workSheet(6:8); %e.g.
Data100
%           StartTempTime = StartTemp;
%           StartTempTime(8) = 'T'; %Data100T

        % = (iSpeedNum-1)*9+(iClampNum-
1)*3+iStartTemp
        % display([workSheet ' Degrees Start Temp'])

        workSheet = workSheetList{iStartTemp};

```

```

        %MasterTemp =
xlsread(MasterFilePath,workSheet, CurrentExcelColumn);
        %MasterForce =
xlsread(MasterFilePath,workSheet, 'G3:G30000');

        %MasterOverFifty = find(MasterForce>50);
        %LengthMaster = length(MasterOverFifty);

        %MasterStart = MasterOverFifty(1);
        %MasterEnd = MasterOverFifty(LengthMaster);

        workSheet = workSheetList{iStartTemp};
        BandedTemp = xlsread(BandedFilePath,
workSheet, CurrentExcelColumn);
        BandedForce = xlsread(BandedFilePath,
workSheet, 'G3:G30000');
        BandedOverFifty = find(BandedForce>50);
        LengthBanded = length(BandedOverFifty);
        BandedStart = BandedOverFifty(1);
        BandedEnd = BandedOverFifty(LengthBanded);

        %VectorLengths(1) = LengthMaster;
        VectorLengths(1) = LengthBanded;
        MinVectorLength = min(VectorLengths);

        BandedTempCut.(StructureName).(ClampNoSpaces)
= BandedTemp(BandedStart:BandedStart+MinVectorLength-1);

BandedTempCut.(StructureName).(ClampNoSpacesTime) =
[0:0.01:(MinVectorLength/100)-0.01];

        if iPlateNum == 1

BandedTempCut.(StructureName).(ClampNoSpaces) =
BandedTempCut.(StructureName).(ClampNoSpaces)/0.85;
        else
        end

%MasterTempCut.(StructureName).(ClampNoSpaces) =
MasterTemp(MasterStart:MasterStart+MinVectorLength-1);

```

```

%MasterTempCut.(StructureName).(ClampNoSpaceTime) =
[0:0.01:(MinVectorLength/100)-0.01];

        clear MinVectorLength zero
        clear MasterTemp MasterForce MasterOverFifty
LengthMaster MasterStart MasterEnd MasterDuration BandedTemp
BandedForce BandedOverFifty
        clear LengthBanded BandedStart BandedEnd
BandedDuration InterpInterval BandedTempInterp
MasterTempInterp CurrentCorrelation WorkSheet

end

        subplot(3,3,(iSpeedNum-1)*3+iStartTemp)
axis([0 15 0 1200])

plot(BandedTempCut.(StructureName).N1500T,BandedTempCut.(Stru
ctureName).N1500,'r')
        hold on

plot(BandedTempCut.(StructureName).N2500T,BandedTempCut.(Stru
ctureName).N2500,'g')

plot(BandedTempCut.(StructureName).N3500T,BandedTempCut.(Stru
ctureName).N3500,'b')
%
plot(MasterTempCut.(StructureName).Data100T,MasterTempCut.(St
ructureName).Data100,'r')
%
plot(MasterTempCut.(StructureName).Data200T,MasterTempCut.(St
ructureName).Data200,'g')
%
plot(MasterTempCut.(StructureName).Data300T,MasterTempCut.(St
ructureName).Data300,'b')
        titlename = strcat([CurrentPlateID,'
',TempNameForPlot,' ',CurrentSpeed])

        if iPlateNum == 1
                titlename = strcat([CurrentPlateID,'
',TempNameForPlot,' via IR',CurrentSpeed])

```

```

        else
        end

        title(titlename)
        xlabel('Time (Sec)')
        ylabel('Temperature (Deg C)')
        axis([0 15 0 1200])

    end

end

    legend('1500 N','2500 N','3500
N','Location','EastOutside')
    saveas(gcf,[CurrentPlateID ' SPEEDvsTEMP' '.emf'])
% saves figure as a jpeg in the folderpath direc
    close
    clear BandedTempCut MasterTempCut
end
toc

```

### For plotting the clamp loads on the friction vs temperature axis

```

tic
RowNum = 0;

%% IMPORT FROM EXCEL

PlateIndex = [{'Plate Std'} {'Plate A'} {'Plate B'} {'Plate
C'} {'Plate D'} {'Plate E'} {'Plate F'} {'Plate G'}];
ExcelIndex = [{'Q3:Q30000'} {'J3:J30000'} {'K3:K30000'}
{'L3:L30000'} {'M3:M30000'} {'N3:N30000'} {'O3:O30000'}
{'P3:P30000'}];

%% FOR EACH PLATE A - G:

for iPlateNum = 1:length(PlateIndex);

    RowNum = 0

    CurrentExcelColumn = ExcelIndex{iPlateNum};
    CurrentPlateID = PlateIndex{iPlateNum};
    CurrentPlateIDNoSpaces = CurrentPlateID(1:5);
    CurrentPlateIDNoSpaces(6) = CurrentPlateID(7);

```

```

display(['Processing ' CurrentPlateID])

SpeedList = [{' 3000rpm'},{' 5000rpm'},{' 7000rpm'}];
SpeedListNoSpaces =
['{3000rpm}','{5000rpm}','{7000rpm}'];

ClampList = [{'1500N'},{'2500N'},{'3500N'}];

workSheetList = [{'Data 100'},{'Data 200'},{'Data 300'}];

scrsz = get(0,'ScreenSize');
figure('Position',[1 scrsz(4) scrsz(3) scrsz(4)])

%% FOR EACH SPEED:

for iSpeedNum = 1:3

    CurrentSpeed = SpeedList{iSpeedNum};
    SpeedNoSpaces = 'RPM';
    SpeedNoSpaces(4:7) = CurrentSpeed(2:5);
    SpeedNoSpacesTime = SpeedNoSpaces;
    SpeedNoSpacesTime(8) = 'T'; %RPM3000T

%% FOR EACH START TEMP:

for iStartTemp = 1:3

    workSheet = workSheetList{iStartTemp};
    TempNoSpaces = strcat('Deg',workSheet(6:8));
    TempNameForPlot = workSheet(6:8);
    TempNameForPlot(4:7) = ' Deg';

%% FOR EACH CLAMP FORCE:

for iClampNum = 1:3
    CurrentClamp = ClampList{iClampNum};
    ClampNoSpaces = 'N';
    ClampNoSpaces(2:5) = CurrentClamp(1:4); %e.g
N1500

    ClampNoSpacesTime = ClampNoSpaces;
    ClampNoSpacesTime(6) = 'T'; %e.g. N1500T
    ClampNoSpacesFric = ClampNoSpacesTime;
    ClampNoSpacesFric(6) = 'F';%e.g. N1500F

```

```

        StructureName =
strcat(TempNoSpaces,SpeedNoSpaces);

        BandedFilePath =
strcat('G:\R_D\Public\Gem\Tests\Test 2\DC0024
Gem\',CurrentPlateID,'\ ',CurrentPlateID,'
',CurrentSpeed,'_ ',CurrentClamp,'.xls');
        MasterFilePath =
strcat('G:\R_D\Public\Gem\Tests\Test 2\DC0024 Gem\Plate
Std\Plate Std',' ',CurrentSpeed,'_ ',CurrentClamp,'.xls');
        %           StartTemp = workSheet(1:4);
        %           StartTemp(5:7) =
workSheet(6:8); %e.g. Data100
        %           StartTempTime = StartTemp;
        %           StartTempTime(8) = 'T';
%Data100T

        % = (iSpeedNum-1)*9+(iClampNum-
1)*3+iStartTemp
        % display([workSheet ' Degrees Start Temp'])

        workSheet = workSheetList{iStartTemp};

        %MasterTemp =
xlsread(MasterFilePath,workSheet, CurrentExcelColumn);
        %MasterForce =
xlsread(MasterFilePath,workSheet, 'G3:G30000');

        %MasterOverFifty = find(MasterForce>50);
        %LengthMaster = length(MasterOverFifty);

        %MasterStart = MasterOverFifty(1);
        %MasterEnd = MasterOverFifty(LengthMaster);

        workSheet = workSheetList{iStartTemp};
        BandedTemp = xlsread(BandedFilePath,
workSheet, CurrentExcelColumn);
        BandedForce = xlsread(BandedFilePath,
workSheet, 'G3:G30000');
        BandedFric = xlsread(BandedFilePath,
workSheet, 'Z3:Z30000');
        BandedOverFifty = find(BandedForce>50);
        LengthBanded = length(BandedOverFifty);
        BandedStart = BandedOverFifty(1);
        BandedEnd = BandedOverFifty(LengthBanded);

```

```

%VectorLengths(1) = LengthMaster;
VectorLengths(1) = LengthBanded;
MinVectorLength = min(VectorLengths);

BandedTempCut.(StructureName).(ClampNoSpaces)
= BandedTemp(BandedStart:BandedStart+MinVectorLength-1);

BandedTempCut.(StructureName).(ClampNoSpacesTime) =
[0:0.01:(MinVectorLength/100)-0.01];

BandedTempCut.(StructureName).(ClampNoSpacesFric) =
BandedFric(BandedStart:BandedStart+MinVectorLength-1);

    if iPlateNum == 1

BandedTempCut.(StructureName).(ClampNoSpaces) =
BandedTempCut.(StructureName).(ClampNoSpaces)/0.85;
        else
        end

%MasterTempCut.(StructureName).(ClampNoSpaces) =
MasterTemp(MasterStart:MasterStart+MinVectorLength-1);

%MasterTempCut.(StructureName).(ClampNoSpacesTime) =
[0:0.01:(MinVectorLength/100)-0.01];

        clear MinVectorLength zero
        clear MasterTemp MasterForce MasterOverFifty
LengthMaster MasterStart MasterEnd MasterDuration BandedTemp
BandedForce BandedOverFifty
        clear LengthBanded BandedStart BandedEnd
BandedDuration InterpInterval BandedTempInterp
MasterTempInterp CurrentCorrelation WorkSheet

    end

```

```

subplot(3,3,(iSpeedNum-1)*3+iStartTemp)

plot(BandedTempCut.(StructureName).N1500,BandedTempCut.(StructureName).N1500F,'r')
    hold on

plot(BandedTempCut.(StructureName).N2500,BandedTempCut.(StructureName).N2500F,'g')

plot(BandedTempCut.(StructureName).N3500,BandedTempCut.(StructureName).N3500F,'b')
    %
plot(MasterTempCut.(StructureName).Data100T,MasterTempCut.(StructureName).Data100,'r')
    %
plot(MasterTempCut.(StructureName).Data200T,MasterTempCut.(StructureName).Data200,'g')
    %
plot(MasterTempCut.(StructureName).Data300T,MasterTempCut.(StructureName).Data300,'b')
    titlename = strcat([CurrentPlateID,'
',TempNameForPlot,' ',CurrentSpeed])

    if iPlateNum == 1
        titlename = strcat([CurrentPlateID,'
',TempNameForPlot,' via IR',CurrentSpeed])
    else
    end

    title(titlename)
    xlabel('Temperature (Deg C)')
    ylabel('Friction')
    axis([0 1500 0 500])

end

end

legend('1500 N','2500 N','3500
N','Location','EastOutside')
saveas(gcf,[CurrentPlateID ' SPEEDvsTEMP-Friction'
'.emf']) %saves figure as a jpeg in the folderpath direc
close
clear BandedTempCut MasterTempCut

```



```
end
toc
```

### For plotting the speeds on the temperature vs time axis

```
tic
RowNum = 0;

%% IMPORT FROM EXCEL

PlateIndex = [{'Plate Std'} {'Plate A'} {'Plate B'} {'Plate
C'} {'Plate D'} {'Plate E'} {'Plate F'} {'Plate G'}];
ExcelIndex = [{'Q3:Q30000'} {'J3:J30000'} {'K3:K30000'}
{'L3:L30000'} {'M3:M30000'} {'N3:N30000'} {'O3:O30000'}
{'P3:P30000'}];

%% FOR EACH PLATE A - G:

for iPlateNum = 1:length(PlateIndex);

    RowNum = 0

    CurrentExcelColumn = ExcelIndex{iPlateNum};
    CurrentPlateID = PlateIndex{iPlateNum};
    CurrentPlateIDNoSpaces = CurrentPlateID(1:5);
    CurrentPlateIDNoSpaces(6) = CurrentPlateID(7);

    display(['Processing ' CurrentPlateID])

    SpeedList = [{' 3000rpm'},{' 5000rpm'},{' 7000rpm'}];
    SpeedListNoSpaces =
[{'3000rpm'},{'5000rpm'},{'7000rpm'}];

    ClampList = [{'1500N'},{'2500N'},{'3500N'}];

    worksheetList = [{'Data 100'},{'Data 200'},{'Data 300'}];

    scrsz = get(0,'ScreenSize');
    figure('Position',[1 scrsz(4) scrsz(3) scrsz(4)])

%% FOR EACH CLAMP FORCE:

    for iClampNum = 1:3
        CurrentClamp = ClampList{iClampNum};
```

```
%% FOR EACH START TEMP:
```

```
    for iStartTemp = 1:3
```

```
        workSheet = workSheetList{iStartTemp};  
        TempNoSpaces = strcat('Deg',workSheet(6:8));  
        TempNameForPlot = workSheet(6:8);  
        TempNameForPlot(4:7) = ' Deg';
```

```
%% FOR EACH SPEED:
```

```
    for ispeedNum = 1:3
```

```
        CurrentSpeed = SpeedList{ispeedNum};  
        SpeedNoSpaces = 'RPM';  
        SpeedNoSpaces(4:7) = CurrentSpeed(2:5);  
        SpeedNoSpacesTime = SpeedNoSpaces;  
        SpeedNoSpacesTime(8) = 'T'; %RPM3000T
```

```
        StructureName = strcat(TempNoSpaces,CurrentClamp);
```

```
        BandedFilePath =
```

```
        strcat('G:\R_D\Public\Gem\Tests\Test 2\DC0024  
Gem\',CurrentPlateID,'\ ',CurrentPlateID,'  
,CurrentSpeed,'_ ',CurrentClamp,'.xls');
```

```
        MasterFilePath =
```

```
        strcat('G:\R_D\Public\Gem\Tests\Test 2\DC0024 Gem\Plate  
Std\Plate Std',' ',CurrentSpeed,'_ ',CurrentClamp,'.xls');
```

```
%           StartTemp = workSheet(1:4);
```

```
%           StartTemp(5:7) = workSheet(6:8); %e.g.
```

```
Data100
```

```
%           StartTempTime = StartTemp;
```

```
%           StartTempTime(8) = 'T'; %Data100T
```

```
% = (ispeedNum-1)*9+(iClampNum-  
1)*3+iStartTemp
```

```
% display([workSheet ' Degrees Start Temp'])
```

**For plotting the speeds on the friction vs temperature axis**

```

tic
RowNum = 0;

%% IMPORT FROM EXCEL

PlateIndex = [{'Plate Std'} {'Plate A'} {'Plate B'} {'Plate
C'} {'Plate D'} {'Plate E'} {'Plate F'} {'Plate G'}];
ExcelIndex = [{'Q3:Q30000'} {'J3:J30000'} {'K3:K30000'}
{'L3:L30000'} {'M3:M30000'} {'N3:N30000'} {'O3:O30000'}
{'P3:P30000'}];

%% FOR EACH PLATE A - G:

for iPlateNum = 1:length(PlateIndex);

    RowNum = 0

    CurrentExcelColumn = ExcelIndex{iPlateNum};
    CurrentPlateID = PlateIndex{iPlateNum};
    CurrentPlateIDNoSpaces = CurrentPlateID(1:5);
    CurrentPlateIDNoSpaces(6) = CurrentPlateID(7);

    display(['Processing ' CurrentPlateID])

    SpeedList = [{' 3000rpm'},{' 5000rpm'},{' 7000rpm'}];
    SpeedListNoSpaces =
    [{'3000rpm'},{'5000rpm'},{'7000rpm'}];

    ClampList = [{'1500N'},{'2500N'},{'3500N'}];

    workSheetList = [{'Data 100'},{'Data 200'},{'Data 300'}];

    scrsz = get(0,'ScreenSize');
    figure('Position',[1 scrsz(4) scrsz(3) scrsz(4)])

%% FOR EACH CLAMP FORCE:

    for iClampNum = 1:3
        CurrentClamp = ClampList{iClampNum};

%% FOR EACH START TEMP:

```

```

for iStartTemp = 1:3

    workSheet = workSheetList{iStartTemp};
    TempNoSpaces = strcat('Deg',workSheet(6:8));
    TempNameForPlot = workSheet(6:8);
    TempNameForPlot(4:7) = ' Deg';

%% FOR EACH SPEED:

    for iSpeedNum = 1:3

        CurrentSpeed = SpeedList{iSpeedNum};
        SpeedNoSpaces = 'RPM';
        SpeedNoSpaces(4:7) = CurrentSpeed(2:5);
        SpeedNoSpacesTime = SpeedNoSpaces;
        SpeedNoSpacesTime(8) = 'T'; %RPM3000T
        SpeedNoSpacesFric = SpeedNoSpacesTime;
        SpeedNoSpacesFric(8) = 'F';

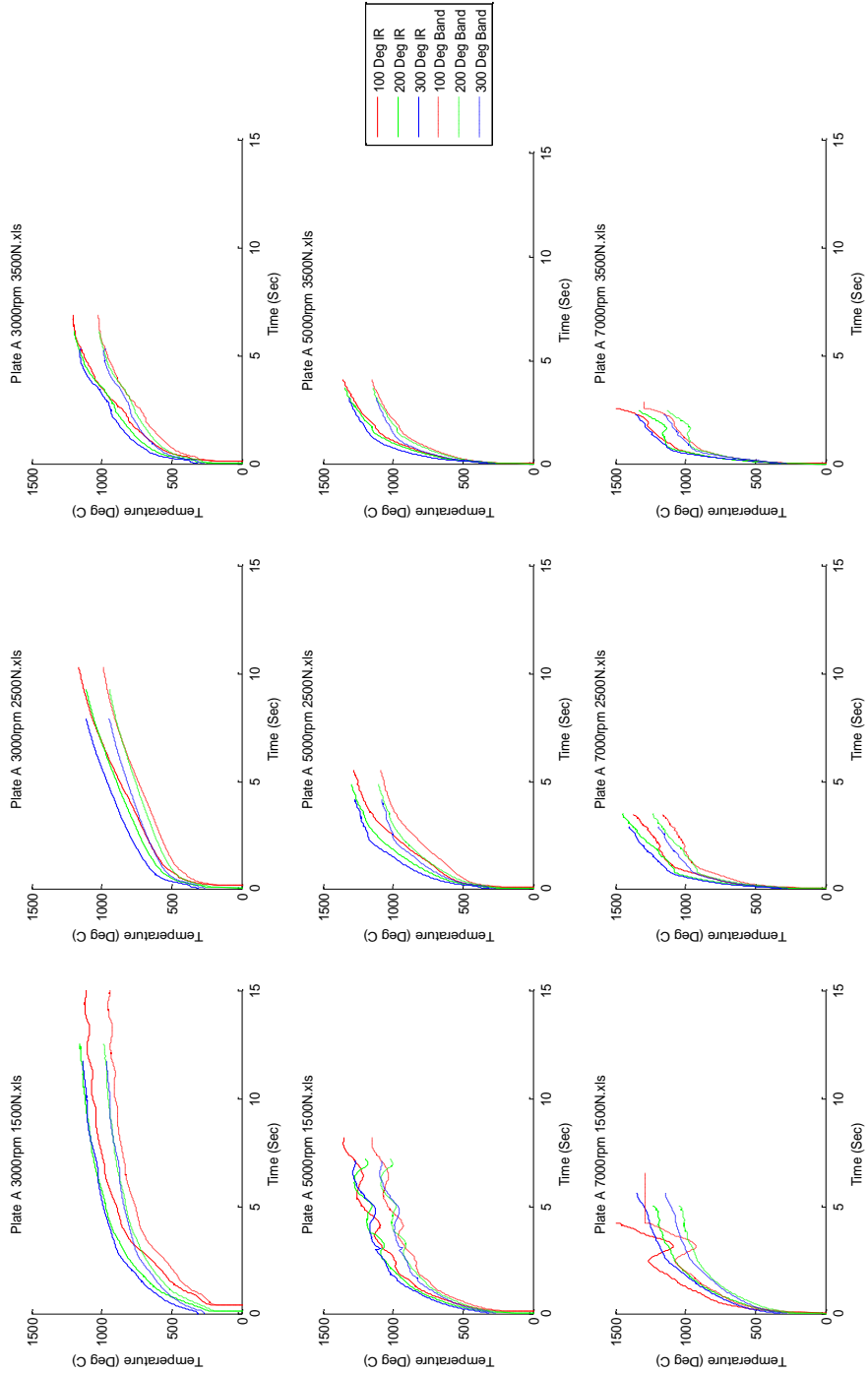
        StructureName = strcat(TempNoSpaces,CurrentClamp);

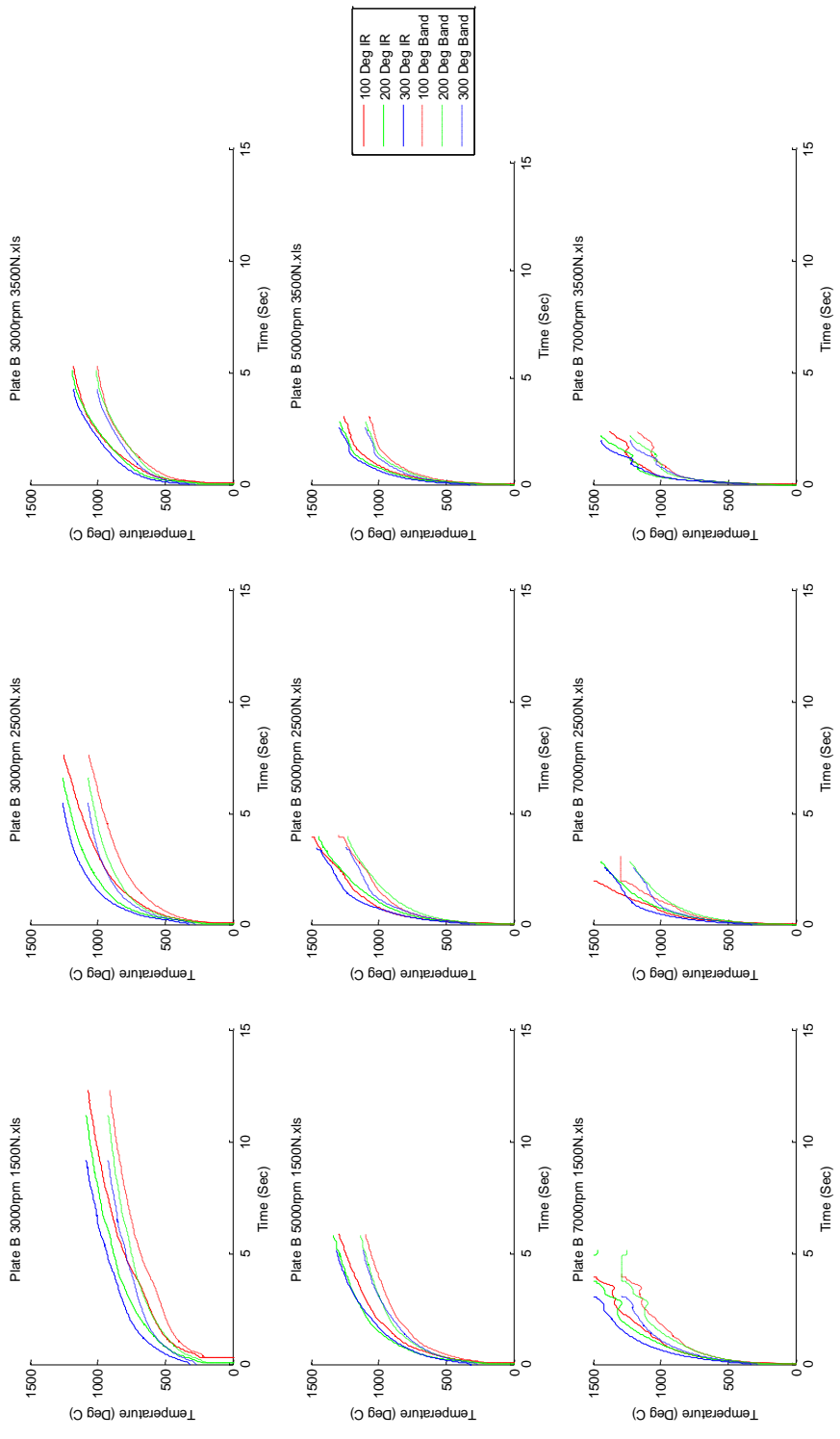
        BandedFilePath =
        strcat('G:\R_D\Public\Gem\Tests\Test 2\DC0024
        Gem\',CurrentPlateID,'\ ',CurrentPlateID,'
        ',CurrentSpeed,'_',CurrentClamp,'.xls');
        MasterFilePath =
        strcat('G:\R_D\Public\Gem\Tests\Test 2\DC0024 Gem\Plate
        Std\Plate Std',' ',CurrentSpeed,'_',CurrentClamp,'.xls');
        %           StartTemp = workSheet(1:4);
        %           StartTemp(5:7) = workSheet(6:8); %e.g.
        Data100
        %           StartTempTime = StartTemp;
        %           StartTempTime(8) = 'T'; %Data100T

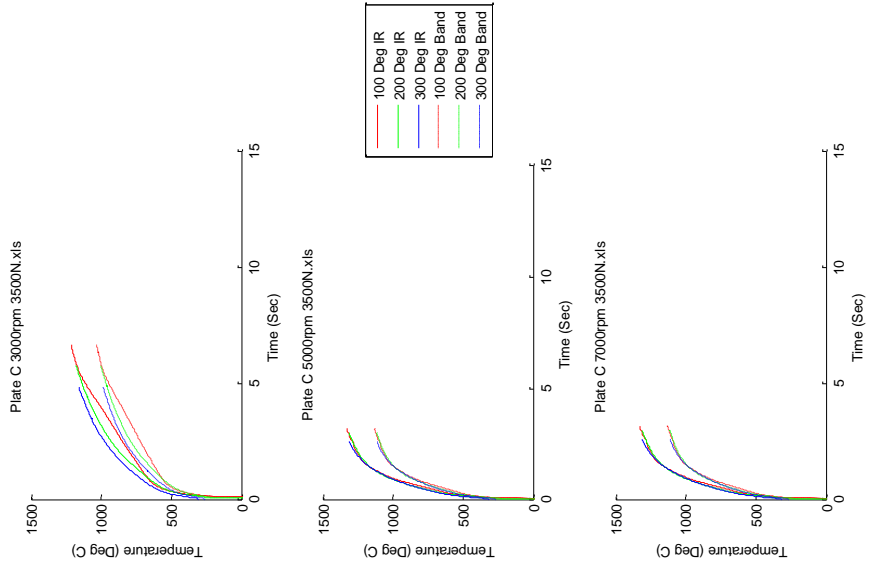
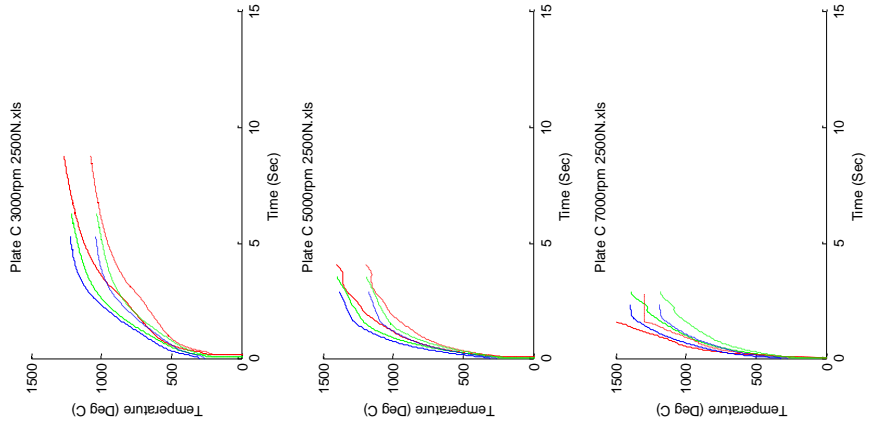
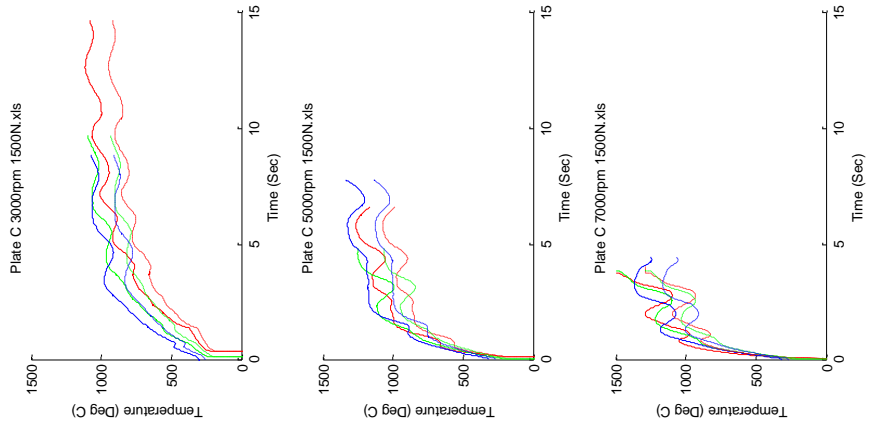
        % = (iSpeedNum-1)*9+(iClampNum-
        1)*3+iStartTemp
        % display([WorkSheet ' Degrees Start Temp'])

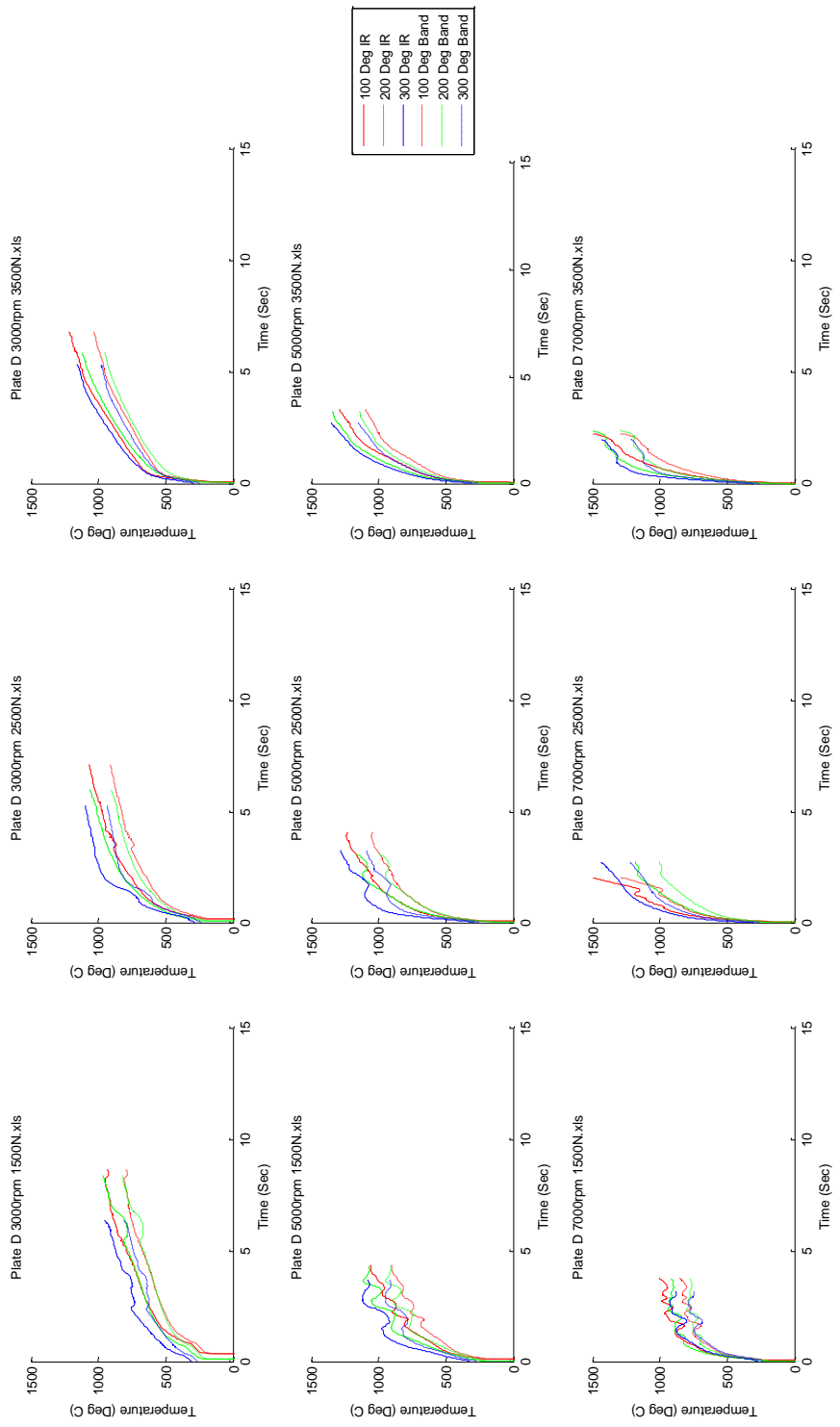
```

# Appendix H - Temperature Effects of Initial Temperature

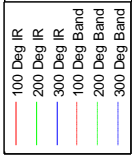
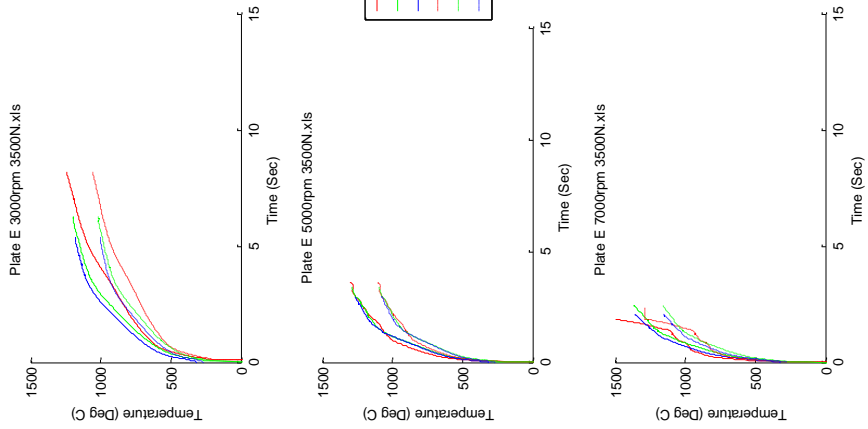
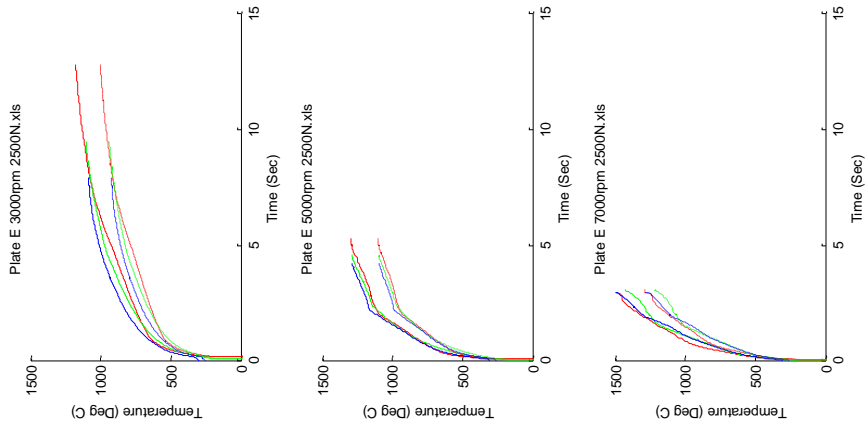
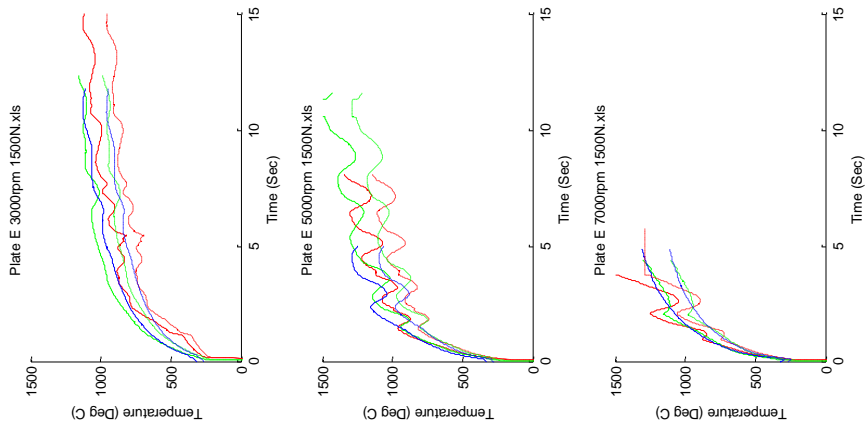


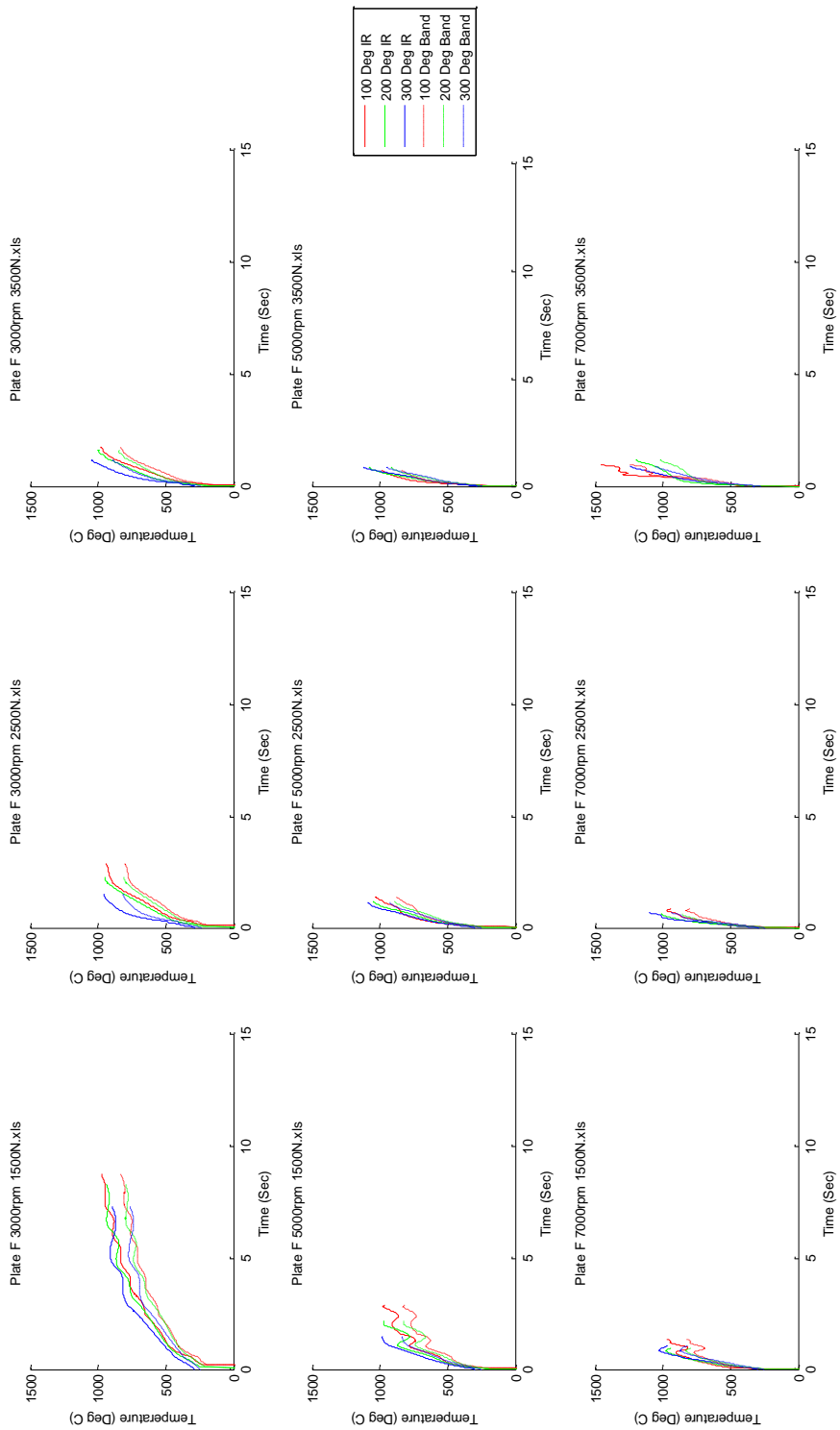


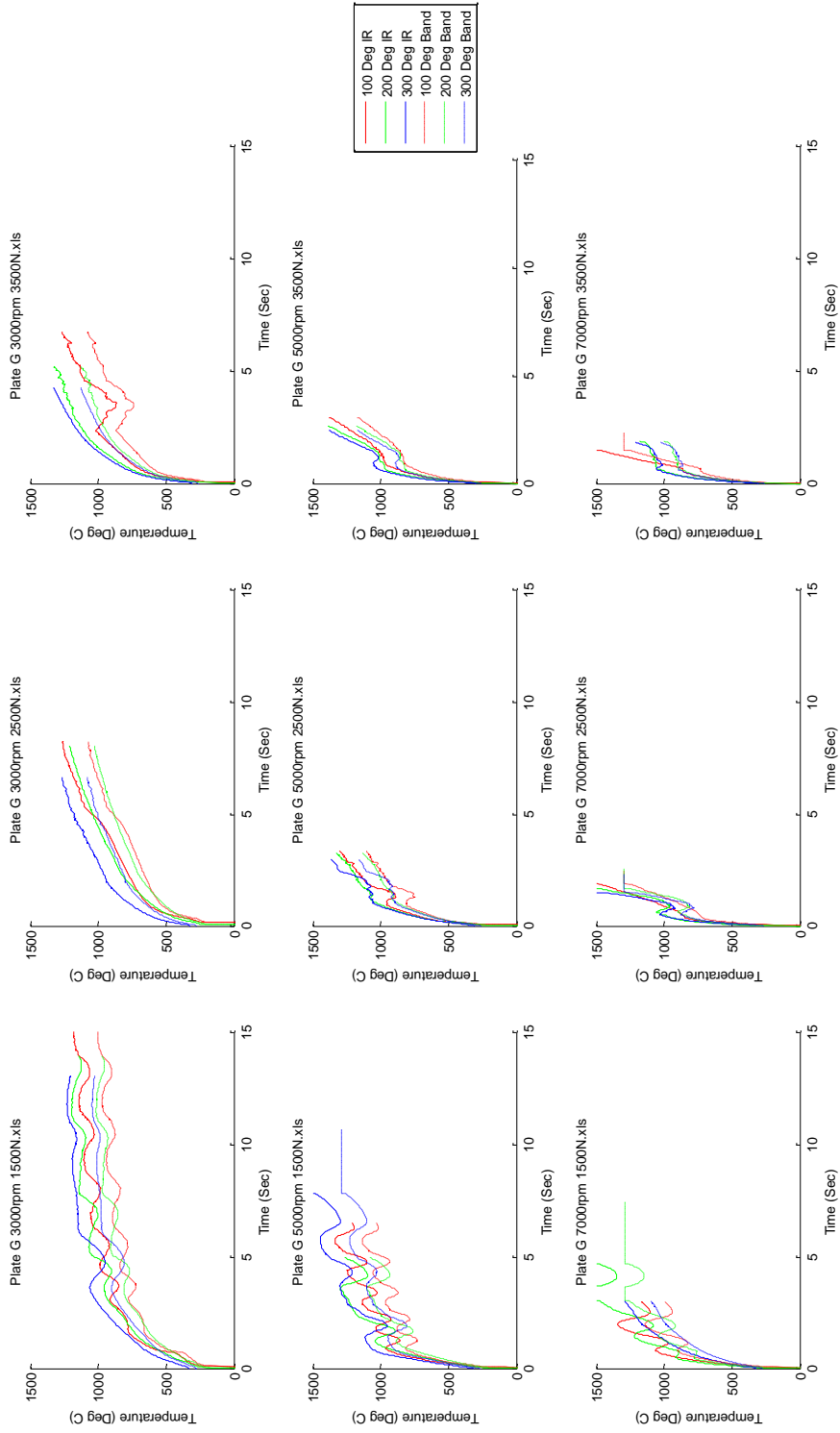


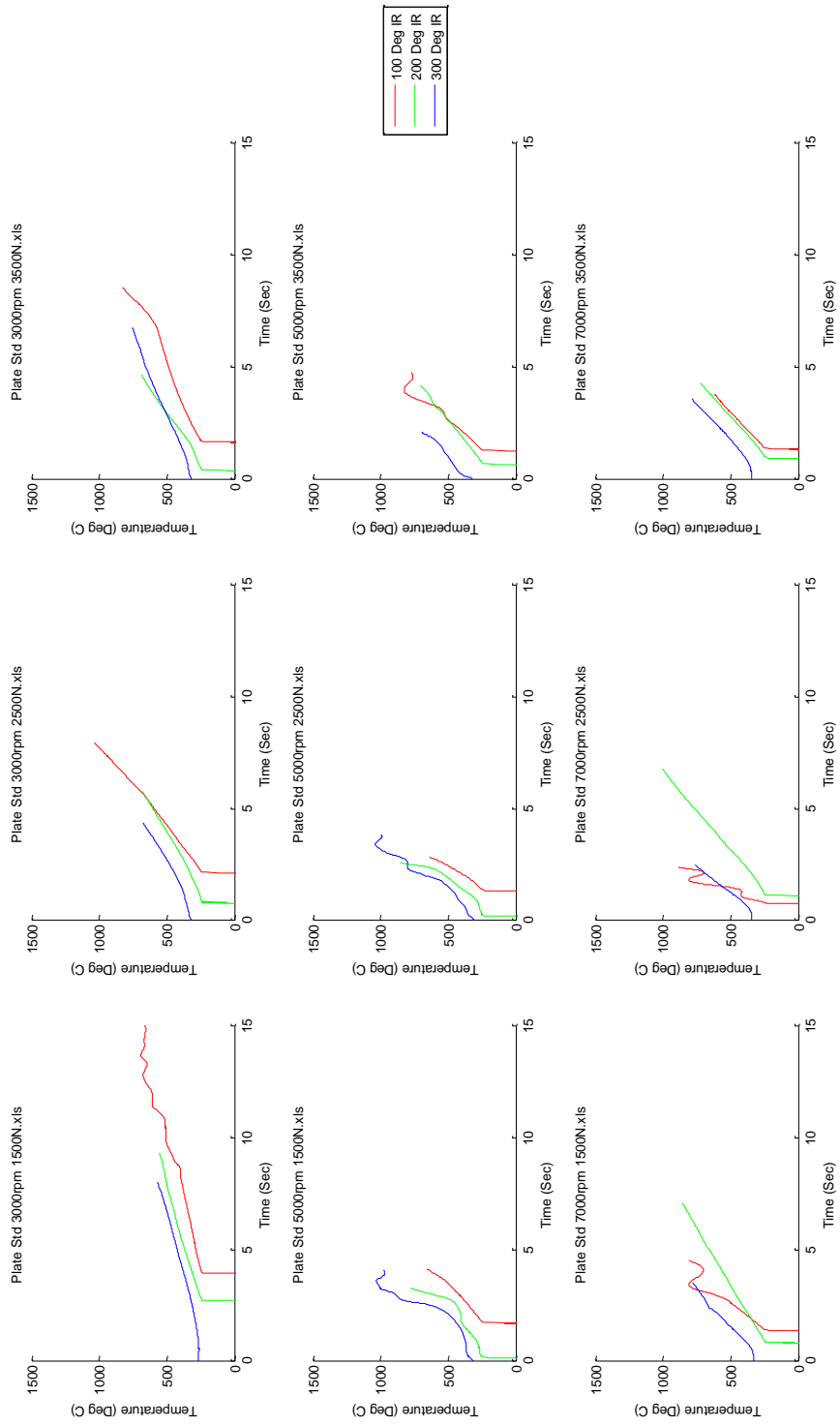


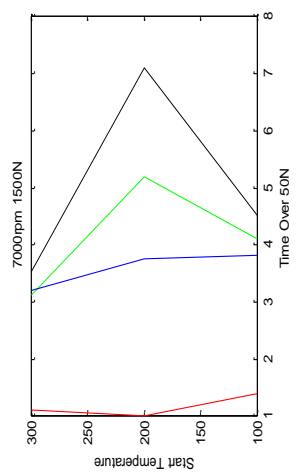
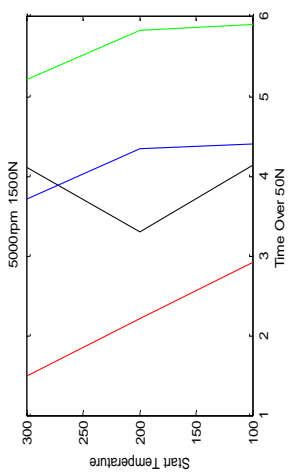
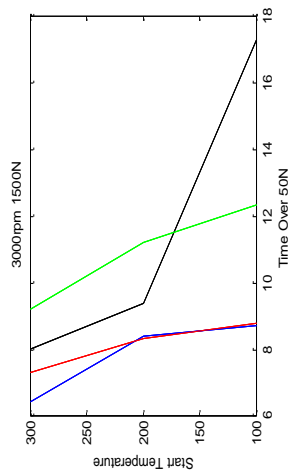
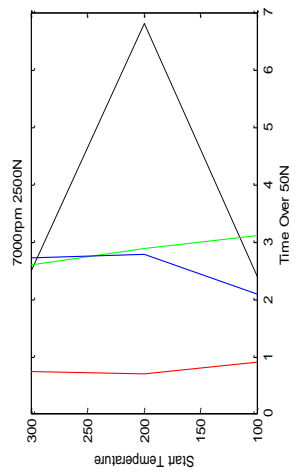
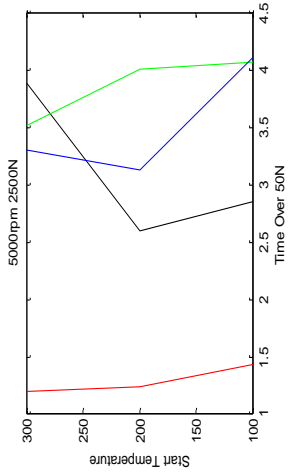
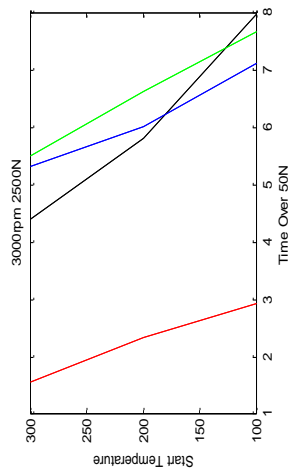
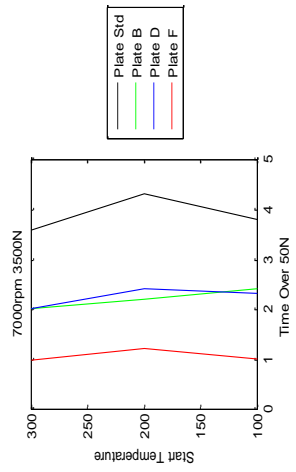
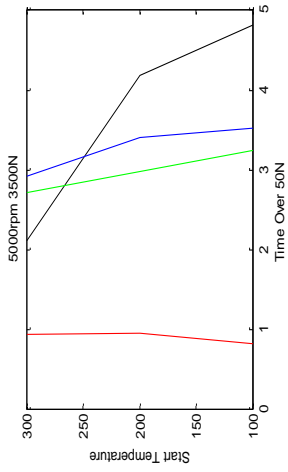
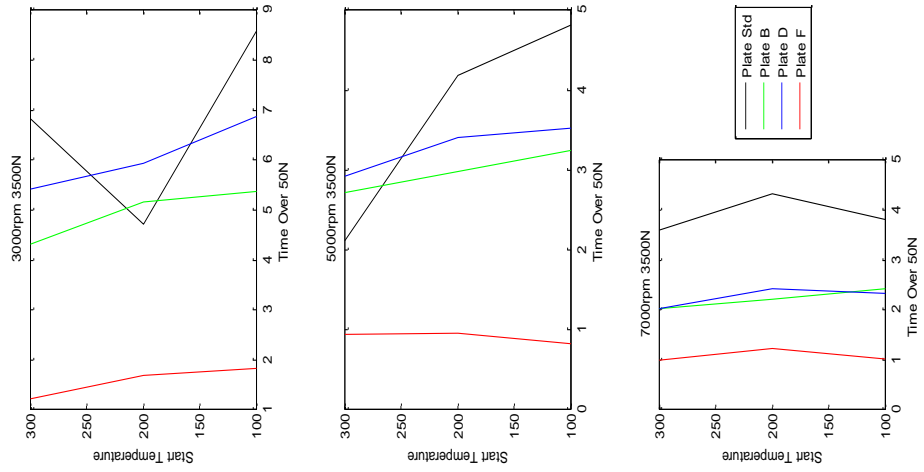




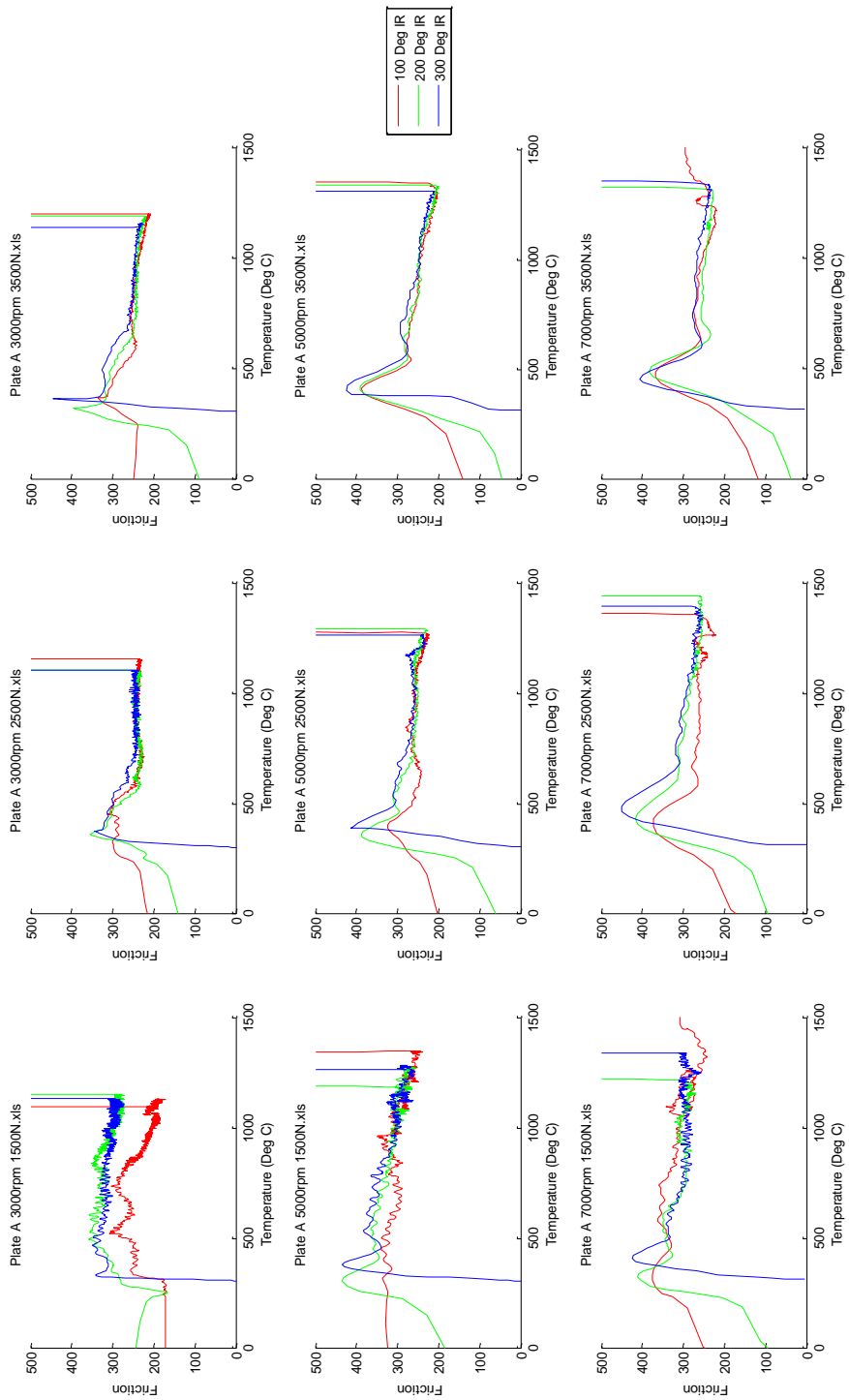


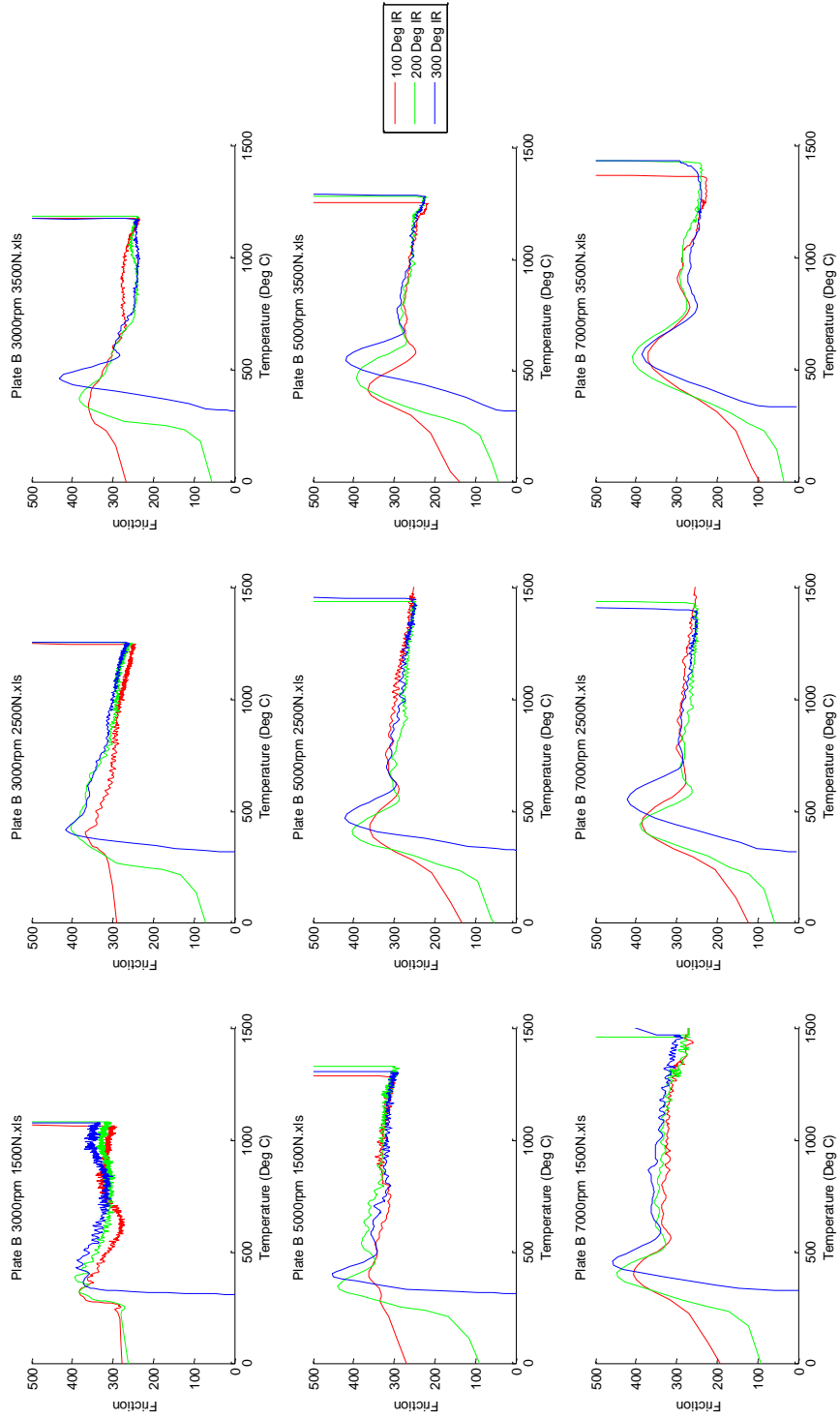


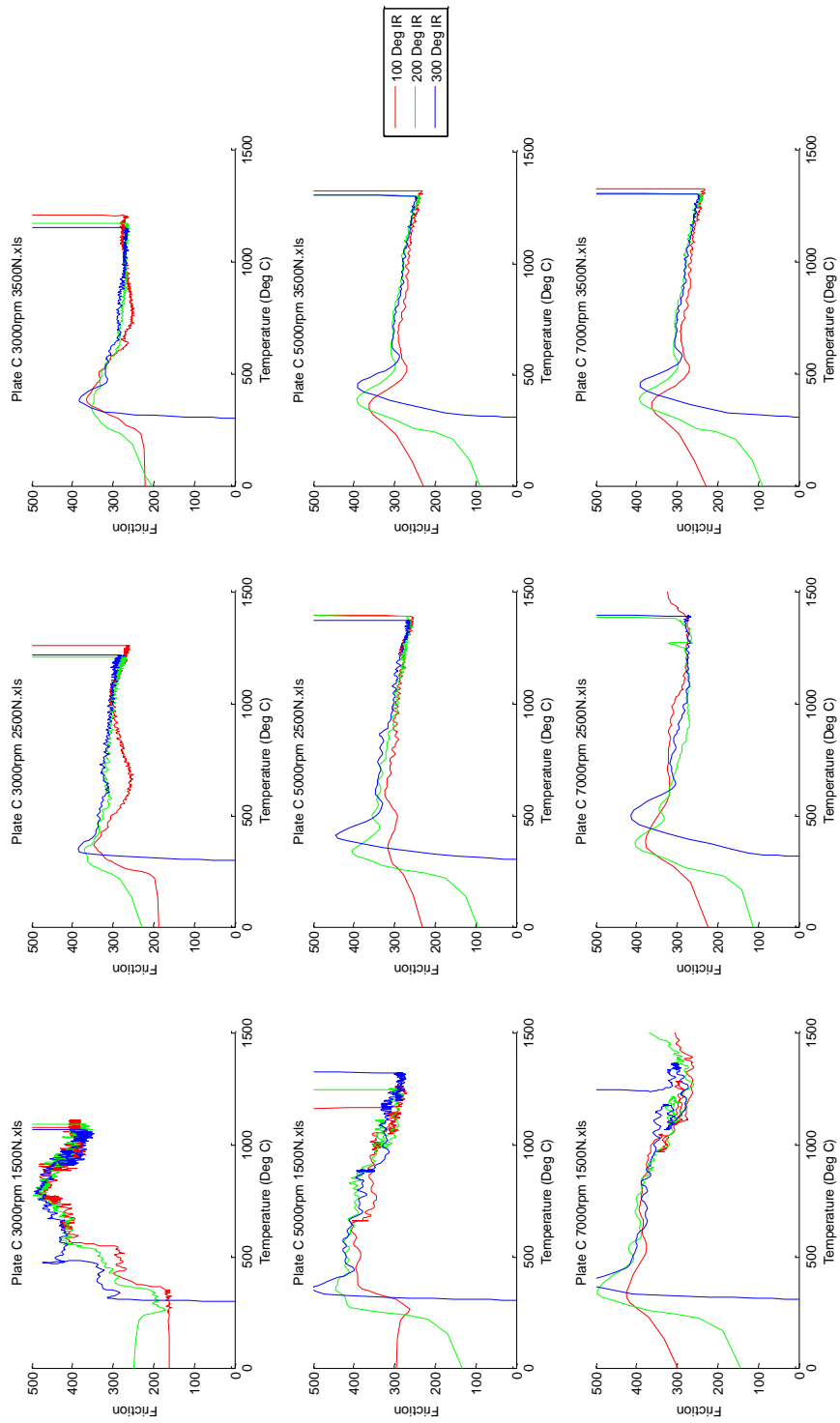




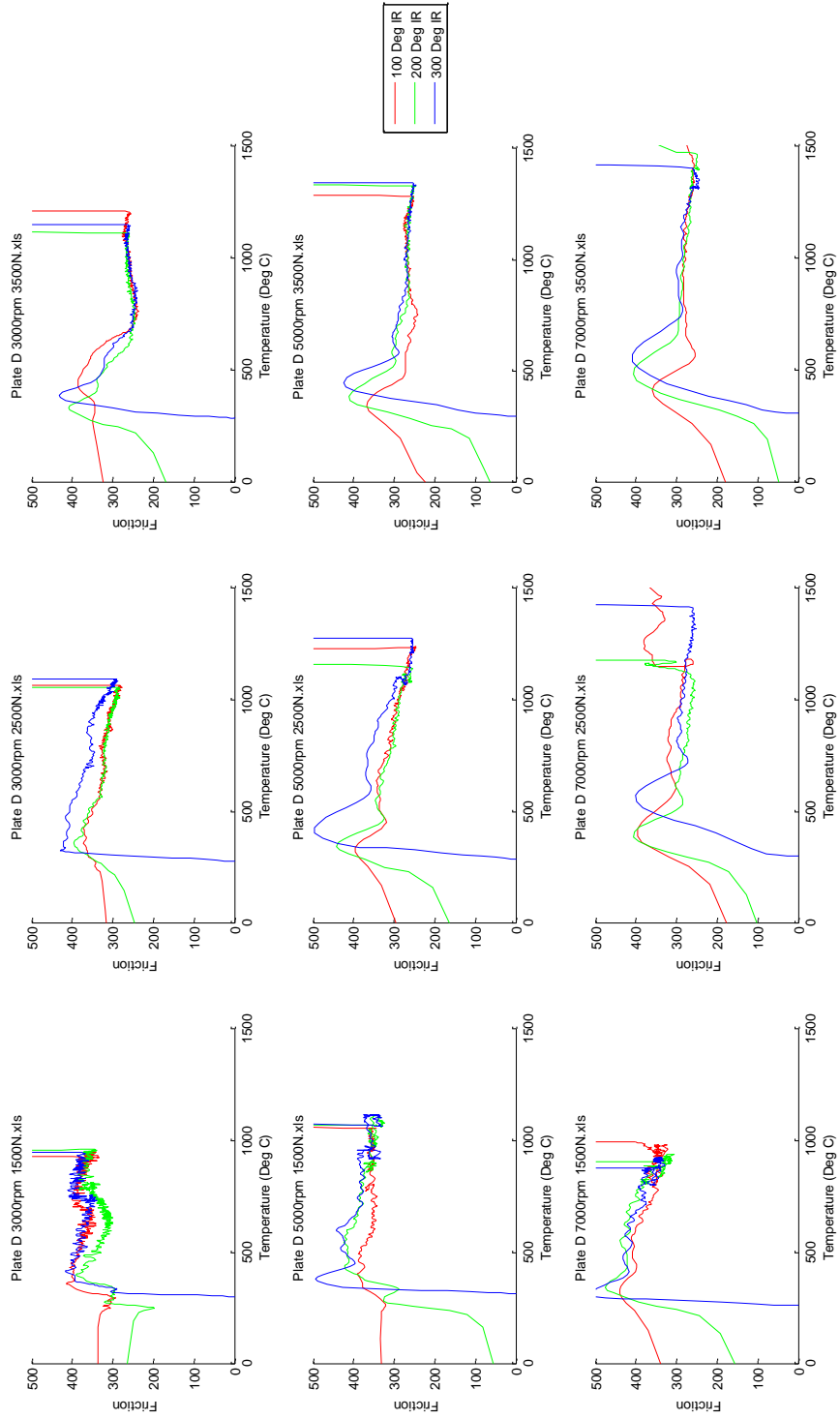
# Appendix I - Friction Effects of Initial Temperature

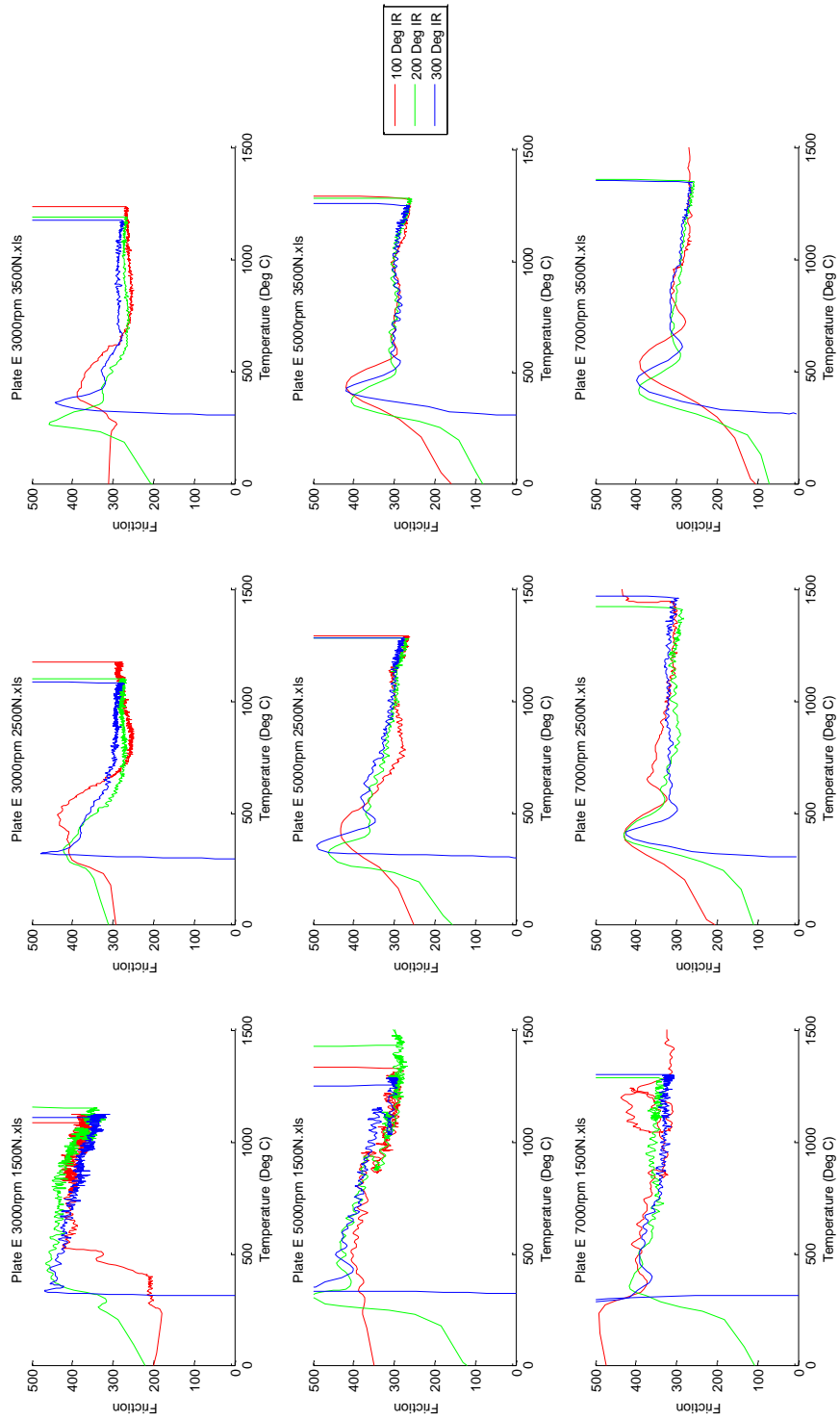


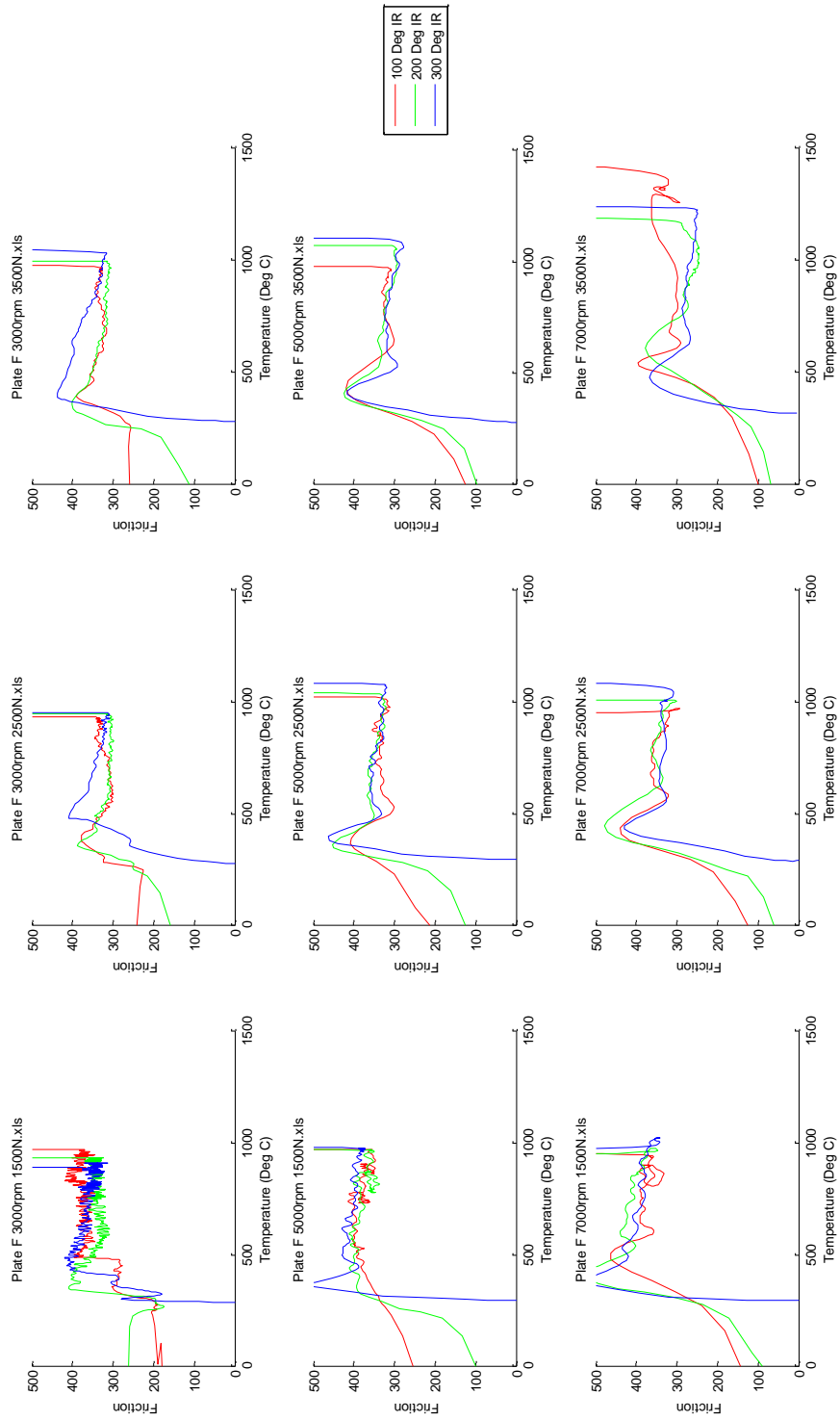


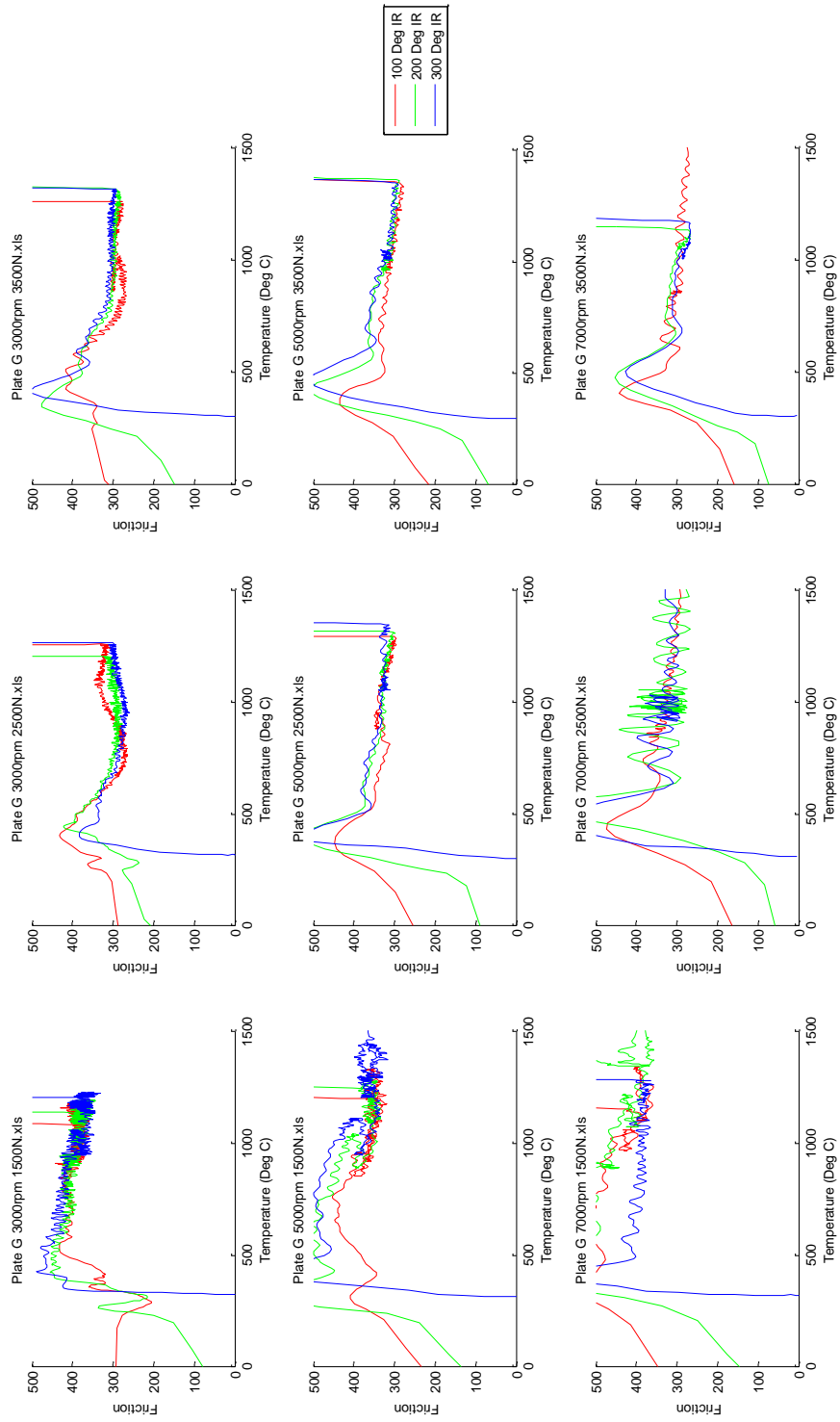


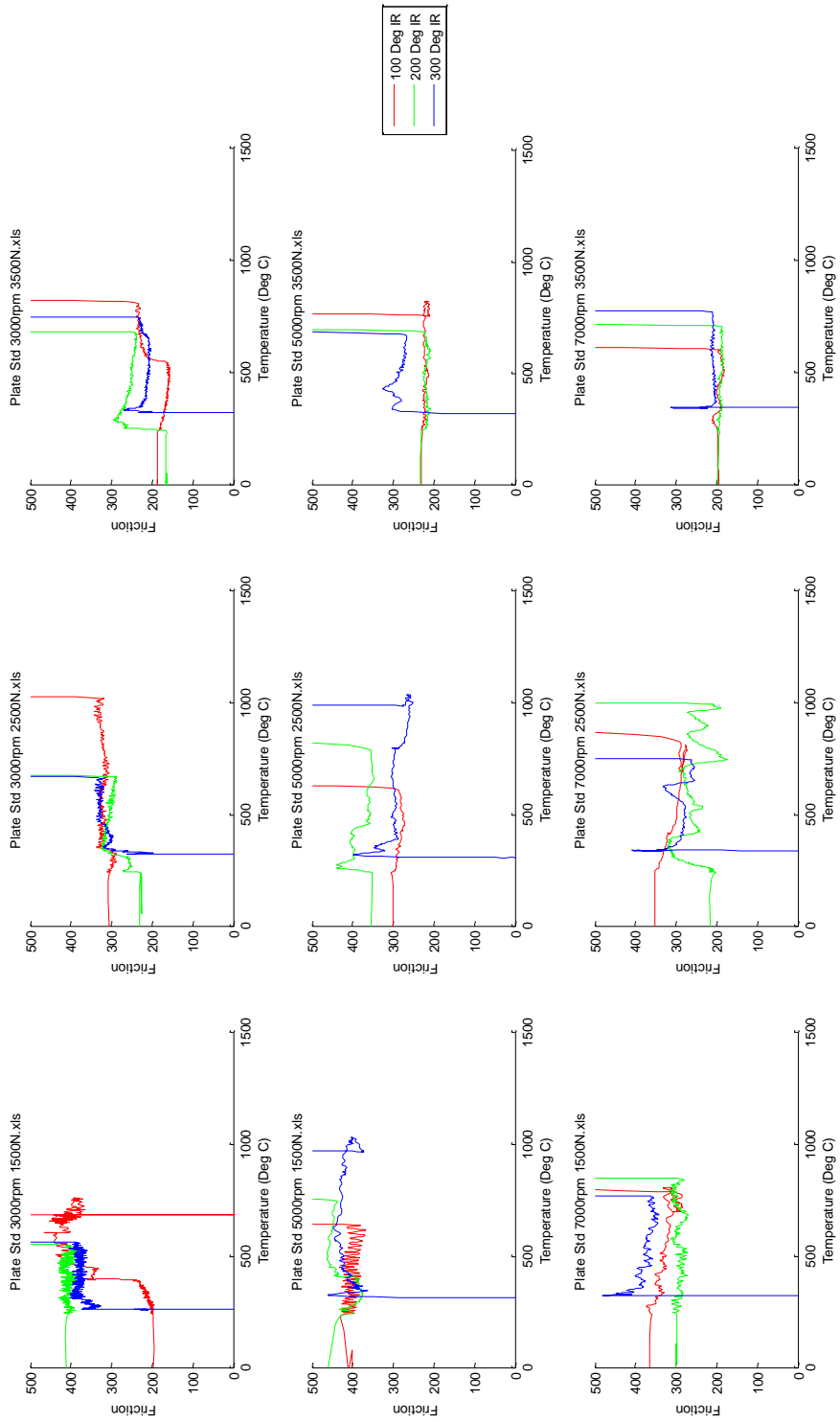




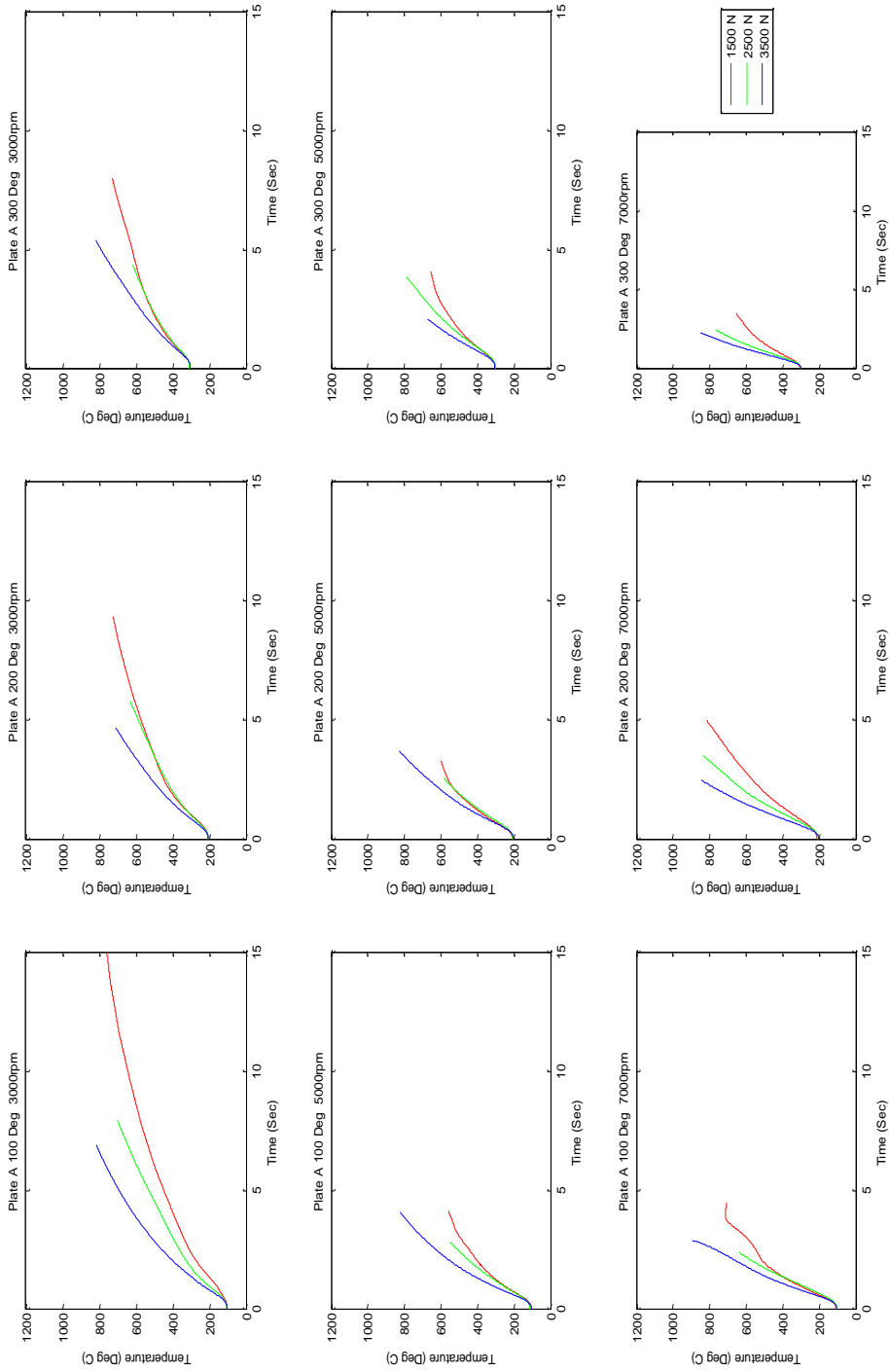


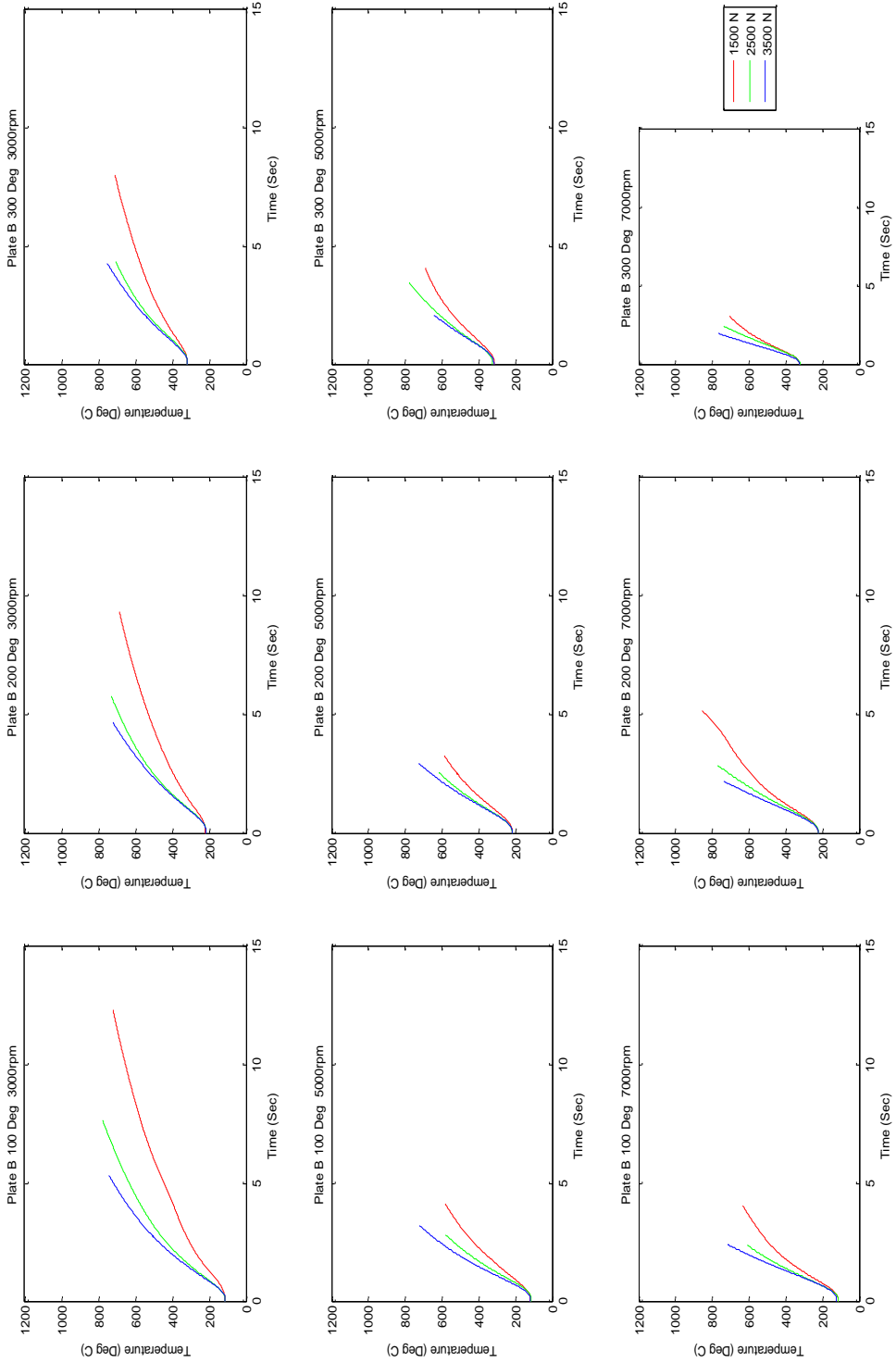


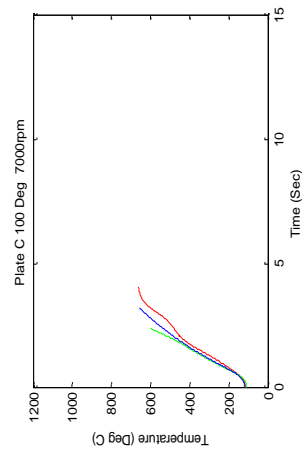
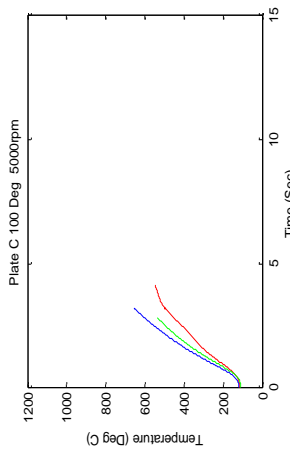
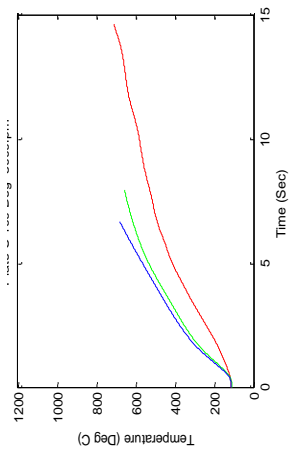
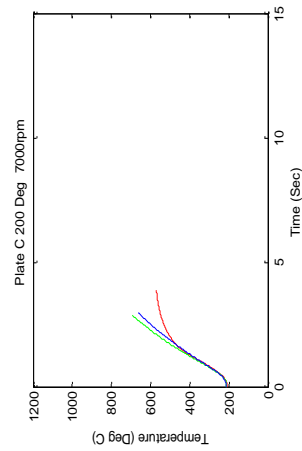
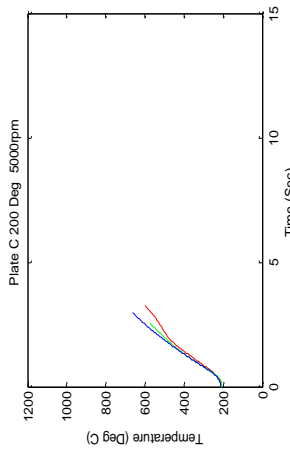
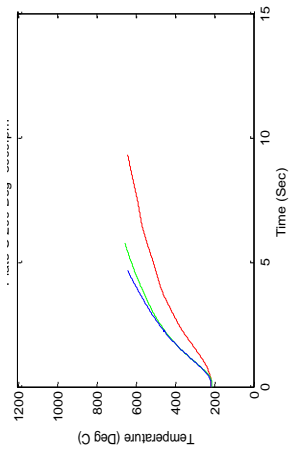
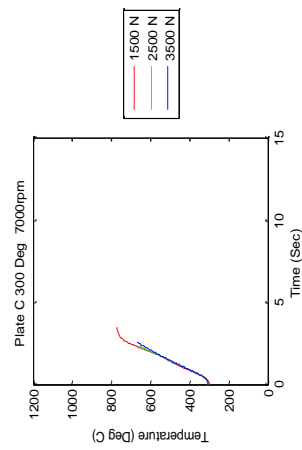
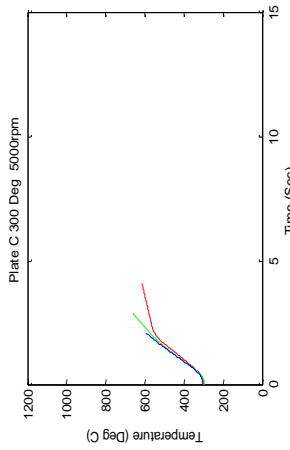
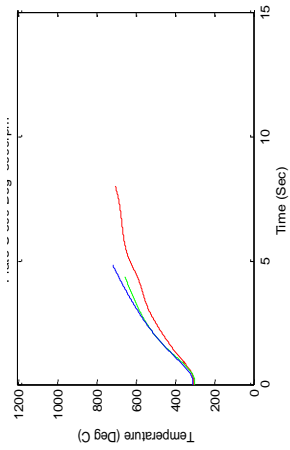




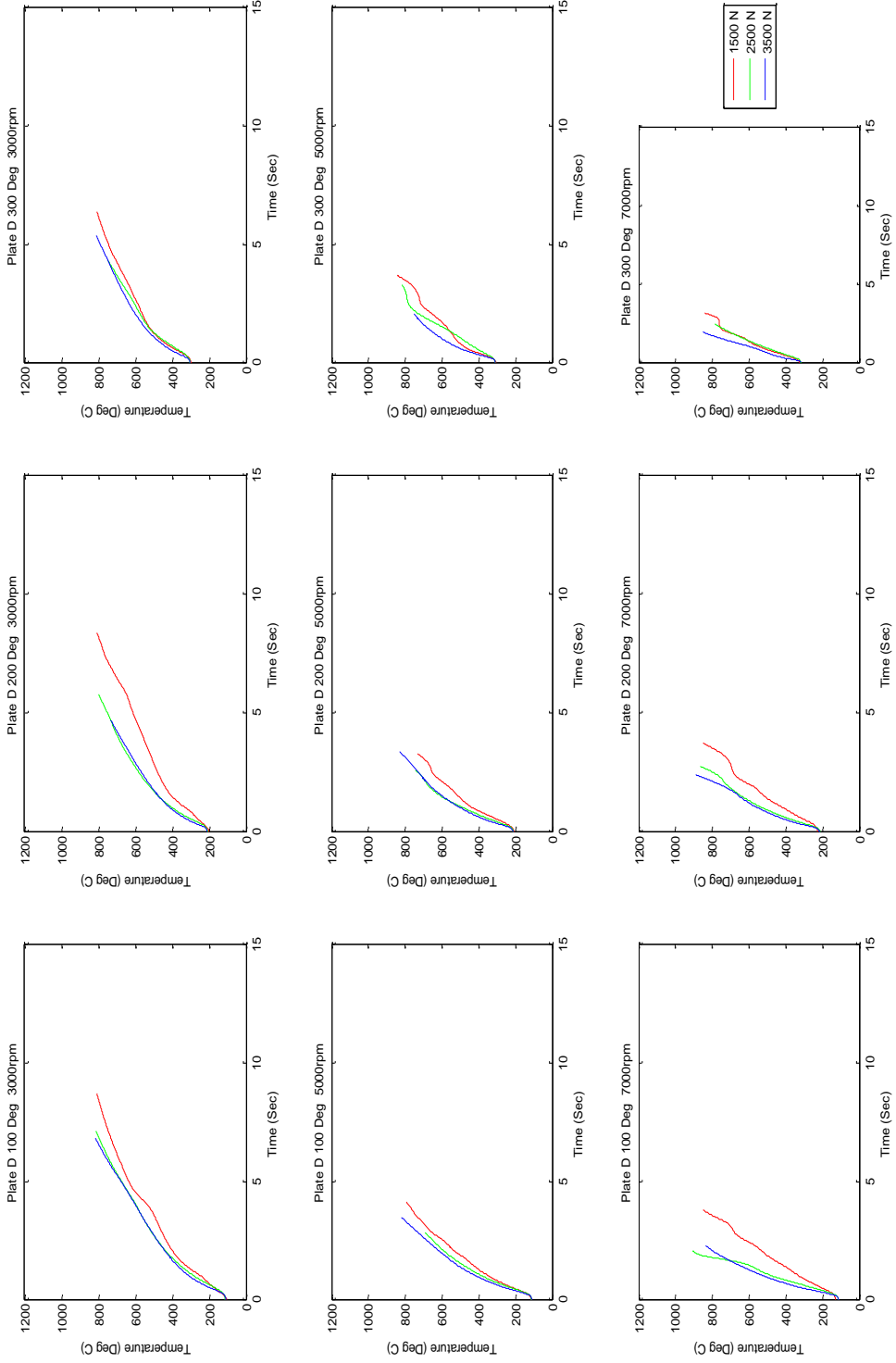
# Appendix J - Temperature Effects of Clamp Load

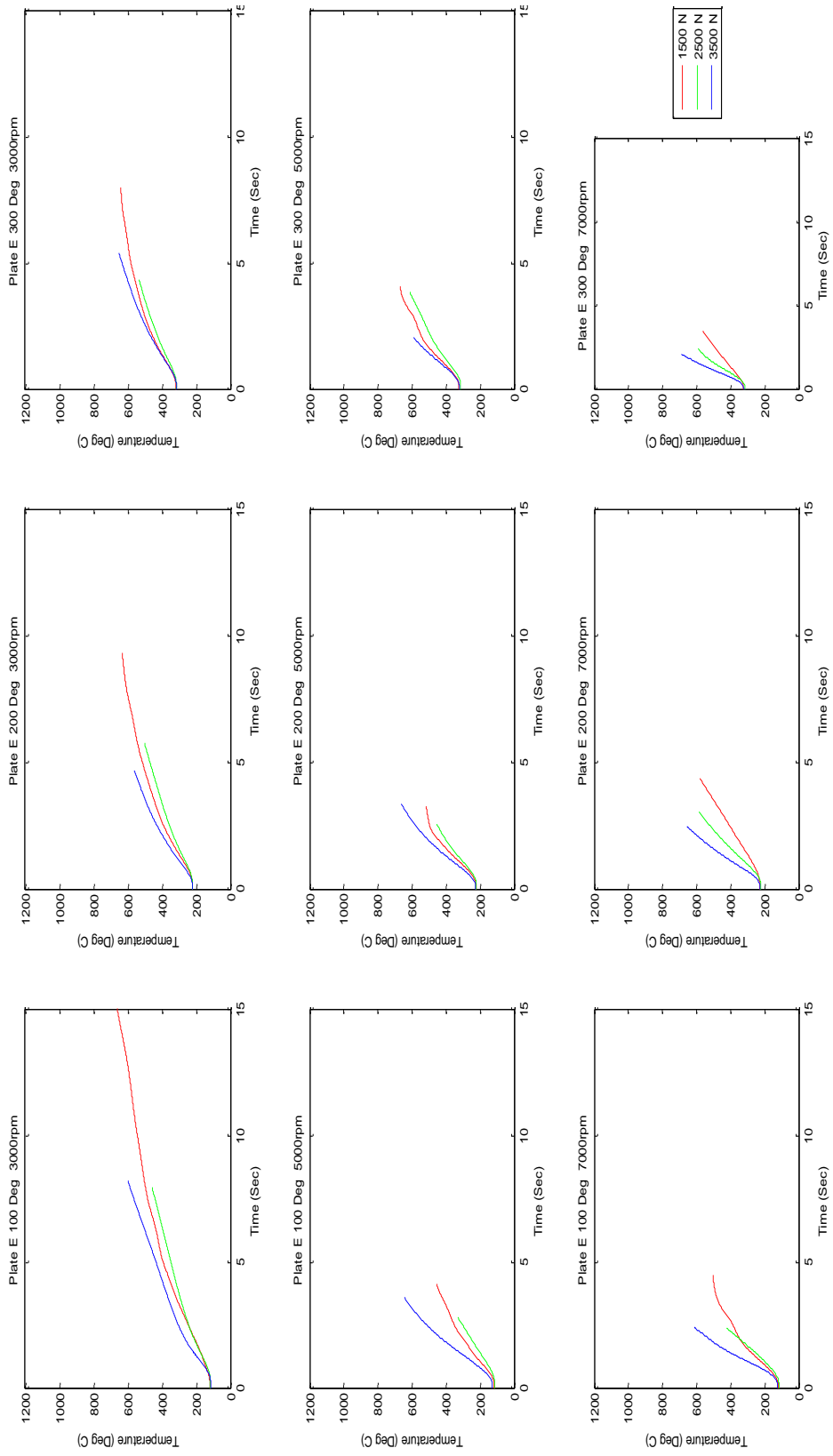


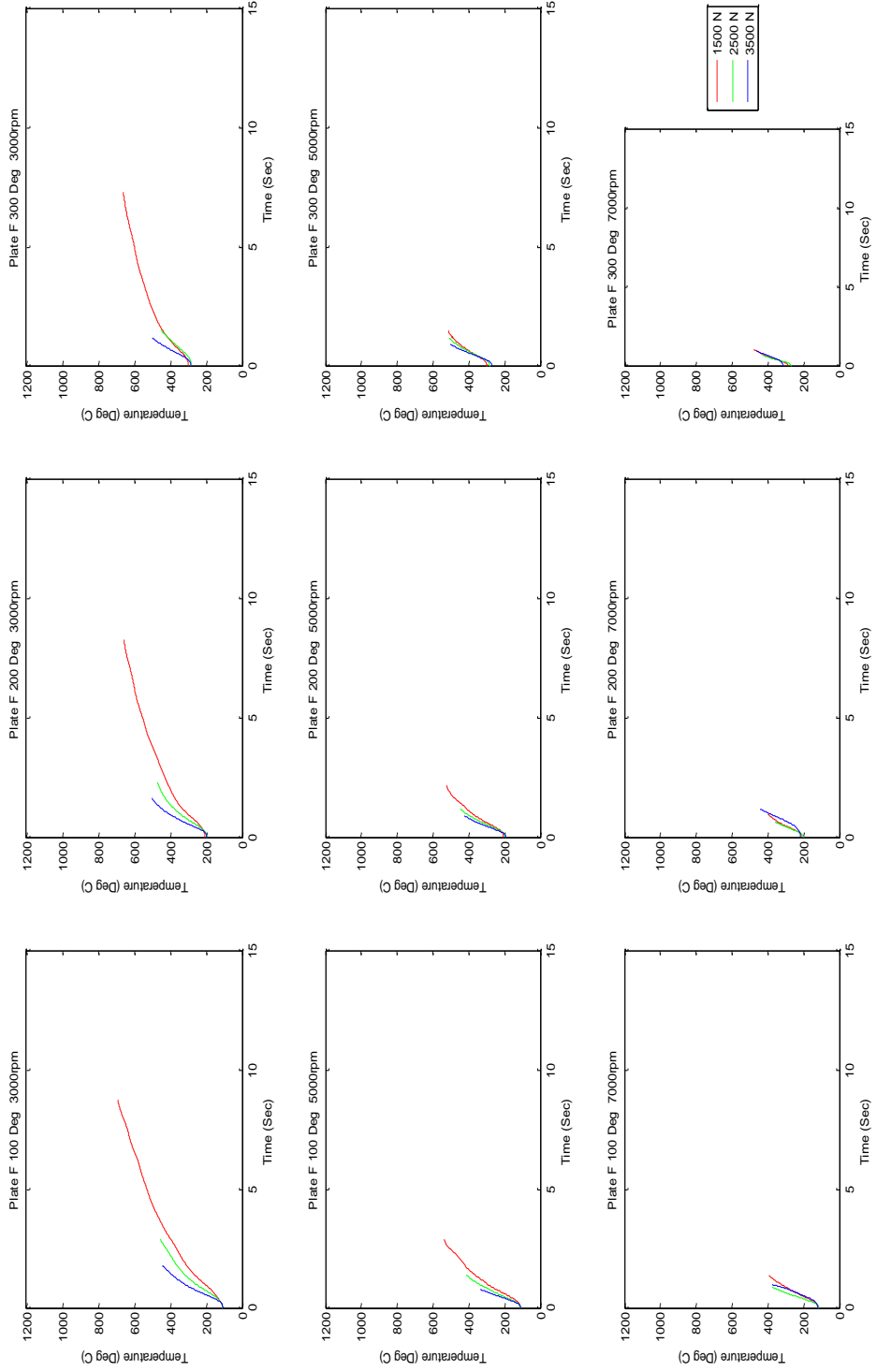


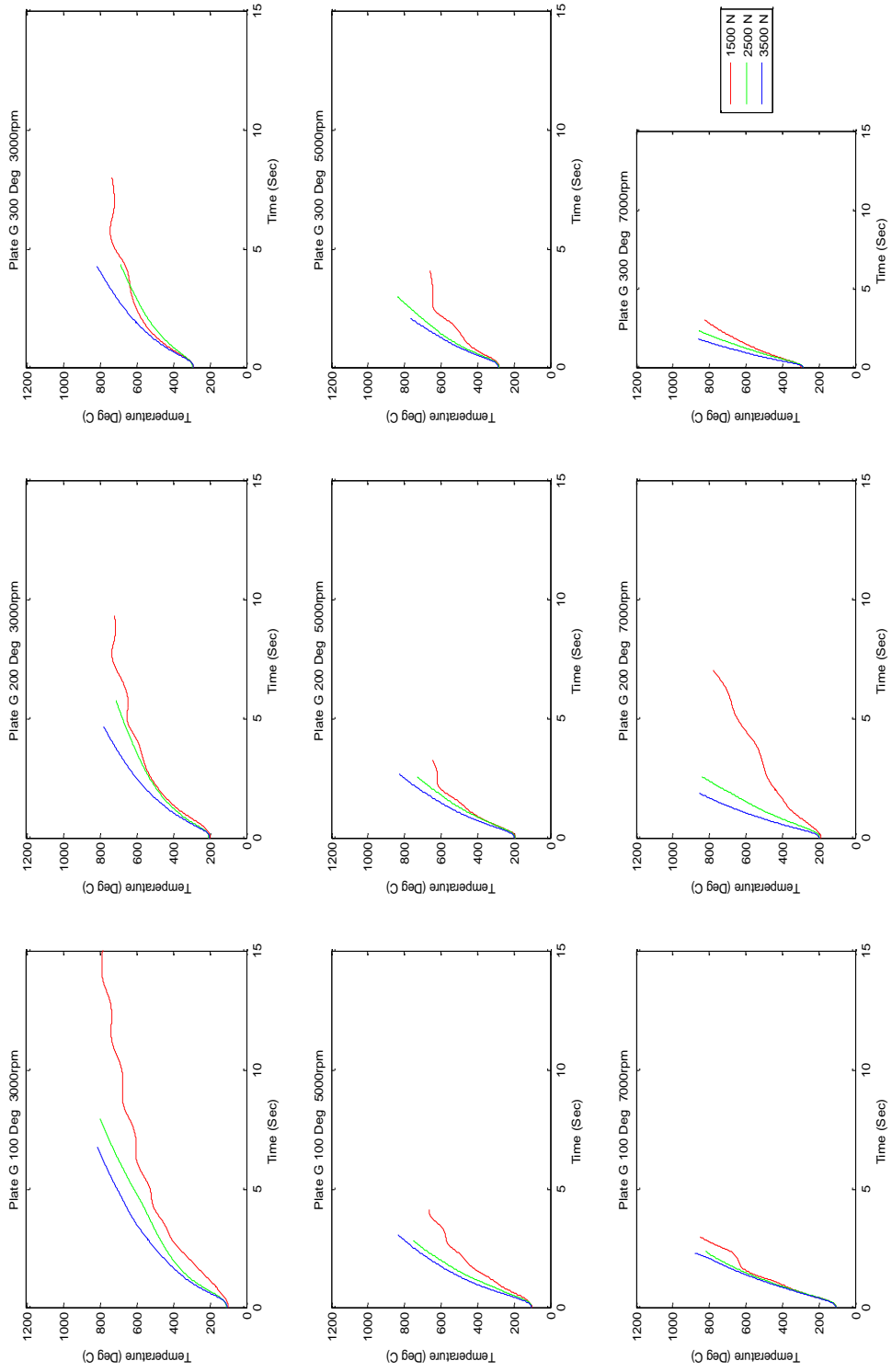


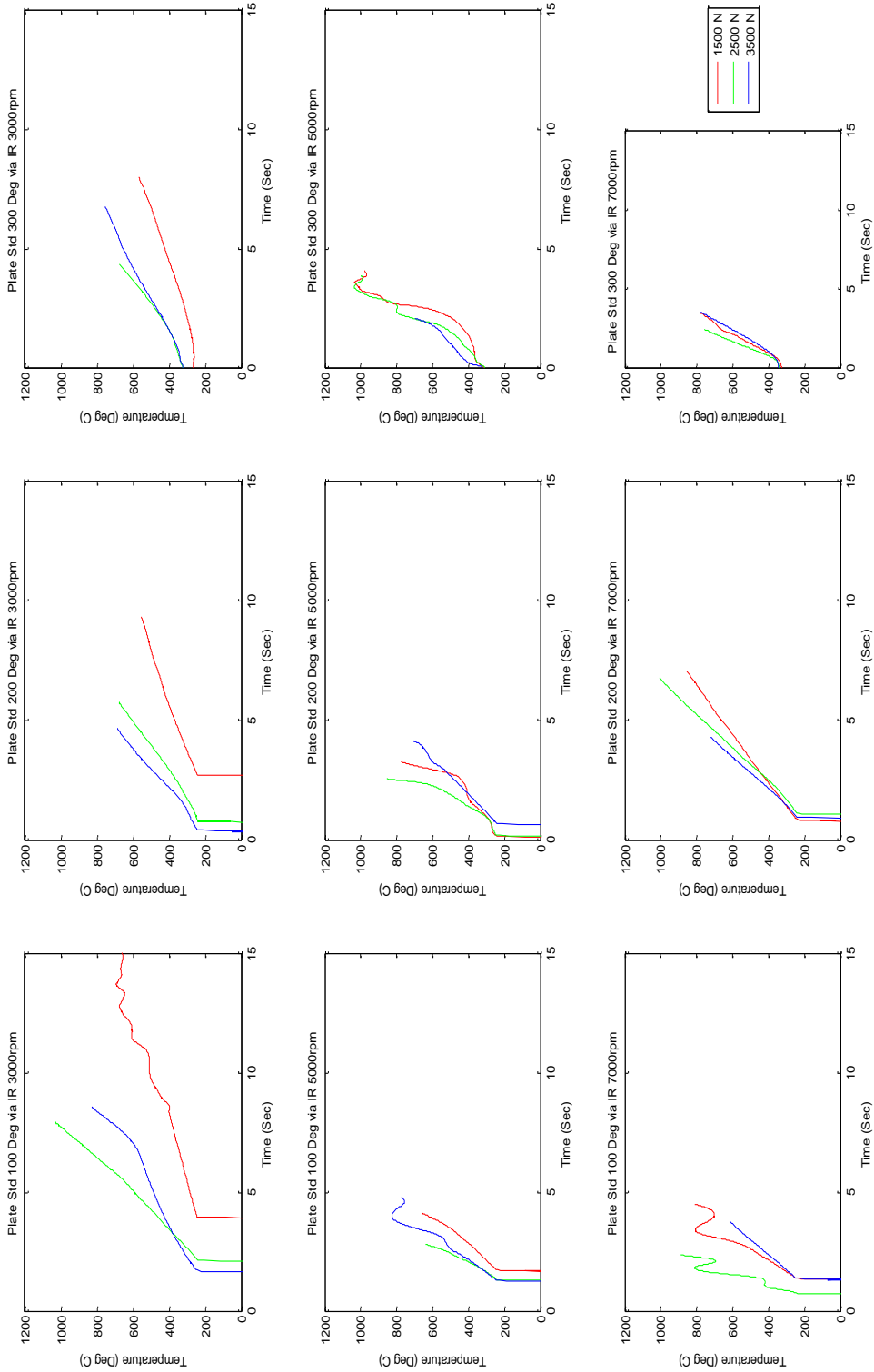


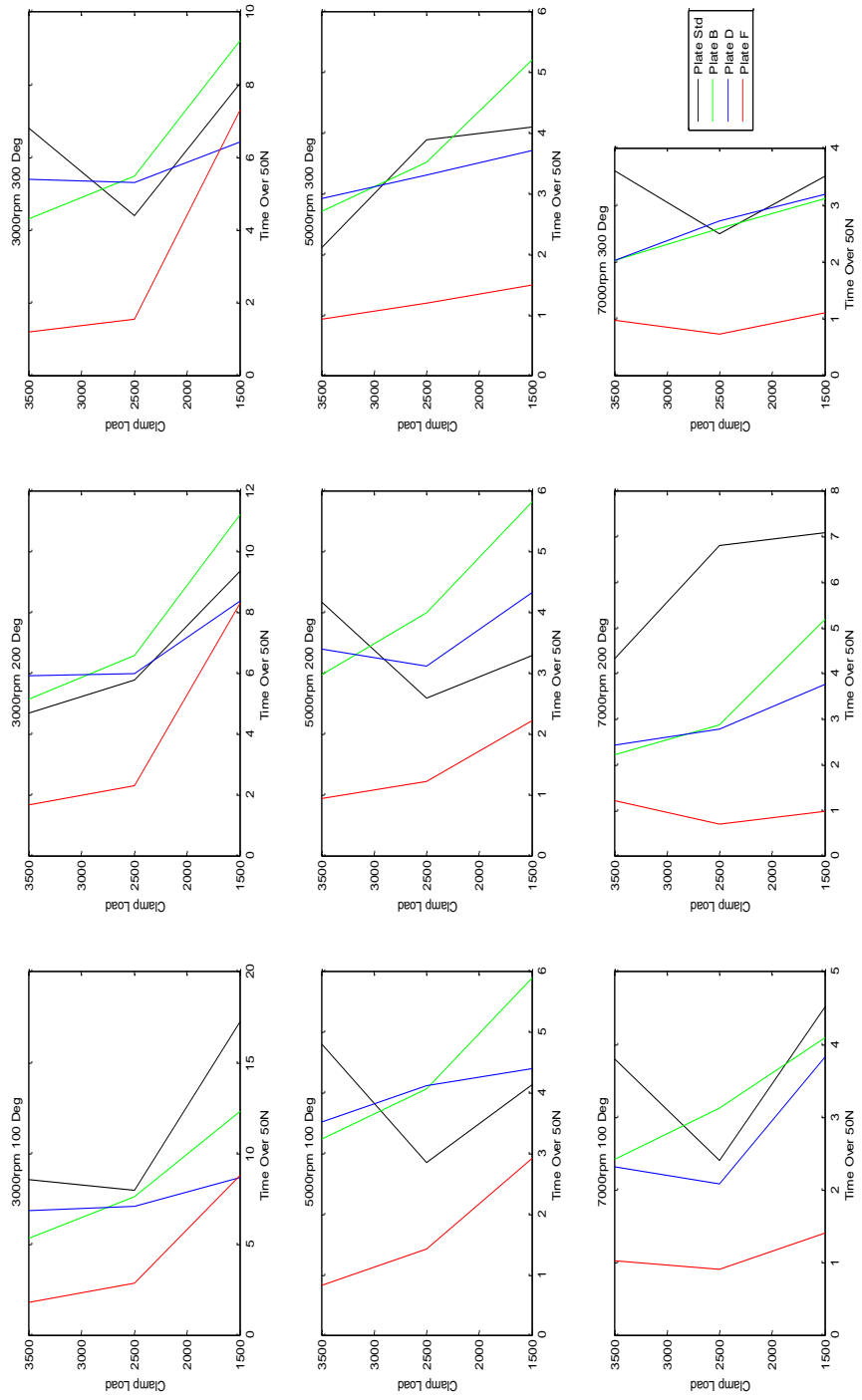




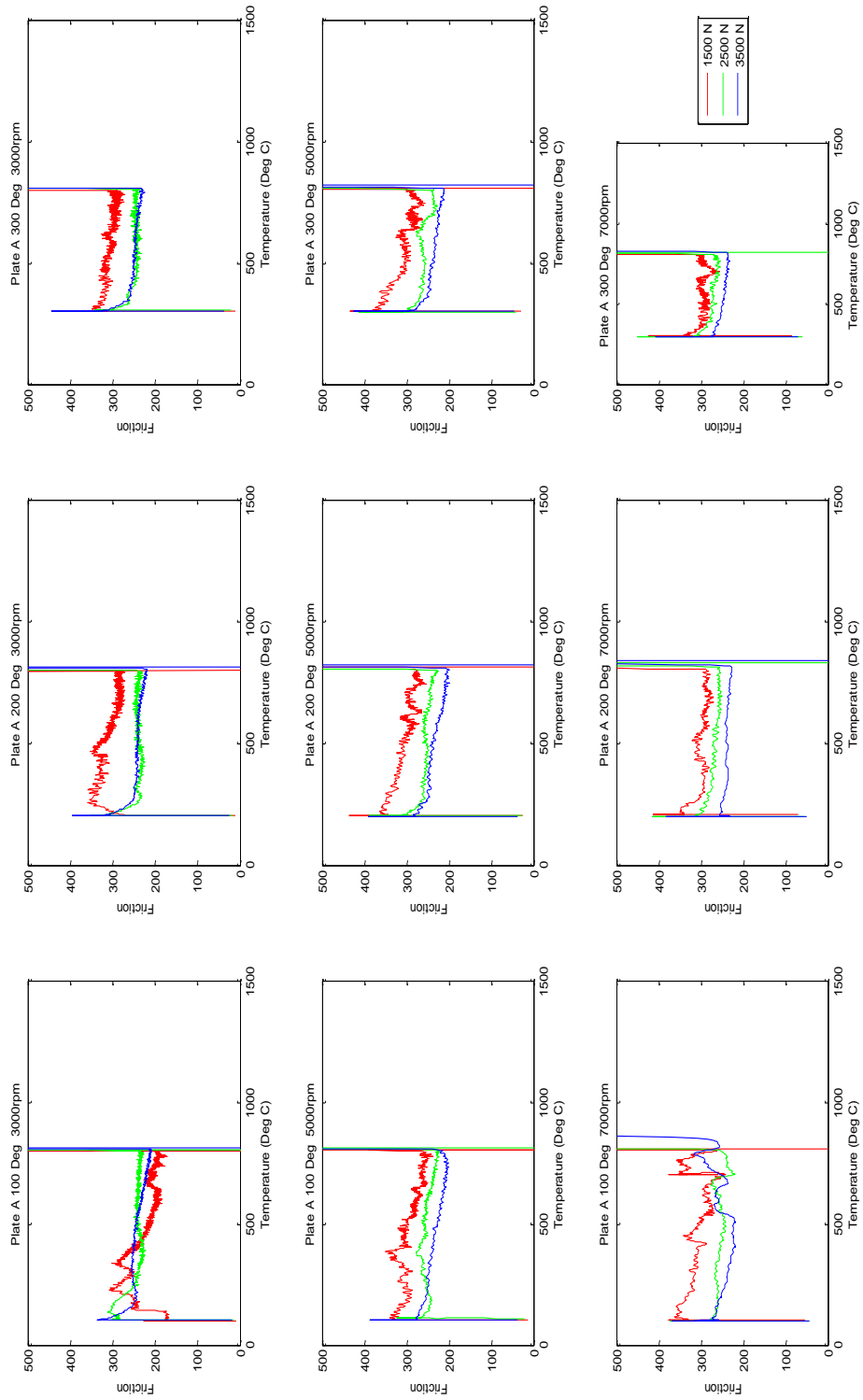


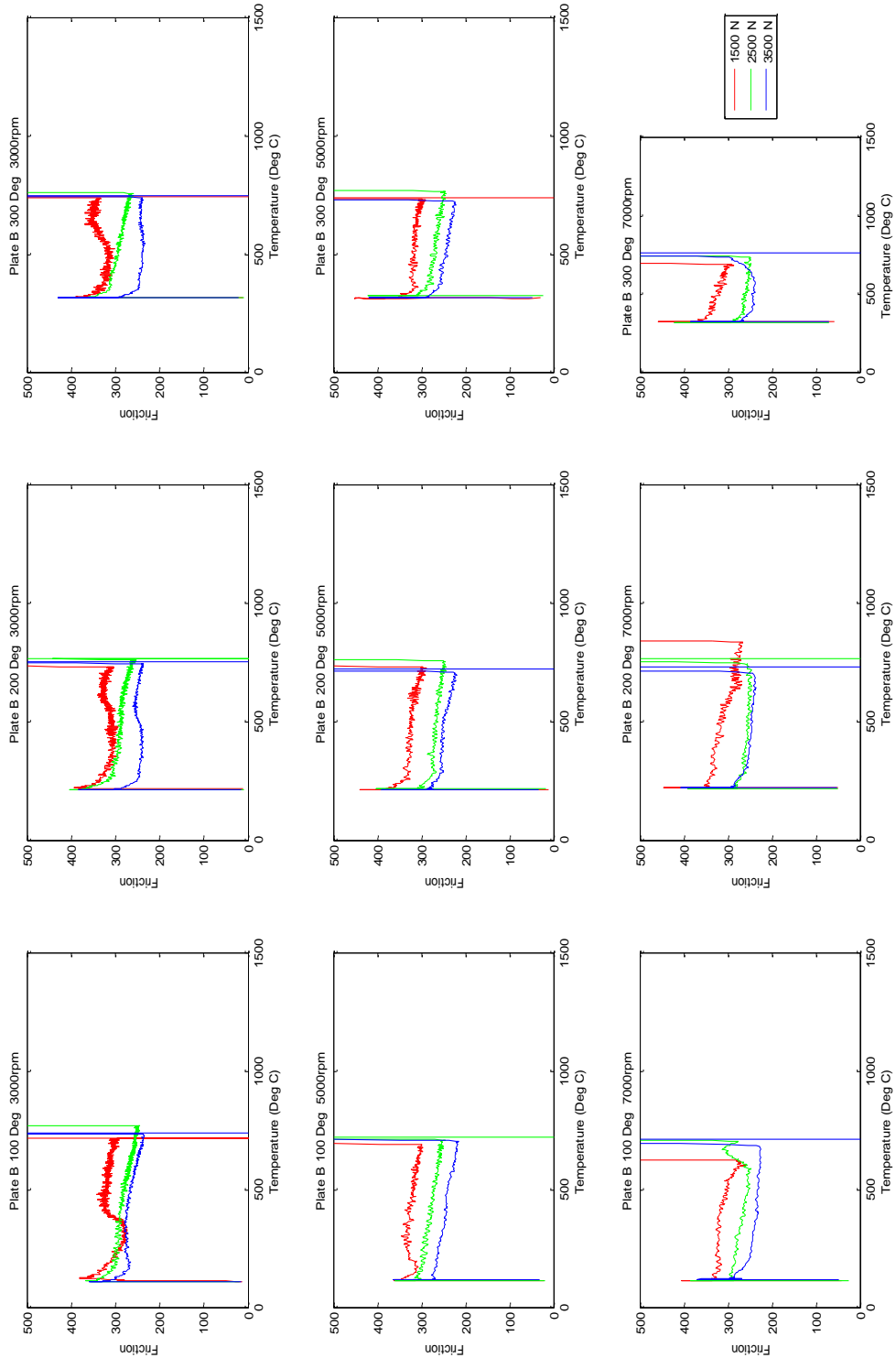




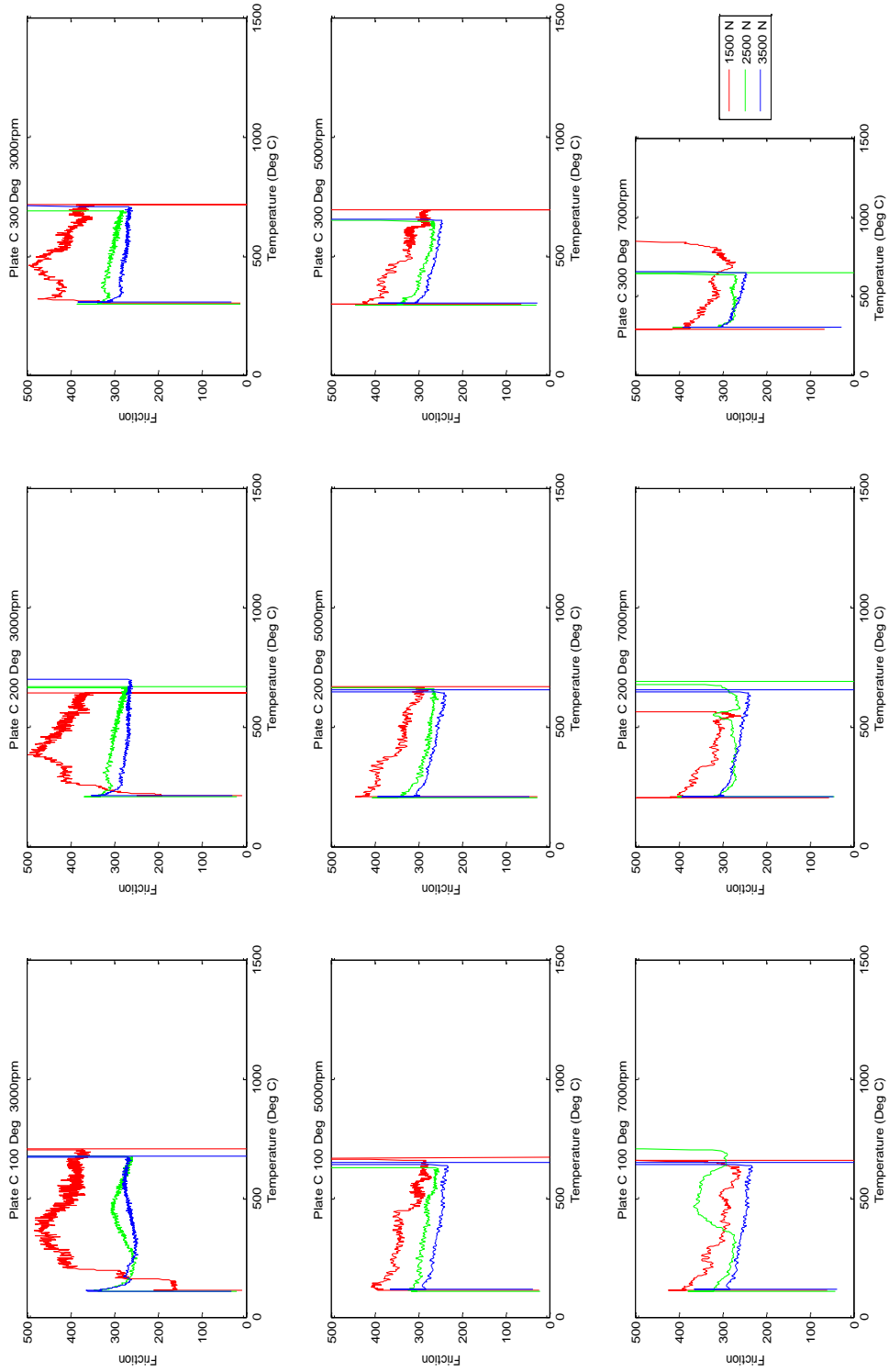


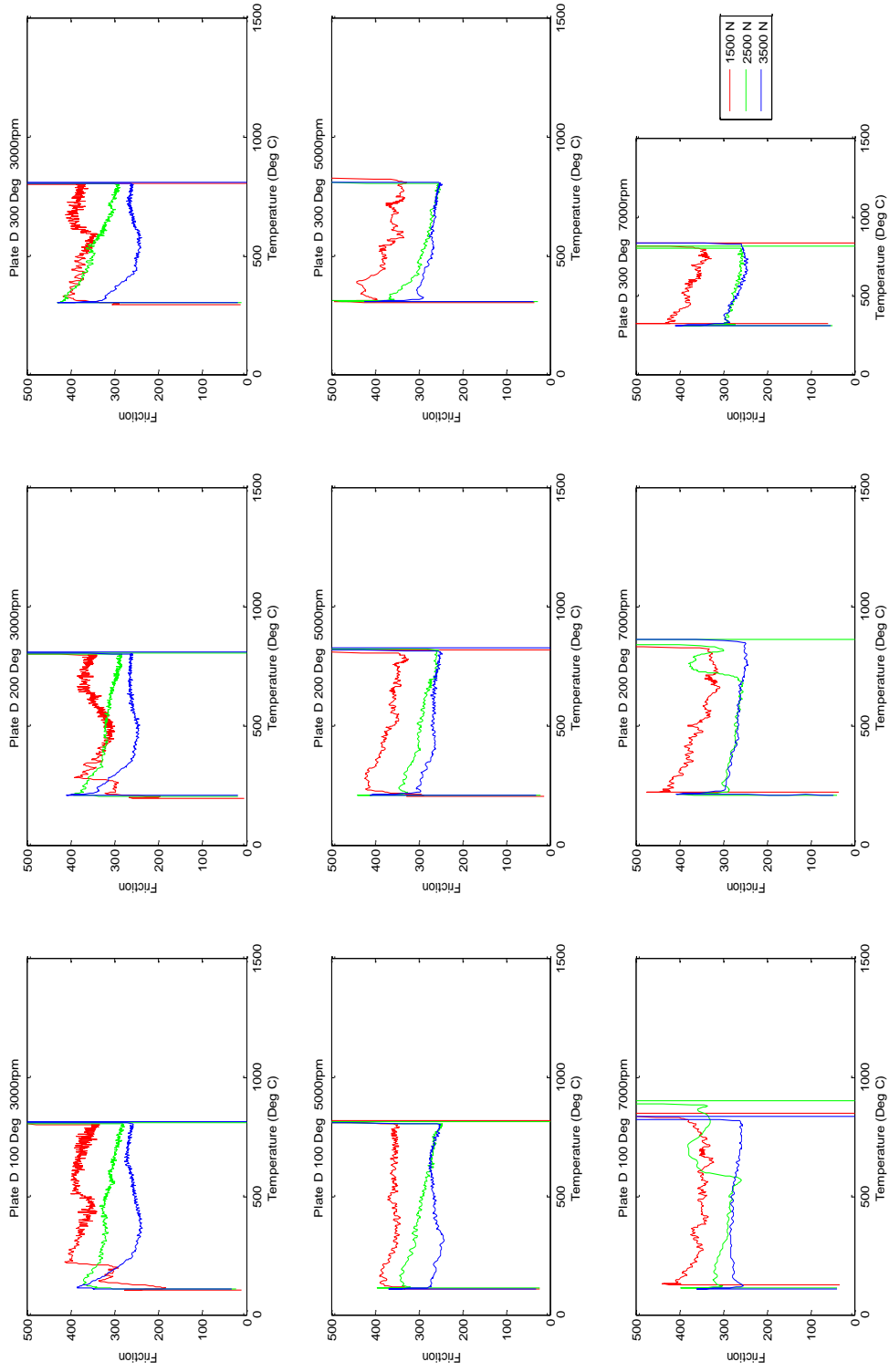
# Appendix K - Friction Effects of Clamp Load

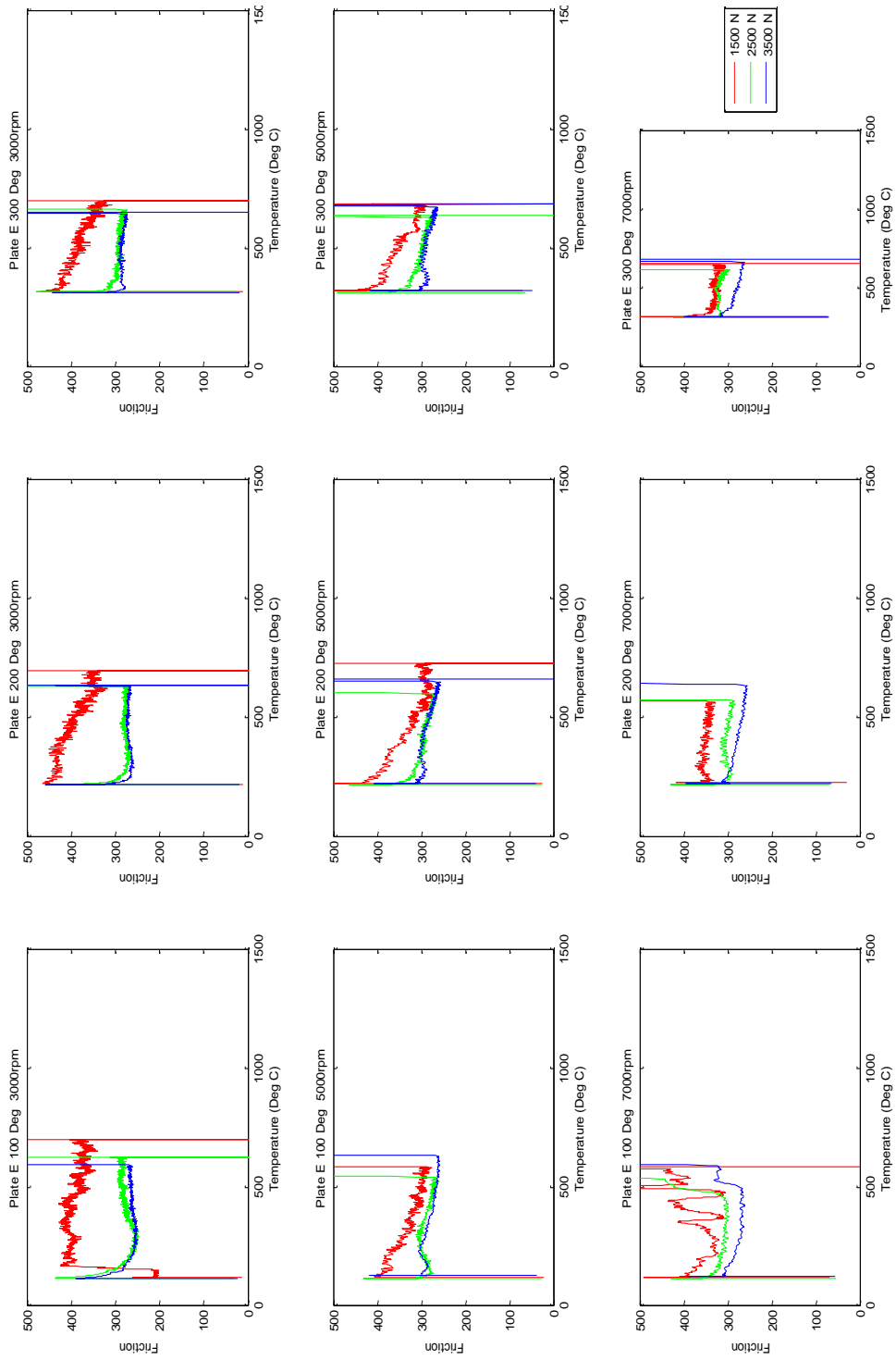


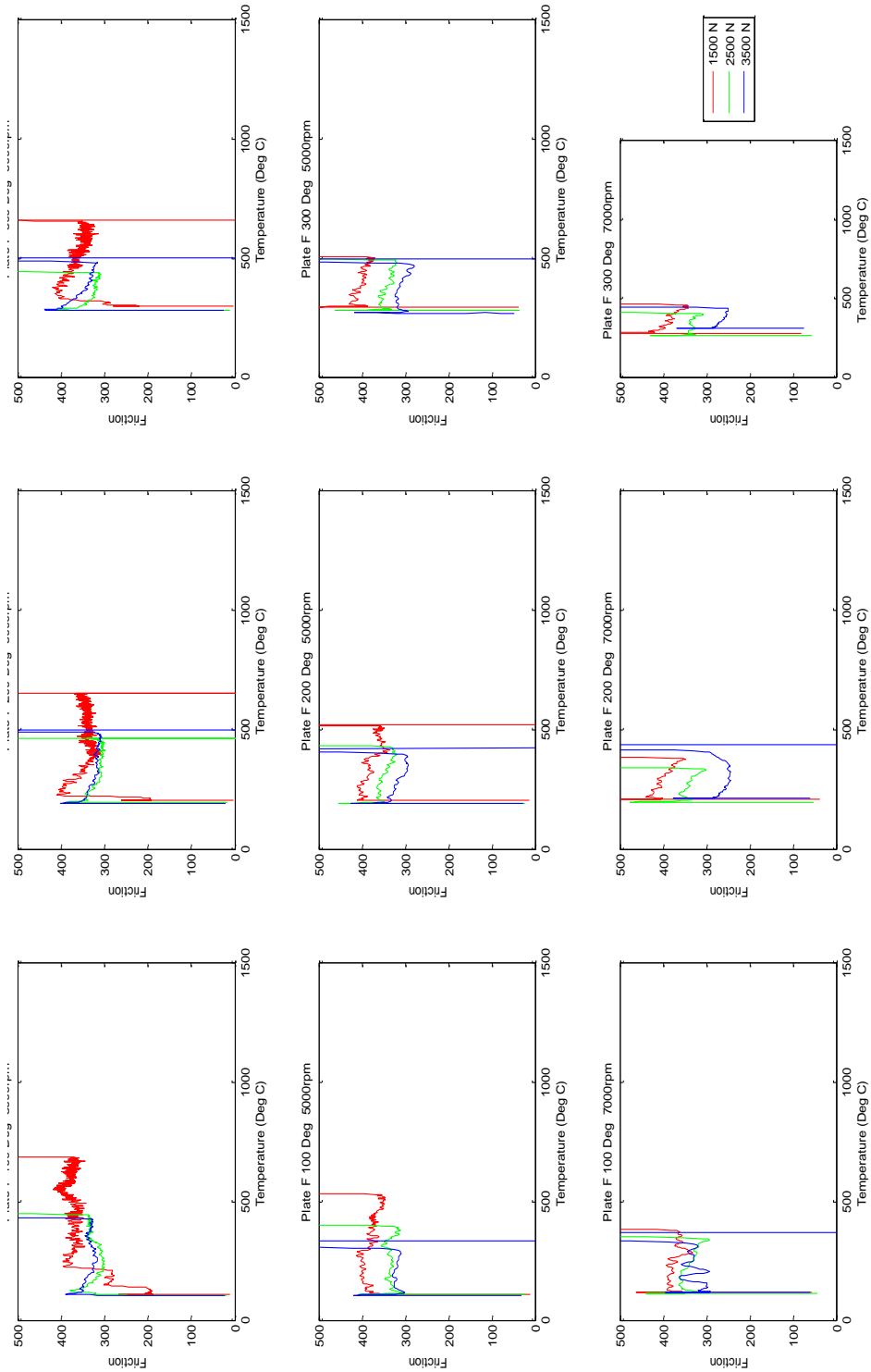


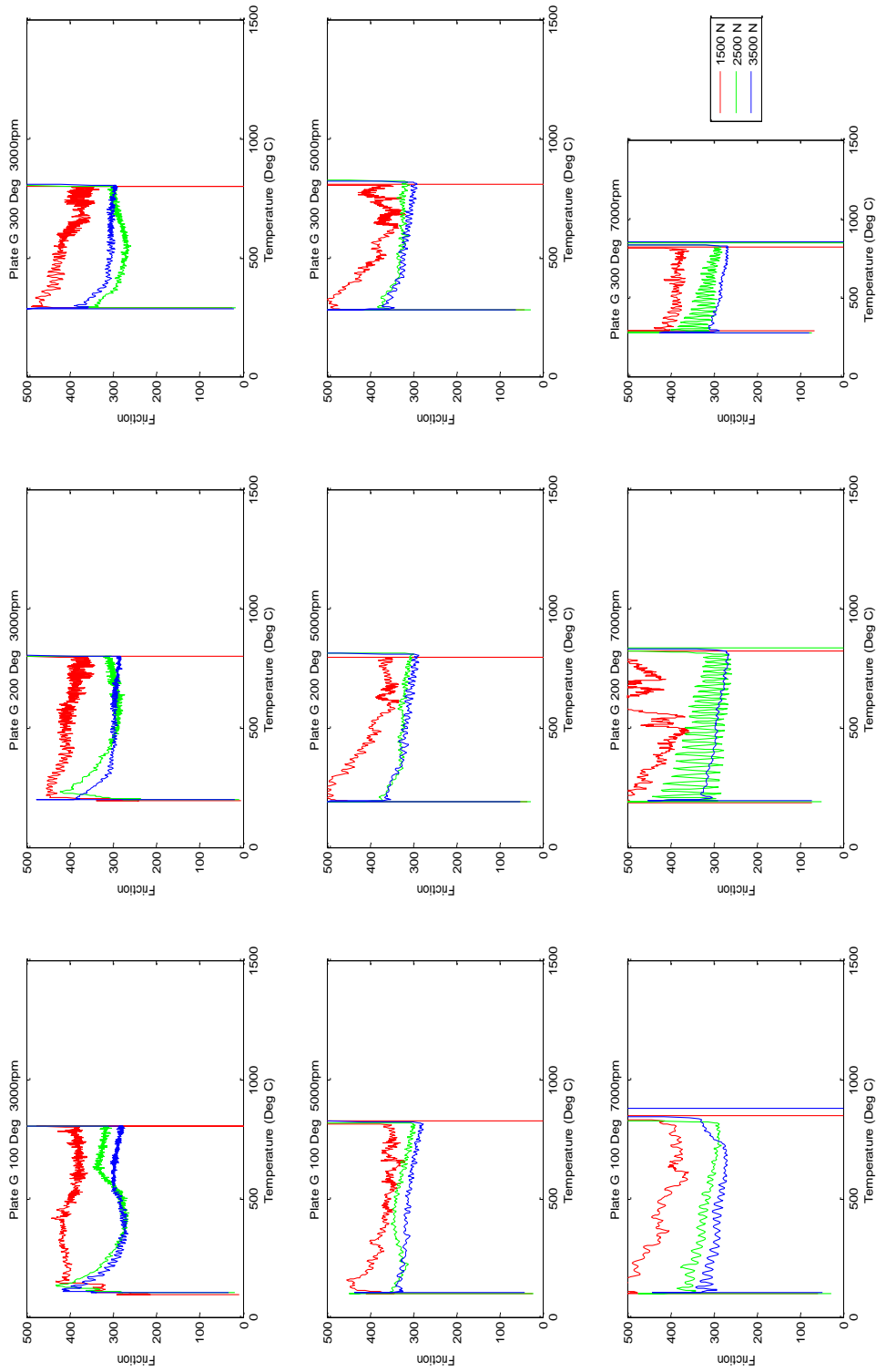


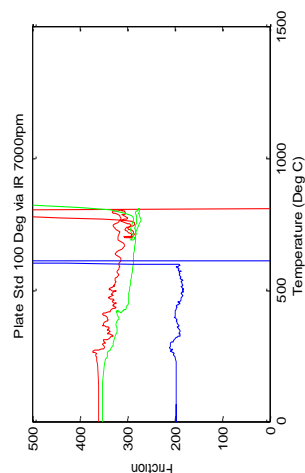
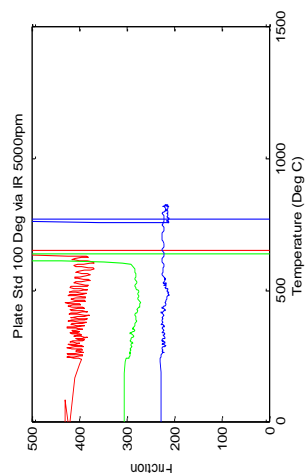
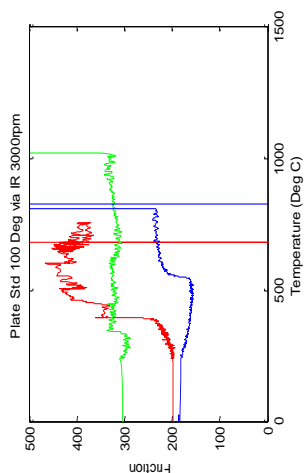
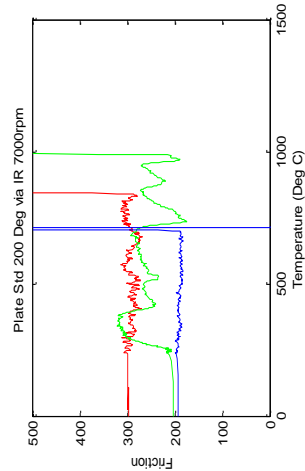
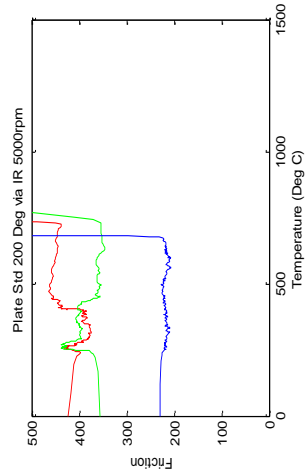
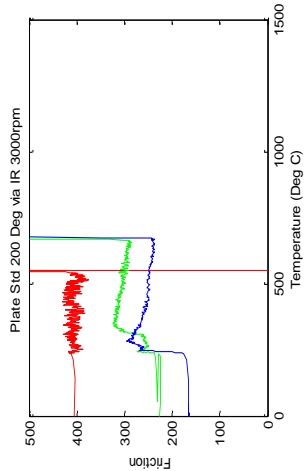
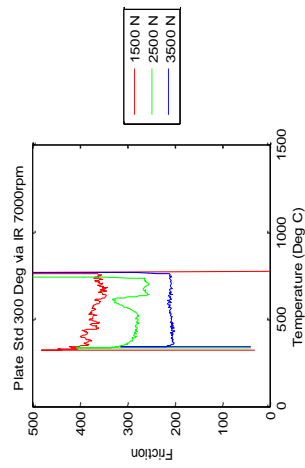
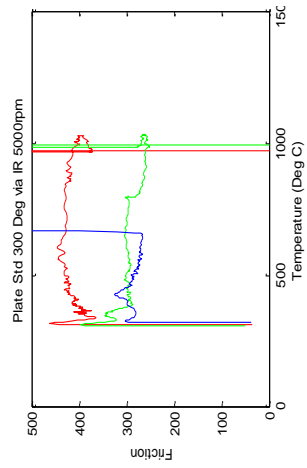
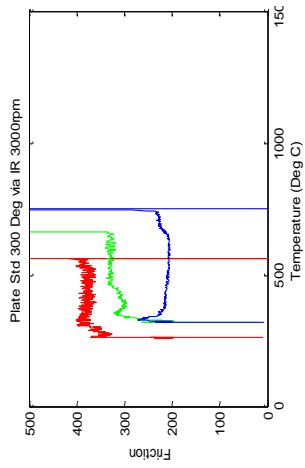




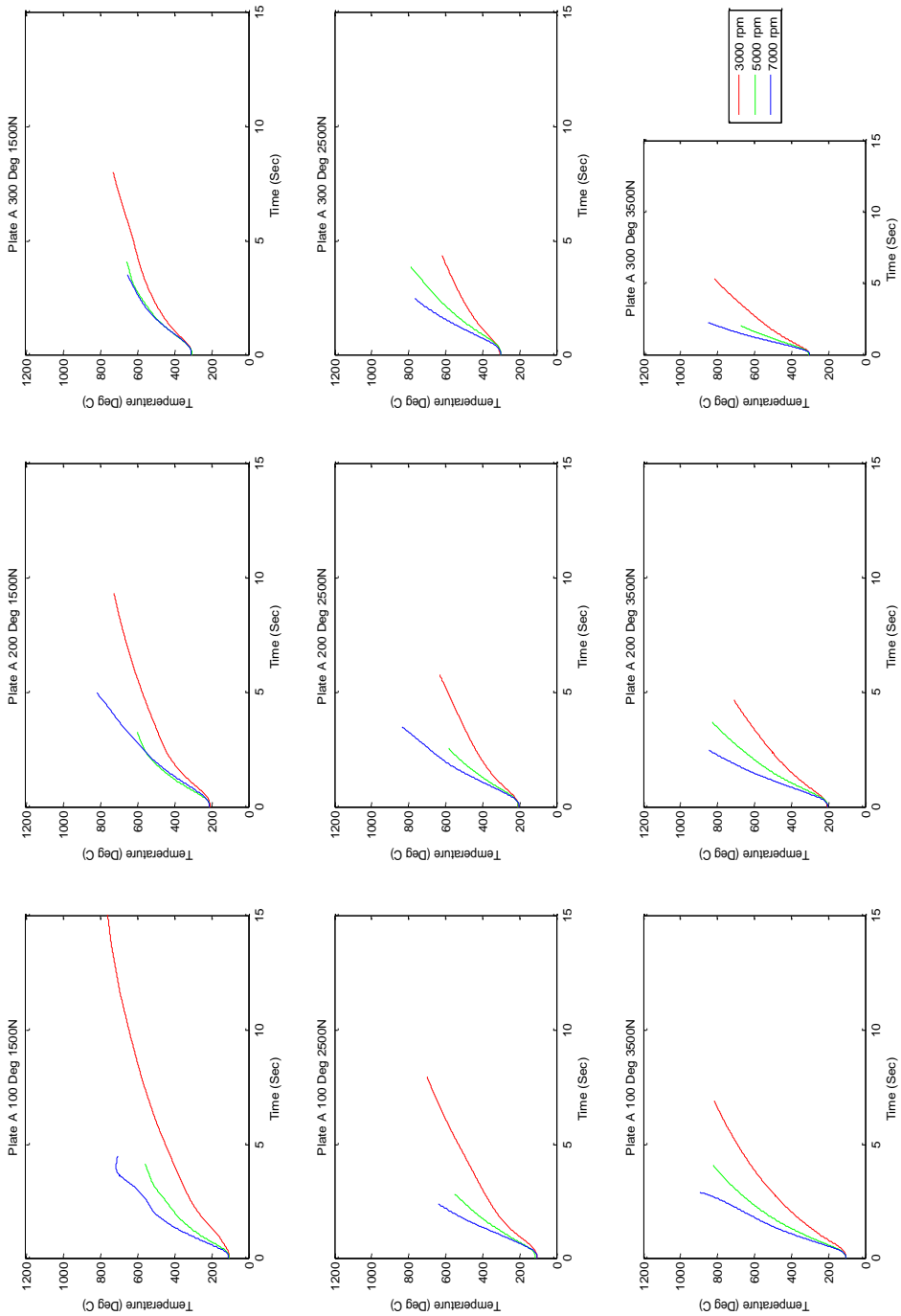


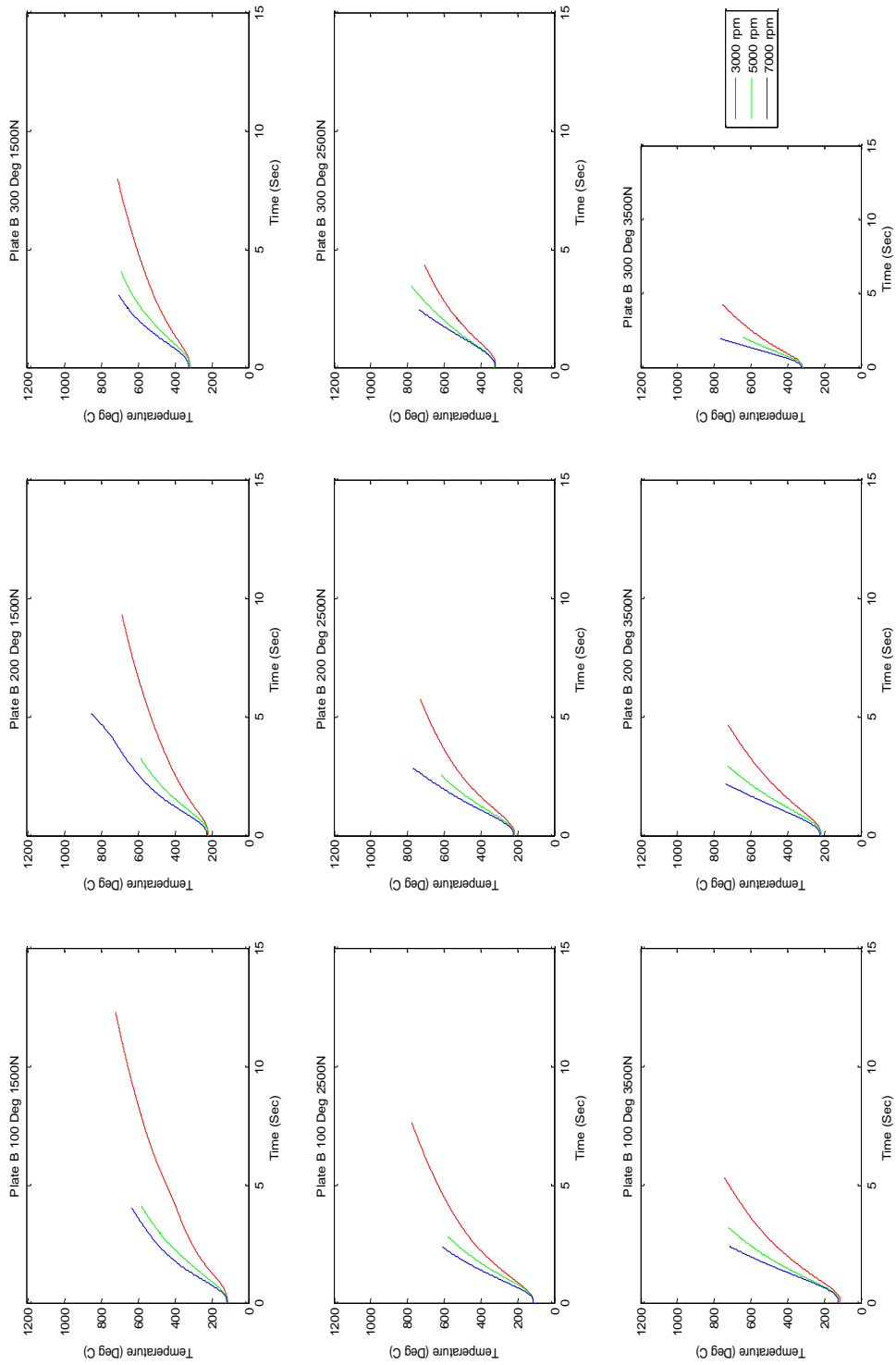




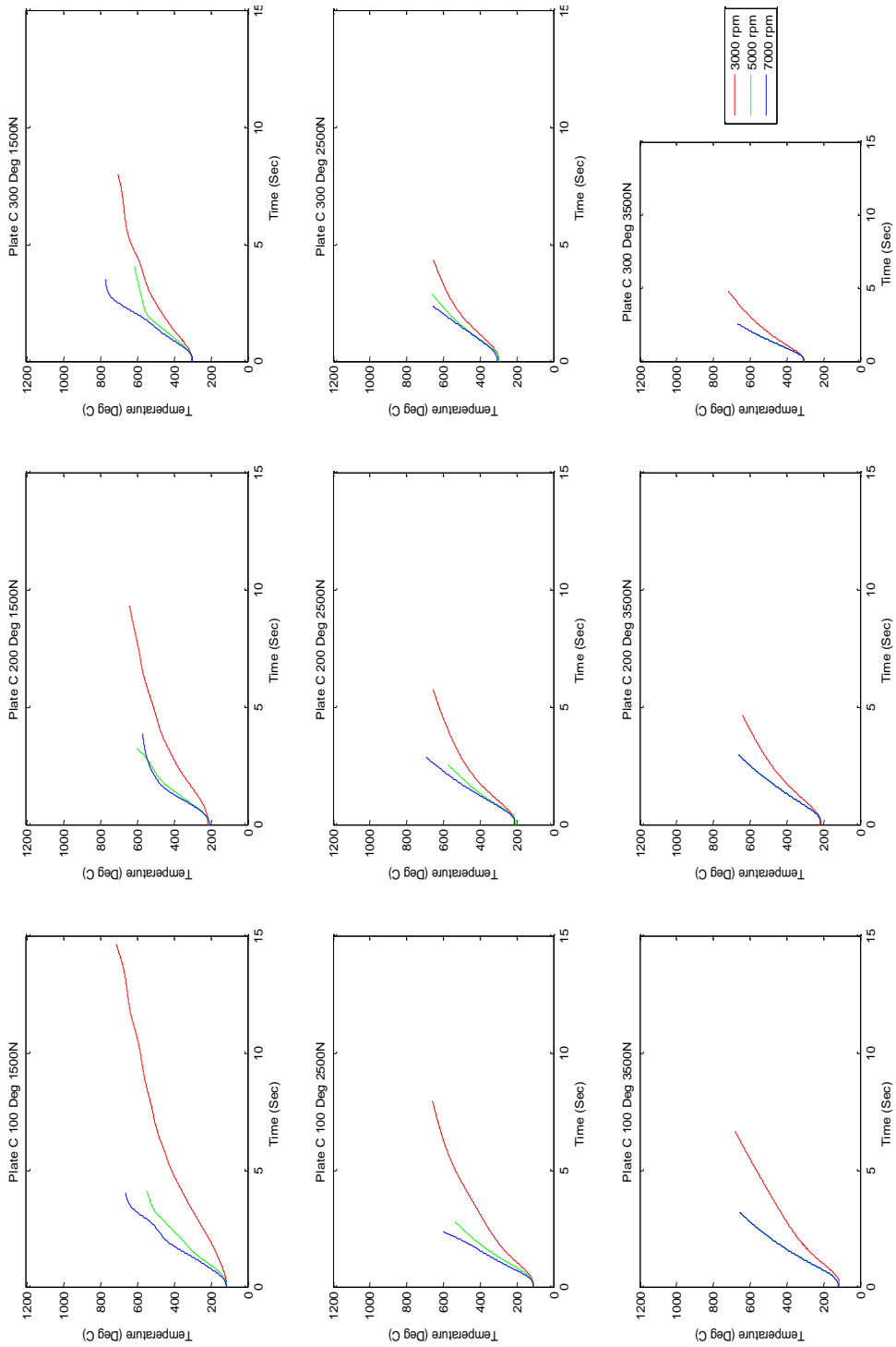


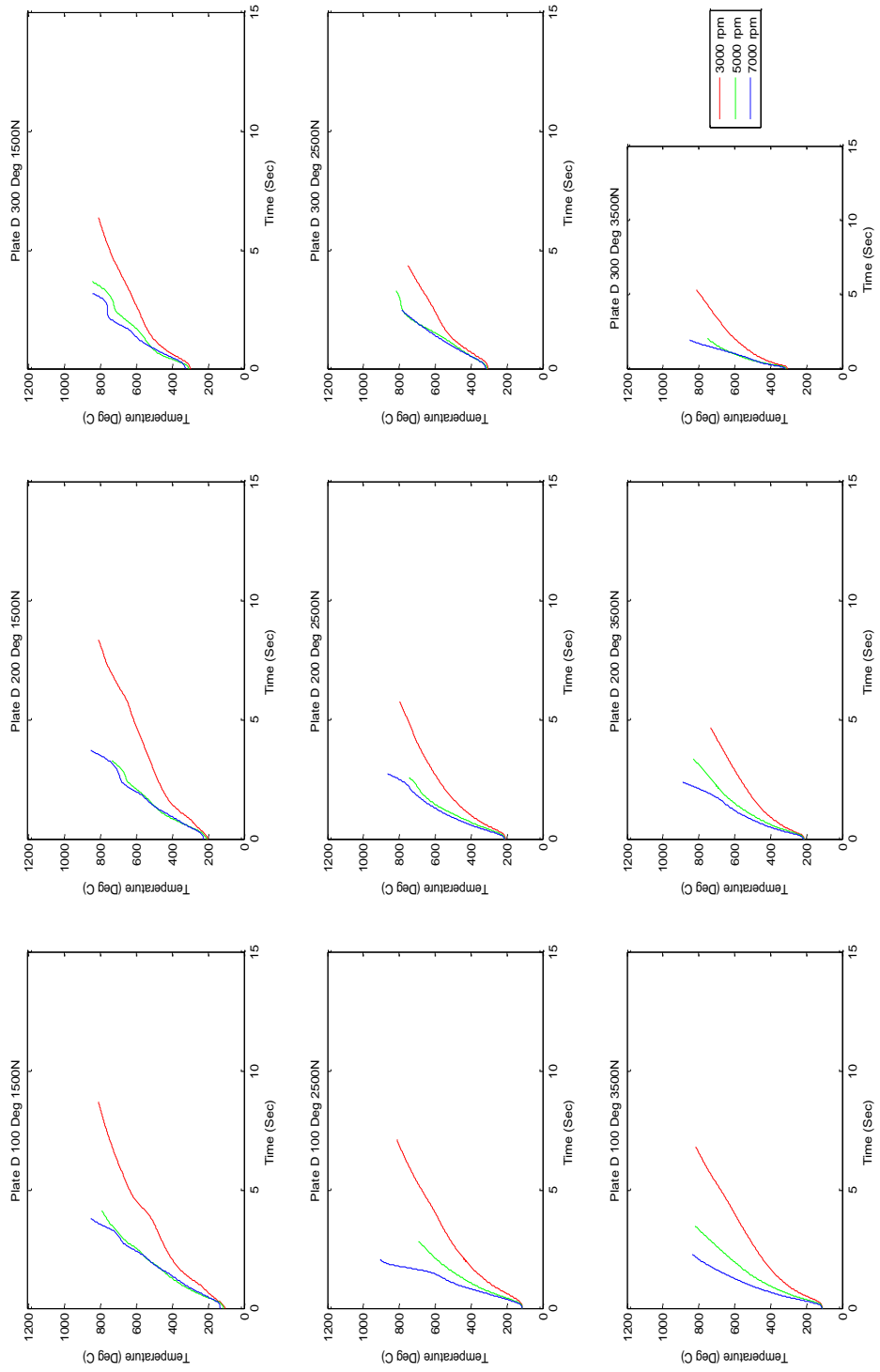
# Appendix L - Temperature Effects of Input Speed

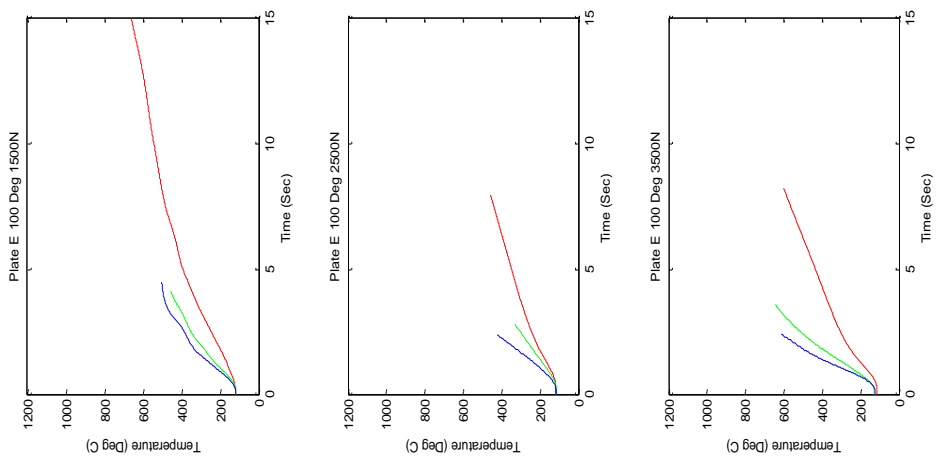
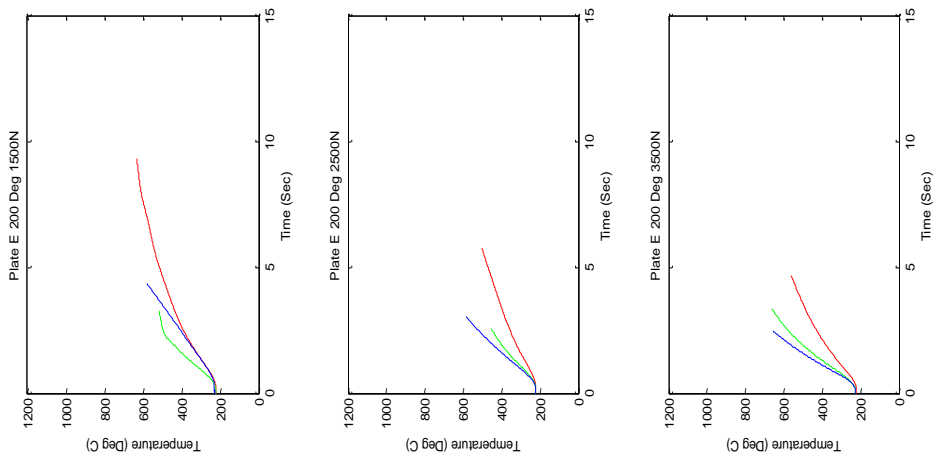
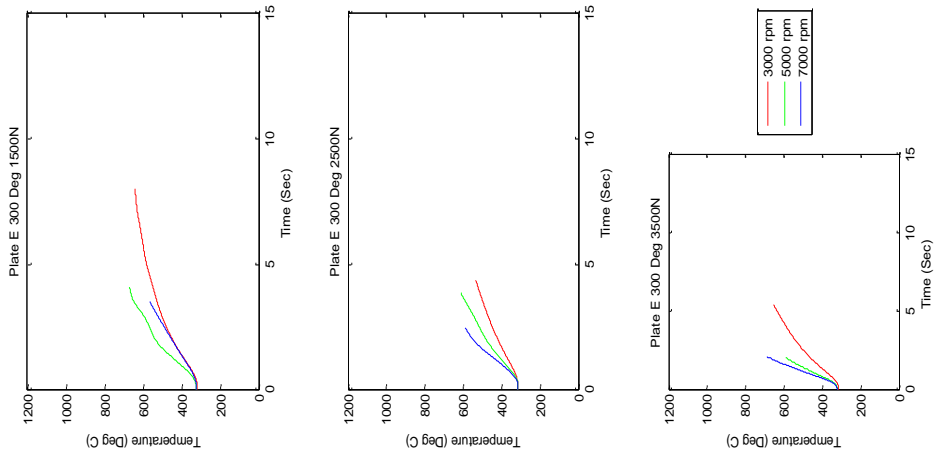


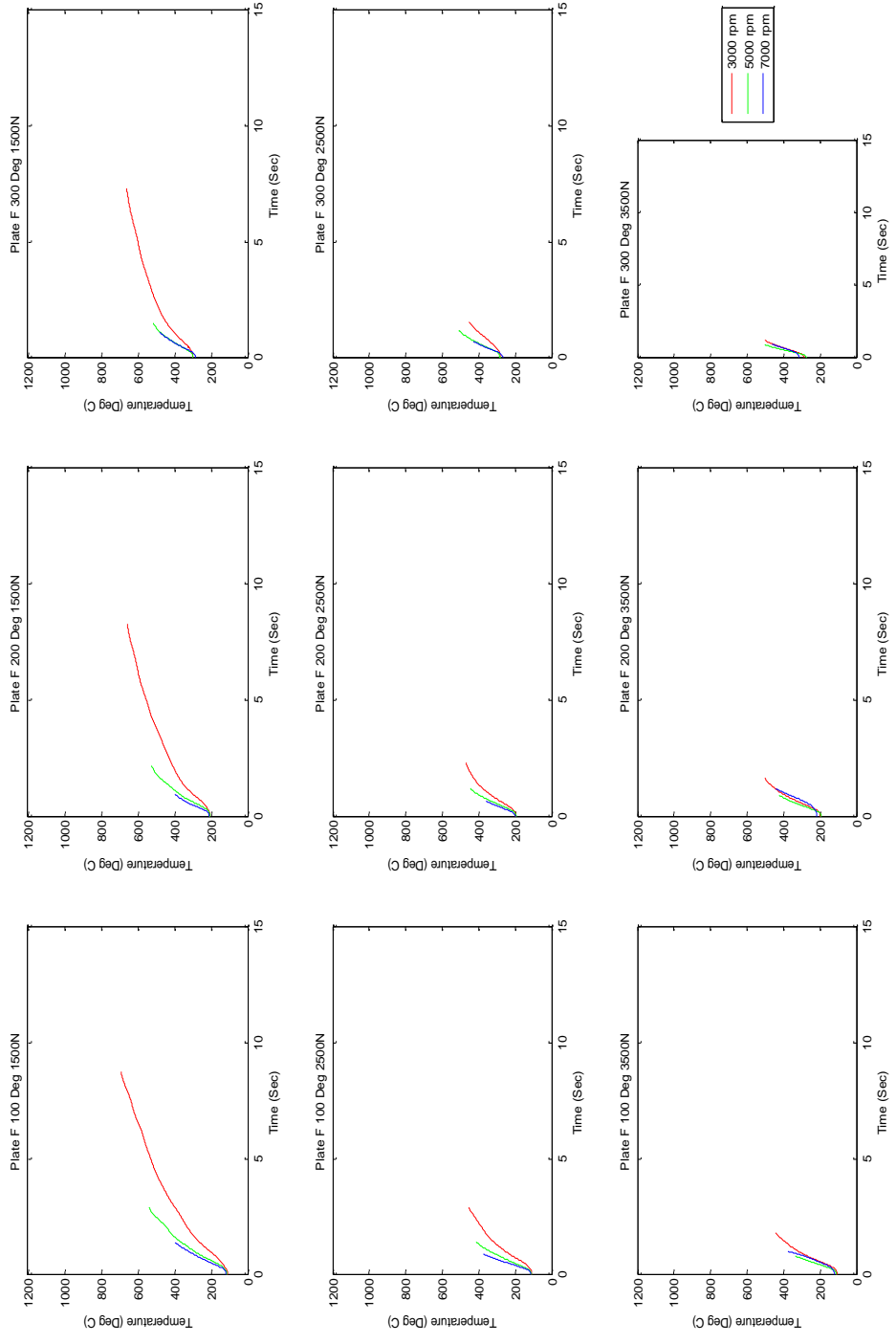


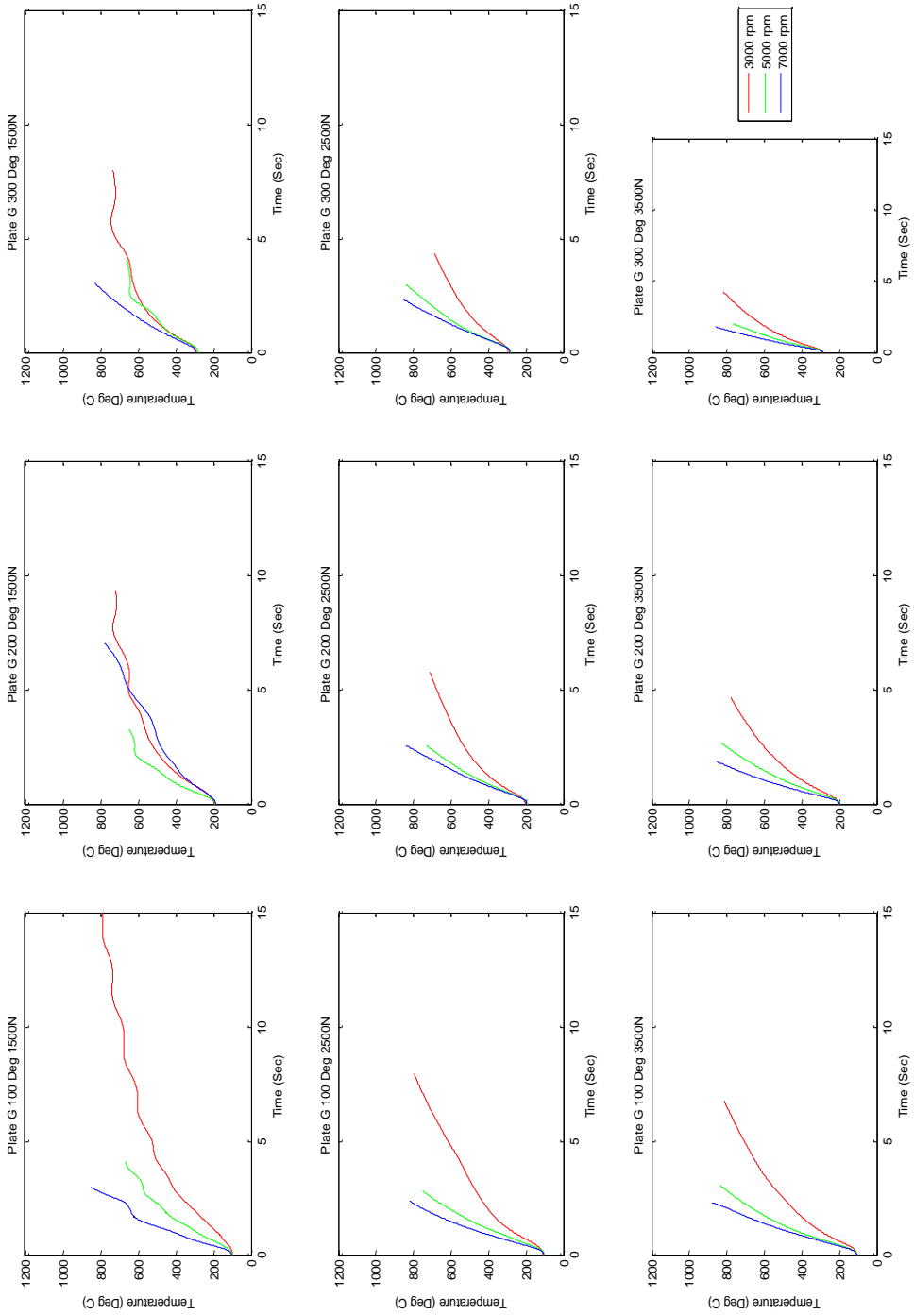


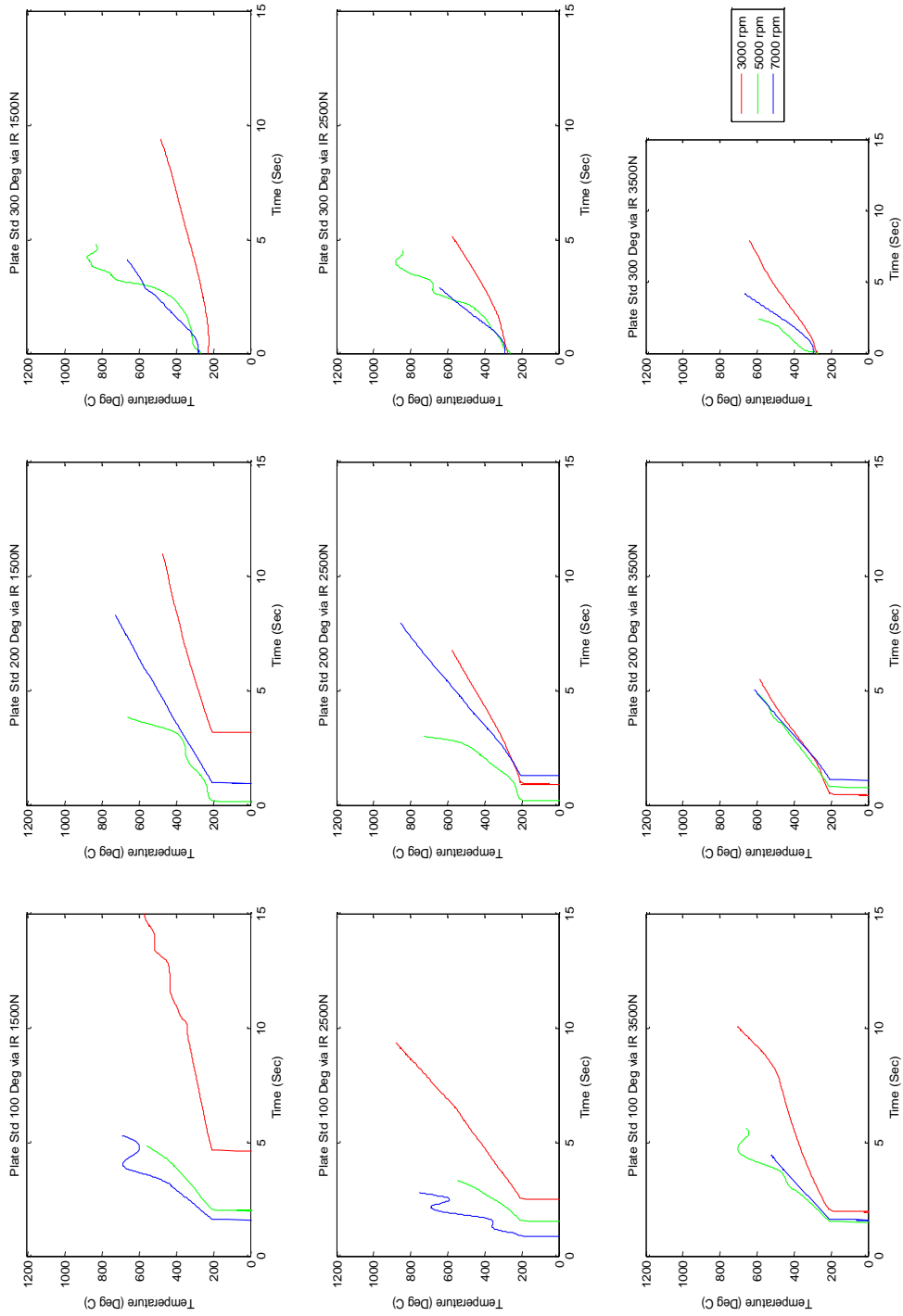


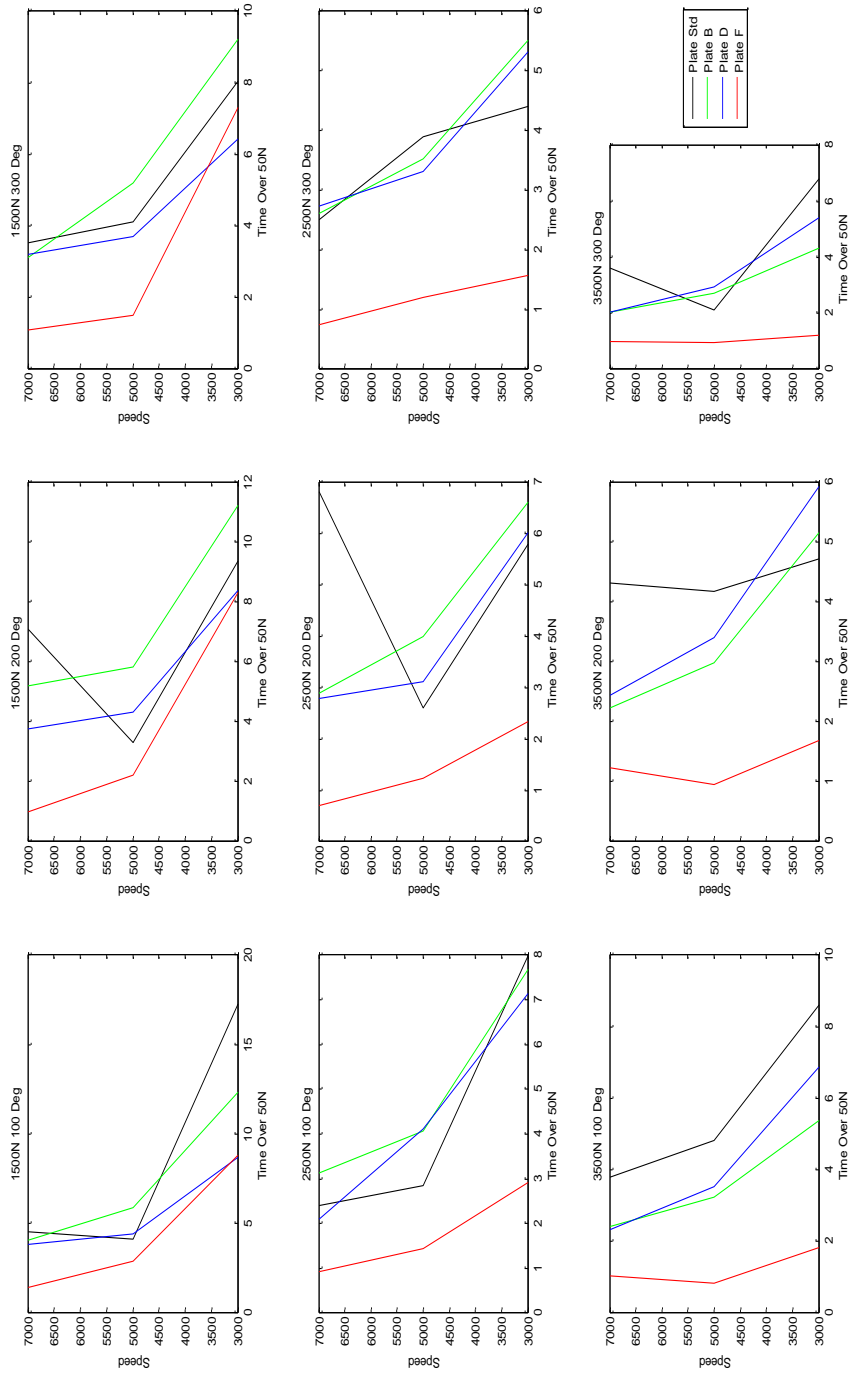




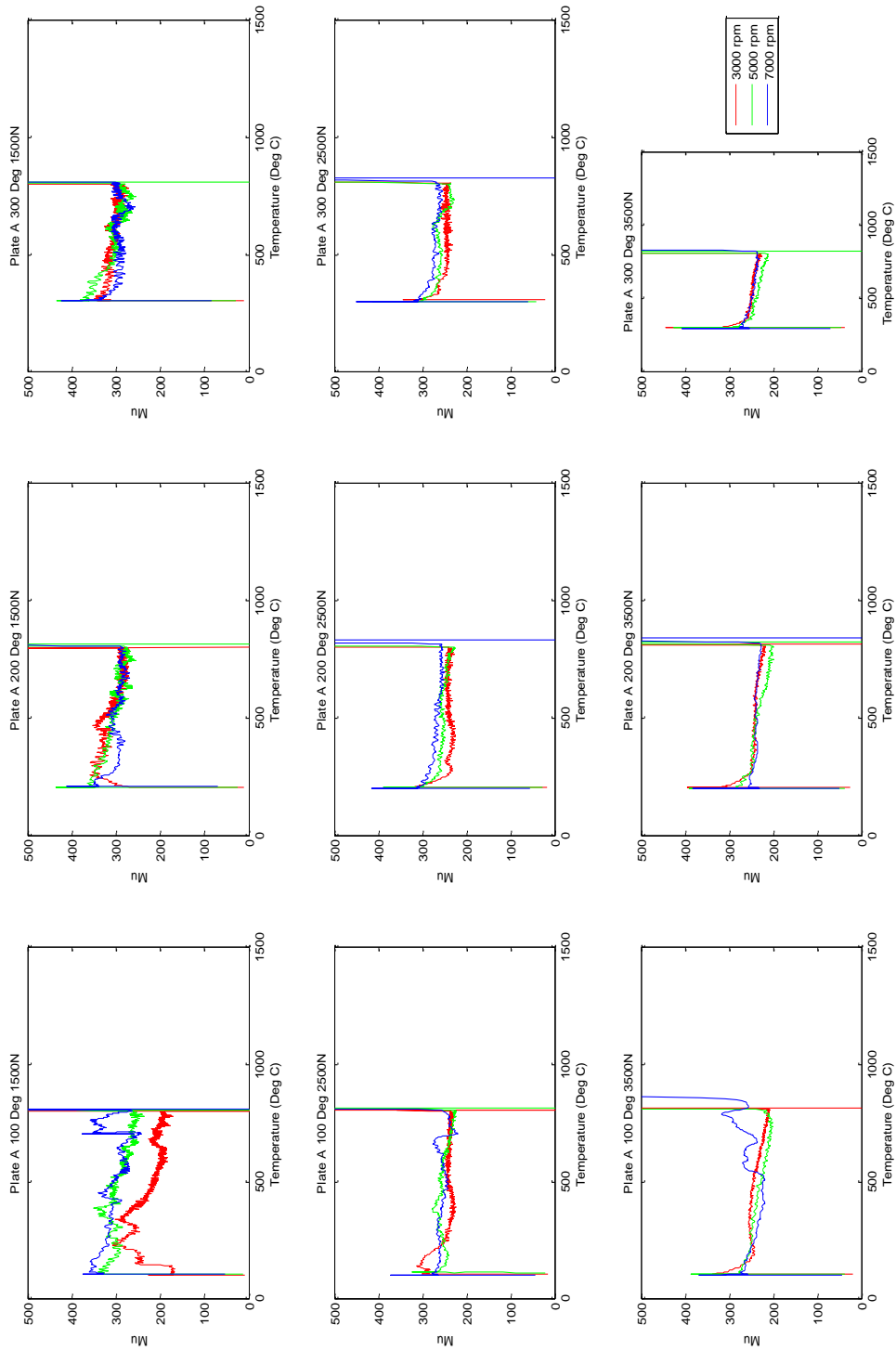




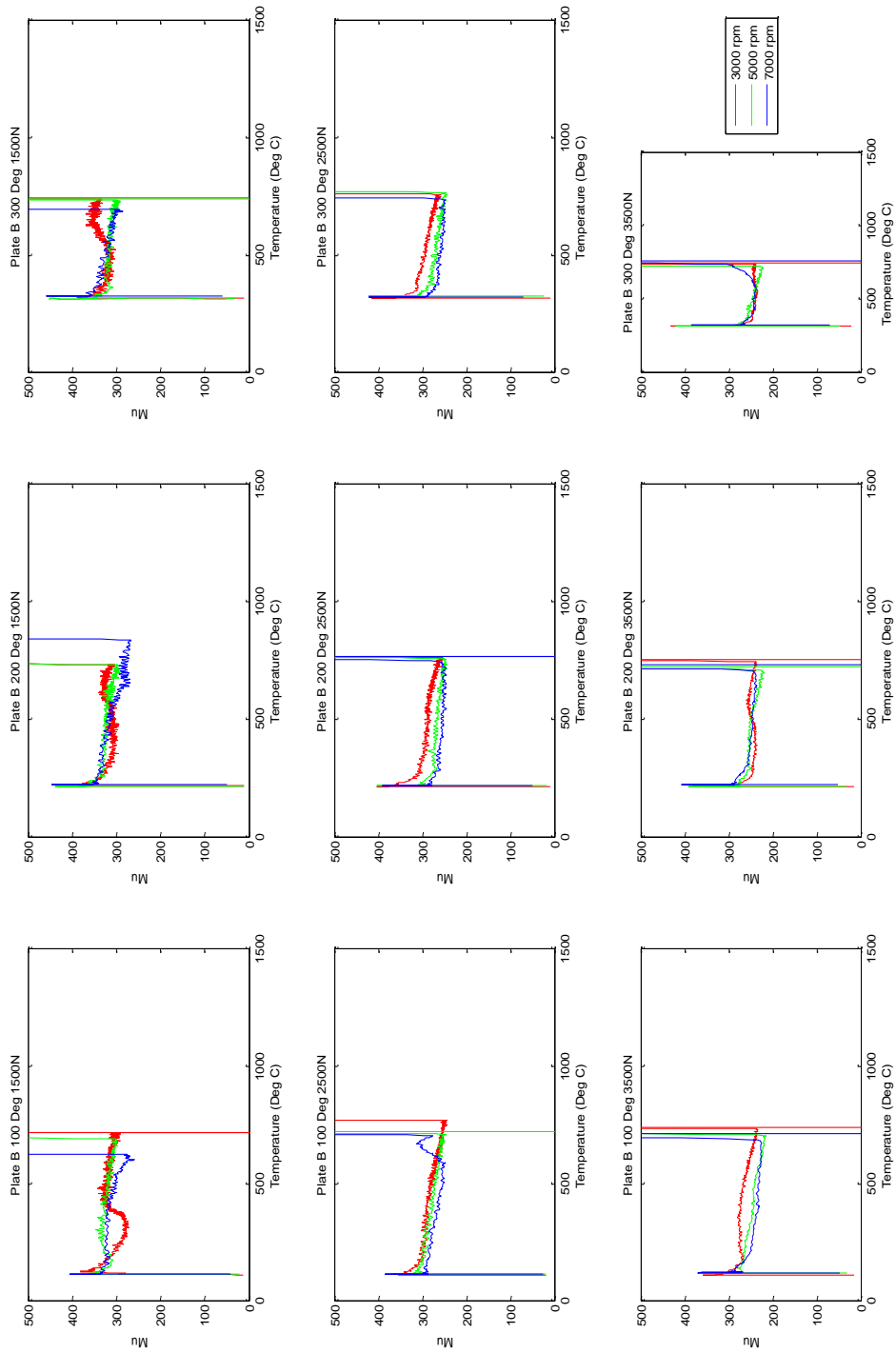


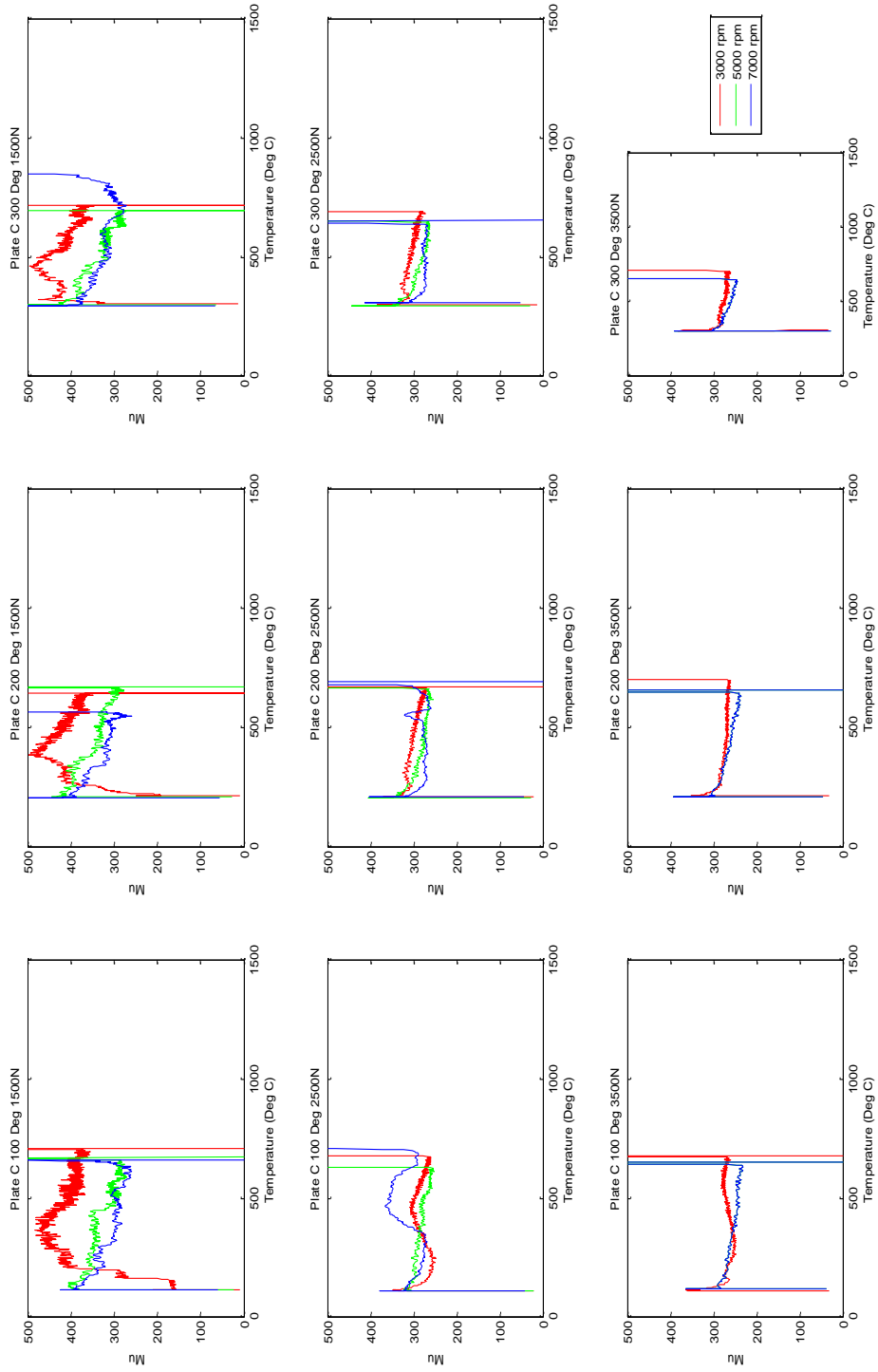


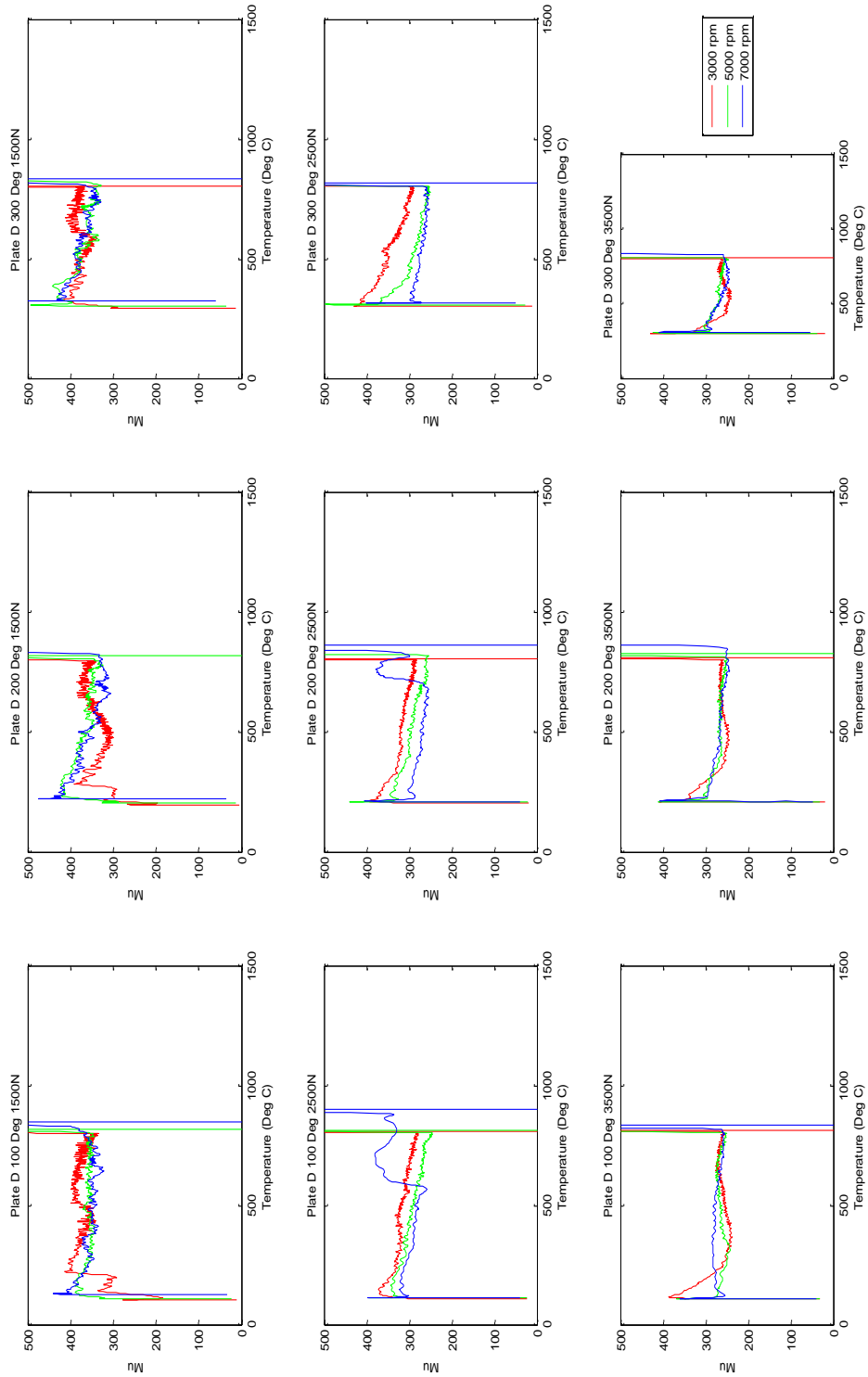
# Appendix M - Friction Effects of Input Speed

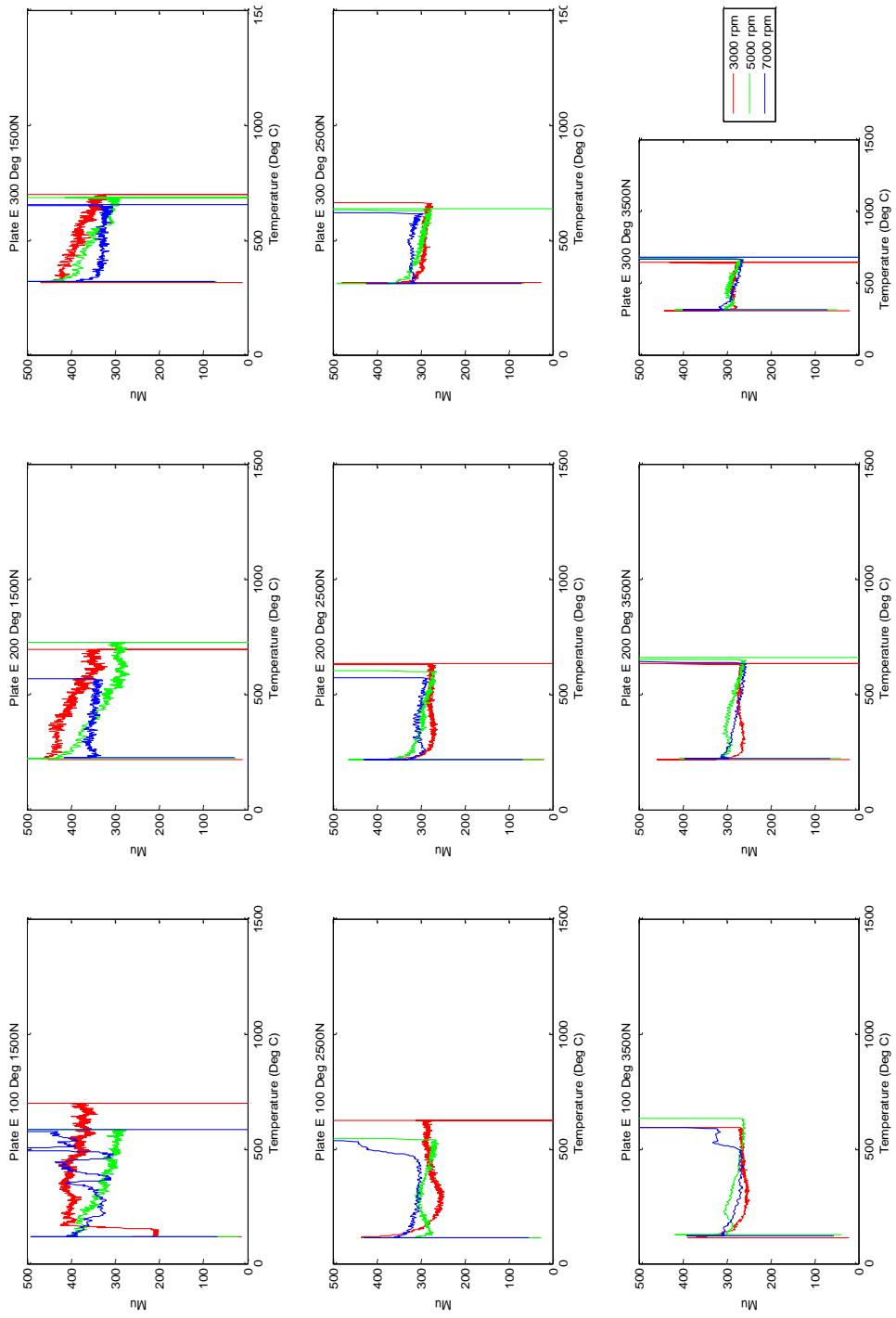


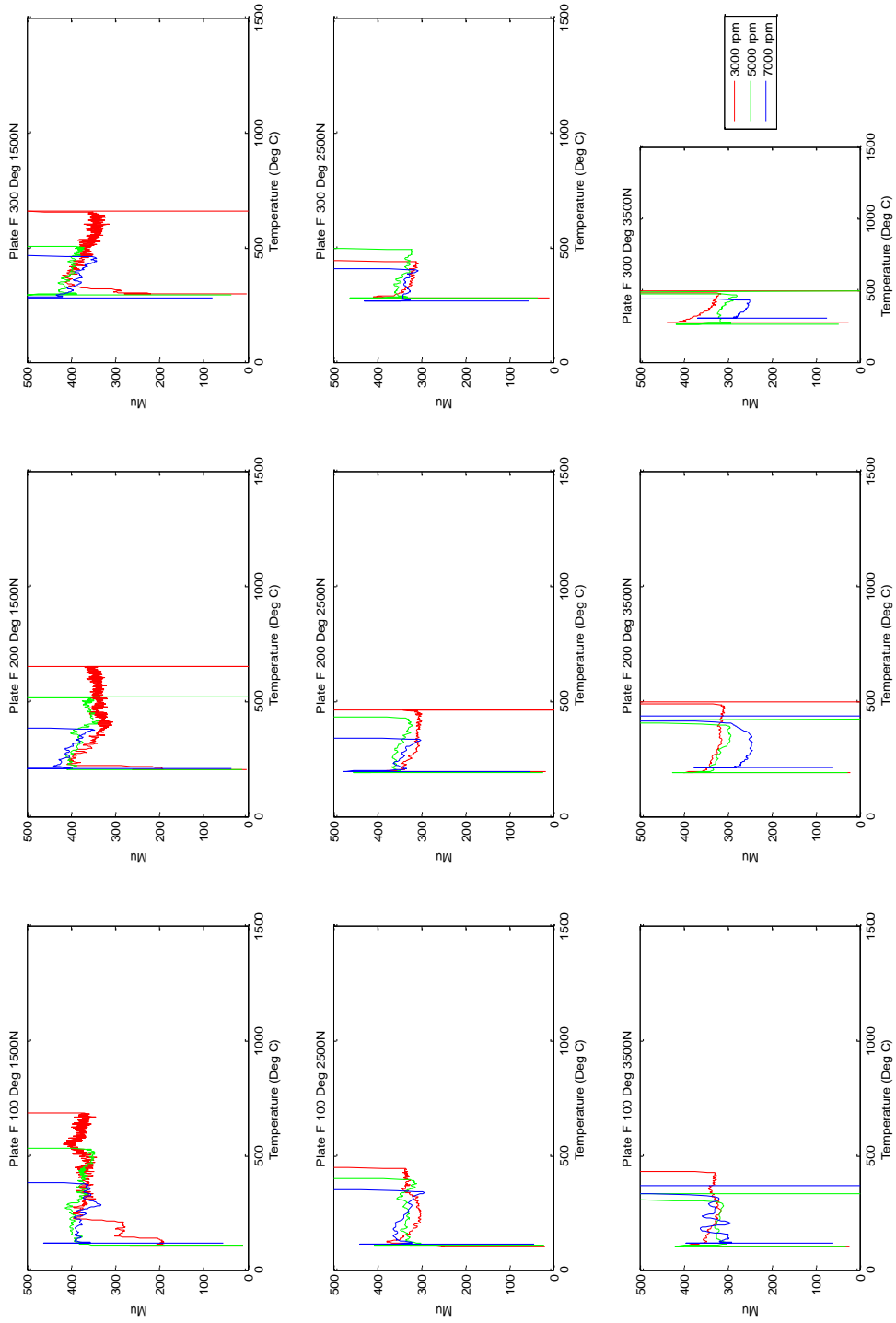


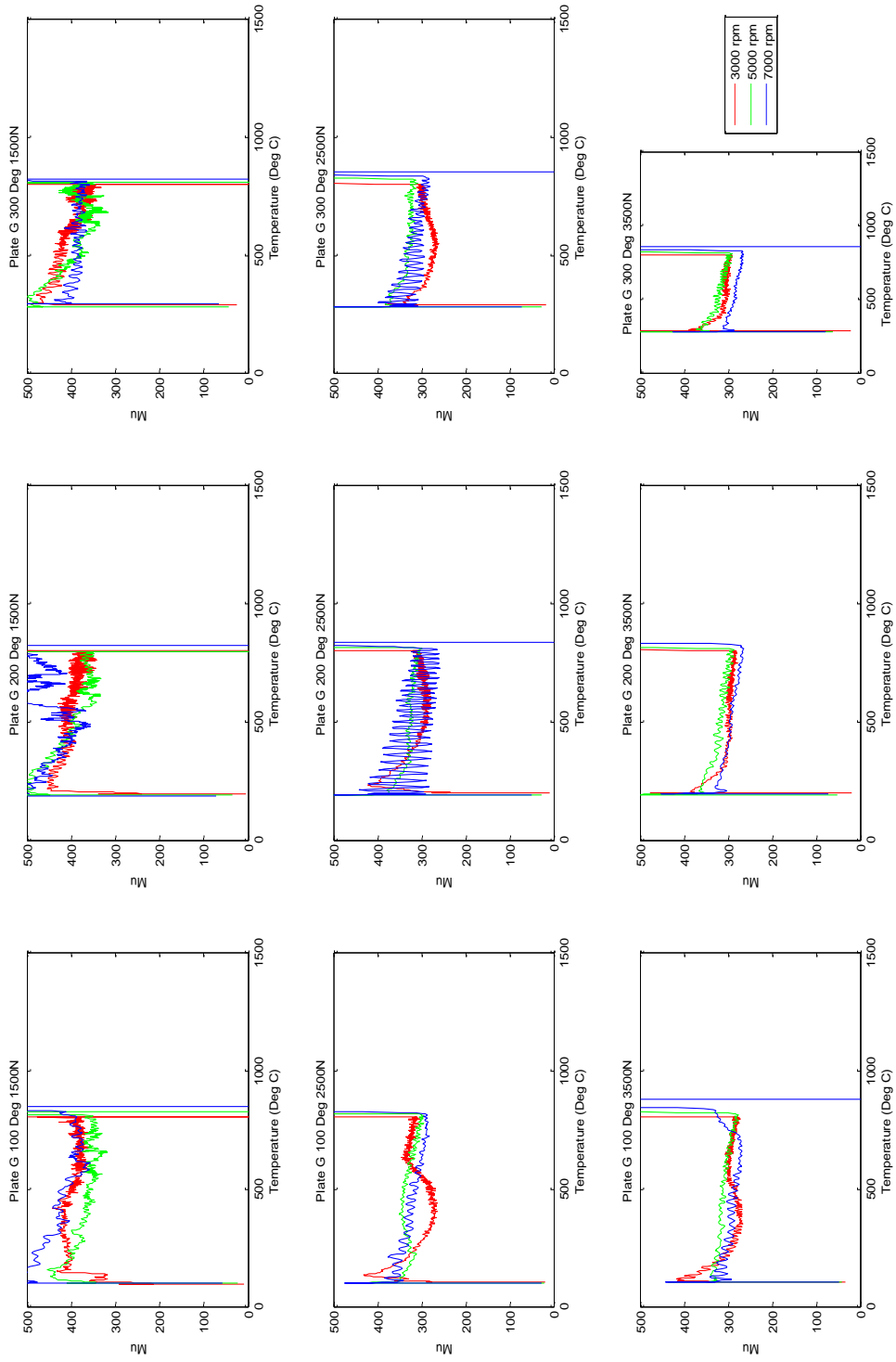


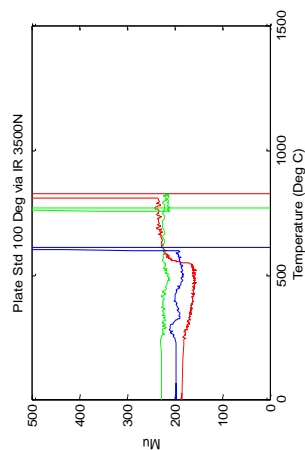
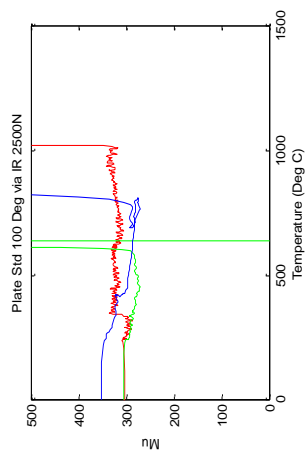
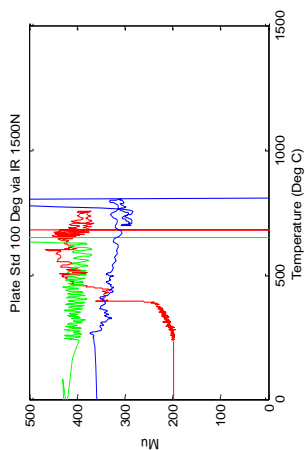
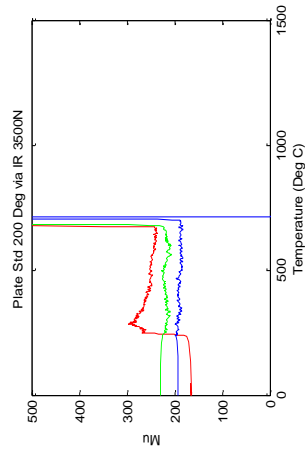
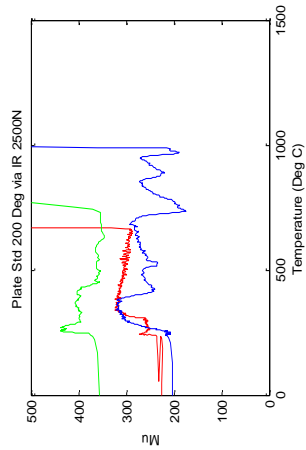
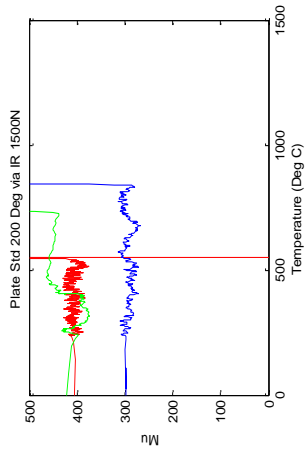
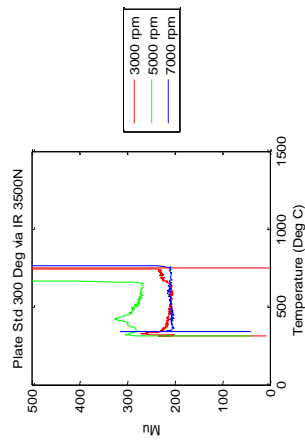
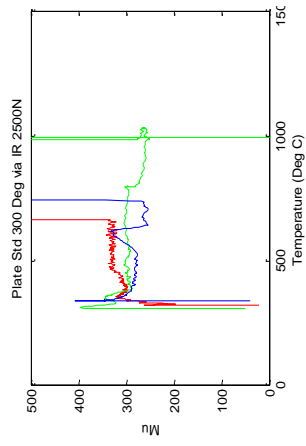
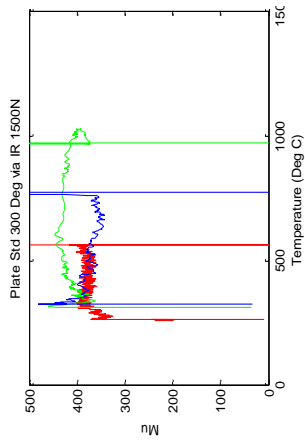




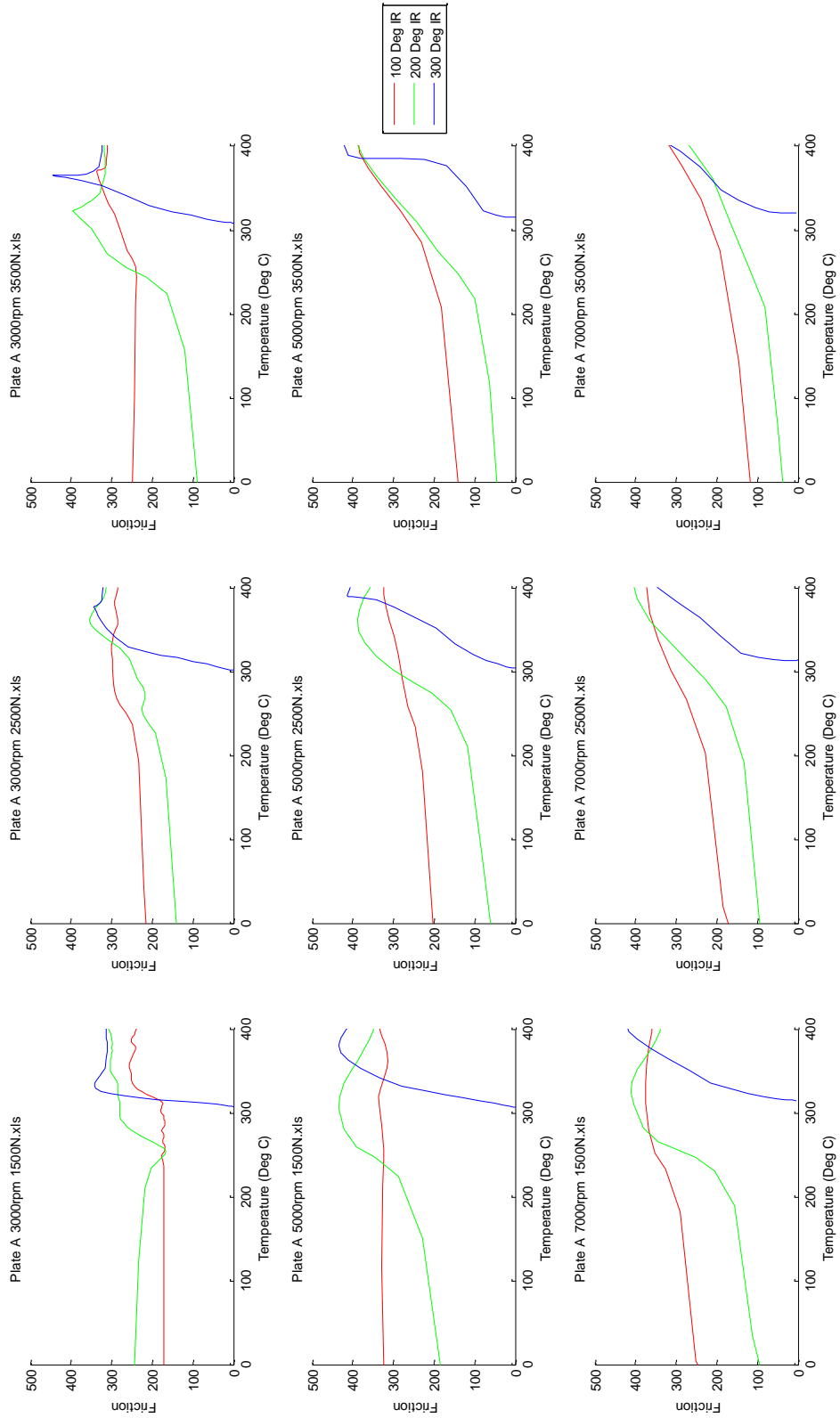




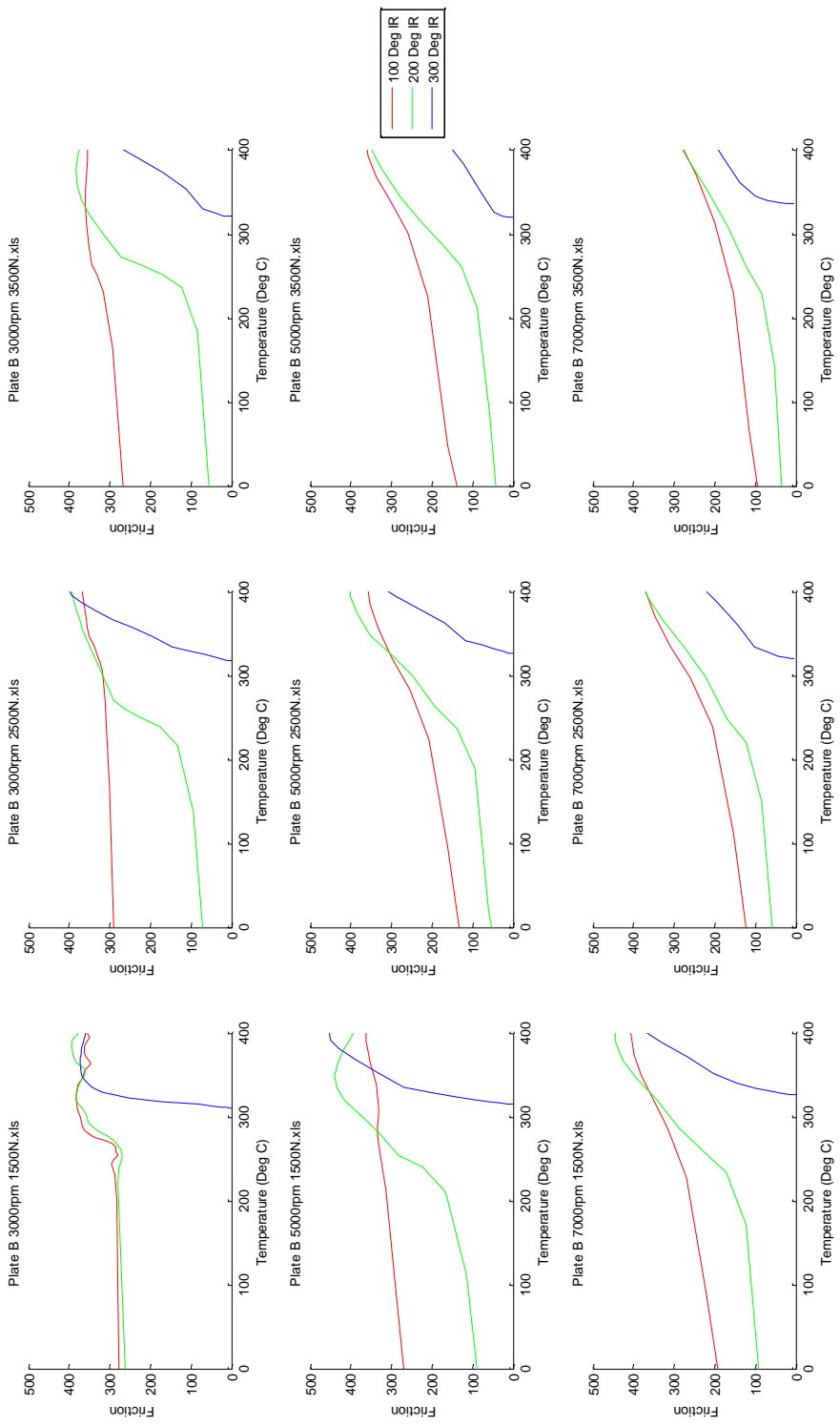


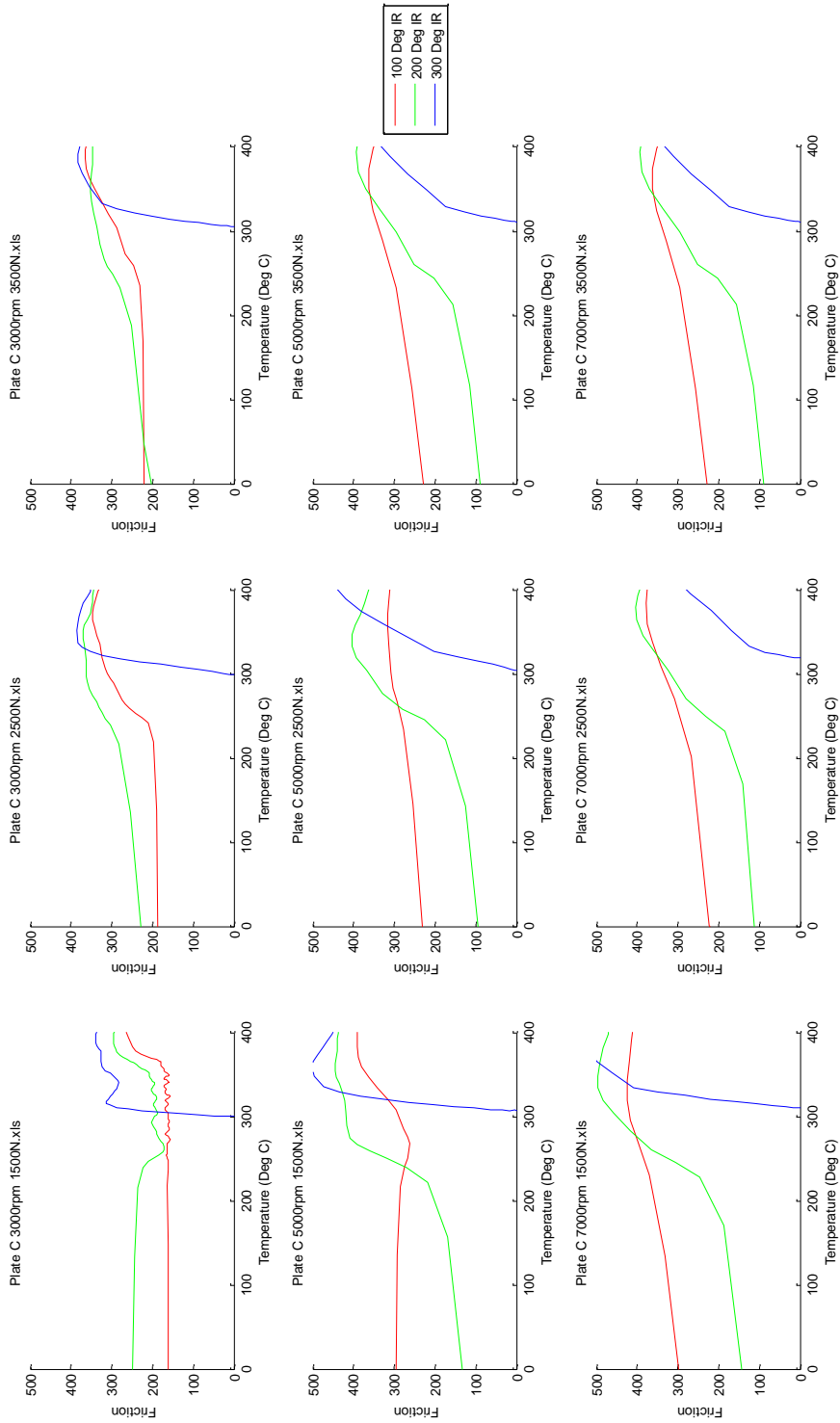


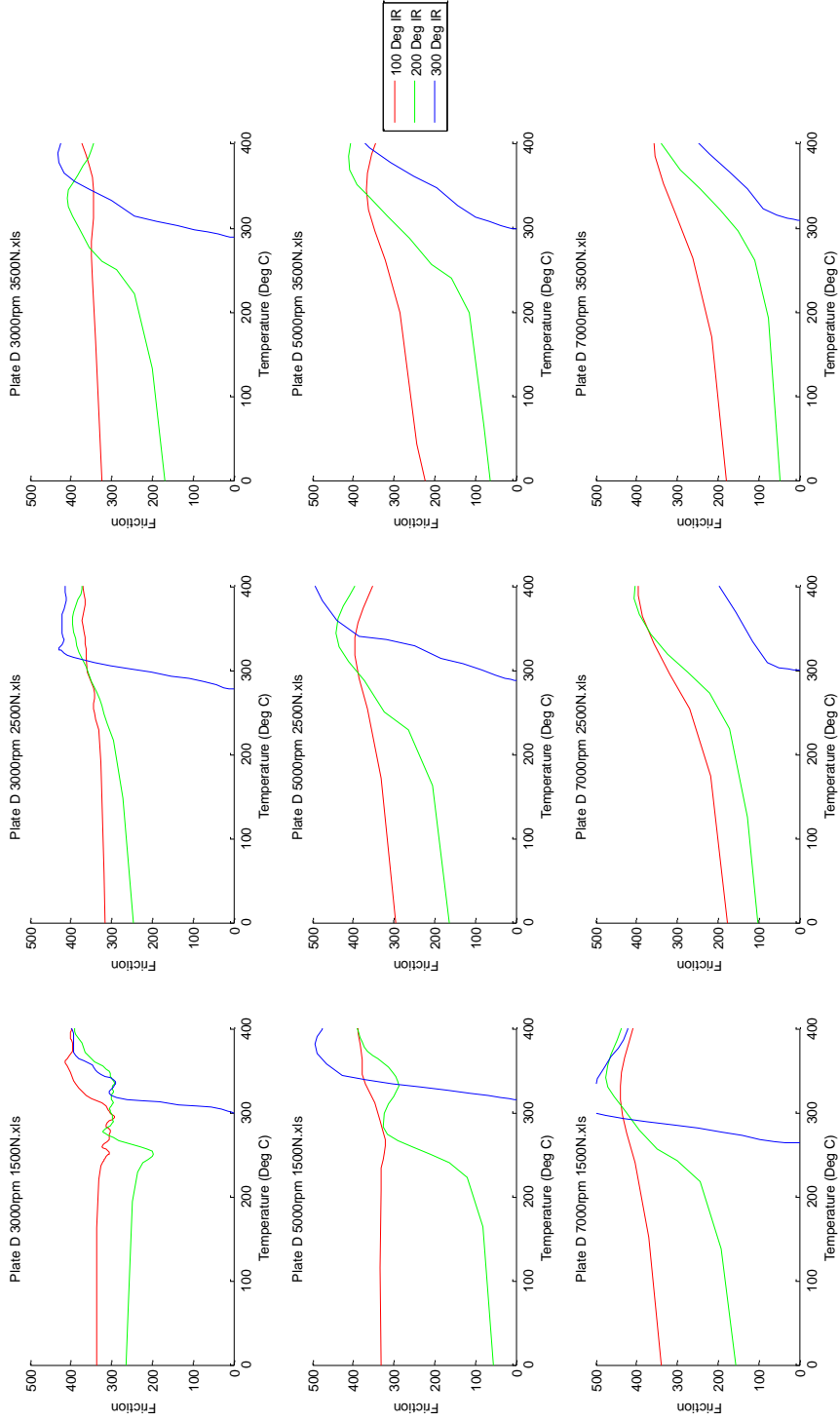
# Appendix N - Friction vs. Temperature Plots for sub 400°C

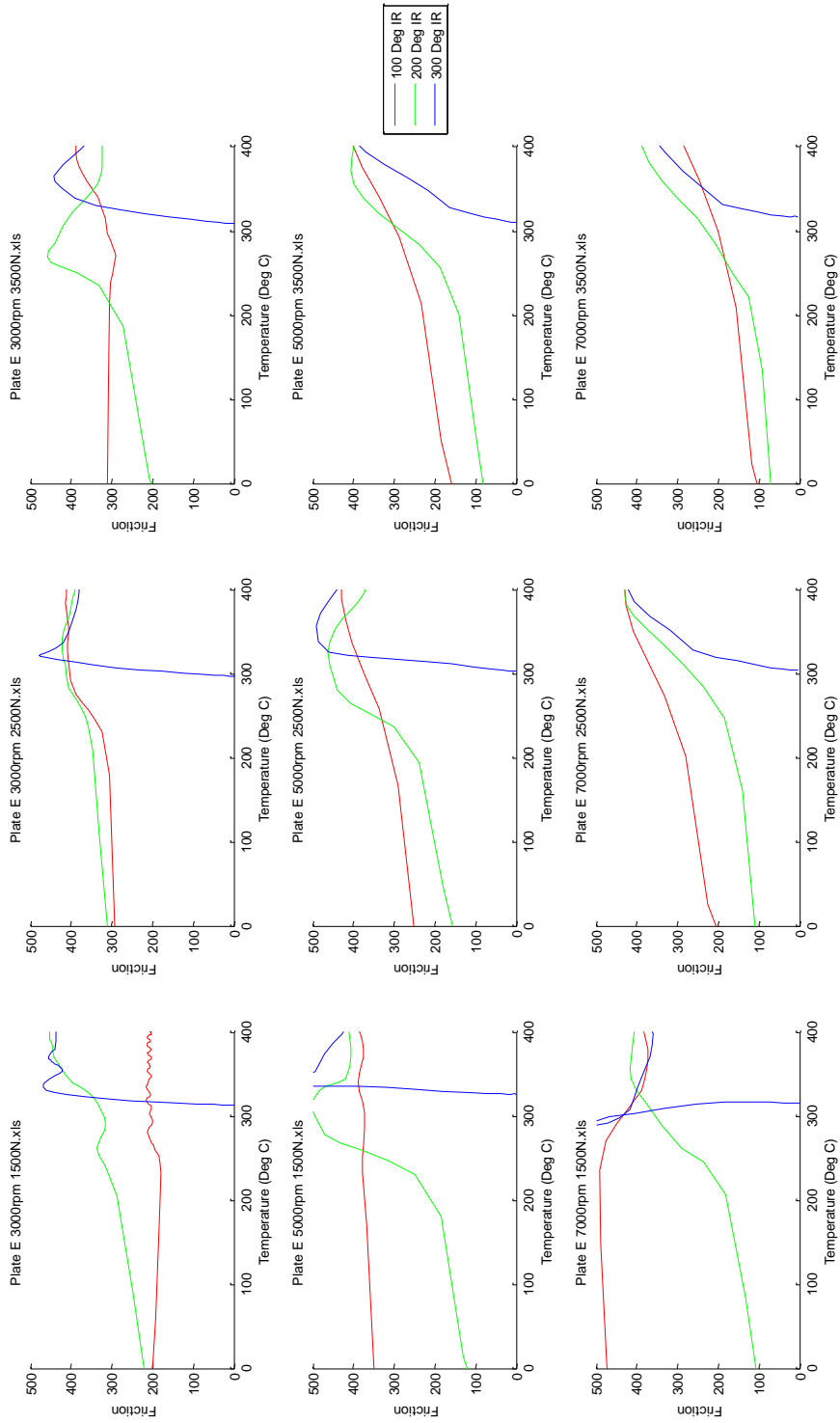


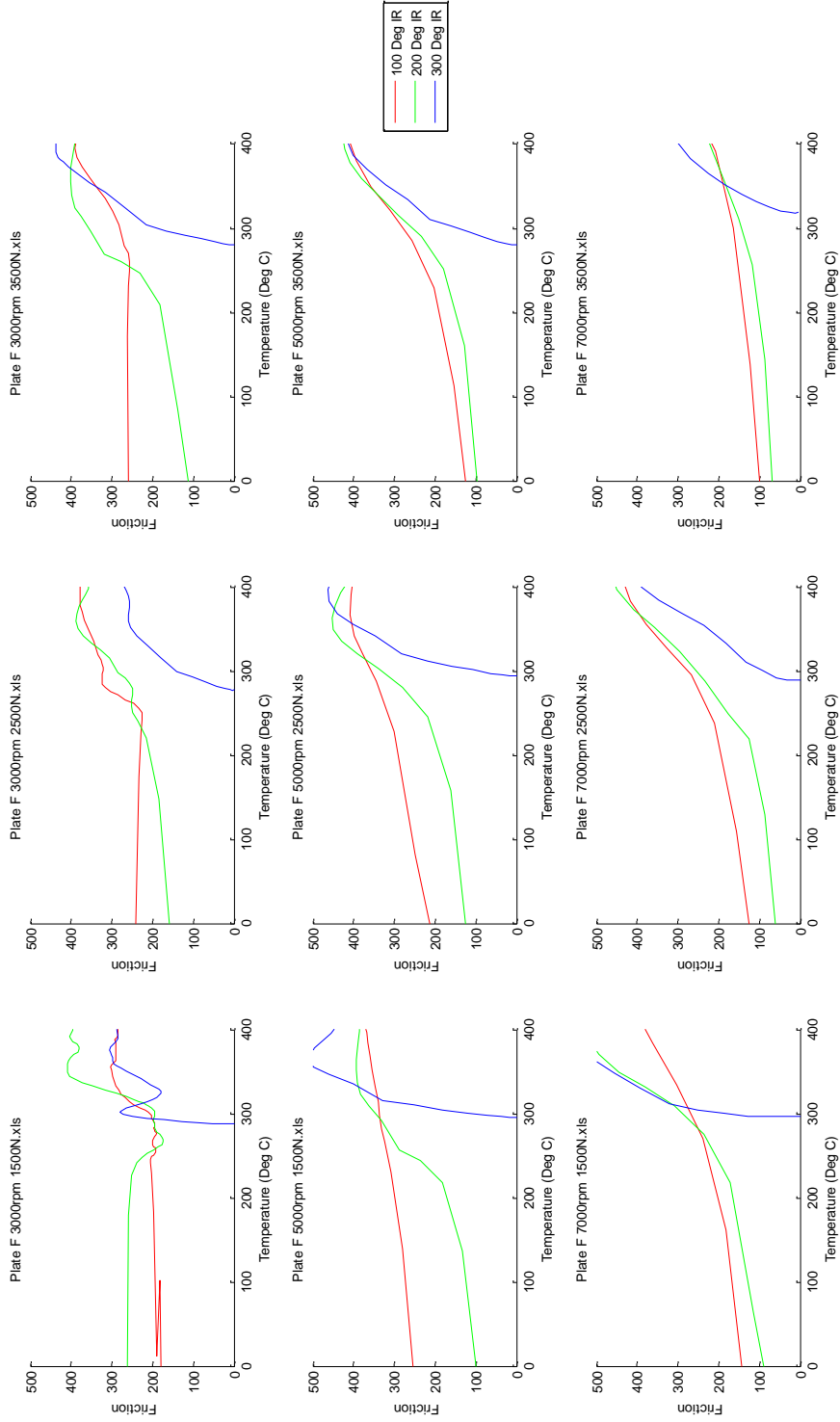


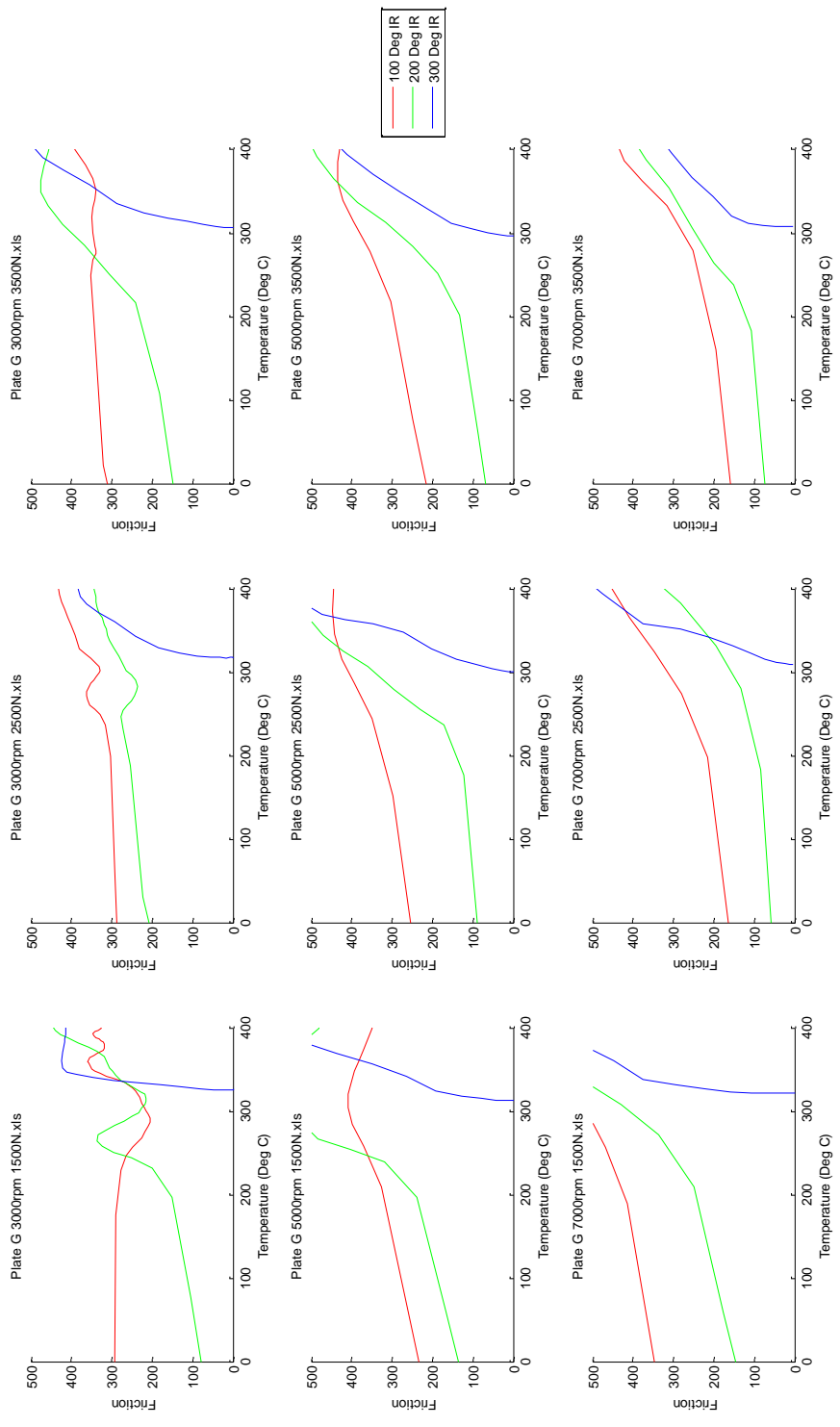


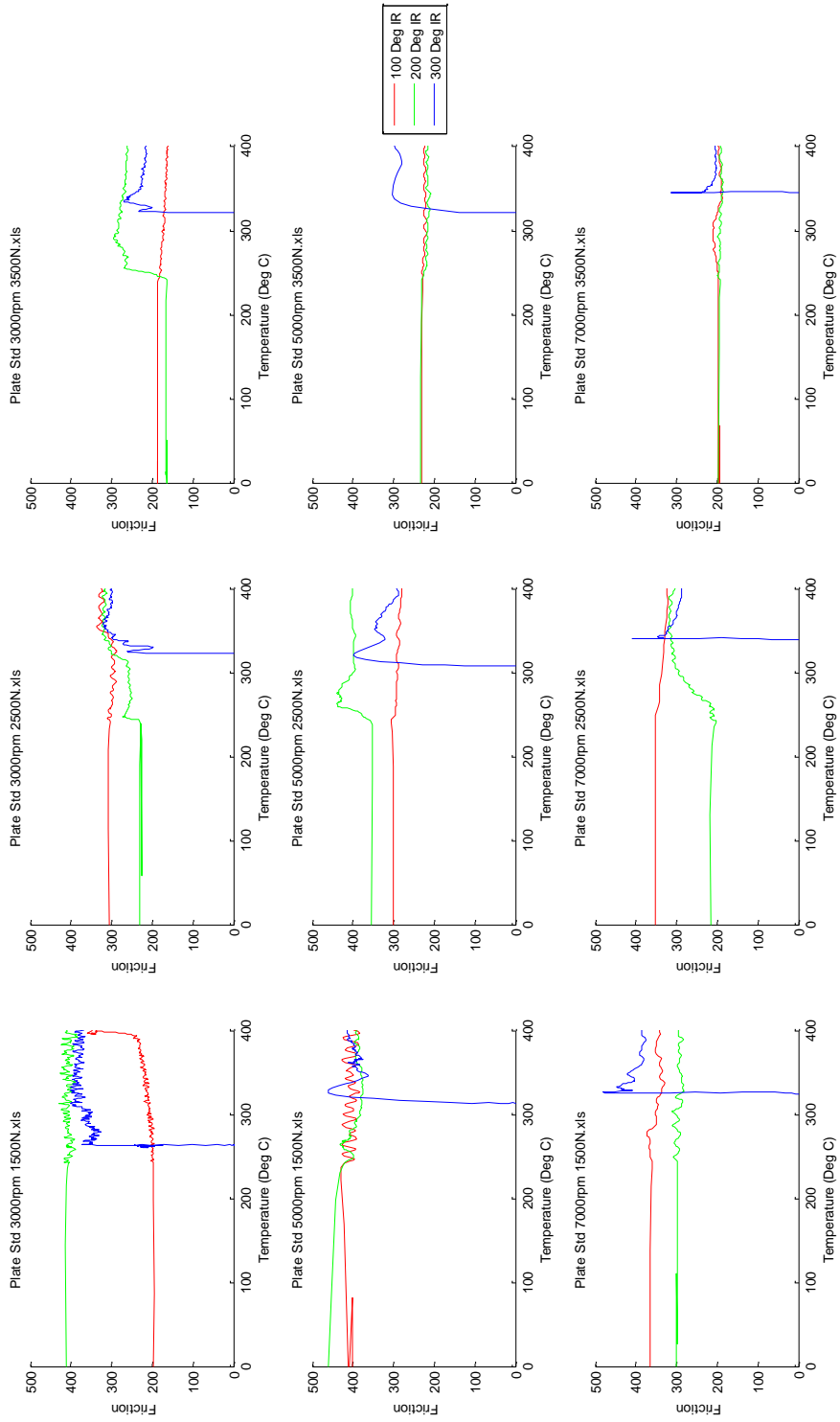












## Appendix O - MATLAB® Code for Results Analysis

### Model

#### MATLAB® Model - Initial Graph Code

```
tic

RowNum = 0;

%% IMPORT FROM EXCEL

PlateIndex = [{'Plate A'} {'Plate B'} {'Plate C'} {'Plate D'}
{'Plate E'} {'Plate F'} {'Plate G'}];

ExcelIndex = [{'J3:J30000'} {'K3:K30000'} {'L3:L30000'}
{'M3:M30000'} {'N3:N30000'} {'O3:O30000'} {'P3:P30000'}];

%% FOR EACH PLATE A - G:

for iPlateNum = 1:length(PlateIndex);

    RowNum = 0

    CurrentExcelColumn = ExcelIndex{iPlateNum};

    CurrentPlateID = PlateIndex{iPlateNum};

    CurrentPlateIDNoSpaces = CurrentPlateID(1:5);

    CurrentPlateIDNoSpaces(6) = CurrentPlateID(7);

    display(['Processing ' CurrentPlateID])

    SpeedList = [{' 3000rpm'}, {' 5000rpm'}, {' 7000rpm'}];

    SpeedListNoSpaces =
    [{'3000rpm'}, {'5000rpm'}, {'7000rpm'}];

    ClampList = [{'1500N'}, {'2500N'}, {'3500N'}];

    worksheetList = [{'Data 100'}, {'Data 200'}, {'Data 300'}];

    scrsz = get(0, 'ScreenSize');

    figure('Position', [1 scrsz(4) scrsz(3) scrsz(4)])
```



```

%% FOR EACH SPEED:

for ispeedNum = 1:3

    CurrentSpeed = SpeedList{ispeedNum};

    SpeedNoSpaces = SpeedListNoSpaces{ispeedNum};

    %% FOR EACH CLAMP FORCE:

    for iClampNum = 1:3

        CurrentClamp = ClampList{iClampNum};

        BandedFilePath = strcat('G:\Gem\Tests\Test
2\DC0024 Gem\',CurrentPlateID,'\ ',CurrentPlateID,'
',CurrentSpeed,'_',CurrentClamp,'.xls');

        MasterFilePath = strcat('G:\Gem\Tests\Test
2\DC0024 Gem\Plate Std\Plate Std', '
',CurrentSpeed,'_',CurrentClamp,'.xls');

        StructureName =
strcat('rpm',SpeedNoSpaces(1:4),CurrentClamp);

%% FOR EACH START TEMPERATURE

    for iStartTemp = 1:3

        workSheet = workSheetList{iStartTemp};

        StartTemp = workSheet(1:4);

        StartTemp(5:7) = workSheet(6:8); %e.g.
Data100

        StartTempTime = StartTemp;

        StartTempTime(8) = 'T'; %Data100T

        % = (ispeedNum-1)*9+(iClampNum-
1)*3+iStartTemp

        % display([workSheet ' Degrees Start Temp'])

CXC

```

```

        workSheet = workSheetList{iStartTemp};

        MasterTemp =
xlsread(MasterFilePath,workSheet, CurrentExcelColumn);

        MasterForce =
xlsread(MasterFilePath,workSheet, 'G3:G30000');

        MasterOverFifty = find(MasterForce>50);

        LengthMaster = length(MasterOverFifty);

        MasterStart = MasterOverFifty(1);

        MasterEnd = MasterOverFifty(LengthMaster);

        workSheet = workSheetList{iStartTemp};

        BandedTemp = xlsread(BandedFilePath,
workSheet, CurrentExcelColumn);

        BandedForce = xlsread(BandedFilePath,
workSheet, 'G3:G30000');

        BandedOverFifty = find(BandedForce>50);

        LengthBanded = length(BandedOverFifty);

        BandedStart = BandedOverFifty(1);

        BandedEnd = BandedOverFifty(LengthBanded);

        VectorLengths(1) = LengthMaster;

        VectorLengths(2) = LengthBanded;

        MinVectorLength = min(VectorLengths);

        BandedTempCut.(StructureName).(StartTemp) =
BandedTemp(BandedStart:BandedStart+MinVectorLength-1);

        BandedTempCut.(StructureName).(StartTempTime)
= [0:0.01:(MinVectorLength/100)-0.01];

        MasterTempCut.(StructureName).(StartTemp) =
MasterTemp(MasterStart:MasterStart+MinVectorLength-1);

```

```
MasterTempCut.(StructureName).(StartTempTime)
= [0:0.01:(MinVectorLength/100)-0.01];
```

```
clear MinVectorLength zero
```

```
clear MasterTemp MasterForce MasterOverFifty
LengthMaster MasterStart MasterEnd MasterDuration BandedTemp
BandedForce BandedOverFifty
```

```
clear LengthBanded BandedStart BandedEnd
BandedDuration InterpInterval BandedTempInterp
MasterTempInterp CurrentCorrelation WorkSheet
```

```
end
```

```
subplot(3,3,(iSpeedNum-1)*3+iClampNum)
```

```
plot(BandedTempCut.(StructureName).Data100T,BandedTempCut.(St
ructureName).Data100,'-.r')
```

```
hold on
```

```
plot(BandedTempCut.(StructureName).Data200T,BandedTempCut.(St
ructureName).Data200,'-.g')
```

```
plot(BandedTempCut.(StructureName).Data300T,BandedTempCut.(St
ructureName).Data300,'-.b')
```

```
plot(MasterTempCut.(StructureName).Data100T,MasterTempCut.(St
ructureName).Data100,'r')
```

```
plot(MasterTempCut.(StructureName).Data200T,MasterTempCut.(St
ructureName).Data200,'g')
```

```
plot(MasterTempCut.(StructureName).Data300T,MasterTempCut.(St
ructureName).Data300,'b')
```

```
titlename = strcat([CurrentPlateID, '
',CurrentSpeed, ' ',CurrentClamp, '.xls'])
```

```
title(titlename)
```

```
xlabel('Time (Sec)')
```

```

ylabel('Temperature (Deg C)')

end

end

legend('Banded 100','Banded 200','Banded 300','Std
100','Std 200','Std 300','Location','EastOutside')

saveas(gcf,[CurrentPlateID '.emf']) %saves figure as a
jpeg in the folderpath direc

close

clear BandedTempCut MasterTempCut

end

toc

```

### **Model Code**

```

tic

RowNum = 0;

%% IMPORT FROM EXCEL

PlateIndex = [{'Plate A'} {'Plate B'} {'Plate C'} {'Plate D'}
{'Plate E'} {'Plate F'} {'Plate G'}];

ExcelIndex = [{'J3:J30000'} {'K3:K30000'} {'L3:L30000'}
{'M3:M30000'} {'N3:N30000'} {'O3:O30000'} {'P3:P30000'}];

%% FOR EACH PLATE A - G:

```

```

for iPlateNum = 1:length(PlateIndex);

    RowNum = 0

    CurrentExcelColumn = ExcelIndex{iPlateNum}

    CurrentPlateID = PlateIndex{iPlateNum};

    CurrentPlateIDNoSpaces = CurrentPlateID(1:5);
    CurrentPlateIDNoSpaces(6) = CurrentPlateID(7);

    display(['Processing ' CurrentPlateID])

    SpeedList = [{' 3000rpm'},{' 5000rpm'},{' 7000rpm'}];
    ClampList = [{'1500N'},{'2500N'},{'3500N'}];
    workSheetList = [{'Data 100'},{'Data 200'},{'Data 300'}];

%% FOR EACH START TEMPERATURE

    for iStartTemp = 1:3

        workSheet = workSheetList{iStartTemp}

        % display(['workSheet ' Degrees Start Temp'])

%% FOR EACH SPEED:

        for ispeedNum = 1:3

            CurrentSpeed = SpeedList{ispeedNum};

%% FOR EACH CLAMP FORCE:

            for iClampNum = 1:3

                CurrentClamp = ClampList{iClampNum};

                RowNum = (ispeedNum-1)*9+(iClampNum-
1)*3+iStartTemp

```

```
BandedFilePath = strcat('G:\Gem\Tests\Test  
2\DC0024 Gem\',CurrentPlateID,'\',CurrentPlateID,'  
,CurrentSpeed,'_',CurrentClamp,'.xls');
```

```
MasterFilePath = strcat('G:\Gem\Tests\Test  
2\DC0024 Gem\Plate Std\Plate Std','  
,CurrentSpeed,'_',CurrentClamp,'.xls');
```

```
workSheet = workSheetList{iStartTemp};
```

```
MasterTemp =  
xlsread(MasterFilePath,workSheet, CurrentExcelColumn);
```

```
MasterForce =  
xlsread(MasterFilePath,workSheet, 'G3:G30000');
```

```
MasterOverFifty = find(MasterForce>50);
```

```
LengthMaster = length(MasterOverFifty);
```

```
MasterStart = MasterOverFifty(1);
```

```
MasterEnd = MasterOverFifty(LengthMaster);
```

```
workSheet = workSheetList{iStartTemp};
```

```
BandedTemp = xlsread(BandedFilePath,  
workSheet, CurrentExcelColumn);
```

```
BandedForce = xlsread(BandedFilePath,  
workSheet, 'G3:G30000');
```

```
BandedOverFifty = find(BandedForce>50);
```

```
LengthBanded = length(BandedOverFifty);
```

```
BandedStart = BandedOverFifty(1);
```

```
BandedEnd = BandedOverFifty(LengthBanded);
```

```
VectorLengths(1) = LengthMaster;
```

```
VectorLengths(2) = LengthBanded;
```

```
MinVectorLength = min(VectorLengths);
```

```
BandedTempCut =  
BandedTemp(BandedStart:BandedStart+MinVectorLength-1);
```

```
MasterTempCut =  
MasterTemp(MasterStart:MasterStart+MinVectorLength-1);
```

```
Correlation.Info{RowNum,1} =  
strcat(CurrentSpeed,CurrentClamp,WorkSheet);
```

```
CurrentCorrelation =  
corrcoef(BandedTempCut,MasterTempCut);
```

```
Correlation.(CurrentPlateIDNoSpaces)(RowNum,1) =  
CurrentCorrelation(1,2)
```

```
clear MasterTemp MasterForce MasterOverFifty  
LengthMaster MasterStart MasterEnd MasterDuration BandedTemp  
BandedForce BandedOverFifty
```

```
clear LengthBanded BandedStart BandedEnd  
BandedDuration InterpInterval BandedTempInterp  
MasterTempInterp CurrentCorrelation WorkSheet
```

```
end
```

```
end
```

```
end
```

```
end
```

```
toc
```

```
%% WRITE TO EXCEL
```

```
success = xlswrite('tempdata.xls', Correlation.Info,  
'Sheet1', 'A2')
```

```
success = xlswrite('tempdata.xls', Correlation.PlateA,  
'Sheet1', 'B2')
```

```
success = xlswrite('tempdata.xls', Correlation.PlateB,  
'Sheet1', 'C2')
```

```
success = xlswrite('tempdata.xls', Correlation.PlateC,  
'Sheet1', 'D2')
```

```
success = xlswrite('tempdata.xls', Correlation.PlateD,  
'Sheet1', 'E2')
```

```
CXCVI
```

```
success = xlswrite('tempdata.xls', Correlation.PlateE,  
'Sheet1', 'F2')
```

```
success = xlswrite('tempdata.xls', Correlation.PlateF,  
'Sheet1', 'G2')
```

```
success = xlswrite('tempdata.xls', Correlation.PlateG,  
'Sheet1', 'H2')
```

## Final Graph Code

```
load 'G:\Gem\Tests\Test 2\DC0024 Gem\Matlab and Associated  
Results\Correlation1D'
```

```
Cor(1:27,1) = Correlation.PlateA(:)
```

```
Cor(1:27,2) = Correlation.PlateB(:)
```

```
Cor(1:27,3) = Correlation.PlateC(:)
```

```
Cor(1:27,4) = Correlation.PlateD(:)
```

```
Cor(1:27,5) = Correlation.PlateE(:)
```

```
Cor(1:27,6) = Correlation.PlateF(:)
```

```
Cor(1:27,7) = Correlation.PlateG(:)
```

```
Cor(1:27,8) = max([Cor], [], 2)
```

```
Cor(1:27,1) = (Cor(1:27,1)==Cor(1:27,8)).*Cor(1:27,1)
```

```
Cor(1:27,2) = (Cor(1:27,2)==Cor(1:27,8)).*Cor(1:27,2)
```

```
Cor(1:27,3) = (Cor(1:27,3)==Cor(1:27,8)).*Cor(1:27,3)
```

```
Cor(1:27,6) = (Cor(1:27,6)==Cor(1:27,8)).*Cor(1:27,6)
```

```
Cor(1:27,5) = (Cor(1:27,5)==Cor(1:27,8)).*Cor(1:27,5)
```

```
Cor(1:27,4) = (Cor(1:27,4)==Cor(1:27,8)).*Cor(1:27,4)
```

```
Cor(1:27,7) = (Cor(1:27,7)==Cor(1:27,8)).*Cor(1:27,7)
```

```
YAxisLowerLim = min(Cor(:,8))-0.01
```



```
bar(Cor(1:27,1:7),6.8)

colormap(lines(7))

set(gca,'ylim',[YAxisLowerLim 1])

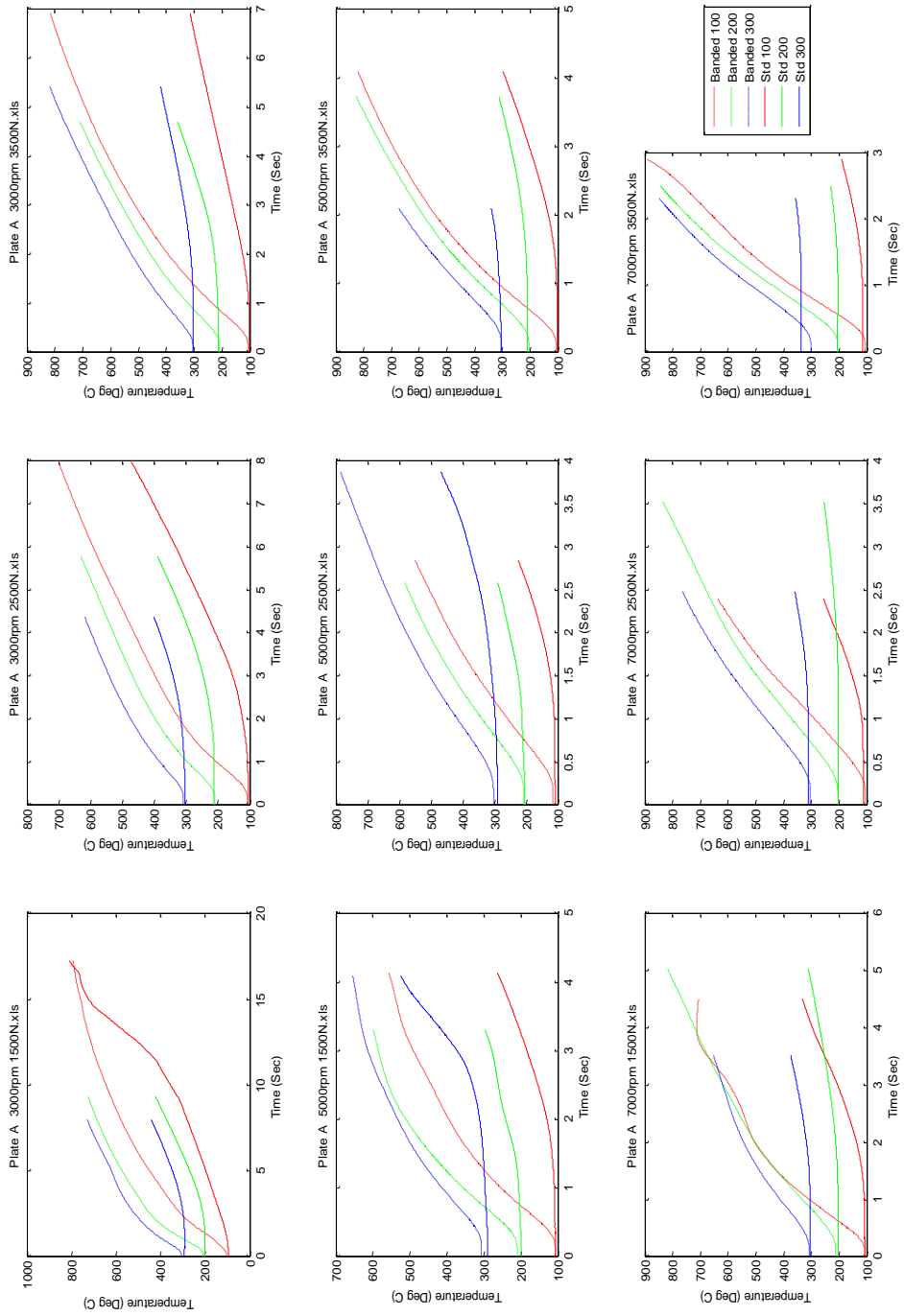
legend('Plate A','Plate B','Plate C','Plate D','Plate
E','Plate F','Plate G','Location','NorthEastOutside')

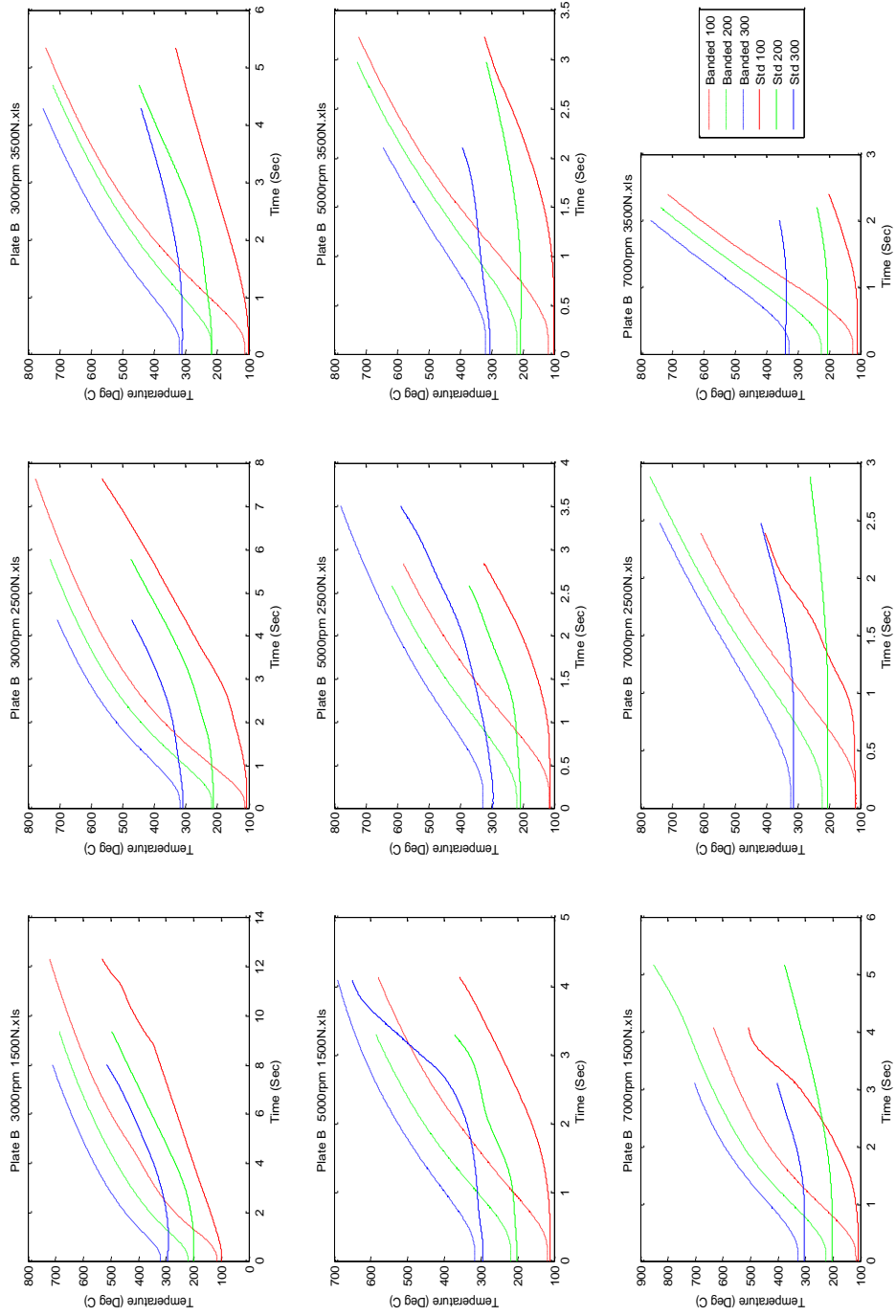
title('Maximum Correlation Coefficients')

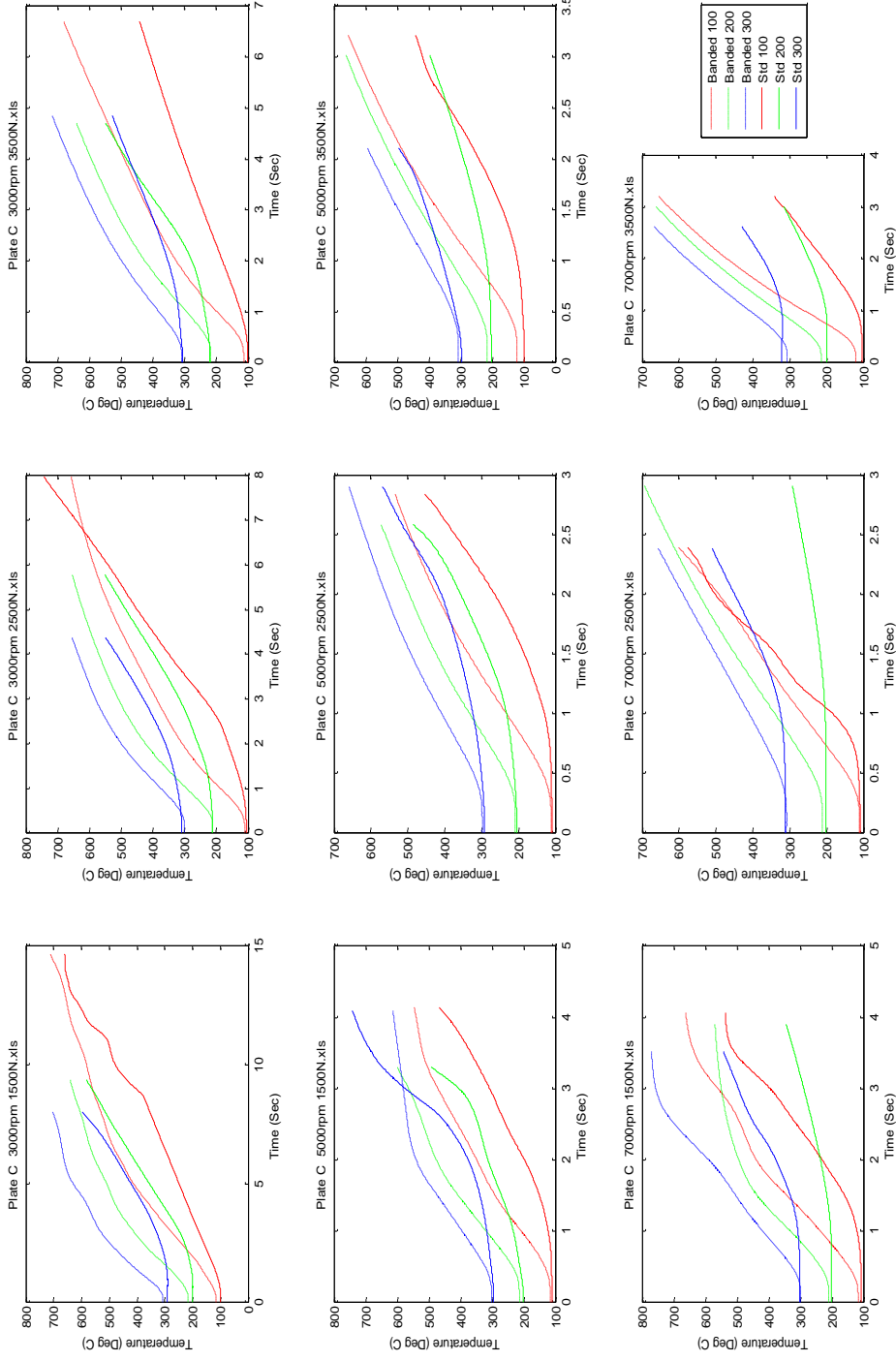
ylabel('Correlation Coefficient')

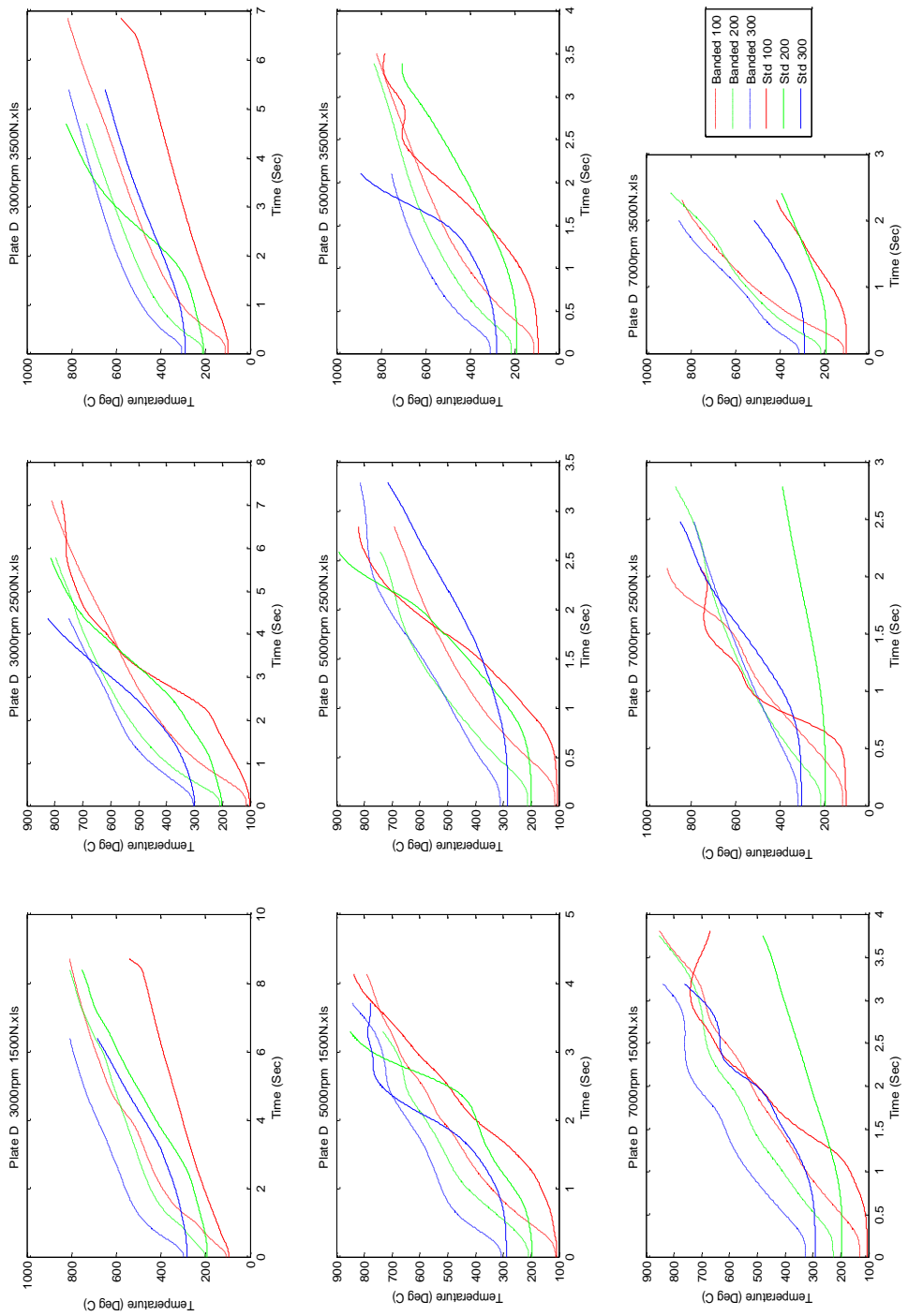
xlabel('Run Number')
```

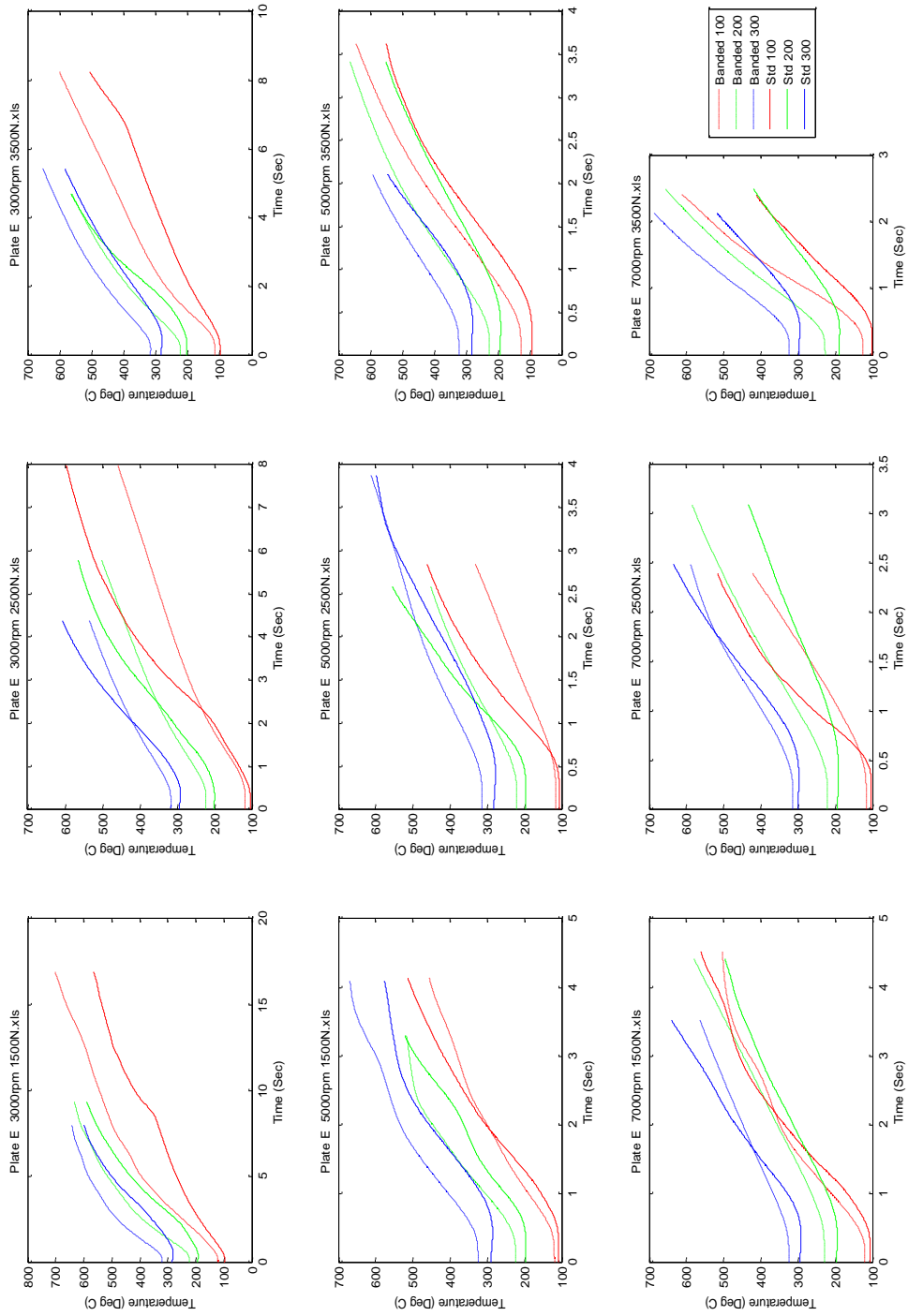
# Appendix P - Results Analysis Model Initial Plots

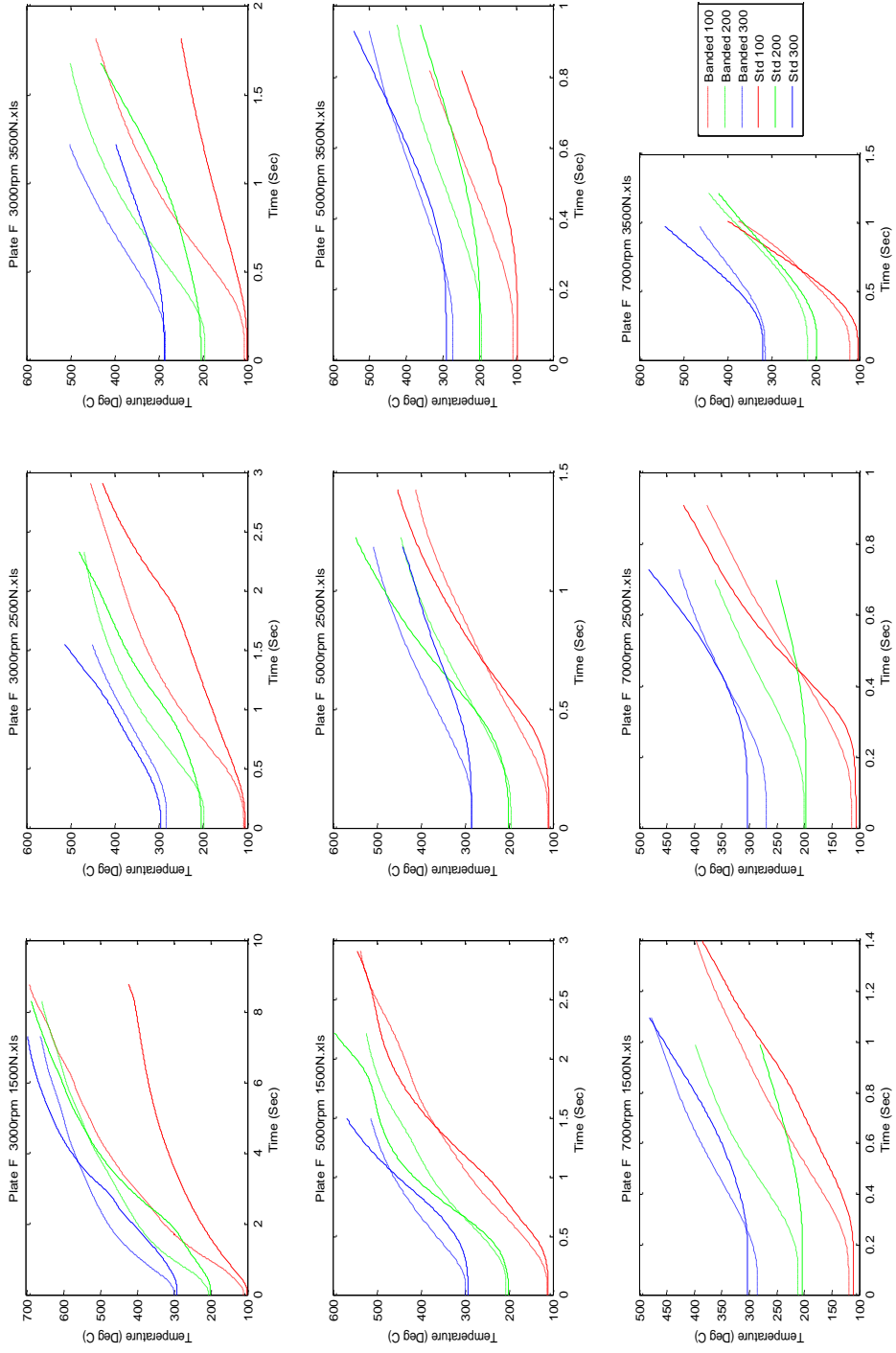


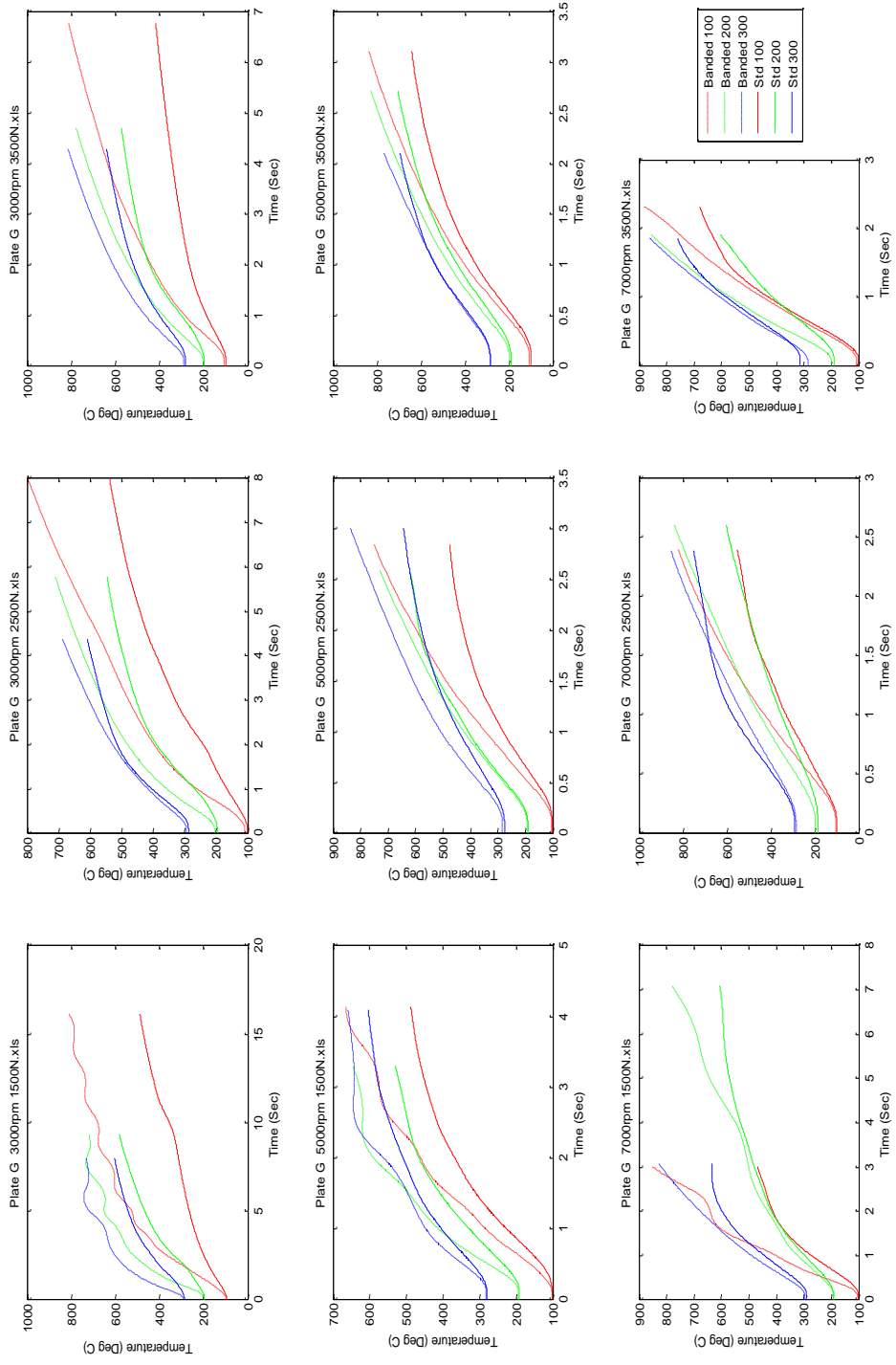






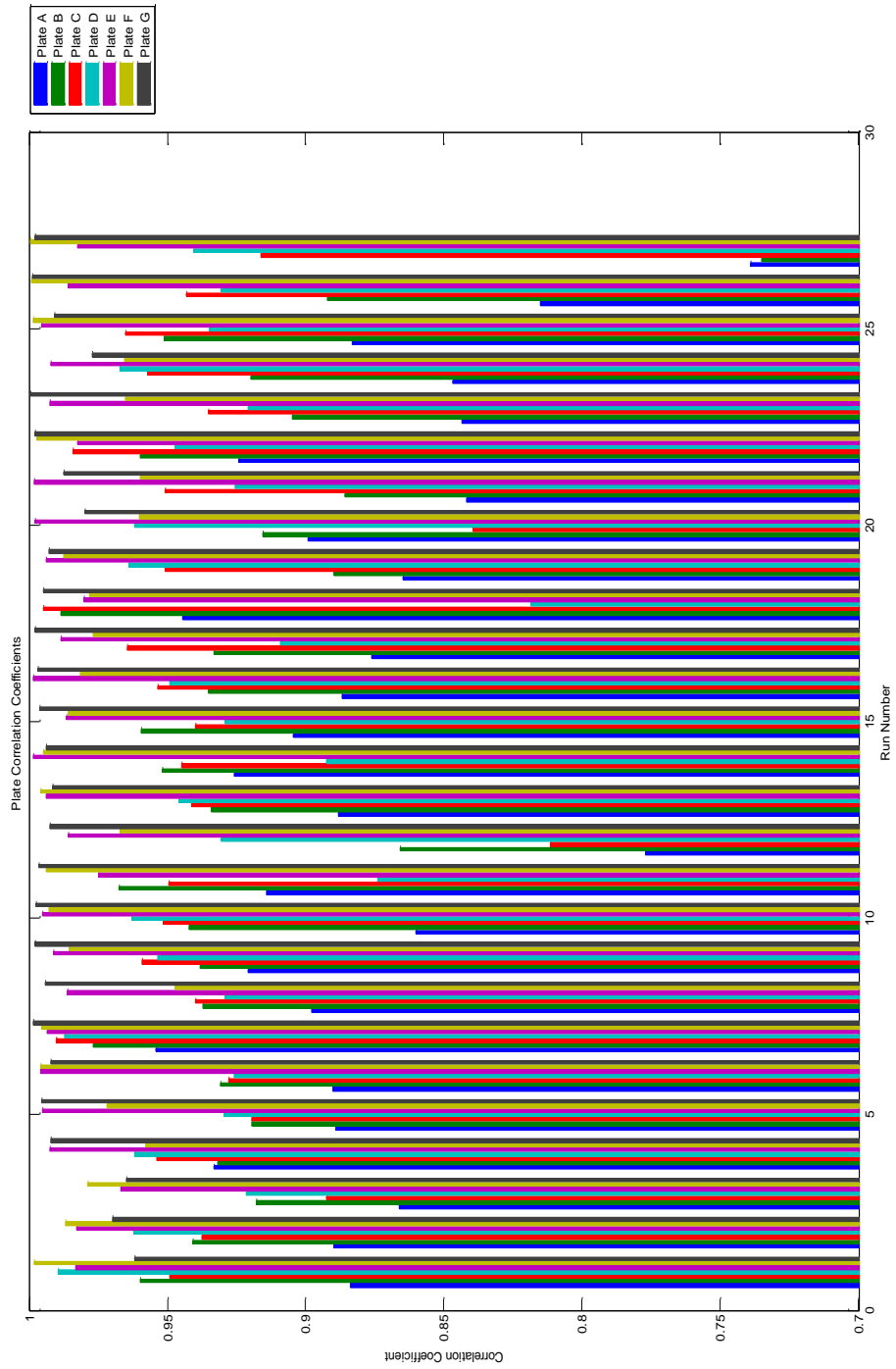


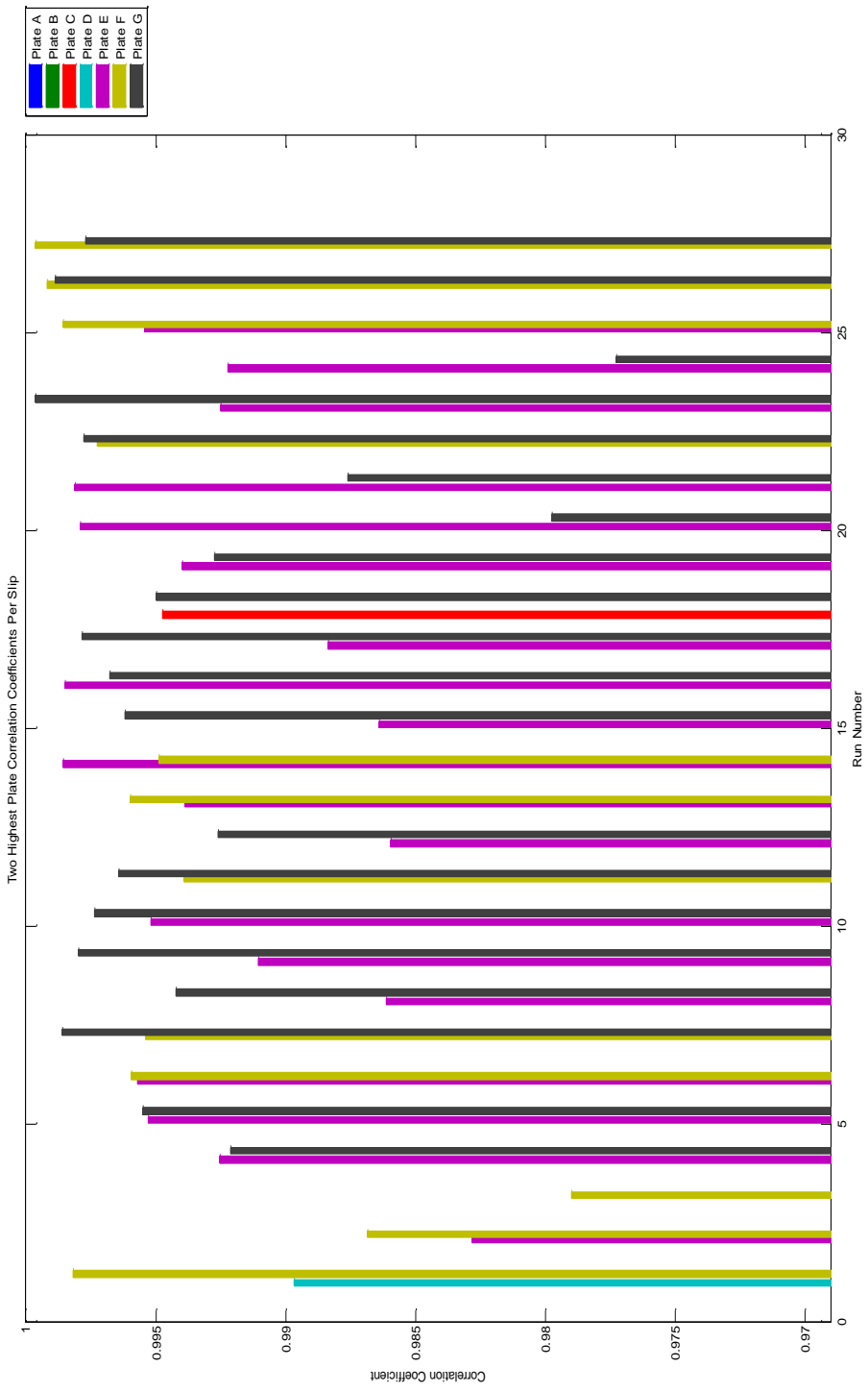






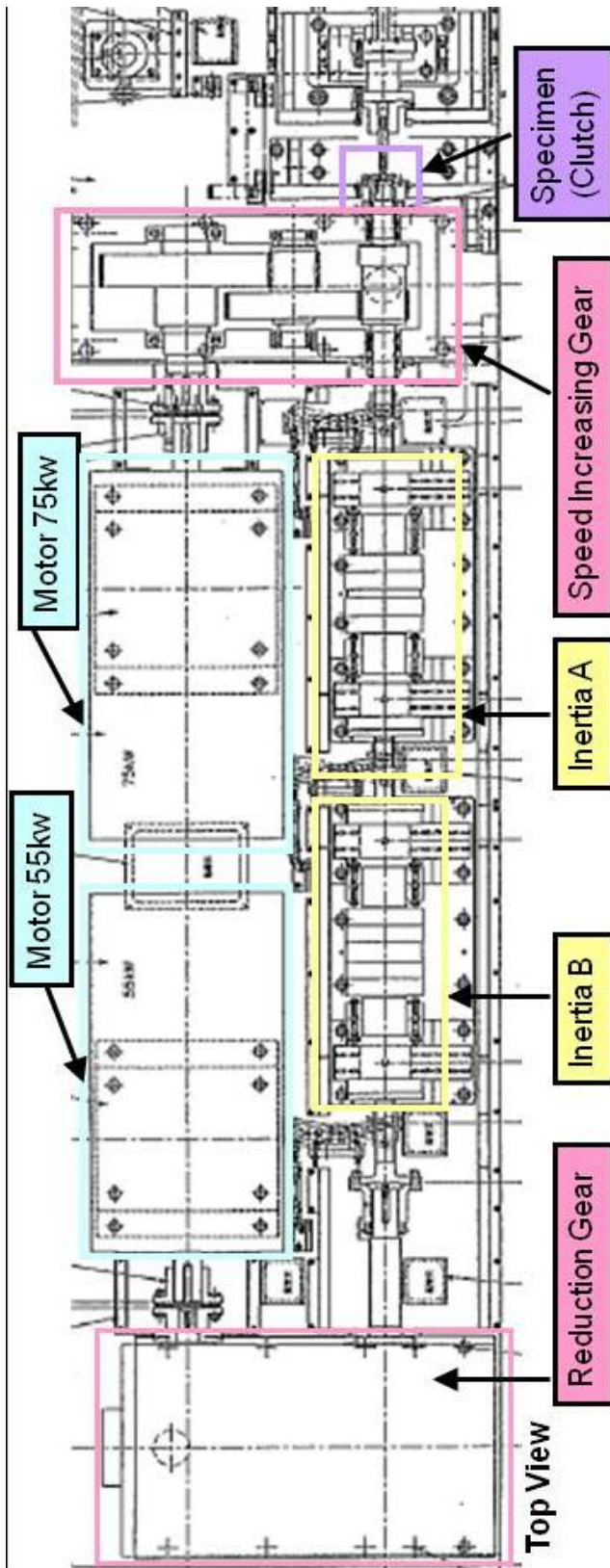
# Appendix Q - Results Analysis Model Evaluated Plots



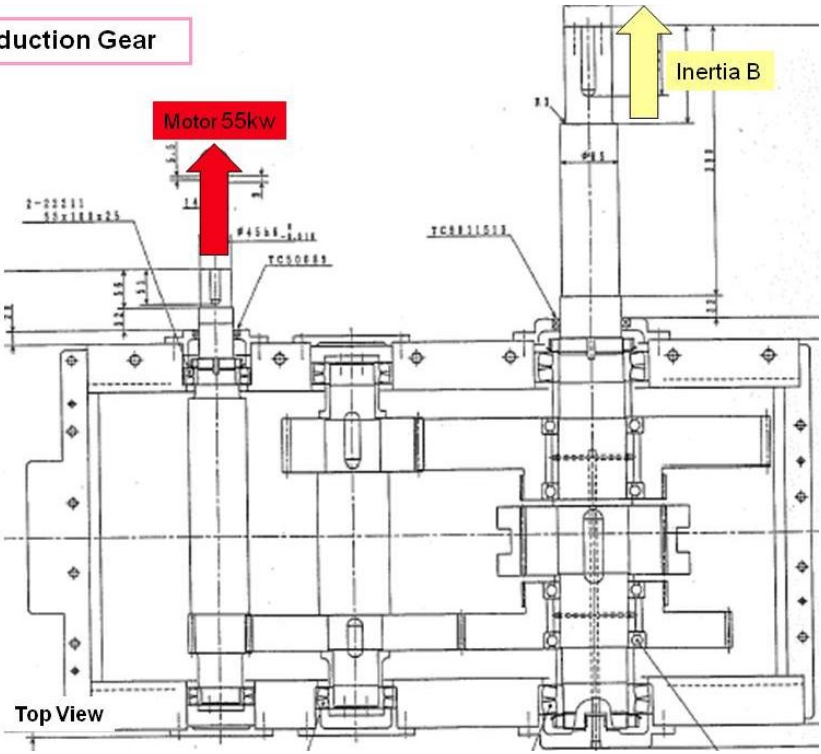




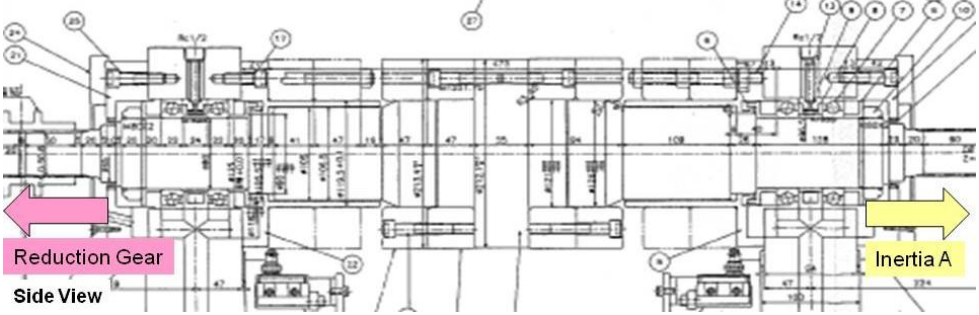
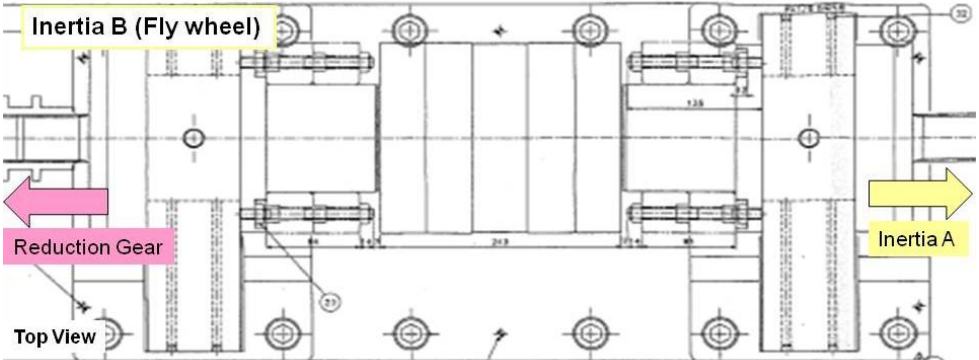
# Appendix R - Technical Drawings of a Clutch Dynamometer

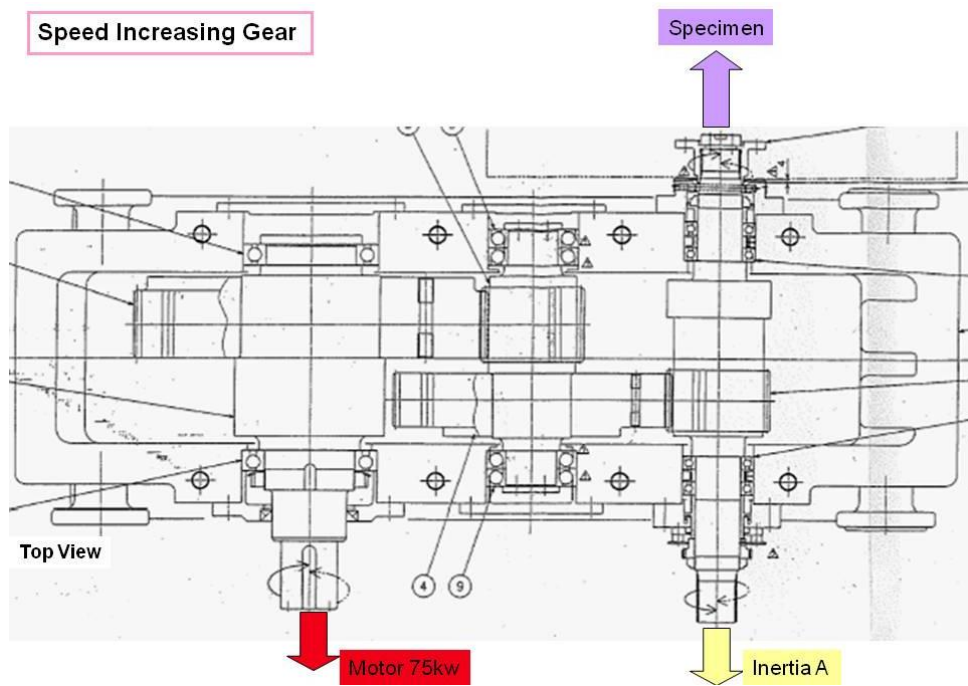
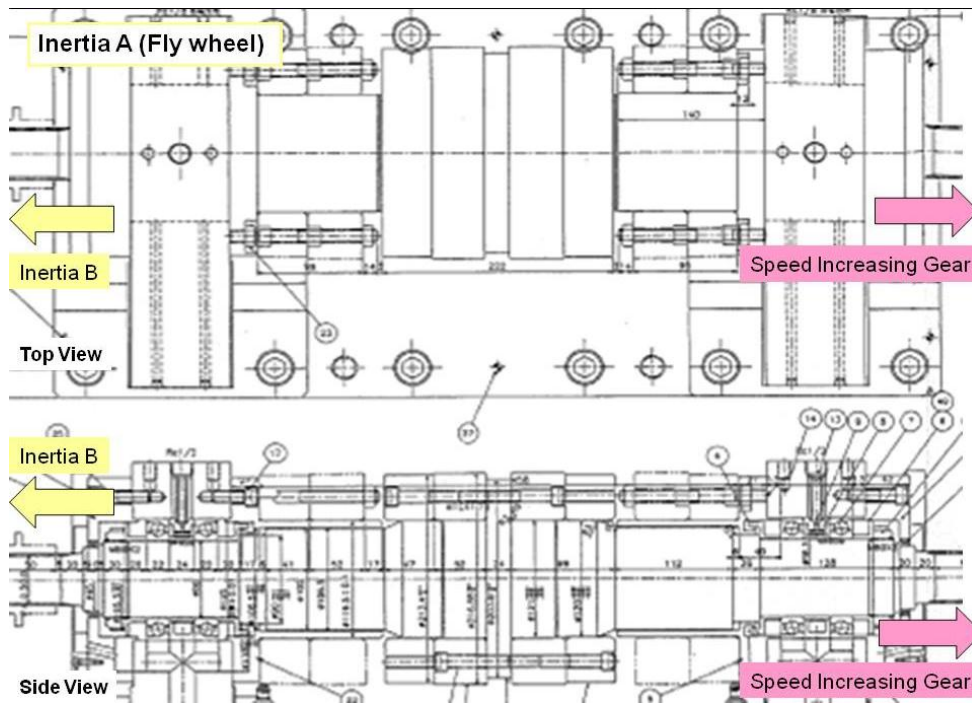


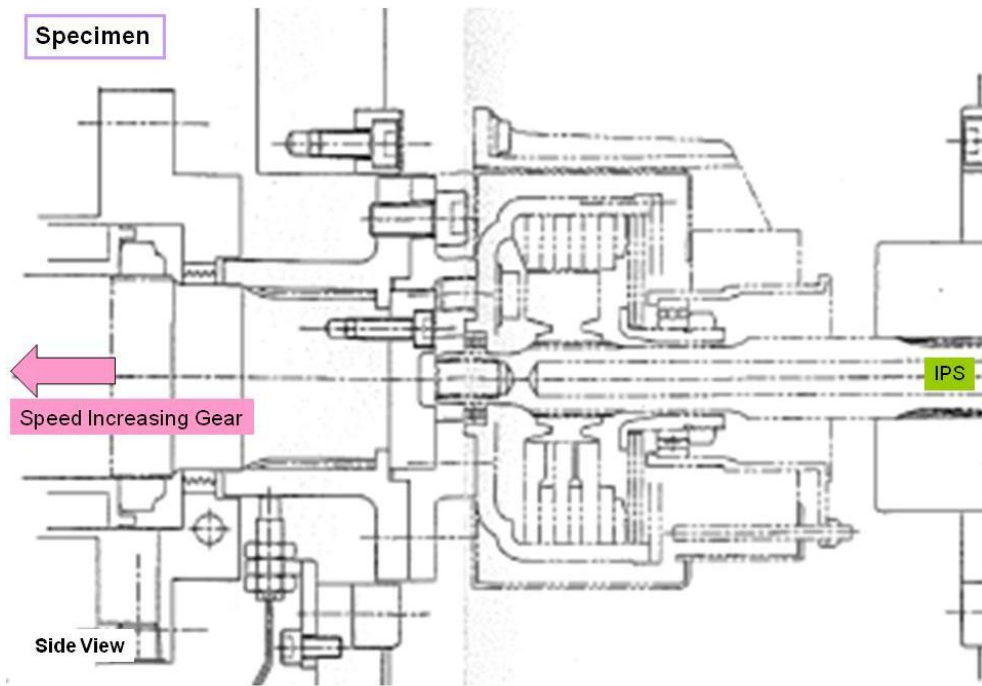
Reduction Gear



Inertia B (Fly wheel)







## Appendix S - Rig Modelling MATLAB® Code

```

% Define functions
function[CluPressurePrev_bar,CluClampLoadPrev_N,CluTorqueNew_Nm,CluSpeedDiff
New_rpm,CluPowerNew_W] = ClutchModel_RigModel
(Time_s,sCluData,dt_s,CluMuPrev,CluSpeedDiffPrev_rpm)

% Define clutch data
% - All clutch information to be stored in structure sCluData

% GEOMETRIC DATA
sCluData.SinglePistonDiameter_mm = 10.5;           % --> Diameter of
single clutch actuation piston [mm]
sCluData.SinglePistonArea_mm2 = 0.25*pi*sCluData.SinglePistonDiameter_mm^2;
% --> Area of single clutch actuation piston [mm^2]
sCluData.NumberOfPistons = 2;                       % --> Total number of
actuation pistons
sCluData.TotalPistonArea_mm2 = sCluData.NumberOfPistons *
sCluData.SinglePistonArea_mm2;
sCluData.DiamInner_mm = 65;                         % --> Inner diameter of
friction material [mm]
sCluData.DiamOuter_mm = 97;                        % --> Outer diameter of
friction material [mm]
sCluData.NumWorkingSurfaces = 6;                   % --> Total number of
working surfaces (1x plate-plate interface = 1 working surface)
sCluData.LeverRatio = 4.73;                        % --> Actuation lever ratio
HGT
sCluData.MeanFrictionRad_mm = (2/3)*(((0.5*sCluData.DiamOuter_mm)^3)-
((0.5*sCluData.DiamInner_mm)^3)) / (((0.5*sCluData.DiamOuter_mm)^2)-
((0.5*sCluData.DiamInner_mm)^2));
sCluData.SingleWorkingSurfaceArea_m2 = (pi/4)*((sCluData.DiamOuter_mm^2)-
(sCluData.DiamInner_mm^2))/1e6;
sCluData.DiscThickness_m = 0.0045;                % --> Thickness of an
individual plate (assumed constant) [m]

sCluData.fInertiaClutchOPS_kgm2 = 0.0003;
sCluData.fInertiaClutchIPS_kgm2 = 0.0016;

% Define rig data

% GEOMETRIC DATA
sCluData.fInertiaRig_kgm2 = 0.42;                  % --> Inertia added to the
clutch rig (Inertia A + Inertia B)
sCluData.fInertiaMotor_kgm2 = 0.2362;             % --> Inertia of the
75kW driving motor and geartrain
sCluData.fSpeedIncreasingRatio = 10.06;           % --> Ratio of the
speed increasing geartrain

% Define initial conditions
% - All initial condition information to be stored in structure sInitialConds

sInitConds.TempAir_degC = 200;                    % --> Initial temperature
of the clutch ambient environment [deg C]
sInitConds.TempBulk_degC = 200;                   % --> Initial
temperature of the clutch bulk [deg C]

```



```

sInitConds.TempSurface_degC = 200; % --> Initial
temperature of the clutch surface [deg C]

sInitConds.CoeffSurfaceState = 0.3; % --> Initial coefficient of
surface state
%sInitConds.CluMu = 0.4

sInitConds.CluSpeedDiff_rpm = 8060;

dt_s = 0.005; % --> Length of each timestep [s]

% Define Functions
function[CluPressurePrev_bar,CluClampLoadPrev_N,CluTorqueNew_Nm,CluSpeedDiff
New_rpm,CluPowerNew_W] =
ClutchModel_RigModel(Time_s,sCluData,dt_s,CluMuPrev,CluSpeedDiffPrev_rpm,RigPr
essureDemand_bar)

TimePressureRise_s = 0.025; % Time taken for the pressure applied by the
rig to reach the maximum value [s]
%RigPressureDemand_bar = 60; % Maximum pressure applied by the rig
during the event [bar]

% If the time at the current timestep is less than the pressure rise time:
% - Calculate the pressure based upon a linear interpolation
% If the time at the current timestep is greater than pressure rise time;
% - Assume pressure is the max pressure
if Time_s < TimePressureRise_s
    CluPressurePrev_bar = RigPressureDemand_bar*(Time_s/TimePressureRise_s);
else
    CluPressurePrev_bar = RigPressureDemand_bar;
end

% Clutch clamp load calculated from:
% - Force = Pressure x Area
CluClampLoadPrev_N =
(CluPressurePrev_bar*1e5)*(sCluData.TotalPistonArea_mm2/1e6)*sCluData.LeverRat
io;
% Clutch torque calculated from:
% - Torque = friction co-efficient x clamp load x number of working surfaces x mean
effective radius
CluTorqueNew_Nm =
CluMuPrev*CluClampLoadPrev_N*sCluData.NumWorkingSurfaces*(sCluData.MeanFri
ctionRad_mm/1e3);

% Convert the clutch speed difference from RPM to radians per second i.e. SI units
CluSpeedDiffPrev_radpers = CluSpeedDiffPrev_rpm*(2*pi/60);

% New clutch speed difference calculated from:
% - Torque = Inertia x angular acceleration
%  $T = I \cdot (\theta \text{ double dot})$ 
%  $T = I \cdot (v_2 - v_1)/dt$ 
%  $v_2 - v_1 = T \cdot dt/I$ 
%  $v_2 = v_1 + (T*dt/I)$ 
CluSpeedDiffNew_radpers = CluSpeedDiffPrev_radpers + (-
CluTorqueNew_Nm*dt_s/(sCluData.fInertiaClutchOPS_kgm2+sCluData.fInertiaRig_kg
m2+(sCluData.fInertiaMotor_kgm2/(sCluData.fSpeedIncreasingRatio^2))));

% New clutch power dissipation calculated from:

```

```
% - Power = Torque x Angular velocity
CluPowerNew_W = CluTorqueNew_Nm*CluSpeedDiffNew_radpers;
```

```
% Convert new speed difference back to rpm from SI unit.
CluSpeedDiffNew_rpm = CluSpeedDiffNew_radpers*(60/(2*pi));
```

```
% Clear unneeded variables
clear CluSpeedDiffNew_radpers CluSpeedDiffOld_radpers
```

```
% ~~~~~
% Ends
```

## Appendix T - Specific Heat and Thermal Diffusivity and Conductivity Test Results

Specific Heat, Thermal Diffusivity and Thermal Conductivity Test Measurements

Test Temperature	Thermal Diffusivity	Specific Heat	Thermal Conductivity
24	6.4	701	8.0
24	6.4	701	8.0
24	6.5	701	8.1
23	6.3	698	7.9
24	6.4	701	8.0
24	6.4	701	8.0
102	6.5	914	10.6
102	6.5	914	10.7
101	6.5	912	10.6
201	6.0	1139	12.1
200	6.0	1137	12.1
199	6.0	1135	12.1
300	5.7	1318	13.3
301	5.6	1320	13.3
301	5.7	1320	13.3
400	5.3	1459	13.6
399	5.3	1457	13.8
398	5.3	1456	13.7
501	5.0	1565	13.9
501	5.0	1565	13.9
501	5.0	1565	13.9
599	4.9	1640	14.2
600	4.8	1640	14.1
601	4.8	1641	14.1
700	4.7	1694	14.0
700	4.7	1694	14.0
700	4.6	1694	13.9

800	4.6	1730	14.2
801	4.6	1731	14.0
801	4.6	1731	14.1
900	4.5	1756	14.0
899	4.5	1756	14.0
899	4.5	1756	14.0
1000	4.5	1777	14.0
1001	4.5	1777	14.2
1001	4.4	1777	13.8
800	4.6	1730	14.0
800	4.6	1730	14.0
802	4.6	1731	14.0
600	5.0	1640	14.4
601	4.8	1641	13.9
599	4.8	1640	14.0
401	5.2	1460	13.6
402	5.3	1461	13.6
402	5.2	1461	13.6
200	6.0	1137	12.1
208	5.9	1153	12.1
208	5.9	1153	12.2
24	6.3	701	7.9
24	6.2	701	7.8
25	6.4	704	8.0

## Appendix U - Thermal Modelling MATLAB® Code

```
function[TempAirNew_degC,TempBulkNew_degC,TempSurfaceNew_degC] =
ClutchModel_ThermalModelSimple(sCluData,TempAirPrev_degC,TempBulkPrev_degC,
TempSurfacePrev_degC,CluPowerNew_W,dt_s)
```

```
% Define clutch data
```

```
% - All clutch information to be stored in structure sCluData
```

```
% GEOMETRIC DATA (RA106 data from Martin Kemp unless otherwise specified in
caps)
```

```
sCluData.SinglePistonDiameter_mm = 10.5; % --> Diameter of
single clutch actuation piston [mm]
```

```
sCluData.SinglePistonArea_mm2 = 0.25*pi*sCluData.SinglePistonDiameter_mm^2;
% --> Area of single clutch actuation piston [mm^2]
```

```
sCluData.NumberOfPistons = 2; % --> Total number of
actuation pistons
```

```
sCluData.TotalPistonArea_mm2 = sCluData.NumberOfPistons *
```

```
sCluData.SinglePistonArea_mm2;
```

```
sCluData.DiamInner_mm = 65; % --> Inner diameter of
friction material [mm]
```

```
sCluData.DiamOuter_mm = 97; % --> Outer diameter of
friction material [mm]
```

```
sCluData.NumWorkingSurfaces = 6; % --> Total number of
working surfaces (1x plate-plate interface = 1 working surface)
```

```
sCluData.LeverRatio = 4.73; % --> Actuation lever ratio
HGT
```

```
sCluData.MeanFrictionRad_mm = (2/3)*(((0.5*sCluData.DiamOuter_mm)^3)-
((0.5*sCluData.DiamInner_mm)^3)) / (((0.5*sCluData.DiamOuter_mm)^2)-
((0.5*sCluData.DiamInner_mm)^2));
```

```
sCluData.SingleWorkingSurfaceArea_m2 = (pi/4)*((sCluData.DiamOuter_mm^2)-
(sCluData.DiamInner_mm^2))/1e6;
```

```
sCluData.DiscThickness_m = 0.0045; % --> Thickness of an
individual plate (assumed constant) [m]
```

```
sCluData.fnertiaClutchOPS_kgm2 = 0.0003;
```

```
sCluData.fnertiaClutchIPS_kgm2 = 0.0016;
```

```
% THERMAL DATA
```

```
sCluData.DensityCC_kgperm3 = 1850; % --> Density of
material [kg/m^3]
```

```
sCluData.Emissivity = 0.8; % --> Emissivity of c-c
```

```
sCluData.CvCCRT_JperkgK = 800; % --> Specific Heat
Capacity at 27degC [J/kg*K]
```

```
sCluData.CvCC1000_JperkgK = 1900; % --> Specific Heat
Capacity at 1000degC [J/kg*K]
```

```
sCluData.ThermalConductivityCCRT_WpermK = 10; % --> Thermal
conductivity perpendicular to friction surface at room temp [W/m.K]
```

```
% Define initial conditions
```

```
% - All initial condition information to be stored in structure sInitialConds
```

```
sInitConds.TempAir_degC = 200; % --> Initial temperature
of the clutch ambient environment [deg C]
```

```
sInitConds.TempBulk_degC = 200; % --> Initial
temperature of the clutch bulk [deg C]
```

```

sInitConds.TempSurface_degC = 200; % --> Initial
temperature of the clutch surface [deg C]

% sInitConds.CluMu = 0.4
sInitConds.CluSpeedDiff_rpm = 8060;
dt_s = 0.005; % --> Length of each timestep [s]

% ~~~~~
% DEFINE MODEL PARAMETERS
SurfaceThickness_m = 0.000010; % Thickness of the surface region [m]
% ~~~~~
% DEFINE ENVIRONMENTAL PROPERTIES
AirConvectiveTransferCoef = 100; % Convective transfer coefficient for air
% ~~~~~
% DEFINE CONSTANTS
StefanBoltzmannConst = 5.6704e-08; % Heat transfer constant of
proportionality [W/m^2.K^4]
% ~~~~~
% OTHER MODEL CALCULATIONS
BulkThickness_m = 0.5*(sCluData.DiscThickness_m - 2*SurfaceThickness_m);
% Thickness of the bulk region [m]
MassBulk_kg =
sCluData.DensityCC_kgperm3*(BulkThickness_m*sCluData.SingleWorkingSurfaceArea
_m2); % Mass of the bulk region [kg]
MassSurface_kg =
sCluData.DensityCC_kgperm3*(SurfaceThickness_m*sCluData.SingleWorkingSurfaceA
rea_m2); % Mass of the surface region [kg]
BulkCircumfSurfaceArea_m2 = BulkThickness_m*(sCluData.DiamOuter_mm/1e3)*pi;
% Exposed radial area of the bulk material [m^2]
% ~~~~~

% ~~~~~
% CONVERT TEMPERATURES FROM CELCIUS TO KELVIN
TempAirPrev_K = TempAirPrev_degC + 273;
TempBulkPrev_K = TempBulkPrev_degC + 273;
TempSurfacePrev_K = TempSurfacePrev_degC + 273;

% ~~~~~
% SPECIFIC HEAT CAPACITY LOOKUP
% ~~~~~
aCvCC = [sCluData.CvCCRT_JperkgK,sCluData.CvCC1000_JperkgK];
aCvTemps_K = [27+273,1000+273];

% If previous surface temperature < 27 deg C
% - Assume Cv is Cv@27degC
% If previous surface temperature > 1000 deg C
% - Assume Cv is Cv@1000degC
% Else assume Cv function is linear and perform interpolation to obtain value for
current surface temperature
if TempSurfacePrev_K < aCvTemps_K(1)
    CvSurface_JperkgK = aCvCC(1);
elseif TempSurfacePrev_K > aCvTemps_K(2);
    CvSurface_JperkgK = aCvCC(2);
else
    CvSurface_JperkgK = interp1(aCvTemps_K,aCvCC,TempSurfacePrev_K);
end

```

```

% Repeat above for bulk
if TempBulkPrev_K < aCvTemps_K(1)
    CvBulk_JperkgK = aCvCC(1);
elseif TempBulkPrev_K > aCvTemps_K(2);
    CvBulk_JperkgK = aCvCC(2);
else
    CvBulk_JperkgK = interp1(aCvTemps_K,aCvCC,TempBulkPrev_K);
end

% ~~~~~~
% HEAT TRANSFER CALCULATIONS
% ~~~~~~

% Assume that entire energy dissipated over the timestep is absorbed into the friction
surface as heat
% - assumptions = zero surface roughness
%           = zero losses to environment
QSurfaceAbsorbed_J = (CluPowerNew_W/12)*dt_s;    % IMPORTANT - divide by 12
as only considering one disc-disc interface (one working surface = two interfaces)

% Heat flux due to conduction from surface to bulk
% - Delta Q = -k.A.(Delta T/Delta x)
% - assumption = uniform conduction through working surface area
QSurfaceConducted_J = -
(sCluData.ThermalConductivityCCRT_WpermK*sCluData.SingleWorkingSurfaceArea_
m2*(TempBulkPrev_K-TempSurfacePrev_K)/BulkThickness_m)*dt_s;

% Heat flux due to convection from surface to bulk
% - Delta Q = A.h.(Delta T)
% - assumption = convection from radial surface of bulk only
QBulkConvected_J =
AirConvectiveTransferCoef*BulkCircumfSurfaceArea_m2*(TempBulkPrev_K-
TempAirPrev_K)*dt_s;

% Heat flux due to radiation
% - Delta Q = A.*sigma*(Delta T)^4
% - assumption = radiation from radial surface of bulk only
QBulkRadiated_J =
BulkCircumfSurfaceArea_m2*StefanBoltzmannConst*sCluData.Emissivity*(TempBulk
Prev_K^4 - TempAirPrev_K^4)*dt_s;

% Flux summation for surface, bulk and ambient environment
% Delta Q = m.Cv.(Delta T)
% - Delta Q = (Heat flux in - heat flux out) over the timestep dt
% For surface:
DeltaTempSurface_K = (QSurfaceAbsorbed_J-
QSurfaceConducted_J)/(MassSurface_kg*CvSurface_JperkgK);
TempSurfaceNew_K = TempSurfacePrev_K + DeltaTempSurface_K;
% New surface temperature = previous surface temperature plus change due to heat
flux
% For bulk:
DeltaTempBulk_K = (QSurfaceConducted_J-QBulkConvected_J-
QBulkRadiated_J)/(MassBulk_kg*CvBulk_JperkgK);
TempBulkNew_K = TempBulkPrev_K + DeltaTempBulk_K;
% For air:

```

CCXX

```
% - assumption = air remains at ambient temp due to air flow i.e. scenario is not a closed system
```

```
TempAirNew_K = TempAirPrev_K;
```

```
% Convert back to deg C from Kelvin
```

```
TempAirNew_degC = TempAirNew_K - 273;
```

```
TempBulkNew_degC = TempBulkNew_K - 273;
```

```
TempSurfaceNew_degC = TempSurfaceNew_K - 273;
```

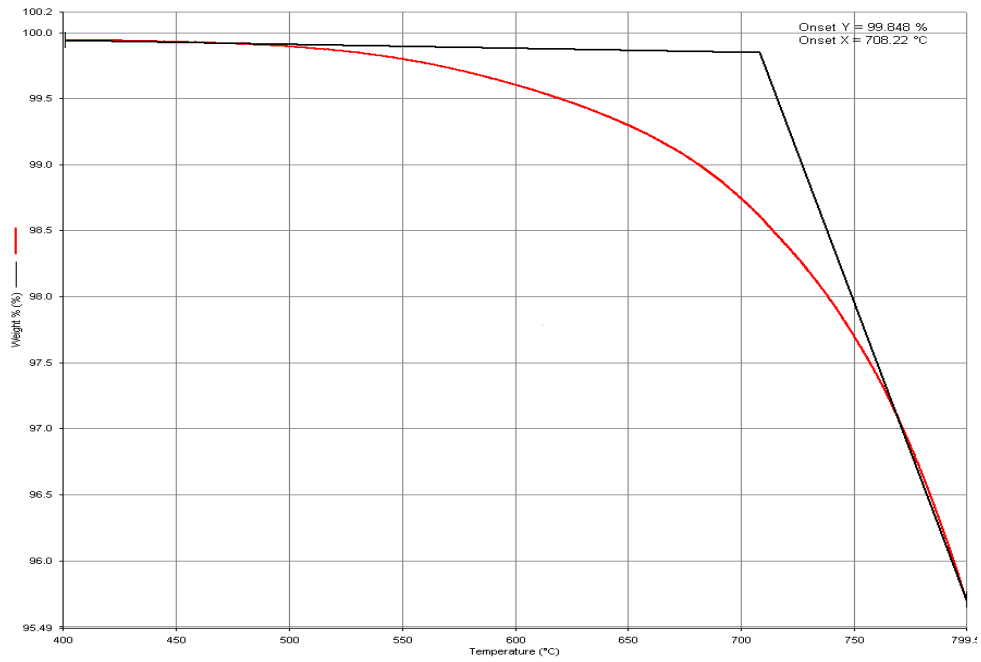
```
% ~~~~~
```

```
% Ends
```

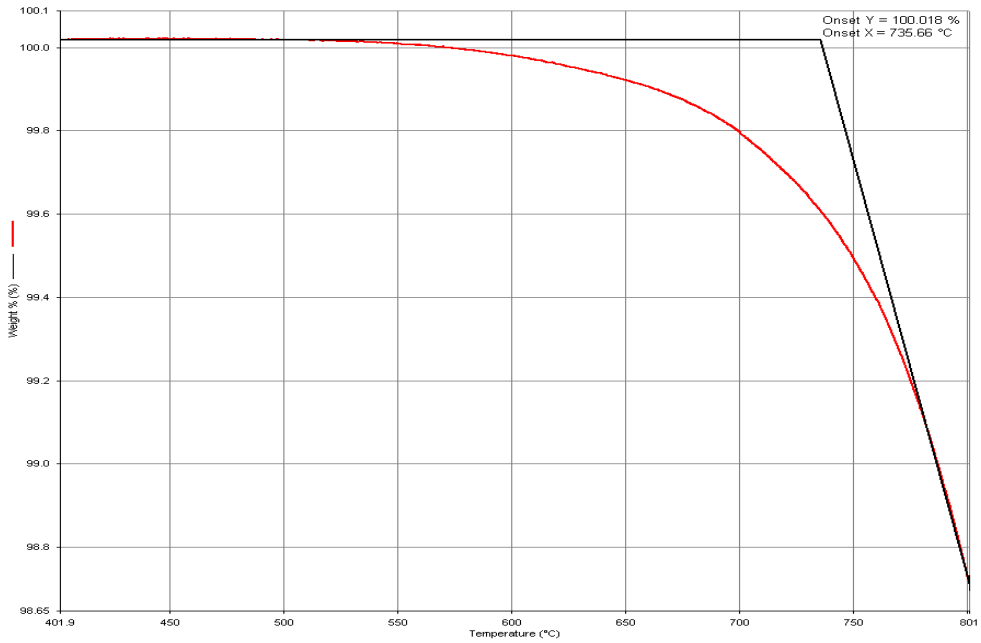


# Appendix V - Thermal Decomposition Test Results

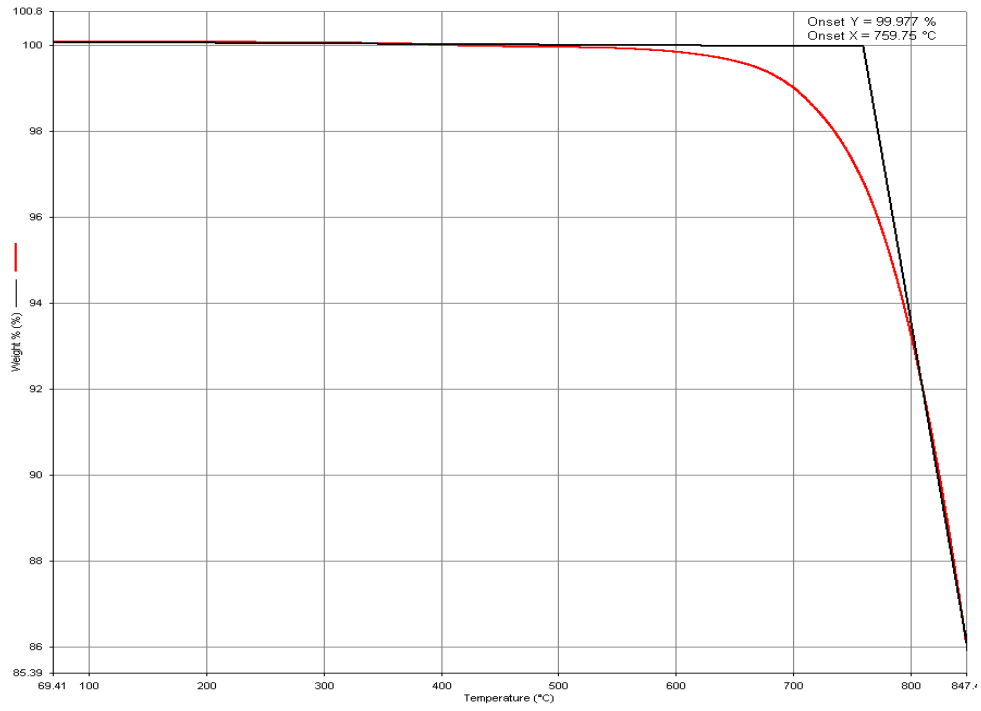
## Thermal Decomposition Sample One



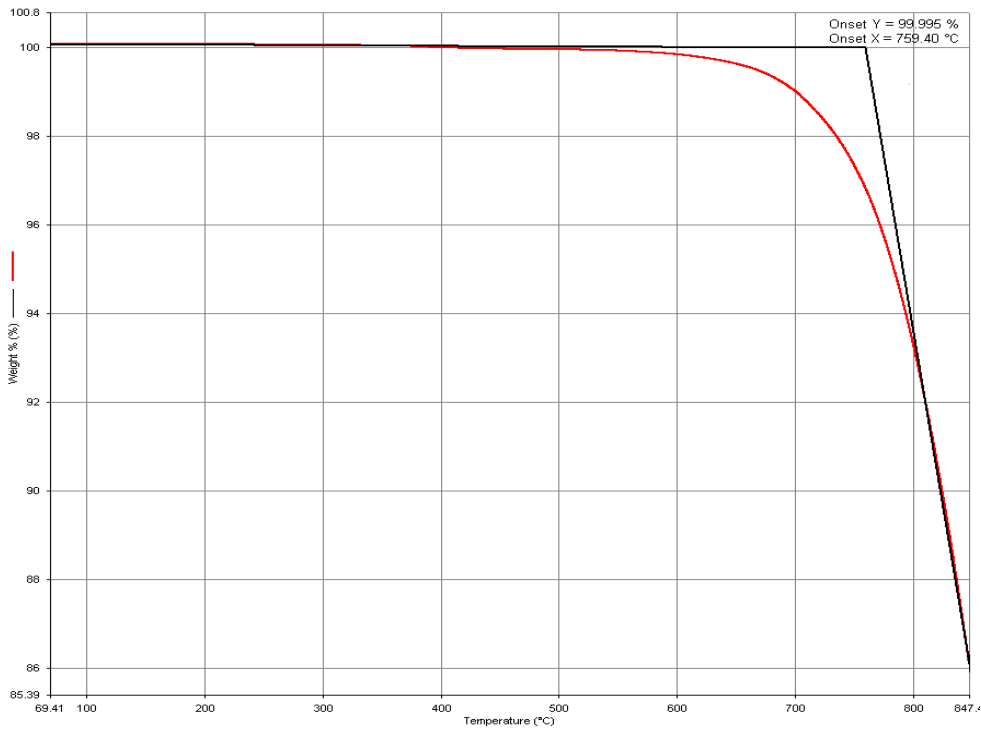
## Thermal Decomposition Sample Two



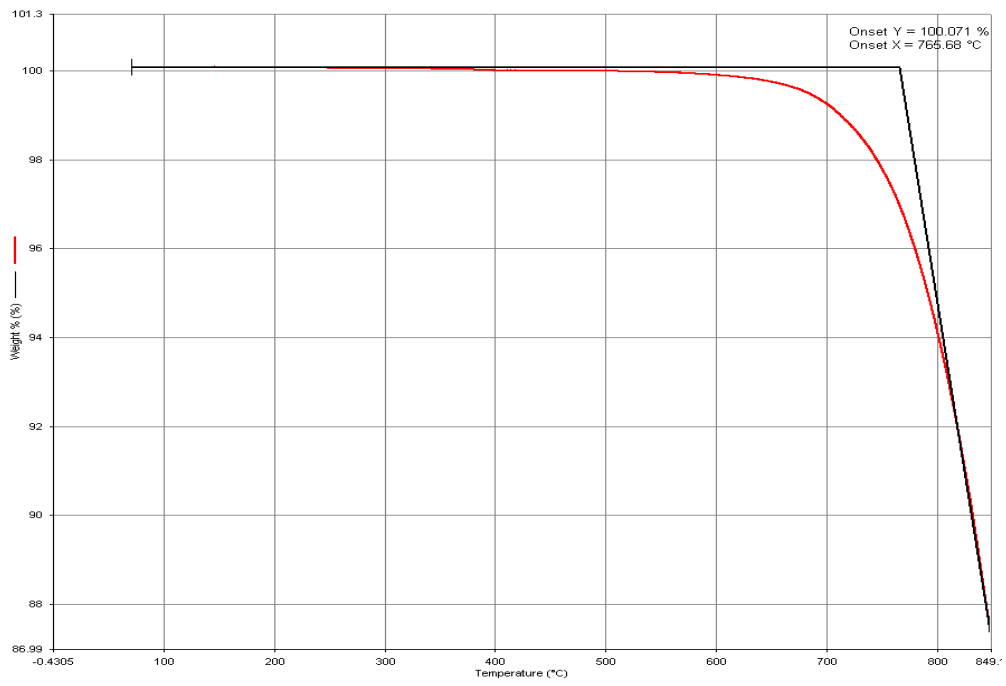
### Thermal Decomposition Sample Three



### Thermal Decomposition Sample Four



## Thermal Decomposition Sample Five



## Appendix W - Surface Modelling MATLAB® Code

### Surface State Model

```
% SYNTAX:
% function[MuAve,MuStart] =
frictionfunction(xDeformation1,yDeformation1,xReformation1,yReformation1,xAbilit
yDeform1,xAbilityReform1,xFriction1,yFriction1,xFriction2,yFriction2)
%
% FILE:
% frictionfunction.m
%
% PURPOSE:
% Predicts the coefficient of friction for a carbon-carbon clutch
% throughout the bedding-in process based upon a simple 'surface-state'
% model.
%
% ARGUMENTS:
% nInitialState - The initial surface state coefficient of the system
% xDeformation1 - x co-ordinate of knee in deformation coefficient curve
% yDeformation2 - y co-ordinate of final point of deformation coefficient curve
% yDeformation1 - y co-ordinate of knee in deformation coefficient curve
% xReformation1 - x co-ordinate of knee in reformation coefficient curve
% yReformation2 - y co-ordinate of final point of reformation coefficient curve
% yReformation1 - y co-ordinate of knee in reformation coefficient curve
% xAbilityDeform1 - x co-ordinate of knee in deformation ability curve
% xAbilityReform1 - x co-ordinate of knee in reformation ability curve
% xFriction1 - x co-ordinate of first knee in coefficient of friction curve
% xFriction2 - x co-ordinate of second knee in coefficient of friction curve
%
% RETURNS:
% aMuAve - Array of average coefficient of friction during each event
% aMuStart - Array of coefficient of friction during first 0.1s of each event
%
% GLOBALS:
% None
%

function[aMuAve,aMuStart] =
frictionfunction(nInitialState,xDeformation1,yDeformation1,yDeformation2,xReforma
tion1,yReformation1,yReformation2,xAbilityDeform1,xAbilityReform1,xFriction1,xFri
ction2)

% Clutch data
ClutchArea_m2 = 0.024429;    % Total area of all clutch working surfaces

% -----
% CYCLE INFORMATION
% - Define the parameters required to generate clutch working cycle

bSameEvents = 1;           % Boolean "All Events The Same?"

dt = 0.1;                  % Time step for the simulation [s]

if bSameEvents == 1
    nEvents = 12;          % Number of events within the cycle?
```

```

nTorque_Nm = 190;      % Torque over the event (assumed constant)
nInputSpeed_rpm = 8000; % Intial clutch input speed [rpm]
nDuration_s = 1;      % Duration of the event [s]
nCooling_s = 4;      % Time between events (i.e. cooling) [s]

eventlength = (nDuration_s + nCooling_s);
aEvent_Speed = zeros(1,eventlength/dt);
aEvent_Torque = zeros(1,eventlength/dt);
aEvent_Slip = zeros(1,eventlength/dt);
aEvent_Speed(1:1+nDuration_s/dt) = [8000:-8000/(nDuration_s/dt):0];
aEvent_Torque(1:1+nDuration_s/dt) = nTorque_Nm;
aEvent_Slip(1:1+nDuration_s/dt) = 1;

aEvent_PowerDensity =
aEvent_Speed.*(2*pi/60).*aEvent_Torque./(1000000*ClutchArea_m2);

aCycle_Time = [dt:dt:(eventlength*nEvents)];
aCycle_Speed = aEvent_Speed;
aCycle_Torque = aEvent_Torque;
aCycle_PowerDensity = aEvent_PowerDensity;
aCycle_Slip = aEvent_Slip;

for iEventCnt = 2:nEvents
    aCycle_Speed(length(aCycle_Speed)+1:length(aCycle_Speed)+(eventlength/dt)) =
aEvent_Speed;

aCycle_Torque(length(aCycle_Torque)+1:length(aCycle_Torque)+(eventlength/dt)) =
aEvent_Torque;

aCycle_PowerDensity(length(aCycle_PowerDensity)+1:length(aCycle_PowerDensity)+
(eventlength/dt)) = aEvent_PowerDensity;
    aCycle_Slip(length(aCycle_Slip)+1:length(aCycle_Slip)+(eventlength/dt)) =
aEvent_Slip;
end

sCycle.Time = aCycle_Time;
sCycle.Speed = aCycle_Speed;
sCycle.Torque = aCycle_Torque;
sCycle.PowerDensity = aCycle_PowerDensity;
sCycle.Slip = aCycle_Slip;
clear aCycle_Time aCycle_Speed aCycle_Torque aCycle_PowerDensity aCycle_Slip

else

end

nPowerTrans = 1;      % Transition power
nPowerMax = 3;      % Max power density considered

sCycle.PowerNormalised = sCycle.PowerDensity./nPowerTrans;

% -----

```

```
% POWER LOOKUP TABLE
```

```
%xDformation1 = 1    % x co-ordinate of the deformation knee  
%yDformation1 = 0.5  % y co-ordinate of the deformation knee  
%xReformation1 = 1.4 % x co-ordinate of the reformation knee  
%yReformation1 = 0.6 % y co-ordinate of the reformation knee
```

```
aLookup_Power = [0:0.1:nPowerMax];  
aLookup_xDformation = [0,xDformation1,nPowerMax];  
aLookup_yDformation = [0,yDformation1,yDformation2];  
aLookup_xReformation = [0,xReformation1,nPowerMax];  
aLookup_yReformation = [0,yReformation1,yReformation2];
```

```
% Plot graph of power against coefficient of deformation/reformation  
Graph_LookupTables = figure;  
subplot(3,1,1);  
plot(aLookup_xDformation,aLookup_yDformation,'color', 'r');  
line(xDformation1,yDformation1, 'Marker', 's', 'MarkerSize', 3, 'MarkerEdgeColor',  
'r', 'MarkerFaceColor', 'r');  
line(nPowerMax,yDformation2, 'Marker', 's', 'MarkerSize', 3, 'MarkerEdgeColor', 'r',  
'MarkerFaceColor', 'r');  
hold on  
grid on  
plot(aLookup_xReformation,aLookup_yReformation,'color', 'g');  
% Add markers to clearly define the location of the knee points  
line(xReformation1,yReformation1, 'Marker', 's', 'MarkerSize', 3, 'MarkerEdgeColor',  
'g', 'MarkerFaceColor', 'g');  
line(nPowerMax,yReformation2, 'Marker', 's', 'MarkerSize', 3, 'MarkerEdgeColor', 'g',  
'MarkerFaceColor', 'g');  
% Add relevant descriptions to the axes  
xlabel('Power Density (MWm^-2)');  
ylabel('Coefficient of surface reformation/deformation');
```

```
% -----  
% ABILITY LOOKUP TABLE
```

```
%xAbilityDeform1 = 0.1  
%yAbilityDeform1 = 0.95  
%xAbilityReform1 = 0.9  
%yAbilityReform1 = 0.95
```

```
aLookup_Power = [0:0.1:3];
```

```
aLookup_xAbilityReform = [1,xAbilityReform1,0];  
aLookup_yAbilityReform = [1,1,0];
```

```
aLookup_xAbilityDeform = [0,xAbilityDeform1,1];  
aLookup_yAbilityDeform = [0,1,1];
```

```
% Plot graph of surface state against ability to deform/reform the surface  
subplot(3,1,2);  
plot(aLookup_xAbilityDeform,aLookup_yAbilityDeform,'color', 'r');  
line(xAbilityDeform1,1, 'Marker', 's', 'MarkerSize', 3, 'MarkerEdgeColor', 'r',  
'MarkerFaceColor', 'r');
```

```

hold on
grid on
plot(aLookup_xAbilityReform,aLookup_yAbilityDeform,'color','g');
% Add markers to clearly define the location of the knee point
line(xAbilityReform1,1,'Marker','s','MarkerSize',3,'MarkerEdgeColor','g',
'MarkerFaceColor','g');
% Add relevant descriptions to the axes
xlabel('Coefficient of Surface State at i-1th timestep');
ylabel('Coefficient of ability to deform/reform');
% -----
% FRICTION LOOKUP TABLE

%xFriction1 = 0.4;
%xFriction2 = 0.6;
%yFriction1 = 0.55;
%yFriction2 = 0.35;

aLookup_xFriction = [0,xFriction1,xFriction2,1];
aLookup_yFriction = [0.6,0.6,0.3,0.3];

subplot(3,1,3);
plot(aLookup_xFriction,aLookup_yFriction);
grid on
% Add markers to clearly define the location of the knee points
line(xFriction1,0.6,'Marker','s','MarkerSize',3,'MarkerEdgeColor','b',
'MarkerFaceColor','b');
line(xFriction2,0.3,'Marker','s','MarkerSize',3,'MarkerEdgeColor','b',
'MarkerFaceColor','b');
% Add relevant descriptions to the axes
xlabel('Coefficient of Surface State');
ylabel('Coefficient of friction');
ylim([0,1]);

sCycle.cDeformation(1,1) = [0];
sCycle.cReformation(1,1) = [0];
sCycle.cAbilityDeform(1,1) = [0];
sCycle.cAbilityReform(1,1) = [0];
sCycle.cChange(1,1) = [0];
sCycle.SurfaceState(1,1) = [nInitialState];
sCycle.Mu(1,1) =
interp1(aLookup_xFriction,aLookup_yFriction,sCycle.SurfaceState(1,1),'linear');

for iTimeStep = 2:length(sCycle.Time)

    PowerDensity = sCycle.PowerDensity(iTimeStep);

    if PowerDensity > nPowerMax
        PowerDensity = nPowerMax;
    end

    sCycle.cDeformation(1,iTimeStep) =
interp1(aLookup_xDeformation,aLookup_yDeformation,PowerDensity,'linear')*dt;
    sCycle.cReformation(1,iTimeStep) =
interp1(aLookup_xReformation,aLookup_yReformation,PowerDensity,'linear')*dt;

```

```

    sCycle.cAbilityDeform(1,iTimeStep) =
interp1(aLookup_xAbilityDeform,aLookup_yAbilityDeform,sCycle.cDeformation(1,iTi
meStep-1),'linear');
    sCycle.cAbilityReform(1,iTimeStep) =
interp1(aLookup_xAbilityReform,aLookup_yAbilityReform,sCycle.cReformation(1,iTi
meStep-1),'linear');

    sCycle.cChange(1,iTimeStep) =
sCycle.cReformation(1,iTimeStep)*sCycle.cAbilityReform(1,iTimeStep) -
sCycle.cDeformation(1,iTimeStep)*sCycle.cAbilityDeform(1,iTimeStep);

    if sCycle.Slip(1,iTimeStep) == 1
        sCycle.SurfaceState(1,iTimeStep) = sCycle.SurfaceState(1,iTimeStep-1) +
sCycle.cChange(1,iTimeStep);
    else
        sCycle.SurfaceState(1,iTimeStep) = sCycle.SurfaceState(1,iTimeStep-1);
    end

    if sCycle.SurfaceState(1,iTimeStep) > 1
        sCycle.SurfaceState(1,iTimeStep) = 1;
    elseif sCycle.SurfaceState(1,iTimeStep) < 0
        sCycle.SurfaceState(1,iTimeStep) = 0;
    end

    sCycle.Mu(1,iTimeStep) =
interp1(aLookup_xFriction,aLookup_yFriction,sCycle.SurfaceState(1,iTimeStep),'linea
r');
    if sCycle.Mu(1,iTimeStep) < 0
        sCycle.Mu(1,iTimeStep) = 0;
    end
end

for iTimeStep = 2:length(sCycle.Time)
    SlipChange(iTimeStep) = sCycle.Slip(iTimeStep)-sCycle.Slip(iTimeStep-1);

end

sCycle.Starts = [1,find(SlipChange == 1)];
sCycle.Ends = find(SlipChange == -1);

for iEventCnt = 1:length(sCycle.Ends)
sCycle.MuAve(iEventCnt) =
mean(sCycle.Mu(sCycle.Starts(iEventCnt):sCycle.Ends(iEventCnt)));
sCycle.MuStart(iEventCnt) =
mean(sCycle.Mu(sCycle.Starts(iEventCnt):sCycle.Starts(iEventCnt)+1));
end

clear SlipChange

aMuAve = sCycle.MuAve(2:end);
aMuStart = sCycle.MuStart(2:end);

```



## Random Number Generator

```
function[RandNum] =  
ClutchModel_RandNumGen(aConfidence,aDiscretisation,nInitialConfidence)  
  
aCumsum = cumsum(aConfidence);  
  
RandNum2 =  
interp1(aCumsum,aDiscretisation,nInitialConfidence+rand(1)*(sum(aConfidence)-  
nInitialConfidence), 'linear');  
  
if isnan(RandNum2) == 1  
    while isnan(RandNum2) == 1  
        RandNum2 =  
interp1(aCumsum,aDiscretisation,nInitialConfidence+rand(1)*(sum(aConfidence)-  
nInitialConfidence));  
    end  
end  
  
RandNum = RandNum2;
```

## Surface State Lookup Table Generator

```
function[mxDeform,myDeform,mzDeform,mxReform,myReform,mzReform,axFriction,  
ayFriction,mDeformCore,mReformCore,aAllGeneratedVals,maxDeform,maxReform] =  
CoordGen_v11(sConfidence);
```

```
%
```

```
~~~~~
```

```
~~~~~
```

```
% GENERATION OF DEFORMATION LOOKUP TABLE
```

```
%
```

```
~~~~~
```

```
~~~~~
```

```
% Define arrays containing x,y and z coordinates of known points
```

```
axKnownVals = [(0:0.1:1),zeros(1,10)];
```

```
ayKnownVals = [zeros(1,11),(0.1:0.1:1)];
```

```
azKnownVals = zeros(1,21);
```

```
OverallLogic = 0;
```

```
while OverallLogic == 0
```

```
    logic = 0;
```

```
    aConfidence = sConfidence.zDeform55;
```

```
    while logic == 0;
```

```
        zDeform55 =
```

```
        ClutchModel_RandNumGen(aConfidence,sConfidence.aDiscretisation,sConfidence.nCo  
n  
fidenceInitial);
```

```
        logic = (zDeform55 > 0)&(1 > zDeform55);
```

```
    end
```

```
    clear aConfidence
```

```
    logic = 0;
```

```
    aConfidence = sConfidence.zDeform5b;
```

```
    while logic == 0;
```

```
        zDeform5b =
```

```
        ClutchModel_RandNumGen(aConfidence,sConfidence.aDiscretisation,sConfidence.nCo  
n  
fidenceInitial);
```

```
        logic = (1 > zDeform5b)&(zDeform5b > zDeform55);
```

```
    end
```

```
    clear aConfidence
```

```
    logic = 0;
```

```
    aConfidence = sConfidence.zDeform5a;
```

```
    while logic == 0;
```

```
        zDeform5a =
```

```
        ClutchModel_RandNumGen(aConfidence,sConfidence.aDiscretisation,sConfidence.nCo  
n  
fidenceInitial);
```

```
        logic = (1 > zDeform5a)&(zDeform5a > zDeform5b);
```

```
    end
```

```
    clear aConfidence
```

```
    logic = 0;
```

```
    aConfidence = sConfidence.yDeformb;
```

```
    while logic == 0;
```

```

yDeformb =
ClutchModel_RandNumGen(aConfidence,sConfidence.aDiscretisation,sConfidence.nCo
nfidenceInitial);
logic = (yDeformb > 0)&(1 > yDeformb);
end
clear aConfidence

```

```

logic = 0;
aConfidence = sConfidence.yDeforma;
while logic == 0;
yDeforma =
ClutchModel_RandNumGen(aConfidence,sConfidence.aDiscretisation,sConfidence.nCo
nfidenceInitial);
logic = (yDeforma > 0)&(yDeformb > yDeforma);
end
clear aConfidence

```

```

logic = 0;
aConfidence = sConfidence.zDeforma5;
while logic == 0;
zDeforma5 =
ClutchModel_RandNumGen(aConfidence,sConfidence.aDiscretisation,sConfidence.nCo
nfidenceInitial);
logic = (zDeforma5 > 0)&(zDeform55 > zDeforma5);
end
clear aConfidence

```

```

logic = 0;
aConfidence = sConfidence.xDeforma;
while logic == 0;
xDeforma =
ClutchModel_RandNumGen(aConfidence,sConfidence.aDiscretisation,sConfidence.nCo
nfidenceInitial);
logic = (xDeforma > 0)&(1 > xDeforma);
end
clear aConfidence

```

```

xDeform1 = 0;
xDeform2 = 0.25;
xDeform3 = 0.5;
xDeform4 = 0.75;
xDeform5 = 1;

```

```

yDeform1 = 0;
yDeform2 = 0.25;
yDeform3 = 0.5;
yDeform4 = 0.75;
yDeform5 = 1;

```

```

axGeneratedVals = [xDeform5,xDeform5,xDeform5,xDeforma];
ayGeneratedVals = [yDeforma,yDeformb,yDeform5,yDeform5];
azGeneratedVals = [zDeform5a,zDeform5b,zDeform55,zDeforma5];

```

```

%nRes = 25;
nMax = 1;
nMin = 0;
nRes = sConfidence.nRes;

[gridx,gridy] = meshgrid([nMin:nMax/nRes:nMax],[nMin:nMax/nRes:nMax]);

gridz =
griddata([axKnownVals,axGeneratedVals],[ayKnownVals,ayGeneratedVals],[azKnown
Vals,azGeneratedVals],gridx,gridy,'invdist');

% mDeform is what will be saved in the sCoord structure
% - gridz can be easily generated later from mDeformCore.
mDeformCore =
[[axKnownVals,axGeneratedVals];[ayKnownVals,ayGeneratedVals];[azKnownVals,azG
eneratedVals]];

zLowCnt = 0;
zHighCnt = 1;
for xCheck = 1:nRes+1

    for yCheck = 1:nRes+1

        z = gridz(xCheck,yCheck);

        if z <= 0
            z = 0;
            zLowCnt = zLowCnt+1;
        end

        if z >= 1;
            z = 1;
            zHighCnt = zHighCnt+1;
        end

        gridz(xCheck,yCheck) = z;
    end

end

zLowCnt_Percent = (zLowCnt/((nRes+1)^2))*100;
zHighCnt_Percent = (zHighCnt/((nRes+1)^2))*100;

if zLowCnt_Percent <= 10
    ResultCheck1 = 1;
else
    ResultCheck1 = 0;
end

if zHighCnt_Percent <= 10
    ResultCheck2 = 1;
else
    ResultCheck2 = 0;
end

```

```

clear zLowCnt_Percent zHighCnt_Percent zLowCnt zHighCnt z

xGradCheck = gridx(size(gridx,1),:);
zGradCheck = gridz(size(gridx,1),:);

for iCnt = 2:length(xGradCheck)
    GradCheck(iCnt-1) = sqrt(zGradCheck(iCnt)-zGradCheck(iCnt-1));
end

clear xGradCheck zGradCheck

ResultCheck3 = isreal(GradCheck);

OverallLogic = (ResultCheck1 == 1 & ResultCheck2 == 1 & ResultCheck3 == 1);
end

mxDeform = gridx;
myDeform = gridy;
mzDeform = gridz;

clear OverallLogic ResultCheck1 ResultCheck2 ResultCheck3
clear axKnownVals axGeneratedVals ayKnownVals ayGeneratedVals azKnownVals
azGeneratedVals

%
%~~~~~
%~~~~~
% GENERATION OF REFORMATION LOOKUP TABLE
%
%~~~~~
%~~~~~

% Define arrays containing x,y and z coordinates of known points
axKnownVals = [(0:0.1:1),zeros(1,10)];
ayKnownVals = [ones(1,11),(0:0.1:0.9)];
azKnownVals = zeros(1,21);

OverallLogic = 0;

while OverallLogic == 0

    logic = 0;
    aConfidence = sConfidence.zReform51;
    while logic == 0;
        zReform51 =
        ClutchModel_RandNumGen(aConfidence,sConfidence.aDiscretisation,sConfidence.nCo
nfidenceInitial);
        logic = (zReform51 > 0)&(1 > zReform51);
    end
    clear aConfidence

    logic = 0;
    aConfidence = sConfidence.zReform5a;

```

```

while logic == 0;
zReform5a =
ClutchModel_RandNumGen(aConfidence,sConfidence.aDiscretisation,sConfidence.nCo
nfidenceInitial);
logic = (zReform5a > 0)&(zReform51 > zReform5a);
end
clear aConfidence

logic = 0;
aConfidence = sConfidence.yReform5a;
while logic == 0;
yReform5a =
ClutchModel_RandNumGen(aConfidence,sConfidence.aDiscretisation,sConfidence.nCo
nfidenceInitial);
logic = (yReform5a > 0)&(1 > yReform5a);
end
clear aConfidence

logic = 0;
aConfidence = sConfidence.zReforma1;
while logic == 0;
zReforma1 =
ClutchModel_RandNumGen(aConfidence,sConfidence.aDiscretisation,sConfidence.nCo
nfidenceInitial);
logic = (zReforma1 > 0)&(zReform51 > zReforma1);
end
clear aConfidence

logic = 0;
aConfidence = sConfidence.xReforma1;
while logic == 0;
xReforma1 =
ClutchModel_RandNumGen(aConfidence,sConfidence.aDiscretisation,sConfidence.nCo
nfidenceInitial);
logic = (xReforma1 > 0)&(1 > xReforma1);
end
clear aConfidence

axGeneratedVals = [1,xReforma1,1];
ayGeneratedVals = [0,0,yReform5a];
azGeneratedVals = [zReform51,zReforma1,zReform5a];

nRes = 25;
nMax = 1;
nMin = 0;

[gridx,gridy] = meshgrid([nMin:nMax/nRes:nMax],[nMin:nMax/nRes:nMax]);

gridz =
griddata([axKnownVals,axGeneratedVals],[ayKnownVals,ayGeneratedVals],[azKnown
Vals,azGeneratedVals],gridx,gridy,'invdist');

% mReformCore is what will be saved in the sCoord structure
% - gridz can be easily generated later from mReformCore.
mReformCore =
[[axKnownVals,axGeneratedVals];[ayKnownVals,ayGeneratedVals];[azKnownVals,azG
eneratedVals]];

```

```

zLowCnt = 0;
zHighCnt = 1;
for xCheck = 1:nRes+1

    for yCheck = 1:nRes+1

        z = gridz(xCheck,yCheck);

        if z <= 0
            z = 0;
            zLowCnt = zLowCnt+1;
        end

        if z >= 1;
            z = 1;
            zHighCnt = zHighCnt+1;
        end

        gridz(xCheck,yCheck) = z;
    end

end

mxReform = gridx;
myReform = gridy;
mzReform = gridz;

OverallLogic = 1;
end

%
%~~~~~
%~~~~~
% GENERATION OF FRICTION LOOKUP TABLE
%
%~~~~~
%~~~~~

xFriction1 = 0;
xFriction2 = 1;

logic = 0;
while logic == 0
    aConfidence = sConfidence.Friction1;
    yFriction1 =
ClutchModel_RandNumGen(aConfidence,sConfidence.aDiscretisation,sConfidence.nCo
nfidenceInitial);
    clear aConfidence

    aConfidence = sConfidence.Friction2;
    yFriction2 =
ClutchModel_RandNumGen(aConfidence,sConfidence.aDiscretisation,sConfidence.nCo
nfidenceInitial);

```

```

clear aConfidence

logic = (yFriction2>0.15)&(yFriction2<0.35)&(yFriction1>0.45)&(yFriction1<0.75);
end

axFriction = [xFriction1,xFriction2];
ayFriction = [yFriction1,yFriction2];

%
~~~~~
% GENERATION OF NORMALISING VALUES
%
~~~~~

logic = 0;
while logic == 0
    aConfidence = sConfidence.maxDeform;
    maxDeform = 800000+(1300000-
800000)*ClutchModel_RandNumGen(aConfidence,sConfidence.aDiscretisation,sConfidence.nConfidenceInitial);
    clear aConfidence

    logic = (maxDeform>800000)&(1300000>maxDeform);
end

logic = 0;
while logic == 0
    aConfidence = sConfidence.maxReform;
    maxReform = 1800+(3000-
1800)*ClutchModel_RandNumGen(aConfidence,sConfidence.aDiscretisation,sConfidence.nConfidenceInitial);
    clear aConfidence

    logic = (maxReform>1800)&(3000>maxReform);
end

aAllGeneratedVals =
[zDeform55,zDeform5b,zDeform5a,yDeformb,yDeforma,zDeforma5,xDeforma,zReform51,zReform5a,yReform5a,zReforma1,xReforma1,yFriction1,yFriction2,maxDeform,maxReform];

```



## Current Data Array Code

```
function[sCoords] = NumGen(nRuns)

Lower = 1;
Upper = 2;

for iCnt = 1:1:nRuns
sLimits.yDeform1 = [0.25,0.4]; %Initially lower limits set to zero
sLimits.yDeform2 = [0.25,0.55];
sLimits.yDeform3 = [0.25,0.65];
sLimits.yDeform4 = [0.25,0.75];
sLimits.yDeform5 = [0.25,0.8];

sLimits.yReform1 = [0,0.25];
sLimits.yReform2 = [0,0.3];
sLimits.yReform3 = [0,0.4];
sLimits.yReform4 = [0,0.9];
sLimits.yReform5 = [0,1];

sLimits.xAbilityDeform1 = 'n/a';
sLimits.xAbilityDeform2 = [0.4,1];
sLimits.xAbilityDeform3 = 'n/a';
sLimits.yAbilityDeform1 = 'n/a';
sLimits.yAbilityDeform2 = [0.5,0.75];
sLimits.yAbilityDeform3 = 'n/a';

sLimits.xAbilityReform1 = 'n/a';
sLimits.xAbilityReform2 = [0,0.6];
sLimits.xAbilityReform3 = 'n/a';
sLimits.yAbilityReform1 = 'n/a';
sLimits.yAbilityReform2 = [0.5,0.75];
sLimits.yAbilityReform3 = 'n/a';

sLimits.xFriction1 = 'n/a';
sLimits.xFriction2 = [0.1,0.7];
sLimits.xFriction3 = [0.3,0.9];
sLimits.xFriction4 = 'n/a';

sLimits.yFriction1 = [0.5,0.7];
sLimits.yFriction2 = [0.4,0.7];
sLimits.yFriction3 = [0.2,0.5];
sLimits.yFriction4 = [0.2,0.35];

xDeform1 = 0;
xDeform2 = 0.25;
xDeform3 = 0.5;
xDeform4 = 0.75;
xDeform5 = 1.0;

xReform1 = 0;
xReform2 = 0.25;
xReform3 = 0.5;
xReform4 = 0.75;
xReform5 = 1.0;
```

```

yReform1 = rand(1)*(sLimits.yReform1(2)-sLimits.yReform1(1));
yReform2 = yReform1 + rand(1)*(sLimits.yReform2(2)-yReform1);

yReform3 = yReform2 + rand(1)*(sLimits.yReform3(2)-yReform2);

yDeform1 = yReform1 + rand(1)*(sLimits.yDeform1(2)-yReform1);
yDeform2 = max(yReform2,yDeform1) + rand(1)*(sLimits.yDeform2(2)-
max(yReform2,yDeform1));
yDeform3 = max(yReform3,yDeform2) + rand(1)*(sLimits.yDeform3(2)-
max(yReform3,yDeform2));
yDeform4 = yDeform3 + rand(1)*(sLimits.yDeform4(2)-yDeform3);
yDeform5 = yDeform4 + rand(1)*(sLimits.yDeform5(2)-yDeform4);

yReform5 = yDeform5 + rand(1)*(sLimits.yReform5(2)-yDeform5);
yReform4 = yReform3 + rand(1)*(yReform5-yReform3);

xAbilityDeform1 = 0;
xAbilityDeform2 =
sLimits.xAbilityDeform2(Lower)+rand(1)*(sLimits.xAbilityDeform2(Upper)-
sLimits.xAbilityDeform2(Lower));
xAbilityDeform3 = 1;
yAbilityDeform1 = 0.5;
yAbilityDeform2 =
sLimits.yAbilityDeform2(Lower)+rand(1)*(sLimits.yAbilityDeform2(Upper)-
sLimits.yAbilityDeform2(Lower));
yAbilityDeform3 = 1;

xAbilityReform1 = 0;
xAbilityReform2 = 1-xAbilityDeform2;
xAbilityReform3 = 1;
yAbilityReform1 = 1;
yAbilityReform2 = yAbilityDeform2;
yAbilityReform3 = 0.5;

xFriction1 = 0;
xFriction2 = sLimits.xFriction2(Lower) + rand(1)*(sLimits.xFriction2(Upper) -
sLimits.xFriction2(Lower));
xFriction3 = max(xFriction2,sLimits.xFriction3(Lower)) +
rand(1)*(sLimits.xFriction3(Upper) - max(xFriction2,sLimits.xFriction3(Lower)));
xFriction4 = 1;

yFriction1 = sLimits.yFriction1(Lower)+rand(1)*(sLimits.yFriction1(Upper)-
sLimits.yFriction1(Lower));
yFriction2 = sLimits.yFriction2(Lower)+rand(1)*(yFriction1-
sLimits.yFriction2(Lower));
yFriction4 = sLimits.yFriction4(Lower)+rand(1)*(sLimits.yFriction4(Upper)-
sLimits.yFriction4(Lower));
yFriction3 = yFriction4 + rand(1)*(min(yFriction2,sLimits.yFriction3(Upper))-
yFriction4);

sCoords.axDeform(iCnt,:) = [xDeform1,xDeform2,xDeform3,xDeform4,xDeform5];
sCoords.ayDeform(iCnt,:) = [yDeform1,yDeform2,yDeform3,yDeform4,yDeform5];

sCoords.axReform(iCnt,:) = [xReform1,xReform2,xReform3,xReform4,xReform5];
sCoords.ayReform(iCnt,:) = [yReform1,yReform2,yReform3,yReform4,yReform5];

```

```

    sCoords.axAbilityDeform(iCnt,:) =
[xAbilityDeform1,xAbilityDeform2,xAbilityDeform3];
    sCoords.ayAbilityDeform(iCnt,:) =
[yAbilityDeform1,yAbilityDeform2,yAbilityDeform3];
    sCoords.axAbilityReform(iCnt,:) =
[xAbilityReform1,xAbilityReform2,xAbilityReform3];
    sCoords.ayAbilityReform(iCnt,:) =
[yAbilityReform1,yAbilityReform2,yAbilityReform3];

    sCoords.axFriction(iCnt,:) = [xFriction1,xFriction2,xFriction3,xFriction4];
    sCoords.ayFriction(iCnt,:) = [yFriction1,yFriction2,yFriction3,yFriction4];

%   for intCnt = 1:51
%
%       x(intCnt) = (intCnt/50)-0.02;
%
%       y(intCnt) = interp1(axFriction(iCnt,:),ayFriction(iCnt,:),x(intCnt),'pchip');
%
%       y2(intCnt) =
interp1(axAbilityDeform(iCnt,:),ayAbilityDeform(iCnt,:),x(intCnt),'pchip');
%       y3(intCnt) =
interp1(axAbilityReform(iCnt,:),ayAbilityReform(iCnt,:),x(intCnt),'pchip');
%
%   end
%
%   figure
%   plot(x,y);
%
%   figure
%   plot(axAbilityDeform(iCnt,:),ayAbilityDeform(iCnt,:));
%   hold on
%   plot(x,y2,'color','r');
%   plot(x,y3,'color','g');
%
%   ax(iCnt,:) = x;
%   ay(iCnt,:) = y;
%
%   ylim([0,1]);

end

```

## Surface Model Code

```
function[CluMuNew,CoefSurfaceStateNew,CoefDeform,CoefReform] =  
ClutchModel_SurfaceModel(iGen,sCluData,CluPowerNew_W,TempSurfaceNew_degC,Coef  
SurfaceStatePrev,sCoordsCurrent)
```

```
% Define clutch data
```

```
% - All clutch information to be stored in structure sCluData
```

```
% GEOMETRIC DATA
```

```
sCluData.SinglePistonDiameter_mm = 10.5; % --> Diameter of  
single clutch actuation piston [mm]
```

```
sCluData.SinglePistonArea_mm2 = 0.25*pi*sCluData.SinglePistonDiameter_mm^2;  
% --> Area of single clutch actuation piston [mm^2]
```

```
sCluData.NumberOfPistons = 2; % --> Total number of  
actuation pistons
```

```
sCluData.TotalPistonArea_mm2 = sCluData.NumberOfPistons *
```

```
sCluData.SinglePistonArea_mm2;
```

```
sCluData.DiamInner_mm = 65; % --> Inner diameter of  
friction material [mm]
```

```
sCluData.DiamOuter_mm = 97; % --> Outer diameter of  
friction material [mm]
```

```
sCluData.NumWorkingSurfaces = 6; % --> Total number of  
working surfaces (1x plate-plate interface = 1 working surface)
```

```
sCluData.LeverRatio = 4.73; % --> Actuation lever ratio  
HGT
```

```
sCluData.MeanFrictionRad_mm = (2/3)*(((0.5*sCluData.DiamOuter_mm)^3)-  
((0.5*sCluData.DiamInner_mm)^3)) / (((0.5*sCluData.DiamOuter_mm)^2)-  
((0.5*sCluData.DiamInner_mm)^2));
```

```
sCluData.SingleWorkingSurfaceArea_m2 = (pi/4)*((sCluData.DiamOuter_mm^2)-  
(sCluData.DiamInner_mm^2))/1e6;
```

```
sCluData.DiscThickness_m = 0.0045; % --> Thickness of an  
individual plate (assumed constant) [m]
```

```
sCluData.fInertiaClutchOPS_kgm2 = 0.0003;
```

```
sCluData.fInertiaClutchIPS_kgm2 = 0.0016;
```

```
% THERMAL DATA
```

```
sCluData.DensityCC_kgperm3 = 1850; % --> Density of Sachs  
material SCM-015 [kg/m^3]
```

```
sCluData.Emissivity = 0.8; % --> Emissivity of c-c (i.e.  
emissive power relative to a black body)
```

```
sCluData.CvCCRT_JperkgK = 800; % --> Specific Heat
```

```
Capacity of SCM-015 at 27degC [J/kg*K]
```

```
sCluData.CvCC1000_JperkgK = 1900; % --> Specific Heat
```

```
Capacity of SCM-015 at 1000degC [J/kg*K]
```

```
sCluData.ThermalConductivityCCRT_WpermK = 10; % --> Thermal  
conductivity of SCM-015 perpendicular to friction surface at room temp [W/m.K]
```

```
% Define initial conditions
```

```
% - All initial condition information to be stored in structure sInitialConds
```

```
sInitConds.TempAir_degC = 200; % --> Initial temperature  
of the clutch ambient environment [deg C]
```

```
sInitConds.TempBulk_degC = 200; % --> Initial  
temperature of the clutch bulk [deg C]
```

```

sInitConds.TempSurface_degC = 200; % --> Initial
temperature of the clutch surface [deg C]

sInitConds.CoeffSurfaceState = 0.3; % --> Initial coefficient of
surface state
%sInitConds.CluMu = 0.4

sInitConds.CluSpeedDiff_rpm = 8060;

dt_s = 0.005; % --> Length of each timestep [s]

PowerDensityMax_Wperm2 = sCoordsCurrent.maxDeform;
TempSurfaceMax_K = sCoordsCurrent.maxReform;

PowerDensity_Wperm2 =
(CluPowerNew_W/sCluData.SingleWorkingSurfaceArea_m2)/12;

CoefPowerDensity = PowerDensity_Wperm2/PowerDensityMax_Wperm2;

if CoefPowerDensity >= 1
    CoefPowerDensity = 1;
end

% Convert the temperature at the current time step to K
TempSurfaceNew_K = TempSurfaceNew_degC + 273;

CoefTempSurface = TempSurfaceNew_K/TempSurfaceMax_K;

if CoefTempSurface >=1
    CoefTempSurface = 1;
end

% Assume surface is only deformed and reformed when plates are in contact.
% - In this model, plates are in contact when slipping occurs.

%CoefDeform =
interp1(sCoords.axDeform(iGen,:),sCoords.ayDeform(iGen,:),CoefPowerDensity,'pchip
');
%CoefReform =
interp1(sCoords.axReform(iGen,:),sCoords.ayReform(iGen,:),CoefTempSurface,'pchip'
);

CoefDeform =
interp2(sCoordsCurrent.mxDeform,sCoordsCurrent.myDeform,sCoordsCurrent.mzDef
orm,CoefPowerDensity,CoefSurfaceStatePrev,'cubic');
CoefReform =
interp2(sCoordsCurrent.mxReform,sCoordsCurrent.myReform,sCoordsCurrent.mzRef
orm,CoefTempSurface,CoefSurfaceStatePrev,'cubic');

%CoefAbilityDeform =
interp1(sCoords.axAbilityDeform(iGen,:),sCoords.ayAbilityDeform(iGen,:),CoefSurface
StatePrev,'pchip');

```

```

%CoefAbilityReform =
interp1(sCoords.axAbilityReform(iGen,:),sCoords.ayAbilityReform(iGen,:),CoefSurface
StatePrev,'pchip');

%DeltaCoefSurfaceState = (CoefReform*CoefAbilityReform) -
(CoefDeform*CoefAbilityDeform);
DeltaCoefSurfaceState = CoefReform - CoefDeform;

CoefSurfaceStateNew = CoefSurfaceStatePrev + DeltaCoefSurfaceState;

if CoefSurfaceStateNew >=1
    CoefSurfaceStateNew = 1;
elseif CoefSurfaceStateNew <= 0
    CoefSurfaceStateNew = 0;
end

CluMuNew =
interp1(sCoordsCurrent.axFriction,sCoordsCurrent.ayFriction,CoefSurfaceStateNew,'c
ubic');

if CluMuNew >= 1
    CluMuNew = 1;
end

```

# Appendix X - Final MATLAB® Model Code

## Initial Conditions Code

```
% ~~~~~  
% SYNTAX:  
% n/a  
%  
% FILENAME:  
% ClutchModel_Init.m  
%  
% FUNCTION:  
% Acts as initialisation file for the Clutch Model. Adds the required  
% geometric, material and rig data to the workspace for use by the model.  
%  
% ARGUMENTS:  
% None  
%  
% RETURNS:  
% None  
%  
% REQUIRED FILES:  
% None  
%  
% REQUIRED GLOBALS:  
% None  
%  
% COMMENTS:  
% None  
%  
% ~~~~~
```

```
ON = 1;  
OFF = 0;
```

```
% ORDER OF PARAMETERS WITHIN INIT FILE:  
% 1) MODEL SETUP  
% 2) LOOKUP TABLE GENERATOR SETUP  
% 3) CLUTCH DATA  
% 4) RIG DATA  
% 5) INITIAL CONDITIONS  
% 6) PLOT OPTIONS
```

```
% ~~~~~  
% 1) MODEL SETUP  
% ~~~~~  
% Define all information required for model to run
```

```
% DISCRETISATION  
dt_s = 0.005; % --> Length of each timestep [s]
```

```
nEvents = 5;
```

```
% LOOKUP TABLE GENERATOR
```

```
CCXLIV
```

```

bRandGen = ON; % --> Define whether lookup
table generator is ON or OFF
nGenerate = 17000; % --> Number of lookup tables
to generate and test

% SAVE FEATURE
bSaveResults = OFF; % --> Define whether save
feature is ON or OFF
nthResultSave = 500; % --> If bSaveResults=ON , save
a file every nth iteration
acstrFilepath = 'C:\Documents and Settings\glawrence\Desktop\Clutch
Model\Results\'; % --> Filepath location for saved files

% Define filename for save - datestamp at time the code commences
DateStamp = clock;
Filename = ['Results_',num2str(DateStamp(1)),'-',num2str(DateStamp(2)),'-
',num2str(DateStamp(3)),'_',num2str(DateStamp(4)),'-
',num2str(DateStamp(5)),'.mat'];
FullFilename = [acstrFilepath,Filename];
clear DateStamp
iSave = 1;

% ~~~~~~
% 2) LOOKUP TABLE GENERATOR SETUP
% ~~~~~~
% Define clutch data
% - All clutch information to be stored in structure sCluData

bConfidenceUpdate = OFF; % --> Define whether
confidence values are updated or remain static

sConfidence.nConfidenceInitial = 40; % --> Initial confidence
weighting
sConfidence.nDiscretisation = 25; % --> Discretisation
resolution used
sConfidence.nConfidenceUpper = 1; % --> Upper limit for
discretisation
sConfidence.nConfidenceLower = 0; % --> Lower limit for
discretisation

sConfidence.aDiscretisation =
[sConfidence.nConfidenceLower,sConfidence.nConfidenceLower+(cumsum(ones(1,sC
onfidence.nDiscretisation))*((sConfidence.nConfidenceUpper-
sConfidence.nConfidenceLower)/sConfidence.nDiscretisation))];
sConfidence.aConfidenceInitial =
ones(1,length(sConfidence.aDiscretisation))*sConfidence.nConfidenceInitial;

sConfidence.nRes = 30;

% ~~~~~~
% 3) CLUTCH DATA
% ~~~~~~
% Define clutch data

```



```

% - All clutch information to be stored in structure sCluData

% GEOMETRIC DATA
sCluData.SinglePistonDiameter_mm = 10.5;           % --> Diameter of
single clutch actuation piston [mm]
sCluData.SinglePistonArea_mm2 = 0.25*pi*sCluData.SinglePistonDiameter_mm^2;
% --> Area of single clutch actuation piston [mm^2]
sCluData.NumberOfPistons = 2;                     % --> Total number of
actuation pistons
sCluData.TotalPistonArea_mm2 = sCluData.NumberOfPistons *
sCluData.SinglePistonArea_mm2;
sCluData.DiamInner_mm = 65;                       % --> Inner diameter of
friction material [mm]
sCluData.DiamOuter_mm = 97;                      % --> Outer diameter of
friction material [mm]
sCluData.NumWorkingSurfaces = 6;                 % --> Total number of
working surfaces (1x plate-plate interface = 1 working surface)
sCluData.LeverRatio = 4.73;                      % --> Actuation lever ratio
sCluData.MeanFrictionRad_mm = (2/3)*{ (((0.5*sCluData.DiamOuter_mm)^3)-
((0.5*sCluData.DiamInner_mm)^3)) / (((0.5*sCluData.DiamOuter_mm)^2)-
((0.5*sCluData.DiamInner_mm)^2))};
sCluData.SingleWorkingSurfaceArea_m2 = (pi/4)*((sCluData.DiamOuter_mm^2)-
(sCluData.DiamInner_mm^2))/1e6;
sCluData.DiscThickness_m = 0.0045;              % --> Thickness of an
individual plate (assumed constant) [m]

sCluData.fInertiaClutchOPS_kgm2 = 0.0003;
sCluData.fInertiaClutchIPS_kgm2 = 0.0016;

% THERMAL DATA
sCluData.DensityCC_kgperm3 = 1850;               % --> Density
[kg/m^3]
sCluData.Emissivity = 0.8;                       % --> Emissivity of c-c (i.e.
emissive power relative to a black body)
sCluData.CvCCRT_JperkgK = 800;                  % --> Specific Heat
Capacity of at 27degC [J/kg*K]
sCluData.CvCC1000_JperkgK = 1900;               % --> Specific Heat
Capacity at 1000degC [J/kg*K]
sCluData.ThermalConductivityCCRT_WpermK = 10;    % --> Thermal
conductivity perpendicular to friction surface at room temp [W/m.K]

% ~~~~~
% 4) RIG DATA
% ~~~~~
% Define rig data
% - All clutch information to be stored in structure sCluData

% GEOMETRIC DATA
sCluData.fInertiaRig_kgm2 = 0.42;                % --> Inertia added to the
clutch rig (Inertia A + Inertia B)
sCluData.fInertiaMotor_kgm2 = 0.2362;           % --> Inertia of the
75kW driving motor and geartrain
sCluData.fSpeedIncreasingRatio = 10.06;         % --> Ratio of the
speed increasing geartrain

```

```

% ~~~~~
% 5) INITIAL CONDITIONS
% ~~~~~
% Define initial conditions
% - All initial condition information to be stored in structure sInitialConds

sInitConds.TempAir_degC = 200;           % --> Initial temperature
of the clutch ambient environment [deg C]
sInitConds.TempBulk_degC = 200;         % --> Initial
temperature of the clutch bulk [deg C]
sInitConds.TempSurface_degC = 200;      % --> Initial
temperature of the clutch surface [deg C]

sInitConds.CoeffSurfaceState = 0.3;     % --> Initial coefficient of
surface state %sInitConds.CluMu = 0.4

sInitConds.CluSpeedDiff_rpm = 8060;

% ~~~~~
% 6) PLOT OPTIONS
% ~~~~~
% Set plot options

% PLOTS
bPlotBestResults = 1;

```

## Random Number Generator

```
function[RandNum] =  
ClutchModel_RandNumGen(aConfidence,aDiscretisation,nInitialConfidence)  
  
aCumsum = cumsum(aConfidence);  
  
RandNum2 =  
interp1(aCumsum,aDiscretisation,nInitialConfidence+rand(1)*(sum(aConfidence)-  
nInitialConfidence), 'linear');  
  
if isnan(RandNum2) == 1  
    while isnan(RandNum2) == 1  
        RandNum2 =  
interp1(aCumsum,aDiscretisation,nInitialConfidence+rand(1)*(sum(aConfidence)-  
nInitialConfidence));  
    end  
end  
  
RandNum = RandNum2;
```

## Surface State Lookup Table Generator

```
function[mxDeform,myDeform,mzDeform,mxReform,myReform,mzReform,axFriction,  
ayFriction,mDeformCore,mReformCore,aAllGeneratedVals,maxDeform,maxReform] =  
CoordGen_v11(sConfidence);
```

```
%
```

```
~~~~~
```

```
~~~~~
```

```
% GENERATION OF DEFORMATION LOOKUP TABLE
```

```
%
```

```
~~~~~
```

```
~~~~~
```

```
% Define arrays containing x,y and z coordinates of known points
```

```
axKnownVals = [(0:0.1:1),zeros(1,10)];
```

```
ayKnownVals = [zeros(1,11),(0.1:0.1:1)];
```

```
azKnownVals = zeros(1,21);
```

```
OverallLogic = 0;
```

```
while OverallLogic == 0
```

```
    logic = 0;
```

```
    aConfidence = sConfidence.zDeform55;
```

```
    while logic == 0;
```

```
        zDeform55 =
```

```
        ClutchModel_RandNumGen(aConfidence,sConfidence.aDiscretisation,sConfidence.nCo  
n  
fidenceInitial);
```

```
        logic = (zDeform55 > 0)&(1 > zDeform55);
```

```
    end
```

```
    clear aConfidence
```

```
    logic = 0;
```

```
    aConfidence = sConfidence.zDeform5b;
```

```
    while logic == 0;
```

```
        zDeform5b =
```

```
        ClutchModel_RandNumGen(aConfidence,sConfidence.aDiscretisation,sConfidence.nCo  
n  
fidenceInitial);
```

```
        logic = (1 > zDeform5b)&(zDeform5b > zDeform55);
```

```
    end
```

```
    clear aConfidence
```

```
    logic = 0;
```

```
    aConfidence = sConfidence.zDeform5a;
```

```
    while logic == 0;
```

```
        zDeform5a =
```

```
        ClutchModel_RandNumGen(aConfidence,sConfidence.aDiscretisation,sConfidence.nCo  
n  
fidenceInitial);
```

```
        logic = (1 > zDeform5a)&(zDeform5a > zDeform5b);
```

```
    end
```

```
    clear aConfidence
```

```
    logic = 0;
```

```
    aConfidence = sConfidence.yDeformb;
```

```
    while logic == 0;
```

```
yDeformb =  
ClutchModel_RandNumGen(aConfidence,sConfidence.aDiscretisation,sConfidence.nCo  
nfidenceInitial);  
logic = (yDeformb > 0)&(1 > yDeformb);  
end  
clear aConfidence
```

```
logic = 0;  
aConfidence = sConfidence.yDeforma;  
while logic == 0;  
yDeforma =  
ClutchModel_RandNumGen(aConfidence,sConfidence.aDiscretisation,sConfidence.nCo  
nfidenceInitial);  
logic = (yDeforma > 0)&(yDeformb > yDeforma);  
end  
clear aConfidence
```

```
logic = 0;  
aConfidence = sConfidence.zDeforma5;  
while logic == 0;  
zDeforma5 =  
ClutchModel_RandNumGen(aConfidence,sConfidence.aDiscretisation,sConfidence.nCo  
nfidenceInitial);  
logic = (zDeforma5 > 0)&(zDeform55 > zDeforma5);  
end  
clear aConfidence
```

```
logic = 0;  
aConfidence = sConfidence.xDeforma;  
while logic == 0;  
xDeforma =  
ClutchModel_RandNumGen(aConfidence,sConfidence.aDiscretisation,sConfidence.nCo  
nfidenceInitial);  
logic = (xDeforma > 0)&(1 > xDeforma);  
end  
clear aConfidence
```

```
xDeform1 = 0;  
xDeform2 = 0.25;  
xDeform3 = 0.5;  
xDeform4 = 0.75;  
xDeform5 = 1;
```

```
yDeform1 = 0;  
yDeform2 = 0.25;  
yDeform3 = 0.5;  
yDeform4 = 0.75;  
yDeform5 = 1;
```

```
axGeneratedVals = [xDeform5,xDeform5,xDeform5,xDeforma];  
ayGeneratedVals = [yDeforma,yDeformb,yDeform5,yDeform5];  
azGeneratedVals = [zDeform5a,zDeform5b,zDeform55,zDeforma5];
```

CCL

```

%nRes = 25;
nMax = 1;
nMin = 0;
nRes = sConfidence.nRes;

[gridx,gridy] = meshgrid([nMin:nMax/nRes:nMax],[nMin:nMax/nRes:nMax]);

gridz =
griddata([axKnownVals,axGeneratedVals],[ayKnownVals,ayGeneratedVals],[azKnown
Vals,azGeneratedVals],gridx,gridy,'invdist');

% mDeform is what will be saved in the sCoord structure
% - gridz can be easily generated later from mDeformCore.
mDeformCore =
[[axKnownVals,axGeneratedVals];[ayKnownVals,ayGeneratedVals];[azKnownVals,azG
eneratedVals]];

zLowCnt = 0;
zHighCnt = 1;
for xCheck = 1:nRes+1

    for yCheck = 1:nRes+1

        z = gridz(xCheck,yCheck);

        if z <= 0
            z = 0;
            zLowCnt = zLowCnt+1;
        end

        if z >= 1;
            z = 1;
            zHighCnt = zHighCnt+1;
        end

        gridz(xCheck,yCheck) = z;
    end

end

zLowCnt_Percent = (zLowCnt/((nRes+1)^2))*100;
zHighCnt_Percent = (zHighCnt/((nRes+1)^2))*100;

if zLowCnt_Percent <= 10
    ResultCheck1 = 1;
else
    ResultCheck1 = 0;
end

if zHighCnt_Percent <= 10
    ResultCheck2 = 1;
else
    ResultCheck2 = 0;
end

```

```

clear zLowCnt_Percent zHighCnt_Percent zLowCnt zHighCnt z

xGradCheck = gridx(size(gridx,1),:);
zGradCheck = gridz(size(gridz,1),:);

for iCnt = 2:length(xGradCheck)
    GradCheck(iCnt-1) = sqrt(zGradCheck(iCnt)-zGradCheck(iCnt-1));
end

clear xGradCheck zGradCheck

ResultCheck3 = isreal(GradCheck);

OverallLogic = (ResultCheck1 == 1 & ResultCheck2 == 1 & ResultCheck3 == 1);
end

mxDeform = gridx;
myDeform = gridy;
mzDeform = gridz;

clear OverallLogic ResultCheck1 ResultCheck2 ResultCheck3
clear axKnownVals axGeneratedVals ayKnownVals ayGeneratedVals azKnownVals
azGeneratedVals

%
% ~~~~~
% ~~~~
% GENERATION OF REFORMATION LOOKUP TABLE
%
% ~~~~~
% ~~~~

% Define arrays containing x,y and z coordinates of known points
axKnownVals = [(0:0.1:1),zeros(1,10)];
ayKnownVals = [ones(1,11),(0:0.1:0.9)];
azKnownVals = zeros(1,21);

OverallLogic = 0;

while OverallLogic == 0

    logic = 0;
    aConfidence = sConfidence.zReform51;
    while logic == 0;
        zReform51 =
        ClutchModel_RandNumGen(aConfidence,sConfidence.aDiscretisation,sConfidence.nCo
        nfidenceInitial);
        logic = (zReform51 > 0)&(1 > zReform51);
    end
    clear aConfidence

    logic = 0;
    aConfidence = sConfidence.zReform5a;

```

CCLII

```

while logic == 0;
zReform5a =
ClutchModel_RandNumGen(aConfidence,sConfidence.aDiscretisation,sConfidence.nCo
nfidenceInitial);
logic = (zReform5a > 0)&(zReform51 > zReform5a);
end
clear aConfidence

logic = 0;
aConfidence = sConfidence.yReform5a;
while logic == 0;
yReform5a =
ClutchModel_RandNumGen(aConfidence,sConfidence.aDiscretisation,sConfidence.nCo
nfidenceInitial);
logic = (yReform5a > 0)&(1 > yReform5a);
end
clear aConfidence

logic = 0;
aConfidence = sConfidence.zReforma1;
while logic == 0;
zReforma1 =
ClutchModel_RandNumGen(aConfidence,sConfidence.aDiscretisation,sConfidence.nCo
nfidenceInitial);
logic = (zReforma1 > 0)&(zReform51 > zReforma1);
end
clear aConfidence

logic = 0;
aConfidence = sConfidence.xReforma1;
while logic == 0;
xReforma1 =
ClutchModel_RandNumGen(aConfidence,sConfidence.aDiscretisation,sConfidence.nCo
nfidenceInitial);
logic = (xReforma1 > 0)&(1 > xReforma1);
end
clear aConfidence

axGeneratedVals = [1,xReforma1,1];
ayGeneratedVals = [0,0,yReform5a];
azGeneratedVals = [zReform51,zReforma1,zReform5a];

nRes = 25;
nMax = 1;
nMin = 0;

[gridx,gridy] = meshgrid([nMin:nMax/nRes:nMax],[nMin:nMax/nRes:nMax]);

gridz =
griddata([axKnownVals,axGeneratedVals],[ayKnownVals,ayGeneratedVals],[azKnown
Vals,azGeneratedVals],gridx,gridy,'invdist');

% mReformCore is what will be saved in the sCoord structure
% - gridz can be easily generated later from mReformCore.
mReformCore =
[[axKnownVals,axGeneratedVals];[ayKnownVals,ayGeneratedVals];[azKnownVals,azG
eneratedVals]];

```



```

zLowCnt = 0;
zHighCnt = 1;
for xCheck = 1:nRes+1

    for yCheck = 1:nRes+1

        z = gridz(xCheck,yCheck);

        if z <= 0
            z = 0;
            zLowCnt = zLowCnt+1;
        end

        if z >= 1;
            z = 1;
            zHighCnt = zHighCnt+1;
        end

        gridz(xCheck,yCheck) = z;
    end

end

mxReform = gridx;
myReform = gridy;
mzReform = gridz;

OverallLogic = 1;
end

%
%~~~~~
%~~~~~
% GENERATION OF FRICTION LOOKUP TABLE
%
%~~~~~
%~~~~~

xFriction1 = 0;
xFriction2 = 1;

logic = 0;
while logic == 0
    aConfidence = sConfidence.Friction1;
    yFriction1 =
    ClutchModel_RandNumGen(aConfidence,sConfidence.aDiscretisation,sConfidence.nCo
nfidenceInitial);
    clear aConfidence

    aConfidence = sConfidence.Friction2;
    yFriction2 =
    ClutchModel_RandNumGen(aConfidence,sConfidence.aDiscretisation,sConfidence.nCo
nfidenceInitial);

```

```

clear aConfidence

logic = (yFriction2>0.15)&(yFriction2<0.35)&(yFriction1>0.45)&(yFriction1<0.75);
end

axFriction = [xFriction1,xFriction2];
ayFriction = [yFriction1,yFriction2];

%
~~~~~
% GENERATION OF NORMALISING VALUES
%
~~~~~

logic = 0;
while logic == 0
    aConfidence = sConfidence.maxDeform;
    maxDeform = 800000+(1300000-
800000)*ClutchModel_RandNumGen(aConfidence,sConfidence.aDiscretisation,sConfidence.nConfidenceInitial);
    clear aConfidence

    logic = (maxDeform>800000)&(1300000>maxDeform);
end

logic = 0;
while logic == 0
    aConfidence = sConfidence.maxReform;
    maxReform = 1800+(3000-
1800)*ClutchModel_RandNumGen(aConfidence,sConfidence.aDiscretisation,sConfidence.nConfidenceInitial);
    clear aConfidence

    logic = (maxReform>1800)&(3000>maxReform);
end

aAllGeneratedVals =
[zDeform55,zDeform5b,zDeform5a,yDeformb,yDeforma,zDeforma5,xDeforma,zReform51,zReform5a,yReform5a,zReforma1,xReforma1,yFriction1,yFriction2,maxDeform,maxReform];

```

## Confidence Update

```
function[sConfidence] =  
ClutchModel_ConfidenceUpdate(sConfidence,nConfidenceUpdate,aAllGeneratedVals)  
%aAllGeneratedVals =  
%[zDeform55,zDeform5b,zDeform5a,yDeformb,yDeforma,zDeforma5,xDeforma,zRefo  
rm51,zReform5a,yReform5a,zReforma1,xReforma1,yFriction1,yFriction2];  
aConfidenceOld = sConfidence.zDeform55;  
nCoord = aAllGeneratedVals(1);  
location = min(find(sConfidence.aDiscretisation>=nCoord));  
aConfidenceNew = aConfidenceOld;  
aConfidenceNew(location) = aConfidenceNew(location)+nConfidenceUpdate;  
sConfidence.zDeform55 = aConfidenceNew;  
clear aConfidenceOld aConfidenceNew nCoord location
```

```
aConfidenceOld = sConfidence.zDeform5b;  
nCoord = aAllGeneratedVals(2);  
location = min(find(sConfidence.aDiscretisation>=nCoord));  
aConfidenceNew = aConfidenceOld;  
aConfidenceNew(location) = aConfidenceNew(location)+nConfidenceUpdate;  
sConfidence.zDeform5b = aConfidenceNew;  
clear aConfidenceOld aConfidenceNew nCoord location
```

```
aConfidenceOld = sConfidence.zDeform5a;  
nCoord = aAllGeneratedVals(3);  
location = min(find(sConfidence.aDiscretisation>=nCoord));  
aConfidenceNew = aConfidenceOld;  
aConfidenceNew(location) = aConfidenceNew(location)+nConfidenceUpdate;  
sConfidence.zDeform5a = aConfidenceNew;  
clear aConfidenceOld aConfidenceNew nCoord location
```

```
aConfidenceOld = sConfidence.yDeformb;  
nCoord = aAllGeneratedVals(4);  
location = min(find(sConfidence.aDiscretisation>=nCoord));  
aConfidenceNew = aConfidenceOld;  
aConfidenceNew(location) = aConfidenceNew(location)+nConfidenceUpdate;  
sConfidence.yDeformb = aConfidenceNew;  
clear aConfidenceOld aConfidenceNew nCoord location
```

```
aConfidenceOld = sConfidence.yDeforma;  
nCoord = aAllGeneratedVals(5);  
location = min(find(sConfidence.aDiscretisation>=nCoord));  
aConfidenceNew = aConfidenceOld;  
aConfidenceNew(location) = aConfidenceNew(location)+nConfidenceUpdate;  
sConfidence.yDeforma = aConfidenceNew;  
clear aConfidenceOld aConfidenceNew nCoord location
```

```
aConfidenceOld = sConfidence.zDeforma5;  
nCoord = aAllGeneratedVals(6);  
location = min(find(sConfidence.aDiscretisation>=nCoord));  
aConfidenceNew = aConfidenceOld;  
aConfidenceNew(location) = aConfidenceNew(location)+nConfidenceUpdate;  
sConfidence.zDeforma5 = aConfidenceNew;  
clear aConfidenceOld aConfidenceNew nCoord location
```

```
aConfidenceOld = sConfidence.xDeforma;  
nCoord = aAllGeneratedVals(7);  
location = min(find(sConfidence.aDiscretisation>=nCoord));
```

```
aConfidenceNew = aConfidenceOld;
aConfidenceNew(location) = aConfidenceNew(location)+nConfidenceUpdate;
sConfidence.xDeforma = aConfidenceNew;
clear aConfidenceOld aConfidenceNew nCoord location
```

```
aConfidenceOld = sConfidence.zReform51;
nCoord = aAllGeneratedVals(8);
location = min(find(sConfidence.aDiscretisation>=nCoord));
aConfidenceNew = aConfidenceOld;
aConfidenceNew(location) = aConfidenceNew(location)+nConfidenceUpdate;
sConfidence.zReform51 = aConfidenceNew;
clear aConfidenceOld aConfidenceNew nCoord location
```

```
aConfidenceOld = sConfidence.zReform5a;
nCoord = aAllGeneratedVals(9);
location = min(find(sConfidence.aDiscretisation>=nCoord));
aConfidenceNew = aConfidenceOld;
aConfidenceNew(location) = aConfidenceNew(location)+nConfidenceUpdate;
sConfidence.zReform5a = aConfidenceNew;
clear aConfidenceOld aConfidenceNew nCoord location
```

```
aConfidenceOld = sConfidence.yReform5a;
nCoord = aAllGeneratedVals(10);
location = min(find(sConfidence.aDiscretisation>=nCoord));
aConfidenceNew = aConfidenceOld;
aConfidenceNew(location) = aConfidenceNew(location)+nConfidenceUpdate;
sConfidence.yReform5a = aConfidenceNew;
clear aConfidenceOld aConfidenceNew nCoord location
```

```
aConfidenceOld = sConfidence.zReforma1;
nCoord = aAllGeneratedVals(11);
location = min(find(sConfidence.aDiscretisation>=nCoord));
aConfidenceNew = aConfidenceOld;
aConfidenceNew(location) = aConfidenceNew(location)+nConfidenceUpdate;
sConfidence.zReforma1 = aConfidenceNew;
clear aConfidenceOld aConfidenceNew nCoord location
```

```
aConfidenceOld = sConfidence.xReforma1;
nCoord = aAllGeneratedVals(12);
location = min(find(sConfidence.aDiscretisation>=nCoord));
aConfidenceNew = aConfidenceOld;
aConfidenceNew(location) = aConfidenceNew(location)+nConfidenceUpdate;
sConfidence.xReforma1 = aConfidenceNew;
clear aConfidenceOld aConfidenceNew nCoord location
```

```
aConfidenceOld = sConfidence.Friction1;
nCoord = aAllGeneratedVals(13);
location = min(find(sConfidence.aDiscretisation>=nCoord));
aConfidenceNew = aConfidenceOld;
aConfidenceNew(location) = aConfidenceNew(location)+nConfidenceUpdate;
sConfidence.Friction1 = aConfidenceNew;
clear aConfidenceOld aConfidenceNew nCoord location
```

```
aConfidenceOld = sConfidence.Friction2;
nCoord = aAllGeneratedVals(14);
location = min(find(sConfidence.aDiscretisation>=nCoord));
aConfidenceNew = aConfidenceOld;
aConfidenceNew(location) = aConfidenceNew(location)+nConfidenceUpdate;
```

```
sConfidence.Friction2 = aConfidenceNew;  
clear aConfidenceOld aConfidenceNew nCoord location
```

## Data Storage Array

```
function[sCoords] = NumGen(nRuns)

Lower = 1;
Upper = 2;

for iCnt = 1:1:nRuns
sLimits.yDeform1 = [0.25,0.4]; %Initially lower limits set to zero
sLimits.yDeform2 = [0.25,0.55];
sLimits.yDeform3 = [0.25,0.65];
sLimits.yDeform4 = [0.25,0.75];
sLimits.yDeform5 = [0.25,0.8];

sLimits.yReform1 = [0,0.25];
sLimits.yReform2 = [0,0.3];
sLimits.yReform3 = [0,0.4];
sLimits.yReform4 = [0,0.9];
sLimits.yReform5 = [0,1];

sLimits.xAbilityDeform1 = 'n/a';
sLimits.xAbilityDeform2 = [0.4,1];
sLimits.xAbilityDeform3 = 'n/a';
sLimits.yAbilityDeform1 = 'n/a';
sLimits.yAbilityDeform2 = [0.5,0.75];
sLimits.yAbilityDeform3 = 'n/a';

sLimits.xAbilityReform1 = 'n/a';
sLimits.xAbilityReform2 = [0,0.6];
sLimits.xAbilityReform3 = 'n/a';
sLimits.yAbilityReform1 = 'n/a';
sLimits.yAbilityReform2 = [0.5,0.75];
sLimits.yAbilityReform3 = 'n/a';

sLimits.xFriction1 = 'n/a';
sLimits.xFriction2 = [0.1,0.7];
sLimits.xFriction3 = [0.3,0.9];
sLimits.xFriction4 = 'n/a';

sLimits.yFriction1 = [0.5,0.7];
sLimits.yFriction2 = [0.4,0.7];
sLimits.yFriction3 = [0.2,0.5];
sLimits.yFriction4 = [0.2,0.35];

xDeform1 = 0;
xDeform2 = 0.25;
xDeform3 = 0.5;
xDeform4 = 0.75;
xDeform5 = 1.0;

xReform1 = 0;
xReform2 = 0.25;
xReform3 = 0.5;
```

```

xReform4 = 0.75;
xReform5 = 1.0;

yReform1 = rand(1)*(sLimits.yReform1(2)-sLimits.yReform1(1));
yReform2 = yReform1 + rand(1)*(sLimits.yReform2(2)-yReform1);

yReform3 = yReform2 + rand(1)*(sLimits.yReform3(2)-yReform2);

yDeform1 = yReform1 + rand(1)*(sLimits.yDeform1(2)-yReform1);
yDeform2 = max(yReform2,yDeform1) + rand(1)*(sLimits.yDeform2(2)-
max(yReform2,yDeform1));
yDeform3 = max(yReform3,yDeform2) + rand(1)*(sLimits.yDeform3(2)-
max(yReform3,yDeform2));
yDeform4 = yDeform3 + rand(1)*(sLimits.yDeform4(2)-yDeform3);
yDeform5 = yDeform4 + rand(1)*(sLimits.yDeform5(2)-yDeform4);

yReform5 = yDeform5 + rand(1)*(sLimits.yReform5(2)-yDeform5);
yReform4 = yReform3 + rand(1)*(yReform5-yReform3);

xAbilityDeform1 = 0;
xAbilityDeform2 =
sLimits.xAbilityDeform2(Lower)+rand(1)*(sLimits.xAbilityDeform2(Upper)-
sLimits.xAbilityDeform2(Lower));
xAbilityDeform3 = 1;
yAbilityDeform1 = 0.5;
yAbilityDeform2 =
sLimits.yAbilityDeform2(Lower)+rand(1)*(sLimits.yAbilityDeform2(Upper)-
sLimits.yAbilityDeform2(Lower));
yAbilityDeform3 = 1;

xAbilityReform1 = 0;
xAbilityReform2 = 1-xAbilityDeform2;
xAbilityReform3 = 1;
yAbilityReform1 = 1;
yAbilityReform2 = yAbilityDeform2;
yAbilityReform3 = 0.5;

xFriction1 = 0;
xFriction2 = sLimits.xFriction2(Lower) + rand(1)*(sLimits.xFriction2(Upper) -
sLimits.xFriction2(Lower));
xFriction3 = max(xFriction2,sLimits.xFriction3(Lower)) +
rand(1)*(sLimits.xFriction3(Upper) - max(xFriction2,sLimits.xFriction3(Lower)));
xFriction4 = 1;

yFriction1 = sLimits.yFriction1(Lower)+rand(1)*(sLimits.yFriction1(Upper)-
sLimits.yFriction1(Lower));
yFriction2 = sLimits.yFriction2(Lower)+rand(1)*(yFriction1-
sLimits.yFriction2(Lower));

```

```
yFriction4 = sLimits.yFriction4(Lower)+rand(1)*(sLimits.yFriction4(Upper)-
sLimits.yFriction4(Lower));
yFriction3 = yFriction4 + rand(1)*(min(yFriction2,sLimits.yFriction3(Upper))-
yFriction4);
```

```
sCoords.axDeform(iCnt,:) = [xDeform1,xDeform2,xDeform3,xDeform4,xDeform5];
sCoords.ayDeform(iCnt,:) = [yDeform1,yDeform2,yDeform3,yDeform4,yDeform5];
```

```
sCoords.axReform(iCnt,:) = [xReform1,xReform2,xReform3,xReform4,xReform5];
sCoords.ayReform(iCnt,:) = [yReform1,yReform2,yReform3,yReform4,yReform5];
```

```
sCoords.axAbilityDeform(iCnt,:) =
[xAbilityDeform1,xAbilityDeform2,xAbilityDeform3];
sCoords.ayAbilityDeform(iCnt,:) =
[yAbilityDeform1,yAbilityDeform2,yAbilityDeform3];
sCoords.axAbilityReform(iCnt,:) =
[xAbilityReform1,xAbilityReform2,xAbilityReform3];
sCoords.ayAbilityReform(iCnt,:) =
[yAbilityReform1,yAbilityReform2,yAbilityReform3];
```

```
sCoords.axFriction(iCnt,:) = [xFriction1,xFriction2,xFriction3,xFriction4];
sCoords.ayFriction(iCnt,:) = [yFriction1,yFriction2,yFriction3,yFriction4];
```

end



## Final Input Model

```
function[CluPressurePrev_bar,CluClampLoadPrev_N,CluTorqueNew_Nm,CluSpeedDiff
New_rpm,CluPowerNew_W] =
ClutchModel_RigModel(Time_s,sCluData,dt_s,CluMuPrev,CluSpeedDiffPrev_rpm,RigPr
essureDemand_bar)

TimePressureRise_s = 0.025;           % Time taken for the pressure applied by the
rig to reach the maximum value [s]
%RigPressureDemand_bar = 60;         % Maximum pressure applied by the rig
during the event [bar]

% If the time at the current timestep is less than the pressure rise time:
% - Calculate the pressure based upon a linear interpolation
% If the time at the current timestep is greater than pressure rise time;
% - Assume pressure is the max pressure
if Time_s < TimePressureRise_s
    CluPressurePrev_bar = RigPressureDemand_bar*(Time_s/TimePressureRise_s);
else
    CluPressurePrev_bar = RigPressureDemand_bar;
end

% Clutch clamp load calculated from:
% - Force = Pressure x Area
CluClampLoadPrev_N =
(CluPressurePrev_bar*1e5)*(sCluData.TotalPistonArea_mm2/1e6)*sCluData.LeverRat
io;

CluTorqueNew_Nm =
CluMuPrev*CluClampLoadPrev_N*sCluData.NumWorkingSurfaces*(sCluData.MeanFri
ctionRad_mm/1e3);

% Convert the clutch speed difference from RPM to radians per second i.e. SI units
CluSpeedDiffPrev_radpers = CluSpeedDiffPrev_rpm*(2*pi/60);

% New clutch speed difference calculated from:
% - Torque = Inertia x angular acceleration
% T = I * (theta double dot)
% T = I * (v2 - v1)/dt
% v2 - v1 = T * dt/I
% v2 = v1 + (T*dt/I)
CluSpeedDiffNew_radpers = CluSpeedDiffPrev_radpers + (-
CluTorqueNew_Nm*dt_s/(sCluData.fInertiaClutchOPS_kgm2+sCluData.fInertiaRig_kg
m2+(sCluData.fInertiaMotor_kgm2/(sCluData.fSpeedIncreasingRatio^2))));

% New clutch power dissipation calculated from:
% - Power = Torque x Angular velocity
CluPowerNew_W = CluTorqueNew_Nm*CluSpeedDiffNew_radpers;

% Convert new speed difference back to rpm from SI unit.
CluSpeedDiffNew_rpm = CluSpeedDiffNew_radpers*(60/(2*pi));

% Clear unneeded variables
clear CluSpeedDiffNew_radpers CluSpeedDiffOld_radpers

% ~~~~~
```

% Ends

## Final Thermal Model

```
function[TempAirNew_degC,TempBulkNew_degC,TempSurfaceNew_degC] =  
ClutchModel_ThermalModelSimple(sCluData,TempAirPrev_degC,TempBulkPrev_degC,  
TempSurfacePrev_degC,CluPowerNew_W,dt_s)
```

```
% ~~~~~  
% DEFINE MODEL PARAMETERS  
SurfaceThickness_m = 0.000010;           % Thickness of the surface region [m]  
% ~~~~~
```

```
% ~~~~~  
% DEFINE ENVIRONMENTAL PROPERTIES  
AirConvectiveTransferCoef = 100;        % Convective transfer coefficient for air  
% ~~~~~  
% DEFINE CONSTANTS  
StefanBoltzmannConst = 5.6704e-08;     % Heat transfer constant of  
proportionality [W/m^2.K^4]  
% ~~~~~
```

```
% OTHER MODEL CALCULATIONS  
BulkThickness_m = 0.5*(sCluData.DiscThickness_m - 2*SurfaceThickness_m);  
% Thickness of the bulk region [m]  
MassBulk_kg =  
sCluData.DensityCC_kgperm3*(BulkThickness_m*sCluData.SingleWorkingSurfaceArea  
_m2); % Mass of the bulk region [kg]  
MassSurface_kg =  
sCluData.DensityCC_kgperm3*(SurfaceThickness_m*sCluData.SingleWorkingSurfaceA  
rea_m2); % Mass of the surface region [kg]  
BulkCircumfSurfaceArea_m2 = BulkThickness_m*(sCluData.DiamOuter_mm/1e3)*pi;  
% Exposed radial area of the bulk material [m^2]  
% ~~~~~
```

```
% ~~~~~  
% CONVERT TEMPERATURES FROM CELCIUS TO KELVIN  
TempAirPrev_K = TempAirPrev_degC + 273;  
TempBulkPrev_K = TempBulkPrev_degC + 273;  
TempSurfacePrev_K = TempSurfacePrev_degC + 273;
```

```
% ~~~~~  
% SPECIFIC HEAT CAPACITY LOOKUP  
% ~~~~~  
aCvCC = [sCluData.CvCCRT_JperkgK,sCluData.CvCC1000_JperkgK];  
aCvTemps_K = [27+273,1000+273];
```

```

% If previous surface temperature < 27 deg C
% - Assume Cv is Cv@27degC
% If previous surface temperature > 1000 deg C
% - Assume Cv is Cv@1000degC
% Else assume Cv function is linear and perform interpolation to obtain value for
current surface temperature
if TempSurfacePrev_K < aCvTemps_K(1)
    CvSurface_JperkgK = aCvCC(1);
elseif TempSurfacePrev_K > aCvTemps_K(2);
    CvSurface_JperkgK = aCvCC(2);
else
    CvSurface_JperkgK = interp1(aCvTemps_K,aCvCC,TempSurfacePrev_K);
end

% Repeat above for bulk
if TempBulkPrev_K < aCvTemps_K(1)
    CvBulk_JperkgK = aCvCC(1);
elseif TempBulkPrev_K > aCvTemps_K(2);
    CvBulk_JperkgK = aCvCC(2);
else
    CvBulk_JperkgK = interp1(aCvTemps_K,aCvCC,TempBulkPrev_K);
end

% ~~~~~
% HEAT TRANSFER CALCULATIONS
% ~~~~~

% Assume that entire energy dissipated over the timestep is absorbed into the friction
surface as heat
% - assumptions = zero surface roughness
%           = zero losses to environment
QSurfaceAbsorbed_J = (CluPowerNew_W/12)*dt_s;    % IMPORTANT - divide by 12
as only considering one disc-disc interface (one working surface = two interfaces)

% Heat flux due to conduction from surface to bulk
% - Delta Q = -k.A.(Delta T/Delta x)
% - assumption = uniform conduction through working surface area
QSurfaceConducted_J = -
(sCluData.ThermalConductivityCCRT_WpermK*sCluData.SingleWorkingSurfaceArea_
m2*(TempBulkPrev_K-TempSurfacePrev_K)/BulkThickness_m)*dt_s;

% Heat flux due to convection from surface to bulk
% - Delta Q = A.h.(Delta T)
% - assumption = convection from radial surface of bulk only
QBulkConvected_J =
AirConvectiveTransferCoef*BulkCircumfSurfaceArea_m2*(TempBulkPrev_K-
TempAirPrev_K)*dt_s;

% Heat flux due to radiation
% - Delta Q = A.*.*.(Delta T)^4
% - assumption = radiation from radial surface of bulk only
QBulkRadiated_J =
BulkCircumfSurfaceArea_m2*StefanBoltzmannConst*sCluData.Emissivity*(TempBulk
Prev_K^4 - TempAirPrev_K^4)*dt_s;

```

```

% Flux summation for surface, bulk and ambient environment
% Delta Q = m.Cv.(Delta T)
% - Delta Q = (Heat flux in - heat flux out) over the timestep dt
% For surface:
DeltaTempSurface_K = (QSurfaceAbsorbed_J-
QSurfaceConducted_J)/(MassSurface_kg*CvSurface_JperkgK);
TempSurfaceNew_K = TempSurfacePrev_K + DeltaTempSurface_K;
% New surface temperature = previous surface temperature plus change due to heat
flux
% For bulk:
DeltaTempBulk_K = (QSurfaceConducted_J-QBulkConvected_J-
QBulkRadiated_J)/(MassBulk_kg*CvBulk_JperkgK);
TempBulkNew_K = TempBulkPrev_K + DeltaTempBulk_K;
% For air:
% - assumption = air remains at ambient temp due to air flow i.e. scenario is not a
closed system
TempAirNew_K = TempAirPrev_K;

% Convert back to deg C from Kelvin
TempAirNew_degC = TempAirNew_K - 273;
TempBulkNew_degC = TempBulkNew_K - 273;
TempSurfaceNew_degC = TempSurfaceNew_K - 273;

% ~~~~~
% Ends

```

## Final Surface Model

```
function[CluMuNew,CoefSurfaceStateNew,CoefDeform,CoefReform] =  
ClutchModel_SurfaceModel(iGen,sCluData,CluPowerNew_W,TempSurfaceNew_degC,  
CoefSurfaceStatePrev,sCoordsCurrent)
```

```
PowerDensityMax_Wperm2 = sCoordsCurrent.maxDeform;  
TempSurfaceMax_K = sCoordsCurrent.maxReform;
```

```
PowerDensity_Wperm2 =  
(CluPowerNew_W/sCluData.SingleWorkingSurfaceArea_m2)/12;
```

```
CoefPowerDensity = PowerDensity_Wperm2/PowerDensityMax_Wperm2;
```

```
if CoefPowerDensity >= 1  
    CoefPowerDensity = 1;  
end
```

```
% Convert the temperature at the current time step to K  
TempSurfaceNew_K = TempSurfaceNew_degC + 273;
```

```
CoefTempSurface = TempSurfaceNew_K/TempSurfaceMax_K;
```

```
if CoefTempSurface >=1  
    CoefTempSurface = 1;  
end
```

```
% Assume surface is only deformed and reformed when plates are in contact.  
% - In this model, plates are in contact when slipping occurs.
```

```
%CoefDeform =  
interp1(sCoords.axDeform(iGen,:),sCoords.ayDeform(iGen,:),CoefPowerDensity,'pchip'  
');  
%CoefReform =  
interp1(sCoords.axReform(iGen,:),sCoords.ayReform(iGen,:),CoefTempSurface,'pchip'  
);
```

```
CoefDeform =  
interp2(sCoordsCurrent.mxDeform,sCoordsCurrent.myDeform,sCoordsCurrent.mzDef  
orm,CoefPowerDensity,CoefSurfaceStatePrev,'cubic');  
CoefReform =  
interp2(sCoordsCurrent.mxReform,sCoordsCurrent.myReform,sCoordsCurrent.mzRef  
orm,CoefTempSurface,CoefSurfaceStatePrev,'cubic');
```

```
%CoefAbilityDeform =  
interp1(sCoords.axAbilityDeform(iGen,:),sCoords.ayAbilityDeform(iGen,:),CoefSurface  
StatePrev,'pchip');  
%CoefAbilityReform =  
interp1(sCoords.axAbilityReform(iGen,:),sCoords.ayAbilityReform(iGen,:),CoefSurface  
StatePrev,'pchip');
```

```
%DeltaCoefSurfaceState = (CoefReform*CoefAbilityReform) -  
(CoefDeform*CoefAbilityDeform);  
DeltaCoefSurfaceState = CoefReform - CoefDeform;
```

```
CoefSurfaceStateNew = CoefSurfaceStatePrev + DeltaCoefSurfaceState;
```

```
if CoefSurfaceStateNew >=1  
    CoefSurfaceStateNew = 1;  
elseif CoefSurfaceStateNew <= 0  
    CoefSurfaceStateNew = 0;  
end
```

```
CluMuNew =  
interp1(sCoordsCurrent.axFriction,sCoordsCurrent.ayFriction,CoefSurfaceStateNew,'c  
ubic');
```

```
if CluMuNew >= 1  
    CluMuNew = 1;  
end
```

## Final Model Code for Thermal Characteristic Generation

```
% ~~~~~  
% SYNTAX:  
% n/a  
%  
% FILENAME:  
% ClutchModel.m  
%  
% FUNCTION:  
% Full clutch model to describe clutch engagement events based upon  
% surface property lookup tables.  
%  
% Can be used to generate and optimise the set of lookup tables, or to  
% simulate rig testing when lookup tables are known and validated.  
%  
% ARGUMENTS:  
% None  
%  
% RETURNS:  
% None  
%  
% REQUIRED FILES:  
% - ClutchModel_Init.m  
% - ClutchModel_ThermalModelSimple.m  
% - ClutchModel_SurfaceModel.m  
% - ClutchModel_LookupGenerator.m  
% - ClutchModel_RandNumGen.m  
%  
% ~~~~~
```

```
% Ensure that the workspace is cleared before use  
close all  
clear all
```

```
% Run the initialization file to populate the workspace  
run ClutchModel_Init
```

```
% Load the data to which the sim results will be correlated  
ClutchPack = 'clutch 1';  
strDataPath = C:\Documents and Settings\glawrence\Desktop\Clutch Model\  
strFullFilename = [strDataPath,ClutchPack,'\','MatlabAnalysisResults.mat'];  
load(strFullFilename,'sData');  
SHGTData = SHGTData(1:nEvents);
```

```
% If not using the random number generator feature, ensure nGenerate is overridden  
if bRandGen == OFF  
    % Load the lookup tables from the filename and filepath described  
    strLookupTableFilepath = 'C:\Documents and Settings\glawrence\Desktop\Clutch  
Model\Results\  
strLookupTableFilename = 'sLookupTables-Results.mat';  
strLookupTableFullFilename = [strLookupTableFilepath,strLookupTableFilename];  
load(strLookupTableFullFilename);
```

```

    % Define how many runs to perform
    nGenerate = length(sCoordsLoad);           % --> If 5 sets in structure, do
5 runs, etc etc.
    sCoords = sCoordsLoad;
end

tic

for iGen = 1:1:nGenerate                       % --> nGenerate = Number of
lookup table datasets to test

    %iGen                                       % --> Unsuppress this if wanting to track
optimisation progress

    % Reset timestep to beginning
    iTimeStep = 1;

    % If lookup table optimisation has been chosen:
    % - Define the confidence levels for each coordinate
    % - Generate each coordinate based on confidence
    if bRandGen == ON

        %
        ~~~~~
        % LOOKUP TABLE GENERATION
        %
        ~~~~~

        % If first generation cycle, we need to set the confidence levels to the initial
        values.
        % - Store all confidence arrays within the structure sConfidence
        if iGen == 1;
            aConfidenceInitial = sConfidence.aConfidenceInitial;

            sConfidence.zDeform55 = aConfidenceInitial;           % -->
sConfidence.zDeform55 = Array of confidence values for the generated coordinate
zDeform55
            sConfidence.zDeform5b = aConfidenceInitial;           % -->
sConfidence.zDeform5b = Array of confidence values for the generated coordinate
zDeform5b
            sConfidence.zDeform5a = aConfidenceInitial;           % -->
sConfidence.zDeform5a = Array of confidence values for the generated coordinate
zDeform5a
            sConfidence.yDeformb = aConfidenceInitial;           % -->
sConfidence.yDeformb = Array of confidence values for the generated coordinate
yDeformb
            sConfidence.yDeforma = aConfidenceInitial;           % -->
sConfidence.yDeforma = Array of confidence values for the generated coordinate
yDeforma
            sConfidence.zDeforma5 = aConfidenceInitial;           % -->
sConfidence.zDeforma5 = Array of confidence values for the generated coordinate
zDeforma5
            sConfidence.xDeforma = aConfidenceInitial;           % -->
sConfidence.xDeforma = Array of confidence values for the generated coordinate
xDeforma

```



```

sConfidence.zReform51 = aConfidenceInitial;
sConfidence.zReform5a = aConfidenceInitial;
sConfidence.zReforma1 = aConfidenceInitial;
sConfidence.yReform5a = aConfidenceInitial;
sConfidence.xReforma1 = aConfidenceInitial;

sConfidence.Friction1 = aConfidenceInitial;
sConfidence.Friction2 = aConfidenceInitial;

sConfidence.maxDeform = aConfidenceInitial;
sConfidence.maxReform = aConfidenceInitial;
end

```

*% Use the function CoordGen to return the lookup table coordinate matrices for this iteration of lookup tables*

```

[mxDeform,myDeform,mzDeform,mxReform,myReform,mzReform,axFriction,ayFriction,mDeformCore,mReformCore,aAllGeneratedVals,maxDeform,maxReform] = CoordGen(sConfidence);

```

*% Save the generated coordinates into the structure sCoords for future analysis*

```

sCoords(iGen,:).mxDeform = mxDeform;
sCoords(iGen,:).myDeform = myDeform;
sCoords(iGen,:).mzDeform = mzDeform;
sCoords(iGen,:).mxReform = mxReform;
sCoords(iGen,:).myReform = myReform;
sCoords(iGen,:).mzReform = mzReform;
sCoords(iGen,:).mDeformCore = mDeformCore;
sCoords(iGen,:).mReformCore = mReformCore;
sCoords(iGen,:).axFriction = axFriction;
sCoords(iGen,:).ayFriction = ayFriction;
sCoords(iGen,:).maxDeform = maxDeform;
sCoords(iGen,:).maxReform = maxReform;

```

```
clear mDeformCore mReformCore
```

*% Generate the structure sCoordsCurrent to store the current coordinates  
% - Reason = to make it easier to pass the coords to future functions*

```

sCoordsCurrent.mxDeform = mxDeform;
sCoordsCurrent.myDeform = myDeform;
sCoordsCurrent.mzDeform = mzDeform;
sCoordsCurrent.mxReform = mxReform;
sCoordsCurrent.myReform = myReform;
sCoordsCurrent.mzReform = mzReform;
sCoordsCurrent.axFriction = axFriction;
sCoordsCurrent.ayFriction = ayFriction;
sCoordsCurrent.maxDeform = maxDeform;
sCoordsCurrent.maxReform = maxReform;

```

*% Now that the current coords have been saved, we can clear the individual matrices*

```
clear mxDeform myDeform mzDeform mxReform myReform mzReform axFriction ayFriction maxDeform maxReform
```

*% If lookup table optimisation has not been chosen:  
% - Load the lookup table coordinates*

```

elseif bRandGen == OFF
    sCoordsCurrent.mxDeform = sCoordsLoad(iGen).mxDeform;
    sCoordsCurrent.myDeform = sCoordsLoad(iGen).myDeform;
    sCoordsCurrent.mzDeform = sCoordsLoad(iGen).mzDeform;
    sCoordsCurrent.mxReform = sCoordsLoad(iGen).mxReform;
    sCoordsCurrent.myReform = sCoordsLoad(iGen).myReform;
    sCoordsCurrent.mzReform = sCoordsLoad(iGen).mzReform;
    sCoordsCurrent.axFriction = sCoordsLoad(iGen).axFriction;
    sCoordsCurrent.ayFriction = sCoordsLoad(iGen).ayFriction;
    sCoordsCurrent.maxDeform = sCoordsLoad(iGen).maxDeform;
    sCoordsCurrent.maxReform = sCoordsLoad(iGen).maxReform;
end

% Now that lookup tables have been created, perform runs in the cycle
% - For each event, find the actuation pressure
% -
for iEvent = 1:nEvents

    %
    ~~~~~
    % CLUTCH ACTUATION PRESSURE PROFILE
    %
    ~~~~~
    % Clutch actuation pressure is not constant throughout HGT events
    % - Events 1 and 2 are performed at 70bar
    % - Subsequent events follow the following cycle:
    % --> 40,70,50,70,60,70 bar
    Event40bar = [3:6:123];
    Event50bar = [5:6:125];
    Event60bar = [7:6:127];
    Event70bar = [1,2:2:128];

    if isempty(find(iEvent == Event70bar))~=1;
        RigPressureDemand_bar = 70;
    elseif isempty(find(iEvent == Event40bar))~=1;
        RigPressureDemand_bar = 40;
    elseif isempty(find(iEvent == Event50bar))~=1;
        RigPressureDemand_bar = 50;
    elseif isempty(find(iEvent == Event60bar))~=1;
        RigPressureDemand_bar = 60;
        % If sim goes beyond limits set above, use a very high value to speed up
        % subsequent events (value tending to zero will make event duration tend to infinity)
    else
        RigPressureDemand_bar = 150;
    end

    iTimeStep = 1;
    CluSpeedDiffPrev_rpm = sInitConds.CluSpeedDiff_rpm;

    while CluSpeedDiffPrev_rpm > 300 % --> Use of 300rpm for
lower limit as HGT have a measurement error below this value

        iTimeStep = iTimeStep + 1;

```

```
Time_s = (iTimeStep-1)*dt_s;  
sEvent(iEvent).aTime_s(iTimeStep,1) = Time_s;
```

```
    %  
    ~~~~~  
    % CLUTCH RIG MODEL  
    %  
    ~~~~~  
    % At each time step, need to provide:  
    % - new rig clamp pressure  
    % - new clutch differential speed  
    % - new clutch torque  
    % - power dissipated over the timestep  
  
    % If we are at the first timestep, all knowns should be set to its initial value  
    if iTimeStep == 2  
  
        sEvent(iEvent).aCluSpeedDiff_rpm(1,1) = sInitConds.CluSpeedDiff_rpm;  
        sEvent(iEvent).aTempAir_degC(1,1) = sInitConds.TempAir_degC;  
        sEvent(iEvent).aTempBulk_degC(1,1) = sInitConds.TempBulk_degC;  
        sEvent(iEvent).aTempSurface_degC(1,1) = sInitConds.TempSurface_degC;  
  
        if iEvent == 1  
            sEvent(iEvent).aCoefSurfaceState(1,1) = sInitConds.CoeffSurfaceState;  
            sEvent(iEvent).aCluMu(1,1) =  
interp1(sCoords(iGen).axFriction,sCoords(iGen).ayFriction,sEvent(iEvent).aCoefSurfa  
ceState(1,1));  
  
        else  
            sEvent(iEvent).aCoefSurfaceState(1,1) = sEvent(iEvent-  
1).aCoefSurfaceState(end);  
            sEvent(iEvent).aCluMu(1,1) =  
interp1(sCoords(iGen).axFriction,sCoords(iGen).ayFriction,sEvent(iEvent).aCoefSurfa  
ceState(1,1));  
        end  
  
    end  
  
    CluSpeedDiffPrev_rpm = sEvent(iEvent).aCluSpeedDiff_rpm(iTimeStep-1,1);  
    CluMuPrev = sEvent(iEvent).aCluMu(iTimeStep-1,1);  
    CoefSurfaceStatePrev = sEvent(iEvent).aCoefSurfaceState(iTimeStep-1);  
  
    [CluPressurePrev_bar,CluClampLoadPrev_N,CluTorqueNew_Nm,CluSpeedDiffNew_rpm,  
CluPowerNew_W] =  
ClutchModel_RigModel(Time_s,sCluData,dt_s,CluMuPrev,CluSpeedDiffPrev_rpm,RigPr  
essureDemand_bar);  
    clear Time_s CluMuPrev  
  
    sEvent(iEvent).aCluPressure_bar(iTimeStep-1,1) = CluPressurePrev_bar;
```

```

sEvent(iEvent).aCluClampLoad_N(iTimeStep-1,1) = CluClampLoadPrev_N;
sEvent(iEvent).aCluTorque_Nm(iTimeStep,1) = CluTorqueNew_Nm;
sEvent(iEvent).aCluSpeedDiff_rpm(iTimeStep,1) = CluSpeedDiffNew_rpm;
sEvent(iEvent).aCluPower_W(iTimeStep,1) = CluPowerNew_W;

```

```

%

```

```

~~~~~
% CLUTCH THERMAL MODEL

```

```

%

```

```

~~~~~
% At each time step, need to provide:

```

```

% - new clutch surface temperature

```

```

% - new clutch bulk temperature

```

```

% - new ambient temperature

```

```

TempAirPrev_degC = sEvent(iEvent).aTempAir_degC(iTimeStep-1,1);

```

```

TempBulkPrev_degC = sEvent(iEvent).aTempBulk_degC(iTimeStep-1,1);

```

```

TempSurfacePrev_degC = sEvent(iEvent).aTempSurface_degC(iTimeStep-1,1);

```

```

[TempAirNew_degC,TempBulkNew_degC,TempSurfaceNew_degC] =

```

```

ClutchModel_ThermalModelSimple(sCluData,TempAirPrev_degC,TempBulkPrev_degC,
TempSurfacePrev_degC,CluPowerNew_W,dt_s);

```

```

sEvent(iEvent).aTempAir_degC(iTimeStep,1) = TempAirNew_degC;

```

```

sEvent(iEvent).aTempBulk_degC(iTimeStep,1) = TempBulkNew_degC;

```

```

sEvent(iEvent).aTempSurface_degC(iTimeStep,1) = TempSurfaceNew_degC;

```

```

clear TempSurfacePrev_degC TempBulkPrev_degC TempAirPrev_degC

```

```

%

```

```

~~~~~
% CLUTCH SURFACE MODEL

```

```

%

```

```

~~~~~
% At each time step, need to provide:

```

```

% - new clutch surface state

```

```

% - new clutch coefficient of friction

```

```

[CluMuNew,CoefSurfaceStateNew,CoefDeform,CoefReform] =

```

```

ClutchModel_SurfaceModel(iGen,sCluData,CluPowerNew_W,TempSurfaceNew_degC,
CoefSurfaceStatePrev,sCoordsCurrent);

```

```

clear CoefSurfaceStatePrev CluPowerNew_W TempSurfaceNew_degC

```

```

TempBulkNew_degC TempAirNew_degC

```

```

sEvent(iEvent).aCluMu(iTimeStep,1) = CluMuNew;

```

```

sEvent(iEvent).aCoefSurfaceState(iTimeStep,1) = CoefSurfaceStateNew;

```

```

sEvent(iEvent).aCoefDeform(iTimeStep,1) = CoefDeform;

```

```

sEvent(iEvent).aCoefReform(iTimeStep,1) = CoefReform;

```

```

clear CoefDeform CoefReform CluMuNew CoefSurfaceStateNew

```

```

    %sEvent(iEvent).aCluMu(iTimeStep,1) = sEvent(iEvent).aCluMu(iTimeStep-
1,1);
    %sEvent(iEvent).aCoefSurfaceState(iTimeStep,1) =
sEvent(iEvent).aCoefSurfaceState(iTimeStep-1,1);

end

%
~~~~~
% OBTAIN MEASUREMENTS FOR CORRELATION PURPOSES
%
~~~~~
% AIM:
% To check accuracy of simulation output against measured output
%
% MEASUREMENTS:
% 1) Determine total event duration
% 2) Grab sim mu at [10,30,50,70,90]% of event duration
% 3) Determine peak mu value in initial and final 0.1s of event
% 4) Determine mean mu for event

fDuration = length(sEvent(iEvent).aTime_s);
sEvent(iEvent).fDuration_s = sEvent(iEvent).aTime_s(end);

aGrabMuPoints_percent = [10,30,50,70,90];
aGrabMuPoints = round(fDuration*(aGrabMuPoints_percent./100));
sEvent(iEvent).aGrabMuVals = sEvent(iEvent).aCluMu(aGrabMuPoints);

sEvent(iEvent).fMuPeakInitial = max(sEvent(iEvent).aCluMu(1:(0.1/dt_s)));
%sEvent(iEvent).fMuPeakFinal =
max(sEvent(iEvent).aCluMu(((sEvent(iEvent).fDuration_s-
0.1)/dt_s):(sEvent(iEvent).fDuration_s/dt_s)));
sEvent(iEvent).fMuAve = mean(sEvent(iEvent).aCluMu);

aDeltaTorqueRange =
find(sEvent(iEvent).aCluSpeedDiff_rpm<=7200&sEvent(iEvent).aCluSpeedDiff_rpm>8
00)';
sEvent(iEvent).fDeltaTorque =
(max(sEvent(iEvent).aCluTorque_Nm(aDeltaTorqueRange))-
(min(sEvent(iEvent).aCluTorque_Nm(aDeltaTorqueRange)));

sEvent(iEvent).aCorrelationData =
[sEvent(iEvent).aGrabMuVals',sEvent(iEvent).fMuPeakInitial,sEvent(iEvent).fMuAve,s
Event(iEvent).fDeltaTorque,sEvent(iEvent).fDuration_s];

sEvent(iEvent).aCorrelationResult = abs(sEvent(iEvent).aCorrelationData-
sHGTDData(iEvent).aCorrelationData)./sHGTDData(iEvent).aCorrelationData;
sEvent(iEvent).fCorrelationResultTotal =
(sum(sEvent(iEvent).aCorrelationResult))/length(sEvent(iEvent).aCorrelationResult)
;
end

```

```

sResults(iGen).sEvent = sEvent;
for iCnt = 1:nEvents
    aCheck(iCnt,1) = sResults(iGen).sEvent(iCnt).fCorrelationResultTotal;
end
%sResults(iGen).CorrTot = sum(aCheck);
sCoords(iGen).AccuracyResult = (sum(aCheck))/nEvents;

if bRandGen == ON
if bConfidenceUpdate == ON
    nConfidenceUpdate = (1-sCoords(iGen).AccuracyResult)^2;
    [sConfidence] =
ClutchModel_ConfidenceUpdate(sConfidence,nConfidenceUpdate,aAllGeneratedVals);

end
end
clear sEvent aCheck nConfidenceUpdate aAllGeneratedVals

if bSaveResults == 1

    % If we are randomly generating results
    if bRandGen == ON

        if iGen == iSave*nthResultSave;
            save(FullFilename,'sCoords','sConfidence');
            iSave = iSave+1;
            SaveText = sprintf('Result saved after %5.0f iterations',iGen)

        end

        elseif bRandGen == OFF
            save(FullFilename,'sCoords','sResults');

        end

    end

    if bRandGen == ON
        clear sResults
    end

end

toc

if bRandGen == ON

for iCnt = 1:length(sCoords)
    aAccuracy(iCnt,1) = sCoords(iCnt).AccuracyResult;
end

```

```

[aAccuracySortedVals,aAccuracySortedPoints] = sort(aAccuracy,'ascend');

nAnalyseBestPercentage = 5; % --> Analyse the best n% of results

nPos = ceil(length(aAccuracySortedVals)*(nAnalyseBestPercentage/100));

clear iCnt

for iCnt = 1:nPos
toget = aAccuracySortedPoints(iCnt);
a = sCoords(toget);
sCoordsLoad(iCnt) = a;
clear a toget
end

strLookupTableSavepath = 'C:\Documents and Settings\glawrence\Desktop\Clutch
Model\Results\';
strFullFilename = [strLookupTableSavepath,'sLookupTables-',Filename];
save(strFullFilename,'sCoordsLoad');
end

if bRandGen == ON

figure
stairs(sConfidence.aDiscretisation,sConfidence.zDeform55,'-', 'color','k')
hold on
stairs(sConfidence.aDiscretisation,sConfidence.zDeform5a,'-', 'color','b')
stairs(sConfidence.aDiscretisation,sConfidence.zDeform5b,'-', 'color','g')

stairs(sConfidence.aDiscretisation,sConfidence.zReforma1,'-', 'color',[0,0.5,0])
stairs(sConfidence.aDiscretisation,sConfidence.yReform5a,'-', 'color','y')
stairs(sConfidence.aDiscretisation,sConfidence.xReforma1,'-', 'color','c')
stairs(sConfidence.aDiscretisation,sConfidence.Friction1,'-', 'color','r')
stairs(sConfidence.aDiscretisation,sConfidence.Friction2,'-', 'color','m')

a = flipud(autumn);

for iCnt = 1:length(sConfidence.aDiscretisation)

    sConfidencePlot(1).Color(1,iCnt) = 1+floor(64*((sConfidence.zDeform55(iCnt)-
sConfidence.nConfidenceInitial)/((sum(sConfidence.zDeform55))-
(sConfidence.nConfidenceInitial*sConfidence.nDiscretisation))));
    sConfidencePlot(2).Color(1,iCnt) = 1+floor(64*((sConfidence.zDeform5a(iCnt)-
sConfidence.nConfidenceInitial)/((sum(sConfidence.zDeform5a))-
(sConfidence.nConfidenceInitial*sConfidence.nDiscretisation))));
    sConfidencePlot(3).Color(1,iCnt) = 1+floor(64*((sConfidence.zReforma1(iCnt)-
sConfidence.nConfidenceInitial)/((sum(sConfidence.zReforma1))-
(sConfidence.nConfidenceInitial*sConfidence.nDiscretisation))));

```

```

    sConfidencePlot(4).Color(1,iCnt) = 1+floor(64*((sConfidence.zDeform5b(iCnt)-
sConfidence.nConfidenceInitial)/((sum(sConfidence.zDeform5b))-
(sConfidence.nConfidenceInitial*sConfidence.nDiscretisation))));
    sConfidencePlot(5).Color(1,iCnt) = 1+floor(64*((sConfidence.yReform5a(iCnt)-
sConfidence.nConfidenceInitial)/((sum(sConfidence.yReform5a))-
(sConfidence.nConfidenceInitial*sConfidence.nDiscretisation))));
    sConfidencePlot(6).Color(1,iCnt) = 1+floor(64*((sConfidence.xReforma1(iCnt)-
sConfidence.nConfidenceInitial)/((sum(sConfidence.xReforma1))-
(sConfidence.nConfidenceInitial*sConfidence.nDiscretisation))));
    sConfidencePlot(7).Color(1,iCnt) = 1+floor(64*((sConfidence.Friction1(iCnt)-
sConfidence.nConfidenceInitial)/((sum(sConfidence.Friction1))-
(sConfidence.nConfidenceInitial*sConfidence.nDiscretisation))));
    sConfidencePlot(8).Color(1,iCnt) = 1+floor(64*((sConfidence.Friction2(iCnt)-
sConfidence.nConfidenceInitial)/((sum(sConfidence.Friction2))-
(sConfidence.nConfidenceInitial*sConfidence.nDiscretisation))));

```

```
end
```

```
figure
```

```
hold on
```

```
for iy = 1:8
```

```
    for ix = 1:length(sConfidence.aDiscretisation)
```

```
        col = [a((sConfidencePlot(iy).Color(ix)),:);
```

```
        plot(ix-0.5,iy,'s','Color',col,'MarkerSize',25,'MarkerFaceColor',col)
```

```
    end
```

```
    line([0,length(sConfidence.aDiscretisation)],[iy-0.5,iy-0.5],'Color','k','LineWidth',3)
```

```
end
```

```
xlim([0,length(sConfidence.aDiscretisation)])
```

```
ylim([0.5,8.5])
```

```
end
```